Universidade do Porto

Faculdade de Engenharia

FEUP

CONVECTION, DIFFUSION AND REACTION:

BRIDGING SCALES IN SCIENCE AND ENGINEERING

A Dissertation presented to the UNIVERSITY OF PORTO

for the degree of Doctor in Chemical and Biological Engineering by

João Pedro Lopes

Supervisor: Prof. Alírio E. Rodrigues, University of Porto

Co-Supervisor: Dr. Silvana S. Cardoso, University of Cambridge

Associate Laboratory LSRE-LCM, Department of Chemical Engineering

Faculty of Engineering, University of Porto

2011

João Pedro Lopes, 2011

Laboratory of Separation and Reaction, Associate Laboratory LSRE/LCM

Department of Chemical Engineering, Faculty of Engineering, University of Porto

Rua Dr. Roberto Frias

4200-465 Porto

Portugal

ABSTRACT

Microchannel reactors are a fundamental building block of chemical reaction engineering. One may find them in a permeable catalytic material as an idealized geometry for a single pore, in a fabricated microreactor, or as a cell in a monolith honeycomb. At different scales, all these structures materialize the concept of process intensification through mass/heat transfer enhancement and/or by miniaturization. The behavior of these systems is determined by the interplay of convection, diffusion and reaction in the open channel and surrounding catalyst domains. In this study, we propose an analysis of these interactions, using scaling and approximate analytical methods. First, we considered the determination of the conversion of reactant in the problem of mass transfer in channel flow with finite linear wall kinetics, for different degrees of the concentration profile development. Then, the analysis was extended to the case where a nonlinear reaction occurs, in the limits of kinetic and mass transfer control. These results were compared with numerical simulations and found to be in reasonable agreement.

A uniformly valid description concerning the degree of development of the concentration (or temperature) profile was also pursued. For this purpose, we developed the application of an asymptotic technique to the series which is the solution of the classical problem. The result can be written as a combination of the predictions from limiting theories and the intermediate region appears well characterized. The extension of this transition zone is bounded between the inlet regime length and the distance at which the profile can be considered fully developed, both given explicitly in terms of the parameters and of an appropriate criterion which can be set as desired.

Concerning the competition between mass transfer towards the catalyst and reaction at the wall, scaling analysis suggests that the correct scales for external and internal transport should be included in the criterion for diffusional limitation. This gives origin to the concept of a rescaled Damköhler number Da^*. These order-of-magnitude predictions are confirmed in more detail by correlations for the degree of mass transfer control θ. It is proposed that boundaries for kinetic and mass transfer control should be plotted for specified values of θ in a diagram, with the Damköhler and Graetz's numbers as axes.

At the scale of the catalyst coating, the internal reaction-diffusion processes were considered and boundaries between limits derived explicitly in terms of the operating temperature. The relationship with regimes defined by external phenomena was examined and the dimensionless group which establishes the overall picture in diffusional limitations at both channel and catalytic coating was identified. An improved calculation method for the effectiveness factor was proposed, based on a typical geometrical characteristic of thin coatings. This has found application in the description of nonlinear kinetics, non-uniform geometries and egg-shell catalyst particles.

The interaction between the same mechanisms appears in the analysis of perfusive catalyst particles and walls, where intraparticular convection is possible due to the existence of 'large pores'. We have derived an expression for the effectiveness factor in a monolith with a permeable wall and shown that the conditions under which the performance enhancement is maximum correspond to strong convective transport, but only if this is 'matched' by a fast reaction. In a slab-shaped catalyst with a zeroth-order exothermic reaction, we estimated the effectiveness factor and maximum temperature in a number of regimes, represented in an operating diagram with axes defined by the intraparticular Peclet number, Thiele modulus and Lewis number.

RESUMO

Um microreactor é um elemento base em engenharia das reacções. Pode ser encontrado num material catalítico permeável como uma geometria idealizada para um poro, num microreactor fabricado, ou como uma célula de um monólito. Em escalas diferentes, todas estas estruturas materializam o conceito de intensificação de processos através da melhoria da transferência de massa/calor e/ou através de miniaturização. O comportamento deste sistemas é determinado pela interação entre convecção, difusão e reacção nos domínios do canal e do catalisador circundante. Neste estudo, propusemos uma investigação destas relações, utilizando análise de escalas e métodos analíticos aproximados. Em primeiro lugar, considerámos a determinação da conversão de reagente no problema de transferência de massa em escoamento num canal, com uma reacção de primeira-ordem na parede, para diferentes graus de desenvolvimento do perfil de concentração. Em seguida, a análise foi alargada ao caso em que uma reacção não-linear ocorre, nos limites de controlo cinético e difusional. Estes resultados foram comparados com simulações numéricas e a concordância entre ambos foi considerada razoável.

Uma descrição uniformemente válida no que diz respeito ao grau de desenvolvimento do perfil de concentração (ou temperatura) também foi procurada. Para atingir esse objectivo, desenvolvemos a aplicação de uma técnica assimptótica à série que é solução do problema. O resultado pode ser escrito como uma combinação das teorias clássicas formuladas em limites, e a região intermédia surge bem caracterizada. A extensão desta zona de transição está limitada entre o comprimento do regime de entrada e a distância à qual o perfil pode ser considerado perfeitamente desenvolvido, ambos formulados explicitamente nos parâmetros e num critério apropriado que pode ser estabelecido como desejado.

No que diz respeito à competição entre transferência de massa para o catalisador e reacção na parede, a análise de escalas sugere que a escala correcta para transporte interno e externo deve ser incluída no critério para limitações difusionais. Isto dá origem ao conceito de número de Damköhler redimensionado Da^*. Estas previsões são confirmadas por correlações para o grau de controlo diffusional θ. É sugerido que os limites para controlo cinético e difusional deverão ser representados para valores específicos de θ num diagrama, com os números de Damköhler e Graetz como eixos.

O processo de reacção-difusão foi considerado à escala da camada catalítica e derivaram-se fronteiras entre os limites em termos da temperatura de operação. A relação com fenómenos externos foi examinada e o grupo adimensional que estabele o quadro completo em termos de limitações difusionais foi identificado. Um método de cálculo melhorado para o factor de eficiência foi proposto, baseando-se na reduzida espessura dos revestimentos catalíticos. Este procedimento encontrou aplicação na descrição de cinéticas lineares e não-lineares, geometrias não-uniformes e partículas catalíticas peliculares.

A interação entre os mesmos mecanismos surge na análise de partículas e paredes com poros largos, onde é possível existir convecção intraparticular. Neste caso, derivámos uma expressão para o factor de eficiência num monólito com parede permeável e mostrámos que as condições em que o aumento do desempenho é máximo correspondem a um forte transporte convectivo, mas apenas se este for acompanhado por uma reacção suficientemente rápida. Num catalisador com geometria de placa plana e uma reacção exotérmica de ordem zero, estimámos o factor de eficiência e a temperatura máxima em vários regimes, representados num diagrama de operação que tem como eixos o número de Peclet intraparticular, o módulo de Thiele e o número de Lewis.

RÉSUMÉ

Un microréacteur est un élément essentiel en ingénierie des réactions. Il peut être trouvé dans un matériau catalytique perméable comme une géométrie idéalisée pour un pore, dans un microréacteur fabriqué, ou comme une cellule d'un monolithe. À des échelles différentes, toutes ces structures matérialisent le concept de l'intensification de procédés en améliorant le transfert de masse/chaleur et/ou grâce à la miniaturisation. Le comportement de ces systèmes est déterminé par l'interaction entre convection, diffusion et réaction dans les domaines du canal et du catalyseur avoisinant. Dans cette étude, nous proposons une analyse des ces interactions en utilisant l'analyse d'échelle et des méthodes analytiques approximées. Premièrement, nous avons considéré la détermination de la conversion du réactif dans le problème du transfert de masse en flux dans un canal, avec une réaction de premier ordre sur la paroi, pour différents degrés de développement du profil de concentration. Ensuite, l'analyse a été étendue au cas où une réaction non-linéaire se produit, dans les limites du contrôle de la cinétique et difusionnel.

Une description uniformément valable en ce qui concerne le degré de développement du profil de concentration (ou température) a également été recherchée. Afin d'atteindre cet objectif, nous avons développé l'application d'une technique asymptotique à la série qui est la solution du problème. Le résultat peut être écrit comme une combinaison de théories classiques formulées en limites, et la région intermédiaire apparaît bien caractérisée. L'étendue de cette zone de transition est limitée entre la longueur du régime à l'entrée et la distance à laquelle le profil peut être considéré comme pleinement développé, ces deux termes sont explicitement formulés dans les paramètres et dans un critère approprié qui peuvent être défini comme désiré.

En ce qui concerne la compétition entre le transfert de masse pour le catalyseur et la réaction sur la paroi, l'analyse d'échelle suggère que l'échelle correcte pour le transport interne et externe doit être inclue dans le critère pour des limitations diffusionnelles. Cela donne lieu à la notion de nombre de Damkohler redimensionné $Da*$. Ces prévisions sont confirmées par corrélations pour le degré de contrôle diffusionnel θ. Il est suggéré que les limites pour un contrôle cinétique et diffusionnel devront être représentées pour des valeurs spécifiques de θ dans un diagramme, avec les numéros de Damkohler et Graetz comme axes.

Le processus de réaction-diffusion a été considéré à l'échelle de la couche catalytique et des frontières entre les limites en termes de température de fonctionnement en ont dérivé. Une méthode de calcul amélioré du facteur d'efficacité a été proposée, basée sur l'épaisseur réduite des revêtements catalytiques. Cette procédure a trouvé une application dans la description de cinétiques linéaires et non linéaires, géométries non-uniformes et particules catalytiques pelliculaires.

L'interaction entre les mêmes mécanismes apparaît dans l'analyse de particules et parois avec de larges pores, où il peut y avoir une convection intraparticulaire. Dans ce cas, nous avons dérivé une expression pour le facteur d'efficacité d'un monolithe avec une paroi perméable et nous avons montré que les conditions dans lesquelles l'augmentation de performance est maximale correspondent à un fort transport convectif, mais seulement si celui-ci est accompagné par une réaction suffisamment rapide. Dans un catalyseur de géométrie de plaque plane et une réaction exothermique d'ordre zéro, nous avons estimé le facteur d'efficacité et la température maximale dans plusieurs régimes, représentés sur un diagramme d'opération avec les nombres de Péclet intraparticulaire, Thiele et Lewis comme axes.

ACKNOWLEDGEMENTS

I would like to acknowledge Prof. Alírio Rodrigues for sharing with me his time and ideas during the supervision of this thesis, but perhaps more importantly, for generously allowing me to build my own path.

I am equally indebted to Dr. Silvana Cardoso for the valuable suggestions provided and for welcoming me into her research group during my visits to the Department of Chemical Engineering and Biotechnology in Cambridge.

Financial support from Fundação para a Ciência e Tecnologia (SFRH/BD/36833/2007) is also thankfully acknowledged.

Finally, I would like to express my gratitude to my family and friends for their understanding, encouragement and genuine affection.

CONTENTS

CHAPTER

ONE

OVERVIEW AND RELEVANCE

Convection, diffusion and reaction are simultaneously present in several chemical engineering phenomena. A well-defined interaction of these mechanisms at several scales is key for the development of strategies for process intensification. Microreaction technology has emerged as one of those strategies, or more generically as a new paradigm for the chemical industry aiming improved performance. One of the main objectives of this thesis is to provide an analysis of the transport-reaction problem in a wall-coated microchannel using approximate analytical techniques. In this chapter, we review the driving forces for miniaturization which can be explained in terms of the length scales governing each transfer mechanism (section 1.1). Then, the practical motivation behind microprocess engineering is briefly illustrated with examples of applications in different fields (section 1.2).

Our analysis also includes the definition of characteristic regimes, which is a topic of great interest in the design and operation of microdevices. Actually, conceptual development of a provess involves several stages in different regimes and a comprehensive description is required. Moreover, microreactors are known for opening new opportunities in parameter spaces which are unfamiliar to the conventional technologies. Some studies which are typically conducted in a widespread range of conditions are detailed in section 1.3.

Process intensification in the sense of enhancement of mass/heat transfer rates can also be accomplished by means of another concept: the promotion of convective transport, where conventionally only diffusion existed to assure transport. This can be implemented in both microreactors with permeable walls and catalyst particles. A review concerning the effect of this additional mechanism inside catalytic structures is presented in section 1.4. Finally, the outline of the thesis is described in detail, along with the specific objectives and methods employed in each chapter (section 1.5).

1.1 OPERATION IN THE MICROSPACE

The 'microspace' results from the reduction of the characteristic dimensions and its implications on flow, mass and heat transfer, coupled with eventual homogeneous and heterogeneous (wall-catalyzed) reactions. The terms 'characteristic length' or 'length scale' refer to the distance over which an appreciable change in a quantity of interest occurs (e.g. changes in velocity, temperature or concentration). In fact, microdevices are composed by structures whose dimensions are of the order of several tens to hundreds of micrometers. As a result they exhibit high surface to volume ratios. If the characteristic geometrical distance is a, then

$$\frac{S_{surf}}{V} \sim \frac{1}{a}. \tag{1.1}$$

Values of this ratio have been reported to be around 10 000 to 50 000 m^2/m^3 (Ehrfeld et al. 2000), which are much larger than the ones for convectional technologies (1 – 10 m^2/m^3). The natural geometry to consider is a channel, and in particular the single channel design is attractive, either as a model for multichannel configurations or as a technology on its own for laboratory and small scale production, with manageable investment costs, safety concerns and control effort. However, apart from specific applications where a precise control of harsh conditions is expensive, parallelization or numbering up is always a possible strategy to increase the productivity.

A consequence of (1.1) is the decrease of the characteristic times for heat / mass transfer and mixing, i.e. enhancement of transport processes. Therefore, microtechnology offers opportunities for process intensification from several perspectives (Charpentier 2005; Becht et al. 2007; Becht et al. 2009; Van Gerven et al. 2009): pure reduction in plant size, increase in selectivity with reduction of waste by rigorous control of residence time and temperature gradients, and maximization of the interfacial area to which driving forces are applied. The timescales for several processes and their dependence on the geometrical characteristics of a microchannel are listed in Table 1.1. If these quantities are combined in the form of ratios, then several dimensionless parameters arise. It is possible to observe that different dependencies are present: second-order (diffusive) processes are more significantly affected from reduction in a. The process with the longest timescale will be controlling, and the design of the microgeometry should take this into consideration.

An analysis based on these time constants for transport phenomena and reactive processes allows one to identify the operations that benefit the most from miniaturization and to compare them with processes occurring at the conventional scale. Many reviews exist in the literature concerning the effect of scaling down. In particular, we highlight the case where a wall-catalyzed reaction occurs in a coated microchannel.

Table 1.1: List of characteristic times for transport-reaction processes

Process X	Timescale, τ_X		
Convection (flow)	$\frac{L}{\langle u \rangle}$		$\sim L$
Viscous diffusion	$\frac{a^2}{\nu}$		$\sim a^2$
Transverse mass diffusion / heat conduction	$\frac{a^2}{D}$;	$\frac{a^2}{\kappa}$	$\sim a^2$
Axial fluid mass diffusion / heat conduction	$\frac{L^2}{D}$;	$\frac{L^2}{\kappa}$	$\sim L^2$
Interphase mass / heat transfer (fully developed profile: $Nu, Sh = \text{constant}$)	$\frac{V/S_{surf}}{k_m} \sim \frac{a^2}{Sh\, D}$;	$\frac{V/S_{surf}}{k_{heat}} \sim \frac{a^2}{Nu\, \kappa}$	$\sim a^2$
Interphase mass / heat transfer (developing profile*: $Nu, Sh \sim \delta^{-1}$)	$\frac{V/S_{surf}}{k_m} \sim \frac{a^2\, \delta}{D}$;	$\frac{V/S_{surf}}{k_{heat}} \sim \frac{a^2\, \delta}{\kappa}$	$\sim a^2\, \delta$
Reaction (ref. coating volume)	$\frac{c_0}{R(c_0)} = \frac{c_0^{1-m}}{k}$		
Homogeneous reaction	$\frac{c_0}{R_{bulk}(c_0)} = \frac{c_0^{1-m}}{k_{bulk}}$		
Wall-catalyzed reaction (no internal diffusion limitations)	$\frac{c_0^{1-m}\, V}{k_{surf}\, S_{surf}} \sim \frac{c_0^{1-m}\, a}{k_{surf}}$		$\sim a$
Heterogeneous reaction in coating (internal diffusion limitations**)	$\frac{c_0}{R_{obs}(c_0)} \sim \frac{a\, c_0^{1-m}}{k_{surf}\, \eta}$		$\sim a$
Heat generation by chemical reaction	$\frac{T_0}{\Delta T_{ad}} \frac{c_0}{R(c_0)} = \frac{\rho\, C_{P,fluid}\, T_0}{(-\Delta H_R)\, R(c_0)}$		
Heat removal by wall conduction (transverse)	$\frac{t_w^2}{\kappa_{wall}}$		
Reactor heat-up	$\frac{\rho_{wall}\, C_{P,wall}\, V_{wall}}{\dot{m}\, C_{P,fluid}}$		

Notes: a and L are the characteristic dimensions in the transverse and axial directions, respectively; for the remaining nomenclature please refer to the Notation section at the end of the chapter; *details on the scale for transport under developing profile conditions ($\sim \delta$) can be found in Chapters 2 and 4; **details concerning the use of the effectiveness factor (η) can be found in Chapters 4 and 5; $R(c_0)$ is expressed as a power-law kinetics in some expressions ($k\, c_0^m$); t_w is the thickness of the catalytic body.

1.1.1 Reactor miniaturization under fixed efficiency

A simple methodology for the design of microreactors, comparison with conventional technologies and identification of the most interesting operations was developed by Commenge et al. (2005). Since in large part this is based on the analysis of the timescales given in Table 1.1, we now summarize the main aspects of this work.

These authors consider reduction of reactor volume (and of the characteristic distance for transfer processes), while keeping efficiency fixed for hydrodynamic and chemically equivalent systems. This naturally requires the definition of both process efficiency and equivalence criteria. According to Commenge et al. (2005), a microstructured reactor is 'equivalent' to a fixed bed packed with nonporous spherical catalyst particles if they present the same porosity, surface area to volume ratio and space time,

$$\varepsilon_{bed} = \varepsilon_{micro}\,,\ \left(\frac{V}{S_{surf}}\right)_{bed} = \left(\frac{V}{S_{surf}}\right)_{micro} \text{ and } \tau_{bed} = \tau_{micro}\,. \tag{1.2}$$

This implies that the cross-sections, heights, catalyst amounts and feed flowrates Q_{feed} of both reactors are the same, and that the particle diameter in the fixed bed is related to the diameter of a cylindrical channel by

$$d_{part} = \frac{3}{2}\,\frac{1-\varepsilon_{micro}}{\varepsilon_{micro}}\,d_{channel}\,. \tag{1.3}$$

Since the spherical particles are only active at the surface, they observe that the two systems related by Eqs.(1.2) and (1.3) present the same conversion for a large range of parameters. In either case, the efficiency is defined as the ratio of two characteristic times, the space time of the process fluid in the system and the one for the operation being considered controlling,

$$NTU = \frac{\tau_{conv}}{\tau_X}\,, \tag{1.4}$$

where $\tau_{conv} = L/\langle u \rangle$ and τ_X is given in Table 1.1 for some common processes. As long as the number of transfer units (NTU) remains constant, the performance is fixed regardless of the scale. Therefore, systems with different dimensions can be compared on the same basis.

For this discussion, the timescales for transport and reaction mechanisms can be grouped in terms of their dependence on the channel characteristic distance a. Then, the implications of reducing a on the reactor volume and pressure drop are examined (Hessel et al. 2004; Commenge et al. 2005; Renken et al. 2008). We write the microstructured reactor volume and pressure drop as

$$V_{reactor} = N_{ch}\,A_{ch}\,L = \tau_X\left(NTU\;Q_{feed}\right) \sim \tau_X \tag{1.5a}$$

$$\Delta P \sim \frac{Q_{feed}\, L}{N_{ch}\, d_{ch}^4} \sim \frac{A_{ch}\, L^2}{\tau_X\, d_{ch}^4\, NTU} \sim \frac{L^2}{\tau_X\, d_{ch}^2} \tag{1.5b}$$

since NTU and $Q_{feed} \sim N_{ch}\, A_{ch}\, L/\tau_X$ are constant (independent from channel dimensions). Control by processes with high order dependences on a, leads to the most expressive reduction of reactor volume with the decrease of the length scale. On the other hand, pressure drop increases unless $N_{ch} \sim L\, a^{-4}$, which according to Eq.(1.5a) leads to $V_{reactor} \sim a^{-2}\, L^2$ (which decreases as τ_X with a if $L \sim a\sqrt{\tau_X}$). For example, if mass transfer towards the coating phase is controlling:

- the reactor volume decreases with a as $V_{reactor} \sim a^2$
- the dependence of pressure drop on a is $\Delta P \sim \frac{L^2}{a^4}$
- miniaturization does not result in a pressure drop increase if $L \sim a^2$ and $N_{ch} \sim a^{-2}$.

Note that here the symbol $\sim$ is used with the meaning "increases/decreases with decrease of a as". Therefore, $L \sim a^2$ means that if a is reduced from 1 mm to 100 μm, L should be reduced from 1 m to 1 cm. This simplified analysis is only possible when there is a clearly controlling mechanism. In general, several effects may appear at leading-order behavior and further assumptions are required. However even for more idealized situations, the design equations need to be written with the correct coefficients and are more complicated than simple scaling rules. Thus, the analysis of regimes which consider the interplay e.g. between mass transfer and reaction are interesting to complement this approach (see Chapters 2 and 3 of this thesis). The definition of the areas where one mechanism is clearly controlling is also of interest (see Chapters 3 and 4 of this thesis). In the same line, Renken et al. (2008) proposed design rules obtained from comparison of the residence time in a microreactor with the time constants for several controlling processes. Note that the system's conversion (and therefore specific productivity) is related with NTU. We now briefly review the implications of scale down in fluid flow, energy consumption, heat and mass transfer, in the absence or presence of chemical reactions in microchannels.

1.1.2 Fluid flow and pressure drop

A major simplification in the modeling of microchannels is to assume a well-defined velocity profile, decoupling fluid mechanics from the problem. Namely, laminar flow is likely to be found since the timescale for viscous diffusion is much smaller than the one for convection, i.e. from Table 1.1:

$$\alpha\, Re_a = \frac{a^2 \langle u \rangle}{\nu\, L} << 1, \tag{1.6}$$

where the two dimensionless parameters are the aspect ratio ($\alpha = a/L$), which is typically small; and the Reynolds number ($Re_a = a\langle u \rangle/\nu$), which is commonly in the laminar range for channel flow. This allows the problem to be treated analytically and the solutions presented in this thesis will rely on this assumption. The effect of simultaneous development of the velocity profile compared with concentration/temperature fields requires numerical evaluation and the importance of this is measured by Prandtl's number for heat transfer or by Schmidt's number for mass transfer:

$$Pr = \frac{\nu}{\kappa} \text{ and } Sc = \frac{\nu}{D}. \tag{1.7}$$

When $Pr \to \infty$ and $Sc \to \infty$, the flow field develops much faster than the concentration or temperature profiles. In the opposing limit ($Pr \to 0$ and $Sc \to 0$), 'plug-flow' can be used as an idealized inlet profile. Solutions obtained for both cases will be presented in Chapters 2, 3 and 4, in the perspective of lower and upper bounds. The entrance length before which the velocity profile can be considered developed is often given by an expression of the type (Bird et al. 2002)

$$\frac{L_e}{a} \sim 0.14\, Re_a, \tag{1.8}$$

here written for flow in a circular channel. There is a similarity between the entrance length of velocity and concentration/temperature profiles. In Chapter 3, the thickness of this region is discussed for the mass/heat transfer problem.

The pressure drop is important to quantify the process energy requirements and sometimes even limiting of the design and performance of a microdevice. It is related to the friction factor by (Bird et al. 2002)

$$\Delta P = f\, \frac{L}{d_h} \frac{\rho \langle u \rangle^2}{2} \tag{1.9}$$

The (Darcy's) friction factor f in a straight channel is inversely proportional to the Reynolds number $\mathrm{Re}_D = \langle u \rangle d_h/\nu$, according to

$$f = \frac{C_f}{\mathrm{Re}_D}, \tag{1.10}$$

where for fully developed velocity profile, the coefficient C_f can be found for several cross-sectional shapes (Shah et al. 1978) (it equals 64 in a circular channel and 96 in a planar channel).

1.1.2.a *Pressure drop reduction*

A significant advantage in the adoption of microreaction technology would be the reduction in energy consumption. It is known that up to a certain extent, this is related to the pressure drop in the system. For 'equivalent' microstructured and packed bed configurations (in the sense detailed in section 1.1.1), the pressure drop from Poiseuille equation for the former is compared with Carman-Kozeney equation for the latter to yield (Commenge et al. 2005),

$$\frac{(\Delta P/L)_{bed}}{(\Delta P/L)_{\mu ch}} = \frac{h_k}{2}. \qquad (1.11)$$

Eq.(1.11) is the ratio between the mean length of passages between particles and the length of a straight capillary tube, given by $h_k/2$. Since $h_k \sim 4.5-5$, the pressure drop can be reduced up to 2.5 times in a microreactor.

1.1.2.b *Scaling effects*

A question that always arises when discussing flow in microchannels, and particularly microflows, is the validity of the continuum theory. The extent of these deviations is assessed by the magnitude of the Knudsen number

$$Kn = \frac{\ell_{mean}}{\ell_{charact}}, \qquad (1.12)$$

and their implications range from wall slip in gas flows to more unclear consequences in liquid flows. The literature presents contradictory conclusions concerning the need to account for these 'new' effects. Doubts related with the accuracy of experimental measurements at small scales with 'large' analysis equipment (Hessel et al. 2004) contribute to the assumption of continuum behavior for (Bruus 2008; Herwig 2008)

$Kn < 10^{-3}$ (gas flows)

and liquid flows with $\sim \ell_{mean,gas}/10$. For mean free path for gases $\ell_{mean} \sim 50\,\text{nm}$, this implies $\ell_{charact} = d_{ch} > 50\,\mu\text{m}$. Since the diameter of the channel at such small scales will be fixed by fabrication and cost limitations, if d_{ch} is between $100\,\mu\text{m}$ and $500\,\mu\text{m}$, then the continuum approach is valid (Mills et al. 2007). In tubes with diameters below $150\,\mu\text{m}$, some deviations of the product of the friction factor and Reynolds number from theoretical values were explained by the failure in accounting for surface roughness (Judy et al. 2002). Other sources of error have been identified (Pfund et al. 2000). A discussion on the importance of effects such as viscous dissipation and the appropriate simplifications of the Navier-Stokes equations at the microscale can be found elsewhere (Herwig 2008).

1.1.3 Presence of wall-catalyzed reactions

Heterogeneous reactions occurring at the microchannel wall or in a catalytic coating attached to this surface are of particular interest due to the large values of the surface to volume ratio, Eq.(1.1). This is in agreement with the generic statement that effects referred to the surface are privileged compared to the ones referred to volume. The dependence of the timescales for these reactions on the channel diameter compared with their homogeneous counterpart (Table 1.1), indicate that benefit from miniaturization does not occur if the controlling timescale is the one for bulk reaction. Actually, there may be a change in mechanism at the microscale and it is possible that a homogeneous reaction becomes heterogeneous. Moreover, uncoated walls (stainless steel, iron,…) can act as catalyst for partial or total combustion (Mills et al. 2007). Therefore, wall catalyzed reactions are of particular interest and their presence introduces additional design considerations which interact with pressure drop, heat and mass transfer.

1.1.3.a *Reactor requirements at the microscale and criteria for miniaturization*

The ideal set of conditions for an industrial reactor to be feasible is well-known (Wörz et al. 2001a; Wörz et al. 2001b). Our expectation is that by reducing the characteristic length scale, some of these requirements are achieved more efficiently or are simply made possible to attain. This is summarized in Table 1.2. It is commonly accepted that the potential of microdevices should be focused towards applications where dramatic improvements result, since the technology is not obviously free of disadvantages and has to compete with already well-established processes, which benefit from the economy of scale. Concerning the nature of the reaction, several authors propose that the main candidates to microprocessing should have the following characteristics:

- fast kinetics;
- exothermic (endothermic) with reasonable (large) reaction heats;
- high temperature;
- complex;
- multiphase;
- hazardous;
- for which conventional technology does not exist or is limited.

Actually, microreactor arrangements may constitute a solution for reactions with a wide range of characteristics. Roberge et al. (2005) classified reactions in three main types according to kinetics, and proposed some examples of how microtechnology can answer the challenges

raised by each one (we have collected this information in Table 1.3). Examples of microprocesses for applications fulfilling these requirements are presented in section 1.2.

Table 1.2: Fulfillment of ideal requirements by microstructured reactors.

Requirement	Purpose	Advantages offered by microspace operation
Residence time needed for reaction	• Attain desired levels of conversion • Selectivity	• Exact control of residence time (minimum backmixing; uniform RTD); • In particular, very short residence times can be achieved; • Transport rates can be matched with kinetics
Efficient heat removal/supply	• Safety (thermal runaway, explosive); • Hot spots reduce selectivity	• Simultaneous micro heat-exchangers; • Large surface to volume ratio, enhanced heat transfer • Selection of wall material and geometry (additional design parameter)
Sufficiently large interface (multiphase systems)	• Improve contact between phases and interphase transport	• large surface to volume ratio in wall-coated systems

Table 1.3: Reaction classification according to Roberge et al. (2005) and respective microreaction engineering approach.

Group	*Reaction characteristics*	*Microtechnology solution*
A	• **Mixing-controlled** • Rapid kinetics • Considerable heat release	Multi-injection principle to spread the reaction over a larger reactor channel length or heat transfer area (Roberge et al. 2008)
B	• **Kinetically controlled** • Slow (reaction time of few minutes) • Require larger residence times with appropriate temperature control	Flexible, modular reactor for reaction with considerable heat release
C	• Hazardous or autocatalytic nature	Small volume systems with excellent temperature control, allowing start under harsh conditions but safe operation

1.1.3.b *Matching transfer rates with kinetics for design*

It is commonly accepted that microreactors should be designed so that mass and heat transfer are fast enough compared to the reaction kinetics. A simple comparison of timescales allows the definition of regions of interest, although a more detailed analysis is required for rigorous design (see e.g. Chapter 2 of this thesis). Hessel et al. (2004) and Commenge et al. (2005) suggest that the dimensioning of the channel diameter should be ruled by these considerations. As can be seen from Table 1.1, heat and mass transfer depend on the channel's diameter as $\sim d_{ch}^2$, while the time constant for an heterogeneous reaction may be proportional to $\sim d_{ch}$. For selected values of d_{ch}, $\tau_{mass\ transfer}$ and $\tau_{heat\ transfer} < \tau_{reaction}$. However, it is recognized that other factors may limit the possible designs, namely: pressure drop, occurrence of clogging/fouling, and uniform distribution of flow entering the microchannels. The first two factors suggest the use of larger diameters, which are also easier to clean (important for pharmaceutical production) and allow high flow rates. For higher throughputs, the 'numbering up' strategy can be used. Herwig (2008) presented a length-time scales plot comparing mixing by molecular diffusion in gases and liquids and the characteristic times for slow and fast homogeneous reactions.

We note that even though it appeared from section 1.1.1 that controlling homogeneous reactions would take no advantage from miniaturization, the fact that 'new' conditions can be applied allows the performance of these processes to be enhanced as well (see sections 1.2.2 and 1.3.2).

1.1.4 Impact on mass transfer

In the case of microdevices operating in laminar flow, transverse mixing is assured only by molecular diffusion, which as shown in Table 1.1 has a characteristic time proportional to the square of the channel's radius or diameter. Jensen (2001) reports that studies with acid-base reactions show that complete mixing in a liquid-phase microreactor with channels 50-400 μm wide occurred in 10 ms. Thus, faster mixing implies channel diameter reduction. This also leads to the increase in pressure drop and a flowrate limitation may appear. This can be surpassed by numbering up, even though other issues such as uniform fluid distribution arise. Therefore, several strategies to improve mixing in microchannel apparatus and networks have been proposed (Hessel et al. 2005b; Falk et al. 2010). The objective is to overcome the limitations in conventional methods, regarding energy consumption, technical feasibility and detrimental effect in the process performance (due to backmixing and axial dispersion).

For the design of a single channel microreactor, the control of the residence time is important for selectivity issues. In preliminary design methods (Hessel et al. 2004; Commenge et al. 2005)

it is proposed that once the required residence time is fixed, the fluid velocity should selected so that minimum dispersion is obtained. It is possible however that excessive pressure drop results from this and a trade-off must be searched.

To highlight the benefits from microstructuring in reducing dispersion, 'equivalent' fixed bed and microreactor (as defined in section 1.1.1) are compared in terms of a dispersion ratio (ratio of the widths of initially delta-like concentration tracers at the reactor exit) (Hessel et al. 2004; Commenge et al. 2005; Renken et al. 2008). In terms of the Peclet number (with D_{ax} as the axial dispersion), an expression for fixed bed reactor of the type

$$Pe = \frac{u\, d_p}{D_{ax}} = f\left(Re, Sc\right)$$

is considered, while for the microchannel the classical Taylor-Aris theory applies (Taylor 1953; Taylor 1954; Aris 1956). For $3 < u\, d/D < 100$, Commenge et al. (2005) observed that the dispersion in a microchannel is smaller than that of a fixed bed reactor with porosity 0.4. These boundaries change for other values of porosity (the range gets broader for smaller porosities, and narrower for higher porosities). The minimum dispersion is attained at $u\, d_{ch}/D \sim 14$ and corresponds to a 40% reduction in dispersion in a microchannel reactor compared to a fixed-bed one.

1.1.5 Implications on heat transfer

Perhaps one of the most important consequences from miniaturization is the enhancement and control of heat transfer rates in both reactive and nonreactive cases. As in the case of mass transfer, higher heat transport rates are possible due to the high values predicted from Eq.(1.1). Very high values of heat transfer coefficient are commonly reported for microgeometries and this has been known for many years (e.g. in the field of electronic microdevices cooling). It is possible to achieve heat transfer coefficients one order of magnitude higher than in conventional heat exchangers (Ehrfeld et al. 2000; Mills et al. 2007).

Concerning the validity of macroscale theory in channels with reduced dimensions, Rosa et al. (2009) provided a critical review, evaluating the importance of scaling effects in single-phase heat transfer in microchannels. They concluded that even though inconsistencies in published results exist, the same theory and correlations are applicable as long as 'scaling effects' are explicitly accounted for or can be safely ignored. These 'scaling effects' included entrance effects, conjugate heat transfer, viscous heating, etc., and although they are likely to be ignored in macro-channels, they now may have a significant influence in heat transfer. They also stress the role of measurement and fabrication uncertainties and the need for reliable experimental

data. Results from single channel designs were found to agree with published correlations better than multichannel configurations and this was attributed to flow maldistribution, 3-dimensional conjugate heat transfer and measurements uncertainties. They expect sub-continuum models to become more important, however probably only relevant at the nano-scale. In particular, these authors review a number of experimental studies in the literature and conclude that in all of them entrance effects need to be accounted for. Conclusions in the same direction are taken in an experimental study from Lee et al. (2005). They assessed a number of classical correlations to describe thermally developing heat transfer in rectangular microchannels with hydraulic diameters ranging from 318 and 903 μm and concluded that these were in good agreement, as long as inlet and boundary conditions are correctly considered. In Chapter 3, we discuss the relevance and extent of inlet effects in the temperature profile.

A major improvement brought by microprocess technology results from combining superior heat transfer capabilities with highly exothermic (endothermic) reactions. Kockmann et al. (2009) discusses heat transfer in microstructures in terms of a volumetric heat transfer coefficient defined as

$$U_V = \frac{\dot{Q}}{V_{int}\,\Delta T} = k_{heat}\frac{S_{ref}}{V_{int}}, \qquad \text{(units of W/m}^3\text{K)}$$

where V_{int} is the internal volume, S_{ref} the area of the reference surface and k_{heat} the heat transfer coefficient (per interface area). Kockmann et al. (2009) report a study from Kinzl which gives a threshold for U_V in microreactors with residence time of $10\,s$ and highly exothermic reactions, so that a mean temperature difference of less than 10 K exists:

$U_V \geq 1\,\mathrm{MW}/\left(\mathrm{m}^3\mathrm{K}\right)$.

Then, they estimate that under typical conditions for organic liquids,

$$U_V = \frac{0.002}{d_{ch}(m)}\,\mathrm{MW}/\left(\mathrm{m}^3\mathrm{K}\right),$$

which is greater than 1 for $d_{ch} < 2$ mm. Therefore, microreactors are also heat exchangers and isothermal operation even for highly exothermic reactions is possible, due to efficient heat removal/supply. As discussed previously, this opens possibilities for dealing with reactions releasing large amounts of heat or with risk of explosion. It also improves selectivity of many processes, due to the reduction or even elimination of hot-spots. Consequently, more aggressive conditions may be employed (see section 1.3.2).

The fastest mechanism for heat removal is by conduction through the walls, as can be seen from the timescale in Table 1.1. Therefore, the channel walls can be designed so that due to its reduced thickness and high-conductivity construction material, no appreciable temperature gradients are registered. In fact, this provides an additional source for control of temperature and

heat supply/removal. Ehrfeld et al. (2000) and Hessel et al. (2004) report several examples of microsystems for carrying out reactions, which are integrated with heat exchangers. This can happen by adjacent heating/cooling gas channels placed in alternating layers with the process channels. Due to the low thermal mass of the thin wall, the thermal response is usually fast (Jensen 2001). Lomel et al. (2006) wrote the characteristic time in both semi-batch and continuous processes for Grignard reaction as a function of the limiting heat transfer timescale. They explained the drastic reduction in operation times as being due to the shorter dimensions of the continuous microprocess, leading to intensified heat transfer and therefore shorter process times. Hardt et al. (2003) explored microstructuring techniques to enhance heat transfer in microdevices by at least one order of magnitude (Nusselt numbers as high as 100 were observed). The performance of the system was also tested in the presence of an endothermic, heterogeneous, gas-phase reaction. When compared to a conventional fixed bed, reduction in the amount of catalyst required and overall equipment size was achieved.

Another direction which takes advantage from excellent thermal behavior is the safe realization of reactions which would result in explosion at the macroscale. Hessel et al. (2004) identified the key features in microchannel reactor which reduce the risk or prevent the occurrence of explosions due to chain reactions or to a large heat release. While molecule collisions with the channel walls may suppress the former, efficient heat transfer is capable of managing the latter. Two timescales that influence the increase in temperature due to a first-order homogeneous exothermic chemical reaction are (Table 1.1):

$$\tau_{generation} \sim \frac{T_{wall}}{\Delta T_{ad}} \tau_{rxn} = \frac{\rho\, C_{P,fluid}\, T_{wall}}{\left(-\Delta H_R\right) k\left(T_{wall}\right)} \tag{1.13}$$

$$\tau_{removal} \sim \frac{d_{ch}}{k_{heat}}.$$

Eq.(1.13) is usually replaced simply by τ_{rxn} and is evaluated here at the wall temperature. Insufficient heat removal or strong heat generation occurs whenever $\tau_{removal} >> \tau_{generation}$, and the maximum temperature difference approaches the adiabatic limit. Nearly isothermal behavior is observed in the reverse case, which is favored by the use of smaller channels.

1.2 APPLICATIONS OF MICROCHANNEL REACTORS

The literature is abundant in applications and proofs of concept of technologies employing microchannel reactors. In fact, several patents have been filled (Hessel et al. 2008a) and some industrial applications were already reported (Hessel et al. 2005b). At the single channel level, several new laboratory or small production scale studies appear on a daily basis. As we will

discuss, the microchannel reactor concept also describes more consolidated technologies, such as monoliths. In this case, there are also many review articles (Hoebink et al. 1998; Nijhuis et al. 2001; Kreutzer et al. 2005; Moulijn et al. 2005; Kreutzer et al. 2006) and dedicated monographs (e.g. Cybulski et al. (1998)).

1.2.1 Practical realizations of the microchannel reactor concept

The description of a system including a channel with the ability to carry reactions due to catalytic activity at its walls is sufficiently general to encompass a series of technologies. In fact, this is an idealized portrait that can act as a fundamental model of several practical solutions in chemical reaction engineering. We however will focus on two approaches in the field of structured reactors: monoliths and microfabricated channels. Usually, both are distinguished by different ranges of characteristic dimensions, being monoliths associated with larger cell hydraulic diameters ($d_{ch} \sim 0.5-1\,\text{mm}$). Nevertheless, in terms of mass/heat transfer intensification with low pressure drops, both technologies claim the same advantages and sometimes the terms are used interchangeably. However, typically the term 'monolith' refers to a honeycomb arrangement composed by several repeating cells, divided by a ceramic or metallic material, e.g. Kolaczkowski (1999) and Chen et al. (2008b). It can be pictured as a catalyst block with a large number of parallel straight channels through which gas flows. On the other hand, microfabricated reactors are typically generated by precision techniques e.g. on a metallic plate. A number of fabrication methods (lithography, machining, micro milling, etc.) is available and details can be found e.g. in Mills et al. (2007) and Ehrfeld et al. (2000). This distinction may pose significant differences in terms of the channel-channel interaction.

The incorporation of catalyst in the walls of these channels also shares similar characteristics. This happens in the case where a high surface area washcoat (e.g. γ-alumina) containing the dispersed catalyst(s) is used, so that sufficient loading is achieved. There are currently a number of techniques available to coat a microchannel with a catalyst layer (wet impregnation, physical and chemical vapor deposition, anodic oxidation, sol-gel, slurry and aerosol techniques) and suitable reviews have been published on the subject (Wunsch et al. 2002; Hessel et al. 2005b). In the case of the monolith, the wall itself may already contain the catalyst as an integral part of its structure. In this case, the boundary conditions are more complex and channel interaction in specific arrangements has to be considered. Problems in microchannel coating are also common to both cases. Rebrov et al. (2009) identified the reproducible preparation of the catalytic coating as a crucial requirement in the fabrication of multi-phase microfluidic devices. Besides reproducibility, other requirements are: homogeneous distribution, mechanical and chemical stability, and sufficient activity to achieve the desired yield under given conditions. The

replacement of the catalyst can also become an arduous task. There is also the possibility of a micropacked bed or a packed monolith. This however typically leads to nonuniform temperature, concentration and flow profiles (leading to increased pressure drop, channeling and favoring the appearance of hot-spots), and are more prone to clog. The step of packing the microchannel also raises some technical issues that require additional study (van Herk et al. 2009). Finally, we refer to another distinction between the two technologies: fabricated microsystems may include other components, such as micromixers, micro-heat exchangers, sensors and controllers (Jensen 2001; McMullen et al. 2010).

1.2.2 Examples of applications

According to the characteristics listed above (section 1.1), we can expect a wide range of reactions to take significant advantages from scaling down. Actually, in the gas-phase, most of them fulfill all the desired features. For example, partial oxidations are typically highly exothermic reactions that required solid catalysts. Selectivity is a major issue, as strong exothermic total oxidation is undesirable. Implementation of more intense conditions is not feasible in conventional technologies due to difficulties in heat management (Becht et al. 2007). In this case, microstructured reactors offer the possibility of enhanced control of residence time and temperature, avoiding hot-spots that harm selectivity and catalyst lifetime.

Several reviews concerning chemicals production on microreactors are available. Srinivasan et al. (1997) discussed ammonia oxidation in an integrated microreactor. Ehrfeld et al. (2000) detailed several examples of studies in gas-phase microreactors. Mills et al. (2007) refer some integrated microreactors for pharmaceuticals manufacture, chemicals production and energy generation. Kockmann et al. (2009) presents some examples of nitrations and organometallic reactions, based on Lonza's industrial experience. Kolb et al. (2007) presents a review of microreactor for gas-phase selective oxidations. Microreactors for preferential oxidation as a gas purification step for fuel cells were also addressed. Other examples can also be found in Kolb et al. (2004), Hessel et al. (2004) and Gokhale et al. (2005). Pennemann et al. (2004) provide a comparison between microreactor and batch reactor (also stirred vessels and fixed bed reactors in some cases) for a large number of industrially relevant organic reactions with data taken from the literature. Their review was divided in 'small-scale applications' (e.g. peptide synthesis, aldol reactions, hydrogenations, dehydrations) and 'lab / pilot scale syntheses' (e.g. nitrations, organomethalic reactions, oxidations, hydrogenations, chlorination and fluorination). This referred to fine chemicals applications with flow rates up to several milliliters per hour and from that to several tens of liters per hour, respectively. While the main concern at the small-scale appears to be conversion (which generally register improvements in microreactors), at larger

scales increase in the process yield and selectivity is also desired (and this is also visible in the results from microdevices). From these examples, it is possible to observe two other important facts: in some cases, the reaction conditions change dramatically (temperature increases from cryogenic to more reasonable values) and the residence times are drastically reduced (from several hours/days to seconds). Mae (2007) gives several examples of organic syntheses in microreactors highlighting the following advantages: shortening of reaction time, solvent-free operation, new synthesis routes, control of unstable intermediates, severe conditions, safe operation under explosive / thermal runaway conditions, and omission of catalysts and reagents. Other examples are given in McMullen et al. (2010). Each case presents particular challenges that microtechnology may solve completely or at least minor its adverse effects. Summary of some particular cases can be found in Table 1.4.

Application of microprocessing in the field of energy generation has gained particular interest and is nowadays a major line of research in the production of purified hydrogen for fuel cells and portable aplications (Kundu et al. 2008). Hessel et al. (2005b) and Kolb et al. (2005) review several examples of microdevices performing steam reforming of methanol, methane and propane. Examples of catalytic combustion and gas purification (CO clean up) are also given. The latter concerns mainly the water-gas shift reaction and preferential CO oxidation (Kim et al. 2008). Ethanol steam reforming has also been studied in the context of renewable fuels from biomass (Casanovas et al. 2008a; Casanovas et al. 2008b; Görke et al. 2009).

Another group of chemical transformations which may take advantage from microstructuring are the ones with biochemical nature (Miyazaki et al. 2006). This may sound as a contradiction when one considers the list of requirements presented in section 1.1.3.a. In fact, biotransformations are typically slow and release small amounts of heat. However, in multiphase systems or multistep synthetic processes the enhancement brought by miniaturization may be visible. Bolivar et al. (2011) presents several examples of liquid/liquid and gas/liquid contacting reactors with enzymatic transformations. In comparison with the reference batch technology, increase of conversion and reaction rate is generally observed and separation is also facilitated. Furthermore, as noted by Thomsen et al. (2009), microsystems become interesting because the biocatalytic step of the process is too slow for integration in conventional continuous flow processes. They performed hydrolysis of lactose and 2-nitrophenyl-beta-D-galactoside (catalyzed by β-glycosidase CelB) in washcoated stainless steel channels with γ-aluminum oxide (to which the enzymes were covalently immobilized). Very fast conversion in the coated microchannels was observed (~10 s to completion). Therefore, microdevices allow the integration of region- and stereoselectivity biocatalysts with continuous industrial production methods. Moreover, scale up is avoided from screening to production stages of the biochemical process. Nevertheless, major challenges in implementation remain such as: selective and reversible enzyme immobilization (with high volumetric activity) and the integration with analytical instruments.

Table 1.4: Role of microreactors in improving the production of some chemicals

Reaction	Features / Challenges	Advantages from microscale operation	Refs. for details
Partial oxidation of proprene to acrolein	• Prevent total oxidation • Quench the reaction after synthesis of unstable desired intermediate • Performed under kinetic control	• Fast heating of inlet gas up to the reaction temperature (enabling the use of short channels and low pressure losses) • Preferred isolation of unstable intermediates	Ehrfeld et al. (2000) Hessel et al. (2004)
Selective partial hydrogena-tion of a cyclic triene	• Avoid consecutive full hydrogenation • Unstable intermediate as target product	• Higher yields (45% increase) of desired product compared with coated granules, wire and foil pieces • Uniform flow pattern, regular pore system, homogeneous catalyst distribution	Ehrfeld et al. (2000) Kolb et al. (2004)
H_2/O_2 reaction	• High temperature • Danger of explosion	• Decrease of residence time to the sub-millisecond range • Ignition only at about 100ºC • Simple and safe design • Improved mass/heat transfer properties	Ehrfeld et al. (2000) Maehara et al. (2008) Voloshin et al. (2009)
Partial hydrogena-tion of benzene	• Avoid full hydrogenation • Very reactive intermediates	• Increase of selectivity (up to 38%)	Ehrfeld et al. (2000) Kolb et al. (2004)
Oxidation of 1-butene to maleic anhydride	• Exothermic reaction • Combined with strongly exothermic total oxidation (hot-spots) • Low selectivity	• Selectivity comparable to fixed bed • Butane concentrations 10 times higher than explosion limit • Space-time yields 5 times higher (shorter residence time)	Hessel et al. (2004) Kolb et al. (2007)
Selective oxidation of ethylene to ethylene oxide	• Step in complex reaction scheme • Increase in selectivity desired • Total conversion to CO_2 favored by high temperatures	• Isothermal conditions (no hot spots) • No inert gas (pure oxygen) with increase in selectivity • Residence times of only a few seconds are required for 29% max. yield of ethylene oxide	Ehrfeld et al. (2000) Kesten-baum et al. (2002) Kolb et al. (2004; 2007)

Table 1.4 (cont.): Role of microreactors in improving the production of some chemicals

Reaction	Features / Challenges	Advantages from microscale operation	Refs. for details
Oxidative dehydrogenation of alcohols	• Low selectivity in large scale pan reactor (45%) • Appreciable temperature rise (150ºC) • Side reactions due to long contact time	• Isothermal conditions • Short residence times (one order of magnitude smaller than multi-tubular reactor) • Conversions higher than 50% and selectivity higher than 90%	Ehrfeld et al. (2000) Hessel et al. (2004) Kolb et al. (2007)
Synthesis of methyl isocyanate	• High temperature • Hazardous gases • Transport and storage risks • Intense cooling needed	• Modular devices including heat exchangers • Smaller hold-up of hazardous chemicals	Ehrfeld et al. (2000) Hessel et al. (2004)
HCN synthesis	• Fast kinetics • High temperature • Hazardous gases • Fast side and consecutive reactions	• High temperatures attained (>1000ºC) • Short contact times (between 0.1 and 1 ms) • Uniform heat distribution (cooling times of 0.1 ms using air, resulting in less than 1.5ºC of difference)	Ehrfeld et al. (2000) Hessel et al. (2004) Kolb et al. (2007)
Nitration of phenol	• Fast kinetics • Large heat release (ΔT ~ 50ºC) • Autocatalytic (longer period required to start) • Decomposition/explosion risk • Prolongated reactant dosing • Low yield (polymeric side products)	• Small internal volumes • High concentration of phenol (90%) • Good temperature control • Almost solvent free • Spontaneous start (controlled backmixing) • Amount of side products reduced by a factor of 10	Kockmann et al. (2009) Halder et al. (2007) (nitration of toluene)
Partial oxidation of methane (syngas generation)	• Very fast reaction (residence time in the order of milliseconds) • Portable, small-scale systems required for on-site small natural gas deposits exploration	• High throughputs and space-time yields • Compactness	Hessel et al. (2004)
Phosgene formation	• Moderately fast and exothermic reaction • Toxic products, storage and shipping difficulties	• Small hold-up • On-site production • High heat dissipation • Kinetic studies in mini fixed-bed reactor	Hessel et al. (2004)

Table 1.4 (cont.): Role of microreactors in improving the production of some chemicals

Reaction	Features / Challenges	Advantages from microscale operation	Refs. for details
Organoli-thium reactions	• Highly exothermic • Unstable intermediates • Batch operation requires cryogenic conditions (-78ºC)	• Operation at -30ºC • Excellent reaction control • Quenching of the intermediate at the end of the reactor	Kockmann et al. (2009)
Grignard reaction	• Very rapid • Highly exothermic (operated at -30ºC in batch); hot spots • Diluted reagents with long dosing times • Reaction type A (Table 1.3)	• Microreactor with multi-injection principle avoids decomposition and undesired side products • Quench of products at the outlet • Good thermal control • Higher yield	Kockmann et al. (2009)
Grignard reaction	• Highly exothermic • Fast • Requires cooling at -40ºC (lab) and -20ºC (industrial)	• Higher S/V ratio (from $4\ \mathrm{m}^{-1}$ at industrial scale to $4000\ \mathrm{m}^{-1}$) • Higher temperature (-10ºC at the microscale) • Drastic reduction of reaction time (from hours to less than 10s) • Increase in yield from 72% to 92% • Increase in the heat transfer coefficient by 1 or 2 orders of magnitude	Lomel et al. (2006)
Dibal-H reduction	• Slow kinetics • Activation of side reactions • Batch operation at -65ºC (complete conversion) • Increasing temperature reduces conversion and yield of main product, due to side reactions	• Same performance of the batch reactor, obtained at higher temperatures (-40ºC)	Kockmann et al. (2009)
Hydrogenation of orto-nitroanisole (pharmaceu-tical)	• Use of hydrogen at high pressure • Highly exothermic • Limited selectivity, downstream purification required • External mass transfer limitation • Poor G/L/S contact • Low yield, oversized reaction volume	• Low hydrogen hold-up • Shorter residence times (minutes instead of hours) • High heat transfer, uniform temperature distribution • Higher selectivity • Move from batch to continuous flow process	Tadepalli et al. (2007a; 2007b)

A similar change in the operating mode of production is expected in the case of pharmaceuticals, where batch technology is dominant. Some examples are given in Table 1.4. Generally, conventional processing is limited in heat transfer and mixing rates (only in stirred vessels), require high dilution, longer dosing times, and hot spots may appear as a result of highly exothermic reactions. Microreactors bring new opportunities from several angles (Kockmann et al. 2009): exploration of new chemical routes with conditions which are not feasible in batch operation, increased safety from controlled operations in small internal volumes, rapid mixing and heat transfer, continuous processing with high flowrates and throughput, and implementation of 'harsher conditions' (e.g. higher concentrations; see section 1.3.2).

An important stage in all microprocesses involving catalytic coatings in microchannels is the testing of the catalyst itself. To perform this in microreactors is desirable, since conditions (temperature, flow…) can be rigorously controlled and extrapolation to the production scale is based on the same geometry. Actually, catalyst screening is among the original applications of microreactors. The areas that showed interest in these devices included combinatorial chemistry (Scheidtmann et al. 2001), high throughput screening (Trapp et al. 2008) and portable analytical measurement devices (Jensen 2001). Monoliths have also been used for the same purposes (e.g. Lucas et al. (2003)).

1.3 CHARACTERISTIC REGIMES IN MICROCHANNEL REACTORS

We have shown that working in the microspace has several advantages. However, many regions may exist in this space, which require characterization. Parametric areas can be distinguished in a number of ways. Scaling analysis leads naturally to the definition of 'regimes', since each mechanism is associated with a timescale (Table 1.1), and these are compared in parameters that arise when making the model dimensionless. The importance of each term is then evaluated by the magnitude of the associated parameter (since correct scaling assumes dependent variables and its derivatives of $O(1)$). In particular when seeking for approximate solutions, a balance between two important effects is often looked for, leaving others ignored or restricted to non-leading order corrections (Lin et al. 1988). These limiting solutions apply in a given regime which is defined a priori. In chemical reactors, the relationship between transport and reaction is often used to define limiting behaviors in the governing equations or in the boundary conditions. In the case of heat transfer, regimes based on the magnitude of conduction to and through the wall or between transport mechanisms/sources of heat are also commonly defined. Mapping of all these regimes in a diagram has the benefits of systematically organizing previous results and

explore new areas, which may have been left ignored in previous studies. The choice of parameters that constitute the axes of this plot also results from scaling.

If a given set of geometric and operation variables is noted by a single point in the aforementioned diagram, then one might question about the likely location of such representation for common conditions in microreactors. Actually, even though some geometric characteristics are shared by all of the designs, many possible operating regimes may prevail. We have already seen some evidences of the flexibility of microreactors concerning operating ranges:

- Even though reactions which are potential candidates to microprocessing possess a defined list of characteristics (section 1.1.3.a) and microreactors can be designed to match these requirements, timescales ratios can still cover several orders of magnitude.
- As we summarized in Table 1.3, some authors proposed microreactor-based solutions for reactions with very different characteristics: from kinetically controlled to transport limited, and even to those exhibiting explosive behavior.
- In many of the studies reported in Table 1.4, several conditions (residence times, temperature,…) are tested and optimized. This may lead to a change in the controlling effect.
- In section 1.2, we have reported applications with distinct purposes, for example screening and chemical production applications. This naturally requires two very different sets of conditions, and consequently two different regimes.

Nevertheless it is interesting to obtain a comprehensive picture of as many regimes as possible, even if this is only done with the purpose of setting boundaries between them. Moreover, one of the promising features of microreactors is the exploration of 'new' process regimes, which are forbidden in conventional technology. These include systems where safety requirements are particularly stringent or where performance enhancement from employing harsher conditions can be attained (section 1.3.2).

1.3.1 Intrinsic kinetic measurements

Apart from the specific applications of microreactors as devices for screening and catalyst testing, measurement of the intrinsic kinetics in a system with the advantages previously mentioned is highly desirable. Their improved mass and heat transfer properties are fundamental in this case, to avoid falsification of the observed kinetics at uniform temperature. The following characteristics should be mentioned:

- isothermal behavior due to improved thermal control;
- controlled thickness of the catalyst layer (sufficiently thin for absence of internal limitations);
- well-defined channel diameter (small enough so that external limitations are absent);
- same geometry as the one found in the full scale process;
- ideal reactor behavior ('plug flow' for $u\,L/D_{Aris} > 100$, with D_{Aris} given by Taylor-Aris theory (Taylor 1953; Aris 1956)).

Several kinetic studies in microreactors/monoliths are available in the literature over a wide range of conditions. In particular, measurements under 'severe conditions' are attractive for a number of reasons. We mention some examples below.

McCarty (1995) used an annular reactor to evaluate kinetics of methane combustion over PdO supported catalysts. The design of the apparatus had a small gap between cylinders (0.1-0.3 mm) and a thin coating (10 μm). Using high flow rates and dilute methane and oxygen in helium, the author claims to have measured the intrinsic rate of methane oxidation up to 900ºC, without contributions from gas-phase reactions. Groppi et al. (2001) used the same configuration to study the same reaction over a PdO/Al_2O_3 catalyst. Beretta et al. (1999) discussed the use of this reactor at high temperatures and high space velocities (GHSV) for kinetic studies of several reactions: catalytic oxidation of CO, catalytic partial oxidation of methane and oxidative dehydrogenation of propane. In this case, a reactor with a thin catalyst layer (50 μm) and small gap (1.1 mm) was used.

The suitability of the structured annular reactor for very fast catalytic combustion reactions was confirmed, since it allowed measurement of kinetic data under conditions closer to the ones in the commercial applications (at higher GHSV and temperature). Extrapolation from lab-scale results can therefore be avoided, as changes in the reaction mechanism may occur (Hayes et al. 1994). In particular, they name the following advantages: (*a*) implementation of very high GHSV with negligible pressure drops (in laboratory fixed beds, ΔP amounted to nearly 1 bar at 400 cm^3 NTP /min in the combustion of methane/bio-gas; and to 0.8 bar in highly diluted bed with GHSV ~10 times higher); (*b*) well defined geometry, flow profile and mass transfer (which they assumed to be given by correlations for Sherwood number at Dirichlet conditions and fully developed concentration profile); (*c*) negligible internal temperature gradients; (*d*) similarity between the coated catalyst tube and the monolith catalysts; (*e*) exclusion of homogeneous reactions; and (*f*) lower dilution of reacting mixture and catalyst compared to a fixed bed.

Groppi et al. (2001) obtained data up to 600ºC at partial conversion (due to high GHSV). The most critical phenomenon was internal diffusion and only by using a thin catalyst layer was kinetics free from mass transfer effects ($t_w \leq 10\,\mu m$ for $\eta \geq 0.9$). External mass transfer limitations played a minor role for channels with a gap between 0.2 – 0.3 mm, which should be kept as small as allowed by pressure drop. Beretta et al. (1999) recognized that depending on the

hydraulic diameter and on the reaction rate at the wall, operation may change from kinetic to diffusional control and that at high temperatures diffusional effects can become important. They proceeded to develop a one-dimensional model from a Sherwood number correlation and concluded that: (a) kinetic regime prevailed up to 450-500ºC, (b) decrease of conversion was thus entirely due to higher GHSV and this widened up the operating window for intermediate conversion values to very high temperatures (200ºC - 900ºC with maximum 65% conversion in CO oxidation and methane partial oxidation); (c) at higher temperatures CO conversion was moderated by the onset of inter-phase mass transfer limitations, and (d) the estimation of intrinsic kinetic constant was in good agreement with the data from fixed bed. Annular reactors have also been considered by other groups (e.g. Yu et al. (2005)).

Germani et al. (2006) studied the kinetics of the water-gas shift reaction over platinum/ceria/alumina catalysts washcoated on stainless steel microchannels. Depite the fact that the catalysts were very active, intrinsic kinetic measurements were performed by employing thin films and favoring plug flow conditions in the channel. The reaction conditions cover a wide range of the operating variables. Sazonova et al. (2009) analyzed the behavior of a LaNiPt-catalyst supported in a honeycomb substrate for methane partial oxidation. In this case, kinetics was measured over the monolith at high temperatures and with millisecond contact times. They used a one-dimensional model to predict the ranges where the process was kinetically controlled in the channel, since the internal resistance was found to be negligible from the low value of Thiele modulus. Görke et al. (2009) highlighted the excellent thermal behavior of Ru/CeO_2 catalyst coated stainless steel microchannels in the evaluation of ethanol reforming kinetics. Employing a very thin catalyst layer ($1\,\mu m$) and short residence times (9 to 42 ms), internal and external diffusional limitations were neglected.

Federici et al. (2011) studied synthesis gas oxidation over a supported Pt/Al_2O_3 catalyst in a micropacked reactor designed for measurement of kinetics of strong exothermic reactions. They intended to avoid the significant temperature gradients that develop and makes it impossible to collect isothermal data. The system was constructed with two thick highly conductive stainless steel walls which guaranteed high heat transfer. A 450 μm gap where the catalyst was placed allowed high heat and mass transfer. Temperatures at the inlet, outlet and inside the bed were measured by installed thermocouples and found to differ by no more than 2ºC from each other. They report complete conversion of CO and H_2 at 325ºC and higher temperatures were not explored as dominant transport effects were expected.

A related topic is the evaluation of internal diffusion limitations in catalyst coatings supported on microchannels. Experimentally, the two most common tests are variation of temperature and catalyst layer thickness. Both quantities are sometimes given as criteria for the chemical regime (specification of a temperature or thickness below which kinetics controls). For example, some authors (Oh et al. 1982; Hayes et al. 1994) consider internal diffusion negligible for $t_w < 50\,\mu m$.

Kapteijn et al. (2005) concluded that washcoat layers thicker than this would lead to mass transfer control in the washcoat, when testing square channel cordierite monoliths with with alumina washcoat layers of various thicknesses (20 - 110 μm) in the Fischer-Tropsch synthesis (in the 180 - 225ºC temperature window). In other studies, diffusional limitations are simply excluded in the view of the thin washcoats employed (Ullah et al. 1992; Uberoi et al. 1996). Walter et al. (2005) considered catalyst coatings of different thickness but with same composition in microchannel reactors. For a constant reactant flow (equal hydrodynamic residence time), internal mass transfer limitation was excluded for thicknesses between 5 and $20 \mu m$. In the selective oxidation of isoprene to citraconic anhydride, the same author excludes limitations for $t_w < 80 \mu m$, based on an analogy with a particle in a fixed bed. Chen et al. (2008a) warn for the fact that internal mass transfer in a metal foam methanol microreformer must be carefully considered and that the critical thickness for absence of diffusional effects was only $8 \mu m$.

However, in other cases internal diffusion limitation can be significant even with very thin washcoat thicknesses (Hayes et al. 1994), when temperature is high (> 700ºC). This refers e.g. to catalytic combustions, which are extremely fast. Hayes et al. (1995) evaluated the extent of intraphase and interphase resistances to the catalytic conversion of low concentrations of carbon monoxide in air in a tube wall reactor (coated with a platinum-alumina deposit). Above 610 K there was strong evidence of both intraphase and interphase resistances to catalytic conversion. In Chapters 4 and 5, we provide a systematic analysis for prediction of the extension of external and internal diffusion limitations.

1.3.2 'New' operating regimes in microprocessing

1.3.2.a *Production in wall-coated microreactors*

It is difficult to define a 'production regime', since this may occur under very diverse conditions. In general, chemical production in microreactors would be in a distinct regime from the one for kinetic measurements and occurs at a different scale than the one found in 'lab-on-a-chip' microfluidic applications. While conversion has to be kept moderate or small to avoid interference of mass transfer effects for evaluation of intrinsic kinetics, blind reduction of channel diameter is also unwise, due to pressure drop and fouling constraints. Lerou et al. (2010) reports two examples of industrial applications of microchannel technology from Velocys, Inc.: the Fisher-Tropsch process and methane steam reforming. Moreover, it was shown how microchannel technology embodies the 'green chemistry' concept. Reports at the

pilot scale have also been provided e.g. by Deshmukh et al. (2010). They have stressed the flexibility in the operation and design of microchannel-based units. The possibility of increasing the production capacity by the increase of the number of channels was also demonstrated. The desired productivity and throughput is achieved by parallelization of a single channel ('numbering up'). A number of issues concerning the flow distribution (Delsman et al. 2004; Rebrov et al. 2007a; Rebrov et al. 2007b), integration and layout of a microplant arise and are out of the scope of this review. The simple single channel configuration can be useful whenever small scale production throughputs are required or for research purposes, since conditions can be better controlled. One of the main advantages of microreactors in terms of the evolution of the process conception is the transferability of data and operating conditions between laboratory, pilot and full production scales.

A particular direction which leads to a more specific definition of production regimes is the 'new window of operation' brought by microprocessing (Hessel 2009). A big contribution to the status of 'innovative process' frequently attributed to microreaction technology is the ability to operate under conditions not reachable efficiently or safely in conventional equipment. In practice, this can have several meanings (Hessel et al. 2004; Commenge et al. 2005; Hessel et al. 2005b; Becht et al. 2007):

- opening of new synthesis routes for known and unknown processes;
- creation of more advantageous contexts for carrying out known processes;
- push of operation conditions beyond conventionally defined safety limits;…

As we have been stressing, fast, highly exothermic, explosive prone reactions are an interesting case-study to illustrate the added-value brought by miniaturization. Generally, one can hope to attain higher selectivity and yields with undiluted reactants and lower energy consumption. We now refer to some perspectives on overcoming the frontiers imposed by traditional designs.

1.3.2.b *'Aggressive' reaction conditions*

The performance limit of a process can be increased by the use of more intense conditions. Here, 'intense' or 'aggressive' can refer to several aspects in a process operation. Some examples include:

- higher temperature and pressure ;
- higher concentration of reactants with less or even in the absence of inerts/solvents;
- shorter dosing of reactants, if any required;
- more active catalysts, higher loading;
- strong heat dissipation for reactions with high heat release;
- rigorous temperature control to reduce side reactions in complex schemes;

- short and defined residence times, from seconds to a few milliseconds;
- different chemical routes;
- fast and controlled thermal ramping for endothermic reactions;
- any effect which enhances reaction rate compared to laboratory experiments;
- any operating range that due to safety issues or unfavorable economics is not feasible in a conventional pilot plant,…

The operation under these conditions may increase the productivity of the process up to 100 times in a single channel (Kockmann et al. 2009). In certain cases, parallelization of channels implies higher investment and control effort and should be avoided or used only as a last measure to increase the mass flow throughput (Kockmann et al. 2009).

Recent work regarding the definition of new process regimes in microreactors include:

- Hessel and co-workers (Hessel et al. 2008b; Hessel 2009; Illg et al. 2010; Hessel et al. 2011) have named as "Novel Process Windows" all the operations described above, which are allowed by microreactors: elevated temperature and pressure; increased concentration or renounce to the use of solvents; explosive or thermal runaway regime; new chemical routes…
- High temperature/pressure in continuous flow organic synthesis (Hessel et al. 2005a; Razzaq et al. 2009; Razzaq et al. 2010);
- Extremely short contact times for highly exothermic and fast benzyl alcohol oxidation (Nieuwland et al. 2010);
- Development of microsystems with separate high pressure (30 MPa, 400 °C) and high temperature (up to 500 °C) regions for supercritical fluid processes (Marre et al. 2010);
- High pressure chemistry in lab-on-a-chip systems (Benito-López et al. 2008);
- Increased temperature in multiphase reactor for the synthesis of tert-butyl peroxy pivalate (Illg et al. 2011).

The term 'superheated processing' is often found and refers to operation under high temperatures and sufficiently high pressures to suppress the evaporation of solvents. This leads to an increase in the reaction rate and safety for endothermic reactions. As we mentioned previously, another group of reactions which reach feasibility at the microscale, are the ones with high safety concerns. This would allow the implementation of on-site processes, avoiding transportation and confining risk to small volumes. Ebrahimi et al. (2009; 2011) considered the production of peracetic acid, which is unstable and explosive. Compared to batch production, the on-site continuous microprocess allowed decrease of reaction time and a small installed volume. However, the evaluation of safety risks based on methods developed for conventional technologies did not apply.

1.4 TRANSPORT ENHANCEMENT IN CATALYTIC STRUCTURES DUE TO INTRAPARTICULAR CONVECTION

As we discussed previously, one of the main motivations behind microprocessing is the elimination of mass transfer resistance by transport rates intensification. Despite the potential of these devices, approaches which take advantage of the economy of scale observed in conventional technology are also desirable. Moreover, packed fixed beds provide a higher active surface area per volume of reactor than washcoated structures. In this context, the search for solutions that reduce mass transfer resistance inside particles includes: (a) use of eggshell catalysts with an accessible thin active layer, or (b) reducing particle size (since the characteristic time for diffusion is proportional to the square of the characteristic particle dimension). These options, however, demand either increase of catalyst volume (if maintenance of activity per volume is desired) or excessive pressure drop. Another possibility is to consider 'large pore' particles through one could force the gas or liquid to flow with a certain intraparticular velocity, reducing diffusional problems without damaging activity. We briefly review this concept and its implications in reaction engineering.

1.4.1 Convection as an additional transport mechanism in 'large-pore' materials

In general, transport in porous catalyst can occur by Knudsen flow, molecular diffusion and viscous flow (Wijngaarden et al. 1998). In particular, the convective regime occurs in pressure-driven flows and both intermolecular and molecule-wall collisions are important. In this case, the idealized pore flow rate depends on the fourth power of the pore radius, and thus the presence of relatively few large pores leads to considerably larger permeability (Wheeler 1951). This implies that whenever total pressure differences across a catalytic material exist, 'forced flow' of molecules is added to purely (Knudsen and molecular) diffusive processes. The total mass transfer rate through a pore cross-section includes contributions from diffusion (due to a difference in partial pressure) and convection. A model for intraparticular convection, diffusion and reaction is written by Wheeler (1951), but not solved. It was suggested that this mechanism would be relevant for materials with large pores (10 000 Å) and high-pressure (100 atm) gas-phase reactions.

Some experimental works conceived to look at the particular effect of internal convection in porous materials (eventually with catalytic properties) have been reported. Hawtin and Murdoch (1964) studied air oxidation in large tubes of graphite. Cogan et al. (1982) looked at the depolymerisation of paraldehyde. Cheng et al. (1987) considered the influence of the porous structure on the effective diffusivity of Rhone Poulenc alumina supports. The effective

diffusivity of a bidisperse catalyst was also determined (Cheng et al. 1989), under reactive conditions with a first-order kinetics (hydrogenation of ethylene) and a non-first-order kinetics (oxidation of ethylene). In both cases, they observed increase of the measured diffusivity with the flowrate of the carrier gas, which was attributed to the presence of convective flow in the macropores. This explanation had already been given by Rodrigues et al. (1982), with the help of the 'augmented diffusivity' concept. Komiyama and Inoue (1974) studied the exchange reaction of H^+ and K^+ on pellets of an exchange resin designed from smaller beads wrapped up in nylon. Prince et al. (1991) considered oxygen consumption in porous culture clumps and found increased rates of nutrient depletion due to internal convective transport through the spheres of entangled rootlets.

Non-reactive experiments with the purpose of evaluating fluid flow inside particles have also been presented. Pfeiffer et al. (1996) measured the volumetric flow rate of liquid and gas through small gigaporous particles by a method that isolated single pellets in a test apparatus. This constituted a confirmation of flow through perfusive particles made at pressure drops experienced during normal HPLC operation, with particles sizes from 30 to 50 μm. From the pressure-flow rate relationship (and CFD model of the test system), the average permeability was measured ($7.89\times10^{-15}\ m^2$). Gustavsson et al. (1998) video recorded the passage of microparticles through the 'superpores' and interstitial pores of agarose beads. These flow-through pores had a diameter which was a substantial fraction of the particle diameter (i.e. to 1/3 to 1/10 of the particle diameter) and together with normal diffusion pores constituted the bidisperse bead (Gustavsson et al. 1997). Other works concerning the fluid mechanics associated with the problem have also been published e.g. by Albusairi et al. (2002; 2004; 2005).

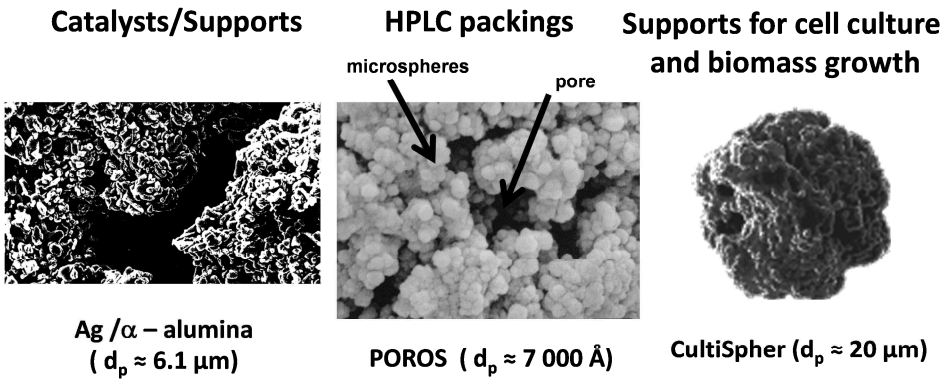

Figure 1.1: Examples of 'large-pore' materials in chemical engineering applications. (a) Silver on alumina catalyst for ethylene oxidation (Nan 1995). (b) Chromatographic material POROS. (c) CultiSpher from Percell Biolytica® (www.percell.se).

Other permeable materials containing large pores (say, with pore diameters greater than 500 Å) have found application for example as, (Figure 1.1):

- catalyst / supports in several reactions (Rodrigues et al. 1982; Quinta Ferreira 1988; Quinta Ferreira et al. 1992; Nan 1995; Costa 2004; Oliveira et al. 2009; Oliveira et al. 2010; Oliveira et al. 2011): ethylene oxidation with silver catalyst supported on α-alumina, butene oxidation to maleic anhydride in V_2O_5, oxidation of o-xylene to phthalic anhydride catalysed by V_2O_5, methane steam reforming…;
- HPLC packings (Afeyan et al. 1990; Lloyd et al. 1990; Carta et al. 1992; Rodrigues et al. 1995; Rodrigues 1996; Rodrigues et al. 1996; Rodrigues 1997; Leitão et al. 2002): polystyrene materials for proteins separation like POROS (from PerSeptive Biosystems, USA) with mean pore diameter of 7 000 Å or PL4000 (from Polymer Laboratories, UK) with pore diameter of 4 000 Å;
- supports for cell culture and biomass growth (Young et al. 1987; Breitenbucher et al. 1990), for example Cultisphere particles are used for Chinese hamster ovary cells culture from Percell Biolytica®; and
- membrane reactors (Coelhoso et al. 1992; Golman et al. 1997; Kobayashi et al. 2001; Kobayashi et al. 2003; Fritsch et al. 2004; Schmidt et al. 2005; Westermann et al. 2009; Nagy 2010a; Nagy 2010b).

1.4.2 Modelling of intraparticular convection coupled with reaction in catalyst particles

The modelling studies in reaction engineering are focused mainly at the particle level. The work from Nir and Pismen (1977) presents the first comprehensive analysis of the impact of intraparticular convection on the performance of catalyst pellets (evaluated by the effectiveness factor). The following remarks were made:

- a dimensionless parameter characterizes the role of convective transport and is defined as $\lambda = u\,L/D_e$, where L is the characteristic dimension of the pellet with diffusivity D_e and u is the intraparticular flow velocity (usually assumed uniform);
- an order-of-magnitude analysis predicted that $\lambda \sim 10$ (appreciable convective effects) when the diameters of powder particles comprising a pellet were around $100\,\mu m$ (if $Re \sim 100$) and $10\,\mu m$ (if $Re \sim 10^3$) in liquid phase, which are close to the ones used in practice;
- results for $\lambda \sim 10-50$ are presented and the higher values are possible in the case of coarse-grained particles exposed to rapid external flow;

- the effect of intraparticular convection is to increase the content of the particle in reactant, and always results in an increase of the effectiveness factor (the minimum effectiveness is obtained for all conditions when $\lambda = 0$);
- the effect of intraparticular flow is not visible in the limits of very slow and fast reaction rates, where the common asymptotes for non-permeable catalyst are observed;
- the maximum enhancement of the effectiveness factor is observed in the region where kinetics just becomes diffusion controlled (intermediate regime);
- the effectiveness factor enhancement is less pronounced in the case of sphere and cylinder geometries, when compared to a slab.

The material balance also includes the Thiele modulus ϕ^2, which compares the magnitudes of reaction and diffusion. Therefore, three regimes can be defined (as in the case of conventional catalyst particles): chemical regime (fast diffusion compared with reaction, where presence of the reactant in the whole slab is assured with concentration near the surface concentration); diffusional regime (where fast reaction leads to a sharp decline in reactant concentration near the surfaces of the slab and only a relatively small fraction of the catalyst is used) and an intermediate regime (where the effect of moderate convection is expected to be more noticeable), Figure 1.2.

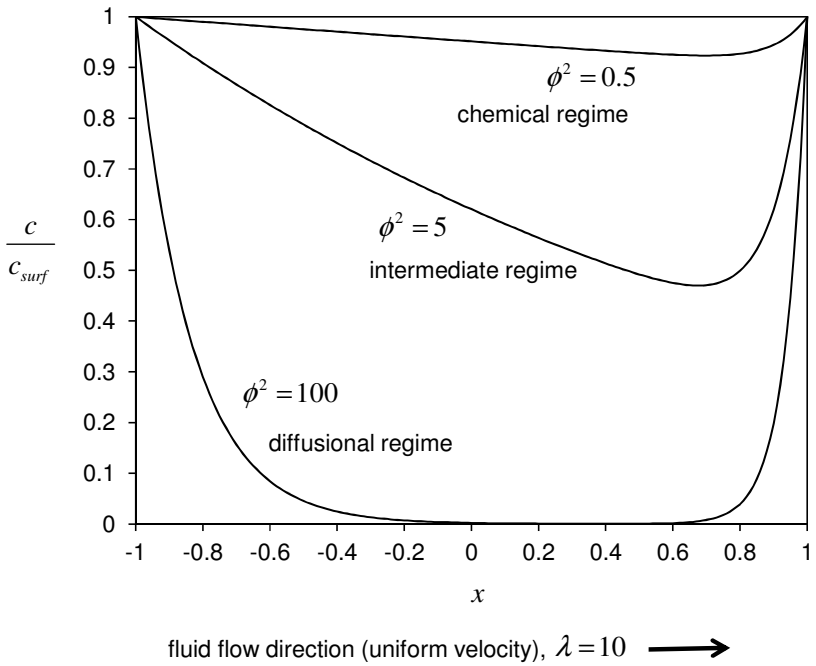

Figure 1.2: Typical concentration profiles in the chemical, intermediate and diffusional regimes for the problem of convection, diffusion and isothermal first-order reaction in a slab shaped particle.

Table 1.5: Modelling studies involving catalytic particles with intraparticular convection

Reference	Details	Geometry
Komiyama et al. (1974)	First-order isothermal reaction	Cylinder parallel to flow
Nir and Pismen (1977)	First-order isothermal reaction	Slab, Sphere and Cylinder perpendicular to flow
Nir (1977)	Sequential first-order isothermal	Slab and Sphere
Rodrigues et al. (1984)	Zero-order isothermal reaction	Slab
Cresswell (1985)	Consecutive-parallel scheme of first-order isothermal reactions	Slab
Quinta Ferreira et al. (1988; Rodrigues et al. 1988)	First-order nonisothermal reaction ** numerical solutions including steady state multiplicity*	Slab
Stephanopoulos et al. (1989)	Zero-order isothermal reaction	Sphere
Chaara et al. (1989)	Reversible first-order bimolecular reaction	Slab
Lu et al. (1993)	First-order isothermal reaction ** transient behaviour and results for augmented diffusivity*	Slab/Sphere analogy
Nan et al. (1995)	First-order isothermal reaction ** combined internal pressure gradients (mole changes from reaction)*	Slab
Nan et al. (1996a)	First-order isothermal reaction	Cylinder (parallel to flow)/ Slab analogy
Nan et al. (1996b)	First-order isothermal reaction ** results for the augmented diffusivity by convection*	Hollow Cylinder (parallel to flow; axial convection)
Moreira et al. (1996)	Isothermal Michaelis-Menten kinetics	Slab
Leitão et al. (1994)	Isothermal first-order reaction ** bidisperse catalysts*	Slab and Sphere
Lopes et al. (1995)	First-order non-isothermal reaction ** numerical solution including internal flow field*	Sphere
Costa (2004)	First-order non-isothermal reaction Consecutive-parallel complex scheme ** numerical solution and multiplicity analysis for external resistance to heat transfer with internally isothermal particle*	Slab
Cardoso et al. (2007)	First-order nonisothermal reaction **perturbation solutions*	Slab
Nagy (2010b)	First-order isothermal reaction with external mass transfer	Slab

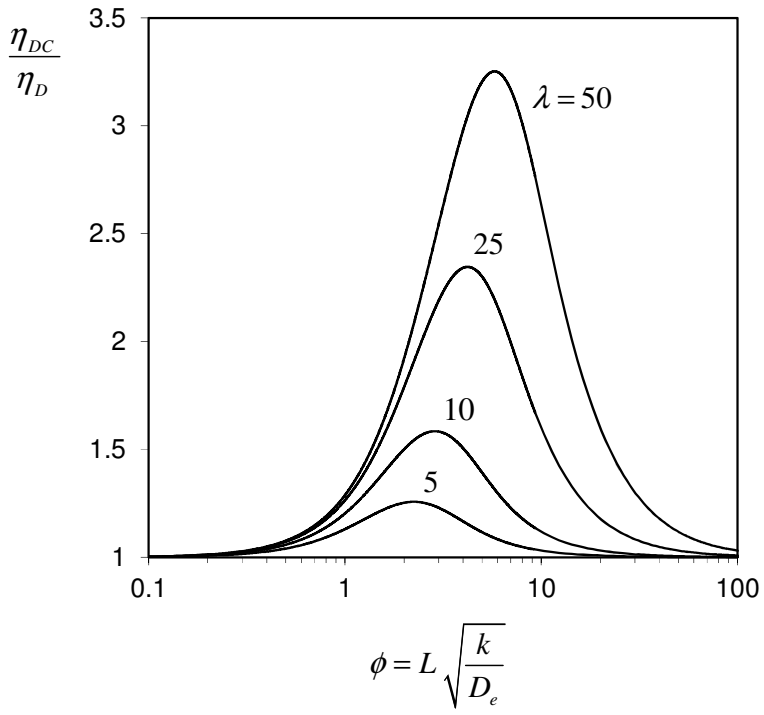

Figure 1.3: Effectiveness factor enhancement in the intermediate region, as calculated by Nir and Pismen (1977).

The main conclusion from Nir and Pismen study is that the effectiveness factor (that measures the performance of the catalyst) is enhanced in the intermediate region of the Thiele modulus. Comparing the effectiveness factor when diffusion and convection are important (η_{DC}) with the situation where convection is negligible (η_D), it is possible to verify that the increase in the effectiveness factor gets more pronounced as the intraparticular Peclet mass number increases (that is, when intraparticular convection gains more and more importance), Figure 1.3.

Subsequent studies extended this approach to other kinetic laws, particle geometries and reaction schemes as can be seen in Table 1.5. Most of them are concerned with isothermal conditions. However, in reactor design where reactions with appreciable heat of reaction occur, it is very important to know the maximum temperature that occurs inside the catalyst particle. In the case where only diffusion/conduction and reaction occur inside the particle, the Damköhler equation (Damköhler 1937) provides a useful relationship between temperature and concentration inside the particle. Without actually solving the equations, Damköhler got a simple expression to estimate the maximum temperature that will occur inside the particle, predicting that it will correspond to the complete consumption of reactant. This expression is function of the Prater parameter, which includes diffusivity, thermal conductivity, heat of reaction and surface conditions. The extension of this solution to the cases where non-negligible internal convection existed has been pursued, either numerically or using approximate analytical methods (Table 1.5).

At the fixed bed reactor level, numerical solution of both steady-state and transient models with different levels of complexity (pseudo-homogeneous and heterogeneous), including thermal effects and runaway behaviour, were also presented (Quinta Ferreira 1988; Rodrigues et al. 1990; Ferreira et al. 1992; Costa et al. 1994; Leitao et al. 1995; Leitão et al. 1995; Quinta-Ferreira et al. 1995; Leitão et al. 1996; Quinta Ferreira et al. 1996a; Quinta Ferreira et al. 1996b; Leitão et al. 1998; Costa 2004).

1.5 THESIS OBJECTIVES AND OUTLINE

The main contribution of this work is to provide a comprehensive description of the transport-reaction processes occurring in a wall-coated microchannel. We focus particularly on an approximate analytical analysis at the individual channel level. As we have described in this chapter, a microchannel with small aspect (diameter-to-length) ratio is an essential building block of all microchemical systems. This geometry allows achievement of high surface-to-volume ratios according to Eq.(1.1), and is convenient due to: easy machining, low pressure drop, natural distribution of flow in parallel processing, and controlled residence time. Other microgeometries such as cavities and wells have been explored for mixing purposes, but are limited to analytical and biotechnological applications. For these reasons, the microchannel will be our object of study. Nevertheless, the adequacy of the 'single channel representation' can obviously be questioned, and it is expected to be limited when modeling arrangements which present strong interchannel interaction due to e.g. nonuniform fluid distribution (Commenge et al. 2002), heat exchange/losses (Di Benedetto et al. 2011) or mass transfer through porous walls (Chen et al. 2008b) exist between channels. These cases are recognizably more expensive from a computational point of view. However, in many situations the channel model is made general enough to at least be included in reactor-level simulations and improve the simulation performance of these systems. Moreover, we have already seen some cases where single channel microreactors may work as mini-plants for production, and this may even be desirable when high control effort and safety requirements are present. In particular, the isothermal microchannel reactor appears as part or on its own in a number of microprocessing studies and applications.

Due to the potential of these units, an improved understanding of their behavior is required and this can be achieved by several modeling methods (Hardt 2000). Numerical solution of the governing equations is able to deal with very complex systems, while exact analytical solutions are limited to idealized models. Our perspective fits in the intermediate region between the two approaches. On one hand, numerically obtained simulations are irremediably tied up with particular values of the (possibly many) parameters and are associated with a certain

computational effort. On the other, exact solutions may result in formulas far too complicated (non-elementary functions, infinite series,…) to extract valuable information. Approximate analytical methods, such as perturbation techniques, play an important role in this context. In this case, selected reductions of the full problem are proposed to describe the solution in tractable terms, in a given regime. Therefore, the functional dependence of quantities of interest (performance) on the model parameter(s) is obtained. Asymptotic methods become particularly interesting when the model contains a parameter which can be assumed to be very small or large (this leads automatically to the definition of a 'regime'). In these cases, the original problem unfolds in a sequence of simpler problems as will be show in several examples throughout the thesis. In these cases different phenomena may dominate over different (local) scales and, while this gives the richest structure in an approximate solution, it is where typically numerical methods encounter most difficulties. Note that even though perturbation solutions may be restricted to smallness of a given parameter, they are uniformly valid in the domain of the problem.

Another class of techniques which cannot be dissociated from asymptotic and perturbation methods is scaling. In fact, the problems studied involve several transport mechanisms coupled with reaction, and the analysis of the magnitude of each term involves the choice of appropriate scales. It is a relationship between these scales which will determine the leading-order behavior or the dominant balance between two effects, being the other(s) negligible at first approximation (but incorporated in corrective terms). The access to these leading-order behaviors (in given, and therefore defined regimes), and the estimation of the order of magnitude of the remaining effects is not provided by numerical techniques. The procedure implies the definition of limits or regimes, and hence is suitable for establishing boundaries between them, which would require extensive numerical simulation in a wide parametric range.

The analysis along these lines also contributes to the rational design of microreactors, which compared to macrosystems are closer to a correct description from first principles (e.g. laminar flow). We have also reported critical reviews pointing out that a 'new' theory is not required, as long as the effects gaining importance from miniaturization are accounted for (sections 1.1.2.b and 1.1.5). Actually, Hessel et al. (2004) distinguish between two descriptions of microreaction technology: 'bottom-up' and 'top-down'. In their opinion, the 'bottom-up' approach has prevailed in most literature, where achievements in specific operating units and applications were reported. They consider desirable that 'top-down' analyses are provided too. These consist in setting requirements related to the process and finding a design which fulfills such aims, subject to constraints and aiming at the minimization of certain cost functions. This is the statement of a design problem, for which we believe that the results in this thesis may contribute.

We aim to achieve further insight into the considered transport-reaction problem with the following two main objectives:

i. provide accurate approximate results from reduced-order models without the need for numerically calculated quantities, and
ii. identify the limits to which the full problem reduces, mapping operating regimes and the transitions between them.

These goals will allow us to analyze relevant process intensification strategies, such as microreactors and flow-through permeable catalyst particles. The relevance of both was highlighted in this chapter, and in practice they are considered as promising directions, particularly for fast reactions with highly active catalysts. For example, information from Velocys, Inc. concerning the choice of reactor design for reactions such as oxidations is presented in Figure 1.4 in terms of the kinetic rate and the amount of pressure drop or temperature variation allowed.

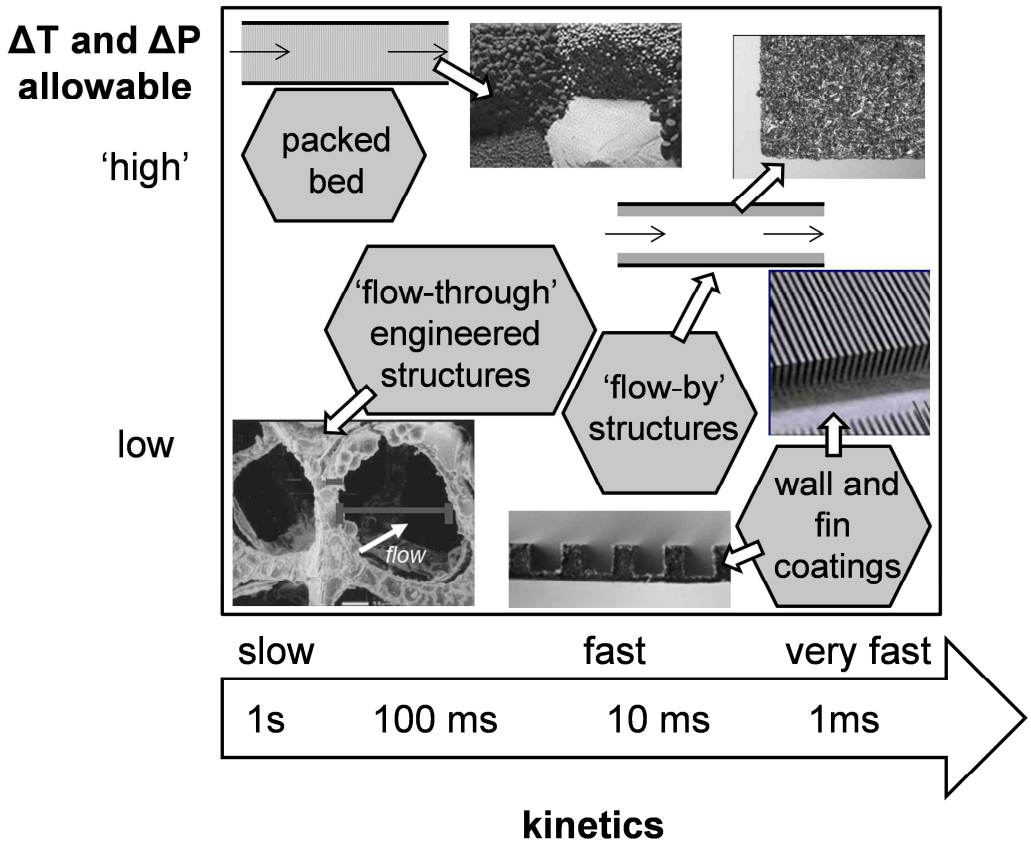

Figure 1.4: Velocys, Inc. catalyst selection strategy. Adapted from J. Lerou, 'Microreaction Engineering: Is small really better?' (www.velocys.com).

In particular, this work proposes:

1. a solution for the transport-reaction problem inside a wall-coated microchannel for finite reaction rates in the fully developed and developing limits of the concentration profile (Chapter 2);
2. a description of conversion in a microchannel when reactions with nonlinear kinetics occur in the asymptotic limits of small and large reaction rates (Chapter 2);
3. a uniform solution which combines classic theories of mass and heat transfer in channel flow and defines ranges of validity for the limits (Chapter 3); and
4. a regime map where a comprehensive picture of the different interphase transport – reaction behaviors is plotted, and boundaries between them derived (Chapter 4).

We also consider the problem at the level of a thin catalytic coating, to achieve:

5. the calculation of the approximate effectiveness factor with linear and nonlinear kinetics and nonuniform geometries (Chapter 5); and
6. the definition of regimes considering the interplay between internal and external mass transfer (Chapter 5).

Furthermore, the existence of intraparticular convection effects is studied in two contexts:

7. calculation of a 'curvature correction' for isothermal linear kinetics in a channel with a thin perfusive wall, and identification of the conditions for maximum enhancement (Chapter 5), and
8. study of the influence of nonisothermal effects in a permeable slab with focus on effectiveness factor and maximum temperature estimation (Chapter 6).

Finally, the main conclusions of our analysis and suggestions for future work are presented in Chapter 7.

NOTATION

a	channel's characteristic (transverse) dimension
A_{ch}	cross-sectional area of the channel
c_0	reference concentration
C_P	fluid specific heat
D	fluid's bulk diffusivity
d_{ch}	channel's hydraulic diameter

d_{part}	particle diameter
GHSV	gas hourly space velocity
h_k	coefficient in Carman-Kozeney equation (double of the ratio between length of passage in porous bed and in straight capillary)
k	reaction rate kinetic constant (referred to catalyst volume)
k_{heat}	heat transfer coefficient
k_m	mass transfer coefficient
k_{surf}	reaction rate kinetic constant (referred to catalyst surface area)
ΔH_R	heat of reaction
ℓ_{mean}	mean free path
L	channel's length, axial characteristic dimension
m	order of reaction with power-law kinetics
$\dot{m}$	mass flowrate
N_{ch}	number of channels
Nu	Nusselt number
NTU	Number of transfer units
ΔP	Pressure drop
Pr	Prandtl's number
Q_{feed}	feed flowrate
$R(c)$	reaction rate (referred to catalyst volume)
Re	Reynold's number
S_{surf}	channel surface area
Sc	Schmidt's number
Sh	Sherwood number
t_w	catalytic coating thickness
T_0	reference temperature
ΔT_{ad}	adiabatic temperature rise
$\langle u \rangle$	average fluid velocity in the channel
V	channel's volume

Greek letters

ε	porosity
δ	boundary layer thickness
κ	fluid thermal diffusivity, $\lambda/(\rho C_P)$
λ	fluid thermal conductivity
η	effectiveness factor
ρ	fluid's density
ν	fluid's kinematic viscosity
τ	timescale, characteristic time, time constant

Subscripts

bulk	conditions in the channel's bulk
surf	conditions at the channel/catalyst interface
wall	referred to wall material

REFERENCES

Afeyan, N. B., S. P. Fulton, N. F. Gordon, I. Mazsaroff, L. Varady and F. E. Regnier (1990). "Perfusion chromatography: An approach to purifying biomolecules." Nature Biotechnology **8**(3): 203-206.

Albusairi, B. and J. T. Hsu (2002). "Application of shape factor to determine the permeability of perfusive particles." Chemical Engineering Journal **89**(1-3): 173-183.

Albusairi, B. and J. T. Hsu (2004). "Flow through beds of perfusive particles: Effective medium model for velocity prediction within the perfusive media." Chemical Engineering Journal **100**(1-3): 79-84.

Albusairi, B. H. and J. T. Hsu (2005). "Dispersion coefficient prediction within a bed packed with perfusive particles." AIChE Journal **51**(5): 1330-1338.

Aris, R. (1956). "On the Dispersion of a Solute in a Fluid Flowing through a Tube " Proceedings of the Royal Society of London A **235**(1200): 67-77.

Becht, S., R. Franke, A. Geißelmann and H. Hahn (2009). "An industrial view of process intensification." Chemical Engineering and Processing: Process Intensification **48**(1): 329-332.

Becht, S., R. Franke, A. Gießelmann and H. Hahn (2007). "Micro process technology as a means of process intensification." Chemical Engineering and Technology **30**(3): 295-299.

Benito-López, F., R. J. M. Egberink, D. N. Reinhoudt and W. Verboom (2008). "High pressure in organic chemistry on the way to miniaturization." Tetrahedron **64**(43): 10023-10040.

Beretta, A., G. Groppi, L. Majocchi and P. Forzatti (1999). "Potentialities and draw-backs of the experimental approach to the study of high T and high GHSV kinetics." Applied Catalysis A: General **187**(1): 49-60.

Bird, R. B., W. E. Stewart and E. N. Lightfoot (2002). Transport Phenomena. New York, John Wiley & Sons, Inc.

Bolivar, J. M., J. Wiesbauer and B. Nidetzky (2011). "Biotransformations in microstructured reactors: more than flowing with the stream?" Trends in Biotechnology.

Breitenbucher, K., M. Siegl, A. Knupfer and M. Radke (1990). "Open-pore sintered glass as a high-efficiency support medium in bioreactors: New results and long-term experiences achieved in high-rate anaerobic digestion." Water Science and Technology **22**(1-2): 25-32.

Bruus, H. (2008). Theoretical Microfluidics. New York, Oxford University Press.

Cardoso, S. S. S. and A. E. Rodrigues (2007). "Convection, diffusion and reaction in a nonisothermal, porous catalyst slab." AIChE Journal **53**(5): 1325-1336.

Carta, G., M. E. Gregory, D. J. Kirwan and H. A. Massaldi (1992). "Chromatography with permeable supports: Theory and comparison with experiments." Separations Technology **2**(2): 62-72.

Casanovas, A., C. de Leitenburg, A. Trovarelli and J. Llorca (2008a). "Catalytic monoliths for ethanol steam reforming." Catalysis Today **138**(3-4): 187-192.

Casanovas, A., M. Dominguez, C. Ledesma, E. Lopez and J. Llorca (2008b). "Catalytic walls and micro-devices for generating hydrogen by low temperature steam reforming of ethanol." Catalysis Today **143**(1-2): 32-37

Chaara, M. and R. Noble (1989). "Effect of Convective Flow Across a Film on Facilitated Transport." Separation Science and Technology **24**: 893-903.

Charpentier, J. C. (2005). "Process intensification by miniaturization." Chemical Engineering and Technology **28**(3): 255-258.

Chen, H., H. Yu, Y. Tang, M. Pan, F. Peng, H. Wang and J. Yang (2008a). "Assessment and optimization of the mass-transfer limitation in a metal foam methanol microreformer." Applied Catalysis A: General **337**(2): 155-162.

Chen, J., H. Yang, N. Wang, Z. Ring and T. Dabros (2008b). "Mathematical modeling of monolith catalysts and reactors for gas phase reactions." Applied Catalysis A: General **345**(1): 1-11.

Cheng, S. and A. Zoulalian (1989). "Influence de la reaction chimique et de la convection interne sur la determination de la diffusivite apparente d'un catalyseur." Chemical Engineering Journal **41**(2): 91-104.

Cheng, S., A. Zoulalian and J. P. Brunelle (1987). Influence of the porous structure of alumina pellets and the internal convective flow on the effective diffusivity of exhaust gas catalyst. Catalysis and Automative Pollution Control. A. Crucq and A. Frennet. Amsterdam, Elsevier Science Publishers B.V.**:** 323-332.

Coelhoso, I., J. Crespo and A. E. Rodrigues (1992). The effect of convective flow on the facilitated transport across a membrane. Meeting of the European Membrane Society. Paris.

Cogan, R., G. Pipko and A. Nir (1982). "Simultaneous Intraparticle Forced Convection, Diffusion and Reaction in a Porous Catalyst - 3." Chemical Engineering Science **37**(2): 147-151.

Commenge, J. M., L. Falk, J. P. Corriou and M. Matlosz (2002). "Optimal Design for Flow Uniformity in Microchannel Reactors." AIChE Journal **48**(2): 345-358.

Commenge, J. M., L. Falk, J. P. Corriou and M. Matlosz (2005). "Analysis of microstructured reactor characteristics for process miniaturization and intensification." Chemical Engineering and Technology **28**(4): 446-458.

Costa, A. C. (2004). Estudo do comportamento estacionário e dinâmico de reactores catalíticos de leito fixo com convecção intraparticular. Universidade de Coimbra. PhD thesis.

Costa, C. A., R. M. Quinta Ferreira and A. E. Rodrigues (1994). "Wrong-way behavior in packed-bed reactors with 'large-pore' catalysts." Chemical Engineering Science **49**(24 B): 5571-5583.

Cresswell, D. L. (1985). "Intra-particle convection: its measurement and effect on catalyst activity and selectivity." Applied catalysis **15**(1): 103-116.

Cybulski, A. and J. Moulijn (1998). Structured Catalysts and Reactors. New York, Marcel Dekker.

Damköhler, G. (1937). "Einfluss von Diffusion, Strömung, und Wärmetransport auf die Ausbeute in Chemisch-Technischen Reaktionen." Chem.-Eng.-Tech **3**(Part 1, Chapter 2): 359-485.

Delsman, E. R., A. Pierik, M. H. J. M. De Croon, G. J. Kramer and J. C. Schouten (2004). "Microchannel plate geometry optimization for even flow distribution at high flow rates." Chemical Engineering Research and Design **82**(2): 267-273.

Deshmukh, S. R., A. L. Y. Tonkovich, K. T. Jarosch, L. Schrader, S. P. Fitzgerald, D. R. Kilanowski, J. J. Lerou and T. J. Mazanec (2010). "Scale-up of microchannel reactors for Fischer-Tropsch synthesis." Industrial and Engineering Chemistry Research **49**(21): 10883-10888.

Di Benedetto, A. and V. Di Sarli (2011). "CFD Modeling and Simulation of a Catalytic Micro-Monolith." International Journal of Chemical Reactor Engineering **9**.

Ebrahimi, F., E. Kolehmainen, P. Oinas, V. Hietapelto and I. Turunen (2011). "Production of unstable percarboxylic acids in a microstructured reactor." Chemical Engineering Journal **167**(2-3): 713-717.

Ebrahimi, F., E. Kolehmainen and I. Turunen (2009). "Safety advantages of on-site microprocesses." Organic Process Research and Development **13**(5): 965-969.

Ehrfeld, W., V. Hessel and H. Löwe (2000). Microreactors: New technology for modern chemistry. Weinheim, Wiley-VCH.

Falk, L. and J. M. Commenge (2010). "Performance comparison of micromixers." Chemical Engineering Science **65**(1): 405-411.

Federici, J. A. and D. G. Vlachos (2011). "Experimental studies on syngas catalytic combustion on Pt/Al2O3 in a microreactor." Combustion and Flame **In Press**.

Ferreira, R. M. Q., A. C. Costa and A. E. Rodrigues (1992). "Dynamic behavior of fixed-bed reactors with ``large-pore" catalysts: A bidimensional heterogeneous diffusion/convection model." Computers and Chemical Engineering **16**(8): 721-751.

Fritsch, D., I. Randjelovic and F. Keil (2004). "Application of a forced-flow catalytic membrane reactor for the dimerisation of isobutene." Catalysis Today **98**(1-2 SPEC. ISS.): 295-308.

Germani, G. and Y. Schuurman (2006). "Water-gas shift reaction kinetics over micro-structured Pt/CeO2/AI2O3 catalysts." AIChE Journal **52**(5): 1806-1813.

Gokhale, S. V., V. K. Jayaraman, R. K. Tayal and B. D. Kulkarni (2005). "Microchannel reactors: Applications and use in process development." International Journal of Chemical Reactor Engineering **3**.

Golman, B., K. Shinohara and M. Kobayashi (1997). "Selectivity and yield of exothermic consecutive reactions in catalytically active porous membrane reactor." Journal of Chemical Engineering of Japan **30**(3): 507-513.

Görke, O., P. Pfeifer and K. Schubert (2009). "Kinetic study of ethanol reforming in a microreactor." Applied Catalysis A: General **360**(2): 232-241.

Groppi, G., W. Ibashi, M. Valentini and P. Forzatti (2001). "High-temperature combustion of CH4 over PdO/Al2O3: Kinetic measurements in a structured annular reactor." Chemical Engineering Science **56**(3): 831-839.

Gustavsson, P. E., A. Axelsson and P. O. Larsson (1998). "Direct measurements of convective fluid velocities in superporous agarose beads." Journal of Chromatography A **795**(2): 199-210.

Gustavsson, P. E., K. Mosbach, K. Nilsson and P. O. Larsson (1997). "Superporous agarose as an affinity chromatography support." Journal of Chromatography A **776**(2): 197-203.

Halder, R., A. Lawal and R. Damavarapu (2007). "Nitration of toluene in a microreactor." Catalysis Today **125**(1-2): 74-80.

Hardt, S. (2000). Microreactors – Modeling and Simulation. Ullmann's Encyclopedia of Industrial Chemistry, Wiley-VCH Verlag GmbH & Co. KGaA.

Hardt, S., W. Ehrfeld, V. Hessel and K. M. Vanden Bussche (2003). "Strategies for size reduction of microreactors by heat transfer enhancement effects." Chemical Engineering Communications **190**(4): 540-559.

Hawtin, P. and R. Murdoch (1964). "The Role of In-pore Mass Transport Resistance in the Reaction of Porous Solids with Gases." Chemical Engineering Science **19**: 819-834.

Hayes, R. E. and S. T. Kolaczkowski (1994). "Mass and heat transfer effects in catalytic monolith reactors." Chemical Engineering Science **49**(21): 3587-3599.

Hayes, R. E., S. T. Kolaczkowski, W. J. Thomas and J. Titiloye (1995). "Intraphase diffusion and interphase mass transfer effects during the catalytic oxidation of CO in a tube wall reactor." Proceedings - Royal Society of London, A **448**(1933): 321-334.

Herwig, H. (2008). Momentum and Heat Transfer in Microsized Devices. Micro Process Engineering: Fundamentals, Devices, Fabrication, and Applications. N. Kockmann. Weinheim, Germany, Wiley-VCH Verlag GmbH**:** 47-70.

Hessel, V. (2009). "Process windows - gate to maximizing process intensification via flow chemistry." Chemical Engineering and Technology **32**(11): 1655-1681.

Hessel, V., B. Cortese and M. H. J. M. de Croon (2011). "Novel process windows - Concept, proposition and evaluation methodology, and intensified superheated processing." Chemical Engineering Science **66**(7): 1426-1448.

Hessel, V., S. Hardt and H. Löwe (2004). Chemical Micro Process Engineering: Fundamentals, Modelling and Reactions. Weinheim, Wiley-VCH.

Hessel, V., C. Hofmann, P. Löb, J. Löhndorf, H. Löwe and A. Ziogas (2005a). "Aqueous Kolbe-Schmitt synthesis using resorcinol in a microreactor laboratory rig under high-p,T conditions." Organic Process Research and Development **9**(4): 479-489.

Hessel, V., C. Knobloch and H. Löwe (2008a). "Review on Patents in Microreactor and Micro Process Engineering." Recent Patents on Chemical Engineering **1**(1): 1-16.

Hessel, V., D. Kralisch and U. Krtschil (2008b). "Sustainability through green processing - Novel process windows intensify micro and milli process technologies." Energy and Environmental Science **1**(4): 467-478.

Hessel, V., H. Löwe, A. Müller and G. Kolb (2005b). Chemical Micro Process Engineering: Processing and Plants. Weinheim, Wiley-VCH.

Hoebink, J. H. B. J. and G. B. Marin (1998). Modeling of Monolithic Reactors for Automotive Exhaust Gas Treatment. Structured Catalysts and Reactors. A. Cybulski and J. Moulijn. New York, Marcel Dekker**:** 209-237.

Illg, T., V. Hessel, P. Löb and J. C. Schouten (2011). "Novel Process Window for the safe and continuous synthesis of tert.-butyl peroxy pivalate in a micro-reactor." Chemical Engineering Journal **167**(2-3): 504-509.

Illg, T., P. Löb and V. Hessel (2010). "Flow chemistry using milli- and microstructured reactors-From conventional to novel process windows." Bioorganic and Medicinal Chemistry **18**(11): 3707-3719.

Jensen, K. F. (2001). "Microreaction engineering-is small better?" Chemical Engineering Science **56**(2): 293-303.

Judy, J., D. Maynes and B. W. Webb (2002). "Characterization of frictional pressure drop for liquid flows through microchannels." International Journal of Heat and Mass Transfer **45**(17): 3477-3489.

Kapteijn, F., R. M. De Deugd and J. A. Moulijn (2005). "Fischer-Tropsch synthesis using monolithic catalysts." Catalysis Today **105**(3-4): 350-356.

Kestenbaum, H., A. L. De Oliveira, W. Schmidt, F. Schüth, W. Ehrfeld, K. Gebauer, H. Löwe, T. Richter, D. Lebiedz, I. Untiedt and H. Zücher (2002). "Silver-catalyzed oxidation of ethylene to ethylene oxide in a microreaction system." Industrial and Engineering Chemistry Research **41**(4): 710-719.

Kim, K. Y., J. Han, S. W. Nam, T. H. Lim and H. I. Lee (2008). "Preferential oxidation of CO over CuO/CeO2 and Pt-Co/Al2O3 catalysts in micro-channel reactors." Catalysis Today **131**(1-4): 431-436.

Kobayashi, M., T. Kanno, J. I. Horiuchi, S. Hoshi, N. Hattori and J. Togawa (2001). Hysteresis kinetics of propene oxidation characterized by a Ag-Re supported membrane reactor. **133:** 105-112.

Kobayashi, M., J. Togawa, T. Kanno, J. I. Horiuchi and K. Tada (2003). "Dramatic innovation of propene epoxidation efficiency derived from a forced flow membrane reactor." Journal of Chemical Technology and Biotechnology **78**(2-3): 303-307.

Kockmann, N. and D. M. Roberge (2009). "Harsh reaction conditions in continuous-flow microreactors for pharmaceutical production." Chemical Engineering and Technology **32**(11): 1682-1694.

Kolaczkowski, S. T. (1999). "Modelling catalytic combustion in monolith reactors - Challenges faced." Catalysis Today **47**(1-4): 209-218.

Kolb, G., V. Cominos, C. Hofmann, H. Pennemann, J. Schürer, D. Tiemann, M. Wichert, R. Zapf, V. Hessel and H. Löwe (2005). "Integrated microstructured fuel processors for fuel cell applications." Chemical Engineering Research and Design **83**(6 A): 626-633.

Kolb, G. and V. Hessel (2004). "Micro-structured reactors for gas phase reactions." Chemical Engineering Journal **98**(1-2): 1-38.

Kolb, G., V. Hessel, V. Cominos, C. Hofmann, H. Löwe, G. Nikolaidis, R. Zapf, A. Ziogas, E. R. Delsman, M. H. J. M. de Croon, J. C. Schouten, O. de la Iglesia, R. Mallada and J. Santamaria (2007). "Selective oxidations in micro-structured catalytic reactors-For gas-phase reactions and specifically for fuel processing for fuel cells." Catalysis Today **120**(1): 2-20.

Komiyama, H. and H. Inoue (1974). "Effects of intraparticle flow on catalytic reactions." Journal of Chemical Engineering of Japan **7**(4): 281-286.

Kreutzer, M. T., F. Kapteijn and J. A. Moulijn (2006). "Shouldn't catalysts shape up? Structured reactors in general and gas-liquid monolith reactors in particular." Catalysis Today **111**(1-2): 111-118.

Kreutzer, M. T., F. Kapteijn, J. A. Moulijn and J. J. Heiszwolf (2005). "Multiphase monolith reactors: Chemical reaction engineering of segmented flow in microchannels." Chemical Engineering Science **60**(22): 5895-5916.

Kundu, A., J. E. Ahn, S. S. Park, Y. G. Shul and H. S. Han (2008). "Process intensification by micro-channel reactor for steam reforming of methanol." Chemical Engineering Journal **135**(1-2): 113-119.

Lee, P. S., S. V. Garimella and D. Liu (2005). "Investigation of heat transfer in rectangular microchannels." International Journal of Heat and Mass Transfer **48**(9): 1688-1704.

Leitao, A., M. Dias and A. Rodrigues (1994). "Effectiveness of bidisperse catalysts with convective flow in the macropores." Chemical Engineering Journal and the Biochemical Engineering Journal **55**(1-2): 81-86.

Leitão, A., M. Li and A. Rodrigues (2002). "The role of intraparticle convection in protein adsorption by liquid chromatography using POROS 20 HQ/M particles." Biochemical Engineering Journal **11**(1): 33-48.

Leitao, A. and A. Rodrigues (1995). "Influence of intraparticle convection on product distribution for series-parallel catalytic reactions." Chemical Engineering Research and Design **73**(A2): 130-135.

Leitão, A. and A. Rodrigues (1995). "Catalytic processes using "large-pore" materials: effects of the flow rate and operating temperature on the conversion in a plug-flow reactor for irreversible first-order reactions." The Chemical Engineering Journal and The Biochemical Engineering Journal **60**(1-3): 111-116.

Leitão, A. and A. Rodrigues (1996). "Modeling of biodegradation/adsorption combined processes in fixed-bed biofilm reactors: Effects of the intraparticle convective flow." Chemical Engineering Science **51**(20): 4595-4604.

Leitão, A. and A. Rodrigues (1998). "Dynamic behaviour of a fixed-bed biofilm reactor: Analysis of the role of the intraparticle convective flow under biofilm growth." Biochemical Engineering Journal **2**(1): 1-9.

Lerou, J. J., A. L. Tonkovich, L. Silva, S. Perry and J. McDaniel (2010). "Microchannel reactor architecture enables greener processes." Chemical Engineering Science **65**(1): 380-385.

Lin, C. C. and L. A. Segel (1988). Mathematics Applied to Deterministic Problems in the Natural Sciences, SIAM.

Lloyd, L. L. and F. P. Warner (1990). "Preparative high-performance liquid chromatography on a unique high-speed macroporous resin." Journal of Chromatography A **512**(C): 365-376.

Lomel, S., L. Falk, J. M. Commenge, J. L. Houzelot and K. Ramdani (2006). "The microreactor: A systematic and efficient tool for the transition from batch to continuous process?" Chemical Engineering Research and Design **84**(5 A): 363-369.

Lopes, J. C. B., M. M. Dias, V. G. Mata and A. E. Rodrigues (1995). "Flow field and non-isothermal effects on diffusion, convection, and reaction in permeable catalysts." Industrial and Engineering Chemistry Research **34**(1): 148-157.

Lu, Z. P., M. M. Dias, J. C. B. Lopes, G. Carta and A. E. Rodrigues (1993). "Diffusion, convection, and reaction in catalyst particles: Analogy between slab and sphere geometries." Industrial and Engineering Chemistry Research **32**(9): 1839-1852.

Lucas, M. and P. Claus (2003). "High throughput screening in monolith reactors for total oxidation reactions." Applied Catalysis A: General **254**(1): 35-43.

Mae, K. (2007). "Advanced chemical processing using microspace." Chemical Engineering Science **62**(18-20): 4842-4851.

Maehara, S., M. Taneda and K. Kusakabe (2008). "Catalytic synthesis of hydrogen peroxide in microreactors." Chemical Engineering Research and Design **86**(4): 410-415.

Marre, S., A. Adamo, S. Basak, C. Aymonier and K. F. Jensen (2010). "Design and packaging of microreactors for high pressure and high temperature applications." Industrial and Engineering Chemistry Research **49**(22): 11310-11320.

McCarty, J. G. (1995). "Kinetics of PdO combustion catalysis." Catalysis Today **26**(3-4): 283-293.

McMullen, J. P. and K. F. Jensen (2010). Integrated microreactors for reaction automation: New approaches to reaction development. **3:** 19-42.

Mills, P. L., D. J. Quiram and J. F. Ryley (2007). "Microreactor technology and process miniaturization for catalytic reactions--A perspective on recent developments and emerging technologies." Chemical Engineering Science **62**(24): 6992-7010.

Miyazaki, M. and H. Maeda (2006). "Microchannel enzyme reactors and their applications for processing." Trends in Biotechnology **24**(10): 463-470.

Moreira, N. E. and F. X. Malcata (1996). "Use of convective flow to enhance the effectiveness factor of poroys slab-shaped beads with immobilized enzyme." Journal of Chemical Engineering of Japan **29**(2): 392-395.

Moulijn, J., M. Kreutzer and F. Kapteijn (2005). "A little structure works wonders." Chemical Engineer(768): 32-34.

Nagy, E. (2010a). "Convective and diffusive mass transport through anisotropic, capillary membrane." Chemical Engineering and Processing: Process Intensification **49**(7): 716-721.

Nagy, E. (2010b). "Mass transfer through a convection flow catalytic membrane layer with dispersed nanometer-sized catalyst." Industrial and Engineering Chemistry Research **49**(3): 1057-1062.

Nan, H. S. (1995). Influence of forced convection on mass transport and reaction in porous catalysts pellets and reactor performance. University of Porto. PhD thesis.

Nan, H. S., M. M. Dias, J. C. B. Lopes and A. E. Rodrigues (1996a). "Diffusion, convection and reaction in catalyst particles: Analogy between slab and cylinder geometries." Chemical Engineering Journal and the Biochemical Engineering Journal **61**(2): 113-122.

Nan, H. S., M. M. Dias, V. G. Mata and A. E. Rodrigues (1996b). "Measurements of effective diffusivity in large-pore permeable pellets with various geometries using the chromatographic method." Chemical Engineering Communications **146**: 201-229.

Nan, H. S., M. M. Dias and A. E. Rodrigues (1995). "Effect of forced convection on reaction with mole changes in porous catalysts." Chemical Engineering Journal and the Biochemical Engineering Journal **57**(2): 101-114.

Nieuwland, P. J., K. Koch, N. Van Harskamp, R. Wehrens, J. C. M. Van Hest and F. P. J. T. Rutjes (2010). "Flash chemistry extensively optimized: High-temperature Swern-Moffatt oxidation in an automated microreactor platform." Chemistry - An Asian Journal **5**(4): 799-805.

Nijhuis, T. A., M. T. Kreutzer, A. C. J. Romijn, F. Kapteijn and J. A. Moulijn (2001). "Monolithic catalysts as more efficient three-phase reactors." Catalysis Today **66**(2-4): 157-165.

Nir, A. (1977). "Simultaneous intraparticle forced convection, diffusion and reaction in a porous catalyst - 2. Selectivity of sequential reactions." Chemical Engineering Science **32**(8): 925-930.

Nir, A. and L. M. Pismen (1977). "Simultaneous intraparticle forced convection, diffusion and reaction in a porous catalyst." Chemical Engineering Science **32**(1): 35-41.

Oh, S. H. and J. C. Cavendish (1982). "Transients of monolithic catalytic converters: Response to step changes in feedstream temperature as related to controlling automobile emissions." Industrial & Engineering Chemistry Product Research and Development **21**(1): 29-37.

Oliveira, E. L. G., C. A. Grande and A. E. Rodrigues (2009). "Steam methane reforming in a Ni/Al2O3 Catalyst: Kinetics and diffusional limitations in extrudates." Canadian Journal of Chemical Engineering **87**(6): 945-956.

Oliveira, E. L. G., C. A. Grande and A. E. Rodrigues (2010). "Methane steam reforming in large pore catalyst." Chemical Engineering Science **65**(5): 1539-1550.

Oliveira, E. L. G., C. A. Grande and A. E. Rodrigues (2011). "Effect of catalyst activity in SMR-SERP for hydrogen production: Commercial vs. large-pore catalyst." Chemical Engineering Science **66**(3): 342-354.

Pennemann, H., P. Watts, S. J. Haswell, V. Hessel and H. Löwe (2004). "Benchmarking of microreactor applications." Organic Process Research and Development **8**(3): 422-439.

Pfeiffer, J. F., J. C. Chen and J. T. Hsu (1996). "Permeability of Gigaporous Particles." AIChE Journal **42**(4): 932-939.

Pfund, D., D. Rector, A. Shekarriz, A. Popescu and J. Welty (2000). "Pressure drop measurements in a microchannel." AIChE Journal **46**(8): 1496-1507.

Prince, C. L., V. Bringi and M. L. Shuler (1991). "Convective Mass Transfer in Large Porous Biocatalysts: Plant Organ Cultures." Biotechnology Progress **7**(2): 195-199.

Quinta-Ferreira, R. M., P. M. Simoes and A. E. Rodrigues (1995). "Simulation of tubular reactors packed with large-pore catalysts with spherical geometry." Computers and Chemical Engineering **19**(Suppl): S351-S356.

Quinta Ferreira, R. M. (1988). Contribuição para o Estudo de Reactores Catalíticos de leito fixo. Efeito da convecção em catalisadores de poros largos e casos de catalisadores bidispersos. University of Porto. PhD Thesis.

Quinta Ferreira, R. M., C. A. Almeida-Costa and A. E. Rodrigues (1996a). "Effect of intraparticle convection on the transient behavior of fixed-bed reactors: Finite differences and collocation methods for solving unidimensional models." Computers and Chemical Engineering **20**(10): 1201-1225.

Quinta Ferreira, R. M., C. A. Almeida-Costa and A. E. Rodrigues (1996b). "Heterogeneous models of tubular reactors packed with ion-exchange resins: Simulation of the MTBE synthesis." Industrial and Engineering Chemistry Research **35**(11): 3827-3841.

Quinta Ferreira, R. M., M. M. Marques, M. F. Babo and A. E. Rodrigues (1992). "Modelling of the methane steam reforming reactor with large-pore catalysts." Chemical Engineering Science **47**(9-11): 2909-2914.

Razzaq, T., T. N. Glasnov and C. O. Kappe (2009). "Accessing novel process windows in a high-temperature/pressure capillary flow reactor." Chemical Engineering and Technology **32**(11): 1702-1716.

Razzaq, T. and C. O. Kappe (2010). "Continuous flow organic synthesis under high-temperature/pressure conditions." Chemistry - An Asian Journal **5**(6): 1274-1289.

Rebrov, E. V., A. Berenguer-Murcia, H. E. Skelton, B. F. G. Johnson, A. E. H. Wheatley and J. C. Schouten (2009). "Capillary microreactors wall-coated with mesoporous titania thin film catalyst supports." Lab on a Chip - Miniaturisation for Chemistry and Biology **9**(4): 503-506.

Rebrov, E. V., R. P. Ekatpure, M. H. J. M. De Croon and J. C. Schouten (2007a). "Design of a thick-walled screen for flow equalization in microstructured reactors." Journal of Micromechanics and Microengineering **17**(3): 633-641.

Rebrov, E. V., I. Z. Ismagilov, R. P. Ekatpure, M. H. J. M. De Croon and J. C. Schouten (2007b). "Header design for flow equalization in microstructured reactors." AIChE Journal **53**(1): 28-38.

Renken, A. and L. Kiwi-Minsker (2008). Chemical Reactions in Continuous–flow Microstructured Reactors. Micro Process Engineering: Fundamentals, Devices, Fabrication, and Applications. N. Kockmann. Weinheim, Germany, Wiley-VCH Verlag GmbH**:** 173-201.

Roberge, D. M., N. Bieler, M. Mathier, M. Eyholzer, B. Zimmermann, P. Barthe, C. Guermeur, O. Lobet, M. Moreno and P. Woehl (2008). "Development of an industrial multi-injection microreactor for fast and exothermic reactions - Part II." Chemical Engineering and Technology **31**(8): 1155-1161.

Roberge, D. M., L. Ducry, N. Bieler, P. Cretton and B. Zimmermann (2005). "Microreactor technology: A revolution for the fine chemical and pharmaceutical industries?" Chemical Engineering and Technology **28**(3): 318-323.

Rodrigues, A., B. Ahn and A. Zoulalian (1982). "Intraparticle Forced Convection Effect in Catalyst Diffusivity Measurements and Reactor Design." AIChE Journal **28**: 541-546.

Rodrigues, A. E. (1996). "Intraparticle Convection in Chromatographic Permeable Packings." ACS Symposium Series **635**: 157-172.

Rodrigues, A. E. (1997). "Permeable packings and perfusion chromatography in protein separation." Journal of Chromatography B: Biomedical Applications **699**(1-2): 47-61.

Rodrigues, A. E., C. Chenou and M. De La Rendueles Vega (1996). "Protein separation by liquid chromatography using permeable POROS Q/M particles." Chemical Engineering Journal and the Biochemical Engineering Journal **61**(3): 191-201.

Rodrigues, A. E., J. M. Loureiro, C. Chenou and M. Rendueles de la Vega (1995). "Bioseparations with permeable particles." Journal of Chromatography B: Biomedical Applications **664**(1): 233-240.

Rodrigues, A. E., J. M. Orfao and A. Zoulalian (1984). "Intraparticle convection, diffusion and zero order reaction in porous catalysts." Chemical Engineering Communications **27**(5-6): 327-337.

Rodrigues, A. E. and R. M. Quinta Ferreira (1988). "Convection, diffusion and reaction in a large-pore catalyst particle." AIChE Symposium Series **84**(266): 80-87.

Rodrigues, A. E. and R. M. Quinta Ferreira (1990). "Effect of intraparticle convection on the steady-state behavior of fixed-bed catalytic reactors." Chemical Engineering Science **45**(8): 2653-2660.

Rosa, P., T. G. Karayiannis and M. W. Collins (2009). "Single-phase heat transfer in microchannels: The importance of scaling effects." Applied Thermal Engineering **29**(17-18): 3447-3468.

Sazonova, N. N., S. N. Pavlova, S. A. Pokrovskaya, N. A. Chumakova and V. A. Sadykov (2009). "Structured reactor with a monolith catalyst fragment for kinetic studies. The case of CH4 partial oxidation on LaNiPt-catalyst." Chemical Engineering Journal **154**(1-3): 17-24.

Scheidtmann, J., P. A. Weiß and W. F. Maier (2001). "Hunting for better catalysts and materials-combinatorial chemistry and high throughput technology." Applied Catalysis A: General **222**(1-2): 79-89.

Schmidt, A., R. Haidar and R. Schomäcker (2005). "Selectivity of partial hydrogenation reactions performed in a pore-through-flow catalytic membrane reactor." Catalysis Today **104**(2-4): 305-312.

Shah, R. K. and A. L. London (1978). Laminar flow forced convection in ducts. New York, Academic Press.

Srinivasan, R., I. M. Hsing, P. E. Berger, K. F. Jensen, S. L. Firebaugh, M. A. Schmidt, M. P. Harold, J. J. Lerou and J. F. Ryley (1997). "Micromachined Reactors for Catalytic Partial Oxidation Reactions." AIChE Journal **43**(11): 3059-3069.

Stephanopoulos, G. and K. Tsiveriotis (1989). "Effect of intraparticle convection on nutrient transport in porous biological pellets." Chemical Engineering Science **44**(9): 2031-2039.

Tadepalli, S., R. Halder and A. Lawal (2007a). "Catalytic hydrogenation of o-nitroanisole in a microreactor: Reactor performance and kinetic studies." Chemical Engineering Science **62**(10): 2663-2678.

Tadepalli, S., D. Qian and A. Lawal (2007b). "Comparison of performance of microreactor and semi-batch reactor for catalytic hydrogenation of o-nitroanisole." Catalysis Today **125**(1-2): 64-73.

Taylor, G. I. (1953). "Dispersion of Soluble Matter in Solvent Flowing Slowly through a Tube." Proceedings of the Royal Society of London A **219**(1137): 186-203.

Taylor, G. I. (1954). "Conditions under Which Dispersion of a Solute in a Stream of Solvent can be Used to Measure Molecular Diffusion " Proceedings of the Royal Society of London A **225**(1163): 473-477.

Thomsen, M. S. and B. Nidetzky (2009). "Coated-wall microreactor for continuous biocatalytic transformations using immobilized enzymes." Biotechnology Journal **4**(1): 98-107.

Trapp, O., S. K. Weber, S. Bauch, T. Bäcker, W. Hofstadt and B. Spliethoff (2008). "High-throughput kinetic study of hydrogenation over palladium nanoparticles: Combination of reaction and analysis." Chemistry - A European Journal **14**(15): 4657-4666.

Uberoi, M. and C. J. Pereira (1996). "External Mass Transfer Coefficients for Monolith Catalysts." Industrial and Engineering Chemistry Research **35**(1): 113-116.

Ullah, U., S. P. Waldram, C. J. Bennett and T. Truex (1992). "Monolithic reactors: mass transfer measurements under reacting conditions." Chemical Engineering Science **47**(9-11): 2413-2418.

Van Gerven, T. and A. Stankiewicz (2009). "Structure, energy, synergy, time-the fundamentals of process intensification." Industrial and Engineering Chemistry Research **48**(5): 2465-2474.

van Herk, D., P. Castaño, M. Quaglia, M. T. Kreutzer, M. Makkee and J. A. Moulijn (2009). "Avoiding segregation during the loading of a catalyst-inert powder mixture in a packed micro-bed." Applied Catalysis A: General **365**(1): 110-121.

Voloshin, Y. and A. Lawal (2009). "Kinetics of hydrogen peroxide reduction by hydrogen in a microreactor." Applied Catalysis A: General **353**(1): 9-16.

Walter, S., S. Malmberg, B. Schmidt and M. A. Liauw (2005). "Mass transfer limitations in microchannel reactors." Catalysis Today **110**(1-2): 15-25.

Westermann, T. and T. Melin (2009). "Flow-through catalytic membrane reactors-Principles and applications." Chemical Engineering and Processing: Process Intensification **48**(1): 17-28.

Wheeler, A. (1951). "Reaction Rates and Selectivity in Catalyst Pores " Advances in Catalysis **3**: 249-327.

Wijngaarden, R. J., A. Kronberg and K. R. Westerterp (1998). Industrial Catalysis. Weinheim, Wiley-VCH.

Wörz, O., K. P. Jäckel, T. Richter and A. Wolf (2001a). "Microreactors - A new efficient tool for reactor development." Chemical Engineering and Technology **24**(2): 138-142.

Wörz, O., K. P. Jäckel, T. Richter and A. Wolf (2001b). "Microreactors, a new efficient tool for optimum reactor design." Chemical Engineering Science **56**(3): 1029-1033.

Wunsch, R., M. Fichtner, O. Görke, K. Haas-Santo and K. Schubert (2002). "Process of applying Al2O3 coatings in microchannels of completely manufactured microstructured reactors." Chemical Engineering and Technology **25**(7): 700-703.

Young, M. W. and R. C. Dean (1987). "Optimization of Mammalian-Cell Bioreactors." Bio-Technology **5**(8): 835-837.

Yu, X., S. T. Tu, Z. Wang and Y. Qi (2005). "On-board production of hydrogen for fuel cells over Cu/ZnO/Al 2O3 catalyst coating in a micro-channel reactor." Journal of Power Sources **150**(1-2): 57-66.

CHAPTER

TWO

MASS TRANSFER IN A WALL-COATED MICROCHANNEL: FINITE REACTION RATES & KINETIC NORMALIZATION

In this chapter, we consider the problem of mass transfer in a channel with wall reaction and present approximate results to describe the conversion profile. We report analytical solutions in both Graetz's and Lévêque's regime in cases where only (semi)numerical studies have been presented before. In particular, for first-order kinetics under conditions of a fully developed concentration profile, an approximate procedure for conversion calculation is proposed for finite reaction rates (section 2.2). When the profile is developing, asymptotic limits are used to formulate accurate approximations in intermediate parametric ranges. Moreover, the effect of finite reaction rates in the corrections due to curvature or velocity profile nonlinearities are reported (section 2.3). Finally, we extend the previous results to an m^{th} order "power-law" wall reaction, so that kinetic normalization is achieved in suitable limits (section 2.4).

2.1 INTRODUCTION

The analysis of flow and mass transfer in a channel with reactive surfaces has been considered useful in modeling several chemical engineering related problems: CVD processes (Van de Ven et al. 1986), electrochemical systems (Newman 1973b), and catalytic monoliths (Tronconi et al. 1992; Bhattacharya et al. 2004b; Berger et al. 2007) among others. Recently, the problem has been again object of great attention in the context of coated-wall microreactors (Hessel et al. 2004; Gervais et al. 2006; Kockmann 2008). In this case, very thin catalytic layers are deposited on microchannels with several cross-sectional shapes, reducing mass transfer resistance, providing good thermal management and lower pressure drops (Chapter 1).

* The contents of this chapter are based on J. P. Lopes, S.S. Cardoso and A. E. Rodrigues (2010), AIChE Journal, DOI: 10.1002/aic.12483

The conceptual descriptions of the problems mentioned above are very similar and they usually involve coupling between flow and mass transfer in the channel domain, with reaction (and eventual further diffusion) at the catalytic layer. The simplest physical picture is the one where reactant species is transported axially by convection and axial diffusion and, towards the walls of the channel, by transverse diffusion. The resulting conservation equation (without the axial diffusion term) has been solved analytically for convective heat transfer in tubes, with uniform wall temperature or flux conditions. Early independent works include the ones by Graetz (1883), Nusselt (1910), and Paneth and Herzfeld (1931) as given credit by Damköhler (1937).

These well-known solutions for the concentration (or temperature) profile involve an infinite sum of terms, each one with coefficients that usually require numerical evaluation (see Table 2.1). Moreover, in the case of a first-order reaction occurring at the walls of the channel, the dependence of such coefficients on the wall kinetic parameter is complex and an explicit relationship has not been obtained for finite reaction rates.

Another issue is that in some cases (especially for short distances from the inlet or high flowrates) a satisfactory solution demands a large number of terms to be retained in the slowly convergent series. For this reason, the analysis of this problem is divided in two main regimes: Graetz's regime (where concentration changes over the length scale of the channel transverse characteristic dimension) and Lévêque's regime (when such variation occurs in a thin region near the walls of the channel). In particular, when only one term in Graetz's series reasonably describes the solution, the concentration profile is said to be "fully developed", while for developing profile conditions, Lévêque's approach (Lévêque 1928) has been extensively used to circumvent the convergence problems associated with the convection-dominated regime. Housiadas et al. (1999) compared several approximations to evaluate the terms in Graetz series with uniform wall concentration, stressing the numerical issues in the accurate calculation of these quantities. In the case of finite reaction rates, a number of studies are available (see Table 2.1), which usually involve numerical evaluation for particular parametric sets. Thus, the effect of kinetics has not been presented explicitly.

In this work, we revisit the problem of convective diffusion inside a wall-coated channel, where an isothermal heterogeneous reaction is occurring. Approximate analytical solutions for the concentration profile inside the channel allow us to obtain accurate estimates for the conversion variation along the channel, with minimal numerical evaluation and explicit parametric dependence. Moreover, asymptotic limits can be identified and help to understand the effects of the following: (a) the *relative importance of mass transport mechanisms* (namely, the length scale over which transverse diffusion effects are relevant, distinguishing two main regimes), (b) *curvature* (considering planar and circular channel geometries), (c) *flow profile* (both plug and laminar flow), (d) *kinetics* (the condition of finite wall reaction rate as an intermediate between uniform wall flux and concentration boundaries), and (e) *reaction rate expression* (in particular, the influence of the order of reaction m in a "power-law" kinetics type).

We use two strategies: (a) calculation of higher-order terms in a perturbative scheme whenever possible (Lévêque's extended regime and corrections for the m order "power law" kinetics in section 2.4); and (b) 'matching' limits by empirical formulas without introducing too much complexity (approximations to eigenvalues and constants in section 2.2). In the case of a first-order reaction, both approaches are done with the purpose of extending the range of validity of asymptotic expansions and describe successfully the solution in intermediate parametric ranges. Although the application of some of these procedures is known in the limiting cases of very slow or fast reactions (Table 2.1), when the reaction rate is finite no approximate solutions exist. In fact, most treatments of the problem require numerical evaluation, which may be inconvenient when: (i) parametric studies in broad ranges are to be performed, (ii) large-scale systems (composed e.g. by several microchannels in a parallel configuration) are being considered, or (iii) numerical difficulties occur, arising e.g. from near zero wall concentration and non-integer reaction exponents. Moreover, this will leave the parametric dependence of the systems' performance implicit. Table 2.1 summarises previous work as well as the contribution of the present work.

2.2 GRAETZ-NUSSELT REGIME (DOMINANT TRANSVERSE DIFFUSION AND CONVECTION)

In a microchannel with small aspect ratio, but when the time constants for transverse diffusion and convection are comparable, the classical Graetz-Nusselt problem (Graetz 1883) is recovered in the channel domain (where $z \sim O(1)$). In this section, we start by identifying the main quantities needed for calculating the concentration profile (and conversion) in the channel. Next, we present our approximate expressions that allow us to estimate conversion as a function of the parameters involved. We then compare our approximate predictions with numerical results from gPROMS®.

Table 2.1:Summary of some relevant previous studies and contribution of the present work.*

Approach	References
Graetz series solution	
Numerical calculation of eigenvalues and constants for specified values of Da and common cross-section geometries (first order wall reaction)	Damköhler (1937) [1]; Carslaw et al. (1959) [2]; Bauer (1976) [3]; Shah et al. (1978) [4]; Özisik et al. (1982) [5] ; Bhattacharya et al. (2004b) [6]
Asymptotic approximations limited to specific ranges (infinitely fast or slow wall reaction rate)	Sellars et al. (1956) [7, 8, 9]; Brown (1960) [7, 10]; Solbrig et al. (1967) [11]; Newman (1973a) [7, 9]; Kays et al. (1980) [12]; Housiadas et al. (1999) [7, 13]; Balakotaiah et al. (2002) [14]; Bhattacharya et al. (2004a) [15]
Uniformly valid analytical approximation for the first eigenvalue and weight for any value of Da with **no** fitting parameters (first order wall reaction)	**This work (section 2.2)**
Lévêque's solution	
Analytical solution with first order wall reaction and Lévêque's original assumptions (additional numerical evaluation required for laminar flow)	Carslaw et al. (1959) [16]; Petersen (1965) [16]; Pancharatnam et al. (1972) [17]; Ghez (1978) [18]
Approximate solution to Lévêque's problem and first-order reaction kinetics **with no** numerical evaluation involved	**This work (section 2.3.2)**
Extended Lévêque solutions in the Dirichlet and Neumann limits (analogy with heat transfer)	Worsoe-Schmidt (1967) [7, 8]; Newman (1969) [7]; Gottifredi et al. (1985) [19]; Shih et al. (1995) [19]
Corrections to extended Lévêque solutions accounting for finiteness of first order reaction kinetics	**This work (sections 2.3.3, 2.3.4 and 2.3.5)**
Reaction kinetics other than first-order	
Numerical	Acrivos et al. (1957) [20] ; Bhattacharya et al. (2004b) [21]
Zero-order reaction	Sellars et al. (1956) [22] ; Siegel et al. (1958) [22] ; Compton et al. (1990) [23] ; Rosner (1966) [24]
Integral equation methods	Chambré et al. (1956) [25] ; Acrivos et al. (1957) [25] ; Katz (1959) [26]; Rosner (1963) [27]; Grau et al. (2001) [28]
Explicit approximations for power-law kinetics in fully developed and developing concentration profile	**This work (section 2.4)**

* Numbers in brackets correspond to details from each reference.

Table 2.1 (continued): Additional details concerning each reference

[1]	Report of the first 3 terms in Graetz series for plug-flow in a circular channel with $Da = 0.1$, 1, 10 and 100 and a plot from where the first 3 eigenvalues can be estimated for $0.1 < Da < 10^3$. See also Paneth et al. (1931).
[2]	First 6 eigenvalues for plug-flow in circular or planar duct for several values of Da.
[3]	First 11 eigenvalues for a parallel plates conduit with homogeneous and heterogeneous first-order reactions (for $Da = 0$, 0.1, 1, 10 and 100) in laminar flow.
[4]	Review of several works in the field of heat transfer with finite wall thermal resistance.
[5]	First 12 eigenvalues for laminar flow inside a circular tube for $Da = 0$, 0.1, 1, 10 and 100, as well as the quantities needed to obtain the first twelve weights w_n.
[6]	First 5 eigenvalues and weights for $Da = 0.01$, 0.1, 1, 10 and 100 in channels with common cross-section shapes (circular, plates, square and equilateral triangle). They also plot λ_1 and w_1 as a function of Da for plug and laminar flows ($10^{-3} < Da < 10^2$).
[7]	Constant wall temperature (Dirichlet) conditions (heat transfer analogy for the case of infinitely fast reactions).
[8]	Constant wall flux (Neumann) condition (heat transfer analogy for the case of slow reactions).
[9]	Asymptotic formulas for higher eigenvalues and constants. Some obtained with the Wentzel-Kramers-Brillouin (WKB) method. See Bender et al. (1978) for more details.
[10]	Numerical calculation.
[11]	Higher eigenvalues through implicit expression which requires numerical evaluation for finite Da.
[12]	Numerical results for uniform temperature and heat flux at the wall of channels with several cross-sectional geometries.
[13]	Extended Lévêque-type solutions for integration constants and eigenfunction derivatives at the wall.
[14]	First five eigenvalues and weights tabulated for $Da = \infty$ and circular, planar, triangular and square geometries.
[15]	Taylor expansions of the first eigenvalue for the kinetic regime ($Da \to 0$), corresponding to the situations of plug and laminar flow inside planar and circular ducts.
[16]	Solution with Laplace transform for plug-flow conditions.
[17]	Inversion of Laplace transformed solution in terms of an infinite summation with coefficients given by recurrence relations (first 24 out of 50 coefficients are tabulated). Laminar flow conditions.
[18]	Analytical solution using Laplace transform for the case of first-order reversible reaction. Asymptotic expansions in the limits of fast and slow reactions are also presented.
[19]	Heat transfer in non-newtonian fluids with constant wall temperature boundary condition.
[20]	Numerical solution of an integral equation for the following reaction schemes: reversible first order, consecutive first-order and irreversible second-order.
[21]	Numerical results for power law kinetics (of orders $m = 1/2$, 1 and 2) for plug flow in a short channel and also for some types of Langmuir-Hinshelwood kinetics, including parameter ranges where the solution exhibited multiplicity behavior.
[22]	Graetz solution with uniform axial heat flux by the eigenfunction expansion method.

Table 2.1 (continued): Additional details concerning each reference

[23]	Analytical solution in Laplace's domain to the problem of mass transfer in a channel cell-crystal-electrode system with zero-order reaction, under Lévêque's assumptions.
[24]	Solutions to the wall concentration profile, for several classes of boundary layer problems, given by $c_{wall} \sim 1 - z/z_0$ for $z < z_0$.
[25]	General solution to a class of laminar boundary layer-type flow fields past solid surfaces where catalytic reactions with arbitrary mechanisms take place. This resulted in a nonlinear Volterra integral equation from where the surface reaction rate can be calculated once the concentration distribution at the wall is known (measured). For first-order reaction, the equation can be solved for certain geometries in terms of a convergent infinite series.
[26]	Considers fully developed laminar flow in a circular tube and from an integral equation, surface concentration can be calculated from the reaction rate (which can be known from the cross-section average concentration). The usefulness of this approach for kinetic studies and reactor design was also discussed for arbitrary reaction rates.
[27]	Solutions in a catalytic flat plate for uniform approaching velocity were obtained for power-law kinetics at the surface in the form $z = f(c_{wall})$.
[28]	Transformation of the original PDE problem with reactions of arbitrary kinetics into a system of integral equations using a Green's function combined with generalized Fourier expansions. The kernels of the integral operators are related to an eigenvalue problem (with homogeneous kinetic-independent boundary conditions). Expressions in the slow, fast and instantaneous reaction regimes were considered to improve the performance of the numerical solution of the resulting integral equations.

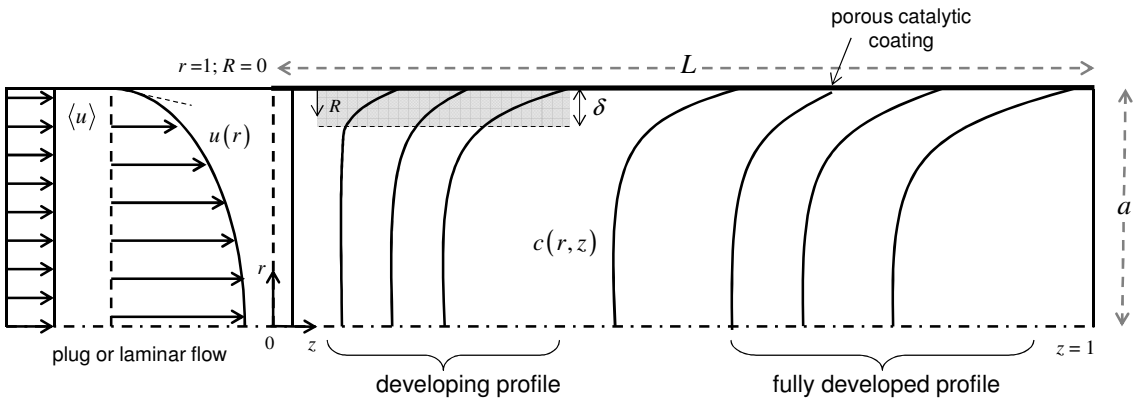

Figure 2.1: Schematic representation of the concentration profile in the channel domain showing the two main mass transfer regimes considered in this work.

2.2.1 Theoretical background

We consider straight parallel plate or circular channels with uniform cross-sectional area, in isothermal steady-state operation, coupled with a first-order heterogeneous reaction in a porous catalytic coating with uniform properties (Figure 2.1). Under these assumptions, the convective diffusion equation is (Deen 1998; Bird et al. 2002)

$$\frac{\partial^2 c}{\partial x^2}+\alpha^2\frac{\partial^2 c}{\partial z^2}=\alpha\, Pe_m\, v(x)\frac{\partial c}{\partial z} \qquad \text{for parallel plates, and} \qquad (2.1a)$$

$$\frac{1}{r}\frac{\partial}{\partial r}\left(r\frac{\partial c}{\partial r}\right)+\alpha^2\frac{\partial^2 c}{\partial z^2}=\alpha\, Pe_m\, v(r)\frac{\partial c}{\partial z} \qquad \text{for a circular channel} \qquad (2.1b)$$

where the dimensionless independent variables are the axial position scaled by the channel length $\left(z=\hat{z}/L\right)$ and the transverse position within the open channel (normalized by channel radius $\left(r=\hat{r}/a\right)$ or half-spacing between plates $\left(x=\hat{x}/a\right)$). The concentration in this domain is written as a fraction of the inlet concentration $\left(c=\hat{c}/c_{in}\right)$. The dimensionless uniform and parabolic velocity profiles are

$$v(r)=\frac{u(r)}{\langle u\rangle}=\begin{cases}\dfrac{S+3}{2}\left(1-r^2\right) & \text{laminar flow}\\ 1 & \text{plug-flow}\end{cases} \qquad (2.2)$$

where $S=0$ for parallel plates, $S=1$ for circular channel and $v(x)=v(r)$.

In Eqs.(2.1) two dimensionless parameters arise: the transverse mass Peclet number ($Pe_m=\langle u\rangle a/D$) and the channel aspect ratio ($\alpha=a/L$). Axial diffusion is negligible up to $O\left(\alpha^2\right)$, i.e. for small aspect ratio channels. In this case ($\alpha<<1$), the inlet Danckwerts' boundary condition is simplified to uniform inlet concentration for $Pe_m>>\alpha$,

$$c(r,0)=1\,. \qquad (2.3)$$

Despite the fact that the two domains (channel and catalytic layer) are coupled, a common approach is averaging the latter by using the effectiveness factor (η) concept. It has been pointed out (Keyser et al. 1991; Bhattacharya et al. 2004b; Hayes et al. 2004) that for a first-order reaction, the flux continuity requirement writes as a finite wall resistance (Robin-type) boundary condition, even when internal diffusion inside the porous coating must be considered. It can thus be written as

$$\left.\frac{\partial c}{\partial r}\right|_{r=1}=-Da\;c(1,z)\,, \qquad (2.4)$$

where the rescaled Damköhler number ($Da^* = Da^{II}\,\eta\,\delta_R$), accounting for the concentration boundary layer thickness ($\delta_R \sim 1$ in the Graetz regime) could have been used instead. Here, the Damköhler number compares the surface reaction timescale with the transverse diffusion one ($Da^{II} = a\,k_{surf}/D$). In terms of the observed reaction kinetics, Da writes as $Da^{II}\,\eta$. Uniform wall flux (Neumann) and uniform wall concentration (Dirichlet-type) boundary conditions are obtained for $Da << 1$ and $Da >> 1$, respectively.

The well-known solution (Graetz 1883; Damköhler 1937) to this problem has the following separable form:

$$c(r,z) = \sum_{n=1}^{\infty} A_n\,\varphi_n(r)\exp\left(\frac{-\lambda_n^{\,2} z}{\alpha\,Pe_{m,\max}}\right) \tag{2.5}$$

where $\varphi_n(r)$ is an eigenfunction in the transverse coordinate (r or x), while the exponential term represents the axial dependence of the concentration profile (being $Pe_{m,\max}$ the transverse Peclet number evaluated at the maximum velocity in the channel). Both transverse and axial contributions are associated with λ_n, the n^{th} eigenvalue (a function of Da, in general), which satisfies Eq.(2.4). The typical dependence of the first eigenvalue on Da is illustrated in Figure 2.2 (full lines correspond to numerical calculations). Two asymptotes are of interest, corresponding to low and high values of Da. For the former, the leading-order behaviour of the first eigenvalue is

$$\lambda_1^2 \sim \sigma\,Da + O\left(Da^2\right) \qquad \text{as } Da \to 0, \tag{2.6}$$

where $\sigma = (S+1)\,u_{\max}/\langle u\rangle$ ($S = 0$ or 1 for parallel plates or circular channel, respectively).

On the other hand, near the Dirichlet limit ($Da >> 1$), the first eigenvalue does not change significantly with Da. Carslaw et al. (1959) and Brown (1960) calculated these values as

$$\lambda_{1,\infty}^2 = \begin{cases} \pi^2/4 & \text{parallel plates} \\ 5.783 & \text{circular channel} \end{cases} \qquad \text{for plug-flow, and} \tag{2.7a}$$

$$\lambda_{1,\infty}^2 = \begin{cases} 2.828 & \text{parallel plates} \\ 7.313 & \text{circular channel} \end{cases} \qquad \text{for laminar flow.} \tag{2.7b}$$

Finally, A_n is the n^{th} integration constant, which can be calculated from the orthogonality condition (e.g. Townsend (1900), Bauer (1976)). The previous results are needed when calculating the mixing-cup concentration:

$$\langle c\rangle(z) = \frac{\int_A u(r)\,c(r,z)\,dA}{\int_A u(r)\,dA}. \tag{2.8}$$

This is related to the conversion of reactant along the channel (with respect to the inlet concentration), $X_R = 1 - \langle c \rangle(z)$. Substituting solution (2.5) into Eq.(2.8) leads to

$$\langle c \rangle(z) = \sum_{n=1}^{\infty} w_n \exp\left(\frac{-\lambda_n^2 \, z}{\alpha \, Pe_{m,\max}} \right) \tag{2.9}$$

where w_n are dependent only on Da for each channel geometry and flow profile, and are called in some references (Bhattacharya et al. 2004b) as the normalized Fourier weights, or are presented as a combination of integration constants and eigenfunctions derivatives at the wall.

The lowest value of w_1 appears in the Dirichlet limit ($w_{1,\infty}$) and is given for plug-flow conditions by(Balakotaiah et al. 2002)

$$w_{n,\infty} = 2 / \lambda_{n,\infty}^2 , \qquad \text{parallel plates} \tag{2.10a}$$

$$w_{n,\infty} = 4 / \lambda_{n,\infty}^2 , \qquad \text{circular channel.} \tag{2.10b}$$

In the next section, we use WKB results (Sellars et al. 1956) to write $w_{n,\infty}$ for laminar flow. More details on the method developed by Wentzel, Kramers and Brillouin (WKB) can be found in Bender et al. (1978). Frequently (Solbrig et al. 1967; Rice et al. 1995; Schmidt 1998; Belfiore 2003; Bhattacharya et al. 2004b), the calculation of $\langle c \rangle(z)$ is simplified by retaining just one term in Eq.(2.9), leading to

$$\langle c \rangle(z) \sim w_1 \exp\left(\frac{-\lambda_1^2 \, z}{\alpha \, Pe_{m,\max}} \right). \tag{2.11}$$

2.2.2 Approximation to the eigenvalues

The calculation of conversion using (2.11) can be done once approximate dependences for λ_1^2 and w_1 on Da are provided. In this section, we will be concerned with the first eigenvalue.

An improved estimate for λ_1 for large Da is obtained here in an iterative manner, starting with the result in the Dirichlet limit as a first guess, $\lambda_1^{(0)} = \lambda_{1,\infty}$. In this case, an approximation for high eigenvalues but $Da/\lambda_1 >> 1$ can be useful to characterise how λ_1 approaches $\lambda_{1,\infty}$ in an intermediate range of Da. For plug-flow between parallel plates, Robin's boundary condition can be expanded for large Da/λ_1 as $\lambda_1 = \arctan\left(Da/\lambda_1 \right) \sim \lambda_1^{(0)} - \lambda_1 / Da + \ldots$. Assuming that it is sufficient to retain these terms in the expansion, the improved result writes as

$$\lambda_1 \sim \lambda_{1,\infty} \frac{Da}{1 + Da} \tag{2.12}$$

which, when compared to the numerical solution presents relative error in the range of $10^{-4} - 5\%$ for $Da > 1.5$. We apply the same procedure for plug flow in a circular channel, after expanding Bessel functions for large argument. The result is similar to that in Eq.(2.12) with $\lambda_1^{(0)} \sim 3\pi/4$ and with a relative error of around 2% for $Da > 2$.

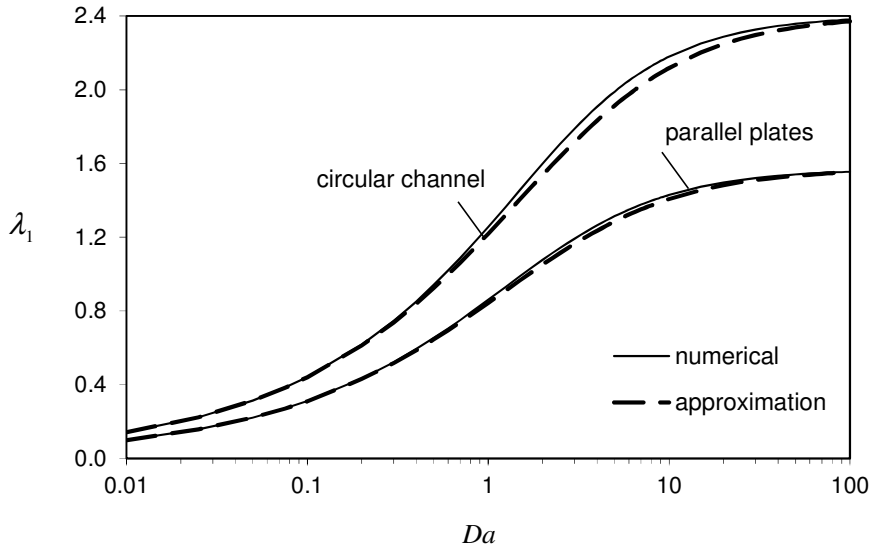

(a)

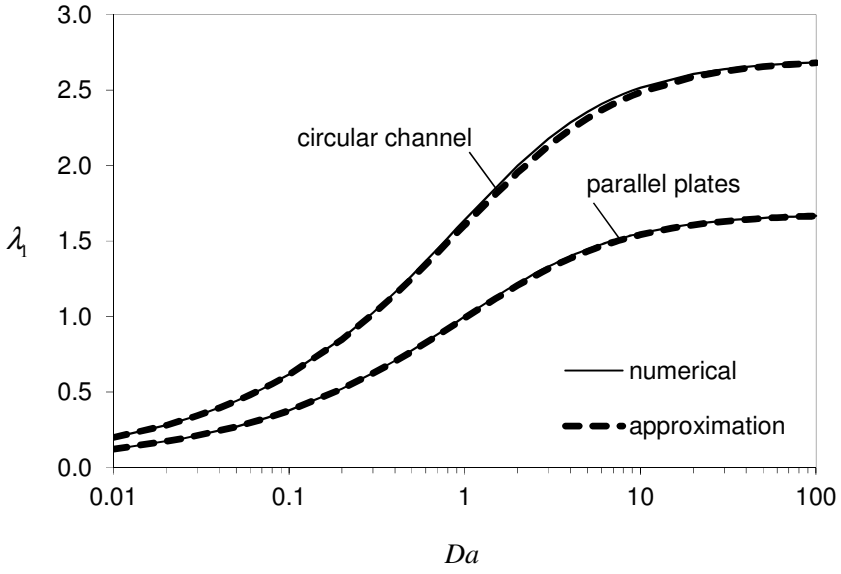

(b)

Figure 2.2: First eigenvalue (λ_1) as a function of the Damköhler number (Da) for plug-flow (a) and laminar flow (b) between parallel plates and inside a circular channel. Numerical results (solid lines) are compared with approximate expression (2.14) (dashed lines).

For laminar flows, we expand hypergeometric functions in $\varphi(x)$ or $\varphi(r)$ for large eigenvalues (Abramowitz et al. 1972) leading to the following form of Robin's condition:

$$\tan \lambda_1 = \frac{1}{2\,\lambda_1} + \frac{Da}{\lambda_1} \qquad \text{(for parallel plates)} \qquad (2.13a)$$

$$\tan\left(\lambda_1 - \frac{\pi}{4}\right) = \frac{Da}{\lambda_1} \qquad \text{(for circular channel)} \qquad (2.13b)$$

For large Da/λ_1, the expansion of $\arctan(x)$ for large argument in Eqs.(2.13) leads to a rational function, which can be corrected to the right Dirichlet limit, yielding a relationship like Eq.(2.12). This result improves the estimate of the eigenvalues for $Da > 1$.

2.2.2.a *Uniformly valid approximation (all values of Da)*

The previous results show that: (a) two asymptotic regions exist, where the eigenvalues are well characterized; and (b) the transition from the $Da \sim 1$ region to the Dirichlet limit is well described by a rational function. An approximate expression of the same form of Eq.(2.12) can be easily conceived using asymptotic methods (e.g. Gottifredi et al.(1986)), so that both limits are fulfilled:

$$\lambda_1^2 \sim \frac{Da\,\sigma}{1 + Da\,\sigma/\lambda_{1,\infty}^2} \qquad (2.14)$$

Eq.(2.14) has higher relative error (compared to numerical results) in the range of $Da \sim 2-3$, which is less than 2.5% or 4% for plug-flow between parallel plates and circular channel, respectively. For laminar flows, the first eigenvalue is predicted with errors just slightly above 1% and 2% for plates and round tube. The numerical results and Eq.(2.14) predictions are plotted in Figure 2.2. Expressions for this type have been also sought in other contexts (Villermaux 1971; Houzelot et al. 1977; Haji-Sheikh et al. 2009), but the final dependence on Da results in much more complicated expressions or are the product of fitting procedures (with numerically evaluated coefficients). Eq.(2.14) gives an extremely simple functional dependence, while retaining the asymptotically correct behaviour.

We note that previous literature is full of procedures for calculation of eigenvalues and weights (or related quantities), due to the high importance of estimating conversion (alternatively, mixing-cup temperature) or Sherwood (and Nusselt) numbers. Table 2.1 provides a short list of some relevant studies concerning the calculation of eigenvalues for Graetz series' terms with first-order wall reaction (more examples could be found in Shah and London (1978) or other textbooks). We distinguish between two approaches.

First, and probably more ubiquitous, examples of numerical calculation for specified values of Da are presented. Secondly, explicit analytical approximations exist but are of extremely limited application, namely high eigenvalues ($n >> 1$) asymptotics in the Dirichlet/Neumann limit, where for example the effect of finite kinetics on the first (lowest) eigenvalue is ignored (see Table 2.1).

The asymptotically correct correlation (2.14) we propose works very reasonably in the intermediate range of $Da \sim 1$. This expression is also attractive when optimal parameter regions are being searched, avoiding extensive numerical evaluation. Moreover, the effects of geometry and flow profile are indicated explicitly.

2.2.3 Approximation to w_n coefficients

Combining Robin's boundary equation with the orthogonality condition, we can obtain a compact result for the integration constant given by

$$A_n = \frac{2\,Da}{\lambda_n\,\varphi_n(1)}\left(\frac{d\,Da}{d\,\lambda_n}\right)^{-1}. \tag{2.15}$$

Therefore, when Da is finite (~ 1), we use Eq.(2.15) to obtain

$$w_n \sim \frac{d\left(\sigma/\lambda_n^2\right)}{d\left(1/Da\right)} \tag{2.16}$$

The typical dependence of the first Fourier weight (which is also the largest one) on Da is represented by a smooth transition between two asymptotic plateaus in the limits of $Da \to 0$ and $Da \to \infty$. The variation in the intermediate range of Damköhler number is not easily obtained and extending the asymptotic expansions in the limits is beneficial for small and large (finite) Da, but unreasonable when $Da \sim 1$.

When $Da << 1$, the first Fourier weight is directly obtained from Eq.(2.16), once we know that the first eigenvalue in this limit is described by Eq.(2.6). Thus,

$$w_1\left(Da \to 0\right) = 1 - O\left(Da^2\right). \tag{2.17}$$

The Dirichlet limit for plug-flow can be found in Eqs.(2.10). For fully developed parabolic flow profile, we follow the WKB method (Sellars et al. 1956) to obtain

$$w_{n,\infty} = \frac{12\left(3^{5/6}\right)}{\sqrt{\pi}\,\Gamma\left(1/6\right)}\,\lambda_{n,\infty}^{-7/3} = 3.0384\,\lambda_{n,\infty}^{-7/3} \qquad \text{parallel plates} \tag{2.18a}$$

$$w_{n,\infty} = \frac{32\left(3^{5/6}\right)}{\sqrt{\pi}\,\Gamma(1/6)}\,\lambda_{n,\infty}^{-7/3} = 8.1023\,\lambda_{n,\infty}^{-7/3} \qquad \text{circular channel.} \tag{2.18b}$$

Even though Eqs.(2.18) were conceived for large eigenvalues (thus, large n), the results for $w_{1,\infty}$ with the appropriate first eigenvalues (Eqs.(2.7)) are in good agreement with numerical solutions for parallel plates ($w_{1,\infty} = 0.9104$) and for circular channel ($w_{1,\infty} = 0.8191$), with maximum relative errors of 1.3% and 0.3%, respectively.

As we saw previously, eigenvalues approach their Dirichlet values $\lambda_{1,\infty}$ according to Eq.(2.12). This is general for the geometries and flow profiles studied, but more accurate for plug-flow, where the Fourier weight tends to its limit value $w_{1,\infty}$, as

$$w_1 = \frac{2\,\sigma}{\lambda_{1,\infty}^2}\left(1+\frac{1}{Da}\right).$$

We can then say generically that,

$$w_1\left(Da \to \infty\right) = w_{1,\infty}\left(1+\frac{1}{Da}\right) \tag{2.19}$$

represents the correct trend in this asymptotic limit. Eq.(2.19) gives less than 5% relative error in the following ranges: $Da \geq 6$ (plug-flow between plates); $Da \geq 3$ (plug-flow inside a circular channel); $Da \geq 15$ (laminar flow between plates); and $Da \geq 8$ (laminar flow inside circular duct).

2.2.3.a *Uniformly valid approximation (all values of Da)*

As expected, the transition from the low-Da asymptote ($w_1 \to 1$) to the high-Da asymptote ($w_1 \to w_{1,\infty}$) in the intermediate region of $Da \sim 1$ is not satisfactorily described by these limits. Table 2.2 contains the asymptotic values $w_{1,\infty}$ for the geometries and flow profiles studied. Both bounds on w_1 ($w_1 = 1$ and $w_1 = w_{1,\infty}$) work as approximations outside the intermediate range of Da,

$$w_1 \sim \begin{cases} 1, & Da \leq Da_{\max} \\ w_{1,\infty}, & Da \geq Da_{\min} \end{cases} \tag{2.20}$$

Values of $Da_{\min}$ and $Da_{\max}$ are given in Table 2.2 for maximum relative errors of the first weight, as given by Eq.(2.20), of around 5% and 1%. We can see that when $Da \sim 1$, no satisfactory approximation is obtained.

Table 2.2: Range of Da in which w_1 can be approximated by either $w_1 = 1$ $\left(Da < Da_{\max}\right)$ or $w_1 = w_{1,\infty}$ $\left(Da > Da_{\min}\right)$.

			error < 5%		error < 1%	
		$w_{1,\infty}$	$Da_{\max}$	$Da_{\min}$	$Da_{\max}$	$Da_{\min}$
plug flow	plates	0.8106	2.5	17	0.8	100
	circular	0.6917	2.1	36	0.7	200
laminar flow	plates	0.9104	5.1	4.1	1.0	34
	circular	0.8191	2.1	12	0.6	70

Note that we have more information when Da is high: the non-leading order variation is of $O\left(Da^{-1}\right)$, while the first Fourier weight deviates very slowly ($O\left(Da^{2}\right)$) from 1 as $Da \to 1$ from 0). Therefore, we construct a uniformly valid approximation from Eq.(2.19):

$$\frac{w_1 - w_{1,\infty}}{1 - w_{1,\infty}} = \frac{w_{1,\infty}}{\left(1 - w_{1,\infty}\right)} \frac{1}{Da} \qquad \text{as } Da \to \infty .$$

A simple expression that also allows the small Da limit to be fulfilled writes as

$$\frac{w_1 - w_{1,\infty}}{1 - w_{1,\infty}} = \frac{1}{1 + \dfrac{1 - w_{1,\infty}}{w_{1,\infty}} Da} \tag{2.21}$$

where $w_{1,\infty}$ is obtained by previously given expressions (independent of Da). Of course Eq.(2.21) is only a particular case of the general empirical equation proposed by Churchill and Usagi (1974) to successfully correlate experimental and numerical data for a wide range of problems (e.g. determination of Sherwood and Nusselt numbers as a function of the Damköhler number for triangular channels (Groppi et al. 1997)). Though a wide variety of problems involving functions that approach constant values in both limits have been successfully dealt by this kind of expressions, to the authors' knowledge it so far has not been applied to the prediction of w_1 as a function of Da in two-dimensional models.

Eq.(2.21) can be generalized to a powered addition of asymptotic limits (Churchill et al. 1974), which results in introducing an extra parameter into the correlation

$$\frac{w_1 - w_{1,\infty}}{1 - w_{1,\infty}} = \left[1 + \left(\frac{1 - w_{1,\infty}}{w_{1,\infty}} Da \right)^{b} \right]^{-1/b} . \tag{2.22}$$

The simplest form to determine b is to ask for the correlation to produce the correct result when the right-hand side of Eq.(2.22) is 2, i.e. when $Da = w_{1,\infty} \big/ \left(1 - w_{1,\infty}\right)$. In that case, $b \approx 1$ for plug flow between parallel plates and for laminar flow (circular and slit ducts), but $b \approx 4$ when plug-flow in a circular channel is being studied. However, the numerical results are still well approximated by (2.22) when b changes around these values.

The correlation given by Eq.(2.21) predicts numerical results for parallel plates with 2.5% maximum error for plug-flow (at $Da \sim 2$), and 2% error for laminar flow (around $Da \sim 8$). For plug-flow inside a circular channel, Eq.(2.22) with $b \approx 4$ gives less than 6% relative error near $Da \sim 7$ (and about 10% had we considered $b \approx 1$). For laminar flow inside a round tube, only 1.4% maximum error is observed near $Da \sim 1$.

2.2.4 One-term approximation for the mixing-cup concentration

The prediction of the exit mixing-cup concentration from Eq.(2.11) (with w_1 from Eq.(2.22) and the first eigenvalue from Eq.(2.14)) is compared with numerical solution of Eqs.(2.1) in Figure 2.3, where the quality of our approximations for the quantities involved in Eq.(2.11) is tested. We also plot the results in a parametric range where the one-term approximation is expected to fail (large αPe_m). The range of $\alpha Pe_m < \left(\alpha Pe_m\right)^*$ where Eq.(2.11) is applicable is identified for the first time for several representative values of Da, as are the magnitudes of error involved.

For $\alpha Pe_m \sim O(1)$, the error associated with the approximation is in the range of error involved in the estimation of eigenvalues and Fourier weights. When αPe_m increases, retaining just one term in Eq.(2.9) is not sufficient (the convection-dominated regime in section 2.3 will be appropriate for this limit). This is particularly noticeable at high Da, for example in the case of plug-flow between parallel plates (Figure 2.3a), where error increases from 4% to 11% at $\alpha Pe_m = 100$, when Da changes from 1 to 10^4. Moreover, in the same situation, less than 5% relative error (in the range of meaningful absolute values for concentration) is obtained only for $\alpha Pe_m < 20$ when $Da = 10$ or $Da = 10^4$. The external mass transfer controlled limit is, therefore, the one where convection-dominated solutions are more relevant, due to the existence of a concentration boundary layer.

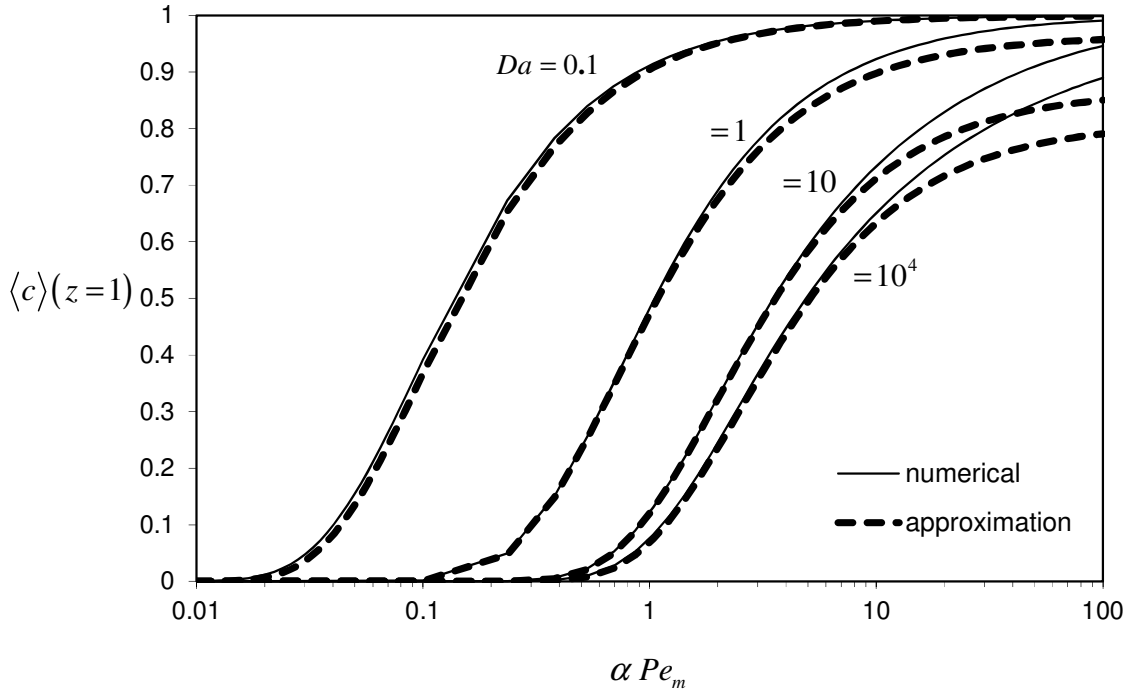

(a) Plug flow between parallel plates

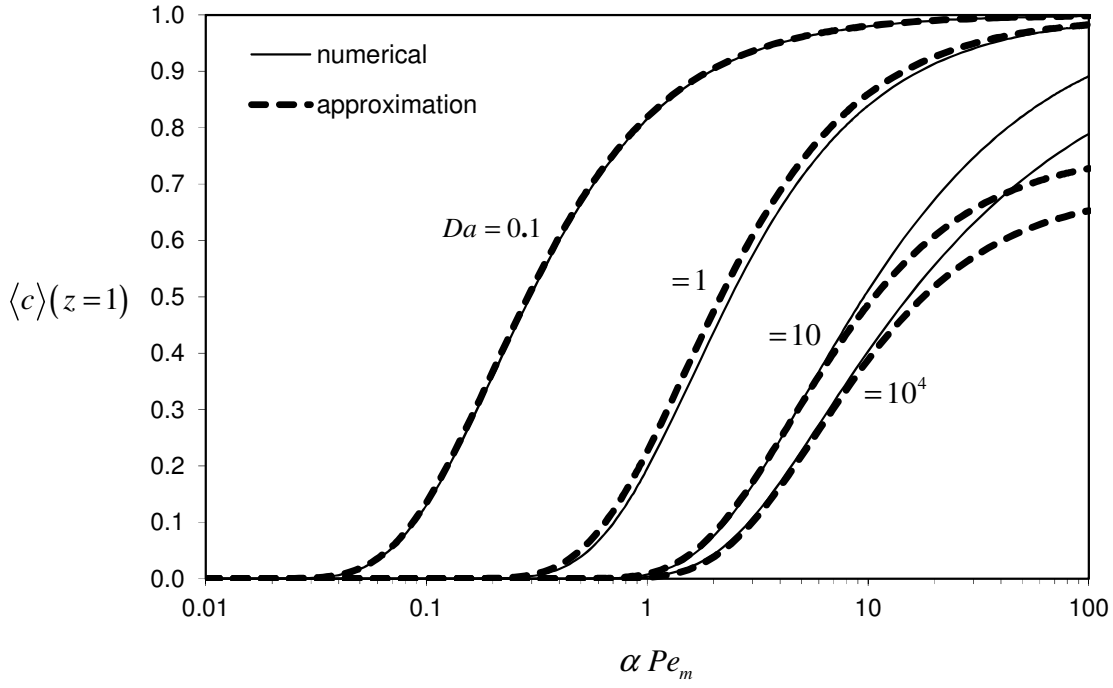

(b) Plug flow inside a circular channel

Figure 2.3: Exit mixing-cup conversion as a function of $\alpha\, Pe_m$ for the channel geometries and flow profiles studied. Curves for several values of $Da = Da^{II}\,\eta$ are plotted, comparing numerical results (full lines) with approximate 1-term expression (Eq.(2.11), dashed lines).

The same remark can be made when plug-flow in a circular tube is considered (Figure 2.3b). The maximum relative errors occur at high αPe_m and Da (around 18% for $Da=10$ and 10^4, but only 0.2% when $Da=1$, at $\alpha Pe_m=100$). Maximum of 5% relative error is obtained for $\alpha Pe_m<10$ when $Da=10$ or 10^4.

For laminar flows (Figure 2.3c and d), the same observations hold in the high Da region: error increases significantly with αPe_m and curvature (maximum errors of 6% in parallel plates and 12% in circular channel, for $\alpha Pe_m=100$ and $Da=10^4$). The range over which is possible to apply the one-term approximation also gets narrower for circular channel (less than 5% error obtained for $\alpha Pe_m<30$ when $Da=10$, and $\alpha Pe_m<20$ when $Da=10^4$), while parallel plates can be represented correctly at least up to $\alpha Pe_m=100$ with less than 5% error for $Da\le 10$ but only up to $\alpha Pe_m=70$, close to the Dirichlet limit ($Da=10^4$).

The introduction of the results for w_1 and λ_1 presented in previous sections into (2.11) allow us to calculate conversion in a channel directly from the governing dimensionless parameters. However, if explicit approximations to conversion are sought (without going through the eigenvalue and weights dependence relationships), simple expressions for kinetic control conditions and mass transfer controlled conditions can provide useful insight. While in the former case, this yields the well-known result for exponential decrease in the equivalent homogeneous model (e.g. Damköhler (1937)):

$$\langle c\rangle(z)\sim\exp\left(\frac{-(S+1)\,Da\,z}{\alpha Pe_m}\right)\qquad(Da\ll 1),\qquad(2.23)$$

for the latter, we obtain

$$\langle c\rangle(z)\sim w_{1,\infty}\exp\left(\frac{-\lambda_{1,\infty}^2\,z}{\alpha Pe_{m,\max}}\right)\left\{1+\frac{1}{Da}\left[1+\frac{(1+S)}{\sigma^2}\frac{\lambda_{1,\infty}^4\,z}{\alpha Pe_m}\right]\right\}+O\left(\frac{1}{Da^2}\right)\quad(Da\gg 1).\qquad(2.24)$$

Eq.(2.24) with an $O(1/Da)$ correction to Dirichlet's limit agrees reasonably well with the numerically calculated data from gPROMS®. For instance, for laminar flow in a circular channel and $Da=20$, Eq.(2.24) gives less than 4×10^{-4} absolute error for $\alpha Pe_m/z<1$. For $\alpha Pe_m/z$ around 1 and up to 20, the approximation predicts less than 2% error. For $Da=10$, the relative error is near 2% when $\alpha Pe_m/z\sim 1$. In the same conditions, maximum error is around 5% for all $\alpha Pe_m/z$ higher than 0.65. For $\alpha Pe_m/z<0.65$, the high relative errors correspond to maximum absolute error of 5×10^{-4}, since concentration is getting negligible on this limit.

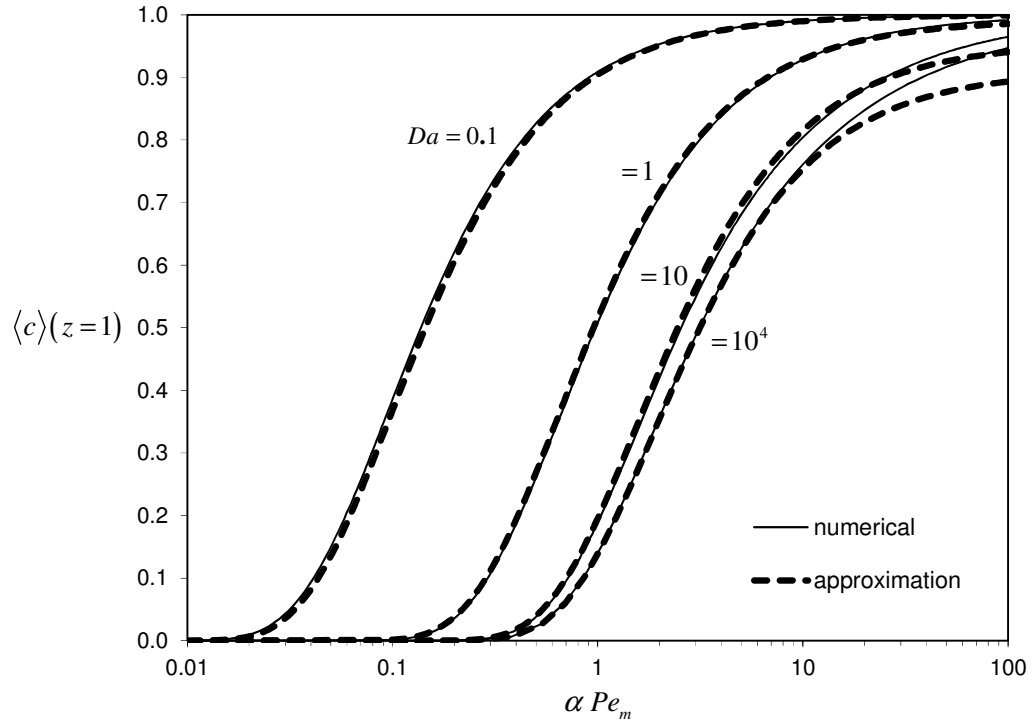

(c) Laminar flow between parallel plates

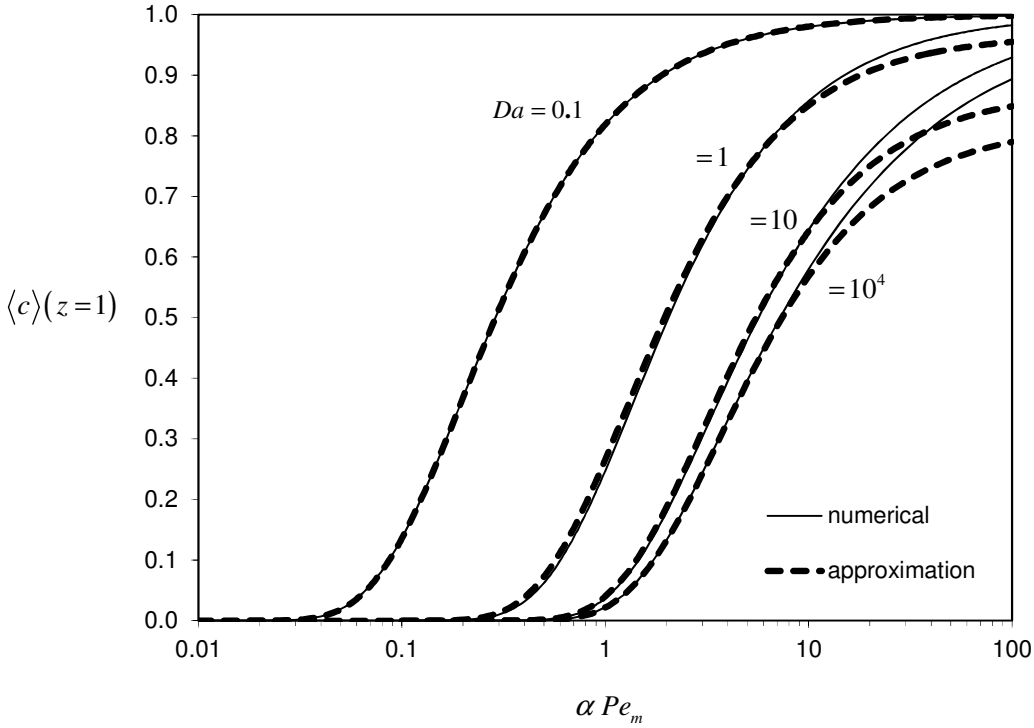

(d) Laminar flow inside a circular channel

Figure 2.3: Exit mixing-cup conversion as a function of $\alpha\, Pe_m$ for the channel geometries and flow profiles studied. Curves for several values of $Da^* = Da = Da^{II}\,\eta$ are plotted, comparing numerical results (full lines) with approximate 1-term expression (Eq.(2.11), dashed lines).

Eq.(2.11) with our approximations for λ_1 and w_1, and in particular limits (2.23) and (2.24), show the dependence of conversion on the Graetz parameter (the reciprocal of $z/\alpha\, Pe_m$) and on Da, for finite kinetic rates (tending to kinetic and mass transfer controlled limits). Explicit analytical expressions without the need of numerical evaluation for this case have not been presented previously. Bhattacharya et al. (2004b) present explicit asymptotic expressions for conversion for a parametric range of $P >> 1$ (their parameter P is equivalent to $\sim \alpha\, Pe_m$) in the Dirichlet ($Da \to \infty$) and Neumann ($Da \to 0$) limits. The applicability of these results in the range of $\alpha\, Pe_m / z \sim 1$ is extremely limited (e.g. more than 20% relative error for $\alpha\, Pe_m < 16$ and $Da = 10$ in round tube with parabolic flow). For a small aspect ratio channel, this merely rewrites Lévêque's regime results, which have been dealt extensively elsewhere (Lévêque 1928; Levich 1962; Cowherd Jr et al. 1965; Petersen 1965; Solbrig et al. 1967; Pancharatnam et al. 1972; Ghez 1978). Therefore, in terms of explicit approximate solutions, the results in this section completes the description of this problem in previous literature, especially in what has been identified (Bhattacharya et al. 2004b) as the parameter regime for the optimal design of catalytic monoliths: $P \sim \alpha\, Pe_m \sim 1$ (e.g. near the mass transfer controlled regime). Moreover, it is possible to identify the effect of design variables on conversion from Eq.(2.11): (a) the channel length L appears only in the argument of the exponential, showing a steeper increase in conversion for longer channels; and (b) the pre-exponential factor is a decreasing function of the channel transverse length a, but the dominant behavior is given by the increase of the time constant for interphase mass transfer in the denominator of the exponential argument, lowering conversion for channels with larger cross-sections. The influences of the fluid velocity inside the channel and of the bulk diffusivity on conversion are reciprocal to those of L or a, respectively. Finally, both diffusivity and kinetic constants depend on the operating temperature, the latter being usually more sensitive. Naturally, higher temperature leads to a steeper decrease of the mixing-cup concentration, as a result of faster reaction.

The dependence of the parameters on the operation and design variables can be nonlinear (e.g. exponential dependence of the kinetic constant on temperature) or appear in several terms of the solution (e.g. the channel radius and bulk diffusivity appear in both Graetz and Damköhler numbers), which complicates the analytical simplified analysis. However, under some assumptions, it is possible to obtain further insight on the effect of physical variables on conversion. When the 1-term Graetz series solution is acceptable, the channel length required to achieve a conversion X_R at a specified fluid velocity $\langle u \rangle$ and constant physical properties is given as a function of the channel radius a, kinetic parameters, geometry, flow profile and temperature by

$$L = \frac{a^2\, u_{\max}}{D}\left(\frac{e^{E/RT}}{\sigma Da_0} + \frac{1}{\lambda_{1,\infty}^2}\right)\left[\ln\left(\frac{w_{1,\infty}}{1-X_R}\right) + \ln\left(\frac{1+\left(1-w_{1,\infty}\right)Da_0\, e^{-E/RT}}{w_{1,\infty}+\left(1-w_{1,\infty}\right)Da_0\, e^{-E/RT}}\right)\right] \qquad (2.25)$$

Alternatively, the operation flow-rate can be calculated for a given channel length L, as a function of e.g. temperature (L and $\langle u \rangle$ can also be combined in the reactor's residence time, τ_{conv}). This assumed a weak dependence of diffusivity on temperature compared to the one of the kinetic constant, which is acceptable. Nevertheless, such dependence (as well as the calculation of the effectiveness factor) can be included, and the result continues explicit for the channel length or fluid velocity. Note that Da_0 is de Damköhler number evaluated with the pre-exponential factor (*Da* at zero activation energy). The values of σ, $\lambda_{1,\infty}^2$ and $w_{1,\infty}$ are known for given flow profile and channel cross-section. Iso-conversion lines in a $T - \langle u \rangle$ operating diagram can be drawn according to the above expression (in this case, for fully developed profile conditions). As an example, consider: $a = 100\,\mu m$, $D = 10^{-5}\ m^2/s$, $Da_0 = 10^6$, $E/R = 10^4\,K$ and specified conversion of $X_R = 0.99$. The following $(T;\tau_{conv})$ operation points should give a performance close to our target: $(300°C;90\,ms)$, $(500°C;2\,ms)$, $(800°C;1.2\,ms)$ and $(1000°C;1.2\,ms)$, for example. This was compared with numerical simulations in a matrix of parameter values $(T \times \tau_{conv})$. The points given by the expression above predicted conversion correctly with maximum of 0.15% of relative error. This line separates two sets of results: when conversion is higher than specified and when conversion is lower than specified. It is obvious that such numerical effort can be avoided: rigorous numerical solution can be restricted to operating points around the given boundary (and not in the complete parametric space).

Another strategy that we explore next, is the use of Lévêque type corrections (constructed for $\alpha\, Pe_m >> 1$) to improve the performance at intermediate values of $\alpha\, Pe_m \sim 1$. To our knowledge, the effect of finite reaction rate conditions in these corrections has not been discussed so far.

2.3 LÉVÊQUE'S REGIME (DOMINANT CONVECTION)

At high flow rates ($\alpha\, Pe_m >> 1$), the transport of reactant towards the walls is now limited by transverse diffusion. If the consumption of reactant at the wall is fast enough, the solution can be decomposed in the transverse direction into two domains: an outer region (which occupies most part of the channel's cross-section, $0 \le r < 1$) and a concentration boundary layer near $r = 1$. In this section, we treat the convection dominated regime as a perturbation problem, allowing us to separate the influence of effects, such as curvature and nonlinearities in the velocity profile, and identify the parametric conditions where they are relevant, under *finite reaction kinetics* conditions. Table 2.1 summarizes some of the previous work invariably associated with Dirichlet and Neumann boundary conditions.

2.3.1 Structure of the perturbation problem in Lévêque's regime

In the presence of significant consumption of reactant (with an associated concentration drop, $\Delta c \sim O(1)$), transverse (and axial) gradients are much larger than $O(1)$ and we stretch the transverse variables in Eqs.(2.1) to obtain a correct rescaling:

$$\frac{\partial^2 c}{\partial X^2} + \alpha^2 \delta_X^2 \frac{\partial^2 c}{\partial z^2} = \alpha\, Pe_m\, v(X)\, \delta_X^2 \frac{\partial c}{\partial z} \qquad \text{for parallel plates} \qquad (2.26a)$$

$$\frac{\partial^2 c}{\partial R^2} - \frac{\delta_R}{1-\delta_R R}\frac{\partial c}{\partial R} + \alpha^2 \delta_R^2 \frac{\partial^2 c}{\partial z^2} = \alpha\, Pe_m\, \delta_R^2\, v(R) \frac{\partial c}{\partial z} \qquad \text{for a circular channel.} \qquad (2.26b)$$

The velocity profiles given by Eq.(2.2) become

$$v(X) = \begin{cases} 3\,\delta_X\, X\left(1 - \dfrac{\delta_X\, X}{2}\right) & \text{laminar flow} \\ 1 & \text{plug-flow} \end{cases} \quad \text{and} \quad v(R) = \begin{cases} 4\,\delta_R\, R\left(1 - \dfrac{\delta_R R}{2}\right) & \text{laminar flow} \\ 1 & \text{plug-flow} \end{cases}$$

where $R = (1-r)/\delta_R$ and $X = (1-x)/\delta_X$ are the transverse stretched spatial variables, and δ_X, $\delta_R << 1$ are the dimensionless thicknesses of the concentration boundary layer near the wall. The only distinguished limit in Eqs.(2.26) reflects a convection-transverse diffusion dominance. Balancing those two terms, the inner layer scales become: $\delta_R \sim \delta_X \sim (\alpha\, Pe_m)^{-1/2}$ for plug flow and $\delta_X \sim (3\,\alpha\, Pe_m)^{-1/3}$ for laminar flow between parallel plates or $\delta_R \sim (4\,\alpha\, Pe_m)^{-1/3}$ if a parabolic velocity profile inside a circular channel is considered. We kept the axial diffusion term in Eqs.(2.1) but near the wall its importance relative to transverse diffusion is $O\left(Pe_{ax}^{-1}\right)$ for plug-flows, while for laminar flows its effect only shows up at $O\left(\alpha^{2/3}/Pe_{ax}^{2/3}\right)$, which are smaller than any other terms calculated next.

We can see the convection-dominated limit as a perturbation problem, where Lévêque's solution is nothing but the leading-order result. The inner problem given by Eqs.(2.26) can be decomposed into subproblems once the dependent variable in this region is expanded as a series in δ, i.e. at the boundary layer ($c^{bl} \equiv c$):

$$c(R, z; \alpha\, Pe_m) = \sum_{n=0}^{\infty} c_n(R, z)\, \delta^n \qquad (2.27)$$

Since the flux continuity at the interface is explicitly free of the perturbation parameter, the appropriate rescaled form for the $O(\delta^n)$ subproblem is (replace R by X for parallel plates)

$$\left.\frac{\partial c_n}{\partial R}\right|_{R=0} = Da^*\, c_n(R=0, z) \qquad (2.28)$$

Here however, $Da* \left(= Da^{II}\ \eta\ \delta_R\right)$ includes the correct length scale for the concentration gradient ($a\ \delta_R$). For $Da* \sim 1$, Eq.(2.28) must retain its full structure, but Neumann and Dirichlet conditions are natural limits for $Da* << 1$ and $Da* >> 1$. Additional details on the definition of regimes from $Da*$ can be found in Chapter 4.

The inlet boundary condition is homogeneous ($c_n\left(R,0\right)=0$) for $n \geq 1$ and the general matching procedure can be reduced in this case to Prandtl's condition for $n=0$:

$c_0\left(R \to \infty, z\right) \to c^{out}\left(r,z\right)=1$ (finite), and (2.29a)

$c_n\left(R \to \infty, z\right)=0 \qquad$ for $n \geq 1$. (2.29b)

Then, the composite solution is simply given by

$$c\left(r,z\right)=c^{out}\left(r,z\right)+c^{bl}\left(R,z\right)-cp$$

where $cp=\lim_{R\to\infty} c_0^{bl}\left(R,z\right)=c^{out}\left(r,z\right)$, and therefore the solution in the boundary layer is uniformly valid over the complete transverse domain. At leading order, the simplified form of the inner equations in the variables X or R becomes independent of the geometry (curvature effects are of $O\left(\delta_R\right)$ and therefore neglected). Moreover, the laminar parabolic velocity profile is linear up to $O\left(\delta_R\right)$ near the wall (Figure 2.1). This reproduces Lévêque's analysis and assumptions (Lévêque 1928).

2.3.2 Approximate solution to Lévêque's problem under finite reaction rate conditions

From previous studies (see Table 2.1), it is clear (especially for laminar flow) that more convenient solutions to the mixing-cup concentration without requiring numerical evaluation are needed, when Da is finite. As shown in section 2.3.1, the correct scaling of Eq.(2.4) includes the thickness of the boundary layer, which is the perturbation parameter in the expansion given by Eq.(2.27). Thus, according to (2.8), the mixing-cup concentration profile is also given by a perturbation series in powers of δ_R. In particular, each coefficient in

$$\left\langle c\right\rangle\left(z\right)=\sum_{n=0}^{\infty}\left\langle c\right\rangle_n\ \delta^n \tag{2.30a}$$

can be obtained from surface conditions from

$$\left\langle c\right\rangle_0\left(z\right)=1-\frac{\left(S+1\right)Da*}{\alpha\ Pe_m\ \delta}\int_0^z c_0\left(0,z\right)\,d\,z\,, \tag{2.30b}$$

$$\left\langle c\right\rangle_n\left(z\right)=-\frac{\left(S+1\right)Da*}{\alpha\ Pe_m\ \delta}\int_0^z c_n\left(0,z\right)\,d\,z\,. \tag{2.30c}$$

2.3.2.a *Plug-flow*

For uniform velocity profile $u(R)=\langle u\rangle$, the result for mixing-cup concentration follows immediately from Eq.(2.30b) and with $c_0(0,z)$ in Carslaw and Jaeger (1959), we obtain

$$\langle c\rangle_0(z)=1-\frac{S+1}{\sqrt{\alpha\, Pe_m}}\left[\frac{2}{\sqrt{\pi}}\sqrt{z}-\frac{1}{Da*}+\frac{e^{(Da*)^2 z}}{Da*}\operatorname{erfc}\left(Da*\sqrt{z}\right)\right] \tag{2.31}$$

Although an exact solution is provided by Eq.(2.31), the limits of $Da*<<1$ and $>>1$ are of interest:

$$\langle c\rangle_0(z)=1-\frac{S+1}{\sqrt{\alpha\, Pe_m}}\left[Da*\,z-\frac{4}{3\sqrt{\pi}}(Da*)^2\, z^{3/2}+O(Da*)^3\right],\ Da*<<1 \text{ or } z<<1 \tag{2.32a}$$

$$\langle c\rangle_0(z)=1-\frac{S+1}{\sqrt{\alpha\, Pe_m}}\left[\frac{2}{\sqrt{\pi}}\sqrt{z}-\frac{1}{Da*}+\frac{1}{\sqrt{\pi}\,z}\frac{1}{(Da*)^2}+O(Da*)^{-3}\right],\quad Da*>>1 \tag{2.32b}$$

An approximation to Eq.(2.31) that 'matches' (not in the asymptotic sense) the leading order estimates in Eqs.(2.32) and still yields a valid estimate even when $Da*\sim 1$ is obtained next. A rational function that respects both limits is of the form:

$$\langle c\rangle_0(z)=1-\frac{S+1}{\sqrt{\alpha\, Pe_m}}\,\frac{Da*\,z}{1+\sqrt{\pi}/2\,\sqrt{z}\,Da*}. \tag{2.33}$$

The exit conversion ($X_c=1-\langle c\rangle(z=1)$) for flow between parallel plates (Figure 2.4) is well described for a large range of parameters by Eq.(2.33), with maximum relative errors of 1.4%, 0.4% and 0.1% for $\alpha\, Pe_m=10,\ 100$ and 1000, respectively, all around $Da*\sim 3$, when compared with numerical results from gPROMS®. These errors can be attributed to the conceived rational approximation, although increase in Peclet number is always beneficial. For $\alpha\, Pe_m=1$ (i.e. outside the asymptotic conditions under which this approximation has been developed), less than 1% error is obtained for $Da*<1$ (point noted by ○ in Figure 2.4).

For plug-flow in a circular channel, the error associated with Eq.(2.33) has contributions due to the uniform approximation itself, to curvature effects and to finite $\alpha\, Pe_m$ values ("1 term" curve in Figure 2.5). In general, the relative error can have several local maximums all located at the intermediate range (~ 1, due to the nature of approximation (2.33)) or reasonably high $Da*$ (due to the ignored curvature effects). In the Dirichlet limit, conversion can be predicted with at most ~ 0.2% of error for high $\alpha\, Pe_m$ (this is ten times the value observed for parallel plates geometry). These results suggest that accounting for the presence of curvature may reduce the error in these approximations (in certain ranges of $Da*$). Also, for all values of $Da*$ and $\alpha\, Pe_m$, the relative errors decrease as we approach the inlet.

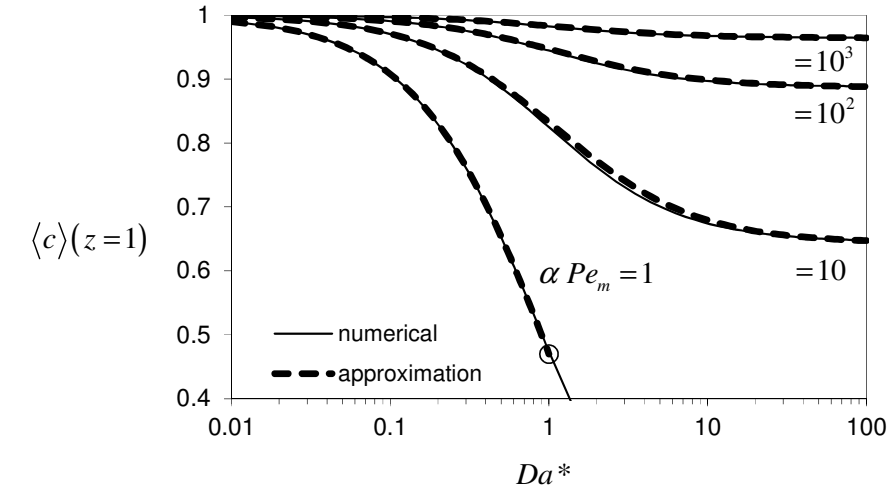

Figure 2.4: Exit mixing-cup concentration $\langle c \rangle (z=1)$ as a function of $Da* = Da^{II}\ \eta / \sqrt{\alpha\, Pe_m}$ for several orders of magnitude of $\alpha\, Pe_m$ in plug-flow between parallel plates. Full lines represent numerical simulation with gPROMS®, while dashed lines refer to Eq.(2.33). The point ○ notes the maximum value of $Da*$ with less than 1% error from using (2.33).

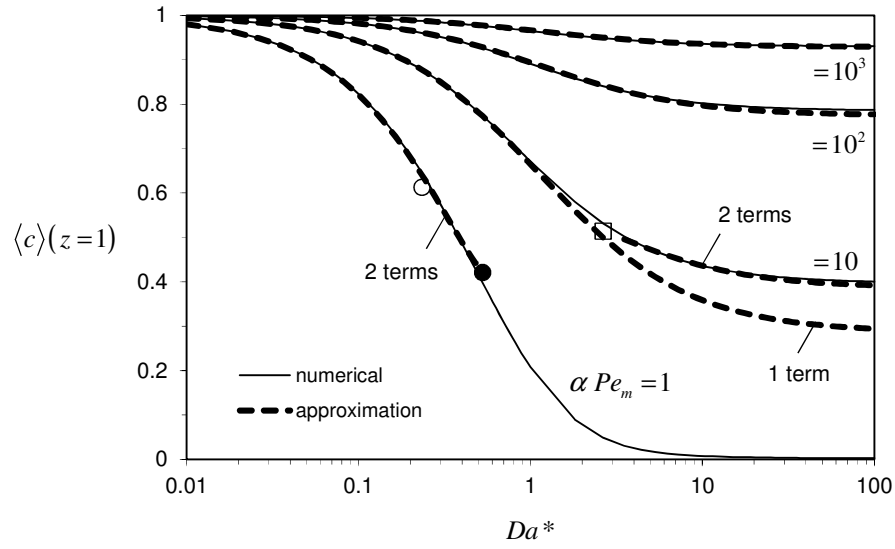

Figure 2.5: Exit mixing-cup concentration $\langle c \rangle (z=1)$ as a function of $Da* = Da^{II}\ \eta / \sqrt{\alpha\, Pe_m}$ for several orders of magnitude of $\alpha\, Pe_m$ in plug-flow inside a circular channel. Full lines represent numerical simulation (gPROMS®), while dashed lines refer to approximate solutions. High values of $\alpha\, Pe_m$ (10^2 and 10^3) are described by Eq.(2.33). For $\alpha\, Pe_m = 1$, Eq.(2.33) has less than 5% relative error (up to the point ○) and the 2-term approximation (with $\langle c \rangle_1$ from Eq.(2.38)) provides less than 5% error (up to ●). For $\alpha\, Pe_m = 10$, the high $Da*$ asymptote second term from Eq.(2.39) is included in the"2 terms" curve after the point □.

2.3.2.b *Laminar flow*

The degree of reactant's conversion can be calculated from Eq.(2.30b) for both limits with the asymptotic expressions for $c_0(0,z)$ presented in Ghez (1978), yielding

$$\langle c\rangle_0(z) = 1 - \frac{(S+1)\,Da^*}{\alpha\, Pe_m\,\delta}\, z + 1.1521\,\frac{(S+1)\,(Da^*)^2}{\alpha\, Pe_m\,\delta}\, z^{4/3} - $$

$$-1.2506\,\frac{(S+1)\,(Da^*)^3}{\alpha\, Pe_m\,\delta}\, z^{5/3} + O\left(\frac{(Da^*)^4\, z^2}{\alpha\, Pe_m\,\delta}\right) \qquad \text{for } Da^*\, z^{1/3} << 1, \quad (2.34a)$$

$$\text{and } \langle c\rangle_0(z) = 1 - 0.8076\,(S+1)\,\frac{z^{2/3}}{\alpha\, Pe_m\,\delta} + 0.5952\,\frac{(S+1)}{Da^*}\,\frac{z^{1/3}}{\alpha\, Pe_m\,\delta} \quad \text{for } Da^*\, z^{1/3} >> 1. \quad (2.34b)$$

where $Da^* = Da^{II}\,\eta\,\delta$ and δ has different definitions according to the geometry and flow profile (section 2.3.1). When compared with the numerical solution of the full model (from gPROMS®), the $O\left(Da^{*2}\right)$ and $O\left(Da^{*-1}\right)$ approximations (obtained truncating Eqs.(2.34) only to leading-order dependence on z) are rather limited in applicability, especially for a circular channel geometry. However, we note that a rational expression (similar to Eq.(2.33)) bringing together the solution for small and large values of $Da^*\, z$, may actually perform better than (or at least, comparably with) the individual limits it is meant to fulfill:

$$\langle c\rangle_0(z) = 1 - \left(\frac{S+1}{\alpha\, Pe_m\,\delta}\right)\frac{Da^*\, z}{1 + 1.2382\, Da^*\, z^{1/3}}. \quad (2.35)$$

Eq.(2.35) predicts conversion in a circular channel with around 1.4% error for $\alpha\, Pe_m = 100$ and ~0.13% for $\alpha\, Pe_m = 1000$, as Da^* increases. For slit channels though, the exit mixing-cup conversion can be reasonably calculated over large parametric ranges (Figure 2.6). For example, up to the Dirichlet limit (large Da^*) maximum relative errors are: 3% for $\alpha\, Pe_m = 10$, ~ 0.1% for $\alpha\, Pe_m = 100$ and ~ 0.01% for $\alpha\, Pe_m = 1000$. In this case, even when $\alpha\, Pe_m = 1$, less than 5% error is achieved for $Da^* < 0.5$. The effect of curvature clearly reduces the accuracy of the approximations (mainly for finite (moderate) values of $\alpha\, Pe_m$), which stresses the importance of a curvature correction.

2.3.3 Higher order corrections to Lévêque's problem

The higher order problem accounting for curvature can be extracted from Eqs.(2.26) (plug-flow profile) at $O\left[\left(\alpha\, Pe_m\right)^{-1/2}\right]$ and is given by

$$\frac{\partial^2 c_1}{\partial R^2} - \frac{\partial c_1}{\partial z} = \frac{\partial c_0}{\partial R} \tag{2.36}$$

with boundary conditions for $n=1$ in Eqs.(2.29). The surface concentration value is calculated inverting Laplace's transform

$$\overline{c}_1(R=0,s) = -\frac{Da*}{2\left(Da*+\sqrt{s}\right)^2 s}.$$

The correction accounting for nonlinearity of the velocity profile at the boundary layer appears at $O(\delta) \sim O\left[\left(\alpha\, Pe_m\right)^{-1/3}\right]$ and is calculated from

$$\frac{\partial^2 c_1}{\partial X^2} - X\,\frac{\partial c_1}{\partial z} = -\frac{X^2}{2}\frac{\partial c_0}{\partial z} \qquad \text{at } O\left[\left(3\alpha\, Pe_m\right)^{-1/3}\right] \text{ for parallel plates, and} \tag{2.37a}$$

$$\frac{\partial^2 c_1}{\partial R^2} - R\frac{\partial c_1}{\partial z} = -\frac{R^2}{2}\frac{\partial c_0}{\partial z} + \frac{\partial c_0}{\partial R} \qquad \text{at } O\left[\left(4\alpha\, Pe_m\right)^{-1/3}\right] \text{ for a circular channel.} \tag{2.37b}$$

Eqs.(2.37) can be solved in Laplace's domain and then inverted for high and low $Da*$.

2.3.4 Effect of curvature in a circular channel with plug flow

The results of interest are the limits of low and high $Da*$ of the mixing-cup concentration which according to Eq.(2.30c) are:

$$\langle c\rangle_1(z) = \frac{(Da*)^2}{\alpha\, Pe_m\,\delta}\left(\frac{z^2}{2} - \frac{16\, z^{5/2}}{15\sqrt{\pi}}\, Da*\right) + O\left(Da*^4\right) \qquad \text{for } Da* << 1 \tag{2.38}$$

$$\langle c\rangle_1(z) = \frac{z}{\alpha\, Pe_m\,\delta}\left(1 - \frac{4}{\sqrt{\pi\, z}}\,\frac{1}{Da*}\right) + O\left(Da*^{-2}\right) \qquad \text{for } Da* >> 1. \tag{2.39}$$

From the previous numerical results, we saw that this correction is mainly needed for $Da* >> 1$ (note that for $Da* << 1$, the correction is of $O\left(Da*^2\right)$). The "curvature correction" can be simplified to $\langle c\rangle_1(z) \sim \frac{z}{\alpha\, Pe_m\,\delta}$, only when $Da* >> 1$.

The high $Da*$ asymptote in Eq.(2.39) improves the approximation even at moderate values of this parameter (□ in Figure 2.5). In particular for $Da* = 100$, the error drops an order of magnitude: from 27% to 1.5% ($\alpha\, Pe_m = 10$), from 1.29% to 0.02% ($\alpha\, Pe_m = 100$) and from 0.14% to 0.03% ($\alpha\, Pe_m = 10^3$). The low $Da*$ term (Eq.(2.38)) is more useful for $\alpha\, Pe_m = 1$ to extend the validity of the approximate solution given by Eq.(2.33) from $Da* < 0.2$ (limit shown by ○) to $Da* < 0.5$ (limit shown by ●), with maximum 5% relative error compared to numerical

results. The contribution of curvature $\delta\langle c\rangle_1$ is more significant at high $Da*$ and is less than 1% of $\langle c\rangle_0$ for $\alpha\, Pe_m/z \geq 100$, however it is less than 30% of $\langle c\rangle_0$ for $\alpha\, Pe_m/z \geq 10$.

2.3.5 Effect of nonlinear velocity profile in laminar flows

In this case, the higher order correction writes in the limits of high and low $Da*$ as

$$\langle c\rangle_1(z) \sim 0.125\frac{(1+S)}{\alpha\, Pe_m\, \delta}(Da*)^2\, z^{5/3} + O\left(Da*^3\right) \qquad \text{for } Da* << 1 \qquad (2.40)$$

$$\langle c\rangle_1(z) \sim \frac{(1+S)\, z}{10\,\alpha\, Pe_m\, \delta}\left(1-\frac{1.615\, z^{-1/3}}{Da*}\right) + O\left(Da*^{-2}\right) \qquad \text{for } Da* >> 1. \qquad (2.41)$$

Again for low $Da*$, the contribution is of $O\left(Da*^2/(\alpha\, Pe_m\, \delta)\right)$ and therefore negligible. However, in the limit of high $Da*$, the correction is more significant.

2.3.5.a *Parallel plates*

Two terms in Eq.(2.41) should be retained in the ranges of $1.8 < Da* < 12$, $4.4 < Da* < 20$ and $0.75 < Da* < 26.5$ for $\alpha\, Pe_m = 10$, 100 and 10^3 (with respective maximum relative errors of 0.20%, 0.03% and 0.009%, respectively). In particular for $Da* = 100$, errors are reduced by one order of magnitude compared to the ones obtained with (2.35). For $\alpha\, Pe_m = 10$, $\langle c\rangle_0(z)$ reasonably describes numerical solutions up to $Da* = 12.7$ (shown in Figure 2.6 by □).

2.3.5.b *Circular channel*

At low $Da*$, the improvement brought by Eq.(2.40) is not particularly visible, as for $\alpha\, Pe_m = 1$, the error is already less than 5% for $Da* < 0.1$ (○ in Figure 7). Eqs.(2.40) and (2.41) result in improvement of the rational function for $\langle c\rangle_0$ (Eq.(2.35)) with transition between asymptotes around $Da* \sim 1$. The effect of correction (2.41) at $Da* = 100$ is quite modest. When $\alpha\, Pe_m$ is not high enough and $Da*$ is large, the Graetz solution is more appropriate to describe accurately the numerical results. In this case (finite $\alpha\, Pe_m$), the penetration of concentration gradients is visible at a length scale comparable to the channel characteristic dimension a, much thicker than $a\,\delta_R$.

The leading order solution at low Da^*, given by the first couple of terms in Eq.(2.34), can be connected to Graetz's estimate at the Dirichlet limit (Eq.(2.11)) with error slightly above 2% for $Da^* = 100$. Such approximation is plotted in Figure 2.7 for $\alpha\, Pe_m = 10$ and writes as:

$$\langle c \rangle(1) \sim 1 - \frac{(S+1)\, Da^*}{\alpha\, Pe_m\, \delta} \frac{w_{1,\infty} \exp\left(\dfrac{-\lambda_{1,\infty}^2}{\alpha\, Pe_{m,\max}} \right)}{1 + \dfrac{(S+1)\, Da^*}{\alpha\, Pe_m\, \delta} - w_{1,\infty} \exp\left(\dfrac{-\lambda_{1,\infty}^2}{\alpha\, Pe_{m,\max}} \right)}. \tag{2.42}$$

As shown in Figure 2.4 to Figure 2.7 and in the previous discussion, the extended Lévêque solutions improve the prediction of conversion significantly even at the exit of the channel. Here, the flow can be already fully developed, so corrections due to velocity profile nonlinearity are important. Improvement resulted for values of $\alpha\, Pe_m$ as low as 10.

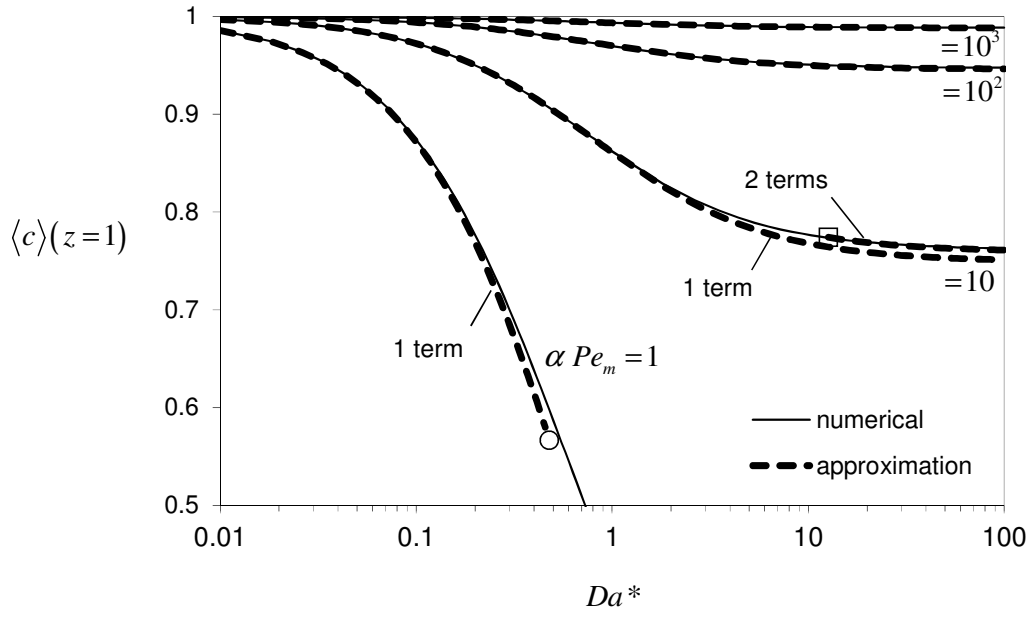

Figure 2.6: Exit mixing-cup concentration $\langle c \rangle(z=1)$ as a function of $Da^* = Da^{II}\, \eta / (3\alpha\, Pe_m)^{1/3}$ for several orders of magnitude of $\alpha\, Pe_m$ for laminar flow between parallel plates. Full lines represent numerical simulation with gPROMS®, while dashed lines refer to approximate solutions. One-term solutions are given by Eq.(2.35). Correction Eq.(2.41) is added to obtain the "2 terms" curve after □.

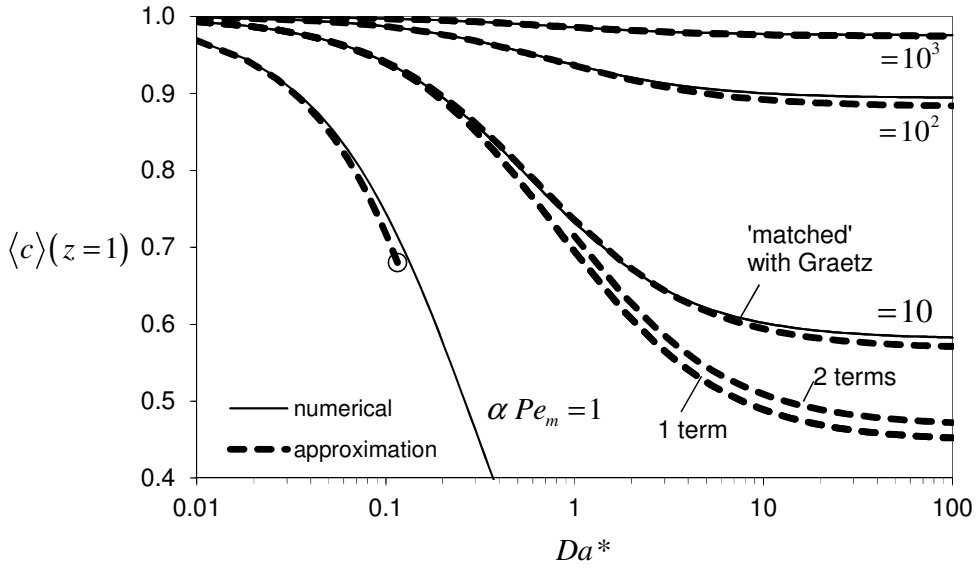

Figure 2.7: Exit mixing-cup concentration $\langle c \rangle (z=1)$ as a function of $Da^* = Da^{II}\, \eta / (4\alpha\, Pe_m)^{1/3}$ for several orders of magnitude of $\alpha\, Pe_m$ for laminar flow inside a circular channel. Full lines represent numerical simulation (gPROMS®), while dashed lines refer to approximate solutions. The correction in Eq.(2.41) is added to Eq.(2.35) to obtain the "2 terms" curve. Eq.(2.42) is also plotted for $\alpha\, Pe_m = 10$.

2.4 KINETIC NORMALIZATION FOR 'POWER-LAW' REACTION RATES

When reactions are unimolecular or when all reactants (species i) except one are present in excess, $R\{c_i(r=1,z)\} = R\{c(r=1,z)\}$. Moreover, if reactant concentration is kept in a restricted range, the so-called 'power-law kinetics' can be used as a reasonable approximation to the actual rate equation: $R\{c(r=1,z)\} = k_{surf}\, c^m(r=1,z)$, where m is the order of reaction.

Concerning the coupled analysis of (channel) flow past a surface where a reaction with arbitrary kinetics is occurring, a great deal of work exists (see Table 2.1). A generic approximate approach to convective-transport problems past catalytic surfaces is to reduce the problem (Lighthill transformation (1950)) to an integral equation relating surface concentration and reaction rate ("integral equation method"), which is usually solved numerically.

Bhattacharya et al. (2004b) present numerical results for power law kinetics (of orders $m = 1/2$, 1 and 2) for plug flow in a short monolith channel and also for some types of Langmuir-Hinshelwood kinetics (with multiplicity behavior). They observed that the same asymptotes for kinetic and mass transfer controlled limits were fulfilled.

In this section, we extend our approximations in fully developed Graetz and Lévêque's regimes to 'power-law' kinetics. Our objectives are the following: (a) to obtain explicit formulas for conversion under kinetic and mass transfer control, and (b) to understand the influence of the reaction rate law through calculation of higher-order contributions in suitable limits.

2.4.1 Developing concentration profile

When the concentration profile is developing, the rescaled wall boundary condition for the nonlinear problem is:

$$\left.\frac{\partial c}{\partial R}\right|_{R=0} = Da^{*}\, c^{m}\left(R=0,z\right) \qquad \text{(power-law kinetics)} \qquad (2.43)$$

In Eq.(2.43), the Da^{*} parameter is defined as usual in Lévêque's regime with the thickness of the boundary layer $\left(=Da^{II}\,\eta\,\delta_R\right)$, however k_{surf} is replaced by $R_{surf}\left(\hat{c}_{in}\right)/\hat{c}_{in}$. To obtain approximate solutions, we must reduce the boundary condition by choosing Da^{*} (or its reciprocal) as perturbation parameter ε. This will not result in any simplification of the complete mass balance in the channel, which is free of ε. Therefore, we start by analyzing Lévêque's regime, where a set of assumptions for $\delta_R \sim \left(\alpha\, Pe_m\right)^{-q} << 1$ ($q=1/2$ for plug flow and $q=1/3$ for laminar flow) allows simplification of the mass balance to Eqs.(2.26).

We consider a perturbation series for concentration of the following form

$$c\left(R,z;\varepsilon\right)=\sum_{n=0}^{\infty} c_n\left(R,z\right)\,\delta_n\left(\varepsilon\right) \qquad (2.44)$$

where, $c_n\left(R,z\right)$ is the solution to the n^{th} subproblem (of $O\left(\delta_n\right)$), ε is the small parameter (which can be either $\varepsilon = Da^{*}$ for kinetic control or $\varepsilon = 1/Da^{*}$ for mass transfer control) and $\delta_n\left(\varepsilon\right)$ are undetermined gauge functions of ε, which will be defined by convenient dominant balances, obeying the following relation $\delta_n\left(\varepsilon\right) >> \delta_{n+1}\left(\varepsilon\right)$ as $\varepsilon \to 0$.

The subproblems appearing after introducing (2.44) into the leading-order problem from Eq.(2.26) and collecting the same order terms are

$$\frac{\partial^2 c_n}{\partial R^2} = \frac{\partial c_n}{\partial z} \qquad \text{(plug flow)} \qquad (2.45a)$$

$$\frac{\partial^2 c_n}{\partial R^2} = R\,\frac{\partial c_n}{\partial z} \qquad \text{(laminar flow).} \qquad (2.45b)$$

Since our perturbation to boundary condition (2.43), associated with the nonlinear kinetics, will render the problem linear, Eqs.(2.45) are amenable to be treated with Laplace transform of $u_n(R,z)=c_n(R,z)-c_n(R,0)$ with respect to z, yielding the following general solutions for the n^{th} subproblem

$$\overline{u}_n(R,s)=const\ e^{-R\sqrt{s}} \qquad \text{(plug flow)} \qquad (2.46a)$$

$$\overline{u}_n(R,s)=const\ \mathrm{Ai}\left(R\,s^{1/3}\right) \qquad \text{(laminar flow).} \qquad (2.46b)$$

Note that $c_n(R,0)=1$ for $n=0$ but $c_n(R,0)=0$ for $n\geq 1$, and therefore $\overline{u}_n(R,s)=\overline{c}_n(R,s)$ (for $n\geq 1$). Solutions (2.46) were obtained so that boundedness as $R\to\infty$ is achieved.

The mixing-cup can be written as

$$\langle c\rangle(z)=1-\frac{(S+1)}{\alpha\, Pe_m\,\delta}\sum_{n=0}^{\infty}\langle c\rangle_n\,\delta_n(\varepsilon), \qquad (2.47)$$

where the contributions from the $O(\delta_n)$ subproblems are

$$\langle c\rangle_n(z)=\int_0^z\left.\frac{\partial c_n}{\partial R}\right|_{R=0}dz=\mathcal{L}^{-1}\left\{\frac{1}{s}\left.\frac{d\overline{c}_n}{dR}\right|_{R=0}\right\}. \qquad (2.48)$$

2.4.1.a *Kinetically controlled regime*

If we seek for a perturbation solution in $\varepsilon=Da^*$, the wall boundary condition (2.43) after introduction of Eq.(2.44) becomes,

$$\sum_{n=0}^{\infty}\left.\frac{\partial c_n}{\partial R}\right|_{R=0}\delta_n=\varepsilon\left(\sum_{n=0}^{\infty}c_n(0,z)\,\delta_n\right)^m \qquad \text{(power law kinetics)} \qquad (2.49)$$

Since both wall concentration and flux are correctly scaled, the left-hand side (LHS) of (2.49) is dominant and therefore the leading order term is unbalanced by any term in the right hand side (RHS) as $\varepsilon\to 0$, i.e.

$$\left.\frac{\partial c_0}{\partial R}\right|_{R=0}\delta_0(\varepsilon)=0 \text{ from where } \left.\frac{\partial c_0}{\partial R}\right|_{R=0}=0 \qquad (2.50)$$

and for convenience, $\delta_0(\varepsilon)\sim 1$. The solution of Eqs.(2.46) subject to (2.50) is, as expected,

$$c_0(R,z)=1. \qquad (2.51)$$

The next subproblem is defined by Eqs.(2.45) with $n=1$ and must be solved with the boundary condition given by

$$\left.\frac{\partial c_1}{\partial R}\right|_{R=0} = c_0^m = 1 . \qquad (2.52)$$

Here, the dominant balance is between the second higher term in the LHS and the higher in the RHS of Eq.(2.49), of order $\delta_1 \sim \varepsilon\,\delta_0$. Up to this order, Lévêque's problem with uniform wall flux is reproduced and for zero-order reactions with nonzero wall concentration, no further corrections from higher subproblems exist. Also so far, the presence of the order of reaction m is not felt, apart from the parameters definition. An higher order kinetics-dependent term is calculated from

$$\left.\frac{\partial c_2}{\partial R}\right|_{R=0} = m\, c_1(0,z) \qquad \text{(power law kinetics),} \qquad (2.53)$$

where $c_2(R,z)$ is the solution at order $\delta_2 \sim \varepsilon^2$. Note that the form of our perturbation expansion, in integer powers of ε ($\delta_n \sim \varepsilon^n$) is independent of m. The Laplace transform of the flux towards the wall is given by

$$\left.\frac{\partial \overline{c}_2}{\partial R}\right|_{R=0} = m\,\overline{c}_1(0,s) = -m\,s^{-3/2} \qquad \text{(plug flow)} \qquad (2.54a)$$

$$\left.\frac{\partial \overline{c}_2}{\partial R}\right|_{R=0} = m\,\overline{c}_1(0,s) = \frac{\mathrm{Ai}(0)}{\mathrm{Ai}'(0)} m\,s^{-4/3} \qquad \text{(laminar flow).} \qquad (2.54b)$$

According to the previous results and from Eqs.(2.47)-(2.48):

$$X_R(z) = \frac{(S+1)}{\alpha\, Pe_m\, \delta}\left[z\, Da^* - \frac{4}{3\sqrt{\pi}}\, m\, z^{3/2}\, Da^{*2} + O\left(Da^{*3}\right)\right] \qquad \text{(plug flow).} \qquad (2.55a)$$

$$X_R(z) = \frac{(S+1)}{\alpha\, Pe_m\, \delta}\left[z\, Da^* - 1.15209\, m\, z^{4/3}\, Da^{*2} + O\left(Da^{*3}\right)\right] \qquad \text{(laminar flow).} \qquad (2.55b)$$

The well-known solutions for first and zero-order reactions are recovered from Eqs.(2.55). The same order terms in Eqs.(2.32) and (2.34) are reproduced for $m=1$, while $\langle c\rangle_2(z) = 0$ for $m=0$.

For the general case of an m^{th} order reaction, more subproblems could be generated and solved in a similar way, however terms up to $O\left[(Da^*)^2\right]$ are enough for our purposes, since the effect of m has already been captured. This term is the basis of the *normalization for kinetic control when the concentration profile is developing* with respect to the reaction rate exponent m.

When flow profile is fully developed in a circular channel (the worst case possible for Lévêque's leading-order problem with linear wall velocity profile and negligible curvature assumptions), the inclusion of $\langle c\rangle_2(z)$ improves the estimate from (2.47) reducing relative errors for $Da^* \sim 0.1$ by about one order of magnitude. In this example, when $m = 1/2$ the

maximum relative error for $Da^* \le 0.1$ reduces from 0.1% to 0.02%, while when $m = 1$ the drop in error is between 0.2% and 0.004%. Finally, for $m = 2$ the predicted error of 0.4% is reduced to less than 0.06%, when our analytical results are compared with numerical simulations in gPROMS® for $\alpha\, Pe_m = 100$.

2.4.1.b *External mass transfer controlled regime*

In the limit of instantaneous reaction at the catalytic surface, we take the perturbation parameter as $\varepsilon = 1/Da^*$ and at leading order ($n = 0$) obtain the Dirichlet problem, given by the $O(1)$ terms in Eqs.(2.32b) and (2.34b). This happens since the RHS in Eq.(2.43) is not balanced by any term in the LHS and so we set $\delta_0 \sim 1$. Thus, at leading order the problem is again independent of the specific form of reaction kinetics, as concentration vanishes at the wall for any form of $R(c)$. We now follow to calculate an higher order term in this limit.

The form of the perturbation expansion and the appropriate wall boundary condition for the next subproblem are determined by introducing (2.44) into (2.43):

$$\sum_{n=1}^{\infty} c_n(0,z)\,\delta_n = \left(\varepsilon \sum_{n=0}^{\infty} \left.\frac{\partial c_n}{\partial R}\right|_{R=0} \delta_n \right)^{1/m} \qquad \text{(power law kinetics)} \qquad (2.56)$$

Requiring the next term in the LHS to balance with the highest in the RHS yields $\delta_1(\varepsilon) \sim \varepsilon^{1/m}$, with $m > 0$ so that $\delta_1(\varepsilon) \to 0$ as $\varepsilon \to 0$. The boundary condition becomes

$$c_1(0,z) = \left(\left.\frac{\partial c_0}{\partial R}\right|_{R=0} \right)^{1/m} \qquad \text{(power law kinetics).} \qquad (2.57)$$

If Eq.(2.56) is expanded for small δ_n and terms organized by order of magnitude it is possible to show that the consistent choices for the form of perturbation series (2.44) are of the form: $\delta_n(\varepsilon) \sim \varepsilon^{n/m}$, for power law kinetics of order m. Note that, as dictated by the dominant balance, the form of the series is dependent on the reaction order in this case. Therefore, subsequent corrections to the leading order term will vanish faster (for the same Da^*) if $m < 1$. For $m = 0$, no corrections to Dirichlet's limit exist, as expected in conditions of reactant exhaustion at the wall.

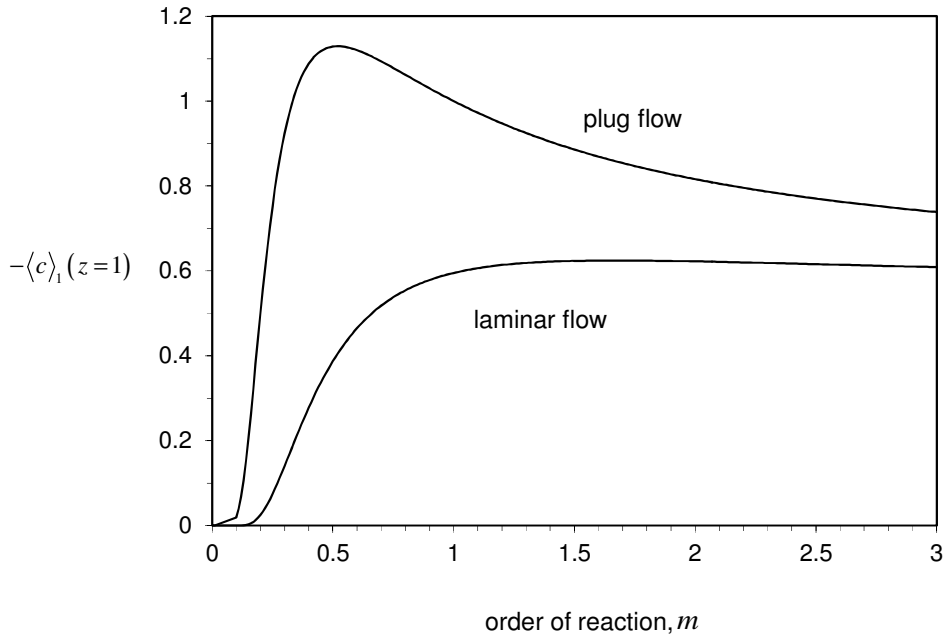

Figure 2.8: Contribution of $O\left(Da^*\right)^{-1/m}$ term at the exit of a channel (with plug or laminar flow), as a function of the reaction order m, Eqs.(2.60).

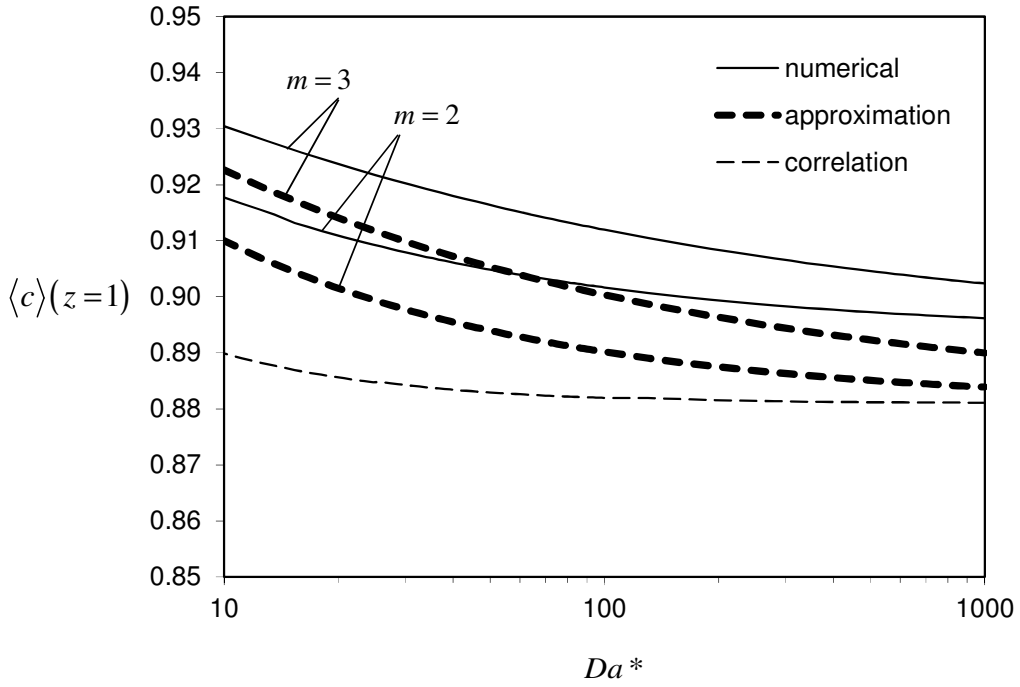

Figure 2.9: Exit mixing-cup conversion $\langle c\rangle(z=1)$ for laminar flow in a circular channel with power law wall kinetics of order $m=2$ and $m=3$ as a function of Da^*. Full lines correspond to gPROMS® simulations with $\alpha\, Pe_m = 100$. Thick dashed lines represent the perturbation solution for conversion with the extra term given by Eq.(2.60b). Eq.(2.35), which reasonably describes lower m kinetics, is also shown (thin dashed line).

At $O\left(\varepsilon^{1/m}\right)$, the particular solutions according to (2.46) subject to Eq.(2.57) are

$$\overline{c}_1(R,s) = s^{\frac{-1}{2m}}\, e^{-R\sqrt{s}} \qquad \text{(plug flow)} \qquad (2.58a)$$

$$\overline{c}_1(R,s) = \left[\frac{\Gamma(2/3)}{3^{2/3}\Gamma(4/3)}\right]^{1/m} s^{\frac{-2}{3m}}\, \frac{\mathrm{Ai}\left(R\, s^{1/3}\right)}{\mathrm{Ai}(0)} \qquad \text{(laminar flow).} \qquad (2.58b)$$

The respective contributions for mixing cup concentrations are calculated from Eq.(2.48):

$$\langle c\rangle_0(z) = \frac{2\sqrt{z}}{\sqrt{\pi}} \qquad \text{(plug flow)} \qquad (2.59a)$$

$$\langle c\rangle_0(z) = \frac{\Gamma(2/3)\, z^{2/3}}{3^{2/3}\Gamma(4/3)\Gamma(5/3)} = 0.807549\, z^{2/3} \qquad \text{(laminar flow)} \qquad (2.59b)$$

$$\langle c\rangle_1(z) = -\frac{z^{\frac{1}{2m}-\frac{1}{2}}}{\Gamma\left(\frac{1}{2}+\frac{1}{2m}\right)} \qquad \text{(plug flow)} \qquad (2.60a)$$

$$\langle c\rangle_1(z) = -\frac{3^{\frac{1}{3}-\frac{2}{3m}}\,\Gamma(2/3)^{1+1/m}}{\Gamma(1/3)\Gamma(4/3)^{1/m}}\, \frac{z^{\frac{2}{3m}-\frac{1}{3}}}{\Gamma\left(\frac{2}{3m}+\frac{2}{3}\right)} \qquad \text{(laminar flow).} \qquad (2.60b)$$

Eqs.(2.59) are the well-known results from the Dirichlet limit (Lévêque 1928; Carslaw et al. 1959). The inversion of Laplace transforms in Eqs.(2.60) is acceptable for $m > 0$. For $m = 1$, the $O(Da^*)^{-1}$ term in Eqs.(2.32b) and (2.34b) is reproduced. The $-\langle c\rangle_1(z=1)$ contribution is plotted in Figure 2.8 as a function of the order of reaction m. The behaviour for plug and laminar flows is slightly different, and the effect of changing m is more pronounced in the former.

The contribution to conversion given by $\langle c\rangle_1(z=1)(Da^*)^{-1/m}$ is more important for $m > 1$. For laminar flow in a round tube ($\alpha\, Pe_m = 100$), the two-term perturbation solution for conversion predicts less than 1.5% of relative error for $Da^* > 1$ when $m = 1/2$ and 1, which is comparable to the errors from Eq.(2.35). However, for $m = 2$ the error involved in the use of rational approximation (2.35) is reduced to half by adding the term in (2.60b), yielding less than 2% relative error for $Da^* > 1$. Figure 2.9 illustrates the improvement in the approximation for $m > 1$ in comparison with the leading-order result (accounted for in Eq.(2.35)).

We note that extended Lévêque solutions in the Dirichlet limit (kinetics-independent) can still be used to improve approximations at high Da^*, as shown previously. Also, since the kinetic and external mass transfer limits are the same, the correlations given by Eqs.(2.33) and (2.35) should be generally valid. However, as we see here, a subdominant contribution accounting for

kinetics ($O\left(Da*\right)^{-1/m}$, in particular when $m>1$) can be beneficial for the approximation. For a given axial position z, Eqs.(2.60) depend only on m and are the basis of our *kinetic normalization in the developing mass transfer controlled concentration profile*.

2.4.1.c *Langmuir kinetics in developing concentration profile conditions*

Langmuir-type kinetics only dependent on the local concentration of one reactant next to the surface can also be considered (although it is known that for some parameter combinations, multiple steady states may show up):

$$R\left\{c\left(R=0,z\right)\right\}=\frac{k_{surf}\ c^{p}\left(0,z\right)}{\left[1+K\,c\left(0,z\right)\right]^{q}},$$

where K, p and q are kinetic parameters. With more or less complexity, this case can be dealt by the same procedure. We restrict the analysis to the equivalence with the "power law" kinetic model in the $Da*<<1$ and $>>1$ limits without considering any multiplicity phenomena. In this case, the wall boundary condition is

$$\left.\frac{\partial c}{\partial R}\right|_{R=0}=Da*\left(1+K\right)^{q}\left.\frac{c^{p}}{\left(1+K\,c\right)^{q}}\right|_{R=0}, \tag{2.61}$$

where p, q and K are the additional kinetic parameters, and $Da*=\frac{a}{D}\frac{R\{\hat{c}_{in}\}}{\hat{c}_{in}}$ with $R\{\hat{c}_{in}\}=k_{s}\ \hat{c}_{in}^{p}/\left(1+K\right)^{q}$. The rate expression in Eq.(2.61) can be thought as a generalized unimolecular decomposition kinetics, reducible to power-law reaction rate when $p=m$ and q or K equals zero.

Under kinetic control, concentration deviates little from the inlet concentration, and a correction to that solution respects the following boundary condition:

$$\left.\frac{\partial c_{1}}{\partial R}\right|_{R=0}=\left(1+K\right)^{q}\frac{c_{0}^{p}\left(0,z\right)}{\left(1+K\,c_{0}^{q}\left(0,z\right)\right)^{q}}=1, \tag{2.62}$$

which is identical to Eq.(2.52). Also at the next order $O\left(Da*\right)^{2}$, the results are the same as the ones in Eqs.(2.55) as long as m is redefined as

$$m=p-\frac{q\,K}{1+K}, \tag{2.63}$$

since at this order the boundary condition is written as

$$\left.\frac{\partial c_{2}}{\partial R}\right|_{R=0}=\left(p-\frac{q\,K}{1+K}\right)c_{1}\left(0,z\right). \tag{2.64}$$

For external mass transfer control conditions ($\varepsilon = 1/Da*$), the $O(\delta_1)$ correction to Dirichlet's limit (Eqs.(2.59)) obeys at the wall,

$$\frac{\varepsilon}{(1+K)^q}\left.\frac{\partial c_0}{\partial R}\right|_{R=0} = \frac{\left(c_1(0,z)\,\delta_1\right)^p}{\left(1+K\,c_1(0,z)\,\delta_1\right)^q} \sim \left(c_1(0,z)\,\delta_1\right)^p . \qquad (2.65)$$

Since $\delta_1 << 1$, the balance in Eq.(2.65) reduces the problem again to "power law" wall kinetics type ($K\,\delta_1 << 1$). In this case, $p = m$ in Eq.(2.57) and $\delta_1 \sim \varepsilon^{1/p}/(1+K)^{q/p}$.

2.4.2 Fully developed concentration profile

We now consider the case where the solution is given by Graetz series and, in particular, when the first term in this series is dominant (i.e. fully developed concentration profile).

In the kinetic and mass transfer controlled limits, the problem is reduced to the well-known cases of heat transfer in tubes with uniform wall flux or temperature. These will be the starting points to build our approximations for power-law kinetics in both regimes, as shown below.

The boundary condition in the higher order subproblems requires a specified wall flux or concentration distribution to be fulfilled. From studies of heat transfer in ducts, it is known that one can deal with arbitrary wall temperature or flux distributions by superposition of fundamental solutions (of Dirichlet and Neumann types). This procedure has been applied to the Graetz problem by several authors (Sellars et al. 1956; Siegel et al. 1958; Carslaw et al. 1959; Shah et al. 1978; Kays et al. 1980; Colle 1988). We will use the same technique to account for the effect of the kinetic rate expression.

2.4.2.a *Kinetically controlled regime*

When reaction is infinitely slow, the mixing-cup and wall concentration are given by $\langle c \rangle_0(z) = 1$. Instead of using $c_0(1,z) = 1$ as $O(1)$ solution, we will adopt Eq.(2.23) to improve our perturbation procedure,

$$c_0(1,z) = \exp\left(\frac{-\sigma\,Da}{\alpha\,Pe_{m,\max}}\,z\right) \qquad \left(\frac{Da\,z}{\alpha\,Pe_m} << 1\right). \qquad (2.66)$$

For power-law kinetics, the first correction that can be calculated is of $O(Da)$ and obeys to Eqs.(2.1) (with $\alpha^2 \to 0$) with the boundary condition:

$$\left.\frac{\partial c_1}{\partial r}\right|_{r=1} = -c_0^m(1,z) = -\exp\left(\frac{-m\,\sigma\,Da}{\alpha\,Pe_{m,\max}}\,z\right). \qquad (2.67)$$

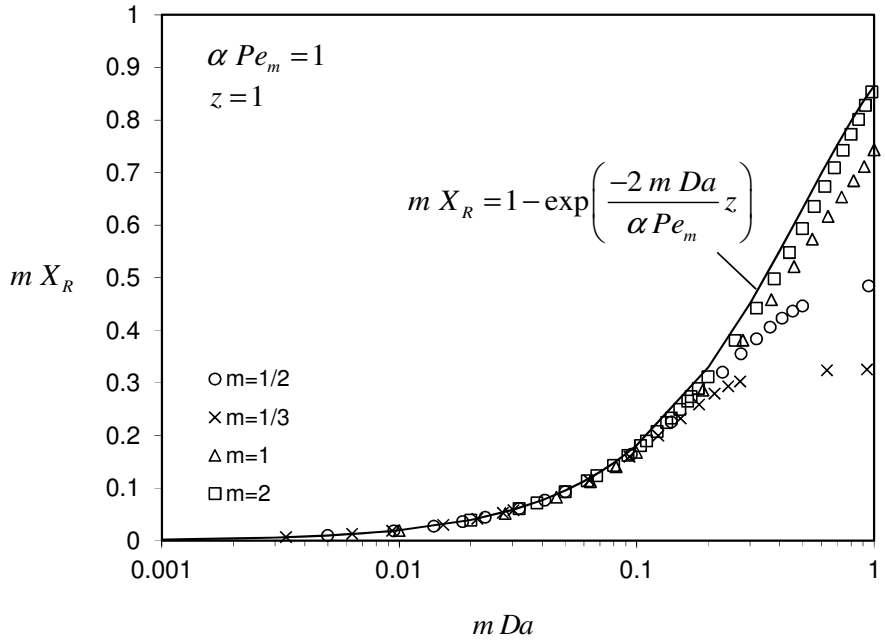

Figure 2.10: Normalization ($m\, X_R - m\, Da$ plot) according to Eq.(2.69) for m th order power-law reactions in the fully developed and kinetically controlled limit. Comparison between analytical prediction (2.69) (line) and numerical results (points). The results refer to laminar flow inside a circular channel with $\alpha\, Pe_m / z = 1$.

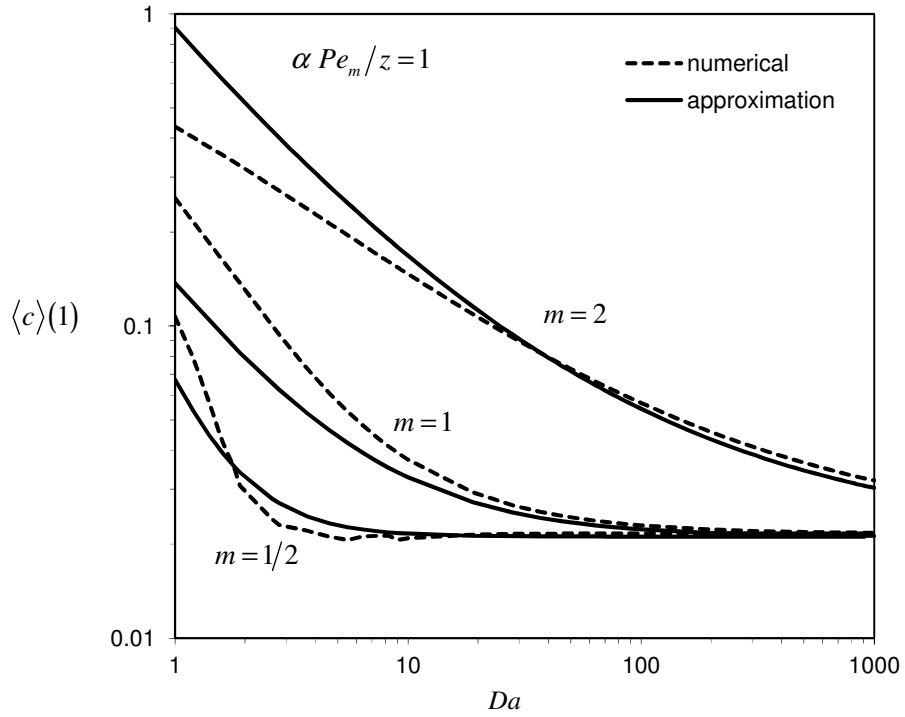

Figure 2.11: Exit concentration as a function of Da, for different orders of reaction m. Comparison between numerical and analytical results. For $m = 2$, the term given by Eq.(2.76) is included in (2.73). The results refer to laminar flow inside a circular channel.

The mixing-cup average calculation at this order can be calculated directly from (2.67), according to

$$\frac{d\langle c\rangle_n}{dz} = \frac{S+1}{\alpha Pe_m}\left.\frac{\partial c_n}{\partial r}\right|_{r=1} \quad \text{and} \quad \langle c\rangle_n(0) = 0 \qquad (n \geq 1). \tag{2.68}$$

In terms of conversion of reactant, $X_R = 1-\langle c\rangle = 1-\langle c\rangle_0 - \langle c\rangle_1 \varepsilon + O(\varepsilon^2)$, the following *normalization under fully developed kinetic control* arises:

$$m\, X_R = 1-\exp\left(\frac{-m(S+1)\,Da}{\alpha Pe_m} z\right). \tag{2.69}$$

Naturally, these results reduce to Eq.(2.23) when $m=1$ and the correction ceases to exist when $m=0$, where the constant flux asymptote is the exact solution (no wall concentration annulment). In Figure 2.10, the relationship between $m\,Da$ and $m\,X_R$ is plotted for several power-law kinetics in laminar flow at the exit of a circular channel ($S=1$). It is possible to see that Eq.(2.69) describes reasonably well all kinetics at least up to $Da \sim 0.1$, even though the curves deviate faster from our approximation as m gets lower. For $Da \leq 0.1$, the maximum relative error between numerical and analytical results are: 1% for $m=2$, 1.6% for $m=1$, 0.6% for $m=1/2$ and 0.5% for $m=1/3$. Further increasing Da results in bigger deviations for the lower values of m. For lower values of $Da/\alpha Pe_m$, maximum relative errors are reduced (e.g. for $Da/\alpha Pe_m = 0.01$, to 0.1% for $m=1$ and 2, and to 0.01% for $m=1/2$ and $1/3$).

2.4.2.b *External mass transfer controlled regime*

For fast wall reaction rates, the leading order problem (obtained by setting $\varepsilon = 1/Da = 0$ in the boundary condition) admits Graetz's constant wall temperature solution, $c_0(r,z)$. We will assume that for $\partial c_0/\partial r|_{r=1}$ in fully developed concentration profile conditions, the first term in the series is enough. The next subproblem appears at $O(\varepsilon^{1/m})$, as before, and the appropriate wall boundary condition requires an exponential variation of surface concentration given by

$$c_1(1,z) = \left[-\left.\frac{\partial c_0}{\partial r}\right|_{r=1}\right]^{1/m} = \left(\frac{w_{1,\infty}\,\lambda_{1,\infty}^2}{\sigma}\right)^{1/m} \exp\left(\frac{-\lambda_{1,\infty}^2\, z}{m\,\alpha Pe_{m,\max}}\right). \tag{2.70}$$

Since the mass balance is free of the small parameter, $c_1(r,z)$ is still governed by Eq.(2.1), which is linear. Consider the fundamental solution for a finite step in wall concentration at the inlet (c_{wall}), given by Graetz's solution with Dirichlet boundary condition:

$$c_{1,\infty}(r,z)=\frac{c_{wall}-c_1(r,z)}{c_{wall}}=\sum_{n=1}^{\infty}A_{n,\infty}\,\varphi_{n,\infty}(r)\,\exp\left(\frac{-\lambda_{n,\infty}^2\,z}{\alpha\,Pe_{m,\max}}\right). \tag{2.71}$$

In the definition from Eq.(2.71), $c_{1,\infty}(r,0)=1$ and $c_{1,\infty}(1,z)=0$ (which are the usual boundary conditions, since the inlet condition is independent of the small parameter and thus $c_1(r,0)=0$).

A solution can now be obtained by superposition of several constant-wall temperature steps (equivalent to Duhamel's principle). The flux towards the wall (which is what we need for calculating the velocity-averaged concentration) can be written as an ordinary Reimann integral, plus a summation with contributions for discontinuous steps (Kays et al. 1980). For our case,

$$-\left.\frac{\partial c_1}{\partial r}\right|_{r=1}=\int_0^z\left.\frac{\partial c_{1,\infty}}{\partial r}\right|_{r=1,z-z'}\frac{d\,c_1(1,z')}{d\,z'}\,dz'+\left.\frac{\partial c_{1,\infty}}{\partial r}\right|_{r=1}\left(\frac{w_{1,\infty}\,\lambda_{1,\infty}^2}{\sigma}\right)^{1/m}, \tag{2.72}$$

where $c_{1,\infty}$ is reaction kinetics independent (Eq.(2.71)), $c_1(1,z)$ is given by Eq.(2.70) and a 'jump' of magnitude $c_1(1,0)$ is considered at $z=0$. The respective contribution to the mixing cup concentration profile can be calculated from Eq.(2.68). From the two first perturbation terms, the mixing-cup concentration profile writes as

$$\langle c\rangle(z)=w_{1,\infty}\exp\left(\frac{-\lambda_{1,\infty}^2\,z}{\alpha\,Pe_{m,\max}}\right)\left\{1+\frac{m}{m-1}\left(\frac{w_{1,\infty}\,\lambda_{1,\infty}^2}{\sigma\,Da*}\right)^{1/m}\left[\exp\left(\frac{m-1}{m}\frac{\lambda_{1,\infty}^2\,z}{\alpha\,Pe_{m,\max}}\right)-1\right]\right\}+O\left(Da*\right)^{-2/m}$$

$$(\,Da*>>1\,) \tag{2.73}.$$

Recall from section 2.2, $w_{n,\infty}\,\lambda_{n,\infty}^2/\sigma=2$ for plug-flow and $w_{n,\infty}\lambda_n^2/\sigma=2.02557\,\lambda_n^{-1/3}$ for laminar flow, both $O(1)$ for $n=1$. When $m=1$, Eq.(2.73) agrees with Eq.(2.24) if estimating w_1 by $w_{1,\infty}$ in the second term is acceptable.

Eq.(2.73) states that the mixing-cup concentration equals the one observed when reactant exhaustion occurs near the wall multiplied by a corrective function dependent on the order of reaction m, the parameters Da and $\alpha\,Pe_m$, and kinetic rate-independent parameters, such as eigenvalues and weights. This function reduces to unity at the Dirichlet limit, and therefore *normalizes our results for developed concentration profile at high* Da.

As we already recognized for the case of developing concentration profile, the corrections in this perturbation series vanish faster for $m<1$ as $\varepsilon\to 0$. For higher orders of reaction, an extra term may be calculated in a simplified form, as detailed below.

At $O(\delta_2)$, the balance between terms in the wall boundary condition yields,

$$\delta_2 \sim \varepsilon^{2/m} \sim Da^{-2/m}, \text{ and} \tag{2.74}$$

$$c_2(1,z) = -\frac{c_1^{\,m-1}}{m}\left.\frac{\partial c_1}{\partial r}\right|_{r=1}. \tag{2.75}$$

The problem can be solved for $\langle c \rangle_2$ by the procedure detailed above. For fully developed flow and high m, the following simplified result can be obtained:

$$\langle c \rangle_2 = \frac{2}{3}\frac{\lambda_{1,\infty}^4\, w_{1,\infty}^3}{m\,\sigma^2} \qquad (m>1). \tag{2.76}$$

The term given by (2.76) can then be added to Eq.(2.73) as $\delta_2 \langle c \rangle_2$. Figure 2.11 compares numerical results for the exit conversion in a circular channel with laminar flow for $\alpha\, Pe_m = 1$ with the above predictions. For $m = 1/2$, less than 5% relative error is observed for $Da > 6$ and the maximum error is around 2% for $Da > 10$. For first-order reactions, the error is near 5% for $Da > 30$, but if $\langle c \rangle_2$ is included this value drops to 3% for $Da > 20$. Second-order reactions clearly benefit from the estimate in Eq.(2.76), as a maximum error around 5% is obtained for $Da > 20$, while 20% relative deviation would have been predicted had the contribution from Eq.(2.76) been ignored.

2.5 CONCLUSIONS

This chapter provides an approximate convenient methodology for the design of microchannel wall-coated reactors. The results presented show that it is possible to describe approximately with analytical techniques the behaviour of a small aspect ratio microchannel ($\alpha << 1$) with a first-order reaction occurring at the walls, for all values of the rescaled Damköhler number (Da^*) and transverse Peclet number (Pe_m). Solutions to Graetz's problem are provided, with dependence of eigenvalues and weights on Da ($= Da^*$). This allows conversion calculation with no numerical evaluation in commonly encountered practical conditions ($\alpha\, Pe_m \sim O(1)$).

Lévêque's regime is treated as a perturbation problem with an uniformly valid leading-order result (over the whole range of Da^* values), followed by corrections accounting for the effect of finite reaction rates in the following contributions: curvature in a circular channel and nonlinear velocity profile in the case of laminar flows. Both higher-order terms proved to be necessary when Da^* is high, and extended Lévêque's results even to $\alpha\, Pe_m \sim O(1)$.

In the last section, we present normalized results for a power law reaction rate expression. The mixing-cup concentration in the kinetic and mass transfer controlled limits, for both developed and developing profiles, was calculated. Different behaviours were observed, namely:

- the form of the perturbation expansion is explicit on the order of reaction m under mass transfer control;
- the correction incorporating m is more important in the mass transfer controlled limit for reactions with $m>1$, which deviate more significantly from Dirichlet limit; and
- under kinetic control, corrections for $m<1$ are especially required since deviations from leading-order result are larger.

Taking into account the appropriate corrections, the description of these limits is successful for a wide range of kinetics.

NOTATION

a	radius of the circular channel or half-spacing between parallel plates
A_n	n^{th} integration constant
$Ai(x)$	Airy function
b	exponent in Eq.(2.22)
c	bulk fluid concentration of reactant species
$\langle c \rangle$	reactant's mixing-cup concentration of the reactant species
$const$	integration constant
D	bulk fluid diffusivity
Da^{II}	(second) Damköhler number
$Da*$	rescaled Damköhler number (Chapter 4)
$erf(x)$	error function
$erfc(x)$	complementary error function
$J_\alpha(x)$	Bessel function of order α
k	intrinsic kinetic constant (with the reaction rate expressed per volume of washcoat)
k_{surf}	intrinsic kinetic constant (with the reaction rate expressed per interface area)
L	length of the channel
LHS	left hand side
m	order of reaction in power-law kinetics
$M(a,b,z)$	confluent (Kummer's) hypergeometric function
Pe_m	transverse Peclet number
Pe_{ax}	axial Peclet number
r	dimensionless transverse coordinate (circular channel geometry)

R	reaction rate
RHS	right hand side
s	Laplace parameter
S	shape parameter: $=0$ for parallel plates; $=1$ for circular channel
$u(r)$	velocity profile inside the channel
$\langle u \rangle$	average velocity inside the channel
$u_{\max}$	maximum velocity inside the channel
$u_n(R,z)$	concentration profile relative to inlet conditions ($=c_n(R,z)-c_n(R,0)$)
$v(r)$	dimensionless velocity profile, normalized by average velocity
x	dimensionless transverse coordinate (parallel plates geometry)
X_R	conversion of reactant
w_n	n^{th} Fourier weight
z	dimensionless axial coordinate

Greek letters

α	aspect ratio of the channel
δ	thickness of the concentration boundary layer; gauge function of ε
ε	perturbation parameter
γ	axial position dependent function in concentration profile
$\Gamma(x)$	gamma function, $\int_0^\infty t^{x-1}\, e^{-t}\, dt$
η	catalytic coating effectiveness factor
φ_n	n^{th} eigenfunction
λ_n	n^{th} eigenvalues
σ	shape/flow parameter, $(S+1)u_{\max}/\langle u \rangle$
τ	time constant

Superscript

^	dimensional quantity
$-$	Laplace transform with respect to z

Subscript

∞	in the Dirichlet limit
max	maximum
n	order in perturbation problem

REFERENCES

Abramowitz, M. and I. A. Stegun (1972). Handbook of Mathematical Functions. Washington, D.C. , National Bureau of Standards

Acrivos, A. and P. L. Chambré (1957). "Laminar boundary layer flows with surface reactions." Industrial & Engineering Chemistry **49**(6): 1025-1029.

Balakotaiah, V. and D. H. West (2002). "Shape normalization and analysis of the mass transfer controlled regime in catalytic monoliths." Chemical Engineering Science **57**(8): 1269-1286.

Bauer, H. F. (1976). "Diffusion, convection and chemical reaction in a channel." International Journal of Heat and Mass Transfer **19**(5): 479-486.

Belfiore, L. A. (2003). Transport Phenomena for Chemical Reactor Design. Hoboken, NJ, John Wiley & Sons, Inc.

Bender, C. M. and S. A. Orszag (1978). Advanced Mathematical Methods for Scientists and Engineers. New York, McGraw-Hill.

Berger, R. J. and F. Kapteijn (2007). "Coated-wall reactor modeling-criteria for neglecting radial concentration gradients. 1. Empty reactor tubes." Industrial and Engineering Chemistry Research **46**(12): 3863-3870.

Bhattacharya, M., M. P. Harold and V. Balakotaiah (2004a). "Mass-transfer coefficients in washcoated monoliths." AIChE Journal **50**(11): 2939-2955.

Bhattacharya, M., M. P. Harold and V. Balakotaiah (2004b). "Shape normalization for catalytic monoliths." Chemical Engineering Science **59**(18): 3737-3766.

Bird, R. B., W. E. Stewart and E. N. Lightfoot (2002). Transport Phenomena. New York, John Wiley & Sons, Inc.

Brown, G. M. (1960). "Heat or mass transfer in a fluid in laminar flow in a circular or flat conduit." AIChE Journal **6**(2): 179-183.

Carslaw, H. S. and J. C. Jaeger (1959). Conduction of Heat in Solids. New York, Oxford University Press.

Chambré, P. L. and A. Acrivos (1956). "On chemical surface reactions in laminar boundary layer flows." Journal of Applied Physics **27**(11): 1322-1328.

Churchill, S. W. and R. Usagi (1974). "A standardized procedure for the production of correlations in the form of a common empirical equation." Industrial and Engineering Chemistry **13**(1): 39-44.

Colle, S. (1988). "The extended Graetz problem with arbitrary boundary conditions in an axially heat conducting tube." Applied Scientific Research **45**(1): 33-51.

Compton, R. G. and P. R. Unwin (1990). "The Dissolution of Calcite in Aqueous Solution at pH < 4: Kinetics and Mechanism." Philosophical Transactions of the Royal Society of London. Series A, Mathematical and Physical Sciences **330**(1609): 1-45.

Cowherd Jr, C. and H. E. Hoelscher (1965). "Kinetics of fast interfacial reactions in laminar tube flow." Industrial and Engineering Chemistry Fundamentals **4**(2): 150-154.

Damköhler, G. (1937). "Einfluss von Diffusion, Strömung, und Wärmetransport auf die Ausbeute in Chemisch-Technischen Reaktionen." Chem.-Eng.-Tech **3**(Part 1, Chapter 2): 359-485.

Deen, W. M. (1998). Analysis of Transport Phenomena. New York, Oxford University Press.

Gervais, T. and K. F. Jensen (2006). "Mass transport and surface reactions in microfluidic systems." Chemical Engineering Science **61**(4): 1102-1121.

Ghez, R. (1978). "Mass transport and surface reactions in Lévêque's approximation." International Journal of Heat and Mass Transfer **21**(6): 745-750.

Gottifredi, J. C. and A. F. Flores (1985). "Extended Leveque solution for heat transfer to non-Newtonian fluids in pipes and flat ducts." International Journal of Heat and Mass Transfer **28**(5): 903-908.

Gottifredi, J. C. and E. E. Gonzo (1986). Application of perturbation and matching techniques to solve transport phenomena problems. Advances in Transport Processes. A. Mujumdar and R. A. Mashelkar. New Delhi, Wiley Eastern. **IV:** 419-464.

Graetz, L. (1883). "Ueber die Wärmeleitungsfähigkeit von Flüssigkeiten." Annalen der Physik und Chemie **18**: 79-94.

Grau, R. J., M. I. Cabrera and A. E. Cassano (2001). "The laminar flow tubular reactor with homogeneous and heterogeneous reactions. I. Integral Equations for Diverse Reaction Rate Regimes." Chemical Engineering Communications **184**: 229-257.

Groppi, G. and E. Tronconi (1997). "Theoretical analysis of mass and heat transfer in monolith catalysts with triangular channels." Chemical Engineering Science **52**(20): 3521-3526.

Haji-Sheikh, A., J. V. Beck and D. E. Amos (2009). "Axial heat conduction effects in the entrance region of circular ducts." Heat and Mass Transfer/Waerme- und Stoffuebertragung **45**(3): 331-341.

Hayes, R. E., B. Liu, R. Moxom and M. Votsmeier (2004). "The effect of washcoat geometry on mass transfer in monolith reactors." Chemical Engineering Science **59**(15): 3169-3181.

Hessel, V., S. Hardt and H. Löwe (2004). Chemical Micro Process Engineering: Fundamentals, Modelling and Reactions. Weinheim, Wiley-VCH.

Housiadas, C., F. E. Larrodé and Y. Drossinos (1999). "Numerical evaluation of the Graetz series." International Journal of Heat and Mass Transfer **42**(15): 3013-3017.

Houzelot, J. L. and J. Villermaux (1977). "Mass transfer in annular cylindrical reactors in laminar flow." Chemical Engineering Science **32**(12): 1465-1470.

Katz, S. (1959). "Chemical reactions catalysed on a tube wall." Chemical Engineering Science **10**: 202-211.

Kays, W. M. and M. E. Crawford (1980). Convective Heat and Mass Transfer. New York, McGraw-Hill.

Keyser, L. F., S. B. Moore and M. T. Leu (1991). "Surface reaction and pore diffusion in flow-tube reactors." Journal of Physical Chemistry **95**(14): 5496-5502.

Kockmann, N. (2008). Transport Phenomena in Micro Process Engineering. Berlin, Springer-Verlag.

Lévêque, M. A. (1928). "Les lois de la transmission de chaleur par convection." Ann. Mines **13**: 201-299.

Levich, V. G. (1962). Physicochemical hydrodynamics. Englewood Cliffs, N.J., Prentice-Hall.

Lighthill, M. J. (1950). "Contributions to the theory of heat transfer through a laminar boundary layer." Proceedings - Royal Society of London, A **202**: 395-377.

Newman, J. (1969). "Extension of the Leveque solution." Journal of Heat Transfer **91**(1): 177-178.

Newman, J. (1973a). The Graetz problem. The Fundamental Principles of Current Distribution and Mass Transport in Electrochemical Cells. A. J. Bard. New York, Dekker. **6:** 187-352.

Newman, J. S. (1973b). Electrochemical Systems. Englewood Cliffs, N.J., Prentice-Hall, Inc.

Nusselt, W. (1910). "Die Abhängigkeit der Wärmeübergangszahl von der Rohrlänge." Zeitschrift des Vereines deutscher Ingenieure **54**: 1154-1158.

Özisik, M. N. and M. S. Sadeghipour (1982). "Analytic solution for the eigenvalues and coefficients of the graetz problem with third kind boundary condition." International Journal of Heat and Mass Transfer **25**(5): 736-739.

Pancharatnam, S. and G. M. Homsy (1972). "An asymptotic solution for tubular flow reactor with catalytic wall at high Peclet numbers." Chemical Engineering Science **27**(6): 1337-1340.

Paneth, F. and K. F. Herzfeld (1931). "Free Methyl and Free Ethyl." Z. Elektrochem. Angew. Phys. Chem. **37**: 577-582.

Petersen, E. (1965). Chemical Reaction Analysis. New Jersey, Prentice-Hall Inc.

Rice, R. G. and D. D. Do (1995). Applied Mathematics and Modeling for Chemical Engineers. New York, John Wiley & Sons.

Rosner, D. E. (1963). "The apparent chemical kinetics of surface reactions in external flow systems: Diffusional falsification of activation energy and reaction order." AIChE Journal **9**(3): 321-331.

Rosner, D. E. (1966). "Effects of convective diffusion on the apparent kinetics of zeroth order surface-catalysed chemical reactions." Chemical Engineering Science **21**(3): 223-239.

Schmidt, L. D. (1998). The Engineering of Chemical Reactions. New York, Oxford University Press.

Sellars, J., M. Tribus and J. Klein (1956). "Heat transfer to laminar flow in a round tube or flat conduit - The Graetz problem extended." ASME Transactions **78**: 441-448.

Shah, R. K. and A. L. London (1978). Laminar flow forced convection in ducts. New York, Academic Press.

Shih, Y. P., C. C. Huang and S. Y. Tsay (1995). "Extended Leveque solution for laminar heat transfer to power-law fluids in pipes with wall slip." International Journal of Heat and Mass Transfer **38**(3): 403-408.

Siegel, R., E. M. Sparrow and T. M. Hallman (1958). "Steady laminar heat transfer in a circular tube with prescribed wall heat flux." Applied Scientific Research **7**: 386-392.

Solbrig, C. W. and D. Gidaspow (1967). "Convective diffusion in a parallel plate duct with one catalytic wall - laminar flow - First order reaction." The Canadian Journal of Chemical Engineering **45**: 35-39.

Townsend, J. S. (1900). "The Diffusion of Ions into Gases " Philosophical Transactions of the Royal Society of London. Series A, Containing Papers of a Mathematical or Physical Character **193**: 129-158.

Tronconi, E. and P. Forzatti (1992). "Adequacy of lumped parameter models for SCR reactors with monolith structure." AIChE Journal **38**(2): 201-210.

Van de Ven, J., G. M. J. Rutten, M. J. Raaijmakers and L. J. Giling (1986). "Gas phase depletion and flow dynamics in horizontal MOCVD reactors." Journal of Crystal Growth **76**(2): 352-372.

Villermaux, J. (1971). "Diffusion in a cylindrical reactor [Diffusion dans un reacteur cylindrique]." International Journal of Heat and Mass Transfer **14**(12): 1963-1981.

Worsoe-Schmidt, P. M. (1967). "Heat transfer in the thermal entrance region of circular tubes and annular passages with fully developed laminar flow." International Journal of Heat and Mass Transfer **10**: 541-551.

CHAPTER

THREE

BRIDGING THE GAP BETWEEN GRAETZ AND LÉVÊQUE'S THEORIES FOR MASS/HEAT TRANSFER

A new approximate solution which bridges the gap between the classical theories of Graetz and Lévêque for heat/mass transfer in channel flow is presented in this chapter. The results include expressions, uniformly valid in the axial direction, for the mixing-cup concentration (or temperature) profile $\langle c \rangle$ when transport towards the wall is slow (Dirichlet limit), and for the Sherwood number Sh when the wall flux can be considered uniform (Neumann limit). The case of a finite wall reaction (Robin's boundary condition) was also explored. The technique employed provides insight into the mathematical structure of both quantities $\langle c \rangle$ (or conversion X_R) and Sh identifying explicitly the contributions from fully developed and developing behaviours, while maintaining accuracy in the transition region. Criteria to bound the different convection-diffusion regimes are suggested, which critically systematize previous results.

3.1 INTRODUCTION

Modeling heat or mass transfer in internal channel flow has been the basis for analyzing heat exchangers and tubular chemical reactors, being therefore of utmost importance for the understanding of a large number of chemical engineering processes. For a channel with high length-to-diameter ratio, in the absence of bulk source terms, the conservation equation translates the balance between convective transport and transfer to or from the wall. This can be formulated as the classical Graetz-Nusselt problem (Graetz 1883; Nusselt 1910), which has been extensively dealt in the literature for several boundary conditions at the channel's surface (a suitable review was provided in Chapter 2).

*The contents of this chapter are partially based on J. P. Lopes, S.S. Cardoso and A. E. Rodrigues (2011), accepted for publication in AIChE Journal.

The simplest cases include the situations of uniform temperature (concentration) or uniform heat (mass) flux evaluated at the wall, Dirichlet and Neumann boundary conditions respectively. In heat exchangers, these boundary conditions can be found when the fluid conductivity is much smaller or larger than the wall conductance. In chemical reactors, a fast heterogeneous reaction in a catalytic layer attached to the duct wall may lead to concentration annulment along most of the surface of a monolith channel or microreactor. Fast reactions are natural candidates for microprocessing due to the fast heat removal and short residence time characteristics of these devices, as mentioned in Chapter 1. Therefore, many processes involving microreactors and catalytic monoliths may occur under external mass transfer control (Kreutzer et al. 2006). A criterion for attaining this regime will be presented in Chapter 4. Alternatively, in the limit of a very slow reaction or when a biochemical reaction kinetics can be reasonably approximated by a zeroth-order reaction, Neumann's boundary condition is appropriate to describe the region where wall concentration exhaustion does not occur. Besides boundary conditions, the heat transfer problem shares similarity with the mass transfer one, i.e. the same equation describes concentration or temperature profiles made dimensionless according to

$$c = \frac{\hat{c}}{\hat{c}_{in}} \text{ or } T = \frac{\hat{T} - \hat{T}_{wall}}{\hat{T}_{in} - \hat{T}_{wall}}. \tag{3.1}$$

The main quantity of interest is the mixing-cup concentration/temperature (velocity profile-averaged value over the transverse length scale), since it describes the performance of the system (conversion) and can easily be measured experimentally (at least at the exit of the channel). From Graetz's series solution, the mixing-cup concentration profile is (Shah et al. 1978)

$$\langle T \rangle(z) \text{ or } \langle c \rangle(z) = \sum_{n=1}^{\infty} w_n \exp\left(\frac{-\lambda_n^2 z}{\alpha Pe_{m,\max}} \right) \tag{3.2}$$

where the coefficients w_n include integration constants and eigenfunction derivatives at the wall (related with Shah and London's G_n by $w_n = 2\sigma G_n / \lambda_n^2$), and λ_n are the eigenvalues associated to the eigenfunctions superposed in an infinite series. For Neumann and Dirichlet wall conditions, these quantities depend only on the channel geometry and on the (flat or parabolic) flow profile. Alternatively, one-dimensional models may be used, with heat or mass transfer coefficients calculated according to correlations for the Nusselt and Sherwood numbers of the form:

$$Sh(z) = (S+1)\frac{k_m(z)\,a}{D} = \frac{-(S+1)\partial c/\partial r\big|_{wall}}{\langle c \rangle(z) - c_{wall}} = \frac{-(S+1)\sum_{n=1}^{\infty} A_n \varphi_n'(1)\gamma_n(z)}{\sum_{n=1}^{\infty} w_n \gamma_n(z) - \sum_{n=1}^{\infty} A_n \varphi_n(1)\gamma_n(z)}, \tag{3.3}$$

where $\gamma_n(z) = \exp\left(\frac{-\lambda_n^2 z}{\alpha Pe_{m,\max}}\right)$ is the part of the solution showing the dependence on the axial coordinate. From Eqs.(3.2) and (3.3), it is possible to see that an inconvenience occurs as $z/\alpha Pe_m \to 0$ in this slowly convergent series. In fact, the number of terms needed to obtain an accurate solution increase sharply as the inlet of the channel is approached or as convection becomes more dominant. In this case, the profile can be obtained by Lévêque's solution (Lévêque 1928; Shah et al. 1978; Rice et al. 1995; Weigand 2004), a simplified treatment concerned with the thin boundary layer that develops near the wall in the thermal entry region. In practical terms, the analysis of the problem in the whole range of Graetz number ($\alpha Pe_m/z$) has been fragmented into two main regions: an entrance length (where Lévêque's solution is valid) and a fully developed section (where only one term from the series in (3.2) is enough). Lévêque's regime and its transition to full development may be significant when millisecond contact time reactors are used, as it is often the case. Rosa et al. (2009) reviewed the importance of several scaling effects in single-phase heat transfer in microchannels. They noted that many prior reviews have reported large discrepancies between experimental, rigorous numerical and analytical results. Then, several effects (arising from working at the microscale) that might be at the origin of such deviations were explored. Concerning inlet effects (development of the temperature profile), the following observations were made: (*a*) the thermal entry length solution must always be considered to describe heat transfer; (*b*) these effects can be especially important in microchannel sinks due to their compactness; (*c*) examination of the range of the Graetz parameter in several experimental works led to the conclusion that most of the times the profile cannot be considered fully developed. In the case of electrochemical microfluidic reactors, Yoon et al. (2006) proposed an improved design based on the analysis of the boundary layer in the Graetz problem. They mention that many microreactors operate in the entrance length regime. Therefore, a non-negligible channel length may be required for the profile to be considered fully developed. A correct description of such cases has relied on the use of compartment models (Gervais et al. 2006; Kockmann 2008), where once a critical value of $(\alpha Pe_m/z)^*$ is identified, Lévêque's solution is used if $\alpha Pe_m/z > (\alpha Pe_m/z)^*$, while the fully developed solution is adequate for $\alpha Pe_m/z < (\alpha Pe_m/z)^*$ (Figure 3.1). This represents a change from high to low conversion asymptotes as the Graetz parameter increases. It also represents the onset of diffusive effects at the global (maximum) transverse scale of the channel, as for $z/\alpha Pe_m < (z/\alpha Pe_m)^*$ these are confined in a boundary layer. When the profile is fully developed, transverse concentration gradients are important over the whole radius of the duct. In this case, a uniform value for Sherwood number is obtained.

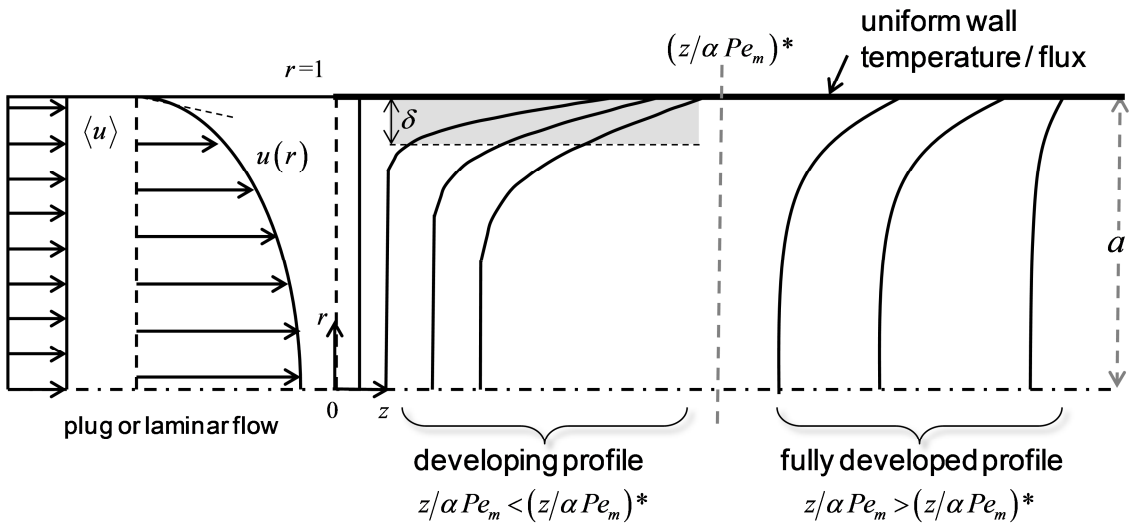

Figure 3.1: Schematic representation of the channel and of the concentration profile, according to a two-compartment model.

A uniformly valid description of this fundamental problem has been pursued in several ways (Shah et al. 1978), of which the most widely used are:

(a) *Numerical calculation of* w_n *and* λ_n $(n>1)$ *to include more terms in* Eq.(3.2): Brown (1960) reports the solution first eleven terms for the Dirichlet problem in laminar flow. Other authors have tabulated eigenvalues and constants for several geometries (see Chapter 2 and references therein).

(b) *Calculation of* w_n *and* λ_n *using of asymptotic relationships for large* n: Sellars et al. (1956) use the WKB method to approximate eigenfunctions, eigenvalues and integration constants in Graetz's series solution. Newman (1973a) extended these approximations, which were used by Shah and London (1978) to estimate λ_n and G_n for $21<n<121$ for a circular channel.

(c) *Matching of developed and developing profile limits by empirical correlations*: This approach has been successfully applied to the prediction of *Sh* number as a function of the Graetz parameter. For example, in Chapter 4 we will provide expressions in the Dirichlet and Neumann limits.

(d) *Extension of Lévêque's solution with higher order perturbation corrections*: This has given origin to what is called Lévêque's series (Shah et al. 1978), which is a perturbation series on powers of the concentration boundary layer thickness, δ:

$$\langle c \rangle (z) = 1 - \sum_{n=0}^{\infty} \langle c \rangle_n \, \delta^n \tag{3.4}$$

where $\langle c \rangle_n (z) = -\dfrac{(S+1)}{\alpha \, Pe_m} \int_0^z \left. \dfrac{d\, c_n}{d\, r} \right|_{wall} d\, z$ and $n \geq 1$.

A reasonable number of terms in series (3.4) has been given by Newman (1969; 1973b) and Worsoe-Schmidt (1967), as reported in Shah and London (1978) for both Dirichlet and Neumann boundary conditions. Note that from the convection-transverse diffusion dominant balance in the boundary layer, $\delta \sim \left[(S+3) \, \alpha \, Pe_m \right]^{-q}$, where: $q = 1/2$ for plug flow, $q = 1/3$ for laminar flow, $S = 0$ in a planar duct and $S = 1$ in a circular channel.

The following disadvantages or limitations of the previous approaches can be enumerated:

- It has been shown (Housiadas et al. 1999) that the evaluation of Graetz series terms with minimum associated error may have to include the use of strategies (a), (b) and (d) simultaneously, depending on the value of n and $z/\alpha \, Pe_m$, for the simpler case of uniform wall concentration (or temperature).

- A significant numerical effort may be associated with (a), since a large number of terms may be required. For example when $z/\alpha \, Pe_m > 10^{-4}$, Shah and London (1978) used 120 terms in Eq.(3.2). Moreover, this gives origin to expressions far too complex with no insight on the contribution from the developing profile.

- An accurate approximation from Eq.(3.4) in the intermediate region demands a large number of terms in this series. For $z/\alpha \, Pe_m < 10^{-4}$, Shah and London (1978) use 7 terms. The higher order terms are meant to account for the effects of channel curvature and velocity profile nonlinearity. Each coefficient is determined by solving a perturbation problem with subdominant terms that depend on solutions calculated previously (Chapter 2). In addition, the approximation generally breaks down in the transition region.

- The formulation of empirical correlations may involve the introduction of fitting parameters to improve the approximation (Chapter 4).

In this work, we present an approximate solution for conversion (section 3.2) and for the Sherwood number (section 3.3) which identifies both fully developed and developing profile contributions, requiring minimum numerical evaluation. This result accelerates the convergence rate of Graetz series producing only two or three terms. It is also free from the limitations of perturbation solutions (which require smallness of a parameter in the governing equations) as a result of the mathematical technique employed, which to our knowledge hasn't been applied to problems of this type so far. Moreover, criteria for the dominance of each contribution and transition between regimes will be provided (section 3.4). This is fundamental for the appropriate choice of correlations in the modelling and interpretation of experimental data. Our procedure consists in asymptotically evaluating the summations in Eqs.(3.2) and (3.3), rewritten as

$$Sh(z) \text{ or } \langle c \rangle (z) \sim \lim_{N \to \infty} \sum_{n=0}^{N} f(n) \tag{3.5}$$

for large N and for each of the geometries and flow profiles studied. This implies that each term in those summations will have to be written explicitly as a function of n. Even though this is only known exactly for the case of plug-flow between parallel plates, accurate solutions can be obtained with some additional assumptions.

3.2 INSTANTANEOUS CONCENTRATION ANNULMENT AT THE WALL (OR UNIFORM WALL TEMPERATURE)

In the case where transverse transport controls, estimates for the eigenvalues and weights in Eq.(3.2) can be analytically calculated in an approximate manner (the subscript ∞ denotes Dirichlet conditions). This is the case where the first weight $w_{1,\infty}$ deviates most from unity ($w_{1,\infty} \le w_1 \le 1$), and where subsequent coefficients decay more slowly (since $\sum w_n = 1$).

3.2.1 Asymptotic dependence of eigenvalues and coefficients

The values for the first eigenvalue can be obtained numerically and are widely tabulated (Carslaw et al. 1959; Brown 1960; Shah et al. 1978):

$$\lambda_{1,\infty}^2 = \begin{cases} \pi^2/4 & \text{(parallel plates)} \\ 5.784 \sim 9\pi^2/16 & \text{(circular channel)} \end{cases} \quad \text{for plug flow,} \tag{3.6a}$$

$$\lambda_{1,\infty}^2 = \begin{cases} 2.828 & \text{(parallel plates)} \\ 7.313 & \text{(circular channel)} \end{cases} \quad \text{for laminar flow.} \tag{3.6b}$$

For laminar flows, the asymptotic predictions from Sellars et al. (1956) for large eigenvalues (yielding $\lambda_{1,\infty}=5/3$ and $\lambda_{1,\infty}=8/3$, respectively) have less than 1% and 3% relative error in comparison with Eq.(3.6b).

The coefficients in Eq.(3.2) are given by

$$w_{n,\infty}=\frac{2(S+1)}{\lambda_{n,\infty}^2} \qquad \text{(plug flow).} \qquad (3.7)$$

Note that $S=0$ for parallel plates and $S=1$ for a circular channel. When the flow profile is fully developed,

$$w_{n,\infty}=4\frac{3^{11/6}}{\sqrt{\pi}\,\Gamma(1/6)}\lambda_{n,\infty}^{-7/3}=3.0384\,\lambda_{n,\infty}^{-7/3} \qquad \text{(parallel plates)} \qquad (3.8a)$$

$$w_{n,\infty}=32\frac{3^{5/6}}{\sqrt{\pi}\,\Gamma(1/6)}\lambda_{n,\infty}^{-7/3}=8.1023\,\lambda_{n,\infty}^{-7/3} \qquad \text{(circular channel)} \qquad (3.8b)$$

for $n=1,2...$. The above results were obtained from WKB theory for large eigenvalues (Sellars et al. 1956), nevertheless in the Dirichlet limit they are acceptable even for $n=1$. Numerical values for $w_{1,\infty}$ are also widely tabulated. These results were also presented in Chapter 2 (sections 2.2.1 and 2.2.3).

Writing the terms in Eqs.(3.2) or (3.3) as $f(n)$ in (3.5) requires some assumptions concerning the spacing between λ_n and λ_{n+1} and the dependence of weights on eigenvalues. The key assumption of our analysis is that the spacing between consecutive eigenvalues can be considered independent of n, i.e.

$$\lambda_{n,\infty}=\lambda_{1,\infty}+(n-1)\Delta\lambda \qquad (n=1,2...) \qquad (3.9)$$

where for large eigenvalues, the uniform spacing is

$$\Delta\lambda=\begin{cases}\pi & \text{(plug-flow)}\\ 4 & \text{(laminar flow)}\end{cases}. \qquad (3.10)$$

When the flow profile is flat, this is exact for parallel plates, but only approximate for a circular channel, since the spacing between eigenvalues is $\Delta\lambda_{n,\infty}\sim\pi-1/(8\pi n^2)+O(n^{-3})$ (i.e. becomes closer to π as $n\to\infty$) from the asymptotic expansion of Bessel functions (Abramowitz et al. 1972). For laminar flows, WKB theory for large eigenvalues predicts a value of $\Delta\lambda$ which is independent of the channel geometry (the curvature effects in the region next to the catalytic wall are $O(\lambda_n^{-2/3})$). Eqs.(3.7)-(3.10) allow us to express the coefficients in the mixing-cup concentration as

$$w_{n,\infty} = w_{1,\infty}\left(1+\frac{\pi(n-1)}{\lambda_{1,\infty}}\right)^{-2} \qquad (n=1,2...) \qquad \text{(plug-flow)} \qquad (3.11a)$$

$$w_{n,\infty} = w_{1,\infty}\left(1+\frac{4(n-1)}{\lambda_{1,\infty}}\right)^{-7/3} \qquad (n=1,2...) \qquad \text{(laminar flow).} \qquad (3.11b)$$

Coefficients and eigenvalues are now a function of n, requiring only the (exact or approximate) knowledge of $\lambda_{1,\infty}$ and $w_{1,\infty}$. Even though these simplifications hold more accurately as $n \to \infty$, we will consider them accurate enough as the basis to build our approximation.

3.2.2 Structure of the mixing-cup concentration/temperature profile

According to the previous section, the terms in the summation in (3.5) are now in appropriate form so that the asymptotic behaviour of the sum as $N \to \infty$ can be determined using the Euler-Maclaurin sum formula (Bender et al. 1978). Retaining the relevant terms, the simplified result for conversion of reactant X_R is obtained:

$$X_R = 1-\langle c \rangle \sim X_{GRAETZ} + X^*_{LEVEQUE} - HOT\,. \qquad (3.12)$$

The following contributions to the conversion profile along the channel can be identified:

- the first term of Graetz's solution is exactly of the same form as that in Eq.(3.2),

  $$X_{GRAETZ}(z) = 1 - w_{1,\infty}\exp\left(\frac{-\lambda^2_{1,\infty}\, z}{\alpha\, Pe_{m,\max}}\right) \qquad (3.13)$$

  with $\lambda^2_{1,\infty}$ and $w_{1,\infty}$ exactly known from Eqs.(3.6) or estimated by asymptotic methods;

- the modified Lévêque's solution, $X^*_{LEVEQUE}$, consists of Lévêque's solution multiplied by a corrective gamma function,

  $$X^*_{LEVEQUE} = \frac{1}{\Gamma(q)}\Gamma\left(q, \frac{\lambda^2_{2,\infty}\, z}{\alpha\, Pe_{m,\max}}\right) X_{LEVEQUE}\,, \qquad (3.14)$$

  Note that $q = 1/2$ for plug flow, $q = 1/3$ for laminar flow and that the original Lévêque solution is given by (Lévêque 1928; Carslaw et al. 1959; Shah et al. 1978):

  $$X_{LEVEQUE}(z) = \frac{2(S+1)}{\sqrt{\pi}}\sqrt{\frac{z}{\alpha\, Pe_m}} \qquad \text{(plug flow)} \qquad (3.15a)$$

  $$X_{LEVEQUE} = \frac{3^{4/3}(S+1)(S+3)}{2^{5/3}\,\Gamma(1/3)}\left(\frac{z}{\alpha\, Pe_{m,\max}}\right)^{2/3} \qquad \text{(laminar flow)} \qquad (3.15b)$$

  with $S = 0$ for plates and $S = 1$ for circular channel;

- the second term of Graetz's solution multiplied by a *compensation function* Δ accounts for the higher order terms (*HOT*) of Eq.(3.2) ignored in (3.13), and not included in (3.14):

$$HOT = w_{2,\infty}\,\Delta \exp\left(\frac{-\lambda_{2,\infty}^2\, z}{\alpha\, Pe_{m,\max}}\right). \tag{3.16}$$

In Eq.(3.16), the second eigenvalue is simply $\lambda_{2,\infty} = \lambda_{1,\infty} + \Delta\lambda$, and is associated with the weight $w_{2,\infty}$ ($= w_{1,\infty}\,\lambda_{1,\infty}^2 / \lambda_{2,\infty}^2$ e.g. for plug-flow). The function Δ appearing in Eq.(3.16) depends linearly on the reciprocal of the Graetz number ($z/\alpha Pe_m \sim Gz^{-1}$) and is defined as

$$\Delta = \Delta_1 + \Delta_2 \frac{z}{\alpha\, Pe_{m,\max}} \tag{3.17}$$

By forcing the inlet boundary condition to be fulfilled, the coefficients in (3.17) can be calculated using only the first eigenvalue and previous relationships to yield

$$\Delta_1 = \frac{1 - w_{1,\infty}}{w_{2,\infty}} \tag{3.18a}$$

$$\Delta_2 = \frac{\Delta\lambda}{6}\,\lambda_{2,\infty}. \tag{3.18b}$$

These results replace the earlier prediction in (3.19) below. Rigorously, the result obtained for Δ_1 can be shown to be associated with the corrective effect accounting for all weights ignored if series (3.2) is truncated after the second term, i.e. by application of the Euler-Maclaurin sum formula to $\Delta_1 = \sum_{n=2}^{\infty} w_{n,\infty} / w_{2,\infty}$:

$$\Delta_1 = \frac{1}{2} + \frac{\pi}{6\,\lambda_2} + \frac{\lambda_2}{\pi} \qquad \text{(plug flow)} \tag{3.19a}$$

$$\Delta_1 = \frac{1}{2} + \frac{7}{9\,\lambda_2} + \frac{3\,\lambda_2}{16} \qquad \text{(laminar flow).} \tag{3.19b}$$

Eqs.(3.19) are the approximate statement that all coefficients add to 1, and therefore Δ_1 can be alternatively calculated from $\sum_{n=1}^{\infty} w_{n,\infty} = w_{1,\infty} + w_{2,\infty}\,\Delta_1 = 1$. Each term in Eq.(3.12) is plotted as a function of $z/\alpha Pe_m$ in Figure 3.2 for a catalytic tubular reactor with parabolic velocity profile. The behavior of the different contributions in Eq.(3.12) is qualitatively the same for both geometries and flow profiles.

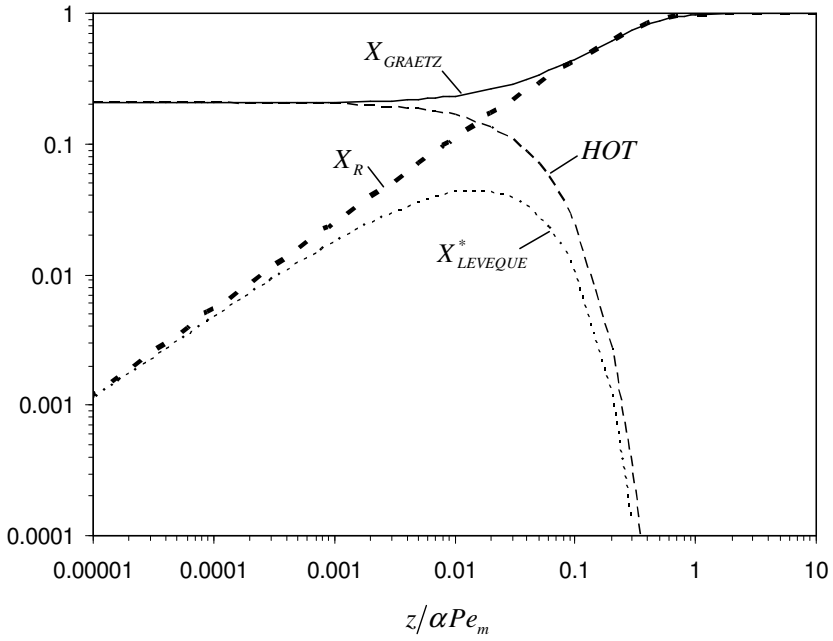

Figure 3.2: Conversion X_R as a function of the reciprocal of Graetz number ($z/\alpha Pe_m$) in an infinitely long circular channel with Dirichlet wall boundary condition, according to Eq.(3.12). The contributions of the one-term Graetz solution X_{GRAETZ}, the higher order terms HOT and the corrected Lévêque solution ($X^*_{LEVEQUE}$) are also plotted as given by Eqs.(3.13) to (3.16).

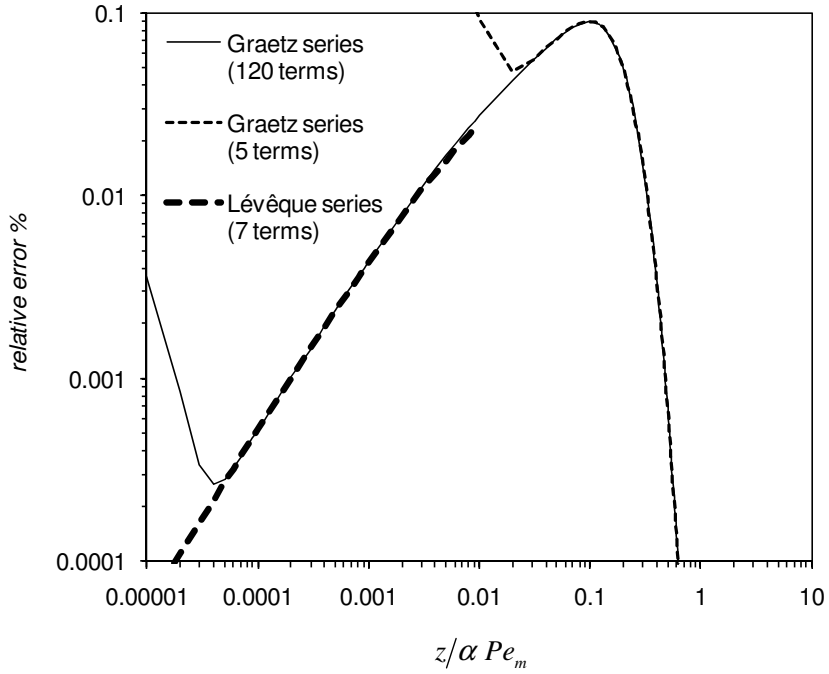

Figure 3.3: Relative error of the improved solution (3.12) with Graetz series (3.2) (with 5 and 120 terms) and with Lévêque's series (3.4) with 7 terms as described in Shah and London (1978). This refers to laminar flow inside a circular channel.

For laminar flows, Shah and London (1978) calculated the mixing-cup temperature profile under these conditions with the 120-term Graetz series (with both numerically and asymptotically determined eigenvalues and coefficients) for $z/\alpha\, Pe_m > 10^{-4}$ and with the 7-term Lévêque series from Worsoe-Schmidt (1967) for $z/\alpha\, Pe_m < 10^{-4}$. In a circular channel, the maximum error of (3.12) compared to Graetz series is 0.09% at $z/\alpha\, Pe_m = 0.1$ (in the intermediate regime between the developing and fully developed limits), as shown in Figure 3.3. For higher $z/\alpha\, Pe_m$, the relative error decays sharply, as the concentration tends to zero. If $z/\alpha\, Pe_m < 6\times10^{-5}$, in the range where Lévêque's extended solution is more appropriate, the relative error is below 3×10^{-4} %, while the deviation from Graetz series solution increases due to the unsuitability of that solution in the entry region. Increasing the number of terms in the series, increases the range where Graetz solution is still a correct estimate, but it is a slowly convergent series: agreement with 5 digits between Eq.(3.2) with 10 and 120 terms only occurs for $z/\alpha\, Pe_m > 0.02$. For lower $z/\alpha\, Pe_m$, the error in using Graetz series increases significantly, and so does the error compared to solution (3.12). Eq.(3.12) has also several advantages over existing solutions from 1D models with coefficients fitted from comparison with particular numerical results. Since the latter are not based on a uniform solution, but only on the asymptotes, they usually result in a compartmented solution with several ranges of Graetz parameter and significant higher error at the endpoints of each interval.

Qualitatively, the behaviour of the error between approximation (3.12) and Graetz and Lévêque's series is identical in a planar duct or when the velocity profile is flat. The maximum deviations from Graetz series are: 0.1% at $z/\alpha\, Pe_m = 0.10$ for plug-flows and 2.6% for laminar flow between parallel plates at $z/\alpha\, Pe_m = 0.01$. The relative error with Graetz's series (for higher values of $z/\alpha\, Pe_m$) and with Lévêque's series (for lower values of $z/\alpha\, Pe_m$) decreases sharply. Nevertheless, the intermediate region is also well described by Eq.(3.12), with low errors from numerical calculations or from Lévêque's extended solution.

Concerning the degree of development of the profile, we observe that the weighing function $\Gamma\left(q, \lambda_{2,\infty}^2\, z/\alpha\, Pe_{m,\max}\right)/\Gamma(q)$ in Eq.(3.14) is related to the fraction of the profile described by the inlet asymptote. If the value of this function is set to 1%, then $z/\alpha\, Pe_m = 0.12$ (laminar flow in a circular channel). If 10%, $z/\alpha\, Pe_m = 0.04$. Then, depending on the level of influence from inlet effects that we are willing to tolerate, the value of the Graetz parameter can be calculated accordingly. This will be further explored in section 3.4.

3.2.3 Lévêque's regime limit

For small $z/\alpha Pe_m$ (large Graetz number), the uniformly valid solution (3.12) reduces to the convective dominated (Lévêque's) limit. The contributions from the 1-term Graetz solution (3.13) and the HOT term (3.16) cancel out as $\sim z/\alpha Pe_m$, and the corrective function in (3.14) tends to unity at the same rate. The result represented by Eq.(3.15) is the leading-order term in the perturbation series given by Eq.(3.4) and tends to zero slower than other terms. Higher order corrections are of $O\left(\delta^n\right)$ and must be obtained by solving a nonhomogeneous PDE. The consistency of our solution in this limit can be tested by expanding Eq.(3.12) in a Taylor series, to yield

$$X_R\left(z\right) = X_{LEVEQUE} - \Phi_1 \frac{z}{\alpha\, Pe_{m,\max}} - \Phi_2 \left(\frac{z}{\alpha\, Pe_{m,\max}}\right)^2 + O\left(\frac{z}{\alpha\, Pe_{m,\max}}\right)^3, \tag{3.20}$$

where Φ_1 and Φ_2 depend on $\lambda_{1,\infty}$, $w_{1,\infty}$ and on the spacing given by (3.10). We note that Eq.(3.20) is written as a series of integer powers of $z/\alpha Pe_m$, which is not the form of (3.4) (where the power in the $O\left(\delta^n\right)$ term depends on $\left(z/\alpha Pe_m\right)^{n/2}$ for plug-flow or on $\left(z/\alpha Pe_m\right)^{n/3}$ for laminar flow). However, both series are in good agreement, as we discuss next.

For plug-flow, the coefficients in (3.20) can be calculated from

$$\Phi_1 = 2\left(S+1\right)\left(\frac{2}{\pi}\lambda_{2,\infty} + \frac{\Delta_2}{\lambda_{2,\infty}^2} - 1 - \Delta_1\right), \text{ and} \tag{3.21a}$$

$$\Phi_2 = 2\left(S+1\right)\left(\frac{\lambda_{1,\infty}^2}{2} + \frac{\Delta_1\,\lambda_{2,\infty}^2}{2} - \Delta_2 - \frac{2\,\lambda_{2,\infty}^3}{3\,\pi}\right). \tag{3.21b}$$

Replacing the approximate results for eigenvalues, weights and with Δ_1 given by Eq.(3.19a), both corrections are identically equal to zero ($\Phi_1 = \Phi_2 = 0$) for parallel plates ($S = 0$), while for circular channel ($S = 1$) the effect of curvature is visible in higher order terms: $\Phi_1 = 1$ and $\Phi_2 = \pi^2/32$. This is consistent with the extended Lévêque terms: for a circular channel, we have calculated the $O\left(z/\alpha Pe_m\right)$ term in Chapter 2, which is exactly reproduced here. In the case of parallel plates there is no room for additional corrections (due to curvature of the channel or profile nonlinearity).

In laminar flow conditions, expressions for Φ_1 and Φ_2 can be deduced as easily. Replacing the values of the first eigenvalue and coefficient, as well as of Δ_2 and Δ_1 from Eqs.(3.18b) and (3.19b), we obtain for parallel plates: $\Phi_1 = 0.1881$ and $\Phi_2 = 0.0285$. The first coefficient is very close to the one given by Newman (1969) and Wørsoe-Smith (1967) reported in Shah and

London (1978): $\Phi_1 = 0.15$. In those solutions, the next term is of $O\left(z/\alpha Pe_{m,\max}\right)^{4/3}$ and the respective coefficient is $\Phi_2 \simeq 0.0342$. Comparing Eq.(3.20) with the extended Lévêque's solution (3.4), this results in a maximum of 0.7% deviation in the range where these predictions have physical meaning. If we compare (3.20) with just two terms from the perturbation series, then a maximum of 3% exists, i.e. the asymptotic expansion tends to our result as the number of terms increases. These corrections account for a nonlinear velocity profile in the boundary layer near the wall, to which the effect of curvature in a circular channel must be added. In this case, $\Phi_1 = 2.7676$ and $\Phi_2 = 0.8513$ in Eq.(3.20). Again, the first coefficient is in reasonable agreement with the results from perturbation procedures (in that case, $\Phi_1 \simeq 2.4$), and the 7-term Lévêque series (Shah et al. 1978) has a maximum of 0.16% error for $z/\alpha Pe_m < 0.01$ and 0.00018% for $z/\alpha Pe_m = 10^{-4}$ when compared to Eq.(3.20). Asymptotic series with fewer terms produce slightly higher errors, proving that extended Lévêque solutions approach our result.

3.2.4 One-term Graetz regime limit

When the concentration profile is fully developed, this is equivalent to retaining only the first term in Graetz series. When $z/\alpha Pe_m$ is large (small Graetz number), Eq.(3.12) can be expanded as

$$X_R \sim X_{GRAETZ} - w_{2,\infty}\left(\Delta - \frac{\lambda_{2,\infty}}{\pi}\right)\exp\left(\frac{-\lambda_{2,\infty}^2\, z}{\alpha Pe_m}\right) \qquad \text{(plug flow)} \qquad (3.22a)$$

$$X_R \sim X_{GRAETZ} - w_{2,\infty}\left(\Delta - \frac{3}{16}\lambda_{2,\infty}\right)\exp\left(\frac{-\lambda_{2,\infty}^2\, z}{\alpha Pe_{m,\max}}\right) \qquad \text{(laminar flow).} \qquad (3.22b)$$

The second term in Eq.(3.22) is exponentially small and the series has the form of the 2-term Graetz solution with a corrective function in the second term, dominated by contribution from HOT in Eq.(3.16). Thus, at leading order, $X_R \sim X_{GRAETZ}$ and the role of the HOT term in (3.12) is to account for the importance of the fully developed profile contribution to the uniformly valid solution. The corrective gamma function "switches off" Lévêque's contribution, which otherwise would be unbounded. Instead, developing profile and higher order terms vanish exponentially.

3.3 UNIFORM WALL MASS / HEAT FLUX

When the mass or heat flux at the wall can be considered uniform, the boundary condition at the wall becomes:

$$\left.\frac{\partial c}{\partial r}\right|_{r=1} = f \,, \tag{3.23}$$

where in the mass transfer problem, $f = 0$ for a channel with inert wall (in the limit of a very slow heterogeneous reaction) or $f = -Da$ if a zeroth-order reaction occurs (without wall concentration annulment). The mixing-cup concentration (or temperature) is given by (Siegel et al. 1958; Bauer 1976; Shah et al. 1978)

$$\langle c \rangle = 1 + f\,\frac{\sigma\, z}{\alpha\, Pe_{m,\max}} \qquad \text{(plug and laminar flow).} \tag{3.24}$$

Contrary to the previous case with Dirichlet boundary condition, $\langle c \rangle$ in Eq.(3.24) does not include contribution from the entry length profile. However, while in the uniform wall concentration situation little insight is obtained by looking at the Sherwood number, here it is useful to analyse this quantity in more detail. We define Sh_H (or Nu_H, for simplicity both noted as Sh) as

$$Sh = \frac{-(S+1)\, f}{\langle c \rangle(z) - c(r=1,z)} \,. \tag{3.25}$$

Considering the full solution for the wall concentration $c(r=1,z)$ (Siegel et al. 1958; Bauer 1976):

$$\frac{1}{Sh} = \frac{1}{Sh_{fd}} + \sum_{n=1}^{\infty} \frac{A_{n,0}\,\varphi_n(1)}{(S+1)} \exp\left(\frac{-\lambda_{n,0}^2\, z}{\alpha\, Pe_{m,\max}}\right), \tag{3.26}$$

where: Sh_{fd} is the fully developed value of Sherwood number given by Eqs.(3.27) below, $A_{n,0}\,\varphi_n(1)$ is the product of the eigenfunction evaluated at the wall and the integration constant for the homogeneous eigenvalue problem in Neumann conditions and $\lambda_{n,0}$ is the associated eigenvalue, evaluated as described in the next section. For both planar ($S = 0$) and circular channels ($S = 1$),

$$Sh_{fd} = (S+3)(S+1) \qquad \text{(plug-flow)} \tag{3.27a}$$

$$Sh_{fd} = \frac{(S+1)(S+5)(S+7)}{5\,S+17} \qquad \text{(laminar flow).} \tag{3.27b}$$

3.3.1 Asymptotic dependence of eigenvalues and coefficients

We will assume again that eigenvalues are equally spaced according to Eq.(3.9). From the same asymptotic behaviour (large eigenvalues), $\Delta\lambda$ takes the same values for flat ($\Delta\lambda=\pi$) and parabolic ($\Delta\lambda=4$) profiles, for both geometries. The first eigenvalue is given by (Sellars et al. 1956; Shah et al. 1978)

$$\lambda_{1,0}^2=\begin{cases}\pi^2 & \text{(parallel plates)}\\ 14.6819 & \text{(circular channel)}\end{cases}\qquad\text{(plug flow)}\qquad(3.28a)$$

$$\lambda_{1,0}^2=\begin{cases}18.3801 & \text{(parallel plates)}\\ 25.6796 & \text{(circular channel)}\end{cases}\qquad\text{(laminar flow).}\qquad(3.28b)$$

Concerning the dependence of $A_{n,0}\,\varphi_n(1)$ on $\lambda_{n,0}$, it can be shown that $-A_{n,0}\,\varphi_n(1)=2\lambda_{n,0}^{-2}$ for plug-flows and $-A_{n,0}\,\varphi_n(1)\sim 2.401\,\lambda_{n,0}^{-5/3}$ for laminar flows (approximately for high eigenvalues). The numerically calculated values for $n=1$ are (Shah et al. 1978):

$$-A_{1,0}\,\varphi_1(1)=\begin{cases}0.20264 & \text{(parallel plates)}\\ 0.136222 & \text{(circular channel)}\end{cases}\qquad\text{(plug flow)}\qquad(3.29a)$$

$$-A_{1,0}\,\varphi_1(1)=\begin{cases}0.2222280 & \text{(parallel plates)}\\ 0.19872216 & \text{(circular channel)}\end{cases}\qquad\text{(laminar flow).}\qquad(3.29b)$$

3.3.2 Uniformly valid approximation to Sherwood/Nusselt number

Obtaining an uniform solution in this case involves the asymptotic evaluation of the summation in Eq.(3.26), which can be written as $\sum_{n=0}^{N} f(n)$ as $N\to\infty$. We apply the Euler-Maclaurin sum formula (Bender et al. 1978) to obtain:

$$\sum_{n=1}^{\infty}\frac{A_{n,0}\,\varphi_n(1)}{(S+1)}\exp\left(\frac{-\lambda_{n,0}^2\,z}{\alpha\,Pe_{m,\max}}\right)=\frac{\Theta_{LEV}}{Sh_{LEV}}+HOT\ .\qquad(3.30)$$

Concerning Eq.(3.30), the following remarks should be made:

- Lévêque's leading-order solution for Sherwood's number, Sh_{LEV}, is given by:

$$Sh_{LEV}=\frac{\sqrt{\pi}}{2}(S+1)\sqrt{\frac{\alpha\,Pe_m}{z}}\qquad\text{(plug flow)}\qquad(3.31a)$$

$$Sh_{LEV}=0.820199\,(S+1)\left(\frac{\alpha\,Pe_{m,\max}}{z}\right)^{1/3}\qquad\text{(laminar flow).}\qquad(3.31b)$$

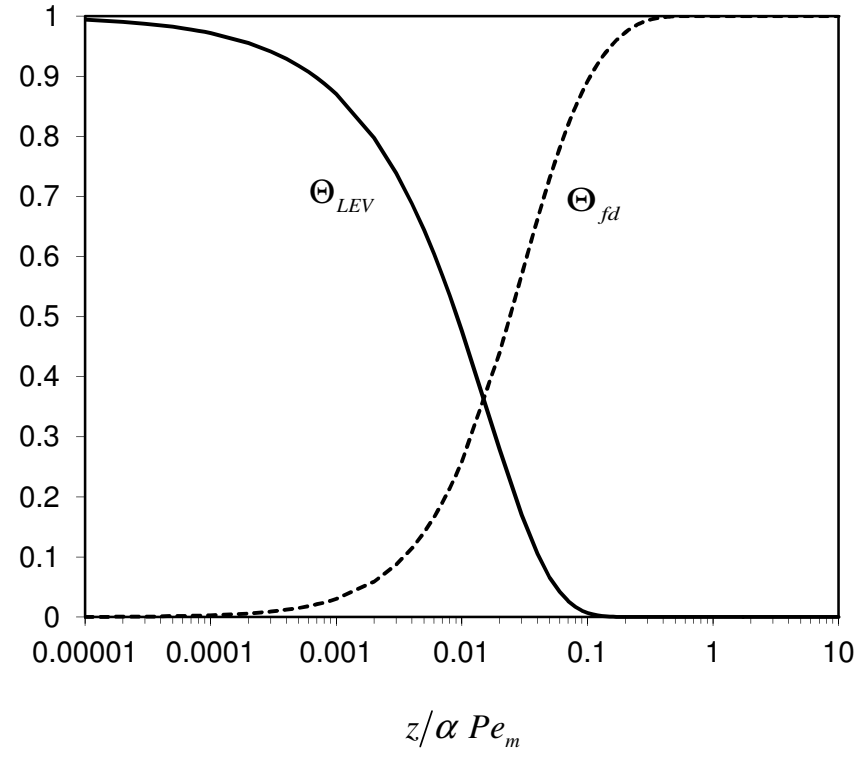

Figure 3.4: Θ_{fd} and Θ_{LEV} as functions of $z/\alpha\, Pe_m$ for laminar flow inside a circular channel.

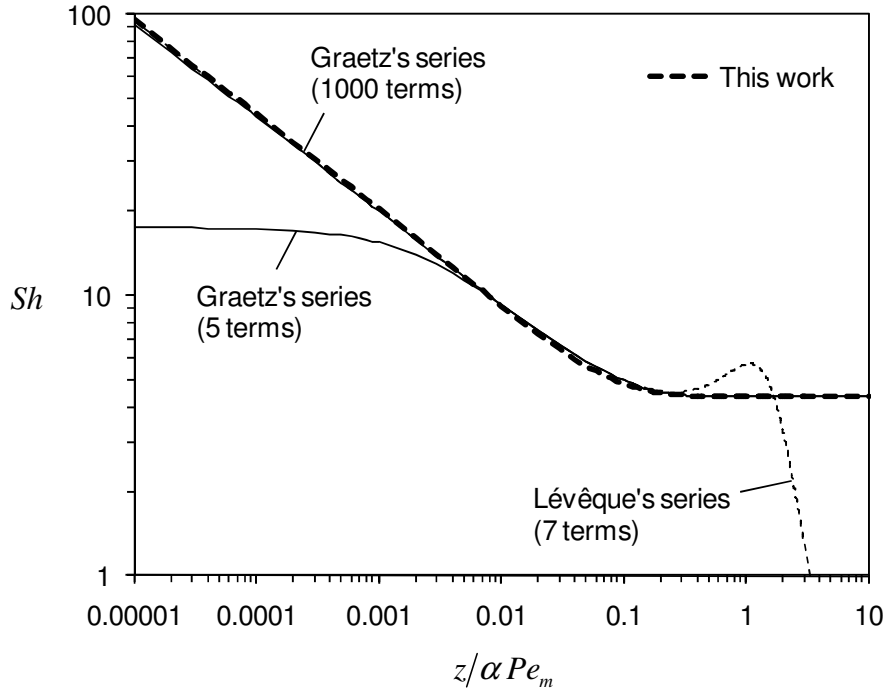

Figure 3.5: Sherwood number (Sh) as a function of $z/\alpha\, Pe_m$ for laminar flow inside a circular channel with uniform wall flux. The result from this work, Eq.(3.35), is compared with the solution from Graetz's series (with 5 and 1000 terms) and with the 7-term Lévêque's series from Shah and London (1978).

- As before, Lévêque's term appears multiplied by a corrective gamma function:

$$\Theta_{LEV} = \frac{1}{\Gamma(1-q)}\,\Gamma\left(1-q, \frac{\lambda_{2,0}^2\, z}{\alpha\, Pe_{m,\max}}\right). \tag{3.32}$$

- the higher-order terms HOT that result from the asymptotic summation are written as:

$$HOT(S+1) = A_{1,0}\,\varphi_1(1)\exp\left(\frac{-\lambda_{1,0}^2\, z}{\alpha\, Pe_{m,\max}}\right) + A_{2,0}\,\varphi_2(1)\left(\Delta_1 + \Delta_2\,\frac{z}{\alpha\, Pe_{m,\max}}\right)\exp\left(\frac{-\lambda_{2,0}^2\, z}{\alpha\, Pe_{m,\max}}\right) \tag{3.33}$$

where $HOT < 0$ and:

$$\Delta_1 = -\frac{A_1\,\varphi_1(1)}{A_2\,\varphi_2(1)} - \frac{S+1}{A_2\,\varphi_2(1)\,Sh_{fd}} \tag{3.34a}$$

$$\Delta_2 = \frac{\Delta\lambda\,\lambda_{2,0}}{6}. \tag{3.34b}$$

The values for Δ_1 were calculated so that the inlet boundary conditions are fulfilled (this substitution is consistent as shown previously).

- $A_{2,0}\,\varphi_2(1)$ and $\lambda_{2,0}$ are calculated from $A_{1,0}\,\varphi_1(1)$, $\lambda_{1,0}$ and the assumption of equally spaced eigenvalues. Moreover, $q = 1/2$ for plug flow, $q = 1/3$ for laminar flow, $S = 0$ for a planar duct and $S = 1$ for a circular channel, as before.

Substituting Eq.(3.30) into (3.26) yields:

$$\frac{1}{Sh} = \frac{\Theta_{fd}}{Sh_{fd}} + \frac{\Theta_{LEV}}{Sh_{LEV}} \tag{3.35}$$

where $\Theta_{fd} = 1 + HOT\,Sh_{fd}$, since the existence of higher-order terms is a measure of the importance of the fully developed contribution. For laminar flow inside a circular channel, the dependence of Θ_{fd} and Θ_{LEV} on $z/\alpha\, Pe_m$ is shown in Figure 3.4. Correlations based on the addition of both developing and fully developed limits are frequently used (e.g. in Chapter 4). Eq.(3.35) provides a justification for the form of such approximations, with additional functions that weigh the importance of each contribution.

The Sherwood number can be calculated as described in Shah and London (1978), using both Graetz (with numerical and asymptotic data) and Lévêque's series. For a circular channel with parabolic velocity profile, Figure 3.5 compares these results with (3.35). In this case, the modulus of the relative error compared with Eq.(3.35) has a maximum of 4% at $z/\alpha\, Pe_m = 0.04$ (corresponding to ~0.236 in absolute error), as shown in Figure 3.6. The error is reduced if a planar channel is considered (maximum of 1.2% at $z/\alpha\, Pe_m = 0.03$) or if the velocity profile is flat (e.g. maximum of 0.114% for $z/\alpha\, Pe_m = 0.03$ in a circular channel).

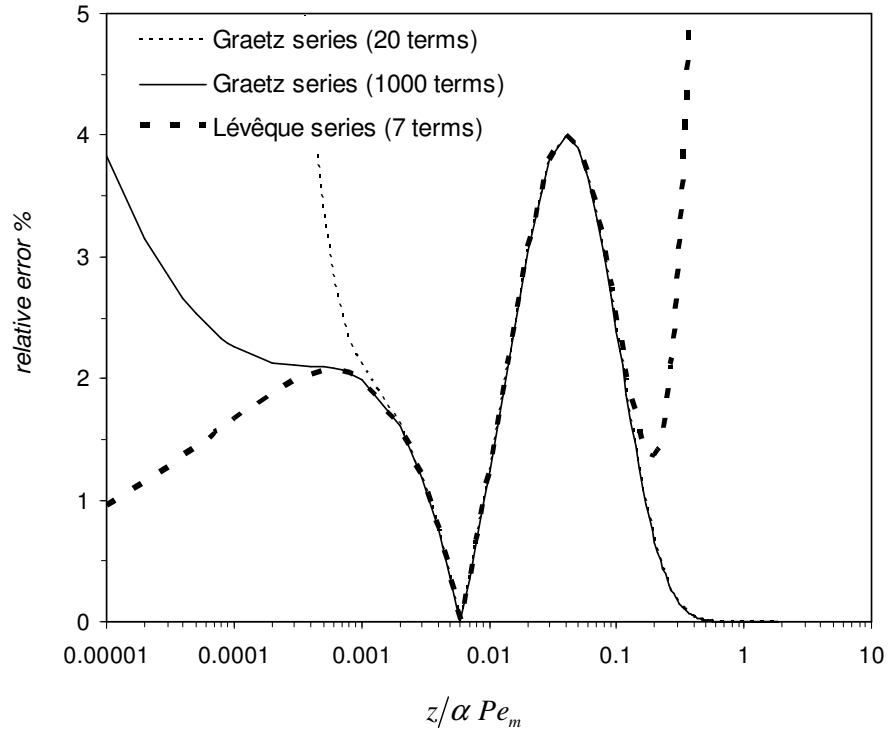

(a)

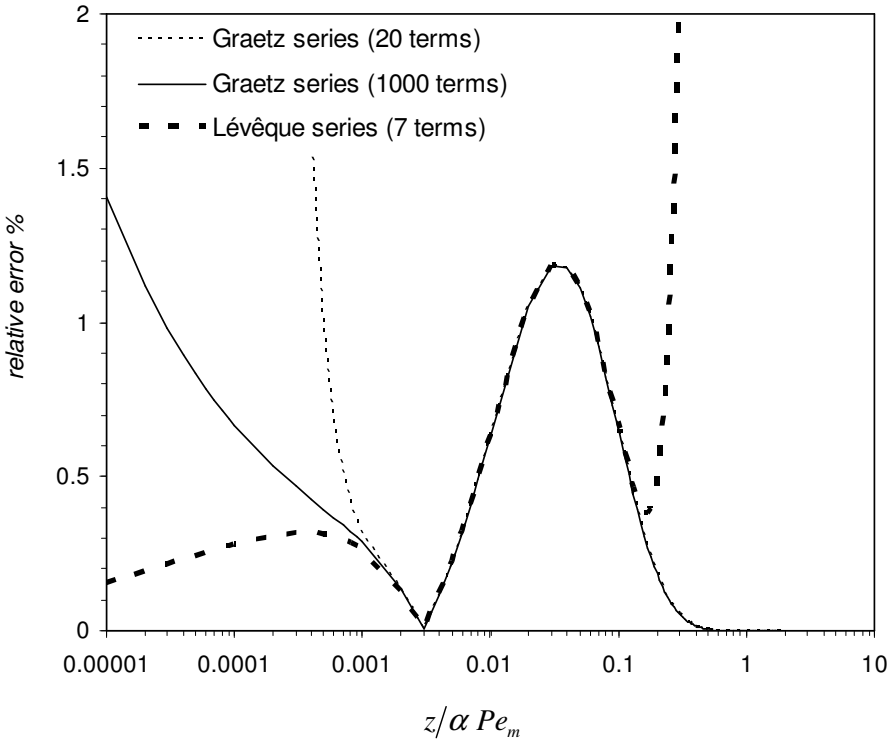

(b)

Figure 3.6:Relative error involved in estimating the Sherwood/Nusselt number with Eq.(3.35), in a circular (a) or planar (b) channel with Neumann wall boundary condition and laminar flow. Comparison of Graetz series (with either 20 or 1000 terms) and with Lévêque's series (7 terms) as given by Shah and London (1978) is shown.

3.3.3 Limiting forms of Eq.(3.35)

According to Eq.(3.35), the Sherwood number reduces to one of its asymptotic forms depending on the behaviour of Θ_{fd} and Θ_{LEV} for $z/\alpha Pe_m \to 0$ and $z/\alpha Pe_m \to \infty$. For small $z/\alpha Pe_m$,

$$\Theta_{LEV} = 1 - \frac{1}{\Gamma(1-q)(1-q)}\left(\frac{\lambda_{2,0}^2\, z}{\alpha Pe_{m,\max}}\right)^{1-q} + \ldots \qquad (z/\alpha Pe_m \to 0) \qquad (3.36a)$$

$$\Theta_{fd} = \frac{A_2\, \varphi_2(1)\Delta_2 + A_1\, \varphi_1(1)\left(\lambda_{2,0}^2 - \lambda_{1,0}^2\right)}{(S+1)}\frac{Sh_{fd}\, z}{\alpha Pe_{m,\max}} + \frac{\lambda_{2,0}^2\, z}{\alpha Pe_{m,\max}} + \ldots \quad (z/\alpha Pe_m \to 0). \qquad (3.36b)$$

For high $z/\alpha Pe_m$,

$$\Theta_{LEV} = \frac{1}{\Gamma(1-q)}\left(\frac{\alpha Pe_{m,\max}}{\lambda_{2,0}^2\, z}\right)^{q} \exp\left(\frac{-\lambda_{2,0}^2\, z}{\alpha Pe_{m,\max}}\right) + \ldots \qquad (z/\alpha Pe_m \to \infty) \qquad (3.37a)$$

$$\Theta_{fd} = 1 - \frac{\left(-A_1\, \varphi_1(1)\right) Sh_{fd}}{(S+1)} \exp\left(\frac{-\lambda_{1,0}^2\, z}{\alpha Pe_{m,\max}}\right) \qquad (z/\alpha Pe_m \to \infty). \qquad (3.37b)$$

As depicted from Eqs.(3.36)-(3.37) and Figure 3.4, when Lévêque's solution is appropriate $\Theta_{LEV} \to 1$ and $\Theta_{fd} \to 0$, while the reverse is observed when the profile is fully developed. In these limits and for laminar flow inside a circular channel, Eq.(3.35) writes as

$$\frac{1}{Sh} \sim \frac{1}{Sh_{LEV}} + 0.23\frac{z}{\alpha Pe_{m,\max}} + \ldots \qquad (z/\alpha Pe_m \to 0) \qquad (3.38a)$$

$$\frac{1}{Sh} \sim \frac{1}{Sh_{fd}} - 0.1\exp\left(\frac{-\lambda_{1,0}^2\, z}{\alpha Pe_{m,\max}}\right) + 0.1\exp\left(\frac{-\lambda_{2,0}^2\, z}{\alpha Pe_{m,\max}}\right) + \ldots \qquad (z/\alpha Pe_m \to \infty). \qquad (3.38b)$$

In (3.38a) the correction includes information from both terms, while in (3.38b) the dominant term (the exponential with $\lambda_{1,0}$ in the argument) results from the fully developed contribution, since Θ_{LEV} decays very sharply.

3.4 TRANSITION CRITERIA BETWEEN REGIMES AND RANGES OF VALIDITY

In the previous sections, we identified the contributions from the entry length and fully developed solutions as a result of the asymptotic technique employed. We now use these results to derive criteria for delimiting regimes.

3.4.1 Dirichlet boundary condition

As we have shown previously, the fully developed contribution (X_{GRAETZ}) can be isolated from the other terms in the uniformly valid approximation (3.12). Therefore, a suitable criterion for evaluating the degree of convective dominance is given by

$$\varphi = \frac{X_{GRAETZ} - X_R}{X_{GRAETZ}}. \tag{3.39}$$

Equivalently, Eq.(3.39) expresses the *degree of transverse transport control* and it is written as the sum of all higher order terms, normalized by the 1-term solution for conversion of reactant. According to the form of our approximate solution for X_R, Eq.(3.12),

$$\varphi \sim \frac{HOT - X^*_{LEVEQUE}}{X_{GRAETZ}} \tag{3.40}$$

Taking into account the dependence of each term in Eq.(3.40) on the Graetz number (Figure 3.2), we note that: when $X_R \to X_{GRAETZ}$, $\varphi \to 0$ (since $HOT \sim X^*_{LEVEQUE} \to 0$ and $X_{GRAETZ} \sim O(1)$) and when $X_R \to X_{LEVEQUE}$, $\varphi \to 1$ (since $X_{GRAETZ} \sim HOT$, while $X^*_{LEVEQUE} \sim X \to 0$). Therefore, φ is bounded and changes from 0 to 1 as $\alpha Pe_m / z$ increases from 0 to ∞. Eq.(3.40) may be accurately evaluated with the results presented earlier (plotted in Figure 3.7 for flow in a circular channel). For a given value of φ, the resulting (nonlinear) expression must be solved for $z/\alpha Pe_m$. Since our purpose is to derive the boundaries that delimit the regions where conversion can be confidently estimated by either X_{GRAETZ} or $X_{LEVEQUE}$, we are interested in the two asymptotes of Eq.(3.40): $\varphi \to 1$ and $\varphi \to 0$.

For plug-flow, expanding Eq.(3.40) around $z/\alpha Pe_m = 0$ or simply taking $X_R \sim X_{LEVEQUE}$ in (3.39) and expanding around the same point yields

$$\frac{z}{\alpha Pe_m} \le \frac{\pi}{4}\left(\frac{1-w_{1,\infty}}{S+1}\right)^2 (1-\varphi)^2 \qquad (\textbf{entrance length} \text{ as } \varphi \to 1). \tag{3.41}$$

Similarly for laminar flow, the critical value of the reciprocal of the Graetz parameter below which Lévêque's approximation can be used is

$$\frac{z}{\alpha Pe_{m,\max}} \le \frac{1.3778}{(S+3)^{1/2}}\left(\frac{1-w_{1,\infty}}{S+1}\right)^{3/2} (1-\varphi)^{3/2} \qquad (\textbf{entrance length} \text{ as } \varphi \to 1). \tag{3.42}$$

For the derivation of a criterion for the applicability of the one-term Graetz regime, we consider: $w_{1,\infty}\exp\left(-\lambda_{1,\infty}^2\ z/\alpha Pe_{m,\max}\right)<<1$, $X^*_{LEVEQUE}\to 0$ but $\Delta_1 >> \Delta_2\ z/\alpha Pe_{m,\max}$. This set of assumptions leads to

$$\frac{z}{\alpha Pe_{m,\max}} \geq \frac{1}{\lambda_{2,\infty}^2}\ln\left(\frac{1-w_{1,\infty}}{\varphi}\right) \qquad \text{(**fully developed regime** as } \varphi\to 0\text{)}, \quad (3.43)$$

valid for plug and laminar flows. Figure 3.7 shows the φ curve vs. the reciprocal of Graetz number for a circular channel. Eqs.(3.42) and (3.43) are able to predict the result from (3.40) with the uniform approximation outlined in section 3.2.2. For parallel plates, the agreement for $\varphi\to 1$ improves because there is no need to account for channel curvature. Plug-flow cases are also better described since no linearization of the velocity profile near the wall is introduced.

Concerning the above criteria, we can make the following remarks:

(a) The variation in the value of $z/\alpha Pe_m$ in Figure 3.7 is more abrupt in the range where the Graetz solution is adequate. This results in a bigger insensitivity to the criteria in this regime, whereas in the definition of the applicability of Lévêque's solution, the arbitrarily fixed value of φ may induce large changes in the entrance length.

(b) The influence of the flow profile in the fully developed boundary is irrelevant. There are numerical difficulties associated with the limit of $\varphi\to 0$ (near zero concentrations), therefore Eq.(3.43) is particularly useful.

(c) The value of φ can be directly related with the relative error that occurs when estimating conversion from the one-term Graetz solution:

$$\varepsilon_{GRAETZ} = \left(X_{GRAETZ} - X_R\right)/X_R = \varphi/(1-\varphi) \sim \varphi. \quad (3.44)$$

(d) The error that results from using Lévêque's approximation (3.15) is given by $\varepsilon_{LEV} = \left|X_{LEV} - X_R\right|/X_R$, which in the limit of $z/\alpha Pe_m \to 0$ relates with φ according to:

$$\varepsilon_{LEV} = \frac{\pi}{4}\ w_{1,\infty}\ \lambda_{1,\infty}^2\ \frac{1-w_{1,\infty}}{(S+1)^2}(1-\varphi)^2 \sim (1-\varphi)^2 \qquad \text{(plug flow)} \qquad (3.45a)$$

$$\varepsilon_{LEV} = 1.3778\ \frac{w_{1,\infty}\ \lambda_{1,\infty}^2\ \sqrt{1-w_{1,\infty}}}{(S+3)^{1/2}\ (S+1)^{3/2}}(1-\varphi)^{3/2} \sim (1-\varphi)^{3/2} \qquad \text{(laminar flow).} \qquad (3.45b)$$

From Eq.(3.45), we can see that the error related with Lévêque's solution is more sensitive to the choice of φ, compared with (3.44). Also, the selection of the same value of φ for plug and laminar flows results in a more conservative criterion for the former.

(e) Depending on the agreement required mainly with Lévêque's original solution, the transition region may extend by several orders of magnitude of $z/\alpha Pe_m$.

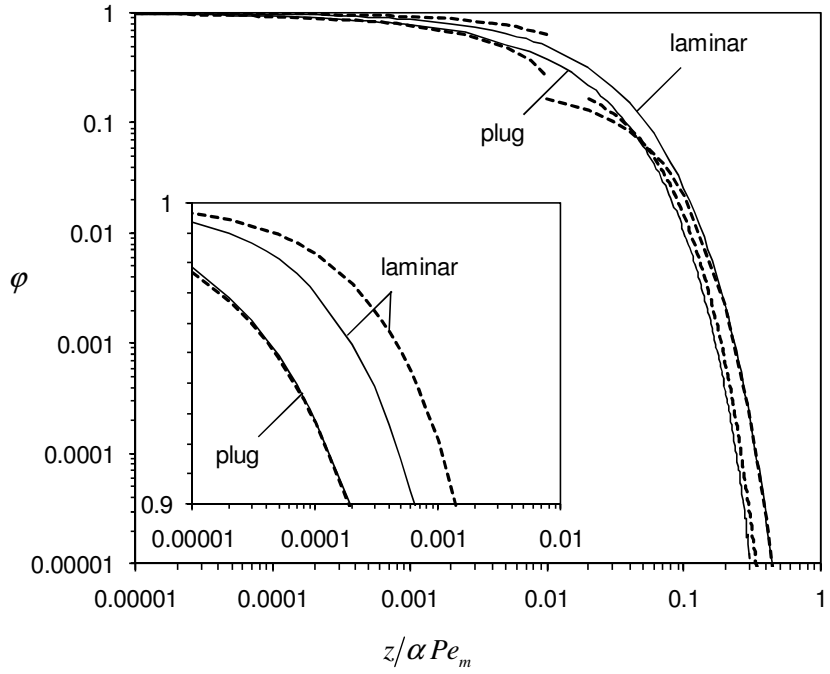

Figure 3.7: Degree of transverse transport control in a circular channel with Dirichlet wall boundary condition. The full lines were calculated according to Eq.(3.12). The limiting forms of the criterion (Eqs.(3.42) and (3.43) given by dashed lines) agree reasonably for $\varphi \to 1$ and $\varphi \to 0$. Both plug and laminar flows are considered.

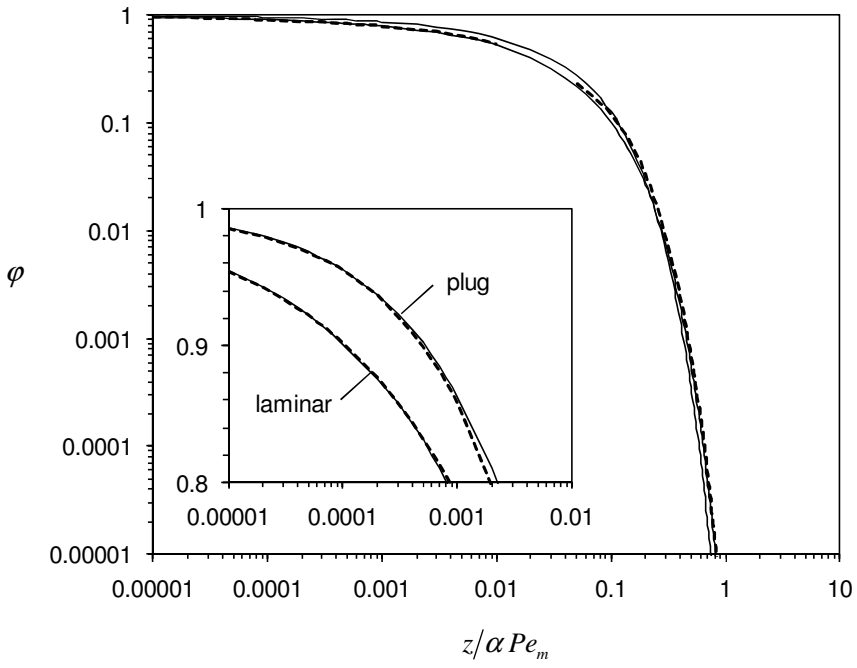

Figure 3.8: Degree of transverse transport control in a circular channel with Neumann wall boundary condition. The full lines were calculated using Eq.(3.35). The dashed lines are given by the limiting forms for $\varphi \to 1$ and $\varphi \to 0$ in Eqs.(3.48) and (3.49). Both plug and laminar flows are considered.

These results define the length of the intermediate region between developing and fully developed profile regimes. Operation and design in this range are of practical interest and haven't been sufficiently characterized. We have described analytically the transition from the low conversion (small temperature change, $\varphi \to 1$) asymptote to the high conversion one ($\varphi \to 0$). The same region marks the transition from low to high pressure drop regimes,

$$\Delta P \big/ \rho \langle u \rangle^2 \sim (\alpha\, Pe_m)^{-1} \sim \begin{cases} (1-\varphi)^{3/2}, \varphi \to 1 \\ -\ln \varphi \quad\;\; , \varphi \to 0 \end{cases}.$$

It is likely that an appropriate trade-off between achieving the required conversion/temperature difference at the minimum pressure drop yields an optimum point in the gap between the two well-described limits. The penalty in conversion so that pressure drop decreases by a certain amount is related to the value of φ, as this measures the degree of agreement with the high conversion (fully developed) asymptote. The simple and accurate results provided can be used in optimization procedures, where many evaluations would be required. This may be particularly useful on the simulation of multi-channel systems, at the integrated reactor level.

Another well-known trade-off occurs between conversion and mass transfer. The effect of an entrance region is to increase the mass/heat transfer rate, compared to the fully developed region, even though this is detrimental to the overall conversion. This increment can be quantified in several ways (e.g. the incremental heat transfer number $N(z)$ given in Shah and London (1978)). Therefore, φ also represents the increment in the transfer rate due to the influence of the inlet and the effect being privileged (high mass transfer rates $\varphi \to 1$, or high conversions $\varphi \to 0$). Setting $\varphi = 0.01$ corresponds to allowing the transfer rate at a given position to be influenced by the inlet by 1%.

3.4.2 Neumann boundary condition

When the flux is uniform throughout the channel, we have separated developing and fully developed contributions in the correlation for Sherwood (or Nusselt) number, Eq.(3.35). In this case, a measure for profile development can be written as

$$\varphi = \frac{Sh - Sh_{fd}}{Sh} = \frac{1/Sh_{fd} - 1/Sh}{1/Sh_{fd}}. \tag{3.46}$$

If $Sh >> Sh_{fd}$ (as it happens in the entrance length), then $\varphi \to 1$. The fully developed region is characterized by low values of φ (since $\varphi \to 0$ as $Sh \to Sh_{fd}$). According to (3.35),

$$\frac{\varphi}{Sh_{fd}} = -HOT - \frac{\Theta_{LEV}}{Sh_{LEV}} \tag{3.47}$$

which can be completely determined with the information in section 3.3.2. This is plotted as a function of $z/\alpha Pe_m$ for a circular channel in Figure 3.8. As previously, the limiting forms of (3.47) are:

$$\frac{z}{\alpha Pe_m} \le \frac{\pi(S+1)^2}{4}\frac{(1-\varphi)^2}{Sh_{fd}^2} \qquad \text{(\textbf{entrance length} as } \varphi \to 1 \text{ for plug flow),} \tag{3.48a}$$

$$\frac{z}{\alpha Pe_{m,\max}} \le 0.55177(S+1)^3\frac{(1-\varphi)^3}{Sh_{fd}^3} \qquad \text{(\textbf{entrance length} as } \varphi \to 1 \text{ for laminar flow),} \tag{3.48b}$$

$$\frac{z}{\alpha Pe_{m,\max}} \ge \frac{1}{\lambda_{1,0}^2}\ln\left(\frac{-A_{1,0}\,\varphi_1(1)}{S+1}\frac{Sh_{fd}}{\varphi}\right) \qquad \text{(\textbf{fully developed regime} as } \varphi \to 0\text{),} \tag{3.49}$$

valid for plug and laminar flows. The calculation of (3.47) from the uniformly valid solution and the limiting forms (3.48) and (3.49) is shown in Figure 3.8 for a circular channel. In the fully developed limit, the curves for plug and laminar flow overlap. The form of the curve in Figure 3.8 is similar to the one in Dirichlet case (previous section) and therefore the same comments are appropriate. Eq.(3.46) directly measures the deviation of the actual Sherwood number from its fully developed value. On the other hand, the relative error associated with Eqs.(3.31) is given by

$$\varepsilon_{LEV} = \frac{Sh - Sh_{LEV}}{Sh} = \frac{1/Sh_{LEV} - 1/Sh}{1/Sh_{LEV}} \sim 1 - \Theta_{LEV}\,. \tag{3.50}$$

Expanding Eq.(3.50) for $z/\alpha Pe_m \to 0$,

$$\varepsilon_{LEV} \sim \frac{1}{\Gamma(1-q)(1-q)}\left(\frac{\lambda_{2,0}^2\, z}{\alpha Pe_m}\right)^{1-q}.$$

Substituting (3.48), ε_{LEV} can be related with φ:

$$\varepsilon_{LEV} \sim (S+1)\frac{\lambda_{2,0}}{Sh_{fd}}(1-\varphi) \sim (1-\varphi) \qquad \text{(plug flow)} \tag{3.51a}$$

$$\varepsilon_{LEV} \sim 0.745201(S+1)^2\frac{\lambda_{2,0}^{4/3}}{Sh_{fd}^2}(1-\varphi)^2 \sim (1-\varphi)^2 \qquad \text{(laminar flow).} \tag{3.51b}$$

For the same value of φ, the criterion is more conservative for laminar flows.

Another interpretation of these results can be given in terms of the mass/thermal boundary layer developing near the interface. The thickness of this region δ is related to the Graetz parameter and it has been shown that it should be included e.g. in the criteria for delimitation of mass

transfer – reaction regimes in a microreactor (Chapter 4). As in the case of the thermal/mass entrance length, there is a lot of disparity in the definitions and values reported concerning δ.

In the case of uniform wall flux, we have obtained an explicit approximation for the Sherwood/Nusselt number. From the theory of interphase transfer coefficients, we define the thickness of the boundary layer ($a\,\delta$) so that the mass/heat transfer coefficient is given by $k_m \sim D/(a\,\delta)$. Thus, the Sherwood/Nusselt number can be written as $Sh(z) = (S+1)/\delta(z)$. The maximum boundary layer thickness is $\delta_\infty = (S+1)/Sh_{fd}$. The normalized thickness so that $\delta^* = 1$ (boundary layer thickness equals the radius of the channel) for fully developed profile is

$$\delta^* = \frac{\delta}{\delta_\infty} = \frac{Sh_{fd}}{Sh}.$$

Introducing Eq.(3.35) or(3.46):

$$\delta^* = \Theta_{fd} + \frac{Sh_{fd}}{Sh_{LEV}}\Theta_{LEV} = 1 - \varphi.$$

In the case of a Dirichlet wall boundary condition, our criterion φ was formulated in terms of conversion values, which makes the relationship with Sherwood number more complex. For simplicity, and since we are looking for an estimate, the following expression is proposed:

$$\delta^* \sim (1-\varphi)^{q/(1-q)},$$

where $q = 1/2$ for plug and $q = 1/3$ for laminar flow. This allows both fully developed and developing dependences of δ^* on the Graetz parameter to be respected. The exact numerical coefficients may differ a little from this estimate, but the correct order of magnitude is kept. We note that according to Eqs.(3.45) at the inlet: $\delta^* \sim \sqrt{\varepsilon_{LEV}}$ for plug flow and $\delta^* \sim \varepsilon_{LEV}^{1/3}$ for laminar flow. On the other hand, according to Eq.(3.44) when the profile is near full development: $\delta^* \sim 1 - \varepsilon_{GRAETZ}$ for plug flow and $\delta^* \sim \sqrt{1-\varepsilon_{GRAETZ}}$ for laminar flow. The correct estimation of this thickness is fundamental for the design of optimized microchannel systems, where the complete or a fraction of the boundary layer is removed or disrupted by the periodic placing of outlets or inlets (Yoon et al. 2006).

Expressing the dependence of Nusselt or Sherwood number on the Graetz parameter is often not achieved by a single expression. Almost all correlations for Sherwood / Nusselt number are given in branches with compartmented ranges of validity (usually, one for fully developed conditions and other(s) for developing profile), and one can find many examples of this in Shah and London's book (Shah et al. 1978). Since each expression is constructed from asymptotic limits, it is recognised that at the intersection of both asymptotes or in the limits of each interval, the error in predicting Sherwood number is maximum. A curious consequence from (3.35) is an estimate for the maximum error associated with this approach.

At the intersection: $Sh_{fd} = Sh_{LEV} = Sh_{est}$ (estimated Sherwood number). Then, the relative error from this approach is given by

$$\text{error} = 1 - \frac{Sh_{est}}{Sh} = 1 - \left(\Theta_{fd} + \Theta_{LEV}\right).$$

This should be evaluated at the intersection point, which is given in Table 3.1 (criterion type B). For laminar flow in a circular channel: $\text{error} \sim 9\%$. In this case, the existence of an uniformly valid solution to the interphase coefficient can reduce the error significantly.

From Figure 3.4, we can observe that Θ_{fd} and Θ_{LEV} intersect at $z/\alpha\, Pe_m \sim 0.01$ at a value of ~ 0.4. At this point, $\varphi \sim 0.5$ which corresponds to the intermediate level of profile development. This validates the roles of Θ_{fd}, Θ_{LEV} and φ as being indicative of the degree of profile development.

3.4.3 Comparison with previous criteria

In most of the chemical engineering literature, the ranges of validity of the entrance and fully developed models have been obtained in a number of ways that we briefly detail below. Table 3.1 situates previous regime boundaries within our criterion by calculating the respective value of φ. Data from the following five "calculation methods" are presented:

A. *Analogy with the momentum boundary layer development length*. For example, Kockmann (2008) scale the entrance length for the concentration profile from the hydrodynamic length yielding in our variables:

$$\frac{z}{\alpha\, Pe_m} \leq 0.05\, \frac{d_h^2}{a^2}.$$

In Table 3.1, we compare this with other criteria for laminar flow in a channel with Dirichlet wall boundary condition.

B. *Intersection of fully developed and Lévêque asymptotes in a* $Sh - \alpha\, Pe_m / z$ *plot.* In Chapter 4, we calculated the value of the Graetz parameter where Lévêque's correlation attained the fully developed value. This is a usual procedure, which however ignores the intermediate region. In this case, transition occurs around $\varphi \sim 0.10$.

C. *Error comparison with numerical solution*. Gervais and Jensen (2006) determined the intersection of absolute error curves from 1D models with developing and fully developed correlations for Sh. Their result for laminar flow between parallel plates with symmetric boundary conditions is in Table 3.1.

D. *Agreement with Sh_{fd} by an arbitrarily defined margin of error*. The reference book from Shah and London (1978) presents the distance required to achieve a local Nusselt number equal to 1.05 of the fully developed temperature profile value. Polyanin et al. (2002) also calculate the length of the thermal initial region so that $Nu = 1.01\, Nu_{fd}$. Table 3.1 contains these results for laminar flow. It can be seen directly in the case of Neumann boundary condition, that our criteria confirms these results.

E. *Agreement between analytical solutions*. Shah and London (1978) give the range of $z/\alpha\, Pe_m$, where the Nusselt number calculated from the 120-term Graetz series equals the one from the 7-term Lévêque series up to 5 or more digits. In addition, Alonso et al. (2010) identified the transition region in laminar flow inside a circular channel with wall concentration annulment ($0.05 \le z/\alpha\, Pe_m \le 0.2$). This is also included in Table 3.1 for comparison.

From these few examples in the literature, we can make the following comments:

(a) As expected, most available information refers to the value of the Graetz parameter below which the fully developed profile is adequate. Much less information concerning the validity of Lévêque's solution is provided. The finite transition region between both regimes is also frequently ignored.
(b) There is a large variation in the boundaries that are provided, sometimes by one-order of magnitude. This is reflected in terms of φ values, and consequently on the relative error incurred by the use of approximations (see e.g. Eqs.(3.44) and (3.45)).
(c) When provided, the boundary for the developing profile given by Lévêque's solution is usually overestimated (values of φ not high enough).

Despite this and the fact that the concept of thermal/mass profile development length is well established, it is a common practice to propose criteria for the negligibility of entrance effects with no relationship to the arbitrary basis on which they were formulated and without the information that the analytical solution provides. Instead, an order of magnitude for the Graetz parameter is often preferred. Recently, Morini (2006) proposed that inlet effects on the average Nusselt number can be neglected if $Gz = \langle u \rangle\, d_h^2 / (D\, L) < 10$. From Figure 3.7, we can see that this corresponds to $(\alpha\, Pe_m)^{-1} > 0.4$ and to a very conservative (low) value of φ. Moreover, order of magnitude results ignore the correct numerical coefficients, which distinguish different shapes and flow conditions.

Table 3.1:Comparison of the ranges of validity given in the literature with our criteria.

Shape	Flow profile	Boundary condition	Criterion type	$\frac{z}{\alpha\, Pe_m}$	φ	Ref.
Circular	Laminar	Dirichlet	A	0.2	0.002	Kockmann (2008)
						Alonso et al. (2010)
			B	0.1021	0.03	Chapter 4
			D	0.22	0.001	Polyanin et al. (2002)
				0.1339	0.01	Shah and London (1978)
			E	$>8\times10^{-5}$	0.974	
				<0.02	0.315	
				>0.05	0.108	Alonso et al. (2010)
		Neumann	B	0.1063	0.09	Chapter 4
			D	0.28	0.01	Polyanin et al. (2002)
				0.1722	0.04	Shah and London (1978)
			E	$>8\times10^{-4}$	0.80	
				<0.02	0.40	
	Plug	Dirichlet	B	0.0381	0.10	Chapter 4
		Neumann	B	0.0491	0.27	
Plates	Laminar	Dirichlet	A	0.8	$\sim10^{-9}$	Kockmann (2008)
			B	0.07	0.07	Chapter 4
			C	0.24	0.001	Gervais and Jensen (2006)
			D	0.1276	0.014	Shah and London (1978)
			E	>0.008	0.58	
				<0.016	0.43	
		Neumann	B	0.0948	0.14	Chapter 4
			D	0.1847	0.045	Shah and London (1978)
			E	>0.008	0.57	
				<0.08	0.17	
	Plug	Dirichlet	B	0.0523	0.1	Chapter 4
		Neumann	B	0.0873	0.26	

We note that in principle the analysis can be extended to channels with different cross-sectional shapes. From WKB theory for large eigenvalues, curvature is negligible at the region near the interface, and therefore the dependence of eigenvalues and weights on n should be approximately the same. The correct values for λ_1 and w_1 can be calculated numerically or taken from the literature (Shah et al. 1978; Kays et al. 1980) for many geometries. Lévêque's solution can also be extended using a normalization based on the friction factor (Shah et al. 1978). At the convective dominated regime, shape effects are negligible at the boundary layer and it is only required to include the correct linearization for the laminar velocity profile. The same applies to other Graetz problems that have appeared in the literature (Weigand et al. 2007; Haji-Sheikh et al. 2009; Aydin et al. 2010; Ray et al. 2010; Vera et al. 2011) and received the same analytical treatment, as long as an asymptotic description of coefficients is available.

3.5 FINITE LINEAR WALL KINETICS

We now extend the approach outlined in sections 3.2 and 3.3 to the case of Robin boundary condition, i.e. when a finite reaction rate occurs at the wall (or for finite wall thermal resistance). In this case, Eq.(2.4) is valid at the wall

$$\left.\frac{\partial c}{\partial r}\right|_{r=1} = -Da\ c(1,z), \tag{2.4}$$

where Da is the Damköhler number for a first-order reaction ($=k_{surf}\ \eta\ a/D$). According to Graetz's series solution, the mixing-cup concentration profile is given by Eq.(3.2), where the eigenvalue λ_n and coefficient w_n are dependent only on Da for each channel geometry and flow profile. In Chapter 2, we have presented empirical correlations that describe the variation of these quantities as a function of Da, between two plateaus in the limits of $Da \to 0$ and $Da \to \infty$, where Neumann and Dirichlet-type boundary conditions are recovered, respectively. In the context of heat transfer, a similar boundary condition applies when the wall resistance (noted by R_w in Shah and London (1978)) is finite. We intend to obtain a solution which is uniformly valid on Da (or R_w) and on Graetz's parameter ($\alpha\ Pe_m/z$).

3.5.1 Assumptions on the dependence of eigenvalues and coefficients

In this case, it is also fundamental to assume that the spacing between consecutive eigenvalues (i.e. between λ_n and λ_{n+1}) is constant. Previously (in the Neumann and Dirichlet limits of

Eq.(2.4)), the asymptotic behavior of eigenfunctions appearing at the wall boundary condition predict nearly uniform spacing as n increases (as the eigenvalues become larger). However, for the first eigenvalues this is also reasonable and in those cases:

$$\lambda_n = \lambda_1 + (n-1)\Delta\lambda \qquad (n = 1, 2...) \tag{3.52}$$

$$\Delta\lambda = \begin{cases} \pi & \text{(plug-flow)} \\ 4 & \text{(laminar flow)} \end{cases} \qquad (\text{as } n \to \infty). \tag{3.10}$$

For finite reaction rate conditions (finite Da), the spacing between the first couple of eigenvalues $\Delta\lambda_n(n, Da)$ may depend not only on n, but also on Da (it has a minimum around $Da \sim 1$, more pronounced for $n = 1$). When $Da \to 0$, $Da \to \infty$ or n is large, Eqs.(3.52) and (3.10) are satisfactorily fulfilled. Since higher eigenvalues are associated with terms of decreasing importance (namely, exponential terms with negative arguments), we will consider that these relationships are also adequate for finite Da. This assumption will reduce the complexity of the final solution as shown below.

Concerning the dependence of coefficients on eigenvalues, the exact values of w_n (when Da finite) are given for *plug flow* by

$$w_n = \frac{2\,\sigma\,Da^2}{\lambda_n^2\left[\lambda_n^2 + Da^2 + Da\,\sigma(1-S)\right]} \qquad (n = 1, 2...). \tag{3.53}$$

Numerically calculated values of λ_1 should be used in Eq.(3.53) for accurate calculations when $n = 1$. When the *flow is fully developed* and for high eigenvalues, WKB theory gives the following results,

$$w_{n,\infty} = 2.02557\,\sigma\,\lambda_{n,\infty}^{-7/3} \qquad (Da \to \infty,\ \lambda_n >> 1) \tag{3.54a}$$

$$w_{n,0} = 2.4010\,\sigma\,Da^2\,\lambda_{n,0}^{-11/3} \qquad (Da \to 0,\ \lambda_n >> 1). \tag{3.54b}$$

When $Da \to 0$, the first eigenvalue also tends to zero according to

$$\frac{\lambda_1^2}{\sigma} = Da - \frac{S+1}{Sh_{fd,0}}Da^2 + O\left(Da^3\right) \tag{3.55}$$

and the estimate from (3.54b) is not adequate. Instead, we use the asymptotic expansion for small eigenvalues,

$$w_1 = 1 - \left(\frac{1+S}{Sh_{fd,0}}\right)^2 Da^2 + O\left(Da^3\right) \tag{3.56}$$

where $Sh_{fd,0}$ is given by Eqs.(3.27). In this limit, (3.53) writes as (*plug-flow*):

$$w_n = 2\,\sigma\,Da^2/\lambda_n^4 \qquad (n > 1 \text{ and } \lambda_n \sim O(1)).$$

3.5.1.a *Simplified dependence of weights*

Taking into account the behavior for large eigenvalues, we assume that higher coefficients can be calculated from the first one according to

$$w_n\ \lambda_n^{\beta} = w_1\ \lambda_1^{\beta} \qquad (n = 2,3...), \tag{3.57}$$

where $\beta_\infty \le \beta \le \beta_0$. According to Eqs.(3.53) and (3.54), β changes from its value in the Dirichlet limit (β_∞) to the one in the small Da asymptote (β_0). For plug-flow,

$$\beta_0 = \beta(n, Da \to 0) = 2 + \frac{\ln\left(\lambda_n^2/\lambda_1^2\right)}{\ln\left(\lambda_n/\lambda_1\right)} = 4 \tag{3.58a}$$

$$\beta_\infty = \beta(n, Da \to \infty) = 2 + \frac{\ln(1)}{\ln\left(\lambda_n/\lambda_1\right)} = 2\,. \tag{3.58b}$$

For laminar flow,

$$\beta_0 = \frac{\ln\left(w_{1,0}/w_{n,0}\right)}{\ln\left(\lambda_{n,0}/\lambda_{1,0}\right)} \sim \frac{\ln w_{n,0}}{\ln \lambda_{1,0}} \sim \frac{\ln Da^2}{\ln \sqrt{Da}} = 4 \tag{3.59a}$$

$$\beta_\infty = \frac{\ln\left(w_{1,\infty}/w_{n,\infty}\right)}{\ln\left(\lambda_{n,\infty}/\lambda_{1,\infty}\right)} = \frac{7}{3}\,. \tag{3.59b}$$

The form of $\beta(Da)$ will be provided in different cases as detailed in the next section.

3.5.2 Contributions to the mixing-cup concentration profile

The assumptions outlined in the previous section allow us to write Eq.(3.2) as $\langle c \rangle = \lim_{N\to\infty} \sum_{n=0}^{N} f(n)$, where:

$$f(n) = \frac{w_1\ \lambda_1^{\beta}}{(\lambda_1 + n\,\Delta\lambda)^{\beta}} \exp\left(\frac{-(\lambda_1 + n\,\Delta\lambda)^2\ z}{\alpha\, Pe_{m,\max}}\right) \qquad (n = 0,1,2...). \tag{3.60}$$

An asymptotic approximation to the summation of terms given by (3.60) can again be obtained by the Euler-Maclaurin sum formula (Bender et al. 1978). After some simplifications and removing the negligible terms, the following expression is obtained:

$$X_R = X_{GRAETZ}\ \Theta_{fd} + LEV\ \Theta_{LEV} \tag{3.61}$$

Each one of the terms in Eq.(3.61) can be calculated as follows. The first term in Graetz series corresponds to the fully developed solution and is given by

$$X_{GRAETZ} = 1 - w_1 \exp\left(\frac{-\lambda_1^2\ z}{\alpha\, Pe_{m,\max}}\right). \tag{3.62}$$

The approximation of the conversion profile by this solution was discussed in Chapter 2 for finite reaction rates. The Θ_{fd} factor measures the importance of (3.62) compared with the other terms in (3.2) that are not retained (far from the inlet), and includes the second term in Graetz's series (this is related to the HOT term in section 3.2.2),

$$\Theta_{fd} = 1 - \frac{w_2\ \Delta \exp\left(-\lambda_2^2\ z/\alpha\ Pe_{m,\max}\right)}{1 - w_1\ \exp\left(-\lambda_1^2\ z/\alpha\ Pe_{m,\max}\right)} \tag{3.63}$$

$$\Delta = \Delta_1 + \Delta_2 \frac{z}{\alpha\, Pe_{m,\max}}. \tag{3.64}$$

From section 3.5.1, w_2 and λ_2 can be easily estimated, if necessary resorting to the definition of β, which is calculated as described in sections 3.5.2.a and 3.5.2.b. The coefficients in (3.64) only require the knowledge of the first eigenvalue according to

$$\Delta_1 = \frac{1 - w_1}{w_2} \tag{3.65a}$$

$$\Delta_2 = \frac{\Delta\lambda}{6}\lambda_2. \tag{3.65b}$$

Rigorously another result is obtained for Δ_1, but is has been shown that replacing it by Eq.(3.65 a) (so as to fulfill the inlet boundary condition) is reasonable (section 3.2.2). The second term in (3.61) is related with the contribution of Lévêque's solution, and includes two factors: the first one (LEV) is a correction/limit of the entry length profile; the second one is a corrective incomplete gamma function, which we have identified as a normalized measure of the importance of LEV (section 3.2.2), as discussed below. Both are given by:

$$LEV = \frac{w_1\ \lambda_1^{\beta}}{\Delta\lambda\,(\beta - 1)} \left(\frac{z}{\alpha\ Pe_{m,\max}} \right)^{(\beta-1)/2} \Gamma\left(\frac{3-\beta}{2} \right) \tag{3.66}$$

$$\Theta_{LEV} = \frac{1}{\Gamma\left(3/2 - \beta/2\right)} \Gamma\left(\frac{3-\beta}{2}, \frac{\lambda_2^2\ z}{\alpha\ Pe_{m,\max}} \right). \tag{3.67}$$

In the *entrance region* of the channel (for small $z/\alpha\ Pe_m$), the conversion of reactant according to Eqs.(3.61) to (3.67), writes as

$$X_R = \frac{w_1\ \lambda_1^{\beta}}{\Delta\lambda\,(\beta - 1)} \left(\frac{z}{\alpha\ Pe_{m,\max}} \right)^{(\beta-1)/2} \Gamma\left(\frac{3-\beta}{2} \right) +$$

$$+ \left[w_1\ \lambda_1^2 + w_2 \left(\lambda_2^2\ \Delta_1 - \Delta_2 \right) + \frac{2\ w_2\ \lambda_2^3}{\Delta\lambda\,(\beta - 1)(\beta - 3)} \right] \frac{z}{\alpha\ Pe_{m,\max}} + O\left(\frac{z}{\alpha\ Pe_m} \right)^2. \tag{3.68}$$

The first term in (3.68) is LEV, while at $O\left(z/\alpha\, Pe_m\right)$ contributions from $X_{GRAETZ}\ \Theta_{fd}$ (the two first terms inside square brackets) and $LEV\ \Theta_{LEV}$ (the third term inside brackets) appear, since

$$\Theta_{LEV} = 1 - \frac{2/(3-\beta)}{\Gamma(3/2-\beta/2)}\left(\frac{\lambda_2^2\, z}{\alpha\, Pe_{m,\max}}\right)^{(3-\beta)/2} + O\left[\left(z/\alpha\, Pe_m\right)^{(3-\beta)/2+1}\right] \tag{3.69a}$$

$$\Theta_{fd} = \left(\lambda_2^2 + \frac{w_1\,\lambda_1^2 - \Delta_2\, w_2}{1-w_1}\right)\frac{z}{\alpha\, Pe_{m,\max}} + O\left[z^2/\left(\alpha\, Pe_m\right)^2\right]. \tag{3.69b}$$

Note that the description of the entry length is greatly influenced by the range of values taken by β. This can be seen namely in the definition of the dominant term in (3.68) and the magnitude (and sign) of Θ_{LEV} in (3.69a).

In conditions *far from the developing length* (i.e. large $z/\alpha\, Pe_m$), the weighting functions of the developing and fully developed solutions change their behavior, confirming their role as measures for the two contributions to the conversion profile. Namely, $\Theta_{fd} \to 1$ and $\Theta_{LEV} \to 0$ according to:

$$\Theta_{LEV} \sim \frac{1}{\Gamma(3/2-\beta/2)}\left(1 - \frac{\beta-1}{2\,\lambda_2^2}\frac{\alpha\, Pe_{m,\max}}{z}\right)\left(\frac{\lambda_2^2\, z}{\alpha\, Pe_{m,\max}}\right)^{(1-\beta)/2} \exp\left(\frac{-\lambda_2^2\, z}{\alpha\, Pe_{m,\max}}\right) \tag{3.70a}$$

$$\Theta_{fd} \sim 1 - w_2\,\Delta \exp\left(\frac{-\lambda_2^2\, z}{\alpha\, Pe_{m,\max}}\right). \tag{3.70b}$$

The values taken by β have little influence in this case (the calculation of w_2 is only slightly changed). Thus, the profile is dominated by the fully developed solution,

$$X_R = X_{GRAETZ} - w_2 \exp\left(\frac{-\lambda_2^2\, z}{\alpha\, Pe_{m,\max}}\right)\left[\Delta - \frac{\lambda_2}{\Delta\lambda}\left(\frac{1}{\beta-1} - \frac{\alpha\, Pe_{m,\max}}{2\lambda_2^2\, z}\right) + O\left(\frac{\alpha\, Pe_m}{z}\right)^2\right]. \tag{3.71}$$

Since there is a significant change in the analysis, depending on the value taken by β, two sets of values are considered separately: $3 < \beta \le \beta_0$ (which includes the kinetic controlled regime) and $\beta_\infty \le \beta < 3$ (representing in the limit, the mass transfer controlled regime). In each region, a calculation procedure for conversion and for the function $\beta(Da)$ is provided. The transition limit (when $\beta = 3$), occurs at a value of Damköhler number Da_T, which we calculate below as being around 1.

3.5.2.a *Values of* $3<\beta\le\beta_0$ *(* $Da<Da_T\sim 1$ *)*

When $\beta>3$, the term in Eq.(3.68) of $O\left(z/\alpha\, Pe_m\right)$ becomes dominant, while *LEV* is of $O\left[\left(z/\alpha\, Pe_m\right)^{(\beta-1)/2}\right]$, representing a correction. In the kinetically controlled limit ($Da\to 0$), the inlet regime described by (3.68) is dominated at $O\left(z/\alpha\, Pe_m\right)$ by $X_{GRAETZ}\,\Theta_{fd}\sim O(Da)$, followed by terms related with Θ_{fd} and $LEV\ \Theta_{LEV}$, both of $O\left(Da^2\right)$. The relative importance of the two latter terms (inside brackets in (3.68)) is given by $\Delta_1(\beta-1)(\beta-3)/2$. Noting that $\Delta_1=(1-w_1)/w_2$ takes its highest value (which may be $>>1$) when Da is low ($\beta\to 4$), it is possible the contribution from $LEV\ \Theta_{LEV}$ to be negligible compared with $X_{GRAETZ}\,\Theta_{fd}$. Also, note that as $\beta\to 3$ the importance of the contribution from $LEV\ \Theta_{LEV}$ at the inlet may increase significantly, leading to an inconvenient singularity. To place this contribution in the correct relative magnitude compared to other terms, we will take

$$\beta=\beta_0=4 \qquad \text{for } Da<Da_T, \tag{3.72}$$

where the transition value Da_T is around 1, although its precise value will be determined in section 3.5.2.b. According to (3.72), the approximation to conversion with an $O\left(Da^2\right)$ term in the *kinetic limit* is given by

$$X_R\sim\frac{\sigma\, Da\, z}{\alpha\, Pe_{m,\max}}-\left(\frac{1+S}{Sh_{fd,0}}+\frac{5}{6}\frac{\sigma^2}{\Delta\lambda^2}\right)\frac{Da^2\, z}{\alpha\, Pe_{m,\max}}+\ldots \qquad (\text{for } z/\alpha\, Pe_m<<1) \tag{3.73a}$$

$$X_R\sim\frac{\sigma\, Da\, z}{\alpha\, Pe_{m,\max}}-\left[\frac{1}{2}\left(\frac{\sigma\, z}{\alpha\, Pe_{m,\max}}\right)^2+\left(\frac{1+S}{Sh_{fd,0}}\right)\frac{z}{\alpha\, Pe_{m,\max}}-\left(\frac{1+S}{Sh_{fd,0}}\right)^2\right]Da^2+\ldots$$

$$(\text{for } z/\alpha\, Pe_m>>1) \tag{3.73b}$$

While the $O\left(Da^2\right)$ term in Eq.(3.73a) has a contribution from the developing parcel $LEV\ \Theta_{LEV}$, (3.73b) only reflects the fully developed profile influence. Examining the solutions in Levêque's regime (Carslaw et al. 1959; Ghez 1978) presented in Chapter 2 for $Da<<1$,

$$X_{LEV}=\frac{\sigma\, Da\, z}{\alpha\, Pe_m}-\frac{4\,\sigma\, Da^2}{3\sqrt{\pi}}\left(\frac{z}{\alpha\, Pe_m}\right)^{3/2}+O(Da)^3 \qquad \text{(plug flow)} \tag{3.74a}$$

$$X_{LEV}=\frac{\sigma\, Da\, z}{\alpha\, Pe_{m,\max}}-0.9144\,\sigma\, Da^2\left(\frac{z}{\alpha\, Pe_{m,\max}}\right)^{4/3}+O\left[Da^3\left(z/\alpha\, Pe_m\right)^{5/3}\right] \qquad \text{(laminar flow)} \tag{3.74b}$$

we observe that the $O\left(Da^2\right)$ corrections to the leading-order behavior are smaller than $O\left(z/\alpha\, Pe_m\right)$. Comparing with Eq.(3.73a), only the leading-order behavior (equal in X_{LEV} and X_{GRAETZ} for $z/\alpha\, Pe_m \to 0$) is reproduced. Therefore, the contribution of LEV is not to represent conversion in Lévêque's limit, but only a $O\left(Da^2\right)$ correction to that solution in an higher order contribution of $O\left(z/\alpha\, Pe_m\right)$.

3.5.2.b *Values of* $\beta_\infty \le \beta < 3$ *(* $Da > Da_T \sim 1$*)*

When $\beta < 3$, the entry length solution (3.68) is given by LEV, followed by a correction of $O\left(z/\alpha\, Pe_m\right)$. In contrast with the kinetic limit (where the leading-order term from X_{LEV} and X_{GRAETZ} is the same), the contributions from fully developed and developing regimes in mass transfer control are completely separable. Actually, $LEV = X_{LEV}$ when Dirichlet boundary condition is applicable (section 3.2.2). Therefore, in this range of β we should take LEV as approximately X_{LEV} (had this been done for $\beta > 3$ and the leading order term would have come up repeated). An approximate solution to Lévêque's problem has been given in Chapter 2:

$$X_{LEV} = \frac{(S+1)\, Da\, z/\alpha\, Pe_m}{1+\sqrt{\pi}/2\, Da\, \sqrt{z/\alpha\, Pe_m}} \qquad \text{(plug flow)} \qquad (2.33)$$

$$X_{LEV} = \frac{\sigma\, Da\, z/\alpha\, Pe_{m,\max}}{1+0.9828\, Da\left(z/\alpha\, Pe_{m,\max}\right)^{1/3}} \qquad \text{(laminar flow).} \qquad (2.35)$$

Eq.(3.61) becomes

$$X_R = X_{GRAETZ}\, \Theta_{fd} + X_{LEV}\, \Theta_{LEV} \qquad (3.75)$$

where all the terms were defined previously in Eqs.(3.62), (3.63) and (3.67). To complete the calculation procedure, namely to calculate w_2 from (3.57) and Θ_{LEV} from (3.67), an estimated relationship for β has to be provided. It is also desirable to know how β varies with Da. In general, $\beta = \beta(n, Da)$ and according to (3.57):

$$\beta(n, Da) = \frac{\ln\left(w_1/w_n\right)}{\ln\left(\lambda_n/\lambda_1\right)}. \qquad (3.76)$$

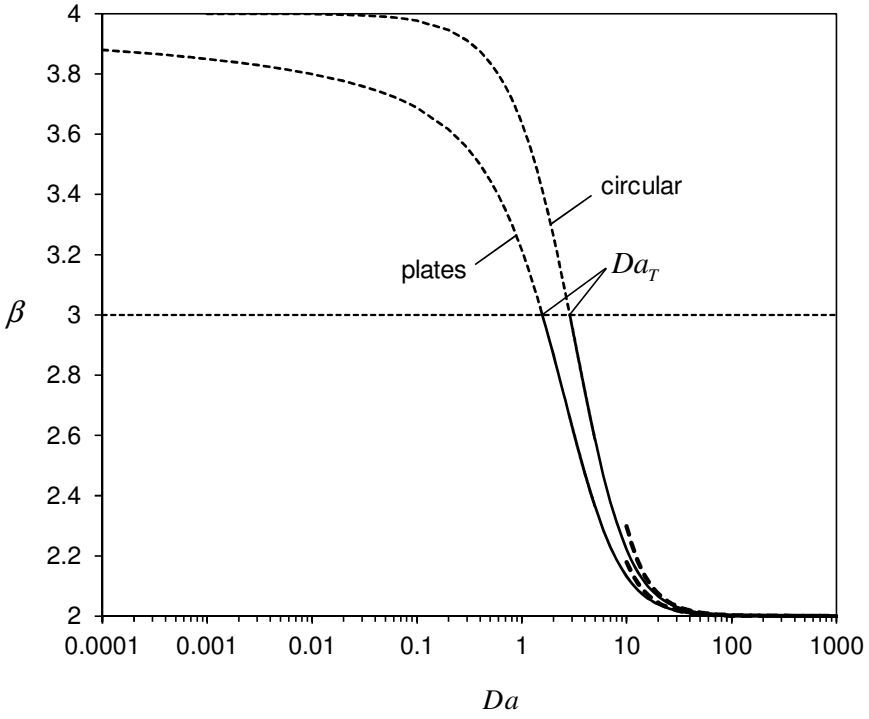

(a) Plug flow

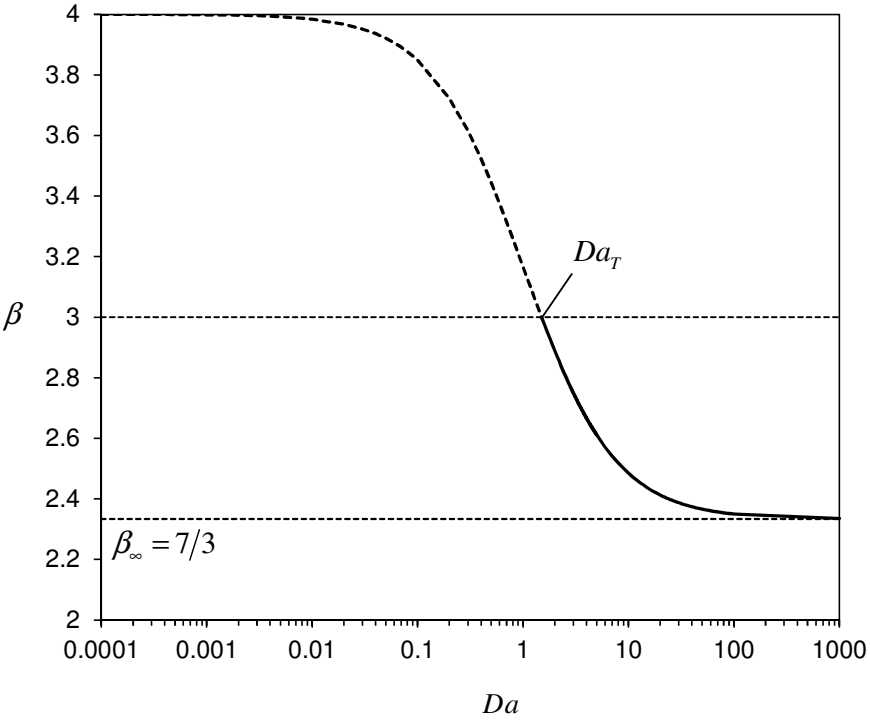

(b) Laminar flow

Figure 3.9: β as a function of the Damköhler number Da. Planar and circular channel with (a) plug flow or (b) laminar flow. Full lines are calculated from Eqs.(3.77) and (3.79) with no numerical evaluation involved (approximation for λ_1 was used). If approximations for large Da are sought, Eq.(3.78) can be used, shown by the dashed lines in (a). For $Da < Da_T$, the dashed variation of β should be replaced by the branch given by $\beta = 4$.

In order to proceed, it is necessary to assume that $\beta(n,Da)=\beta(Da)$, i.e. β is independent of n. Moreover, since the purpose of defining β is to correctly estimate coefficients that get significantly smaller as n increases (according to (3.60)), then $\beta(n,Da)\sim\beta(n=2,Da)$. Higher weights tend to zero fast, so the approximation benefits from accurately estimating the second weight. For plug-flow, according to Eq.(3.53):

$$\beta=2+\frac{1}{\ln\left(\lambda_2/\lambda_1\right)}\ln\left(\frac{\lambda_2^2+Da^2+Da\,\sigma(1-S)}{\lambda_1^2+Da^2+Da\,\sigma(1-S)}\right) \qquad \text{(plug flow).} \qquad (3.77)$$

Note that in Eq.(3.77): $\lambda_2=\lambda_1+\Delta\lambda$ and λ_1 can be estimated as described in section 3.5.1 (numerically or approximately). Figure 3.9a shows the plot according to (3.77) as well as the limiting form for large Da :

$$\beta=\beta_\infty+\frac{\lambda_{1,\infty}+\lambda_{2,\infty}}{\ln\left(\lambda_{2,\infty}/\lambda_{1,\infty}\right)}\frac{\Delta\lambda}{Da^2}+O\left(Da^{-3}\right) \qquad \text{(plug-flow, } Da\to\infty\text{).} \qquad (3.78)$$

with $\lambda_{2,\infty}=\lambda_{1,\infty}+\Delta\lambda$ (plug). Eq.(3.78) is useful for $Da>20$. Alternatively, the coefficient β can be fitted obviously in a number of ways. For simplicity and with minimum numerical evaluation, the following empirical correlation for laminar flow is proposed:

$$\beta(Da)=\frac{\beta_0+\beta_\infty\,Da}{1+Da} \qquad \text{(laminar flow).} \qquad (3.79)$$

Eq.(3.79) represents numerical results of (3.76) with $n=2$, very accurately for $Da>Da_T$. Also, in laminar flow insensitivity to the channel's geometry is observed. Note that for high Da , Eq.(3.79) writes as $\beta(Da)=\beta_\infty+(\beta_0-\beta_\infty)/Da$, which is of the same form of the expansion of (3.76) for $Da\to\infty$. Eq.(3.79) is plotted in Figure 3.9b for laminar flow. It also fulfills our requirements of simple evaluation, without introducing additional parameters and avoiding fitting. From (3.77) and (3.79) with $\beta(Da_T)=3$, the value of Damköhler number which marks the transition is $Da_T=1.5$ for laminar flow, $Da_T\simeq1.6$ for plug flow between parallel plates and $Da_T\simeq2.9$ for plug flow inside a circular channel.

The variation of Θ_{fd} and Θ_{LEV} with Da and $z/\alpha\,Pe_m$ is plotted in Figure 3.10 and Figure 3.11, respectively. The weighting function of the fully developed profile Θ_{fd} changes significantly at low kinetic rates, with increasing importance as $Da\to0$, where $\Theta_{fd}\to1$ closer to the inlet. The behavior of Θ_{LEV} also changes significantly, with $Da=Da_T$ being the turning point between negative and positive values. When $\beta>3$, $-\Theta_{LEV}$ decreases as $z/\alpha\,Pe_m$ and Da increases. When $\beta<3$, Θ_{LEV} increases with Da and it approaches unity at much higher $z/\alpha\,Pe_m$ for high Da, than it does for intermediate values.

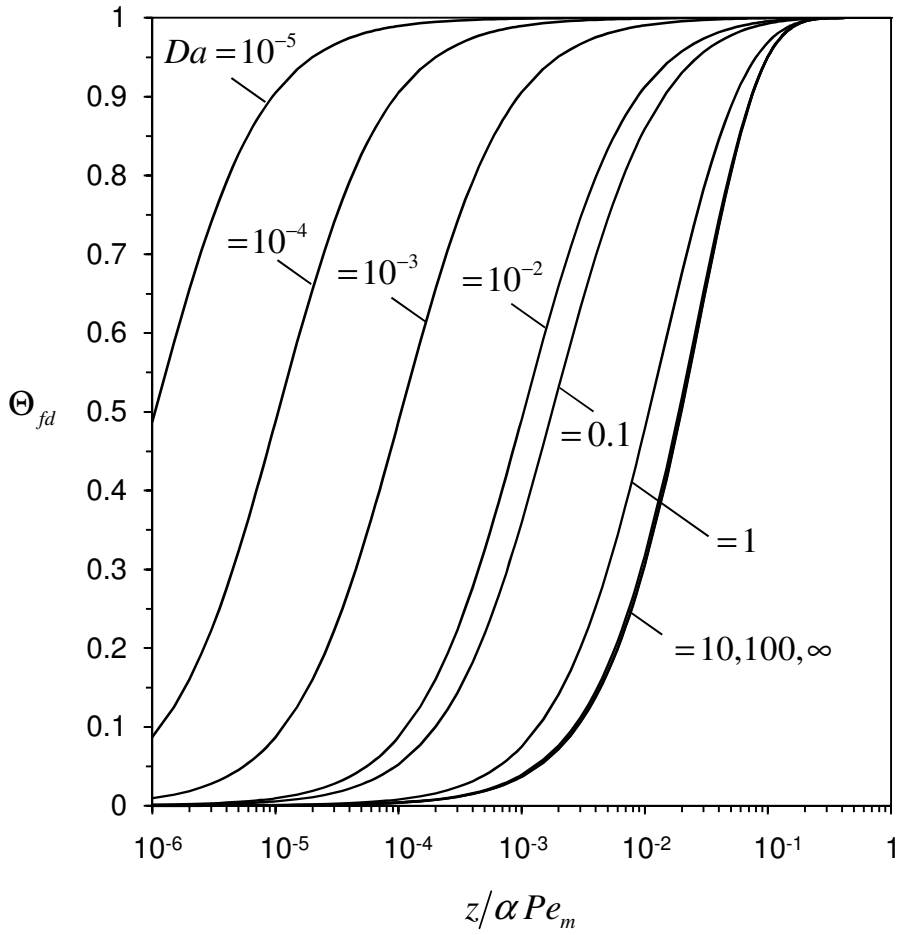

Figure 3.10: Θ_{fd} as a function of Graetz's parameter reciprocal $z/\alpha Pe_m$. Curves are plotted for several values of Da in laminar flow inside a circular channel.

3.5.2.c *Limit of* $\beta \to 3$ *(* $Da = Da_T$ *)*

At $Da = Da_T$, the conversion calculation from Eqs.(3.61) and (3.75) should be comparable with each other. This is approximately true since: $X_R \sim X_{GRAETZ}\ \Theta_{fd}$ (note that $\Theta_{LEV}(\beta = 3) \to 0$ and $-\Theta_{LEV}(\beta = 4)$ takes its lowest value). This point represents a change in the contribution from the developing profile parcel. As Da increases, a subdominant correction converts into a leading-order contribution to conversion, becoming more and more important as Da increases ($Da > Da_T$). Assuming that some correction exists at $Da = Da_T$, Eq.(3.61) should be used (with $\beta = 4$) for this value of Damköhler's parameter.

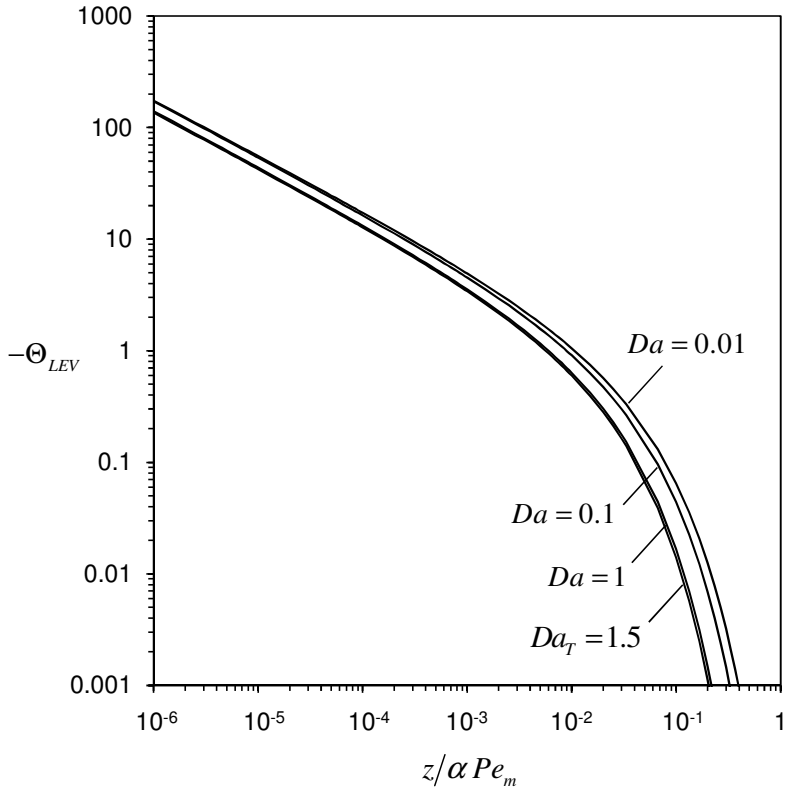

(a) $Da < Da_T$

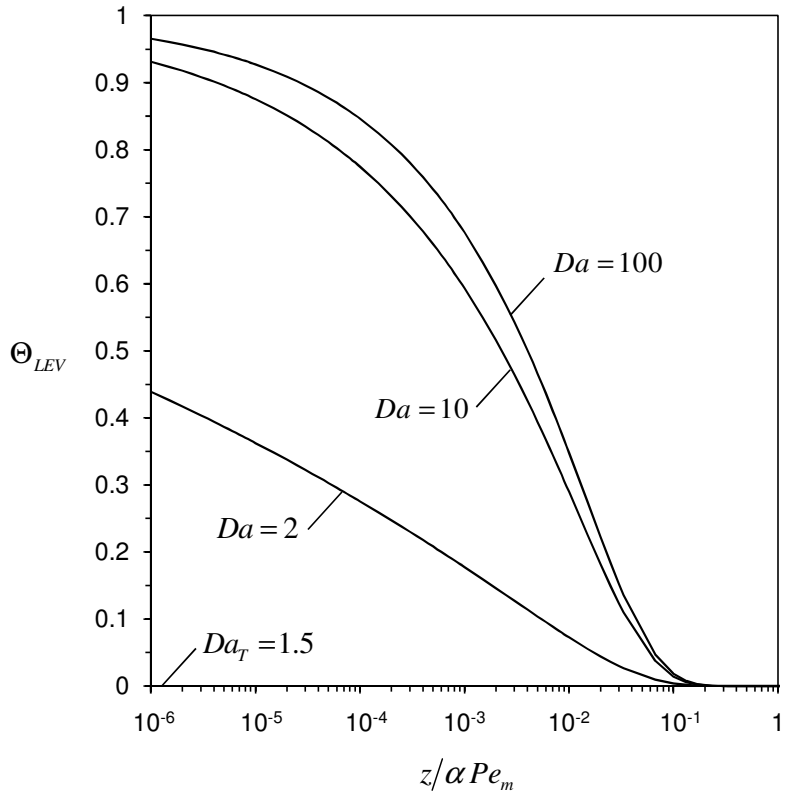

(b) $Da > Da_T$

Figure 3.11: Θ_{LEV} as a function of Damköhler and Graetz's parameters. (a) For $Da < Da_T$, where $\beta = \beta_0 = 4$. (b) For $Da > Da_T$, where $\beta(Da)$ is given by Eqs.(3.77) and (3.79).

3.5.3 Calculation procedure for the conversion profile

According to this analysis, the estimation of conversion for given values of Da and $z/\alpha\, Pe_m$ can be summarized into the following steps:

1. For a given Da, calculate w_1 and λ_1 numerically or approximately according to the results in section 3.5.1.
2. Choose a suitable value for β, according with the value of Da_T:

$$\beta = \begin{cases} \beta_0 = 4 & Da \le Da_T \\ \beta(Da) & Da > Da_T \end{cases}$$

   where $\beta(Da)$ is given by Eq.(3.77) for plug flow and by Eq.(3.79) for laminar flow.

3. The second weight w_2 and eigenvalue λ_2 can be simply calculated from step 1, using Eqs.(3.52) and (3.57) with the appropriate value of β.
4. For each value of Da and $z/\alpha\, Pe_m$, calculate Θ_{fd} and Θ_{LEV}. These functions are plotted in Figure 3.10 and in Figure 3.11 for laminar flow inside a circular channel.
5. Calculate conversion according to Eq.(3.61) for $Da \le Da_T$, and with (3.75) for $Da > Da_T$, evaluating X_{GRAETZ} and LEV or X_{LEV} with Eqs.(3.62) and (3.66) or (2.33, 2.35), respectively.

For laminar flow inside a circular channel, where a first-order heterogeneous reaction occurs, Figure 3.12 compares the uniform solution calculated as described above, with Graetz's series with 1 and 12 terms for several values of Da. The terms in Graetz's series used for comparison were calculated numerically when available (Özisik et al. 1982) or from asymptotic relationships (section 3.5.1). The $\Theta_{LEV}\, LEV$ or $\Theta_{LEV}\, X_{LEV}$ terms are also shown. It is possible to observe the increase in the importance of this term as Da increases. The consistent evolution of its magnitude legitimates our choice for the calculation at Da_T and the substitution of LEV by X_{LEV} when $Da > Da_T$. Note that this replacement allows the inlet region to be described correctly for $Da > Da_T$ (where Θ_{LEV} is not vanishingly small). The convergence of Graetz's series also gets worse as Da increases. In particular, the adequacy of the first term in the series becomes extremely limited as the reaction rate increases. The agreement of our solution increases as more terms in Graetz's series are considered, meaning that the approximate result is at least comparable with the exact solution with a reasonable number of terms which depend on numerically calculated quantities. Similar behavior for other geometries and flow profiles is observed.

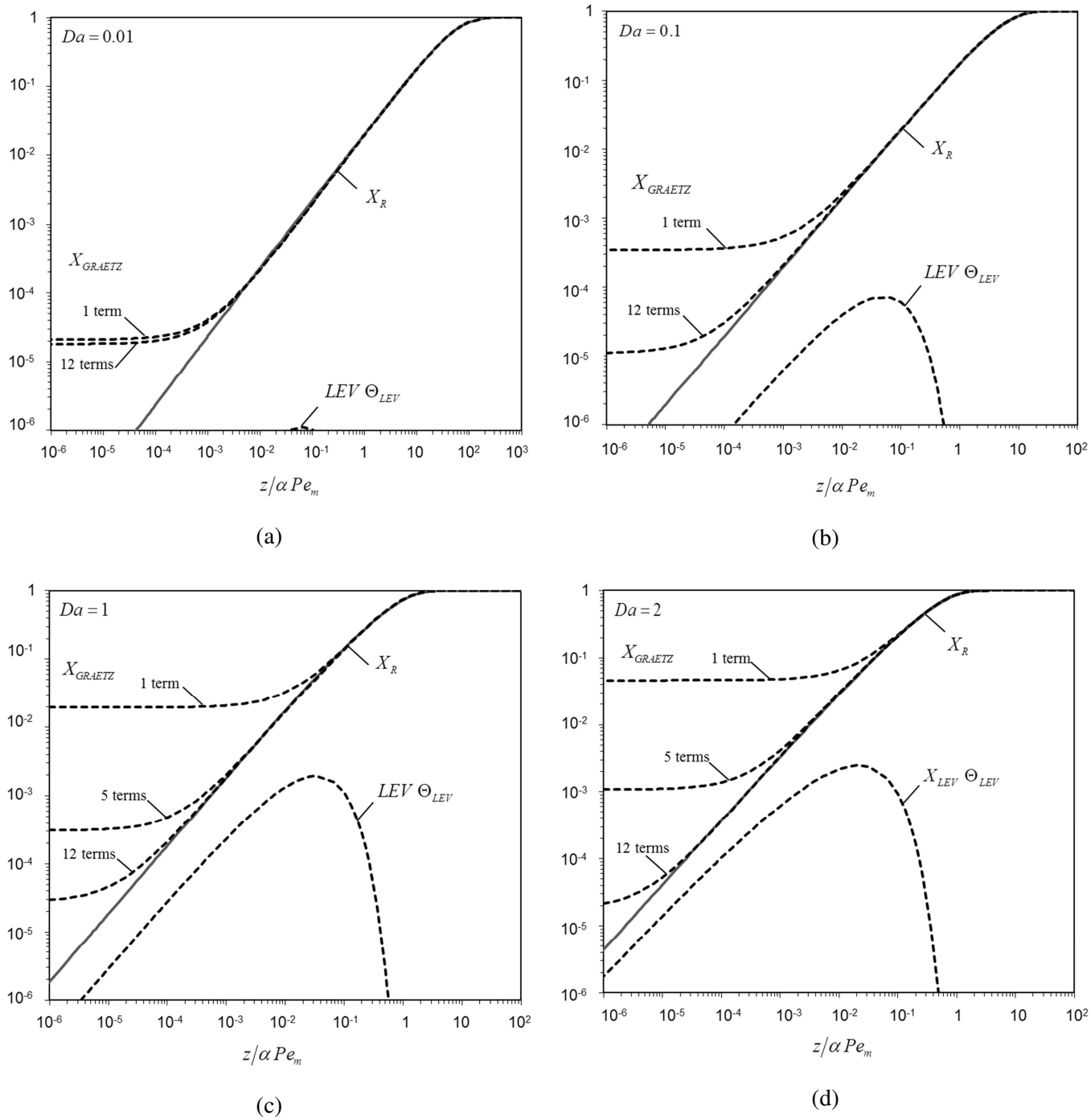

Figure 3.12: Conversion in laminar flow inside a circular channel with first-order wall reaction as a function of Graetz's parameter $z/\alpha Pe_m$ for several values of Damköhler's number Da. Graetz series solution (3.2) with 1, 5 and 12 terms is shown.

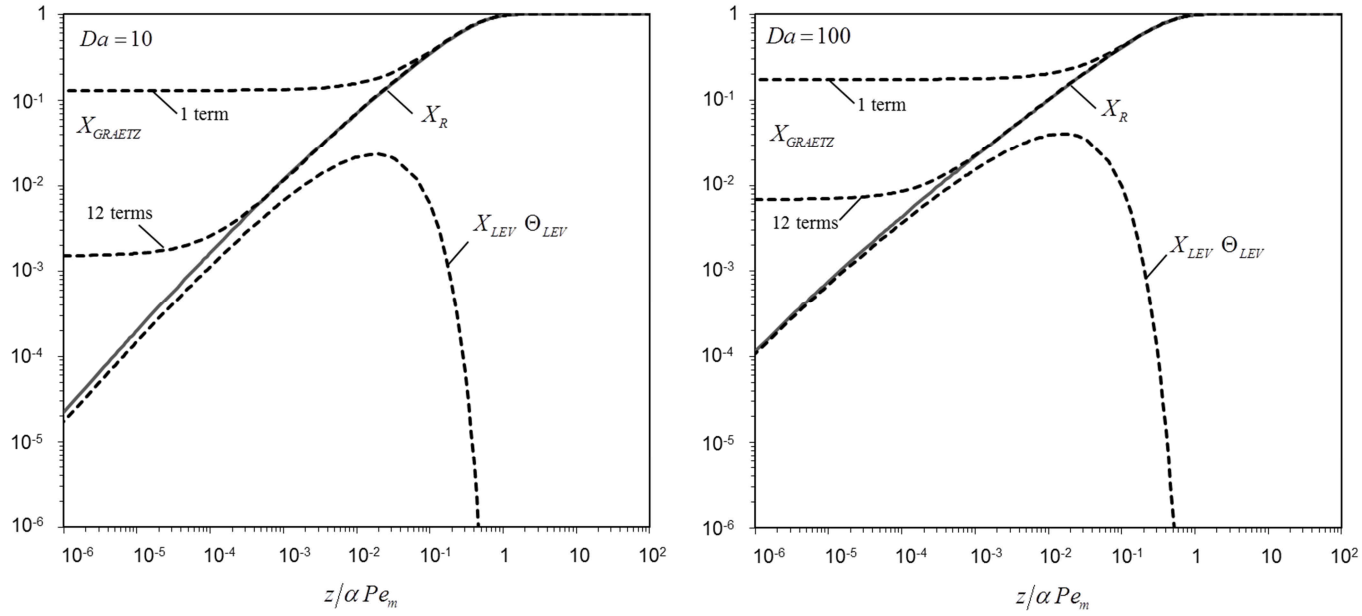

(e) (f)

Figure 3.12: Conversion in laminar flow inside a circular channel with first-order wall reaction as a function of Graetz's parameter $z/\alpha\, Pe_m$ for several values of Damköhler's number Da. Graetz series solution (3.2) with 1, 5 and 12 terms is shown.

3.5.4 Developing length of the concentration profile

By explicitly identifying the contribution from the fully developed profile (the first term in Graetz series), it is possible to estimate the length of profile development. We are particularly interested in understanding the applicability of the fully developed asymptote as $Da \to 0$. This is motivated by the fact that the results from the Neumann boundary condition in section 3.3 do not reflect several remarks that have been made in this work and in the literature. Namely,

(a) the error in estimating conversion with one term in Graetz series when $\alpha\, Pe_m/z$ increases is more significant for high values of Da (as seen in Chapter 2);

(b) at leading-order as $Da \to 0$, fully developed and Lévêque solutions coincide near the inlet (see section 3.5.2.a);

(c) Θ_{fd} (which measures the importance of the fully developed limit) reaches values close to 1 at lower $z/\alpha\, Pe_m$ when $Da \to 0$ (Figure 3.10); and

(d) Gervais and Jensen (2006) concluded that the importance of the fully developed description increases when $Da \to 0$, comparing simplified models with the numerical solution.

Moreover, it is also recognized (Gervais et al. 2006) that the critical value of Graetz's parameter at which Lévêque's model is no longer satisfactory cannot be determined from a straightforward approach when Da is finite, and that the required numerical evaluation is tedious. Nevertheless, they show that terms in Graetz series, other than the first, decay much faster for lower Da, and this results in reduction of the absolute error of the fully developed asymptote by one order-of-magnitude at the inlet.

We can make use of the degree of transverse control introduced previously and given by Eq.(3.39), which is related to the relative error of the one-term Graetz solution by Eq.(3.44). We will focus on the derivation of the profile development length (i.e. low values of φ or ε_{GRAETZ}). In the kinetic limit ($Da \to 0$), low error of the Graetz asymptote is obtained near the inlet ($z/\alpha\, Pe_m \to 0$). In these conditions, we assume $LEV\ \Theta_{LEV} << X_{GRAETZ}\ \Theta_{fd}$, and therefore:

$$\varepsilon_{GRAETZ} \sim \left|\Theta_{fd}^{-1} - 1\right| \sim Da\, \frac{\alpha\, Pe_{m,\max}}{\sigma\, z} \left(\frac{1+S}{Sh_{fd,0}}\right)^2 \tag{3.80}$$

For $z/\alpha\, Pe_m \sim O(1)$, $\varepsilon_{GRAETZ} \to 0$ faster, so Eq.(3.80) can be defined as a boundary. At the diffusional limit ($Da \to \infty$), when the fully developed solution is appropriate: $\Theta_{LEV} \to 0$ and Θ_{fd} is reasonably insensitive to kinetics as shown in Figure 3.10. Therefore, the Dirichlet limit detailed in section 3.4.1 is recovered again and the length of development is nearly insensitive to the fast kinetics:

$$\varepsilon_{GRAETZ} \sim 1 - \Theta_{fd} \sim w_{2,\infty}\, \Delta_\infty \exp\left(\frac{-\lambda_{2,\infty}^2\, z}{\alpha\, Pe_{m,\max}}\right) \sim \left(1 - w_{1,\infty}\right) \exp\left(\frac{-\lambda_{2,\infty}^2\, z}{\alpha\, Pe_{m,\max}}\right). \tag{3.81}$$

Other limits are more complex. We propose a formula that correlates both behaviours from (3.80) and (3.81) as

$$\frac{\alpha\, Pe_{m,\max}}{z} = \frac{\varepsilon_{GRAETZ}}{Da}\, \sigma\, \frac{Sh_{fd,0}^2}{(1+S)^2} + \lambda_{2,\infty}^2 \left[\ln\left(\frac{1 - w_{1,\infty}}{\varepsilon_{GRAETZ}}\right)\right]^{-1} \tag{3.82}$$

which is valid for small ε_{GRAETZ} and can be written explicitly for Da. For circular channel with laminar flow, the $Da\left(z/\alpha\, Pe_m\right)$ curves for several values of ε_{GRAETZ} are plotted in Figure 3.13. Qualitatively, this represents the expected trend even though quantitatively some adjustments may be required.

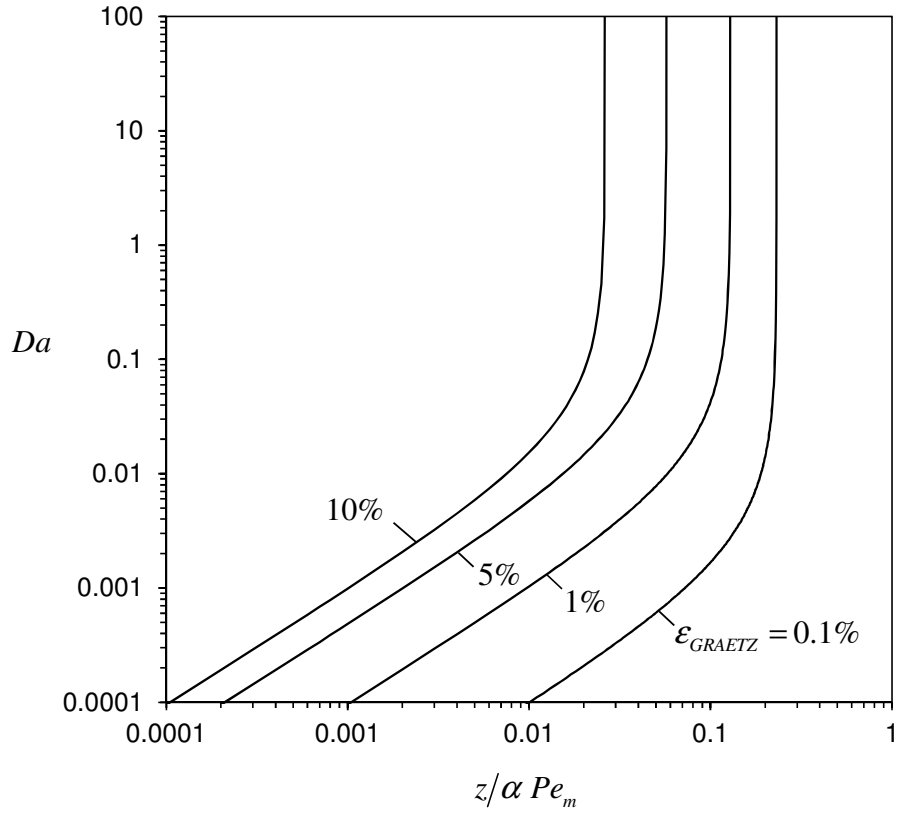

Figure 3.13: Boundaries in the $Da - z/\alpha\, Pe_m$ diagram where conversion is described by the fully developed asymptote with different relative errors. For $z/\alpha\, Pe_m$ greater than the specified in the boundaries, the relative error is reduced.

3.5.5 Other cross-sectional geometries

Concerning the effect of the channel's cross-section geometry on the previous results, we note that:

- the asymptotic predictions in section 3.5.1 using WKB theory for large eigenvalues reduce curvature effects near the channel wall to a subdominant term and the same comment holds for Lévêque's leading order solutions;
- β and its influence in the final result are nearly insensitive to the shape of a straight channel;
- the shape factors S and σ appearing in all the expressions in sections 3.5.1 and 3.5.2 can be determined by an analogy with $f\,Re$ values (Shah et al. 1978); and
- the values for w_1 and λ_1 can be calculated numerically for several known channel geometries (see references in Chapter 2).

Therefore, the analysis herein presented is likely to be extendable to other channel geometries.

3.6 CONCLUSIONS

We have derived an approximate analytical solution to Graetz's problem in terms of a combination of the fully developed and developing (Lévêque's) limits. Our solutions for the mixing-cup concentration/temperature profile or for Sherwood number, as a function of the axial distance, have the following features: (a) accurate results are obtained over the full range of the Graetz number ($\alpha\, Pe_m / z$); (b) relative error does not increase sharply in any specific range; (c) both limiting regimes are respected and the gap between them is well described; and (d) the form of the analytical solution is much simpler than any of the existing (involving a large number of terms with numerically determined coefficients) and minimum numerical evaluation is required. Mixing-cup concentrations are described with a maximum of 0.1% relative error (except for laminar flow between parallel plates, where the error is higher but still tolerable). When the wall boundary condition is of Neumann type, a solution for the Sherwood number based on adding the entrance length and fully developed terms is given. Each term has an associated weighting function, for which analytical expressions are provided. We have also extended the analysis to the case where a finite reaction rate at the wall occurred.

Finally, we define criteria for transition between regimes which reflect the relative errors obtained by using the fully developed or Lévêque solutions. Explicit expressions for the length of the profile development zone are provided as a function of a desired degree of agreement with the fully developed solution, channel geometry, flow profile and boundary condition type. Previous disperse results in the literature are framed in a common analysis. Ranges of validity for the developing profile asymptote are given, as well as estimates for the length of the transition region. The approach presented can be extended to the analysis of Graetz or other chemical engineering problems.

NOTATION

a	radius of the circular channel or half-spacing between parallel plates
A_n	n^{th} integration constant
c	bulk fluid concentration of reactant species
$\langle c \rangle$	reactant's mixing-cup concentration of the reactant species
c_{in}	inlet reactant concentration
D	bulk fluid diffusivity
d_h	hydraulic diameter
Da	Damköhler number
$f\ Re$	product of the friction factor and Reynolds number

G_n	coefficients used by Shah and London (1978)in the mixing-cup temperature profile ($= -A_n / 2\, d\,\varphi_n / d\,r\big\|_{r=1}$)
HOT	higher order terms
k_m	interphase transfer constant
L	length of the channel
Pe_m	transverse Peclet number ($= a\langle u\rangle / D$ or $= a\langle u\rangle / \kappa$)
q	exponent in Lévêque's dependence on Graetz's parameter
r	dimensionless transverse coordinate ($= \hat{r} / a$)
S	shape parameter: $=0$ for parallel plates; $=1$ for circular channel
Sh	Sherwood number
T	temperature of the fluid
$\langle T\rangle$	mixing-cup temperature of the fluid
$u(r)$	velocity profile inside the channel
$\langle u\rangle$	average velocity inside the channel
$v(r)$	dimensionless velocity profile, normalized by average velocity
X_R	conversion of reactant
w_n	n^{th} coefficient related with Shah and London's (1978) notation by $= 2\sigma G_n / \lambda_n^2$
z	dimensionless axial coordinate
$z/\alpha\, Pe_m$	reciprocal of Graetz's parameter

Greek letters

α	aspect ratio of the channel
β	coefficient in Eq.(3.57)
Δ	compensation function
$\Delta\lambda$	spacing between eigenvalues
ε	relative error
δ	thickness of the concentration/thermal boundary layer
$\Gamma(z)$	Gamma function, $\int_0^\infty t^{z-1}\, e^{-t}\, dt$
$\Gamma(a,z)$	Incomplete Gamma function, $\int_z^\infty t^{a-1}\, e^{-t}\, dt$
γ	axial contribution to terms in Graetz's solution
κ	thermal diffusivity
φ	degree of transverse transport control
φ_n	n^{th} eigenfunction
λ_n	n^{th} eigenvalues
σ	shape/flow parameter, $(S+1)u_{\max} / \langle u\rangle$

Superscript

^	dimensional quantity
‘	derivative

Subscript

fd	fully developed
In	inlet
GRAETZ	Graetz series (1 term)
LEV	Lévêque's solution
max	maximum (referred to maximum velocity)
surf	at the wall of the channel
wall	at the wall of the channel
0	in the Neumann limit
∞	in the Dirichlet limit

REFERENCES

Abramowitz, M. and I. A. Stegun (1972). Handbook of Mathematical Functions. Washington, D.C. , National Bureau of Standards

Alonso, M., F. J. Alguacil and C. H. Huang (2010). "Analytical approximation to the fully developed concentration profile of diffusive aerosol particles in laminar flow in a circular tube." Journal of Aerosol Science **41**(4): 413-417.

Aydin, O. and M. Avci (2010). "On the constant wall temperature boundary condition in internal convection heat transfer studies including viscous dissipation." International Communications in Heat and Mass Transfer **37**(5): 535-539.

Bauer, H. F. (1976). "Diffusion, convection and chemical reaction in a channel." International Journal of Heat and Mass Transfer **19**(5): 479-486.

Bender, C. M. and S. A. Orszag (1978). Advanced Mathematical Methods for Scientists and Engineers. New York, McGraw-Hill.

Brown, G. M. (1960). "Heat or mass transfer in a fluid in laminar flow in a circular or flat conduit." AIChE Journal **6**(2): 179-183.

Carslaw, H. S. and J. C. Jaeger (1959). Conduction of Heat in Solids. New York, Oxford University Press.

Gervais, T. and K. F. Jensen (2006). "Mass transport and surface reactions in microfluidic systems." Chemical Engineering Science **61**(4): 1102-1121.

Ghez, R. (1978). "Mass transport and surface reactions in Lévêque's approximation." International Journal of Heat and Mass Transfer **21**(6): 745-750.

Graetz, L. (1883). "Ueber die Wärmeleitungsfähigkeit von Flüssigkeiten." Annalen der Physik und Chemie **18**: 79-94.

Haji-Sheikh, A., J. V. Beck and D. E. Amos (2009). "Axial heat conduction effects in the entrance region of circular ducts." Heat and Mass Transfer/Waerme- und Stoffuebertragung **45**(3): 331-341.

Housiadas, C., F. E. Larrodé and Y. Drossinos (1999). "Numerical evaluation of the Graetz series." International Journal of Heat and Mass Transfer **42**(15): 3013-3017.

Kays, W. M. and M. E. Crawford (1980). Convective Heat and Mass Transfer. New York, McGraw-Hill.

Kockmann, N. (2008). Transport Phenomena in Micro Process Engineering. Berlin, Springer-Verlag.

Kreutzer, M. T., F. Kapteijn and J. A. Moulijn (2006). "Shouldn't catalysts shape up? Structured reactors in general and gas-liquid monolith reactors in particular." Catalysis Today **111**(1-2): 111-118.

Lévêque, M. A. (1928). "Les lois de la transmission de chaleur par convection." Ann. Mines **13**: 201-299.

Morini, G. L. (2006). "Scaling effects for liquid flows in microchannels." Heat Transfer Engineering **27**(4): 64-73.

Newman, J. (1969). "Extension of the Leveque solution." Journal of Heat Transfer **91**(1): 177-178.

Newman, J. (1973a). The Graetz problem. The Fundamental Principles of Current Distribution and Mass Transport in Electrochemical Cells. A. J. Bard. New York, Dekker. **6:** 187-352.

Newman, J. S. (1973b). Electrochemical Systems. Englewood Cliffs, N.J., Prentice-Hall, Inc.

Nusselt, W. (1910). "Die Abhängigkeit der Wärmeübergangszahl von der Rohrlänge." Zeitschrift des Vereines deutscher Ingenieure **54**: 1154-1158.

Özisik, M. N. and M. S. Sadeghipour (1982). "Analytic solution for the eigenvalues and coefficients of the graetz problem with third kind boundary condition." International Journal of Heat and Mass Transfer **25**(5): 736-739.

Polyanin, A. D., A. M. Kutepov, A. V. Vyazmin and D. A. Kazenin (2002). Hydrodynamics, mass and heat transfer in chemical engineering. London, Taylor & Francis.

Ray, S. and D. Misra (2010). "Laminar fully developed flow through square and equilateral triangular ducts with rounded corners subjected to H1 and H2 boundary conditions." International Journal of Thermal Sciences **49**(9): 1763-1775.

Rice, R. G. and D. D. Do (1995). Applied Mathematics and Modeling for Chemical Engineers. New York, John Wiley & Sons.

Rosa, P., T. G. Karayiannis and M. W. Collins (2009). "Single-phase heat transfer in microchannels: The importance of scaling effects." Applied Thermal Engineering **29**(17-18): 3447-3468.

Sellars, J., M. Tribus and J. Klein (1956). "Heat transfer to laminar flow in a round tube or flat conduit - The Graetz problem extended." ASME Transactions **78**: 441-448.

Shah, R. K. and A. L. London (1978). Laminar flow forced convection in ducts. New York, Academic Press.

Siegel, R., E. M. Sparrow and T. M. Hallman (1958). "Steady laminar heat transfer in a circular tube with prescribed wall heat flux." Applied Scientific Research **7**: 386-392.

Vera, M. and A. Liñán (2011). "Exact solution for the conjugate fluid-fluid problem in the thermal entrance region of laminar counterflow heat exchangers." International Journal of Heat and Mass Transfer **54**(1-3): 490-499.

Weigand, B. (2004). Analytical Methods for Heat Transfer and Fluid Flow Problems Berlin, Springer.

Weigand, B. and G. Gassner (2007). "The effect of wall conduction for the extended Graetz problem for laminar and turbulent channel flows." International Journal of Heat and Mass Transfer **50**(5-6): 1097-1105.

Worsoe-Schmidt, P. M. (1967). "Heat transfer in the thermal entrance region of circular tubes and annular passages with fully developed laminar flow." International Journal of Heat and Mass Transfer **10**: 541-551.

Yoon, S. K., G. W. Fichtl and P. J. A. Kenis (2006). "Active control of the depletion boundary layers in microfluidic electrochemical reactors." Lab on a Chip - Miniaturisation for Chemistry and Biology **6**(12): 1516-1524.

CHAPTER

FOUR

CRITERIA FOR KINETIC AND MASS TRANSFER CONTROL IN A WALL-COATED MICROREACTOR

Analytical expressions for distinguishing between different reaction and mass transport regimes in an isothermal microchannel reactor with first-order wall reaction are presented in this chapter. These expressions are explicit functions of the Damköhler number (Da) and of the Graetz parameter ($\alpha Pe_m/z$), as well as of the degree of mass transport control (θ) which is usually set arbitrarily. The power law addition of contributions from fully developed and developing concentration profile conditions allows a correct description for all values of $\alpha Pe_m/z$.

As we will see, the scaling analysis suggests that the relative importance of mass transfer effects compared to reaction should be assessed by the *rescaled Damköhler number* Da^*, defined with the correct scales for external and internal diffusion. It is also shown that a $Da-\alpha Pe_m/z$ parametric map is appropriate for identifying the boundaries between regimes, which can be directly calculated from the dimensionless parameters in a very convenient manner.

4.1 INTRODUCTION

Coated-wall microchannel reactors have been put forward as a promising design concept (Jensen 2001; Kreutzer et al. 2006; Rebrov et al. 2009) for technologies related with energy generation (Casanovas et al. 2009; Karakaya et al. 2009; Avci et al. 2010; Jang et al. 2010; Snytnikov et al. 2010; Karakaya et al. 2011), biocatalysis (Thomsen et al. 2009), systems with strict safety requirements (Inoue et al. 2007) or environmental applications (Hernández Carucci et al. 2009) (see Chapter 1 for additional references). As we have pointed out, attaching a catalytic coating to the walls of the channel provides significant higher accessible surface area without increasing pressure drop. Moreover the benefits from miniaturization, such as

* The contents of this chapter are partially based on J. Lopes, S. Cardoso and A. Rodrigues (2011), Chemical Engineering Journal, DOI: 10.1016/j.cej.2011.05.088

enhancement of transfer rates and nearly isothermal behaviour, are also observed. However, the introduction of the catalyst may lead to the appearance of external (as well as internal) mass transfer limitations.

As detailed in Chapter 1, working on the microscale (channels with diameters in the order of $a \sim 100\,\mu m$) privileges surface effects (such as an heterogeneous reaction) over homogenous processes dependent on the channel volume. In the analysis of the competition between surface reaction and transport towards the catalytic surface, two limiting regimes are usually identified by the chemical reaction engineering community (Tronconi et al. 1992; Hayes et al. 1994; Heck et al. 2001; Balakotaiah et al. 2002): the kinetically controlled regime (when reaction is slow compared to radial mass transport) and the mass transfer controlled regime (when reaction is comparatively fast). The definition of operating regimes is of extreme importance for almost all studies involving catalytic monoliths or microchannel reactors. For example,

1. *measurement of intrinsic kinetic parameters*: the presence of significant radial concentration gradients makes it impossible to measure directly the intrinsic activity and selectivity of the catalytic layer (Berger et al. 2007). To be certified that mass transfer and kinetics are independently evaluated, a number of methods are available (Bennett et al. 1991; Hayes et al. 1995; Beretta et al. 1999; Kölbl et al. 2004; Pfeifer et al. 2005; Walter et al. 2005), involving a selective enhancement of mass transfer or reaction rates;
2. *measurement of mass transfer parameters*: at high temperatures, when the different mass transfer resistances must be accounted for, the evaluation of transport parameters may lead to inconsistent results if wall concentration annulment is incorrectly assumed (Votruba et al. 1975; Bennett et al. 1991; Ullah et al. 1992; Hayes et al. 1994; Uberoi et al. 1996). This has led to controversy in literature, where observed Sherwood numbers were lower than the theoretical minimum due to failing in accounting for finite wall reaction rates;
3. *design of the microreactor and choice of operating conditions*: the geometric and operating parameters are included in the dimensionless numbers of the model and must be chosen so that the required performance is achieved. The change in operating conditions may lead to a change in the regime, which might take conversion to follow a different asymptote;
4. *appropriate selection of models for simulation and optimization*: the assumption that for a sufficiently high inlet temperature, the whole microchannel operates in mass transfer control has given origin to analyses (e.g. Balakotaiah et al. (2002)) whose validity must be checked. Since the asymptotic behaviour of the quantities involved in estimating conversion is accurately known in the kinetic and mass transfer controlled limits, it is important to understand when these simplified solutions can be safely used.

It is clear that criteria for kinetic and mass transfer control are desirable, especially if they can be evaluated a priori and without the need for numerical evaluation. The objectives of this chapter are: (a) to identify the different regimes of operation based on the length scales over which the different mass transfer mechanisms dominate and their relationship with the

characteristic time for wall reaction; (b) to discuss criteria for distinguishing between those regimes in limiting cases and provide uniformly valid correlations; and finally (c) plot these results on a parametric map and compare them with existing alternatives in the literature.

4.2 SCALING AND OPERATING REGIMES DEFINITION

We consider the two-dimensional convection-diffusion problem described earlier (section 2.2.1), in the geometry represented in Figures 2.1 and 3.1. The complete description of mass transport includes diffusion in both directions (Eqs.(2.1)). In this case, the problem of determining the species (reactant) concentration distribution under several wall boundary conditions is known as the extended Graetz problem (Papoutsakis et al. 1980a; Papoutsakis et al. 1980b; Polyanin et al. 2002). However, in many practical parameter ranges, the full solution is unnecessary and simplification in appropriate regimes may be sought. These particular regimes are defined assuming that the physical situation is mainly due to the balancing of two out of the three original terms in the mass conservation equation, in geometries such as parallel plates or circular channels. It is also conceivable that one term is solely dominant at a global scale, while a richer structure is only necessary to describe events at a local scale (Bender et al. 1978).

4.2.1 Global scale regimes

When appreciable concentration change ($\Delta \hat{c} \sim O(\hat{c}_{in})$) occurs over the length of the channel L and over the maximum transverse distance a, the relative magnitude of the characteristic time for transport by axial diffusion ($\tau_{axial,diff} = L^2/D$) compared to the one by transverse diffusion ($\tau_{transv,diff} = a^2/D$) is related to the channel's aspect ratio:

$$\alpha^2 = \left(\frac{a}{L}\right)^2 . \tag{4.1}$$

Timescales for both transport processes in the axial direction are compared by

$$\frac{\alpha}{Pe_m} = \frac{D}{L\langle u\rangle} = \frac{\tau_{conv}}{\tau_{axial,diff}} . \tag{4.2}$$

This implies that concentration gradients in the axial and radial directions are correctly nondimensionalized by the natural scales for concentration and length (i.e. $\partial \hat{c}/\partial \hat{z} \sim \hat{c}_{in}/L$ and $\partial \hat{c}/\partial \hat{r} \sim \hat{c}_{in}/a$), as well as the second derivatives ($\partial^2 \hat{c}/\partial \hat{z}^2 \sim \hat{c}_{in}/L^2$ and $\partial^2 \hat{c}/\partial \hat{r}^2 \sim \hat{c}_{in}/a^2$).

From this straightforward scaling analysis, axial diffusion becomes subdominant in the outer governing equations (2.1), whenever long microchannels ($\alpha << 1$) and/or high axial Peclet number regimes ($Pe_{ax} = Pe_m/\alpha >> 1$) are encountered. Our analysis applies in these conditions and therefore this mechanism is considered negligible. For typical dimensions of a laboratory scale monolith / microreactor ($a \sim 100\,\mu\text{m}$, $L \sim 10\,cm$) with a gas-phase process ($D \sim 10^{-4}\ m^2/s$): $\alpha \sim 0.001$ and $\tau_{trans,diff} \sim 0.1\,ms$. The timescales for convection and reaction can vary significantly with operating conditions (e.g. $\tau_{conv} \sim 10\,ms$ when $\langle u \rangle = 1\,m/s$) and catalyst properties (loading, distribution…), respectively. Thus, although α is small, the remaining parameters can cover a broad range of values.

At global scales, the remaining processes are compared by the transverse Peclet number multiplied by the aspect ratio (whose magnitude regulates the convective-diffusive dominant balance) and by the Damköhler number which translates the competition between transport towards the wall and surface reaction. These dimensionless numbers are defined as:

$$\alpha\, Pe_m = \frac{\langle u \rangle a^2}{L\, D} = \frac{\tau_{transv,diff}}{\tau_{conv}} \tag{4.3a}$$

$$Pe_m = \frac{\langle u \rangle a}{D} = Re_a\, Sc \tag{4.3b}$$

$$Da = \frac{a\, k_{surf}\, \eta}{D}, \tag{4.4}$$

where $Re_a = \langle u \rangle a\rho/\mu$ is the Reynolds number and $Sc = \mu/(\rho D)$ is the Schmidt number. The presence of the catalytic coating is accounted for by including the effectiveness factor (η), as usual. The definition of global scale regimes is readily obtained from the mass balance equation (2.1) in the channel domain when the spatial independent variables are normalized by their respective maximum values ($z = \hat{z}/L$ and $r = \hat{r}/a$ in the axial and transverse direction, respectively). Then, convection and transverse diffusion (*Graetz's regime*) balance when $\alpha Pe_m \sim 1 >> \alpha^2$. If in addition we consider one mechanism dominance regimes at global scale, convection is dominant (*Lévêque's regime*) when $\alpha Pe_m >> \alpha^2, 1$; while fast transverse diffusion occurs for $\alpha^2, \alpha Pe_m << 1$. We note that the solutions from these problems are included in the more complete Graetz regime. Nevertheless, the simplified limits they give origin to can be useful. For example, the series solution of the Graetz problem (1883) includes the results from Lévêque's analysis (1928) if an infinite number of terms were to be retained. On the other hand, approximate one-term truncated results are often used, which are also a reduction of the convection-transverse diffusion dominated case. The *one-term Graetz series regime* (for $z/\alpha Pe_m >> 1$) yields the fully developed concentration profile.

All these regimes are defined based on the magnitude of the quantities defined in Eqs.(4.3a) and (4.4). These two parameters define an $\alpha Pe_m - Da$ operating map, which we will later present. Actually, if a variable axial length scale is adopted, the behaviour at global transverse scale depends on the Graetz parameter, $\alpha Pe_m / z$.

4.2.2 Local scale regimes

Regimes that neglect transverse diffusion at first approximation are not able to fulfil one or more boundary conditions in this direction. This is usually accompanied by the appearance of a boundary layer around one endpoint of the domain, with thickness much smaller than the global scale adopted to normalize position in this direction. The behaviour in these inner regions is described by Eqs.(2.26), which are obtained once the independent variable is stretched as $R = (r_0 \mp r)/\delta_R$, where r_0 is the endpoint near where the boundary layer develops with thickness $\delta_R << 1$ ($R > 0$). This new variable rescales the derivatives on the original mass balance equations correctly, and therefore sharp concentration variation of $O(\hat{c}_{in})$ over the inner layer thickness is typical. Given the symmetry condition at $r = 0$, we can exclude the appearance of local regions near this point. In fact, only at $r_0 = 1$ it is possible to obtain a distinguished limit. The contributions of curvature in a circular channel or nonlinear velocity profile in laminar flows are of $O(\delta_R)$ and $O(\delta_R^2)$ respectively, and therefore negligible in transverse inner regions at first approximation (see section 2.3.1).

When convection dominates at the outer scale (*Lévêque's regime*), concentration decay occurs near the wall, where transverse diffusion is required to become important if significant reactant consumption occurs. This is translated into the following scaling relationship:

$$\alpha Pe_m \, \delta_R^2 \, |v(R)| \sim 1 >> (\alpha \, \delta_R)^2 ,$$

where the scale $|v(R)|$ is taken from the linearized velocity profile near the wall

$$v(R) = \frac{u(R)}{\langle u \rangle} \sim \begin{cases} (S+3)\,\delta_R \, R & \text{laminar flow} \\ 1 & \text{plug-flow} \end{cases}$$

with $S = 0$ for parallel plates; $S = 1$ for a circular channel. Therefore, the characteristic length scale of the inner layer is $\delta_R \sim (\alpha Pe_m)^{-1/2}$ for plug flow and $\delta_R \sim \left[(S+3)\,\alpha Pe_m\right]^{-1/3}$ for laminar flow.

The natural scale a is correct for making the governing equations dimensionless if the maximum concentration variation occurs over the maximum transverse distance in the channel

$\left(\partial \hat{c}/\partial \hat{r} \sim \hat{c}_{in}/a\right)$. However, when transverse boundary layers occur (e.g. in the convective limit, $\alpha\, Pe_m >> 1$), concentration variation occurs over a length scale that can be much smaller than the channel radius, while for $\alpha\, Pe_m \sim O(1)$, $\delta_R \sim O(1)$. So, in general, the characteristic length for diffusion in the channel's transverse direction is $\ell_{channel} \sim a\,\delta_R$.

4.2.3 Interphase mass transport - wall reaction regimes

The flux continuity condition is responsible for the coupling of the channel and catalytic coating domains. Introducing the effectiveness factor concept (that averages the reaction-diffusion processes in the coating):

$$\left.\frac{\partial c}{\partial r}\right|_{r=1} = -Da\, c(1,z) \qquad \text{(slab and annular geometry)} \qquad (2.4)$$

where Da is given by Eq.(4.4). This has been recognised previously in the literature (Keyser et al. 1991; Bhattacharya et al. 2004; Hayes et al. 2004). However, a fair comparison between the fluxes at both sides of the interface requires rescaling of Eq.(2.4)), when concentration boundary layers near the interface appear. In that case, Eq.(2.4) writes as

$$\left.\frac{\partial c}{\partial R}\right|_{R=0} = Da\,\delta_R\, c(1,z), \qquad (4.5)$$

with $R = (1-r)/\delta_R$. The parameter group that defines different operating regimes can be rewritten as a *rescaled Damköhler number* ($Da^* = Da\,\delta_R$), which can be understood as an "effective" quantity:

$$Da^* = \frac{\ell_{channel}\, k_{surf,obs}}{D} = \frac{(a\,\delta_R)(k_{surf}\,\eta)}{D}, \qquad (4.6a)$$

where the characteristic dimension and the reaction constant in the original definition are corrected by the presence of external and internal mass transfer limitations, respectively. On the other hand, it can be seen as the original parameter simply referred to a different length scale,

$$Da^* = \frac{k\,\ell^2}{D} = \frac{k\,\ell_{channel}\,\ell_{coating}}{D} = \frac{\tau^*_{transv,diff}}{\tau_{rxn}} \qquad (4.7b)$$

where $\ell = \sqrt{\ell_{channel}\,\ell_{coating}}$ is the geometric mean between diffusion characteristic lengths at the channel ($\ell_{channel} = a\,\delta_R$) and washcoat ($\ell_{coating} = \eta\, V_{coat}/S_{ext}$) and not simply a^2 (the maximum distance for diffusion in the channel).

The rescaled Damköhler number Da^* can act as a "wall-reaction model" constant in Robin's boundary condition, which can assume different forms at leading order:

$Da^* << 1$, Neumann type boundary condition (i.e. $\partial c/\partial r\big|_{r=1} = 0$) (4.8)

$Da^* \sim 1$, Robin type boundary condition (i.e. $\partial c/\partial R\big|_{r=1} = -Da^* c(1,z)$) (4.9)

$Da^* >> 1$, Dirichlet type boundary condition (i.e. $c(1,z) = 0$) (4.10)

As Da^* increases, the boundary condition type moves from Neumann to Robin and for high Damköhler number to Dirichlet type, i.e. from impermeable interface (Eq. (4.8)) to wall-reaction model boundary condition (4.9) and finally to instantaneous reaction at the washcoat interface (Eq. (4.10)). These regimes reproduce the two classical limiting situations concerning the competition between the effective reaction rate at the wall (eventually lumping internal reaction and diffusion in the catalytic coating) and mass transport in the channel:

- (external) *kinetic regime*, where the concentration profile is essentially uniform in the transverse direction (and close to the inlet concentration value), and
- (external) *mass transfer controlled regime*, where appreciable decay of concentration is observed from the centre of the channel to the value at the wall (which is close to zero).

Naturally, a transition regime between both limits is also present, generically described by Eq.(4.9). Figure 4.1 shows the concentration profile in the limits of fully developed (one-term from Graetz's series solution) and developing (Lévêque's) conditions for several values of Da and Da^*, respectively.

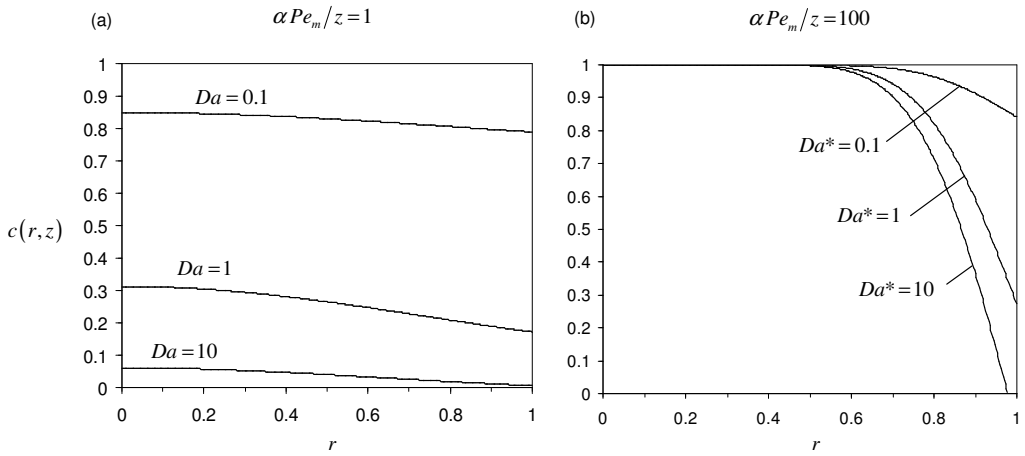

Figure 4.1: Transverse concentration profile for several values of the wall-reaction constant, Da^*. (a) Fully developed concentration profile, $Da^* = Da$. (b) Developing concentration profile, $Da^* = Da\,\delta_R$ with $\delta_R \sim (\alpha Pe_m)^{-1/2}$ for plug flow and $\delta_R \sim \left[(S+3)\,\alpha Pe_m\right]^{-1/3}$ for laminar flow ($S = 0$ for parallel plates; $S = 1$ for circular channel). The results were obtained with gPROMS® for laminar flow inside a circular duct.

4.3 DEGREE OF EXTERNAL MASS TRANSPORT LIMITATION

Delimiting boundaries between the regimes defined above in the parametric map involves establishing a rather arbitrary numerical criterion for the *degree of mass transfer control*. It is convenient to express it as the driving force for transverse transport normalized by its maximum value (the mixing-cup concentration alone):

$$\theta(z)=\frac{\langle c\rangle(z)-c(1,z)}{\langle c\rangle(z)}. \tag{4.11}$$

This measure of the decrease of reactant concentration across the transverse direction is bounded between the cases of complete kinetic or mass transfer control. In particular, when the wall reaction is slow compared to transverse transport, $\langle c\rangle(z)\to c(1,z)$ with $\langle c\rangle(z)$ finite, and $\theta=0$. If complete consumption of reactant occurs near the wall ($c(1,z)\to 0$), then $\theta=1$. Once convenient approximations for the mixing-cup and surface concentrations are provided, iso-θ lines of the form $Da=Da(\alpha\, Pe_m/z,\theta)$ can be drawn in the $\alpha\, Pe_m/z-Da$ plot.

According to Graetz's complete solution (Graetz 1883), Eq.(4.11) writes as

$$\theta=1-\frac{\displaystyle\sum_{n=1}^{\infty}A_n\,\varphi_n(1)\exp\left(-\frac{\lambda_n^2\,z}{\alpha\, Pe_{m,\max}}\right)}{\displaystyle\sum_{n=1}^{\infty}\frac{-\varphi'_n(1)\,A_n}{\lambda_n^2/\sigma}\exp\left(-\frac{\lambda_n^2\,z}{\alpha\, Pe_{m,\max}}\right)} \tag{4.12}$$

where A_n are integration constants and λ_n^2 are the eigenvalues associated with the n^{th} eigenfunction $\varphi_n(r)$, which also appears evaluated at $r=1$, as well as its derivative $\varphi'_n(1)$. Without any further simplification, it is not possible to obtain an explicit relationship between $z/\alpha\, Pe_m$ and Da (which is implicitly present through complex dependences of A_n and λ_n^2, for Robin boundary condition). Moreover, in this diagram the Dirichlet limit represents only the limiting trend at $Da\to\infty$.

4.3.1 Fully developed concentration profile

The simplest result that can be extracted from Eq.(4.12) corresponds to *fully developed concentration profile* conditions, i.e. retaining only one term in the numerator and denominator.

This is equivalent to the one-term Graetz regime discussed previously, and the results in this section are valid for values of $z/\alpha Pe_m$ greater than the transition values in Table 4.1 or in the regions defined in Chapter 3. Since $c_{surf}/\langle c \rangle$ is independent of the Graetz number (i.e. of the duct length) in this limit, θ depends only on Da for fully developed profile.

4.3.1.a *Fully developed conversion profile for linear kinetics*

As we have discussed in Chapter 2, the mixing-cup concentration profile is given by Eq.(2.11), where the first eigenvalue λ_1 is a function of Da, and this dependence is described by (2.14):

$$\lambda_1^2 = \frac{Da\,\sigma}{1 + Da\,\sigma/\lambda_{1,\infty}^2}, \tag{2.14}$$

where we recall that:

$$\sigma = \frac{u_{\max}}{\langle u \rangle}(S+1) \tag{4.13a}$$

$$S = \begin{cases} 0, & \text{parallel plates} \\ 1, & \text{circular channel} \end{cases}, \text{ and} \tag{4.13b}$$

$$u_{\max}/\langle u \rangle = (S+3)/2 \text{ for laminar flow.} \tag{4.13c}$$

The Dirichlet values $\lambda_{1,\infty}^2$ and $w_{1,\infty}$ are known and tabulated, even though approximate analytical calculation is also possible (Chapter 2).

Concerning the asymptotic behavior of eigenvalues, the following limiting expressions add an extra term to the leading-order result implicit in Eq.(2.14):

$$\lambda_1^2 = \sigma\,Da - \sigma\,b\,Da^2 + O(Da^3) \qquad \text{for } Da << 1 \tag{4.14a}$$

$$\lambda_1^2 = \lambda_{1,\infty}^2 \left(\frac{Da}{1+Da} \right)^2 \qquad \text{for } Da >> 1. \tag{4.14b}$$

These expressions were obtained from expansion in appropriate limits of Bessel functions $J_k(x)$ and confluent hypergeometric functions $M(a,b,z)$. The coefficient in Eq.(4.14a) is given here as a function of the shape parameter S (defined in Eq.(4.13b)):

$$b = \frac{1}{3+S} \qquad \text{(plug flow)} \tag{4.15a}$$

$$b = \frac{9}{S+7} - \frac{4}{S+5} \qquad \text{(laminar flow).} \tag{4.15b}$$

Note that this relates to Eq.(3.55), where $b = (1+S)/Sh_{fd,0}$.

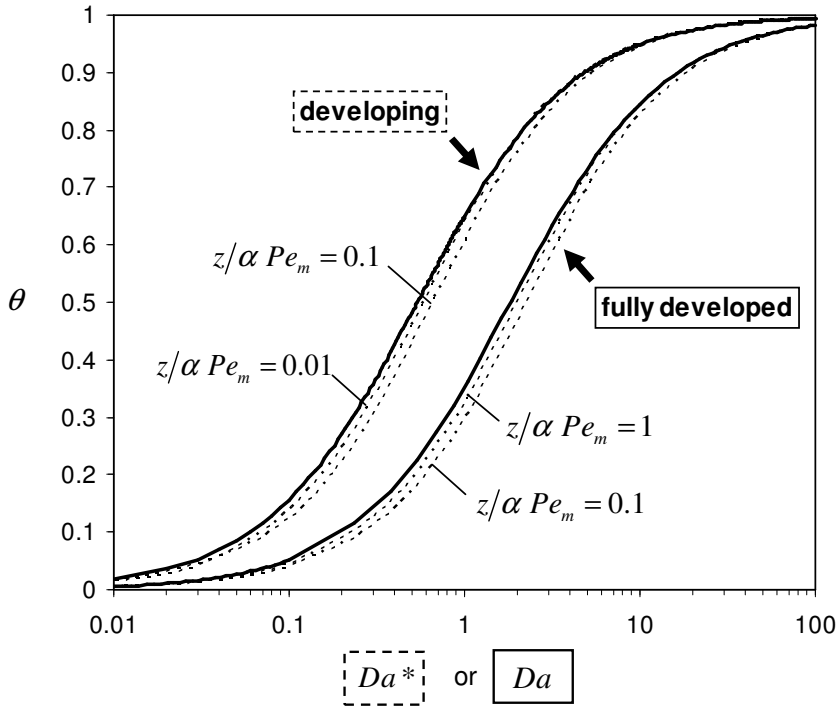

Figure 4.2: Degree of mass transfer control (θ). Analytical boundaries for the cases of fully developed and developing concentration profile (full lines) are given by Eqs.(4.18) and (4.22). Numerical results for finite values of $z/\alpha\, Pe_m$ are given by the dashed lines. The curves corresponding to developing profile are plotted as a function of the rescaled Damköhler number (axial position dependent), Da^*, given by Eq.(4.20). The curves for fully developed profile are plotted in terms of the Damköhler number, Da (not position dependent). This example refers to laminar flow inside a circular channel with small aspect ratio.

Table 4.1: Values of coefficients in Eqs.(4.17) for both flow profiles and geometries and respective concentration profile entry length.

Geometry	Flow profile	b	$\lambda_{1,\infty}^2/\sigma$	$z/\alpha\, Pe_m$	
				Kinetic control	Mass transfer control
Plates	Plug	1/3	2.4674	0.0873	0.0523
	Laminar	17/35	1.8853	0.0948	0.0699
Circular channel	Plug	1/4	2.8915	0.0491	0.0381
	Laminar	11/24	1.8283	0.1063	0.1021

4.3.1.b *Degree of mass transfer control in a fully developed concentration profile*

In this limit, Eq.(4.12) reduces to

$$Da = \frac{\lambda_1^2}{\sigma(1-\theta)}. \tag{4.16}$$

For a first-order wall reaction, the previous approximations to the first eigenvalue given by Eqs.(4.14) can be used to obtain:

$$\theta = b\,Da \qquad \text{(kinetic control, } Da \to 0\text{)} \tag{4.17a}$$

$$\theta = 1 - \frac{\lambda_{1,\infty}^2}{\sigma}\frac{Da}{(1+Da)^2} \sim 1 - \frac{\lambda_{1,\infty}^2}{\sigma\,Da} \qquad \text{(mass transfer control, } Da \to \infty\text{).} \tag{4.17b}$$

The degree of mass transfer control changes from $\theta \sim Da$ in kinetic control to $\theta \sim 1 - 1/Da$ in the mass transfer controlled regime. For delimitation of the two main regimes, the limits of $\theta \to 0$ and $\theta \to 1$ are enough, however for all values of Da the boundaries can be evaluated by

$$Da \sim \frac{\lambda_{1,\infty}^2}{\sigma}\left(\frac{\theta}{1-\theta}\right), \tag{4.18}$$

once the approximate uniformly valid dependence given by Eq.(2.14) is used. Obviously, this is a very simple empirical correlation which respects the limiting trends, but is more exact in the mass transfer controlled limit, as more information from Eq.(4.17b) is present. When $Da \to 0$, the coefficient should correct to $1/b$. Nevertheless, $\lambda_{1,\infty}^2/\sigma \sim 1/b \sim O(1)$ for the geometries and velocity profiles studied as can be seen in Table 4.1. Comparing the values for the coefficients in the previous criteria, we can see that for the same θ, the possible Da values are bounded between laminar (lower limit) and plug (upper limit) flows.

For $Da \sim 1$ the correlation in (4.18) reasonably describes numerical results. In Figure 4.2, the set of curves corresponding to fully developed conditions include correlation (4.18) (full line) and numerically calculated results with gPROMS® (dashed lines) for laminar flow inside a circular channel. The values of θ are plotted as a function of Da for two values of the Graetz parameter. Increasing $z/\alpha Pe_m$ (>0.1) improves the agreement with Eq.(4.18) as the profile becomes more developed. In the kinetic controlled limit, this criterion is slightly conservative.

4.3.2 Developing concentration profile

When $\alpha Pe_m / z >> 1$, Lévêque's solution must be used to approximate the concentration profile as described in previous sections. The minimum values of the Graetz parameter for which the following results apply are presented in Table 4.1 and are derived in section 4.3.2.c.

4.3.2.a *Degree of mass transfer control when the profile is developing*

For first-order wall reaction, exact as well as approximate solutions have been presented (Chapter 2). When reaction kinetics is the rate limiting step, the results for surface and mixing-cup concentration in the limit of small Da are introduced into Eq.(4.11) to yield

$$\theta(z) \sim \frac{2}{\sqrt{\pi}} \sqrt{\frac{z}{\alpha\, Pe_m}}\, Da \sim 1.1284\, Da^* \qquad \text{(plug-flow, } Da^* \to 0\text{)} \qquad (4.19a)$$

$$\theta(z) \sim \frac{3^{2/3}}{\Gamma(2/3)} Da \left(\frac{z}{2\,\alpha\, Pe_{m,\max}} \right)^{1/3} \sim 1.5361\, Da^* \qquad \text{(laminar flow, } Da^* \to 0\text{).} \qquad (4.19b)$$

Note that in Eqs.(4.19) we have defined the rescaled Damköhler number in terms of a variable axial length scale $\hat{z}$ ($z = \hat{z}/L$):

$$Da^* = Da \left(\frac{z}{\alpha\, Pe_m} \right)^q \qquad \text{(plug-flow)} \qquad (4.20a)$$

$$Da^* = Da \left(\frac{z}{2\alpha\, Pe_{m,\max}} \right)^q \qquad \text{(laminar flow),} \qquad (4.20b)$$

where $q = 1/2$ for plug-flow and $q = 1/3$ for laminar flow. In terms of this variable, the asymptote presents the same trend observed in fully developed conditions (where there is no effect of the axial distance, $q = 0$): $\theta \sim Da^*$.

In the external mass transfer limited regime, introducing the results for the conversion profile (Chapter 2) and expanding for large Da:

$$\theta(z) \sim 1 - \frac{1}{Da\sqrt{\pi}} \sqrt{\frac{\alpha\, Pe_m}{z}} = 1 - \frac{0.5642}{Da^*} \qquad \text{(plug-flow, } Da^* \to \infty\text{)} \qquad (4.21a)$$

$$\theta(z) \sim 1 - \frac{3^{1/3}}{\Gamma(1/3)\, Da} \left(\frac{2\alpha\, Pe_{m,\max}}{z} \right)^{1/3} = 1 - \frac{0.5384}{Da^*} \qquad \text{(laminar flow, } Da^* \to \infty\text{),} \qquad (4.21b)$$

with the same definition from Eqs.(4.20).

By analogy with Eq.(4.18), correlations for all values of $Da*$ are of the form

$$\theta \sim \frac{1}{1+1/\left(Da*\sqrt{\pi}\right)} \qquad \text{(plug-flow)} \qquad (4.22a)$$

$$\theta \sim \frac{1}{1+0.53837/Da*} \qquad \text{(laminar flow).} \qquad (4.22b)$$

Again Eq.(4.22) include more information from (4.21) than it does from (4.19), but it is acceptable to describe the $Da* \sim 1$ range, as shown in Figure 4.2. The dashed lines for $\alpha\, Pe_m / z > 10$ represent numerical results obtained with gPROMS® for laminar flow inside a circular channel, which agree reasonably with the analytical prediction in Eqs.(4.22) (full line). The transition between both sets of curves (at $z/\alpha\, Pe_m = 0.1$) will be detailed in section 4.3.2.c.

4.3.2.b *Interpretation of the degree of mass transport control in terms of time constants*

Generically, we can say that for any degree of development of the profile, correlations for θ are of the following form:

$$\theta \sim \frac{Da*}{1+Da*}. \qquad (4.23)$$

This differs from the actual results by coefficients which are around unity and includes the ones in fully developed profile conditions, since in that limit: $Da* = Da$. We have defined the rescaled Damköhler number as the ratio of the effective characteristic time for transverse diffusion to the one for reaction. Therefore, in terms of time constants

$$\theta \sim \frac{\tau^*_{transv,diff}}{\tau_{rxn} + \tau^*_{transv,diff}},$$

i.e. θ is the fraction of the time constant for the overall mass transfer-reaction process allocated to transport across the transverse length over which significant variation of concentration takes place. As discussed in section 4.2.3, $\tau^*_{transv,diff}$ is defined as an average of the characteristic lengths in the channel and catalytic coating domains, which may be much smaller than a or t_w if external and/or internal concentration boundary layers exist. This confirms our initial scaling analysis for the limits of control by slow mass transfer ($\tau^*_{transv\ diff} >> \tau_{rxn}$) or slow reaction ($\tau_{rxn} >> \tau^*_{transv\ diff}$), now supported on a more detailed analysis of the problem.

4.3.2.c *Criteria for concentration profile development from θ curves*

The numerical results for $z/\alpha\, Pe_m = 0.1$ are plotted for both developing and fully developed profile conditions in Figure 4.2, for the case of laminar flow inside a circular channel. It is possible to observe that as long as this transition is well identified, our correlations are able to describe correctly both limits and therefore all the values of the Graetz parameter.

Criteria for concentration profile development can be obtained from the intersection of the fully developed and developing asymptotes for $Da \to 0$ and $Da \to \infty$ above detailed (for the same θ). Using Eqs.(4.17a) and (4.19), the transition values at kinetic control are obtained:

$$\frac{z}{\alpha\, Pe_m} = \frac{\pi}{4(3+S)^2} \qquad \text{(plug-flow, } Da \to 0\text{)} \qquad (4.24a)$$

$$\frac{z}{\alpha\, Pe_{m,\max}} = 0.5518\left(\frac{9}{S+7} - \frac{4}{S+5}\right)^3 \qquad \text{(laminar flow, } Da \to 0\text{).} \qquad (4.24b)$$

Similarly from Eqs.(4.17) and (4.21), in mass transfer controlled conditions:

$$\frac{z}{\alpha\, Pe_m} = \frac{\sigma^2}{\pi\, \lambda_{1,\infty}^4} \qquad \text{(plug-flow, } Da \to \infty\text{)} \qquad (4.25a)$$

$$\frac{z}{\alpha\, Pe_{m,\max}} = 0.3121\left(\frac{\sigma}{\lambda_{1,\infty}^2}\right)^3 \qquad \text{(laminar flow, } Da \to \infty\text{).} \qquad (4.25b)$$

The results for the concentration profile development length are given in Table 4.1. According to this calculation, the transition from fully developed to developing occurs around the same values for Dirichlet and Neumann boundary conditions (very weak dependence on Da). This calculation method was also considered in Chapter 3.

4.3.3 Iso-θ curves in the $Da - \alpha\, Pe_m/z$ diagram

The previous limits can also be correlated in a single expression for all values of Graetz's parameters as criteria for kinetic and mass transfer controlled limits. An empirical expression that matches satisfactorily the asymptotes could be a generic power law addition. This procedure yields the following boundaries:

(a) **kinetic control** ($\theta \to 0$, for all values of $\alpha\, Pe_m / z$)

$$Da = \frac{\theta}{1-\theta}\left[\frac{1}{b^n} + \left(\frac{\sqrt{\pi}}{2}\sqrt{\frac{\alpha\, Pe_m}{z}}\right)^n\right]^{1/n} \qquad \text{(plug flow, } n \sim 2\text{)} \qquad (4.26a)$$

$$Da = \frac{\theta}{1-\theta}\left[\frac{1}{b^n} + 0.8202^n\left(\frac{\alpha\, Pe_{m,\max}}{z}\right)^{n/3}\right]^{1/n} \qquad \text{(laminar flow, } n \sim 4\text{)} \qquad (4.26b)$$

(b) **mass transfer control** ($\theta \to 1$, for all values of $\alpha\, Pe_m / z$)

$$Da = \frac{\theta}{1-\theta}\left[\left(\frac{\lambda_{1,\infty}^2}{\sigma}\right)^n + \left(\frac{1}{\sqrt{\pi}}\sqrt{\frac{\alpha\, Pe_m}{z}}\right)^n\right]^{1/n} \qquad \text{(plug flow, } n \sim 2\text{)} \qquad (4.27a)$$

$$Da = \frac{\theta}{1-\theta}\left[\left(\frac{\lambda_{1,\infty}^2}{\sigma}\right)^n + 0.6783^n\left(\frac{\alpha\, Pe_{m,\max}}{z}\right)^{n/3}\right]^{1/n} \qquad \text{(laminar flow, } n \sim 4\text{)} \qquad (4.27b)$$

(c) **mixed control** ($0 < \theta < 1$, for all values of $\alpha\, Pe_m / z$)

For $Da^* \sim 1$, either correlation (4.26) or (4.27) can be used, as mentioned in previous sections.

The values of b and $\lambda_{1,\infty}^2 / \sigma$ can be found in Table 4.1, and we will take $n = 2$ for plug flow and $n = 4$ for laminar flow, even though other choices around these values do not affect the agreement with numerical results significantly. However, since the change between asymptotes becomes sharper when n increases, it is possible the transition to be more abrupt for laminar flow, than for plug flow.

For specified values of Da and a distribution of the axial coordinate $z/\alpha\, Pe_m$, the model can be solved numerically (simulated with gPROMS®) and a value for θ calculated from Eq.(4.11). In Figure 4.3 and Figure 4.4, we compare those results as a function of $z/\alpha\, Pe_m$ for several $Da = \text{constant}$ curves, with the predictions from Eqs.(4.26) and (4.27).

Eqs.(4.26) and (4.27) provide expressions of the type $Da = Da\left(\alpha\, Pe_m / z, \theta\right)$, which for given values of the degree of mass transport control are the boundaries for operating regimes in the $Da - \alpha\, Pe_m / z$ diagram (Figure 4.5). The transition between developing and fully developed profile calculated in the previous section is also plotted. Note that Eqs.(4.26) and (4.27) could be as easily written explicitly for $\alpha\, Pe_m / z$.

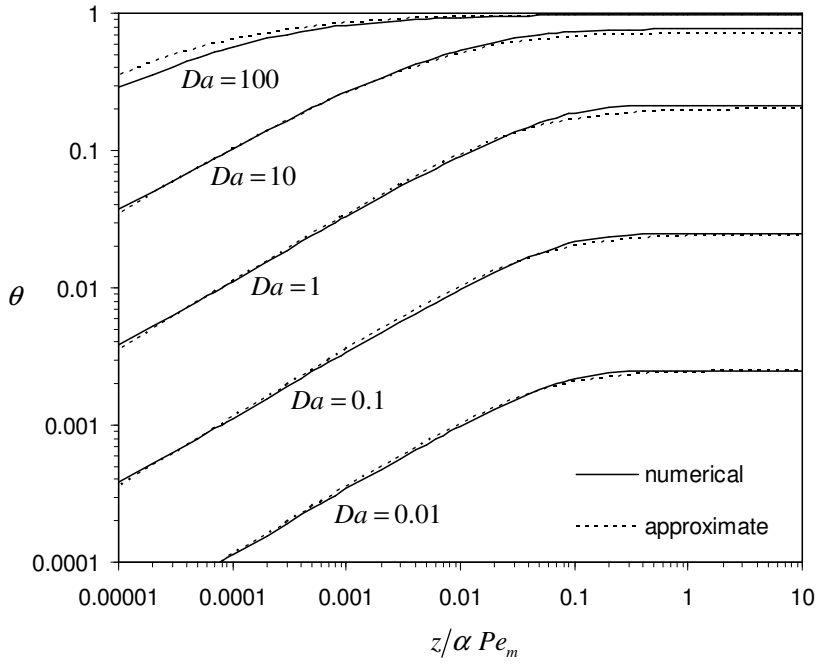

Figure 4.3: Degree of mass transport control θ for plug flow inside a circular channel. Numerical and analytical results (Eqs.(4.26)-(4.27)) are plotted as a function of the Graetz parameter ($\alpha Pe_m/z$) for several values of the Damköhler number Da .

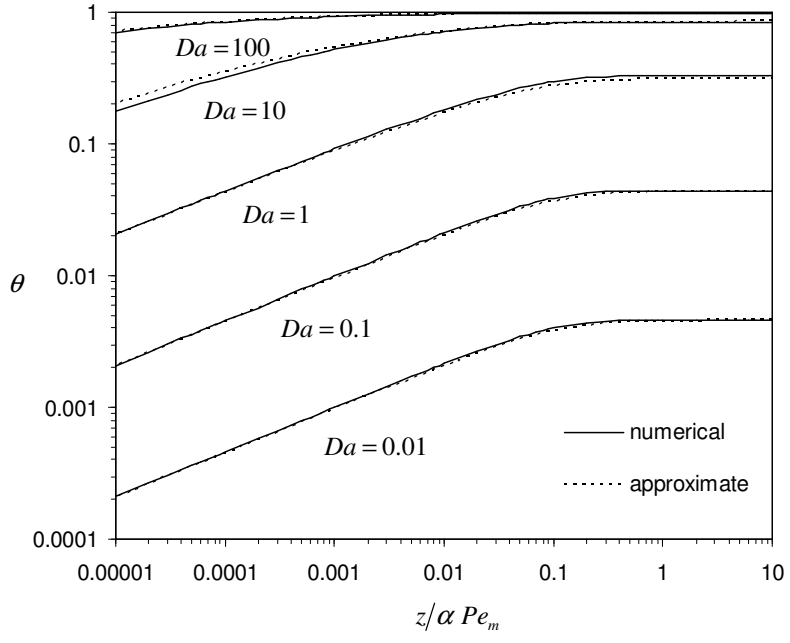

(a)

Figure 4.4: Degree of mass transport control θ for laminar flow inside a circular channel. Numerical and analytical curves are plotted as a function of the Graetz parameter ($\alpha Pe_m/z$) for several values of the Damköhler number Da . (a) Correlation (4.26) describes the low θ asymptote.

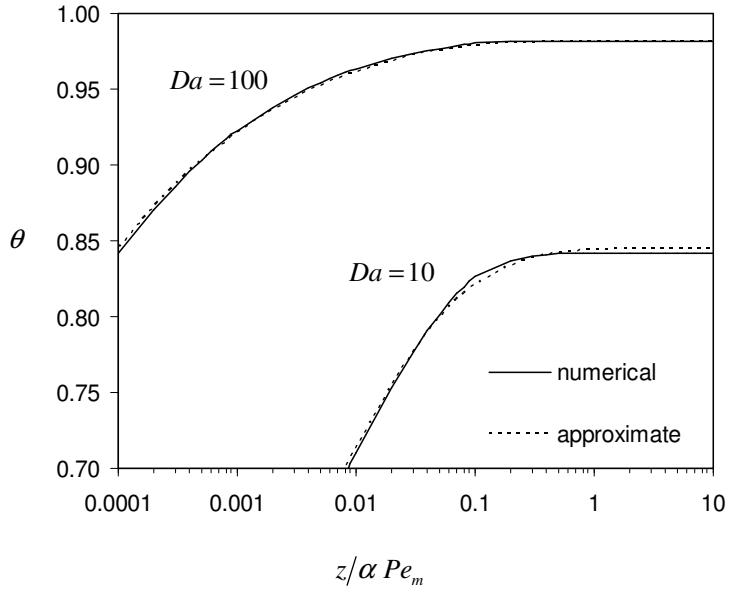

(b)

Figure 4.4: Degree of mass transport control θ for laminar flow inside a circular channel. Numerical (dashed) and analytical (full) curves are plotted as a function of the Graetz parameter ($\alpha\, Pe_m / z$) for several values of the Damköhler number Da . (b) For θ close to unity, correlation (4.27) is appropriate.

4.4 COMPARISON WITH PREVIOUS CRITERIA IN THE LITERATURE

Damköhler (1937) provides order of magnitude criteria for when conversion is solely determined by transport mechanisms or reaction:

$Da^{II} \leq 0.1$ reaction rate controlling (4.28a)

$Da^{II} \geq 100$ diffusion rate transverse to the flow controlling (4.28b)

$0.1 < Da^{II} < 100$ both reaction and diffusion rates are controlling, (4.28c)

where $Da^{II} = k_{surf}\, a / D$ is the second Damköhler number. The values have been estimated for plug-flow in a cylindrical tube with first-order reaction occurring at the wall, though it is recognised that exact numerical values would require further calculation. Moreover, the controlling regimes are related exclusively with the magnitude of Da^{II}. For parabolic velocity profile in a cylindrical tube, the limiting behaviour at diffusional control is different, namely conversion is lower in this case and concentration annulment near the wall is reached at lower Da^{II}. Obviously, Eq.(4.28) reproduces the scaling laws (in terms of Da^{II} or Da with effectiveness factor around unity) for fully developed concentration profile and the values chosen are sensible when compared with Eqs.(4.17) and (4.18).

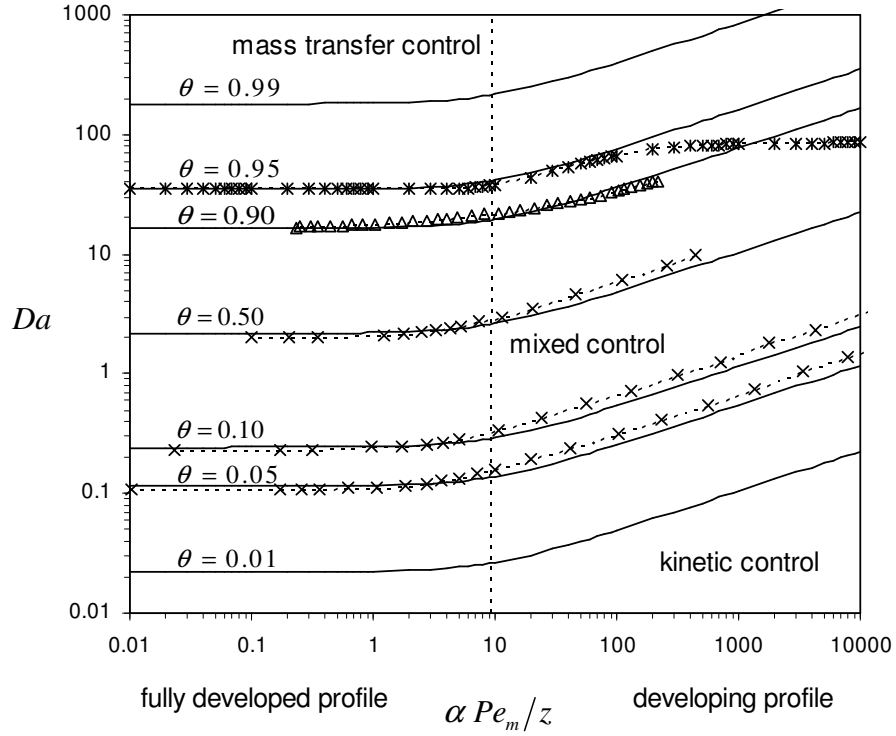

Figure 4.5: $Da-\alpha\, Pe_m/z$ diagram for laminar flow inside a circular channel. The boundaries for kinetic and mass transfer controlled regimes are plotted for several values of the degree of mass transport control. The values of the Graetz parameter for which the concentration profile can be considered fully developed is also plotted (dashed line). The dashed lines $-\times-$ refer to numerically calculated results extracted from Berger and Kapteijn (2007) for the same values of their criterion for kinetic control Δ_k (0.05, 0.10 and 0.50). The dashed line $-*-$ represents the criterion for attaining mass transfer control involving the calculation of Sherwood number with 4 terms from the Graetz series solution (Balakotaiah et al. 2002). Numerical results from Joshi et al. (2010) for $\theta = 0.90$ (CO oxidation) are also plotted ($-\triangle-$).

For linear kinetics, the criteria in terms of θ is related with Sh number. Hayes and Kolaczkowski (1994) propose a criterion for mass transfer control in terms of a ratio between the concentration at the wall and the average radial concentration. For a first-order reaction, this dimensionless concentration ratio was plotted as a function of the Damköhler number in Robin boundary condition at the wall (Da). The numerical simulations were done in a wide parametric range ($1 < 2Da < 10^3$), however, only under conditions of fully developed concentration profile (where an uniform value of Sherwood number could be used). The Sherwood number numerically calculated from a 2D model (Sh) was compared with the one which would give the same conversion profile if wall concentration annulment occurred (Sh_{app}). This is given as a function of Da, and since

$$Sh = Sh_{app}\left(1-\frac{Sh_{app}}{Da\left(S+1\right)}\right)^{-1} > Sh_{app},$$

the actual (theoretical) mass transfer coefficient is higher than the apparent one. Both curves approach as Da increases, and it was considered that for $2Da>100$ the results were similar, which corresponded to $c_{wall}/\langle c\rangle < 0.03$ (their criterion for mass transfer control). Naturally, the setting of this boundary must be recognised as arbitrary, but it is possible to read from their $c_{wall}/\langle c\rangle - Da$ plot the value of Da required to achieve mass transfer control for specified values of $(1-\theta)$. Since these results are for fully developed concentration profile conditions, they can be compared with our correlation Eq.(4.18) (Figure 4.6).

Walter et al. (2005) tested the presence of mass transfer limitations in the oxidation of isoprene. They excluded these limitations based on the criterion from Damköhler (1937) (Eqs.(4.28)) and extrapolated the boundary limit of Hayes and Kolaczkowski (1994) to the kinetic regime: $c_{wall}/\langle c\rangle > 0.97$. This required the simulation of concentration profiles at a given axial position (they report results for $\hat{z}=500\mu m$) and sets of experiments with different inert gases. Based on their information, we calculate the two dimensionless parameters as being: $Da=0.021$ and $\alpha\, Pe_m = 0.026$. At the exit (20 mm), the profile is fully developed and the value of θ is given e.g. by Eq.(4.17a) as being $\theta \sim 0.01$ ($c_{wall}/\langle c\rangle \sim 0.99$). For shorter axial distances, the Graetz parameter will increase, locating the operating point in a curve with θ closer to zero (conditions even further controlled by kinetics).

The kinetic study of ethanol reforming from Görke et al. (2009) was determined not to be falsified by external mass transfer by modifying the criterion of Mears (for internal diffusion) as

$$\frac{R_{EtOH}}{k_g\, c_{EtOH,in}}\left(\frac{V_{cat}}{S_{ext}}\right) < 0.05,$$

where is $c_{EtOH,in}$ is the inlet concentration of ethanol, R_{EtOH} is the effective (measured) reaction rate, V_{cat}/S_{ext} is the volume of catalyst per interfacial area and k_g is a mass transfer coefficient. If for scaling purposes we normalize the reaction rate by its (maximum) value at inlet conditions ($R_{EtOH} \sim R_{in}$), the criterion can be rewritten as

$$\frac{Da'}{Sh'} < 0.05$$

where $Sh' = k_g\, a/D$, $Da' = a\, R_{in,surf}/\left(D\, c_{EtOH,in}\right)$, $R_{in,surf} = R_{in}\, V_{cat}/S_{ext}$ and a is an appropriate scale for transverse length (we take it as being half of the hydrodynamic diameter of the square microchannel). This can be approximated to our criterion as

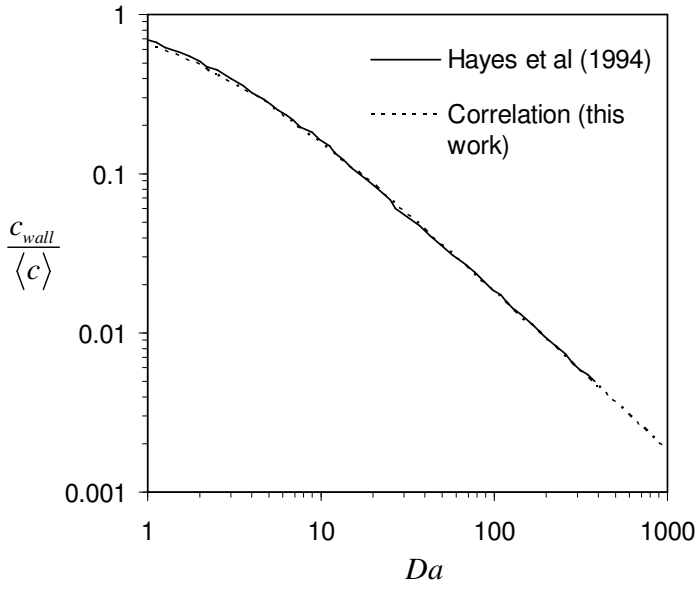

Figure 4.6: Ratio between wall concentration and mixing-cup concentration as a function of Damköhler number in fully developed concentration profile conditions. Numerical data from Hayes and Kolaczkowski (1994) (full line) and correlation (4.18) (dashed line) are shown for laminar flow inside a circular channel with first-order wall reaction.

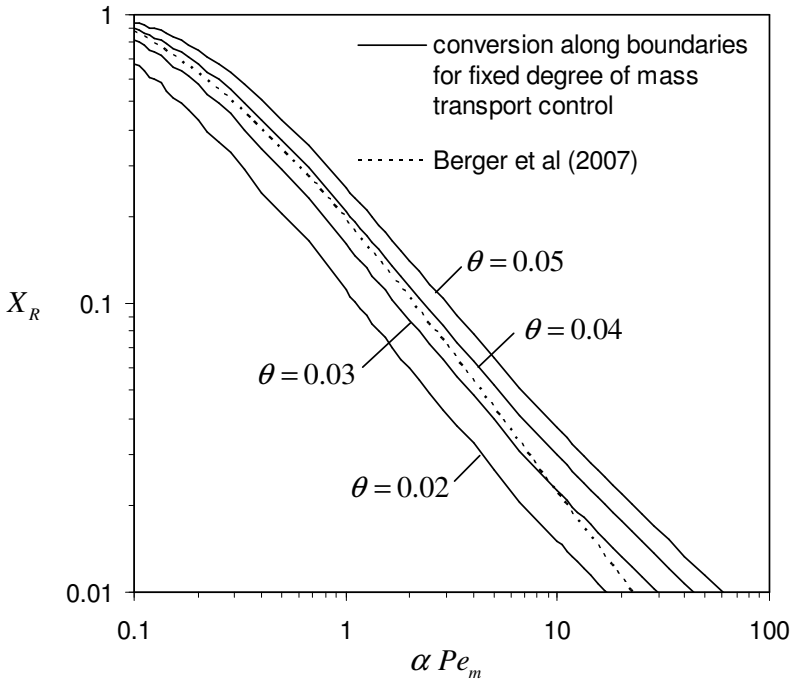

Figure 4.7: Conversion of reactant X_R as a function of $\alpha\, Pe_m$ for fixed values of θ in kinetic control. The correlations from Berger and Kapteijn (2007) for negligible radial gradients in fully developed profile for laminar flow inside a circular channel with first-order wall reaction are also presented.

$$\frac{Da'}{Sh'} = \frac{\theta}{1-\theta} < 0.05$$

which for low θ, simplifies to $\theta < 0.05$. They calculated the values for their criterion at 650ºC and the highest value obtained for their experimental conditions was 0.011. From their results for the mass transfer coefficient, we calculate the maximum value of $Da' \sim 0.02$. Using Eqs.(4.17a) or (4.26b), for a square microchannel (since $S \sim 1$ from its relationship with $a\, S_{ext}/V_{ch}$, we take value of b for a circular channel, $11/24$) we calculate $\theta = 0.01$, which reproduces their result.

Balakotaiah and West (2002) also use the same concentration ratio expressed as

$$\frac{c_{wall}}{\langle c \rangle} = 1-\theta = \frac{1}{1+(S+1)\,Da/Sh(P)} \tag{4.29}$$

where $P \sim \alpha\, Pe_m$. Then, they arbitrarily take as a practical criterion for mass transfer control: $(S+1)\,Da/Sh(P) \geq 10$, which corresponds to $\theta \geq 0.91$. Even though a criterion for kinetic control is given, $(S+1)\,Da/Sh(P) \leq 0.1$ ($\theta \leq 0.09$), the Sh number is also a function of Da for finite reaction rates. The calculation of Sherwood number is performed from Graetz series solution at Dirichlet wall condition, and the first 4 terms are given for some common geometries. Unfortunately a large number of terms may need to be retained if developing profile and transition to fully developed profile conditions are to be described accurately. Several approximations are reviewed and discussed to make the procedure more convenient and include also the case of finite Schmidt number, but they result in more complicated (non explicit) dependences on P than the one presented in Eq.(4.27). In this case, for $\theta = 0.95$ and Sh calculated from the 4-terms Graetz series, the $Da - P$ boundary ($-*-$) is plotted in Figure 4.5. It is clear that regime delimitation from the existing Sh number correlations or given by Graetz series solution is not adequate for developing or near developed profile conditions. Moreover, this does not allow direct calculation for example, of the duct length above which the process can be considered diffusionally limited or below which kinetic control prevails. The same difficulty holds in the analysis of the feed flowrate effect, for given kinetic parameters, physical properties, pressure and temperature.

Gervais and Jensen (2006) determined the transition point between fully developed and developing regimes in the Dirichlet limit, for laminar flow between parallel plates. The value reported by those authors ($z/\alpha\, Pe_m = 0.24$) differs from the one in Table 4.1 for the same conditions (0.07). This is due to the different criteria adopted as discussed in Chapter 3.

Berger and Kapteijn (2007) present an extensive numerical study to derive a criterion for neglecting radial concentration gradients in a coated wall reactor. A channel with several shapes (cylindrical, annular, square, rectangular and triangular) was considered, where an nth order reaction occurred. The presence of mass transfer limitations was assessed comparing the results

from the 2D simulations with the pseudo-homogeneous solution in kinetic control and plug-flow. This was measured by two criteria: (a) relative deviation of conversion calculated from the two models, Δ_X; and (b) relative deviation of the reaction rate constant that would be calculated from the conversion values as if radial gradients were absent, Δ_k. Contours for several values of Δ_X and Δ_k (≥ 0.05) are presented (for first-order reaction at the exit of a cylindrical tube) in diagrams with axes related to the model parameters: Da and $Da/\alpha\, Pe_m$. The criterion in terms of conversion is less strict for $Da > \alpha\, Pe_m$ than Δ_k, due to the approach of full conversion. For $Da > 0.1\,\alpha\, Pe_m$, the criterion Δ_k becomes independent of $Da/\alpha\, Pe_m$. Even though the criteria are different, we take the results from Berger and Kapteijn (2007) and compare them for the same values of $\Delta_k = \theta$. As shown in Figure 4.5 (dashed lines $-\times-$), the agreement is very reasonable. They also present expressions in terms of observable quantities (namely, conversion X_R) so that $\Delta_k < 0.05$, valid for $0.10 < X_R < 0.80$:

$$X_R < \frac{0.23}{0.16 + \alpha\, Pe_m} \qquad \text{(circular channel, first-order wall reaction),} \qquad (4.30a)$$

$$X_R < 1 - \exp\left(\frac{-0.22}{\alpha\, Pe_m}\right) \qquad \text{(circular channel, first-order wall reaction).} \qquad (4.30b)$$

Eqs.(4.30) are a useful but conservative criterion as they correspond to the case of fully developed profile. We compare these two expressions with conversion calculated as a function of the Graetz parameter for Da values so that θ is fixed (between 0.02 and 0.05), according to Eq.(4.26b) (Figure 4.7). Both correlations (4.30) are practically identical and the results are close to our prediction for $\theta \sim 0.04$ and $\alpha\, Pe_m < 1$.

Joshi et al. (2010) present a comprehensive study of the spectrum of characteristic regimes observed in a catalytic monolith. Increasing the temperature, the monolith operation may change from kinetically controlled to internal, and then external, mass transfer limited. Transition regimes between them are naturally present. Criteria were again presented in terms of concentration ratios, or equivalently in terms of the resistances to reaction and mass transfer, which are plotted as a function of the monolith temperature. For a first-order reaction it writes as: $\theta \leq 0.09$ and $\eta \geq 0.9$ for kinetic regime; $\theta \geq 0.9$ and $\eta \leq 0.1$ for external diffusional regime; and, $\theta \leq 0.09$ and $\eta \leq 0.1$ for internal diffusional regime. Then, for a given system (e.g. CO oxidation), numerical simulations were performed and the boundaries between regimes plotted in temperature-X diagrams (X can be washcoat diffusivity, thickness, catalyst loading or channel length and diameter). Other systems or criteria require a whole new set of simulations over large parametric ranges. Moreover, with their standard set of parameters, simulations are in fully developed concentration profile conditions in most part of the channel. The effect of the channel's length includes some results in developing profile range, as shown in Figure 4.5.

4.5 INLET EFFECTS

The remarks in section 4.2.1 concerning the negligible influence of axial diffusion referred to a global scale in this direction (the channel's length L). Local scales with respect to the transverse coordinate were examined in sections 2.3.1 and 4.2.2. In this section, we look at inner regions in the axial direction, which will include axial diffusion in their description.

In section 4.2.1, several convection-diffusion regimes were identified as reductions of the most general case, when $\alpha^2 \sim \alpha Pe_m \sim O(1)$. In practice, longitudinal diffusive transport is required to describe short wide channels, and in this case the aspect ratio α (~ 1) must be considered as an independent parameter (and not only associated with Pe_m). This discussion was limited to the effect of different magnitude relationships between the dimensionless parameters in the mass balance. However, the inlet boundary condition (of Danckwerts' type) is also affected

$$\frac{\partial c}{\partial z} = \frac{Pe_m}{\alpha} v(r)(c-1) \qquad \text{(at the channel inlet, } z=0\text{).} \tag{4.31}$$

At outer axial and transverse scales, Eq.(4.31) reduces to

$$c(r,0) = 1, \qquad \text{when } Pe_{ax} = Pe_m/\alpha >> 1 \text{ or} \tag{4.32a}$$

$$\partial c(r,0)/\partial z = 0, \qquad \text{when } Pe_{ax} << 1. \tag{4.32b}$$

Eq.(4.31) maintains its structure if $Pe_{ax} \sim O(1)$. At the channel's 'closed' outlet, the boundary condition is independent of parameter, as in (4.32b).

4.5.1 Local (inner) scaling in the axial and radial directions

The scaling analysis in section 2.3.1 and 4.2.2 searched for the existence of transverse boundary layers (i.e. in r). Here, we admit that inner regions in the axial direction also exist and look for distinguished limits. In this case, the independent variables in Eqs.(2.1) are stretched around (r_0, z_0) as

$$R = \frac{r_0 \mp r}{\delta_R} \qquad \text{in the transverse direction} \tag{4.33}$$

$$Z = \frac{z_0 \mp z}{\delta_Z} \qquad \text{in the axial direction,} \tag{4.34}$$

for simplicity, r is the transverse coordinate for both circular and planar channels. The thickness of an eventual axial boundary layer is δ_Z (in dimensional form given by $\delta_Z L$). This region is governed by

$$\frac{\partial^2 c}{\partial R^2}+\left(\alpha \frac{\delta_R}{\delta_Z}\right)^2 \frac{\partial^2 c}{\partial Z^2}=\alpha Pe_m \frac{\delta_R^2}{\delta_Z} v(R)\frac{\partial c}{\partial Z} \qquad \text{(parallel plates)} \qquad (4.35a)$$

$$\frac{\partial^2 c}{\partial R^2}-\frac{\delta_R}{1-\delta_R R}\frac{\partial c}{\partial R}+\left(\alpha \frac{\delta_R}{\delta_Z}\right)^2 \frac{\partial^2 c}{\partial Z^2}=\alpha Pe_m \frac{\delta_R^2}{\delta_Z} v(R)\frac{\partial c}{\partial Z} \qquad \text{(circular channel),} \qquad (4.35b)$$

where as usual, $v(R)$ is given by

$$v(R)=\begin{cases}(S+3)\delta_R R\left(1-\dfrac{\delta_R R}{2}\right) & \text{laminar flow}\\ 1 & \text{plug-flow}\end{cases}. \qquad (4.36)$$

In the simpler cases, points (r_0, z_0) near the boundary of the domain are susceptible of presenting boundary layers if diffusive (second-order) processes are absent at global scale leading-order behaviour. It is possible to establish dominant balances from (4.35), thus the transverse diffusion-convection description that we have found previously in section 4.2.2 occurs when

$$\alpha Pe_m \frac{\delta_R^2}{\delta_Z}\left|v(R)\right| \sim 1 >> \left(\alpha \frac{\delta_R}{\delta_Z}\right)^2, \qquad (4.37)$$

where the scale for velocity profile is $\left|v(R)\right|$, the linear leading order term in Eq.(4.36). This relationship implies that at least convection is dominant at the outer scale, compared to radial diffusion, $\alpha Pe_m >> 1$. It is not possible to independently determine both thicknesses in (4.37), but $\delta_Z >> \delta_R^2\left|v(R)\right|, \alpha\,\delta_R$. When $\delta_Z \sim O(1)$, the previous results are obtained.

4.5.1.a *Inlet boundary layer*

A boundary layer next to $z=0$ is expected if the outer channel equation is generally not able to fulfil both axial boundary conditions (it can be shown that at $z=1$ no distinguished limit can be obtained). Consider the presence of significant reactant consumption near the inlet at an outer transverse scale. Then, the possible dominant balances are extracted from inner equations (4.35) with $\delta_R \sim 1$. Moreover, Danckwerts' inlet condition (4.31) rescales according to Eqs.(4.33) and (4.34) as

$$\frac{\partial c}{\partial Z} = \frac{Pe_m}{\alpha}\,\delta_Z\,(c-1) \qquad \text{(at } Z=0 \text{ for plug-flow)} \qquad (4.38a)$$

$$\frac{\partial c}{\partial Z} = (S+3)\frac{Pe_m}{\alpha}\,\delta_Z\,\delta_R\left(1-\frac{\delta_R R}{2}\right)R\,(c-1) \qquad \text{(at } Z=0 \text{ for laminar flow).} \qquad (4.38b)$$

The following structures for a solution valid at $\hat{r} \sim O(a)$ are possible:

(a) Transverse and axial diffusion balance in an inner layer with thickness comparable to the channel radius in a small aspect ratio channel ($\delta_Z \sim \alpha$), when $Pe_m << 1$. This makes the LHS term in (4.38) dominant and transverse boundary conditions are still able to be fulfilled ($\delta_R \sim 1$).

(b) Axial diffusion dominates with convection in region with $\delta_Z \sim \alpha/Pe_m$ for $Pe_m >> 1$. Although Eq.(4.38) must be obeyed without further simplification, in general no conditions at the channel wall can be fulfilled. In those cases a transverse boundary layer with $\delta_R << 1$ arises, that should match the solution obtained here (outer transverse domain) as $R \to \infty$. This case will be detailed in the next section.

(c) Since axial diffusion must be retained to fulfil boundary and matching conditions, the remaining possibility is solving Eqs.(4.35) with $\delta_Z \sim \alpha/Pe_m$, which cannot be avoided when $Pe_m \sim 1$ and $\alpha << 1$. No transverse boundary layers exist, but the extended Graetz problem has to be solved in a semi-infinite domain.

4.5.1.b *Inner region at the channel-catalytic coating interface near the inlet ($z=0$ and $r=1$)*

The general concentration profile (for any magnitude of the reaction constant time) near the inlet at high Pe_m is composed by two spatial regions of distinct nature: an axial boundary layer at the outer transverse scale (from the dominant balance defined in (b) in the previous section) and a transverse boundary layer near the interface (superposed with the inner axial region), which we describe next.

In Eqs.(4.35) we consider a transverse diffusion-convection balance that does not reproduce previously identified regimes. This dominance is expressed by

$$\frac{\delta_Z}{\delta_R^2} \sim \alpha\, Pe_m \qquad \text{(plug flow)} \qquad (4.39a)$$

$$\frac{\delta_Z}{\delta_R^3} \sim (S+3)\,\alpha\, Pe_m \qquad \text{(laminar flow),} \qquad (4.39b)$$

Scaling relationships (4.39) relate δ_R and δ_Z. Even though this is in agreement with the first two terms in (4.37), previously we have ignored axial diffusion, which can be done when: $\delta_Z >> \alpha / Pe_m$ (plug flow) and $\delta_Z >> \alpha \Big/ \left[(S+3) Pe_m \delta_R \right]$ (laminar flow), i.e. when the thickness of the axial boundary layer near the interface is much larger than the one in the outer transverse scale (when $R \to \infty$). For an axial boundary layer, this case does not have sufficient structure to fulfil conditions at $R \to 0$ and $R \to \infty$.

To determine all the inner length scales, we employ an additional balance. A distinguished limit may be obtained if one demands both terms in the inlet (Danckwerts') boundary condition to balance yielding

$$\delta_Z \sim \frac{\alpha}{Pe_m} = \frac{1}{Pe_{ax}} \qquad \text{(plug-flow)} \qquad (4.40a)$$

$$\delta_Z \, \delta_R \sim \frac{\alpha}{(S+3) Pe_m} \qquad \text{(laminar flow),} \qquad (4.40b)$$

which means that axial diffusion must be included in the previous balance, if a distinct solution exists. The scaling from Eqs.(4.39) to(4.40) defines inner regions near $z = 0$ and $r = 1$, with the following characteristic lengths ($Pe_m >> 1$):

$$\delta_Z \sim \frac{\alpha}{Pe_m} = \frac{1}{Pe_{ax}} \quad \text{and} \quad \delta_R \sim \frac{1}{Pe_m} \qquad \text{(plug-flow)} \qquad (4.41)$$

$$\delta_Z \sim \frac{\alpha}{\sqrt{Pe_m}} = \sqrt{\frac{\alpha}{Pe_{ax}}} \quad \text{and} \quad \delta_R \sim \frac{1}{\sqrt{Pe_m}} \qquad \text{(laminar flow).} \qquad (4.42)$$

The $(S+3)$ factor in Eq.(4.42) was omitted for simplicity. The rescaled equations by these factors translate the penetration of reactant on a small fraction of the channel starting at the interface with the catalytic coating. For $z >> \delta_Z$, these inlet effects disappear and for $Pe_m >> 1$, this happens first in all of the transverse scale for plug flow or in the channel's core for laminar flow (near the wall, the axial boundary layer is thicker). The scaling for this region is relevant when there is an $O(1)$ concentration drop near the wall and at the inlet. We now discuss the relationship of this analysis with the reaction time constant.

4.5.2 Rescaled Damköhler number for inlet effects

We have seen that at the inlet, due to axial diffusion effects, the transverse scale over which concentration changes from the channel's core ($c = 1$) to the value at the surface ($c_{wall} < 1$) is different from the one predicted in section 4.2.2.

For purpose of regime definition, these scales should be included into the rescaled Damköhler number defined in Eq.(4.7),

$$Da^* = \frac{a\left(k_{surf}\,\eta\right)}{D\,Pe_m} = \frac{k_{surf}\,\eta}{\langle u \rangle} \qquad \text{(plug-flow)} \qquad (4.43)$$

$$Da^* = \frac{a\left(k_{surf}\,\eta\right)}{D\sqrt{Pe_m}} = \sqrt{Pe_m}\,\frac{k_{surf}\,\eta}{\langle u \rangle} \qquad \text{(laminar flow).} \qquad (4.44)$$

We note that since $Pe_m >> 1$, for the same values of kinetic constant and average velocity, Da^* is much higher for laminar flow than it is for plug-flow. Therefore, inlet mass transfer effects are much more severe for a parabolic velocity profile. Note that 'inlet' refers to the point where the flow meets the catalyst and this may happen in an intermediate section of the microchannel, where the flow is already fully developed. Examples of coatings at the reactor midsection include combustion channels in microdevices for steam reforming, e.g. Moreno et al. (2010).

We simulated the inlet concentration profile in a circular channel with plug and laminar flows with gPROMS®. From these results, the degree of mass transfer control θ could be calculated according to (4.11). This is represented in Figure 4.8a as a function of Da. The same values of θ are plotted in Figure 4.8b against Da^*, defined in (4.43) and (4.44). It is possible to observe that this scaling brings the curves together, regardless of the flow profile. We note that the $\theta(Da^*)$ dependence can be described by an expression of the form of (4.23), apart from specific numerical coefficients.

The reduced problem at the inlet section includes the wall boundary condition (4.5) and the different mass transfer-reaction regimes can be defined as in (4.8)-(4.10). In the case of significant consumption of reactant, the penetration of concentration gradients near the inlet occurs in a region with 'area':

$$\ell_{radial}\,\ell_{axial} = \left(a\,\delta_R\right)\left(L\,\delta_Z\right) \sim \frac{a^2}{Pe_m^2} \qquad \text{(plug flow) and}$$

$$\ell_{radial}\,\ell_{axial} = \left(a\,\delta_R\right)\left(L\,\delta_Z\right) \sim \frac{a^2}{Pe_m} \qquad \text{(laminar flow).}$$

For $Pe_m >> 1$, this area is larger for laminar flow.

A simple estimate for Sherwood number is obtained by replacing the mass transfer coefficient by $k_m \sim D/\ell_{film}$, where ℓ_{film} is the thickness according to the 'film model' (here taken as $a\,\delta_R$). Therefore, near the inlet:

$$Sh \sim (S+1)\,\delta_R^{-1} \sim \begin{cases} Pe_m & \text{(plug-flow)} \\ \sqrt{Pe_m} & \text{(laminar flow)} \end{cases} \qquad \text{for } 0 < z < \delta_Z . \qquad (4.45).$$

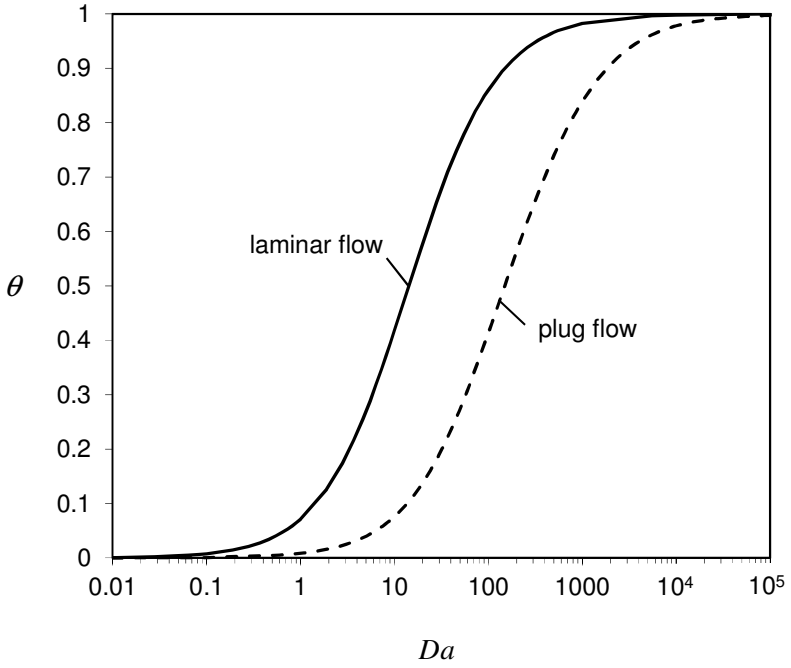

(a)

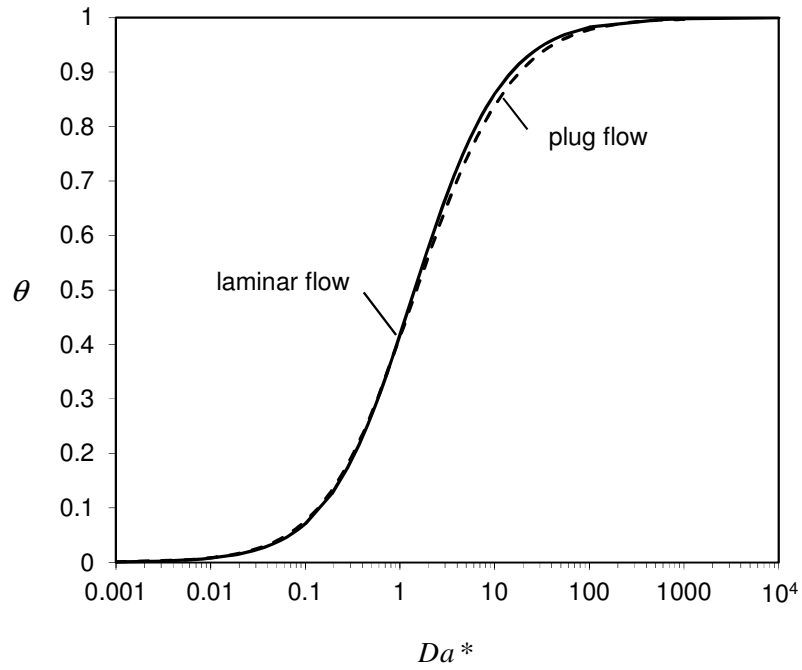

(b)

Figure 4.8: Degree of mass transfer control θ at the inlet of a circular channel as a function of (a) the Damköhler number evaluated with global scales, Eq.(4.4); and (b) the rescaled Damköhler number defined in Eqs.(4.43) and (4.44). Numerical simulations were performed for $\alpha = 0.01$ and $Pe_m = 100$.

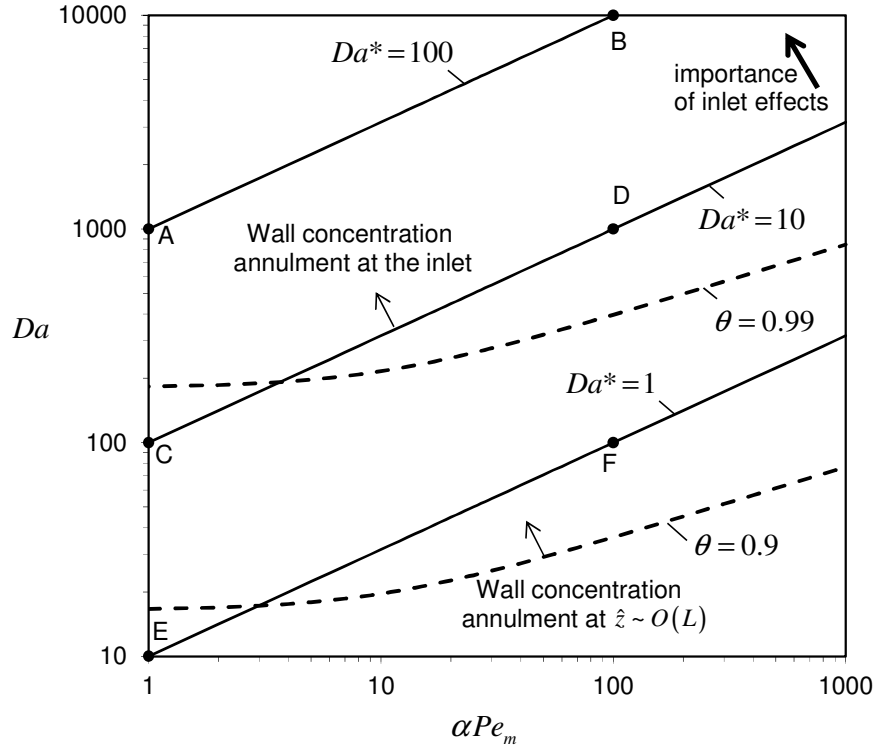

Figure 4.9: Inlet effects in the Da - αPe_m diagram. For $\alpha = 0.01$, the lines for fixed values of Da^* are plotted according to (4.44). The boundaries of the outer domain ($z \sim 1$) for $\theta = 0.9$ and $\theta = 0.99$ are also plotted, given by Eq.(4.27b). Laminar flow inside a circular channel was considered.

These dependencies are different to the ones predicted by Lévêque's analysis, and from the one by Gupta et al. (2001), where for laminar flow $Sh \sim Pe_m^{2/3}$. Other scaling analysis are available but don't predict the same area of influence for this effect, e.g. Leal (2007) overestimates the axial length of this region ($\ell_{axial} \sim a$) and neglects axial diffusion. Thus, the structure of these inner regions is different.

Nevertheless, we are interested in the influence of these effects on the definition of the mass transfer – reaction regimes. In particular, for large Pe_m significant decrease of concentration in the aforementioned boundary layer occurs at the inlet mass transfer controlled regime defined generically by $Da^* >> 1$. In a $Da - \alpha Pe_m$ diagram, this boundary can be plotted for a given value of α ($= 0.01$), as shown in Figure 4.9. Concentration at the channel's surface reaches annulment for approximately $Da^* \sim 10$, while downstream wall concentration annulment is reached for lower Da (less severe conditions). Examples of the nonuniform inlet transverse concentration profile for selected points in Figure 4.9 are shown in Figure 4.10.

It is possible to observe that the pairs of operating points lying in the same boundary present approximately the same surface concentration (and hence the same value of θ, since $\langle c \rangle \sim 1$). This confirms our scaling and proves the usefulness of the rescaled Damköhler number in analysing axial diffusion governed inner regions.

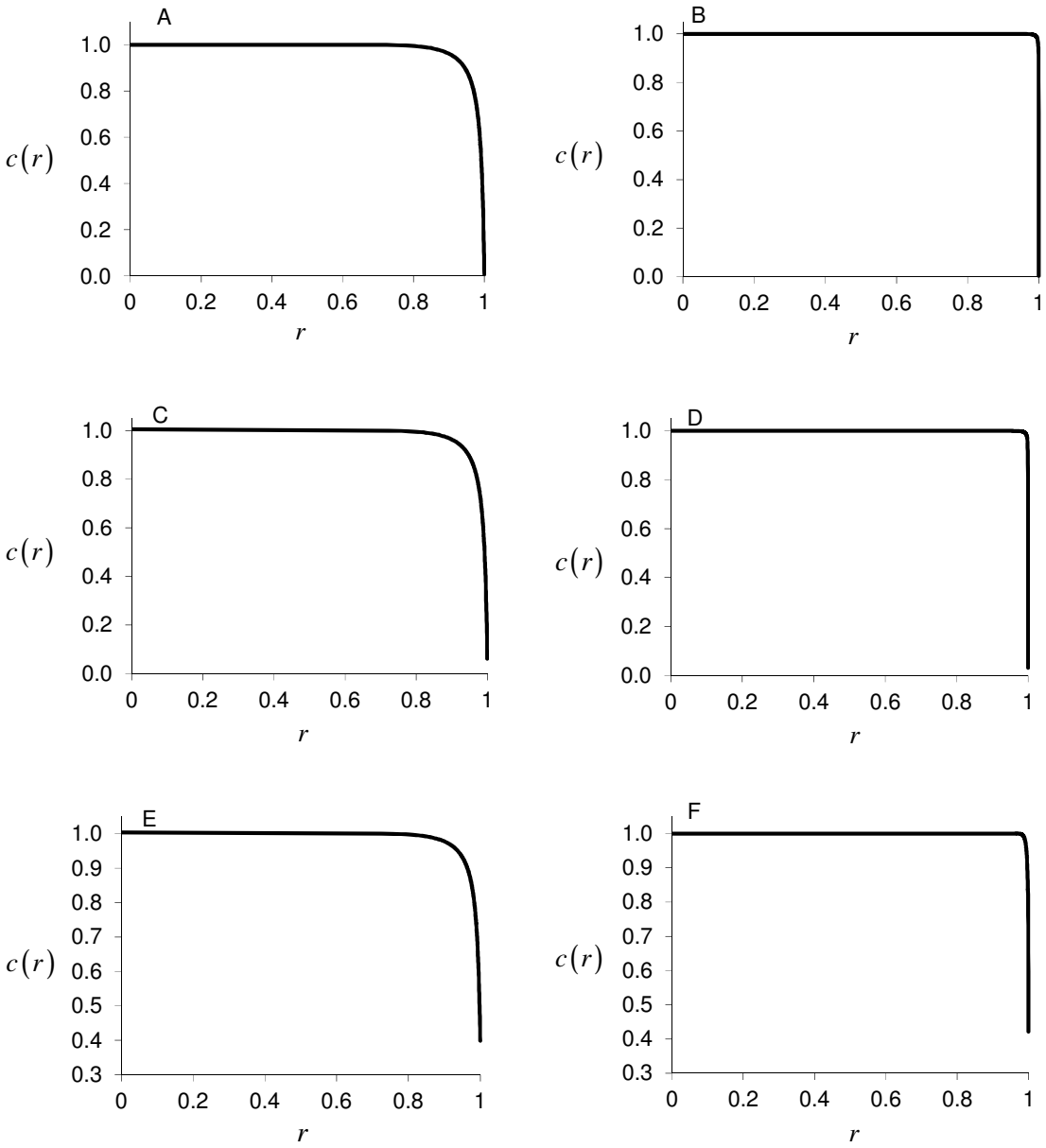

Figure 4.10: Inlet radial concentration profiles $c(r)$ at several points of the $Da - \alpha Pe_m$ diagram plotted in Figure 4.9.

Nonuniform inlet transverse concentration profile can be included in the analytical solution of the outer profile. However, the influence of this effect on an averaged quantity, such as conversion, is expected to be modest. Therefore, the interest in this region should be explored in the context of local phenomena, such as ignition/extinction in nonisothermal problems, as discussed in the suggestions for future work presented in Chapter 7.

4.6 CONCLUSIONS

The analysis of mass transfer and reaction in microchannel reactors, and interpretation of experimental work depend strongly on the correct definition of kinetic and mass-transfer controlled regimes. The existing studies in the literature usually involve the arbitrary setting of a criterion (written here as the degree of mass transfer control θ), and numerical calculations for a specified system are performed or simplified correlations are presented but in limited ranges. The approach presented in this chapter has some clear interesting advantages compared to what exists in the literature so far. We highlight the following features:

- The presented criteria are able to describe developing profile conditions (when mass transfer is confined to a boundary layer near the wall) and the transition region close to developed profile;
- The boundaries between regimes are given explicitly in terms of the dimensionless parameters (the Damköhler number Da and Graetz's parameter $\alpha Pe_m/z$) and θ;
- When the criteria values are changed, it is not necessary to evaluate numerically the conversion or Sherwood number, or repeat calculations over large parameter ranges; and
- Even though transition criteria for kinetic and mass transfer controlled regimes are of particular importance, the results are not limited to uniform wall flux or concentration boundary conditions (we have seen that results also apply for $0<\theta<1$ when the rescaled Damköhler number Da^* is ~ 1).

We have also shown that a $Da-\alpha Pe_m/z$ parametric map summarizes the behaviour of a microchannel with small aspect ratio and that criteria using dimensionless parameters should include the correct scale for diffusion in the channel.

Finally, the effects related to the magnitude of axial diffusion near the inlet were considered. In particular:

- a scaling analysis was formulated to understand the nature and location of this region;
- the rescaled Damköhler number concept was extended to the inlet; and
- the areas where this region of influence is significant were identified in a parametric map.

NOTATION

a	radius of the circular channel or half-spacing between parallel plates
A_n	n^{th} integration constant
b	coefficient defined in Eq.(4.15)
c	bulk fluid concentration of reactant species
$\langle c \rangle$	reactant's mixing-cup concentration of the reactant species
c_{in}	inlet reactant concentration
D	bulk fluid diffusivity
$Da*$	rescaled Damköhler number
k	intrinsic kinetic constant (with the reaction rate expressed per volume of washcoat)
$J_k(x)$	Bessel function of the first kind (order k)
ℓ	characteristic length
L	length of the channel
LHS	left hand side
$M(a,b,z)$	confluent (Kummer's) hypergeometric function
n	exponent in Eqs.(4.26) and (4.27)
Pe_m	transverse Peclet number
Pe_{ax}	axial Peclet number
r	dimensionless transverse coordinate
R	dimensionless transverse coordinate rescaled by δ_R
$R_{in,surf}$	reaction rate evaluated at inlet conditions, referred to catalyst surface area
Re_a	Reynolds number based on characteristic length a
RHS	right hand side
S	shape parameter: $=0$ for parallel plates; $=1$ for circular channel
S_{ext}	geometric area of the channel-washcoat surface
Sc	Schmidt number
Sh	Sherwood number
$u(r)$	velocity profile inside the channel
$\langle u \rangle$	average velocity inside the channel
$v(r)$	dimensionless velocity profile, normalized by average velocity
V_{coat}	volume of the catalytic coating
X_R	conversion of reactant
w_n	n^{th} weight
z	dimensionless axial coordinate
Z	dimensionless axial coordinate rescaled by δ_Z

Greek letters

α	aspect ratio of the channel
δ	thickness of the concentration boundary layer
η	catalytic coating effectiveness factor
φ_n	n^{th} eigenfunction
λ_n	n^{th} eigenvalues
μ	dynamic viscosity
ρ	density of the fluid
σ	shape/flow parameter, $(S+1)u_{\max}/\langle u \rangle$
τ	time constant
θ	degree of mass transfer control

Superscript

^	dimensional quantity

Subscript

∞	in the Dirichlet limit
max	maximum (referred to maximum velocity)
surf	channel – coating interface, per interface area

REFERENCES

Avci, A. K., D. L. Trimm and M. Karakaya (2010). "Microreactor catalytic combustion for chemicals processing." Catalysis Today **155**(1-2): 66-74.

Balakotaiah, V. and D. H. West (2002). "Shape normalization and analysis of the mass transfer controlled regime in catalytic monoliths." Chemical Engineering Science **57**(8): 1269-1286.

Bender, C. M. and S. A. Orszag (1978). Advanced Mathematical Methods for Scientists and Engineers. New York, McGraw-Hill.

Bennett, C. J., S. T. Kolaczkowski and W. J. Thomas (1991). "Determination of heterogeneous reaction kinetics and reaction rates under mass transfer controlled conditions for a monolith reactor." Process Safety and Environmental Protection: Transactions of the Institution of Chemical Engineers, Part B **69**(4): 209-220.

Beretta, A., G. Groppi, L. Majocchi and P. Forzatti (1999). "Potentialities and draw-backs of the experimental approach to the study of high T and high GHSV kinetics." Applied Catalysis A: General **187**(1): 49-60.

Berger, R. J. and F. Kapteijn (2007). "Coated-wall reactor modeling-criteria for neglecting radial concentration gradients. 1. Empty reactor tubes." Industrial and Engineering Chemistry Research **46**(12): 3863-3870.

Bhattacharya, M., M. P. Harold and V. Balakotaiah (2004). "Shape normalization for catalytic monoliths." Chemical Engineering Science **59**(18): 3737-3766.

Casanovas, A., C. de Leitenburg, A. Trovarelli and J. Llorca (2009). "Ethanol steam reforming and water gas shift reaction over Co-Mn/ZnO catalysts." Chemical Engineering Journal.

Damköhler, G. (1937). "Einfluss von Diffusion, Strömung, und Wärmetransport auf die Ausbeute in Chemisch-Technischen Reaktionen." Chem.-Eng.-Tech **3**(Part 1, Chapter 2): 359-485.

Gervais, T. and K. F. Jensen (2006). "Mass transport and surface reactions in microfluidic systems." Chemical Engineering Science **61**(4): 1102-1121.

Görke, O., P. Pfeifer and K. Schubert (2009). "Kinetic study of ethanol reforming in a microreactor." Applied Catalysis A: General **360**(2): 232-241.

Graetz, L. (1883). "Ueber die Wärmeleitungsfähigkeit von Flüssigkeiten." Annalen der Physik und Chemie **18**: 79-94.

Gupta, N. and V. Balakotaiah (2001). "Heat and mass transfer coefficients in catalytic monoliths." Chemical Engineering Science **56**(16): 4771-4786.

Hayes, R. E. and S. T. Kolaczkowski (1994). "Mass and heat transfer effects in catalytic monolith reactors." Chemical Engineering Science **49**(21): 3587-3599.

Hayes, R. E., S. T. Kolaczkowski, W. J. Thomas and J. Titiloye (1995). "Intraphase diffusion and interphase mass transfer effects during the catalytic oxidation of CO in a tube wall reactor." Proceedings - Royal Society of London, A **448**(1933): 321-334.

Hayes, R. E., B. Liu, R. Moxom and M. Votsmeier (2004). "The effect of washcoat geometry on mass transfer in monolith reactors." Chemical Engineering Science **59**(15): 3169-3181.

Heck, R. M., S. Gulati and R. J. Farrauto (2001). "The application of monoliths for gas phase catalytic reactions." Chemical Engineering Journal **82**(1-3): 149-156.

Hernández Carucci, J. R., K. Eränen, D. Y. Murzin and T. O. Salmi (2009). "Experimental and modelling aspects in microstructured reactors applied to environmental catalysis." Catalysis Today **147**(SUPPL.): S149-S155.

Inoue, T., M. A. Schmidt and K. F. Jensen (2007). "Microfabricated multiphase reactors for the direct synthesis of hydrogen peroxide from hydrogen and oxygen." Industrial and Engineering Chemistry Research **46**(4): 1153-1160.

Jang, J. Y., Y. X. Huang and C. H. Cheng (2010). "The effects of geometric and operating conditions on the hydrogen production performance of a micro-methanol steam reformer." Chemical Engineering Science **65**(20): 5495-5506.

Jensen, K. F. (2001). "Microreaction engineering-is small better?" Chemical Engineering Science **56**(2): 293-303.

Joshi, S. Y., M. P. Harold and V. Balakotaiah (2010). "Overall mass transfer coefficients and controlling regimes in catalytic monoliths." Chemical Engineering Science **65**(5): 1729-1747.

Karakaya, M. and A. K. Avci (2011). "Microchannel reactor modeling for combustion driven reforming of iso-octane." International Journal of Hydrogen Energy **36**(11): 6569-6577.

Karakaya, M., A. K. Avci, A. E. Aksoylu and Z. I. Önsan (2009). "Steady-state and dynamic modeling of indirect partial oxidation of methane in a wall-coated microchannel." Catalysis Today **139**(4): 312-321.

Keyser, L. F., S. B. Moore and M. T. Leu (1991). "Surface reaction and pore diffusion in flow-tube reactors." Journal of Physical Chemistry **95**(14): 5496-5502.

Kölbl, A., P. Pfeifer, M. Kraut, K. Schubert, M. Fichtner, M. A. Liauw and G. Emig (2004). "Examination of external mass transport in a microchannel reactor by pressure variation." Chemical Engineering and Technology **27**(6): 671-675.

Kreutzer, M. T., F. Kapteijn and J. A. Moulijn (2006). "Shouldn't catalysts shape up? Structured reactors in general and gas-liquid monolith reactors in particular." Catalysis Today **111**(1-2): 111-118.

Leal, L. G. (2007). Advanced Transport Phenomena: Fluid Mechanics and Convective Transport Processes. Cambridge, Cambridge University Press.

Lévêque, M. A. (1928). "Les lois de la transmission de chaleur par convection." Ann. Mines **13**: 201-299.

Moreno, A. M. and B. A. Wilhite (2010). "Autothermal hydrogen generation from methanol in a ceramic microchannel network." Journal of Power Sources **195**(7): 1964-1970.

Papoutsakis, E., D. Ramkrishna and H. C. Lim (1980a). "The extended Graetz problem with Dirichlet wall boundary conditions." Applied Scientific Research **36**(1): 13-34.

Papoutsakis, E., D. Ramkrishna and H. C. Lim (1980b). "Extended Graetz problem with prescribed wall flux." AIChE Journal **26**(5): 779-787.

Pfeifer, P., A. Kölbl and K. Schubert (2005). "Kinetic investigations on methanol steam reforming on PdZn catalysts in microchannel reactors and model transfer into the pressure gap region." Catalysis Today **110**(1-2): 76-85.

Polyanin, A. D., A. M. Kutepov, A. V. Vyazmin and D. A. Kazenin (2002). Hydrodynamics, mass and heat transfer in chemical engineering. London, Taylor & Francis.

Rebrov, E. V., A. Berenguer-Murcia, A. E. H. Wheatley, B. F. G. Johnson and J. C. Schouten (2009). "Thin catalytic coatings on microreactor walls a way to make industrial processes more efficient." Chimica Oggi **27**(4): 4-7.

Snytnikov, P. V., D. I. Potemkin, E. V. Rebrov, V. A. Sobyanin, V. Hessel and J. C. Schouten (2010). "Design, scale-out, and operation of a microchannel reactor with a Cu/CeO2-x catalytic coating for preferential CO oxidation." Chemical Engineering Journal **160**(3): 923-929.

Thomsen, M. S. and B. Nidetzky (2009). "Coated-wall microreactor for continuous biocatalytic transformations using immobilized enzymes." Biotechnology Journal **4**(1): 98-107.

Tronconi, E. and P. Forzatti (1992). "Adequacy of lumped parameter models for SCR reactors with monolith structure." AIChE Journal **38**(2): 201-210.

Uberoi, M. and C. J. Pereira (1996). "External Mass Transfer Coefficients for Monolith Catalysts." Industrial and Engineering Chemistry Research **35**(1): 113-116.

Ullah, U., S. P. Waldram, C. J. Bennett and T. Truex (1992). "Monolithic reactors: mass transfer measurements under reacting conditions." Chemical Engineering Science **47**(9-11): 2413-2418.

Votruba, J., J. Sinkule, V. Hlavacek and J. Skrivanek (1975). "Heat and mass transfer in monolithic honeycomb catalysts-I." Chemical Engineering Science **30**(1): 117-123.

Walter, S., S. Malmberg, B. Schmidt and M. A. Liauw (2005). "Mass transfer limitations in microchannel reactors." Catalysis Today **110**(1-2): 15-25.

CHAPTER

FIVE

EFFECTIVENESS FACTOR FOR THIN CATALYTIC COATINGS

The classical theory of diffusion and reaction inside catalytic pellets, based on the effectiveness factor η concept, is applied here to thin coatings supported on microchannels or nonporous pellets. We take advantage of a distinct geometrical characteristic in these systems to simplify the general problem. In particular, an approximate method for the evaluation of η is proposed for linear and some nonlinear kinetics (sections 5.3), in uniform (section 5.4) and nonuniform (section 5.5) geometries. We also complement the analysis of the mass transfer-reaction regimes presented in Chapter 4. In section 5.6, we show that by incorporating the internal diffusion-reaction behaviors, it is possible to identify by scaling arguments the controlling process which defines the maximum temperature for kinetic control and the minimum one for both channel and catalyst domains to be under mass transfer control. The previously presented results in Chapter 4 are written explicitly for the temperature of operation. Finally, we apply our analysis to a permeable catalytic coating, where intraparticular convection exists (section 5.7).

5.1 INTRODUCTION

As mentioned in Chapter 1, an attractive design concept in many reactor technologies is the one where a thin layer of catalyst is attached to an impermeable/inert support. This can be the surface of an inert nonporous pellet (the so called egg-shell catalysts) or the wall of a channel, through which a stream carrying the reactant flows. The latter case would correspond to the picture found in monoliths and microreactors, where a catalytic washcoat is used to increase the specific surface area without increasing pressure drop significantly, compared to the case of microchannel fixed bed reactors (Jensen 2001; Kapteijn et al. 2001; Schouten et al. 2002; Kiwi-Minsker et al. 2005; Kolb et al. 2007; Rebrov et al. 2009b).

Concerning the former, Gavriilidis et al. (1992) showed that the optimal activity distribution for ethylene epoxidation was a thin layer at the external surface of the pellet. Both situations aim to reduce the internal mass transfer resistance and the fraction of unutilized catalyst. In the case of structured reactors, the characteristic dimensions for external and internal mass transfer can be varied somewhat independently (Kreutzer et al. 2006). However, the modeling and design of these units has long being recognized to depend on the coupled analysis of both domains: channel and catalytic coating. The presence of internal diffusional limitations has also been described in many practical situations (Hayes et al. 1994; Leung et al. 1996; Groppi et al. 2001; Kapteijn et al. 2005; Tomasic et al. 2006; Kalluri et al. 2009; Mogalicherla et al. 2010; Santos et al. 2011; Scheuer et al. 2011), where large reaction rates and high temperatures prevail.

The reaction-diffusion model for the catalytic coating has relied in the concept of the effectiveness factor η. This results from the averaging of the coating domain in the transverse direction. Successful approaches relying on the η concept are employed with the expectation that both domains are decoupled, being the internal problem considered separately and if possible with minimum evaluation. The issue of the numerical effort associated with the calculation of η should not be underestimated, despite the evolution in computational tools. In real scale applications, the complexity of the models has increased and the time allowed for solving them decreased. The effective reaction rate (calculated from the intrinsic reaction rate at surface conditions and η) may have to be evaluated a huge number of times, especially if optimization is pursued. At the same time, faster simulators are required for real time control strategies. For these reasons, analytical or semi-analytical solutions for η have been proposed for several geometries and kinetics. In general, some features are desired in an approximate calculation procedure:

(a) *Accurate solution at least for some classes of nonlinear kinetics*. The actual form of the reaction rate expression can be very complex and the estimation of η in these cases becomes more challenging. Nevertheless in some concentration ranges, 'power-law' kinetics or Langmuir-type expressions are reasonable fittings (Bouzek et al. 1996). Even in these cases, numerical solution may pose difficulties, especially when concentration tends to zero somewhere inside the catalyst. Keegan et al. (2003) presented an approximation divided into two ranges of Thiele modulus and tested it for several kinetics. It is possible to observe that the error increases for low values of the reaction order, significant inhibition in Langmuir-Hinshelwood kinetics, nonisothermal effects, and in intermediate values of Thiele modulus.

(b) *Satisfactory approximation for nonuniform geometries*. The washcoat in a real channel is nonuniform. Most incorporation procedures result in accumulation of material in the corners of the channel, where the coating becomes thicker. The calculation of an area-averaged effectiveness factor in such geometries has to be carried out numerically. The best alternative to the complete two-dimensional calculation is the 'slice method' presented by Papadias et al.

(2000b). This was used to model isothermal kinetics in several real and idealized nonuniform washcoats (Papadias et al. 2000b; Hayes et al. 2004; Hayes et al. 2005). However, in some cases its application to nonlinear kinetics implies additional numerical evaluation and a reasonably high number of slices may be required.

(c) *Uniform description in the whole range of Thiele modulus*. General solutions for arbitrary geometries and kinetics are often considered in the chemical and diffusional limits. The literature is profuse in normalizations based on these asymptotes. However, it is well known that the maximum error from the approximation is situated in the region where neither reaction nor mass transfer is controlling. Different descriptions depending on the value of a critical Thiele modulus are also not convenient.

(d) *Evaluation with minimum information or numerical effort*. Complex fitting procedures for parameters characterizing shape are often found in the literature. Sometimes this is the result of perturbation procedures for small and high Thiele modulus. In the case of reaction nonlinearities, preliminary numerical evaluations are sometimes required (Hayes et al. 2005).

In this work, we propose a different methodology for the calculation of the effectiveness factor in a catalytic coating, which on one hand avoids some of the disadvantages in current methods and on the other, improves existing ones. Our analysis is based on a typical geometrical feature of a catalytic coating supported on a wall: small thickness (t_w) compared to the characteristic distance for diffusion in the open channel (a). In fact, thin coatings are preferred for a number of reasons. Internal mass transfer limitations are greatly reduced and heat removal/supply is facilitated. Clogging and nonuniform deposition occur less frequently, e.g. preparation of polymer monoliths require walls to be thin (Podgornik et al. 2000) so that an uniform structure is obtained. Moreover, issues regarding the adherence of the coating to the surface may lead to a preference for thinner layers (Yu et al. 2005). Typical values of the ratio between the coating thickness and channel radius (characteristic dimension) are given in Table 5.1. Another characteristic of the channels where most catalysts are supported is the small radius-to-length ratio (α).

Advantage may be taken from these characteristics, namely in the simplification of the 2D or 3D reaction-diffusion problem inside the catalytic body. In fact, the low values of ε ($=t_w/a$) are often used as a criterion for approximating the washcoat by a slab geometry. Groppi et al. (2001) finds this approximation acceptable if $a/t_w > 50$. This reduction of the actual geometry to an equivalent slab is common practice and is convenient for several reasons: the calculation (even if numerical) is easier and many exact and approximate solutions exist, inclusive for nonlinear kinetics. Even when non-uniformities in the washcoat have to be accounted for, the well-known results for slab geometry are employed as a part of the solution, e.g. in the 'slice method' from Papadias et al. (2000b) (see section 5.5 for details).

Table 5.1: Range of values for the geometric parameters in a wall-coated channel ($\varepsilon = t_w/a$ and $\alpha = a/L$) from some examples in the literature (estimated).

Reference	Nature of coating and support	$\varepsilon = t_w/a$	$\alpha = a/L$
Ouyang et al. (2005)	Pt/Al_2O_3 coating on silicon microreactor	0.008 - 0.02	0.006
Yu et al. (2005)	$Cu/ZnO/Al_2O_3$ coating in annular microreactor	0.04 - 0.16	0.002
Walter et al. (2005)	$V_{75}Ti_{25}O_x/Al_2O_3$ washcoat on a semi elliptic channel	0.03 - 0.12	0.009
Germani et al. (2006)	$Pt/CeO_2/Al_2O_3$ coating in microchannels	0.1 - 0.14	0.005
Tomasic et al. (2006)	Cu/ZSM5 zeolite on cordierite monolith	0.35 - 1	0.01
Görke et al. (2009)	Rh/CeO_2 coating on microstructured foil	0.01	0.001
Thomsen et al. (2009)	γ-Al_2O_3 microchannel coating	0.07 - 0.13	0.008
Rebrov et al. (2009a)	Pd/TiO_2 in fused silica capillary channel	0.001	<<1
Vita et al. (2010)	Pt/CeO_2 catalyst supported on a cordierite monolith	0.06 - 0.11	0.095
Mogalicherla et al. (2010)	Pd/Al_2O_3 monolith with square channels	0.011 - 0.063	0.004 - 0.02
Protasova et al. (2011)	Au/TiO_2 and Pt-Sn/TiO_2 films in silica capillaries	0.0007	<<1

The major difference of these approaches to the one presented in our work is that instead of reducing the actual geometry to the planar case, we use a two-term expansion to estimate the effectiveness factor with coefficients written in terms of the solution for a slab. This will require the calculation of a 'curvature correction' (section 5.3), which measures the deviation from the leading-order result (slab). These results are applied to uniform (section 5.4) and nonuniform geometries (section 5.5), and yield improved procedures for the evaluation of the effectiveness factor, compared to the additional information and computation time required by the present methods.

In section 5.6, we use the approximations to the effectiveness factor to determine the conditions under which the channel-coating system can be considered to operate in the chemical or diffusional regime. In many cases, this is controlled by the internal mass transfer-reaction regimes and is important for applications such as intrinsic kinetics measurement in microdevices and evaluation of the washcoat diffusional limitations. Finally, we evaluate an opportunity for performance enhancement in catalytic coatings, by allowing the existence of transverse intraparticular convection due to a pressure gradient (section 5.7). The operating conditions under which the influence of this effect is maximized are identified.

5.2 PROBLEM FORMULATION

The reaction-diffusion equations in the catalytic coating have to be written in general for the 3 coordinates. To reduce the order of the complete model, we use the one-dimensional cylinder model presented in section 5.2.1. The calculation of effectiveness factors from this approach is discussed in section 5.2.2.

5.2.1 One-dimensional cylindrical model for a catalytic coating

The one-dimensional generalized cylinder model (1DGC) has been widely used for the calculation of effectiveness factors in catalyst particles with arbitrary shape (Datta et al. 1985; Burghardt et al. 1996; Keegan et al. 2003; Mariani et al. 2003; Mariani et al. 2008a; Mariani et al. 2009a; Mariani et al. 2009b). The model and its assumptions are detailed in the previous references, yielding the following form of the governing equation:

$$\frac{\partial^2 c'}{\partial r^2} + \frac{\varepsilon\,\sigma}{1+\varepsilon\, r}\frac{\partial c'}{\partial r} + (\alpha\,\varepsilon)^2 \frac{\partial^2 c'}{\partial z^2} = \phi_{in}^2\, R_{in}(c'). \tag{5.1}$$

Eq.(5.1) is made dimensionless using the following normalization for dependent and independent variables (dimensional variables are capped):

$$r = \frac{\hat{r} - a}{t_w}, \qquad z = \frac{\hat{z}}{L} \qquad \text{and} \qquad c' = \frac{\hat{c}}{c_{in}}; \tag{5.2}$$

where t_w is the characteristic length scale in the transverse direction inside the washcoat, a is the external diffusion length scale in the open channel, L is the channel's length in the axial direction and c_{in} is the inlet concentration per volume of washcoat (related with the channel's inlet concentration C_{in} by the porosity of the catalyst layer: $c_{in} = \varepsilon_P\, C_{in}$).

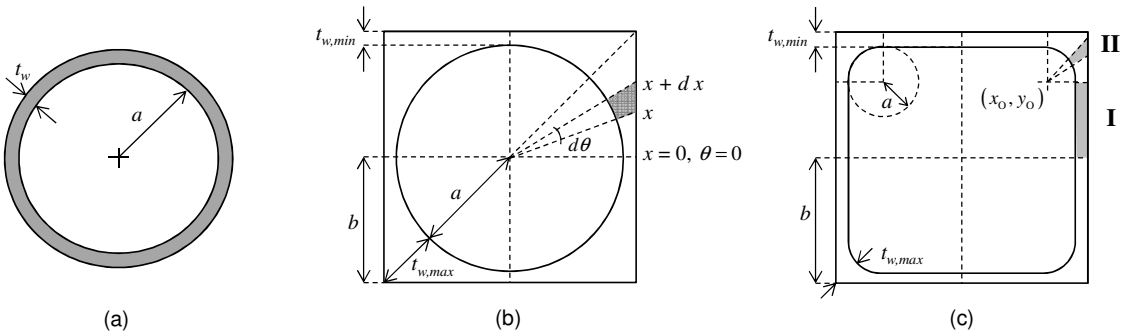

Figure 5.1: Geometries of the washcoats studied. (a) Uniform annular catalyst layer (circle in circle). (b) Circle in square. (c) Square with rounded corners.

Figure 5.1 shows some common washcoat geometries and their dimensions. The reaction rate expression can be generically expressed by

$$R_{in}(c') = \frac{R_V(c_{in}\, c')}{R_V(c_{in})} = \frac{(1+k')^p\,(c')^m}{(1+k'\,c')^p}, \tag{5.3}$$

where the dimensional reaction rate (per unit of washcoat volume) is $R_V(\hat{c}) = k_1\,\hat{c}^m\,(1+k_2\,\hat{c})^{-p}$ with $k' = k_2\,c_{in}$. The timescales for reaction (at inlet conditions) and transverse diffusion are compared by the Thiele modulus (evaluated at the inlet),

$$\phi_{in}^2 = \frac{t_w^2\,R_V(c_{in})}{C_{in}\,D_{eff}}.$$

Additionally, this choice of scales leads to the appearance of two geometrical parameters,

$\varepsilon = \frac{t_w}{a}$ (transverse length scales ratio) and (5.4a)

$\alpha = \frac{a}{L}$ (channel's aspect ratio). (5.4b)

As discussed in section 5.1, both parameters are typically small for supported catalytic coatings. The magnitude of $(\alpha\,\varepsilon)^2$ measures the importance of axial diffusion, over the full length of the washcoat, which is therefore negligible ($\tau_{transv}/\tau_{axial} << 1$). Thus, the axial dependence in the concentration profile, results then from the concentration continuity condition at the interface : $c'(r=0,z) = c_{surf}(z)$. Normalization by surface conditions yields the following dimensionless model:

$$\frac{d^2c}{dr^2}+\frac{\varepsilon\sigma}{1+\varepsilon r}\frac{dc}{dr}=\phi^2\,R(c) \tag{5.5a}$$

$$c(r=0)=1 \tag{5.5b}$$

$$\left.\frac{\partial c}{\partial r}\right|_{r=1}=0 \tag{5.5c}$$

where,

$$c(r)=\frac{c'(r,z)}{c_{surf}(z)} \tag{5.5d}$$

$$R(c)=\frac{R_{in}(c_{surf}\,c)}{R_{in}(c_{surf})}=\left(\frac{1+K}{1+K\,c}\right)^p c^m \qquad (\text{with } K=k'\,c_{surf}) \tag{5.5e}$$

$$\phi^2=\phi_{in}^2\,\frac{R_{in}(c_{surf})}{c_{surf}}=\frac{t_w^2\,R_V(\hat{c}_{surf})}{\hat{c}_{surf}\,D_{eff}} \tag{5.5f}$$

with ε from (5.4a). In the above equations, two parameters (t_w and σ) are directly related with the reduction to the one-dimensional model adopted. The success of the simplification relies on the judicious choice of these quantities. According to the same model, t_w and σ are tied up by an expression for the volume to surface ratio of the catalytic body . Then, the ratio between V/S for the actual geometry (where S is the area of the surface in contact with the reacting species) and for a slab with thickness t_w (the same characteristic transverse length) is

$$\upsilon=\frac{V}{t_w\,S}=\frac{1}{\varepsilon(\sigma+1)}\left[(1+\varepsilon)^{\sigma+1}-1\right]. \tag{5.6}$$

For thin coatings, (5.6) expands as

$$\upsilon\sim 1+\frac{\sigma\varepsilon}{2}+\sigma(\sigma-1)\frac{\varepsilon^2}{6}+O(\varepsilon^3). \tag{5.7a}$$

Note that for an annular washcoat in a cylindrical channel: $\sigma=1$ and $\upsilon=1+\varepsilon/2$ as expected. If only the first two terms are retained in (5.7a), then a simple relationship between υ and σ is obtained:

$$\sigma=\frac{2}{\varepsilon}(\upsilon-1). \tag{5.7b}$$

Thus, the problem is determined once the characteristic length for diffusion is chosen. Since this is the length scale over which concentration decays inside the washcoat, t_w can be equal to the maximum distance measured in the normal direction to the interface with the channel. Examples will be given in sections 5.4 and 5.5.

Eqs.(5.7) represent the simplest way of calculating σ for catalytic coatings. In the literature, many evolved approaches have been pursed to fit σ so that more accurate predictions from the 1DGC model can be obtained. For example, Mariani et al. (2003) calculated it to fulfill the low reaction rate asymptotics of the actual pellet. In later work from the same group, Mariani et al. (2008b; 2009a) matched the behavior at high reaction rates. More recently, they also used information from both regimes (Mocciaro et al. 2011), with emphasis on the prediction of effectiveness factors in multihole and multilobe particles. According to their analysis, negative values of their parameter σ are not likely to be obtained for catalytic pellets, but can be found for washcoats in monolith reactors. The corrective coefficients that appear in the higher order terms of the perturbation series for low and high ϕ are not useful as shape factors, in the sense that geometries with similar behavior at high reaction rates may present significantly deviation in the chemical regime (Keegan et al. 2005).

5.2.2 Effectiveness factor

The effectiveness factor compares the amount of reactant consumed (in the presence of diffusional limitations) with the one that would have been converted had surface conditions prevailed everywhere inside the catalyst. It can be calculated from

$$\eta = \frac{1}{A}\int_A R(c)\, dA\,.$$

According to the 1DGC model, averaging the mass balance yields

$$\eta = \frac{1}{\upsilon}\int_0^1 (1+\varepsilon\, r)^{\sigma}\, R(c)\, dr = \frac{-1}{\phi^2\, \upsilon}\left.\frac{d\,c}{d\,r}\right|_{r=0}\,. \tag{5.8}$$

5.3 PERTURBATION SOLUTION FOR THIN CATALYTIC COATINGS

An approximate solution to (5.5) can be constructed by a regular perturbation method for small values of ε. This will unfold the original problem into a sequence of (simpler) subproblems, once the perturbation series

$$c(r;\varepsilon) = \sum_{n=0}^{\infty} c_n(r)\, \varepsilon^n \tag{5.9}$$

is introduced into the model and terms with the same order are collected. Generically, the $O(\varepsilon^n)$ subproblem is described by

$$O(\varepsilon^n): \qquad \frac{d^2 c_n}{d r^2} - \frac{\phi^2}{n!}\frac{d^n R}{d \varepsilon^n}\bigg|_{\varepsilon=0} = -\sum_{q=0}^{n} \frac{1}{(n-q)!}\frac{d^{n-q}}{d \varepsilon^{n-q}}\left(\frac{\varepsilon \sigma}{1+\varepsilon r}\right)\bigg|_{\varepsilon=0} \frac{d c_q}{d r} \tag{5.10a}$$

$$c_0(r=0)=1 \text{ and } c_n(r=0)=0 \text{ for } n>0 \tag{5.10b}$$

$$\frac{d c_n}{d r}\bigg|_{r=1} = 0. \tag{5.10c}$$

The terms in the LHS of (5.10a) are dominant (diffusion in the normal direction and reaction), while the curvature term in the RHS appears as an higher-order correction (note that this side is annulled for $n=0$). From (5.8), a perturbation series for the effectiveness factor is also obtained,

$$\eta = \sum_{n=0}^{\infty} \eta_n \, \varepsilon^n \qquad \text{where } \eta_n = \frac{-1}{\phi^2 \upsilon}\frac{d c_n}{d r}\bigg|_{r=0}. \tag{5.11}$$

In theory, one may calculate as many terms as desired (numerically or analytically when possible). However, more terms in (5.11) may reduce the accuracy of the approximation as ε increases and, as we will show, a two-term expansion with analytically calculated terms is enough for our purposes.

The leading-order term from (5.10) yields the classical reaction-diffusion problem in a catalyst slab ($a \to \infty$). Exact and approximate analytical solutions for this problem have been provided in the literature for several forms of $R(c)$ (Petersen 1965; Bischoff 1967; Aris 1975; Gottifredi et al. 1981; Gottifredi et al. 1986; Gottifredi et al. 2005a; Gottifredi et al. 2005b; Magyari 2008). If required, numerical solution for the case of planar geometry can be obtained with considerably less effort. Therefore, we focus on the higher-order correction that appears at $O(\varepsilon)$, accounting for geometry effects.

5.3.1 Linear kinetics

When kinetics is first-order in the reactant concentration, the solution to the subproblems in (5.10) can be obtained analytically. The leading-order term has a familiar form:

$$c_0(r) = \frac{\cosh\left[\phi(1-r)\right]}{\cosh\phi} \text{ and } \eta_0 = \frac{\tanh\phi}{\upsilon\phi}. \tag{5.12}$$

Note that, this is equivalent to setting $\varepsilon = 0$ in the original problem and therefore $\upsilon = 1$, so that $\eta_0 = \eta_{slab} = \tanh\phi/\phi$ (Thiele 1939; Aris 1975; Froment et al. 1979). For the subproblem obtained when $n=1$:

$$c_1(r) = -\frac{\sigma\, e^{2\phi}}{\left(e^{2\phi}+1\right)^2}\, r\left[\cosh\left(\phi(2-r)\right)+\cosh(\phi\, r)-2\frac{\sinh(\phi\, r)}{\phi\, r}\right] \text{ and} \tag{5.13}$$

$$\eta_1 = \frac{\sigma}{2\,\upsilon}\frac{\tanh^2\phi}{\phi^2} = \frac{\sigma}{2\,\upsilon}\eta_{slab}^2 . \tag{5.14}$$

According to Eq.(5.11), the two-term perturbation series for the effectiveness factor can be written as:

$$\eta = \frac{\eta_{slab}}{\upsilon} + \frac{\varepsilon\,\sigma}{2\,\upsilon}\eta_{slab}^2 + O\left(\varepsilon^2\right).$$

Attending to the fact that for thin catalytic coatings the shape factor is given by Eq.(5.7b),

$$\eta \sim \frac{\eta_{slab}}{\upsilon}\left[1+(\upsilon-1)\,\eta_{slab}\right]. \tag{5.15}$$

Eq.(5.15) relates the effectiveness factor for a thin catalytic coating, described by the 1DGC model, with the one calculated for a slab catalyst, with thickness equal to the characteristic length t_w. This dimension is one of the two pieces of information concerning geometry: the other is the V/S ratio which can be quantified explicitly for simple geometries or analyzed digitally and measured for more complex ones. We must stress the fact that (5.15) is *valid for all values of the Thiele modulus* and is not limited to high or low reaction rates. In section 5.3.2, we understand how this relationship holds for nonlinear kinetics.

A final remark should be made to note that the 1DGC model admits an exact analytical solution for linear kinetics. This solution is an adaptation of previous analytical work for the hollow cylinder geometry and can be written in terms of a combination involving modified Bessel functions with complex arguments and whose order may be integer or fractional. Naturally, these transcendental functions aren't of convenient evaluation and an expansion for small ε is not easily obtained from the full solution. Moreover, the complex form of the exact solution does not inspire an approximation for more complex situations, such as the nonlinear kinetics examined in the next section. Apart from its simplicity, the perturbation solution has another advantage: it writes the effectiveness factor for the actual geometry in terms of its most elementary representation, a 1D slab.

5.3.2 Nonlinear kinetics

We would now like to understand if Eq.(5.15) holds for the case of nonlinear kinetics, with η_{slab} being the effectiveness factor for a slab under the same (nonlinear) conditions experienced by the actual geometry. In the case of first-order reactions, it is not the reaction term which

introduces complexity into the solution of the full problem. However, when kinetics is nonlinear, an exact solution to the leading-order problem of (5.10) may not be possible or convenient. Therefore, a perturbation scheme which affects the relative magnitude of reaction to diffusion is required. We expect maximum deviation to appear when kinetics is comparable with transport rates, but as we mentioned we want to avoid having to solve the 2D nonlinear problem. Alternatively, we consider the asymptotic limits of the solution for small and large Thiele modulus.

5.3.2.a *Chemical regime*

In the $\phi << 1$ limit, we look for a perturbation solution with the following form

$$c(r;\phi) = \sum_{n=0}^{\infty} c_n(r)\,\phi^{2n} \,. \tag{5.16}$$

This is a regular problem, where the leading order solution is naturally $c_0(r) = 1$, since reaction is much slower than transverse diffusion inside the washcoat. The $O(\phi^2)$ correction yields a result for the effectiveness factor which is independent of the reaction rate expression ($\eta = 1$). The deviation from unity is achieved in the next subproblem, where the curvature term was retained, making the solution valid for all values of ε. With these results, the series for the effectiveness factor becomes:

$$\eta = \frac{-1}{\upsilon}\sum_{n=0}^{\infty} \left.\frac{dc_n}{dr}\right|_{r=0} \phi^{2(n-1)} = 1 - \phi^2\, R'(1)\,\Lambda + O(\phi^4), \tag{5.17}$$

where the coefficient Λ is only related with the shape of the coating,

$$\Lambda(\varepsilon,\sigma) = \frac{1-\sigma+(1+\varepsilon)^{2(1+\sigma)}(3+\sigma)-(1+\varepsilon)^{1+\sigma}\left[4+\varepsilon(2+\varepsilon)(\sigma+1)^2\right]}{\varepsilon^2\left[(1+\varepsilon)^{1+\sigma}-1\right](\sigma+1)(\sigma-1)(\sigma+3)}. \tag{5.18}$$

In the limit of thin coatings, using Eq.(5.7b),

$$\Lambda(\varepsilon\to 0,\sigma) = \frac{1}{3}\left(1+\frac{\varepsilon\,\sigma}{2}\right) + O(\varepsilon^2) \sim \frac{\upsilon}{3}. \tag{5.19}$$

For a slab catalyst ($a \to \infty$), $\Lambda(\varepsilon = 0, \sigma = 1) = 1/3$ and the expansion from Aris (1975) is reproduced. If the limit of Eq.(5.18) when $\varepsilon \to \infty$ is taken, then the result obtained for solid catalyst bodies using the 1DGC model is retrieved:

$$\Lambda(\varepsilon\to\infty,\sigma) = \frac{1}{(\sigma+3)(\sigma+1)} = \frac{\upsilon}{\sigma+3}. \tag{5.20}$$

Note that in (5.20), υ is referred to the surface area in contact with reactants, i.e. for solid catalyst particles, $\upsilon=(1+\sigma)^{-1}$. The quantity Λ is related to the so called 'first Aris number' (Wijngaarden et al. 1998) or to the γ parameter from Mariani et al. (2003):

$$An_1=\gamma=\frac{\Lambda}{\upsilon^2}=\frac{1}{\upsilon(\sigma+3)}=\frac{\sigma+1}{\sigma+3}.$$

The normalization proposed by Eq.(5.17) accounts for generic shape and kinetics in two separable factors: (a) geometry effects induce a change in Thiele modulus for a slab, ϕ^2 now appears as $\upsilon\phi^2$ (i.e. the characteristic length is taken as the geometric average between t_w and V/S); (b) kinetic effects are expressed through $R'(1)$, which from Eq.(5.5e), is simply:

$$R'(1)=m-\frac{p\,K}{1+K}.$$

Introducing the expansion for η_{slab} in the chemical regime for any kinetics into Eq.(5.15) yields

$$\eta=1-\frac{R'(1)\,\phi^2}{3}\left(2-\frac{1}{\upsilon}\right)+O\left(\phi^4\right)$$

The correct factor for geometry given by (5.18) agrees with this one as $\upsilon\to 1$ (i.e. as $\varepsilon\to 0$)

$$\frac{2\upsilon-1}{\upsilon}\sim\upsilon+O\left(\varepsilon^2\right).$$

The expansions agree up to $O\left(\varepsilon^2\right)$, which is smaller than any contribution in Eq.(5.15). Thus, it is possible to conclude that the result from section 5.3.1 is still valid for nonlinear kinetics in the chemical regime.

5.3.2.b *Diffusional regime*

In the limit of a very fast reaction ($\phi^2>>1$), it is well-known that a boundary layer develops near the interface to match the dead core (the only solution from $R(c)=0$) with the surface condition (5.5b). This region is described by (5.5), with stretching of the transverse coordinate ($R=r/\delta$, where $\delta\sim\phi^{-1}$ is the thickness of the inner region):

$$\frac{d^2c}{dR^2}-R(c)=-\frac{\varepsilon\,\sigma}{\phi+\varepsilon\,R}\frac{dc}{dR},$$

where the singular perturbation series for concentration writes as $c(R;\varepsilon)=\sum_{n=0}^{\infty}c_n(R)\,\phi^{-n}$. The curvature term (which accounts for geometry effects) is of $O(\varepsilon/\phi)$, which is small in this limit

even for $\varepsilon \sim 1$. The leading-order problem resembles the reaction-diffusion in a slab, which has been treated in a detailed manner by several authors. The analysis at this order results in a very well-known normalization for arbitrary kinetics given by

$$\eta_0 = \frac{-1}{\phi \upsilon} \frac{d c_0}{d R}\bigg|_{R=0} = \frac{1}{\phi \upsilon} \sqrt{2 \int_0^1 R(c_0)\, d c_0} \,. \tag{5.21}$$

This can be rewritten as $\eta_0 = \eta_{slab}/\upsilon$, which is the first term from (5.15). For kinetics of the form of Eq.(5.5e): $\int_0^1 R(c_0)\, d c_0 = \frac{(1+K)^p}{1+m}\, {}_2F_1(1+m, p, 2+m, -K)$ with $m > -1$ or simply $(1+m)^{-1/2}$ for power-law kinetics.

To obtain an higher order term capturing the effect of geometry, we follow Wedel and Luss (1980) to write the solution of

$$\frac{d^2 c_1}{d R^2} - \frac{d R}{d c}\bigg|_{c_0} c_1 = -\varepsilon\, \sigma \frac{d c_0}{d R}$$

as $\frac{d c_1}{d R}\Big|_{R=0} = \frac{\varepsilon\, \sigma}{d c_0 / d R|_{R=0}} \int_{c_0 \to 1}^{c_0 \to 0} \left(\frac{d c_0}{d R} \right) d c_0$.

We make the following approximation in the boundary layer:

$$\frac{d c_0}{d R} \Big/ \frac{d c_0}{d R}\bigg|_{R=0} = \int_R^\infty R(c_0)\, dR \Big/ \int_0^\infty R(c_0)\, dR \sim R(c_0),$$

which yields the following two term solution for the effectiveness factor:

$$\eta = \frac{1}{\phi \upsilon} \sqrt{2 \int_0^1 R(c_0)\, d c_0} + \frac{\varepsilon\, \sigma}{\phi^2 \upsilon} \int_0^1 R(c_0)\, d c_0 + O\left(\phi^{-3}\right). \tag{5.22}$$

In terms of the kinetically generalized Thiele modulus (independent of shape) defined by Petersen (1965), Bischoff (1967) and Aris (1975)

$$\Phi = \frac{\phi}{\sqrt{2 \int_0^1 R(c_0)\, d c_0}}, \tag{5.23}$$

Eq.(5.22) writes as

$$\eta = \frac{1}{\Phi \upsilon} + \frac{\varepsilon\, \sigma}{2 \upsilon} \frac{1}{\Phi^2} + O\left(\phi^{-3}\right) = \frac{1}{\Phi \upsilon} + \frac{\upsilon - 1}{\upsilon} \frac{1}{\Phi^2} + O\left(\phi^{-3}\right). \tag{5.24}$$

Since in this limit a slab with arbitrary kinetics is described by $\eta_{slab} = 1/\Phi$, Eq.(5.15) is recovered. The separable geometric factors coincide with our analysis in section 5.3.1.

5.3.2.c *Monotonous $\eta(\phi^2)$ curves ("normal" kinetics)*

Since Eq.(5.15) holds for nonlinear kinetics in the chemical and diffusional regimes even at higher orders ($O(\phi^2)$ and $O(\phi^{-2})$, respectively), we can expect the intermediate region to be described at least approximately by the same equation. However, it is known from other shape normalizations that maximum deviation is found when $\phi \sim 1$. Also, the error of the approximation increases when kinetics present strong inhibition or multiplicity effects (Keegan et al. 2003). In this work, we address the case of 'monotonous $\eta(\phi^2)$ curves', where reaction rate is an increasing function of the reactant's concentration.

The solution requires the calculation of the effectiveness factor for the nonlinear reactive slab, which can be solved numerically with considerably less effort than the original problem. Approximations are also available (Gottifredi et al. 1981; Gottifredi et al. 1986; Haynes Jr 1986; Wijngaarden et al. 1998; Gottifredi et al. 2005a; Lee et al. 2006). Here we present a different derivation in terms of a generalized Thiele modulus with respect to kinetics, which should be introduced into a function which fulfills the asymptotic limits for a slab. We choose the simple solution for first-order reaction,

$$\eta_{slab}(\Phi) = \frac{\tanh \Phi}{\Phi}, \tag{5.25}$$

where the *normalized Thiele modulus with respect to kinetics* Φ is:

$$\frac{\Phi^2}{\phi^2} = \frac{R'(1)}{1+\phi^2} + \left[2\int_0^1 R(c_0)\, d\, c_0 \right]^{-1} \frac{\phi^2}{1+\phi^2}. \tag{5.26}$$

As expected, $\Phi = \phi$ when the reaction is first-order. For power-law kinetics,

$$\frac{\Phi^2}{\phi^2} = \frac{m}{1+\phi^2} + \frac{m+1}{2}\frac{\phi^2}{1+\phi^2}. \tag{5.27}$$

We note that our normalization includes the classical result from Petersen (1965) and Bischoff (1967), which is more rigorous as $\phi \to \infty$. However, (5.27) predicts the effectiveness factor in the intermediate and low range of ϕ much better. For a slab geometry, introducing the generalized Thiele modulus into Eq.(5.25) results in comparable result to the empirical correlation from Gottifredi et al. (1986) particularly for $m > 1$ (around 0.55% maximum error for $m = 2$). Our result is particularly better than the existing approximate solutions for low m (even though the maximum error also increases as the order of reaction becomes lower than 1). The effectiveness factor is predicted by (5.25) with less than 1% error (for $m = 3/4$) and less than 2.6% for $m = 1/2$. As $m \to 0$, the transition between asymptotes becomes much sharper and the smooth transition from our normalization becomes less accurate (5.3% error for $m = 1/3$

and 7% for $m=1/4$). In those cases, a better approximation may be obtained by combining both limits in a powered addition as

$$\left(\frac{\Phi^2}{\phi^2}\right)^b = \left(\frac{m}{1+\phi^2}\right)^b + \left(\frac{m+1}{2}\frac{\phi^2}{1+\phi^2}\right)^b \tag{5.28}$$

with $b>1$. We do not consider b a fitting parameter, since the final result is pretty insensitive to virtually any value chosen, provided that it is reasonably higher than 1. In the cases examined, the maximum error changes from 3.38% to 3.44% when b changes from 2 to 100 (for $m=1/3$). The same observation holds for $m=1/4$ (maximum error 3.7% at least for $b\geq 2$).

Wijngaarden et al. (1998) compared several modified Thiele modulus that bring the effectiveness factor curves together for several reaction kinetics in the low and high region of η (equivalently, the zero-th and first Aris numbers). Approximations in these two limits are also given, but with excessive error in the intermediate range. A better estimate using information from both asymptotes is proposed, but it requires an iterative procedure. For a first-order reaction, the maximum error is 2.2% for a slab. They also used the same formula for the hollow cylinder, with maximum error of 4.4%. Generally, other approximations are of less convenient evaluation or have higher errors associated than the one proposed.

For this case, the effectiveness factor for slab geometry is always expected to be less than 1. Then from Eq.(5.15): $\upsilon^{-1}<\eta/\eta_{slab}<1$. The maximum deviation from the slab geometry is

$$\left|\frac{\eta-\eta_{slab}}{\eta}\right| = \upsilon - 1 \sim \frac{\varepsilon\,\sigma}{2}. \tag{5.29}$$

For $\varepsilon=0.1$, a cylindrical catalyst coating deviates from the slab geometry by approximately 5%. Eq.(5.29) allows an estimate of the maximum thickness admissible for the actual geometry to be represented by a slab, for a specified amount of relative error. Note that for "abnormal kinetics" (with inhibiting or nonisothermal effects), the analysis predicts that at least for some values of the Thiele modulus where $\eta_{slab}>1$, it is possible that $\eta/\eta_{slab}>1$. In these cases, advantage from using thicker coatings may exist.

5.3.3 Egg-shell catalysts

If the internal core of a pellet consists in a nonporous/inert solid ($0\leq\hat{r}\leq a$), with the catalytic material only in an outer layer ($a\leq\hat{r}\leq a+t_w$), then a similar problem is obtained but with reverse boundary conditions on both surfaces, given by

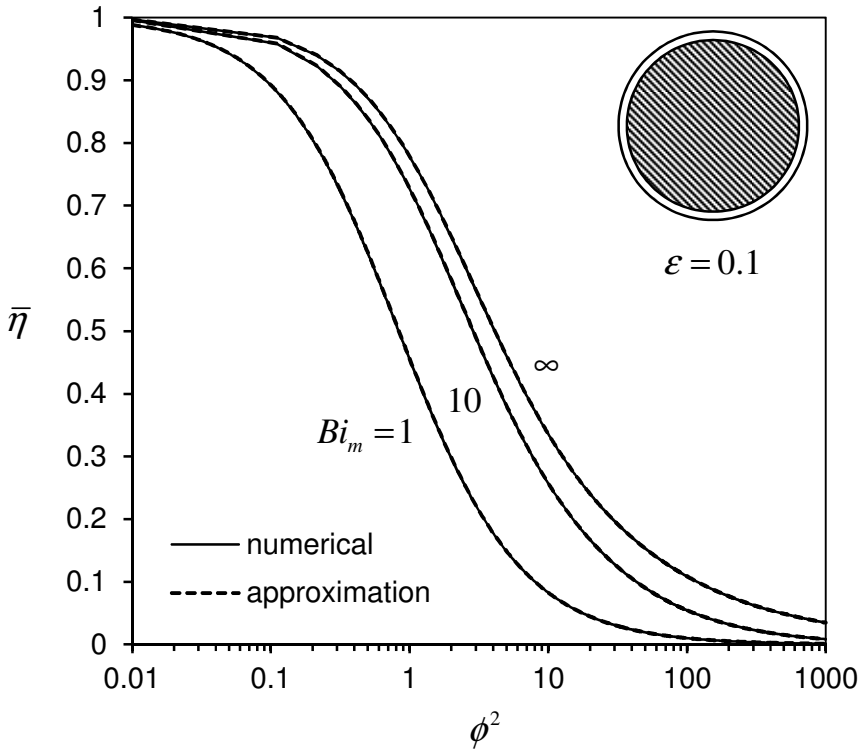

(a)

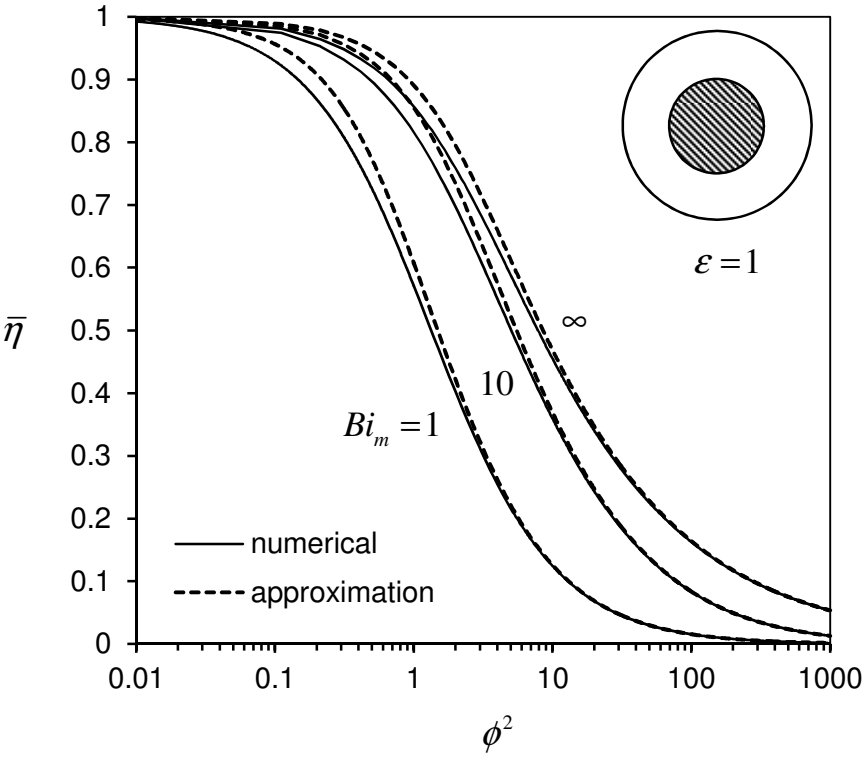

(b)

Figure 5.2: Effectiveness factor of a spherical catalytic layer supported on an impermeable core with a first-order reaction. Numerical simulations with gPROMS® are compared with (5.32) as a function of ϕ^2 for several values of Bi_m and $\varepsilon = 0.1$ (a) or $\varepsilon = 1$ (b).

$$c(r=1)=1 \tag{5.30a}$$

$$\left.\frac{\partial c}{\partial r}\right|_{r=0}=0 \tag{5.30b}$$

The surface reaction is now referred to the external surface and the effectiveness factor becomes:

$$\eta=\frac{1}{\phi^2\,\upsilon}\left.\frac{d\,c}{d\,r}\right|_{r=1}\text{, where } \upsilon=\frac{V}{S_{ext}\,t_w}\sim 1-\frac{\varepsilon\,\sigma}{2} \text{ as } \varepsilon\to 0\,. \tag{5.31}$$

The shape exponent σ is used in the reaction-diffusion equation as in (5.1). The reference to the outer surface yields a change in the sign associated with σ, and this is why in the 1DGC model for washcoats: $\sigma<0$ (Keegan et al. 2005). Following our perturbation procedure as outlined in section 5.3.1, Eq.(5.15) is found to still apply as long as υ is defined as in (5.31).

An asymptotic solution at the diffusional regime according to (5.23) is known for several kinetic expressions arising in enzymatic reactions occurring in pellicular catalysts (Horvath et al. 1973; Vos et al. 1990). There isn't any reason for the results in section 5.3.2 not to be valid for egg-shell catalysts and therefore (5.15) can be used for some nonlinear kinetics, as discussed previously. If external mass transfer resistance is also considered, then the approximate expressions for the effectiveness factor are more complex. We can also show that in the case of finite external mass transfer, Eq.(5.15) is again obtained (the superscript – denotes reference to bulk fluid conditions)

$$\overline{\eta}=\frac{\overline{\eta}_{slab}}{\upsilon}\left[1+(\upsilon-1)\,\overline{\eta}_{slab}\right], \tag{5.32}$$

with the well-known solution for a slab with linear kinetics (Aris 1975),

$$\overline{\eta}_{slab}=\frac{Bi_m}{\phi^2+Bi_m\,\phi\coth\phi}\,.$$

The mass Biot number for external mass transfer is given by $Bi_m=k_m\,t_w/D_{eff}$. For a spherical geometry, $\sigma=2$ and $\upsilon=\dfrac{1+\varepsilon+\varepsilon^2/3}{1+2\,\varepsilon+\varepsilon^2}\sim 1-\varepsilon$, the effectiveness factor predicted from (5.32) is compared with numerical results in Figure 5.2, when a first-order reaction is occurring.

5.4 UNIFORM ANNULAR COATING

The simplest case possible, apart from the slab catalyst layer, is the one of an annular washcoat. Uniform annular catalyst layers are found when a circular channel is perfectly coated or in the case of egg-shell catalysts in noncircular channels (Kreutzer et al. 2006).

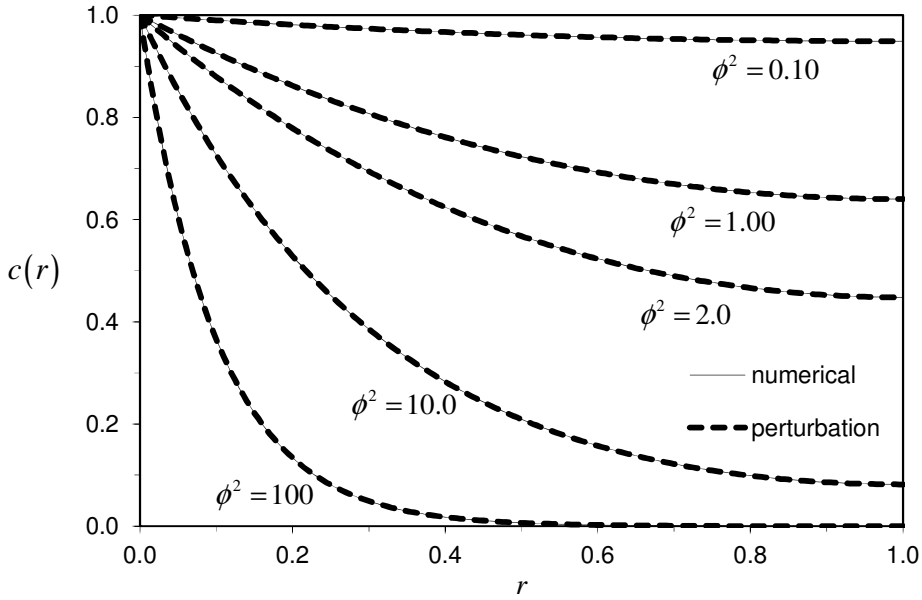

Figure 5.3: Internal concentration profiles $c(r) = \hat{c}/\hat{c}_{surf}$ in the catalytic layer coating of a long cylindrical microchannel ($\alpha = 0.01$). Numerical results obtained with gPROMS® (full lines) overlap with the two-term perturbation solution (dashed lines), Eq.(5.34), for $\varepsilon = 0.1$ and a wide range of values for the Thiele modulus.

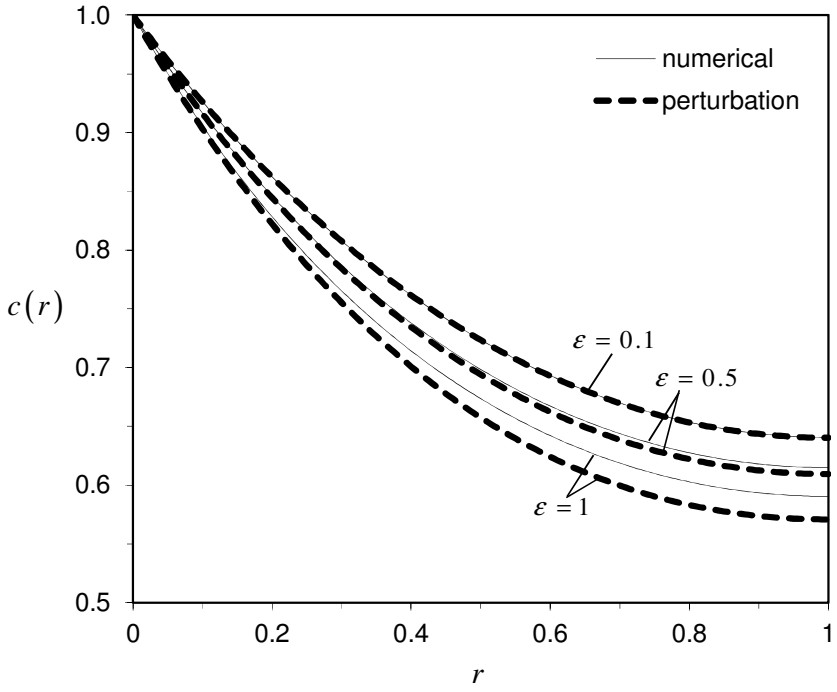

Figure 5.4: Perturbation solution for $c(r)$ with an $O(\varepsilon)$ correction due to curvature for the concentration profile, Eq.(5.34), with $\phi^2 = 1$, $\alpha = 0.01$ and for different values of the ratio between catalytic coating thickness and channel radius, ε. Numerical results obtained with gPROMS® (full lines) are in reasonable agreement with the approximate solution (dashed lines) for $\varepsilon = 0.1$, $\varepsilon = 0.5$ and $\varepsilon = 1$.

In the latter situation, the channel is first modified by introduction of a low BET material coating, which blocks the macroporosity of the channel walls and rounds the shape of the channel, filling the poorly used regions. Pérez-Cadenas et al. (2005) have shown the superior performance of these catalysts in the hydrogenation of fatty acid methyl esters compared with a square channel cordierite monolith. Better utilization and distribution of the catalytic layer was observed, as well as higher selectivity to the desired products. This case can also appropriately model diffusion and reaction in Raschig rings and hollow cylinders with internal flux (Mariani et al. 2003), in the limits of small aspect ratio ($t_w << L$).

This shape is schematically represented in Figure 5.1a and has very well-defined geometric characteristics:

$t_w =$ thickness of the annular catalyst layer (5.33a)

$$\upsilon = 1 + \frac{\varepsilon}{2} \tag{5.33b}$$

and therefore $\sigma = 1$.

5.4.1 Linear kinetics

According to the results presented in section 5.3.1, the internal concentration profile and the effectiveness factor curve are given by:

$$c(r;\varepsilon) = \frac{\cosh\left[\phi(1-r)\right]}{\cosh\phi} - \varepsilon \frac{e^{2\phi}}{\left(e^{2\phi}+1\right)^2} r\left[\cosh\left(\phi(2-r)\right) + \cosh(\phi r) - 2\frac{\sinh(\phi r)}{\phi r}\right] + O\left(\varepsilon^2\right) \tag{5.34}$$

$$\eta = \frac{1}{1+\varepsilon/2}\left(\frac{\tanh\phi}{\phi} + \frac{\varepsilon}{2}\frac{\tanh^2\phi}{\phi^2}\right) + O\left(\varepsilon^2\right). \tag{5.35}$$

The two-term expansion (5.34) is plotted in Figure 5.3 for $\varepsilon = 0.1$ and several values of ϕ^2 (from 0.1 to 100). The inclusion of the second term reduces the maximum relative error from 0.16% to 0.004% for $\phi^2 = 0.1$ and from near 5% to less than 0.1% when $\phi^2 = 100$ (in the region of virtually zero concentrations, corresponding to absolute error of 10^{-8}). Figure 5.4 compares the performance of the approximation for several values of the perturbation parameter ε. Naturally, better agreement is obtained as $\varepsilon \to 0$, but even for values as high as $\varepsilon = 1$ the maximum error reduces from around 10% to 3%, when the $O(\varepsilon)$ correction is added.

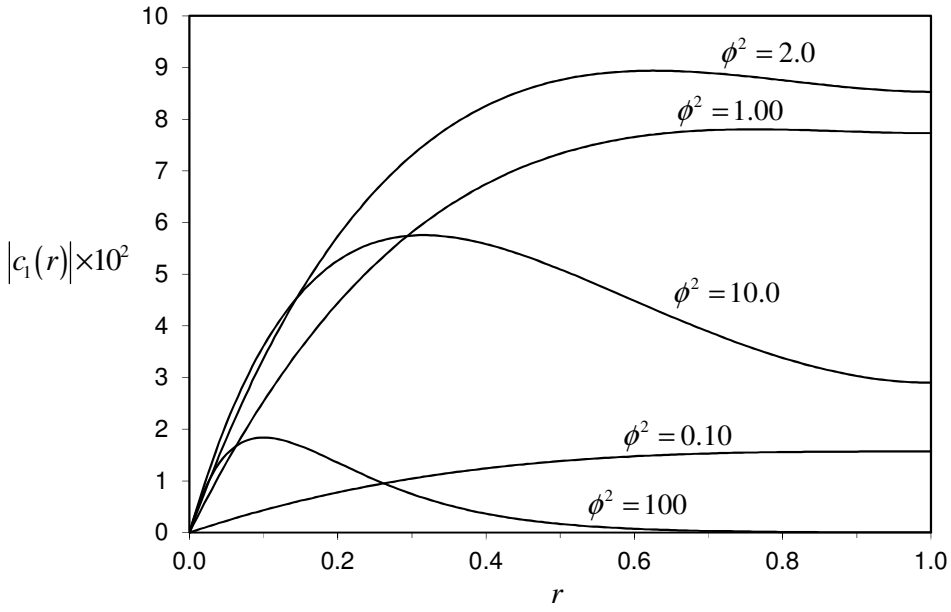

Figure 5.5: Magnitude of the $O(\varepsilon)$ correction to the transverse concentration profile in a slab coating due to the weak presence of curvature.

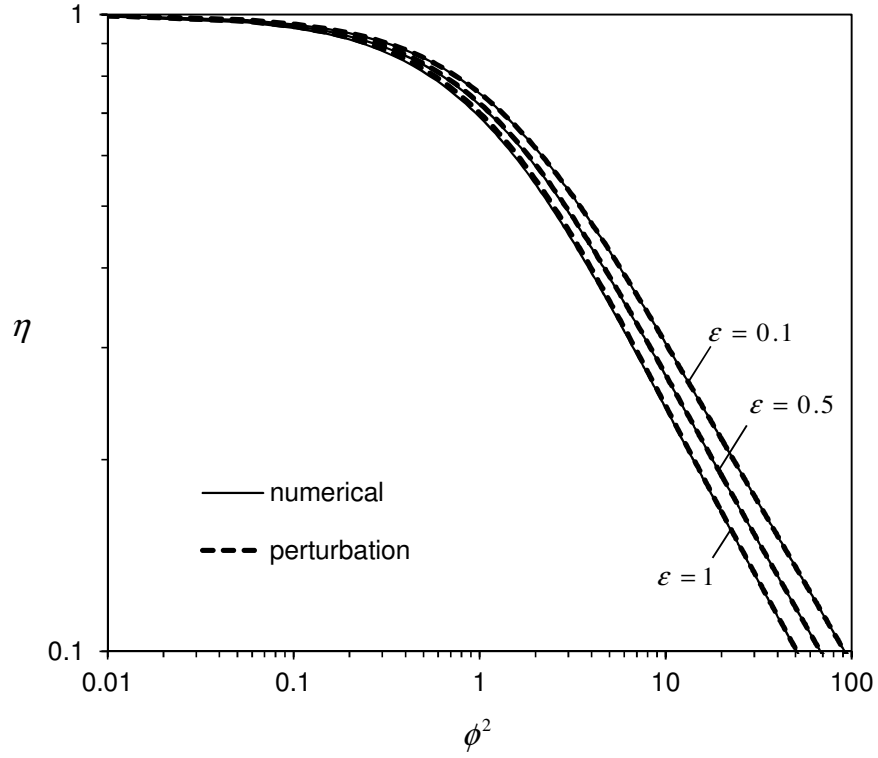

Figure 5.6: η vs. ϕ^2 curve for a long catalytic annular region ($\alpha = 0.01$) for $\varepsilon = 0.1$, $\varepsilon = 0.5$ and $\varepsilon = 1$. Numerical results are in good agreement with perturbation series given by Eq.(5.35).

The $c_1(r)$ term in Eq.(5.34) is negative and its absolute value register a maximum, except for low ϕ (where $c_1(r)$ is maximum at $r=1$). The curvature importance increases with the distance from the interface, as long as reasonably high transverse concentration gradients are present. The position where the correction is maximum $r_{\max}$ marks the transition from a region of high transverse gradients to another where the concentration profile starts to flatten out. For $\phi>1$, $r_{\max}$ is the reactant penetration length (ϕ^{-1}). The η vs. ϕ^2 curve is plotted in Figure 5.6 with less than 3% maximum relative error for $\varepsilon=1$ and only around 1% for $\varepsilon=0.1$, compared to numerical results. We note that other methods in the literature for calculating the effectiveness factor have some drawbacks compared with our approach, namely: (a) the use of the geometrical Thiele modulus in $\eta=\tanh\phi_g/\phi_g$ leads to considerable high errors in the intermediate range of ϕ ; (b) analytical results from Lewis et al. (1974) and Wijngaarden et al. (1998) imply the inconvenient evaluation of modified Bessel functions or infinite series of these functions; (c) the 1DGC solution for the effectiveness factor (Burghardt et al. 1996) with a value of σ fitted to the chemical regime is again written in terms of Bessel functions (with fractional or integer orders) with (Mariani et al. 2003):

$$\sigma=\frac{-\varepsilon(2+\varepsilon)\left[6+\varepsilon(2+\varepsilon)\left(9+4\varepsilon+2\varepsilon^2\right)\right]+12(1+\varepsilon)^4\ln(1+\varepsilon)}{\varepsilon(2+\varepsilon)\left[2+\varepsilon(2+\varepsilon)\left(3+4\varepsilon+2\varepsilon^2\right)\right]-4(1+\varepsilon)^4\ln(1+\varepsilon)},$$

and $\varepsilon<0.4$ so that the error does not exceed 0.7%. Therefore, our method is simple, its evaluation is convenient, does not require fitting to any particular regime (it is valid for the whole range of ϕ) and is accurate.

5.4.2 Nonlinear kinetics

The treatment for nonlinear kinetics follows the analysis in section 5.3.2. As discussed there, the effectiveness factor depends on υ (here given by Eq.(5.33b)) and on η_{slab} (calculated numerically or with Φ in Eq.(5.25)), according to (5.15). Table 5.2 shows the maximum deviations observed between our solution and the numerical calculations for some kinetic forms. The reaction-diffusion problem was solved numerically with DASOLV routine from gPROMS® with discretization of the spatial coordinate r by orthogonal colocation in finite elements. The polynomial was second order and 1000 elements (first-order reaction) or 500 elements (remaining kinetics) were used. As expected, the factors that contribute to an increase in the relative deviation are: increase in the coating thickness (ε), intermediate values of Thiele modulus ($\phi^2 \sim 1-10$) and 'abnormal kinetics' (the two last cases in Table 5.2), where the approximation is only acceptable for lower values of ε .

Table 5.2: Maximum relative errors associated with effectiveness factor calculations from Eq.(5.15) for an annular catalyst layer with several kinetic expressions.

Reaction kinetics			Calculation method for η_{slab}	$\varepsilon = \frac{t_w}{a}$	Maximum error from Eq.(5.15)
Power-law, $R(c) = c^m$					
m					
0.75			Analytical (approximate): Eqs.(5.25) - (5.27)	0.01	0.89%
				0.1	0.78%
				0.5	1.02%
				1	2.14%
1			Analytical (exact): Eq.(5.25) with $\Phi = \phi$	0.01	0.10%
				0.1	0.11%
				0.5	0.58%
				1	1.68%
2			Numerical	0.01	0.02%
				0.1	0.2%
				0.5	0.7%
				1	1.1%
			Analytical (approximate): Eqs.(5.25) - (5.27)	0.01	0.67%
				0.1	0.63%
				0.5	1.17%
				1	1.58%
"Langmuir-Hinshelwood" type, $R(c) = \frac{(1+K)^p c^m}{(1+K c)^p}$					
m	p	K			
1	1	1	Analytical (approximate): Eqs.(5.25) - (5.26)	0.01	1.63%
				0.1	1.52%
				0.5	2.59%
				1	4.42%
1	2	5	Numerical	0.01	0.34%
				0.1	3.36%
1	2	10	Numerical	0.01	0.58%
				0.1	5.73%

5.5 NONUNIFORM COATINGS

The best method to deal with the calculation of the effectiveness factor in nonuniform coatings appears to be the so-called 'slice method' from Papadias et al. (2000a; 2000b). Briefly, the domain is divided into a series of slices, then the average effectiveness factor is calculated from the mass/volume weighed summation of all pieces and is given by

$$\eta = \sum_{i=1}^{N} w_i \, \eta_i \ . \tag{5.36}$$

The method was applied to several geometries (Papadias et al. 2000a; Papadias et al. 2000b; Hayes et al. 2005) and was also included in monolithic reactor simulation (Gonzo 2008; Gonzo et al. 2011). However, so far each slice has been treated as a slab, and η_i calculated accordingly, referred to the geometric characteristic length.

We propose a modification to the method, which consists in calculating η_i from Eq.(5.15). This introduces another parameter into the model, the characteristic length for diffusion of each slice, which together with the volume-to-surface ratio characterizes each segment i:

$t_{w,i}$ = maximum transverse distance normal to the interface in i (5.37a)

$$\upsilon_i = \frac{V_i}{t_{w,i} \, A_i} \ . \tag{5.37b}$$

The volume fraction of each slice is $w_i = V_i / V$ and A_i is the fluid-solid interfacial area. The original treatment assumes $\upsilon_i = 1$ and $\eta_i = \eta_{slab,i}\left(\phi_i\right)$, with ϕ_i referred to $t_{w,i}$.

5.5.1 Circular channel in square geometry

An extreme case of nonuniform deposition of washcoat in a rectangular channel is the 'circle in square' geometry, depicted in Figure 5.1b. The dimensionless local thickness in terms of the angular coordinate is

$$\varepsilon(\theta) = \frac{t_w(\theta)}{a} = \left(1 + \varepsilon_{\min}\right) \sec\theta - 1 \, ,$$

where $\varepsilon_{\min} = t_{w,\min} / a$ and due to symmetry of this geometry, $0 \le \theta \le \pi/4$. A differential slice i corresponding to an angular change of $d\theta$ has the following geometric features, according with Eqs.(5.37):

$$t_{w,i} = t_w\left(\theta + d\theta\right) = b \sec\left(\theta + d\theta\right) - a \tag{5.38a}$$

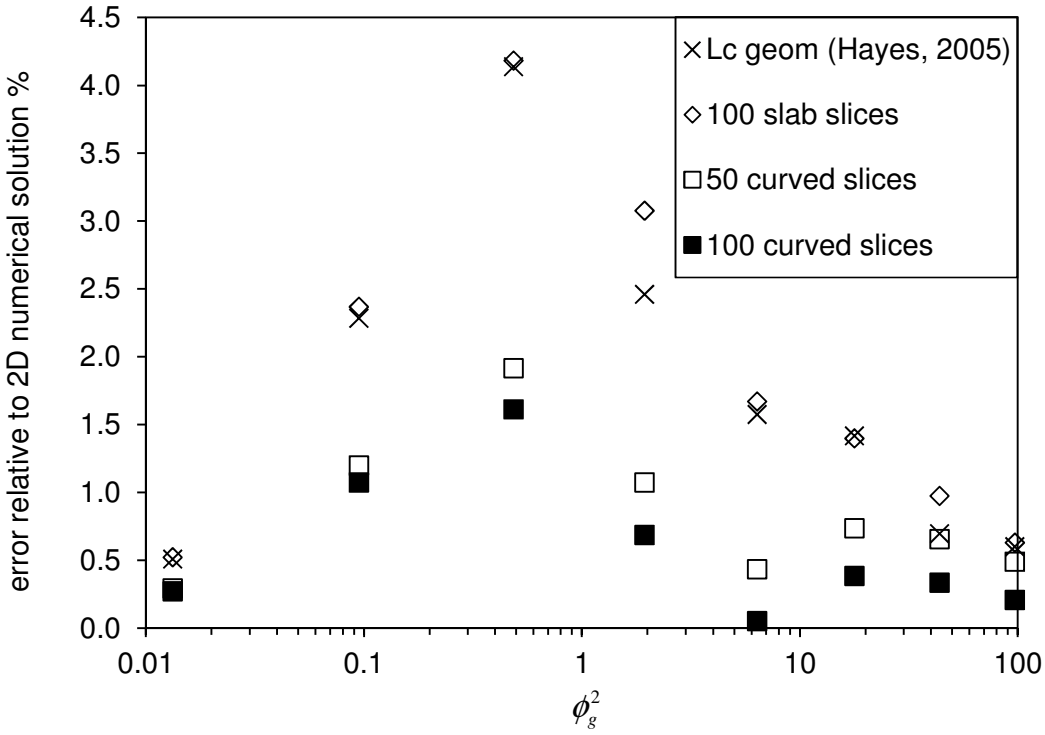

Figure 5.7: Error of several calculation methods for the effectiveness factor relative to the result obtained with a 2D numerical solution from Hayes et al. (2005) for several values of the Thiele modulus ϕ_g^2. The washcoat geometry is a circle in square (Figure 5.1b) and first-order kinetics is considered. The approximate methods used to estimate η include: the conventional 'slice method' used by Hayes et al. (2005) and with 100 slab slices; and Eqs.(5.36) and (5.38) for 50 and 100 curved slices.

$$\upsilon_i = \frac{dV/dA}{t_{w,i}} = \frac{1}{t_{w,i}}\left[\frac{b^2}{2a}\frac{\tan(\theta+d\theta)-\tan\theta}{d\theta} - \frac{a}{2}\right]. \tag{5.38b}$$

Eq.(5.38a) expresses a scaling for the transverse coordinate, where its value is normalized by the maximum value registered inside a slice (this occurs on the upper value taken by θ). Assuming (as in previous literature) that the slices are equally parted (all slices have the same $d\theta$):

$$w_i = \frac{dV}{V} = \frac{b^2\left[\tan(\theta+d\theta)-\tan\theta\right]-a^2\,d\theta}{b^2-\pi\,a^2/4}. \tag{5.38c}$$

The conventional 'slice method' treats each slice as a slab with $t_{w,i} = dV/dA$ and $\upsilon_i = 1$, whereas Eqs.(5.38) add a curvature correction to each segment. Figure 5.7 compares several approximate methods for calculating the effectiveness factor with the 2D numerical solution

(finite element method) from Hayes et al. (2005). For a square with $b = 0.5\,\text{mm}$ and $\varepsilon_{\min} = 0.021$, the conventional slice method was also employed by Hayes et al. (2005) (using the geometrical characteristic length). We add the result for 100 slab slices for comparison, as well as the calculation from Eqs.(5.36) and (5.38) for 50 and 100 curved slices.

We can observe that the number of slices required to achieve a desired level of accuracy decreases sharply when the curvature effect of each slice is taken into account. The improvement is particularly noticeable in the intermediate region of Thiele modulus, where 50 annular slices have less than half the error associated compared to 100 slab slices. The level of effort added by our approach is negligible and the improvement is significant, even for the simpler case of linear kinetics. Hayes et al. (2005) also report another approach, which however requires a preliminary step of numerical evaluation, and has higher error associated in the intermediate region (comparable with 100 slab slices).

5.5.2 Square channel with rounded corners

This geometry is closer to the actual geometries found in practical cases, where the washcoat accumulation is more pronounced only at the corners. Chou and Stewart (1986) considered this shape and performed numerical calculations with external mass transfer resistance. Papadias et al. (2000b) and Hayes et al. (2005) calculated the effectiveness factor using the slice method, where each section was treated as a slab. We divide the geometry (see Figure 5.1c) into two domains: a planar one characterized by a uniform (minimum) thickness (domain **I** in Figure 5.1c), and a circular fillet with center at (x,x) and where the washcoat thickness increases (shown as domain **II**). Due to symmetry, the angular coordinate in domain **II** is $0 \le \theta \le \pi/4$.

Each domain and slice i (a section of **II** between θ and $d\theta$) is described by:

$$t_{w,i} = \begin{cases} t_{w,\min} & \text{domain } \mathbf{I} \\ \dfrac{t_{w,\min} + a}{\cos(\theta + d\theta)} - a & \text{domain } \mathbf{II} \end{cases} \tag{5.39a}$$

$$\upsilon_i = \begin{cases} 1 & \text{domain } \mathbf{I} \\ \dfrac{1}{2\,d\theta} \dfrac{(1+\varepsilon_{\min})^2 \left[\tan(\theta + d\theta) - \tan\theta\right] - d\theta}{(1+\varepsilon_{\min})\sec(\theta + d\theta) - 1} & \text{domain } \mathbf{II} \end{cases} \tag{5.39b}$$

$$w_i = \begin{cases} \dfrac{2\,\varepsilon_{\min}(\beta - 1 - \varepsilon_{\min})}{2\,\varepsilon_{\min}(\beta - 1 - \varepsilon_{\min}) + (1+\varepsilon_{\min})^2 - \pi/4} & \text{domain } \mathbf{I} \\ \dfrac{(1+\varepsilon_{\min})^2 \left[\tan(\theta + d\theta) - \tan\theta\right] - d\theta}{2\,\varepsilon_{\min}(\beta - 1 - \varepsilon_{\min}) + (1+\varepsilon_{\min})^2 - \pi/4} & \text{domain } \mathbf{II} \end{cases} \tag{5.39c}$$

where the ratio between the radius of the rounded corner and the half side of the square channel is $\beta = b/a$ and the minimum dimensionless thickness is $\varepsilon_{\min} = t_{w,\min}/a$. Domain **I** is treated as a single slice, while the number of slices taken to describe domain **II** is chosen so that $N_{slices} = \pi/4/d\theta$. Both contributions are added according to

$$\eta = w_I\, \eta_I + \sum_{i=1}^{Nslices} w_{i,II}\, \eta_{II,i}\,, \tag{5.40}$$

where $\eta_I = \eta_{slab}\left(t_{w,\min}\right)$ and $\eta_{II,i}\left(\eta_{slab}, \upsilon_i\right)$ is the effectiveness factor for an annular slice, given by Eq. (5.15). One of the geometries studied by Papadias et al. (2000b) has the following geometric features: $\varepsilon_{\min} = 0.056$, $\beta = 1.39$ and $a = 0.36$ mm. For a first-order reaction, they considered 30 planar slices but also solved the reaction – diffusion 2D problem numerically (finite element method with an uniform mesh of 8640 triangular elements for $\eta > 0.2$, and an adaptive mesh with maximum of 90 000 elements for low η). A maximum error of 4.9% was reported, which occurs in a temperature range between 450 and 500 K. We compare the solution obtained with 30 annular slices in Eq.(5.40): in the same range, the maximum error observed is 1.5%. Hayes et al. (2005) presented results for this geometry with $\varepsilon_{\min} = 0.030$, $\beta = 1.44$ and $a = 0.347$ mm. With respect to their 2D numerical solution, a maximum error of 1.6% is observed with 100 annular slices, while 3.6% deviation occurs when planar slices are considered. In both cases, the inclusion of the $O(\varepsilon)$ correction, improves the solution.

It should be further noted that: (a) the errors tend to decrease when the fraction of washcoat described by a planar wall with uniform thickness increases (i.e. maximum errors are observed for the case of circular channel in square geometry) and (b) in principle, the improvement in the results is also valid for nonlinear kinetics, where the effectiveness factor in a slab geometry is calculated either numerically or by the approximation in section 5.3.2.c.

5.6 INTERPLAY BETWEEN INTERNAL AND EXTERNAL MASS TRANSFER – REACTION REGIMES

The delimitation of the regimes arising from the interaction between mass transfer and reaction appears in the literature in a number of ways, most of them equivalent. We use the concentration gradient at the catalytic surface to evaluate the extension of mass transfer limitations. This is rigorously related to the effectiveness factor for arbitrary kinetics, according to Eq.(5.8). A scaling relationship is obtained from this condition: $\eta\,\phi^2 << 1$ for kinetic control and $\eta\,\phi^2 >> 1$ for diffusional control, which reproduces the Weisz-Prater criterion for catalytic pellets (Weisz et al. 1954).

The effectiveness factor is an average of the reaction rate inside the catalytic layer referred to surface conditions. For a first-order reaction,

$$\eta = \frac{\langle c \rangle}{c_{surf}} . \tag{5.41}$$

Moreover, the internal regimes are related with the external ones by the flux continuity condition:

$$\left. \frac{\partial c_{ch}}{\partial r_{ch}} \right|_{r_{ch}=1} = \frac{D_{eff}}{\varepsilon D} \left. \frac{\partial c'}{\partial r} \right|_{r=0} , \tag{5.42}$$

where the dimensional variables in the channel are $\hat{c}_{ch} = c_{ch} C_{in}$ and $\hat{r} = r_{ch} a$; and D is the bulk fluid diffusivity. The parameter which governs the magnitude of internal and external mass transport limitations is

$$\frac{D_{eff}}{\varepsilon D} = \frac{Da}{\eta \phi^2 \upsilon} , \tag{5.43}$$

where Da is the Damköhler number for a wall-coated microchannel reactor. If a concentration boundary layer with thickness δ develops at the channel's inlet regime, then the rescaled Damköhler number is appropriate ($Da^* = Da\, \delta$) (Chapter 4). In terms of timescales for internal and external diffusion, $\tau_{int} / \tau_{ext} = \varepsilon^2 D / D_{eff}$.

For the external (channel) domain, we have used the concept of the degree of mass transfer control θ (Chapter 4), which is related to the ratio between the average concentration in the channel and its surface value:

$$\theta = 1 - \frac{c_{surf}^{ch}}{\left\langle c^{ch} \right\rangle} . \tag{5.44}$$

The value of this parameter ranges from 0 in the external kinetic limit to 1 under severe mass transfer limitations.

Frequently, the criteria are given in terms of operating variables, e.g. the temperature above which diffusional effects are present in a particular system. Under some assumptions, the criteria formulated in dimensionless manner can be rewritten explicitly for the relevant quantities characterizing geometry and operation. In the definitions of both Thiele modulus and Damköhler's number, the temperature dependence of the time constant for reaction (evaluated at the surface) is written as

$$\frac{R_V\left(\hat{c}_{surf}\right)}{\hat{c}_{surf}} \sim \exp\left[\frac{-E}{R_G}\left(\frac{1}{T} - \frac{1}{T_0}\right)\right] \lim_{T \to T_0} \frac{R_V\left(\hat{c}_{surf}\right)}{\hat{c}_{surf}} ,$$

where T_0 is a reference temperature, E is the activation energy and R_G is the ideal gas constant. When kinetics is of 'power-law' type, $T_0 \to \infty$ is a convenient choice and

$$\frac{R_V\left(\hat{c}_{surf}\right)}{\hat{c}_{surf}} \sim k_0 \left(\hat{c}_{surf}\right)^{m-1} e^{\frac{-E}{R_G T}},$$

where k_0 is the pre-exponential factor in the Arrhenius law. In more complex kinetics, with other temperature-dependent constants, T_0 should be chosen at a value in the range predicted by the expressions below. The same applies to the calculated values of diffusivity, but if required a simplified iterative procedure may be used. If all the correct dependences need to be considered, then the problem is still reduced and consists in solving a nonlinear algebraic equation, instead of the full convection-diffusion-reaction problem at both channel and washcoat domains.

5.6.1 Kinetic regime

We now discuss the operating boundary for the kinetic regime for different magnitudes of $D_{eff}/(\varepsilon D)$, i.e. change in the controlling behavior from internal to external mass transfer.

5.6.1.a *External mass transfer faster than internal diffusion*

If the effective diffusivity in the catalyst layer is much smaller than the bulk diffusivity (for example, in some zeolite washcoats) and the coating is not extremely thin, then it is likely that $D_{eff}/(\varepsilon D) << 1$. This means that internal diffusion is the rate-limiting step. Therefore, it is possible that no external mass transfer limitations are observable in the channel, but internal concentration gradients exist. For the whole phenomena to be under kinetic control the following condition is sufficient (from (5.43), Da is even smaller): $\eta \phi^2 \upsilon << 1$.

For a specified value of the effectiveness factor (close to unit) given by Eq.(5.17), and considering Arrhenius-type temperature dependence only in the kinetic constant k yields the following expression

$$T_\eta \le \frac{E/R_G}{\ln\left(\frac{\Phi_0^2 \Lambda}{1-\eta}\right)}, \tag{5.45}$$

as the temperature range for which the washcoat (and hence the channel) is free from mass transport limitations. In (5.45), the temperature independent Thiele modulus is defined as

$$\phi_0^2 = \frac{t_w^2}{D_{eff}} \lim_{T \to T_0} \frac{R_V\left(\hat{c}_{surf}\right)}{\hat{c}_{surf}} e^{E/(R_G T_0)} \text{ and} \tag{5.46a}$$

$$\Phi_0^2 = R'(1)\,\phi_0^2 . \tag{5.46b}$$

The shape factor is defined in (5.18), but for thin catalytic coatings is simply $\Lambda = \upsilon/3$. For power-law kinetics associated with only one constant, (5.46a) is simply $\phi_0^2 = t_w^2\, k_0 \left(\hat{c}_{surf}\right)^{m-1} \Big/ D_{eff}$.

Joshi et al. (2010) simulated numerically the oxidation of CO in a circular channel with first-order kinetics. The values reported for diffusivities and geometric characteristics yield $D_{eff}/(\varepsilon D) \sim 0.24$. In these conditions, the temperature below which kinetically controlled conditions prevails is according to (5.45): $T_\eta \leq 187$ºC ($\eta \geq 0.91$). The simulations performed by these authors in channels with different lengths showed very weak dependence of the temperature for kinetic control on the channel dimension (L from 0.01 to 10 cm), with variation between 189ºC and 185ºC, approximately. Our estimate is therefore very reasonable (maximum 1% relative error) given the assumptions, and circumvent the need for numerical solution of the channel-washcoat problem for an extended range of parameters and the rejection of the values which do not lead to the specified η and θ (or alternatively, the need for iterative calculation).

Groppi et al. (2001) studied the kinetics of methane combustion in an annular microreactor with a surface coated with a PdO/Al_2O_3 catalyst layer. They found up that the limiting condition for intrinsic kinetics evaluation was internal diffusion and this could only be achieved by keeping $t_w \leq 10\,\mu$m (so that the effectiveness factor is kept above 0.9). The same qualitative conclusion can be reached taking their data and calculating according to (5.43):

$$\frac{D_{eff}}{\varepsilon\, D} \leq 0.19 . \tag{5.47}$$

Note that in (5.47), ε is the ratio between the catalyst layer thickness and the gap between outer and inner cylinders radii, while the importance of curvature should be evaluated by another parameter (defined as the catalyst thickness divided by the inner cylinder radius). In their conditions, for effectiveness factor greater than 0.9 and $t_w \sim 10\,\mu$m, the maximum temperature for kinetic control from (5.45) is $T_\eta \leq 854$K (581ºC).

The temperature in their simulations was 873K and the effectiveness factor is higher than 0.9 if $t_w \leq 9\,\mu$m micrometers, which is in good agreement with their simulations. Therefore, we may expect that their measurements up to about 600ºC, are free from diffusional limitations in line with their predictions. Note that the geometrical parameter in this case is defined as

$$\upsilon = \frac{2\, r_{in} + t_w}{2\, r_{in} + 2\, t_w}$$

where r_{in} is the radius of the internal cylinder in which the catalyst layer with thickness t_w is supported.

As seen above, the relevant condition in practice for attaining kinetic regime in both domains is not related with channel characteristics. Therefore, the usual strategy of working at high flowrates to ensure kinetic control in the channel (or decrease its length) will not sort much effect in this case. This can be noticed from the numerical solution of the problem, since near or in developing profile conditions, the limiting temperature remains unaffected. We note that when Da is small, the parameter which governs the regime definition in the channel at *developing concentration profile conditions* (Da^*) is even smaller (since it appears multiplied by the normalized thickness of the boundary layer, $\delta << 1$).

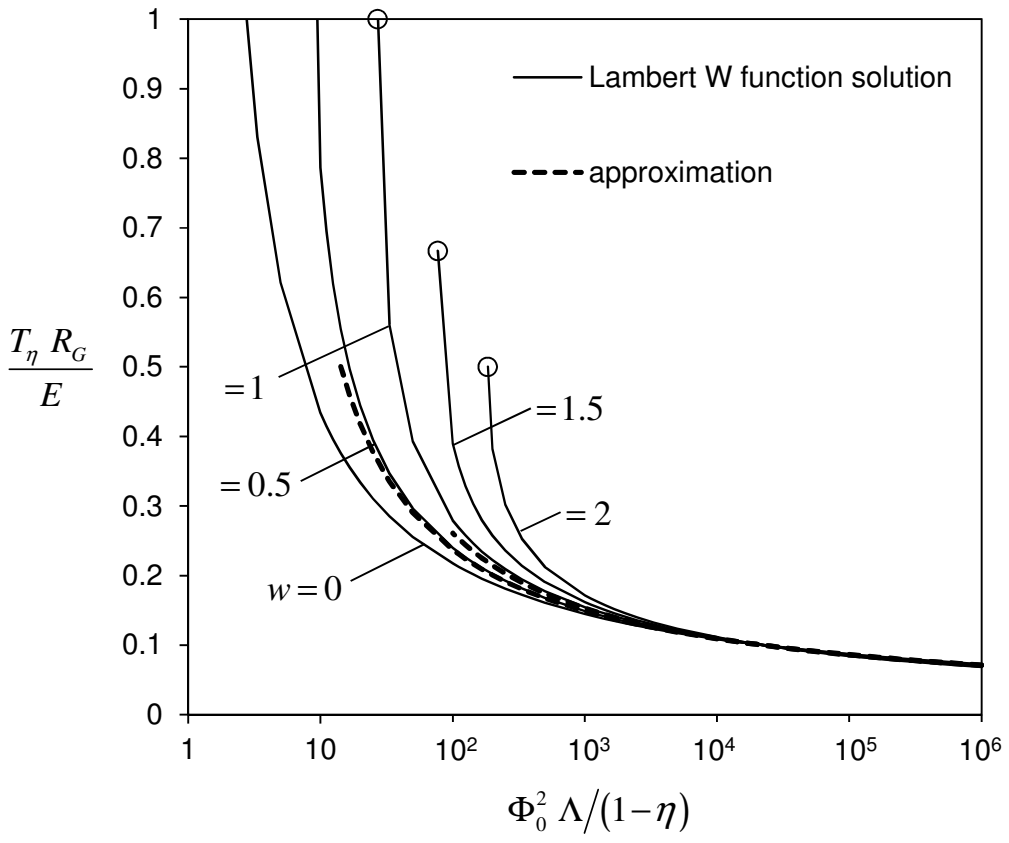

Figure 5.8: Effect of temperature-dependent effective diffusivity on the kinetic regime boundary. The solution involving the Lambert W function Eq.(5.49) is shown for $\gamma_0 = 10$ and several values of the power w in (5.48). The limiting coordinates below which real values are not obtained are depicted by ○. The approximation in (5.50) and the result for $w = 0$ from (5.48) are also represented.

If the effective diffusivity also presents a pronounced temperature dependence given by

$$\frac{D_{eff}}{D_{eff,0}} = \left(\frac{T}{T_0} \right)^w , \tag{5.48}$$

an estimate for T_η is still possible in terms of the Lambert W function from *Mathematica*® or *Matlab*®,

$$T_\eta \leq \frac{E/R_G}{-w\, W\left[\frac{-E}{R_G\, T_0\, w} \left(\frac{1-\eta}{\Phi_0^2\, \Lambda} \right)^{1/w} \right]} \tag{5.49}$$

which requires numerical evaluation and yields real values for $\Phi_0^2\, \Lambda/(1-\eta) > (e\, \gamma_0/w)^w$. An approximate solution is obtained if the dependence in (5.48) is recognized to be subdominant compared with the one expressed by Arrhenius law for the kinetic constant. This is constructed in an iterative manner, with (5.45) as a starting point and writes as

$$T_\eta \leq \frac{E/R_G}{\ln\left(\frac{\Phi_0^2\, \Lambda}{1-\eta} \right) + w \ln\left[\frac{R_G\, T_0}{E} \ln\left(\frac{\Phi_0^2\, \Lambda}{1-\eta} \right) \right]} . \tag{5.50}$$

Note that in Eqs.(5.49) and (5.50), D_{eff} in (5.46a) is evaluated as $D_{eff,0}$. The same approximate treatment can apply to the case where other kinetic constants exhibit strong temperature dependence, e.g. K in Eq.(5.5e). For a fixed value of $\gamma_0 = E/(R_G\, T_0)$, $T\, R_G/E$ can be plotted as a function of $\Phi_0^2\, \Lambda/(1-\eta)$ for several values of w. The results from Eqs.(5.45), (5.49) and (5.50) are plotted in Figure 5.8 for $\gamma_0 = 10$. Our approximate expression (5.50) is valid for weak $D_{eff}(T)$ dependences (low values of w) and high $\phi_0^2\, \Lambda/(1-\eta)$. Actually, for $\Phi_0^2\, \Lambda/(1-\eta) >> 1$, which is the case since $\eta \to 1$ and $\phi_0^2 = \lim_{T\to\infty} \phi^2$ is usually large, this effect is negligible and the results are well described by (5.45). The typical diffusion mechanism inside a washcoat usually yields values of $w \sim 0.5$. We also note that in this regime, $D_{eff}/(\varepsilon D) << 1$, so the magnitude of the effective diffusivity is expected to be low. Moreover, the effect loses relevance if the reaction activation energy is large. The net result from considering temperature dependence of diffusivity is to increase the temperature below which kinetic control prevails. Therefore, strong dependence of the effective diffusivity on temperature is useful for kinetic measurements.

5.6.1.b *Internal diffusion faster than external mass transfer*

If $D_{eff}/(\varepsilon D) >> 1$ (e.g. in the limit of an extremely thin washcoat), then from (5.43) $Da >> \eta \phi^2 \upsilon$, and it is possible to observe limitation in the interphase mass transfer to a catalytic coating controlled by kinetics. In this case, it suffices to require the negligibility of concentration gradients in the channel. In Chapter 4, we have provided correlations for θ of the form: $Da = f(\theta, \alpha\, Pe_m/z)$, where $\alpha\, Pe_m/z$ is Graetz's parameter ($\alpha\, Pe_m = a^2 \langle u \rangle / (L D)$). Alternatively, a uniformly valid solution for Sherwood number with Neumann boundary condition at the wall could be used. We are going to consider the case of fully developed laminar flow inside a circular channel, however the analysis is similar for the other cases discussed in Chapter 4 and can be easily generalized. Ignoring the temperature dependence on parameters other than the kinetic constant k, the reference Damköhler number writes as ($k_{surf,0} = k_0\, t_w\, \upsilon$):

$$Da_0 = \frac{k_{surf,0}\, a}{D} \lim_{T \to T_0} \frac{R_V(\hat{c}_{surf})}{k_0\, \hat{c}_{surf}} e^{E/(R_G T_0)}. \tag{5.51}$$

Note that since internal transport is very fast, $\eta \to 1$. The temperature below which kinetic controls is

$$T_\theta = \frac{E/R_G}{\ln(Da_0/Da)} = \frac{E/R_G}{\ln\left(Da_0 \frac{1-\theta}{\theta}\right) - \frac{1}{n}\ln\left[\left(\frac{24}{11}\right)^n + 1.033^n \left(\frac{\alpha\, Pe_m}{z}\right)^{n/3}\right]}. \tag{5.52}$$

The coefficient n takes the value of 4 for laminar flow and the degree of mass transfer control θ should be set to a low value (kinetic conditions). The following limits of (5.52) can be obtained

$$T_\theta = \frac{E/R_G}{\ln\left(\frac{11}{24}\frac{Da_0}{\theta}\right)} \qquad \text{(fully developed profile, } \alpha\, Pe_m/z << 1\text{)} \tag{5.53a}$$

$$T_\theta = \frac{E/R_G}{\ln\left[\frac{Da_0}{1.033\,\theta}\left(\frac{z}{\alpha\, Pe_m}\right)^{1/3}\right]} \qquad \text{(developing profile, } \alpha\, Pe_m/z >> 1\text{).} \tag{5.53b}$$

The leading-order estimate is naturally,

$$T_\theta = \frac{E/R_G}{\ln(Da_0/\theta)}. \tag{5.53c}$$

The numerical coefficients in (5.53a) and (5.53b) are related with Sherwood's number under constant wall flux conditions from fully developed and Lévêque's solutions (Shah et al. 1978).

Contrary to the previous case (section 5.6.1.a), the operating boundary depends on channel geometry and conditions, but doesn't include information from the catalytic coating. From (5.52), T_θ decreases with $z/\alpha\, Pe_m$, until reaching its asymptotic value given by (5.53a). Increasing the flow rate, so that operation occurs at the inlet regime described by (5.53b) is beneficial, since it increases T_θ, allowing kinetic measurements at higher temperatures. We note that the effects of the channel's diameter and bulk diffusivity (affected by changes in the pressure or in the nature of the inert gas) are associated, and therefore it is unnecessary to conduct preliminary parametric studies where they are varied independently. The same comment applies to the effect of channel's length, tied with the average velocity in the time constant $L/\langle u \rangle$. To account for the temperature dependence of molecular diffusivity, a similar procedure to the one outlined previously can be obtained for fully developed profile . In this case, $w \sim 1.5$ is a typical value.

Joshi et al. (2011) studied hydrogen oxidation on Pt/Al_2O_3 monolith, where advantage from working at higher flowrates was explored for the purpose of kinetic measurements. In the single channel experiments and at operating temperatures between 20ºC and 500ºC:

$$\frac{D_{eff}}{\varepsilon\, D} \sim 2-5$$

according with their expressions for diffusivities. They reported a characteristic length for diffusion in the washcoat of 25 mm, which is extraordinarily high. We have replaced this value by 25 microns, which is much more reasonable and calculated t_w accordingly (otherwise we would fall in the case explored in section 5.6.1.a). Using Eq.(5.52), a maximum temperature around 6ºC is still required for kinetic control ($\theta \le 0.1$) to prevail inside the square channel (numerical coefficients were adapted for this geometry (Shah et al. 1978)). For $\theta \le 0.25$, $T \le 24^\circ\mathrm{C}$.

5.6.1.c *Internal and external mass transfer rates comparable*

In general, if neither internal nor external mass transfer dominate, the regime will be the 'same' in the channel and in the catalytic coating, or at least it is not possible to identify *a priori* the limiting condition for kinetic control. Therefore, if $D_{eff}/(\varepsilon D) \sim 1$ and consequently $Da \sim \eta\, \phi^2 \upsilon << 1$, the maximum temperature so that concentration gradients are absent from both domains is

$$T = \min\left(T_\eta, T_\theta\right), \tag{5.54}$$

where low values of $(1-\eta)$ and θ should be set in Eqs.(5.45) and (5.52), for the coating and channel respectively. A magnitude relationship between T_η and T_θ can be written for fully developed concentration profile as

$$T_\eta < T_\theta \qquad \text{if } \frac{D_{eff}}{\varepsilon D} < 0.7273\, R'(1)\frac{\theta}{1-\eta} \tag{5.55a}$$

$$T_\eta > T_\theta \qquad \text{if } \frac{D_{eff}}{\varepsilon D} > 0.7273\, R'(1)\frac{\theta}{1-\eta}, \tag{5.55b}$$

and for developing profile conditions as

$$T_\eta < T_\theta \qquad \text{if } \frac{D_{eff}}{\varepsilon D} < 0.344\, R'(1)\left(\frac{\alpha\, Pe_m}{z}\right)^{1/3}\frac{\theta}{1-\eta} \tag{5.56a}$$

$$T_\eta > T_\theta \qquad \text{if } \frac{D_{eff}}{\varepsilon D} > 0.344\, R'(1)\left(\frac{\alpha\, Pe_m}{z}\right)^{1/3}\frac{\theta}{1-\eta}. \tag{5.56b}$$

For simplicity, the arbitrary criteria can be set to the same value at both channel and washcoat, i.e. $\theta \sim 1-\eta << 1$. Eq.(5.19) was used for thin catalytic coatings, but the result without this substitution is easily obtained by multiplying the right hand side of (5.55) and (5.56) by $3\Lambda/\upsilon$.

When Eqs.(5.55a) or (5.56a) apply, a conservative estimate for the kinetic regime boundary is obtained as discussed in section 5.6.1.a. On the other hand, if (5.55b) or (5.56b) describe a particular situation, then the results in section 5.6.1.b are appropriate. Note that $D_{eff}/(\varepsilon D)$ needs to take really high values for (5.56b) to apply ($\alpha\, Pe_m >> 1$), otherwise kinetic control in the washcoat is always limiting.

5.6.2 Diffusional regime

In the washcoat, the temperature above which diffusional effects are present (associated with a low value of η) is

$$T_\eta = \frac{E/R_G}{2\ln\left[\dfrac{\Phi_0\,\upsilon\,\eta}{1+\upsilon(\upsilon-1)\eta}\right]}. \tag{5.57}$$

To obtain Eq.(5.57), we have used Eq.(5.24) where the Thiele modulus is given by

$$\Phi_0^2 = \left(2\int_0^1 R(c_0)\,dc_0\right)^{-1}\phi_0^2, \tag{5.58}$$

and here ϕ_0^2 is referred to the value in (5.46a). The relationship between the prediction from (5.57) and the extent of diffusional limitations in the channel is discussed below for several values of $D_{eff}/(\varepsilon D)$.

5.6.2.a *External mass transfer faster than internal diffusion*

As before, using the scaling from (5.43) it is possible to observe that the presence of internal strong concentration gradients ($\eta\phi^2 >> 1$) does not imply necessarily that the transport in the channel is limited. Therefore, both domains are diffusion-controlled when $T > T_\theta$ given by (for selected values of θ close to 1):

$$T_\theta = \frac{E/(2R_G)}{\ln(Da_0/Da)} = \frac{E/(2R_G)}{\ln\left(Da_0\dfrac{1-\theta}{\theta}\right) - \dfrac{1}{4}\ln\left[11.1735 + 0.5334\left(\dfrac{\alpha\, Pe_m}{z}\right)^{4/3}\right]} \tag{5.59}$$

Eq.(5.59) made use of the correlation developed in Chapter 4, shown here for laminar flow inside a circular channel. The Damköhler number Da_0 is defined as

$$Da_0 = \frac{Da_0^{II}}{\Phi_0} = \left(2\int_0^1 R(c_0)\,dc_0\right)^{1/2} \frac{\upsilon\, a\sqrt{D_{eff}}}{D} \sqrt{\lim_{T\to T_0}\frac{R_V(\hat{c}_{surf})}{\hat{c}_{surf}}}\; e^{E/(2R_G T_0)} \tag{5.60a}$$

or for a 'power-law kinetics':

$$Da_0 = \frac{Da_0^{II}}{\Phi_0} = \left(2\int_0^1 R(c_0)\,dc_0\right)^{1/2} \frac{\upsilon\, a}{D}\sqrt{k_0(\hat{c}_{surf})^{m-1} D_{eff}}\,. \tag{5.60b}$$

In these expressions, the effectiveness factor in the definition of Da was given by $\eta \sim 1/\Phi$, with Φ related with Φ_0 from (5.58).

The temperature below which mass transfer limitations are negligible in the channel, but washcoat diffusion is present, is given from the correlation also employed in (5.52) (for a low value of θ),

$$T_\theta = \frac{E/(2R_G)}{\ln(Da_0/Da)} = \frac{E/(2R_G)}{\ln\left(Da_0\dfrac{1-\theta}{\theta}\right) - \dfrac{1}{4}\ln\left[\left(\dfrac{24}{11}\right)^4 + 1.033^4\left(\dfrac{\alpha\, Pe_m}{z}\right)^{4/3}\right]}\,, \tag{5.61}$$

with Da_0 from Eq.(5.60). Santos and Costa (2011) quantified the magnitudes of the reaction, internal and external mass transfer resistances for a set of parameters corresponding to experiments in a three-way catalyst for the conversion of pollutants in automotive catalytic converters. They noted that external mass transfer controlled regime was difficult to achieve,

but most of their points lied in what they defined as a mixed control between internal and external mass transfer control (which corresponds to the overall mass transfer resistances representing 90% of the total resistance). Their values of $D_{eff}/(D\varepsilon)$ are low and their observations are consistent with the presence of strong intraphase mass transfer resistances in comparison with the external one. In fact, according to (5.57), the effectiveness factor is lower than 0.1 for temperatures above 536ºC, and lower than 0.33 for temperatures higher than 363ºC. External mass transfer control ($\theta \geq 0.9$) is not achieved in their experiments, since for this to happen $T > 1400$ºC from (5.59). The maximum value of θ registered was near 0.75.

5.6.2.b *Internal diffusion faster than external mass transfer*

Due to the reduced characteristic dimensions of catalytic coatings, it is possible that internal diffusion proceeds faster than the external one (in the sense of "diffusion velocity" mentioned earlier) and thus possibly eliminates the existence of any internal gradient, while in the channel they may exist. In this case, both domains will be under diffusion control when temperature exceeds that calculated from (5.57). More likely, diffusion limitations occur in the channel, but not on the catalytic coating and the temperature associated with a given value of mass transfer control θ is given by

$$T_\theta = \frac{E/R_G}{\ln(Da_0/Da)} = \frac{E/R_G}{\ln\left(Da_0\dfrac{1-\theta}{\theta}\right) - \dfrac{1}{4}\ln\left[11.1735 + 0.5334\left(\dfrac{\alpha\, Pe_m}{z}\right)^{4/3}\right]}, \tag{5.62}$$

where Da_0 is given by (5.51). Tomasic et al. (2002) studied NO decomposition over zeolite ZSM5 supported on a cordierite monolith. They have also performed 2D numerical simulations and reported interphase mass transfer limitations, but negligible internal diffusional effects (except for the highest temperature and thickest catalytic coating where $\eta = 0.72$). One of the monolith samples presented $\eta = 0.99$ but θ very close to 1. According to our analysis, this was due to the high value of effective diffusivity found by these authors ($D_{eff} \sim 8\times10^{-6}$ m^2/s), leading to $D_{eff}/(\varepsilon D) > 1$ for their conditions. We note that for this condition to be achieved, it is not required for the effective diffusivity to achieve unrealistic high values, since ε (which in their case was around 0.1 – 1) is often small enough.

The turning point in the magnitude relationship between the behaviors in sections 5.6.2.a and 5.6.2.b is obtained by comparing (5.57) with (5.59):

$$T_\eta > T_\theta \qquad \text{if } \frac{D_{eff}}{\varepsilon D} > \frac{Sh_\infty}{(S+1)\upsilon}\frac{\eta}{1-\theta} \tag{5.63a}$$

$$T_\eta < T_\theta \qquad \text{if } \frac{D_{eff}}{\varepsilon D} < \frac{Sh_\infty}{(S+1)\upsilon}\frac{\eta}{1-\theta}, \tag{5.63b}$$

where Sh_∞ is Sherwood number under Dirichlet wall boundary condition and $S=1$ in a circular channel. The reversed roles of our criteria η and θ can be seen in comparison with Eqs.(5.55).

5.6.3 Mapping of operating regimes

Figure 5.9 shows the previously identified boundaries for a first-order reaction and for two values of $\varepsilon D/D_{eff}$, corresponding to different controlling behaviors. The activation temperature (E/R_G) was chosen to be 10^4 K, although this value doesn't need to be specified (the temperature axis could have been normalized as $T\,R_G/E$). The temperature dependence of quantities other than the kinetic constant is neglected. The reaction occurs in a cylindrical catalyst layer with $\varepsilon = 0.1$.

Figure 5.9a is plotted for a fixed value of Thiele modulus (and thus, Damköhler's number Da_0 is also fixed). For high $\varepsilon D/D_{eff}$, the kinetic regime is determined by the internal process, while mass transfer control is harder to be achieved in the channel. The influence of the flowrate and other operating conditions in $\alpha\, Pe_m$ has no effect in improving the parametric area for kinetic measurements, since the boundary for $\theta = 0.1$ is in the intermediate regime of the catalytic coating. Nevertheless, $\varepsilon D/D_{eff} = 10$ is high enough for the effectiveness factor to be described by $\eta \sim 1/\phi$, and therefore even though $\eta > 0.1$, the value of θ is close to 0.1 from Eq.(5.61). The reverse picture is found when $\varepsilon D/D_{eff}$ is low (Figure 5.9b), where external mass transfer control is easier to achieve, while the washcoat may be in an intermediate regime. However, the curve for $\theta = 0.9$ is sufficiently close to the internal diffusional regime for $\eta \sim 1/\phi$ and hence transport in the channel is limiting, with already moderate to severe internal diffusion control. The value considered for this case ($\varepsilon D/D_{eff} = 0.5$) is not low enough for Eq.(5.62) to apply (the washcoat is not free from limitations in this case). However, it is possible to see the transition in the controlling behavior, which changes between the coating and the channel as the Peclet number increases. This point is predicted from Eqs.(5.63). This confirms that when the channel is operated at the entrance length regime, mass transfer controlled conditions are harder to be achieved.

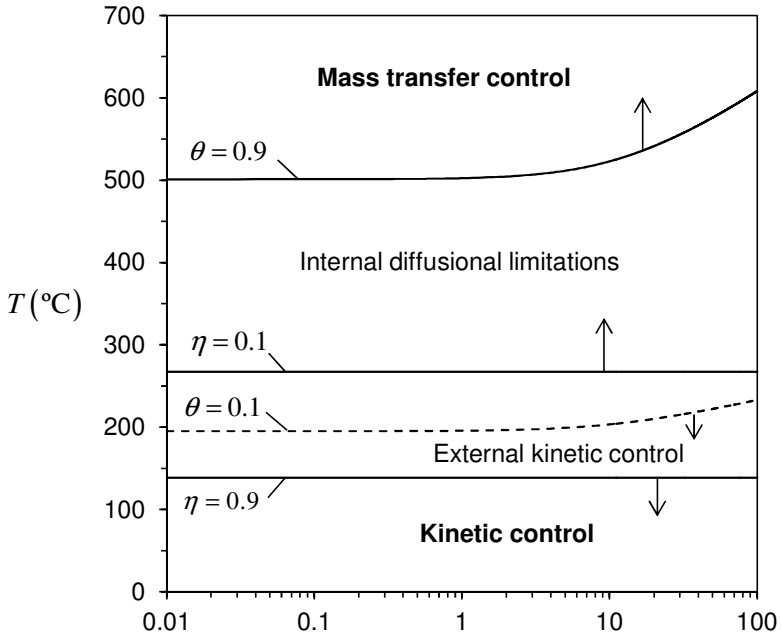

(a) $\frac{D_{eff}}{\varepsilon\, D} = 0.1$ and $\phi_0 = 10^5$.

Lines: $\eta = 0.9$ from (5.45); $\eta = 0.1$ from (5.57); $\theta = 0.1$ from (5.61); $\theta = 0.9$ from (5.59).

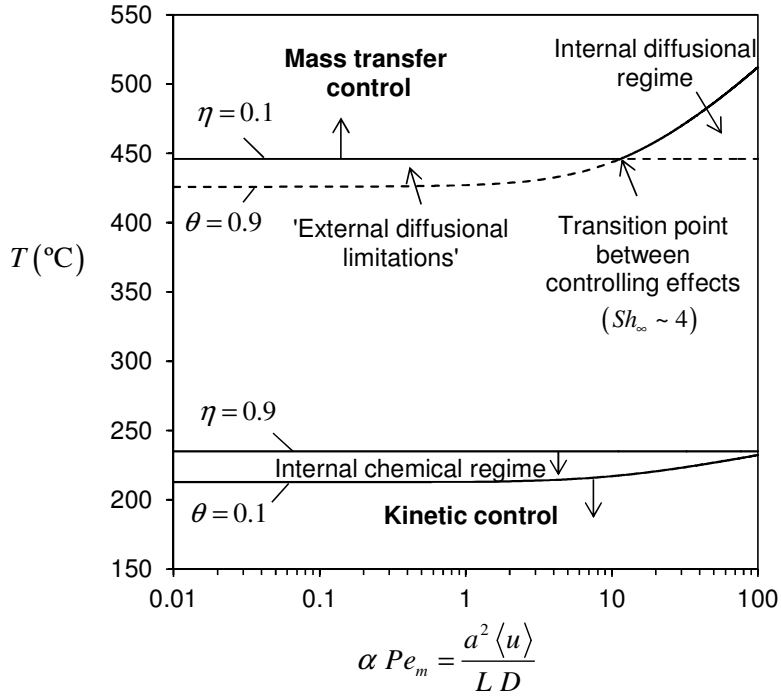

(b) $\frac{D_{eff}}{\varepsilon\, D} = 2$ and $\phi_0 = 10^4$.

Lines: $\eta = 0.9$ from (5.45); $\eta = 0.1$ from (5.57); $\theta = 0.1$ from (5.52); $\theta = 0.9$ from (5.59).

Figure 5.9: Mapping of operating regimes: Temperature - $\alpha\, Pe_m$ diagrams (figures (a) and (b))

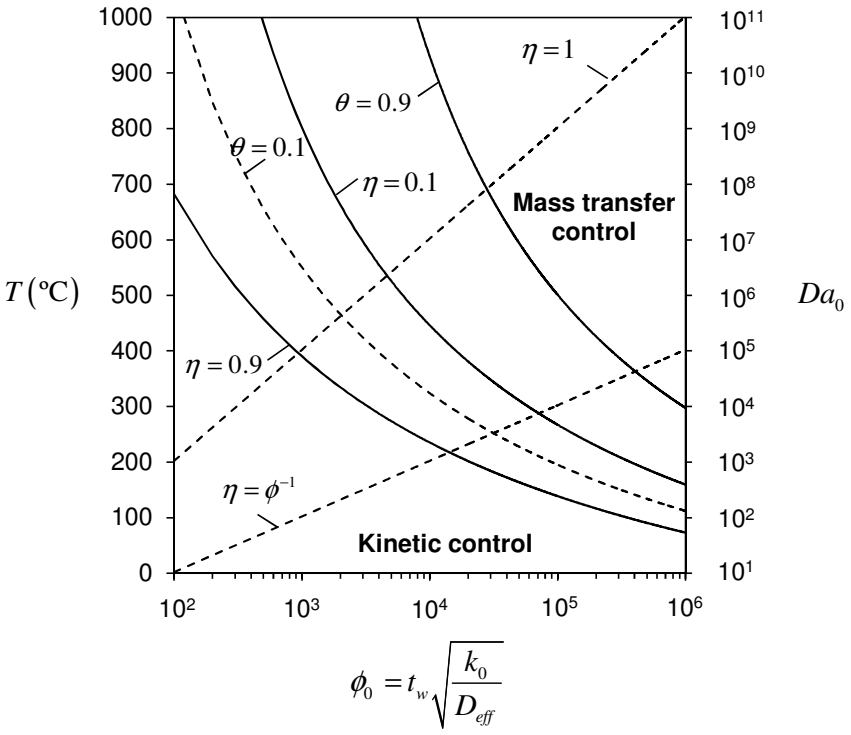

(c) $\dfrac{D_{eff}}{\varepsilon\, D} = 0.1$ and $\alpha\, Pe_m = 0.1$.

Lines: $\eta = 0.9$ from (5.45); $\eta = 0.1$ from (5.57); $\theta = 0.1$ from (5.61); $\theta = 0.9$ from (5.59).

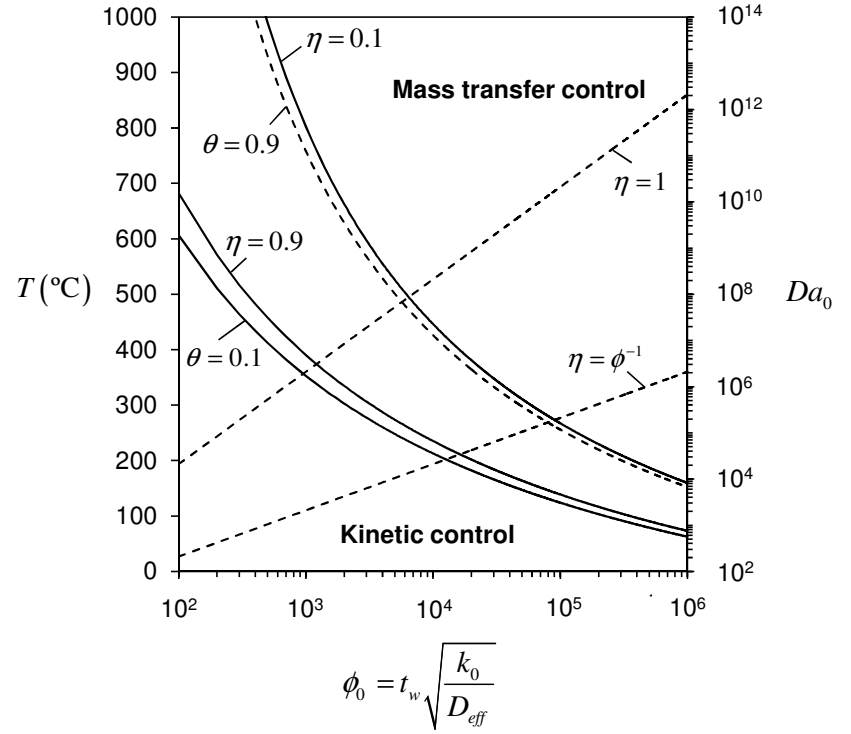

(d) $\dfrac{D_{eff}}{\varepsilon\, D} = 2$ and $\alpha\, Pe_m = 0.1$.

Lines: $\eta = 0.9$ from (5.45); $\eta = 0.1$ from (5.57); $\theta = 0.1$ from (5.52); $\theta = 0.9$ from (5.62).

Figure 5.9: Mapping of operating regimes: Temperature - ϕ_0 diagrams (figures (c) and (d))

Concerning the processes which determine the definition of completely kinetic or mass transfer controlled regimes, the above conclusions can also be taken from 5.9c and 5.9d. In this case for fixed $\varepsilon D/D_{eff}$ and variable ϕ_0, Da_0 also varies according to (5.43). For chemical ($\eta \sim 1$) and diffusional ($\eta \sim 1/\phi$) internal regimes, the value of Da_0 is given by the dashed lines, which should be read on the right side scale.

To evaluate the accuracy of these boundaries, numerical simulations for fixed values of ε, α, ϕ_0 and $\varepsilon D/D_{eff}$ were performed for several values of αPe_m. Temperature was set so that the simulation parameters lied in each of the defined limits. The channel and washcoat mass balances were solved with concentration and flux continuity conditions (Eq.(5.42)). From these results, the effectiveness factor and the degree of mass transfer control were calculated and compared with the specified values. Minor differences were observed.

5.7 PERFUSIVE CATALYTIC COATINGS AND MONOLITHS

Wall-coated microchannel reactors with thin catalyst layers, hollow catalyst pellets or egg-shell particles are some of the strategies for reduction of the internal mass transfer resistance that have appeared in the last decades in the field of reaction engineering. Other approaches also have been proposed, namely the introduction of macroporosity into the catalytic washcoat (Wang et al. 2010). In fact, bimodal catalysts in which the pore size distribution includes both macropores (providing pathways for fast intraparticular diffusion) and mesopores (providing high surface area for efficient metal dispersion) are still being studied and synthetized (Wang et al. 2008; Tao et al. 2011; Zhou et al. 2011). In this case the transport in the macropores may also rely on viscous flow due to internal pressure variation (changes in the number of moles from reaction).

Another possibility arises when the material is permeable, and therefore intraparticular flow due to an external pressure difference is observed. The effect of this additional transport mechanism was explored originally in the context of permeable catalytically active pellets with the usual geometries of slab, cylinder and sphere (Nir et al. 1977; Rodrigues et al. 1982; Lu et al. 1993; Nan et al. 1996a). However, other shapes are interesting for reduction of mass transfer resistance, even when they rely on diffusion alone. The hollow cylinder (and multihole pellets in general) has been pointed out as the most frequent shape found in practice (Wijngaarden et al. 1998), and in some cases selected as the optimal geometry (Soltan Mohammadzadeh et al. 2002) due to its improved mass transfer features, convenient manufacture, low pressure drop and capability of inducing larger transverse mixing and bed porosities. If internal convection is superposed to this, further advantage may be taken from the catalyst. Nan et al. (1996b)

quantified the augmented diffusivity due to convection in the axial direction for a hollow cylinder analytically and experimentally using the chromatographic method. In this section, we obtain a solution that applies to a long hollow cylindrical particle with radial convective flow.

The same picture with convective and diffusive fluxes acting in the same direction is found in other cases, for example: 'open-wall' monoliths, tubular reactors with porous catalytic walls or membrane reactors. Lathouder et al. (2004) used a highly porous acicular mullite honeycombs as support for enzyme immobilization (Figure 5.10b). They point out the advantages of the open microstructure compared with the conventional 'small pore' monoliths, namely: higher catalyst loading, reduced pressure drop, slower decrease in activity with time, and improved mass transfer in the cases where limitations existed. In the monoliths used, the pore diameter ranged from $5\,\mu m$ to $16\,\mu m$. Bakker et al. (2005) studied the hydrodynamic properties of this 'open wall' monolith and promoted radial convection by using gas-liquid Taylor flow. Bakker et al. (2007) conducted a selective hydrogenation in the same type of monoliths. They reported an intrinsic permeability of $40\times10^{-12}\,m^2$ and interstitial voids with $45\,\mu m$, and used the pressure pulsing from Taylor flow to induce fluid velocities inside the wall of $10\ mm/s$. This effect was observed to reduce mass transfer limitation, increase activity and the maximum yield. Khassin et al. (2003; 2005a; 2005b) also made use of the 'permeable monolith' concept for the Fischer-Tropsch synthesis. Porous wall tubular reactors have been also studied for quite a long time (Shah et al. 1971; Cedro III et al. 1974). In these configurations, suction or injection of reactant, product or inerts is explored with advantages over solid wall reactors. Recently, new applications include microchannel enzyme reactors (Chen et al. 2010a), bioreactors (Chen et al. 2010b) or porous ceramic mesoreactors for multiphase G/L/S reactions (Aran et al. 2011) (Figure 5.10c). Membrane reactors are also deeply related with these technologies and its modeling can be very similar (Nagy 2010a; Nagy 2010b). In the cases where the performance of the membrane reactor is severely limited by diffusion, the advantages of perfusion have been well documented, for example in oxygen transport in hollow fiber bioreactors (Coletti et al. 2006; Chen et al. 2009). Flow-through catalytic membrane reactors have been also studied for gas-phase reactions, destruction of VOCs and harmful chemicals (Westermann et al. 2009; Motamedhashemi et al. 2011). In some cases, the performance increased in comparison with conventional wall-coated monoliths.

In the context of separation technologies, perfusion chromatography explored the same concept, e.g. for purification of proteins (Afeyan et al. (1990a; 1990b; 1991)). Recently, flow-through monolithic structures and columns operating in radial mode have also been explored for the purification of proteins (Lee et al. 1990; Podgornik et al. 2004), DNA and viruses (Trilisky et al. 2009a; Trilisky et al. 2009b). A technology based on this concept is commercialized by BIA Separations (www.biaseparations.com) and is based on their proprietary CIM Convective Interaction Media® (Figure 5.10a) (CIM). This also relates to the previously discussed work,

since recently these configurations were used as immobilized enzyme reactors (Podgornik et al. 2002; Vodopivec et al. 2003; Platonova et al. 2009).

It is clear from the literature that the presence and improvement resulting from convective flow has interest for a number of technologies. At the channel level, this extra mass transfer mechanism can be beneficial, as it disrupts the boundary layer that forms in the transverse direction. In some sense, this is related to other approaches for performance enhancement in microchannel reactors (Yoon et al. 2006). In this section we propose a simplified expression for the effectiveness factor in a cylindrical permeable catalyst layer (section 5.7.2). We then quantify the performance enhancement in the effectiveness factor (section 5.7.3).

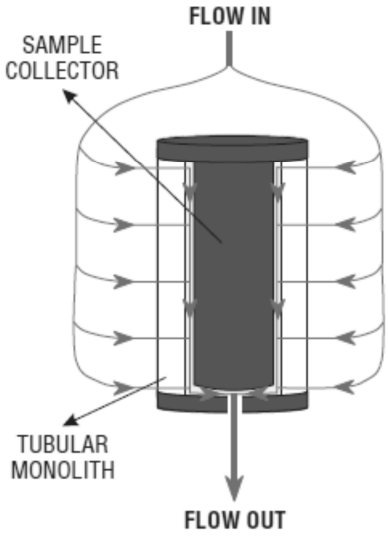

(a) CIM® tube monolithic column from BIASeparations.

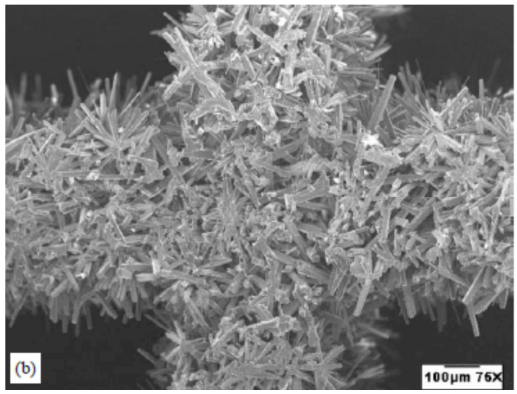

(b) Acicular mullite ceramic honeycomb (De Lathouder et al. 2004).

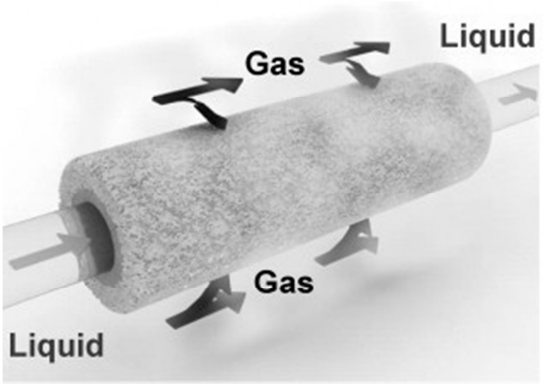

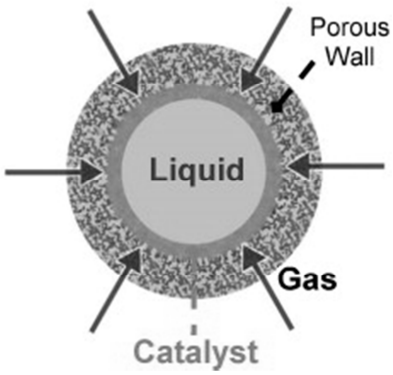

(c) Porous ceramic mesoreactors for gas/liquid/solid hydrogenation (Aran et al. 2011).

Figure 5.10: Examples reproduced from the literature of materials and technologies where intraparticular flow inside catalytic monoliths or coatings is present.

5.7.1 Model equations for a perfusive hollow cylinder

We consider a single circular channel made of a permeable material with catalytic properties, in which a first-order isothermal reaction occurs (see Figure 5.11). The reactant stream that flows through the channel penetrates the washcoat with interstitial radial velocity $\hat{u}_i$, given by Darcy's law. As we will discuss below, the characteristic distances for transport in other directions are much larger than the one in the radial direction. The equation of motion for an homogeneous porous media (with permeability B) and the continuity equation yield (Kelsey et al. 1990)

$$\hat{u}_i(r,z) = \frac{u_{wall}(z)}{1+\varepsilon\, r}, \tag{5.64}$$

where the variables were defined as before (dimensional variables are capped), $r = (\hat{r}-a)/t_w$ and $z = \hat{z}/L$. The velocity at the internal wall $u_{wall}(z)$ is obtained by integration over the radial coordinate,

$$u_{wall}(\hat{z}) = \frac{B}{\varepsilon_P\, \mu}\, \frac{(P_{in}-P_{out})}{a\ln(1+\varepsilon)},$$

where $P_{in}(z)$ is the pressure on the channel's lumen side and $P_{out}(z)$ is the pressure on the external side of the channel ($P_{in}-P_{out}$ is the trans-membrane pressure). Flow across the wall from inside the channel occurs whenever $P_{in} > P_{out}$. Note that in the limit of a flat wall ($a \to \infty$): $u_{wall}(\hat{z}) = B(P_{in}-P_{out})/(\varepsilon_P\, \mu\, t_w)$. We use the radial average of velocity as a scale for $\hat{u}_i$:

$$\langle \hat{u}_i \rangle(z) = \frac{B(P_{in}-P_{out})}{\varepsilon_P\, \mu\, t_w\, \upsilon}\, \frac{\varepsilon}{\ln(1+\varepsilon)}.$$

The velocity profile in (5.64) is then made dimensionless according to:

$$u_i(r) = \frac{\hat{u}_i(r,z)}{\langle \hat{u}_i \rangle(z)} = \frac{\upsilon}{1+\varepsilon\, r}. \tag{5.65}$$

For thin walls (small ε), $u_i(r) \sim \upsilon(1-\varepsilon\, r) + O(\varepsilon^2)$. The dimensionless mass conservation equation inside an annular element of the washcoat (with volume $dV = 2\pi\, \hat{r}\, d\hat{r}\, d\hat{z}$) is

$$\frac{1}{1+\varepsilon\, r}\frac{\partial}{\partial r}\left[(1+\varepsilon\, r)\frac{\partial c}{\partial r}\right] - \frac{P}{1+\varepsilon\, r}\frac{\partial c}{\partial r} - \phi^2\, c = P_{ax}(\alpha\,\varepsilon)^2\frac{\partial c}{\partial z} - (\alpha\,\varepsilon)^2\frac{\partial^2 c}{\partial z^2} \tag{5.66a}$$

Our solution applies to small values of $P_{ax}(\alpha\,\varepsilon)^2$ or $(\alpha\,\varepsilon)^2$, rendering the terms on the right hand side of (5.66a) negligible, and therefore we scale concentration by its value at the internal wall: $c(r,z) = \hat{c}(r,z)/\hat{c}_1(z)$.

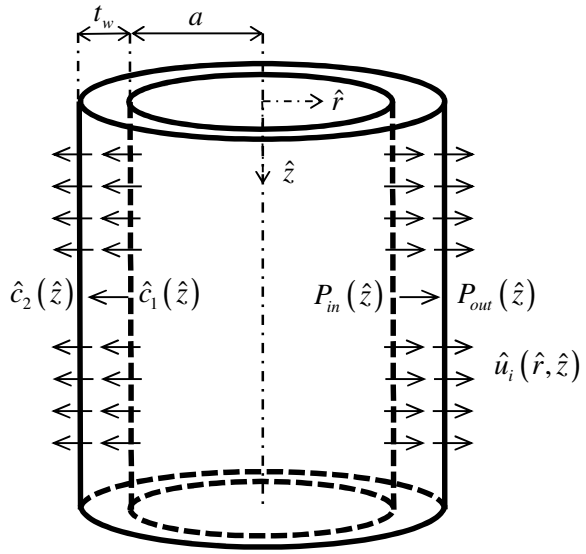

Figure 5.11: Perfusive monolith with wall thickness t_w and radius of the circular open channel a. Intraparticular flow direction is represented for $P_{in} > P_{out}$ with velocity profile $\hat{u}_i$. Surface concentrations are $\hat{c}_1$ and $\hat{c}_2$.

For simplicity , we solve the problem for the case of specified concentration at both surfaces of the channel:

$c = 1$ at $r = 0$ (5.66b)

$c = c_2(z)$ at $r = 1$. (5.66c)

These surface concentrations are determined when solving the internal and external convection-diffusion problems. The parameters (and/or functions of the axial variable) appearing in Eqs.(5.66) are:

Intraparticular radial Peclet number: $$P = \frac{\varepsilon_P \langle \hat{u}_i \rangle t_w \upsilon}{D_{eff}} = \frac{B(P_{in} - P_{out})}{\mu D_{eff}} \frac{\varepsilon}{\ln(1+\varepsilon)} \quad (5.67a)$$

Intraparticular axial Peclet number: $$P_{ax} = \frac{\varepsilon_P u_{ax} L}{D_{ax}} \quad (5.67b)$$

Thiele modulus: $$\phi^2 = \frac{t_w^2 k}{D_{eff}} \quad (5.67c)$$

Washcoat-channel length scales ratio: $$\varepsilon = \frac{t_w}{a} \quad (5.67d)$$

Aspect ratio: $$\alpha = \frac{a}{L}\sqrt{\frac{D_{ax}}{D_{eff}}} \quad (5.67e)$$

Ratio of surface concentration distributions: $$c_2 = \frac{\hat{c}_2}{\hat{c}_1} \quad (5.67f)$$

When neglecting axial diffusion and convection, besides typical geometrical features ($t_w << L$), we have assumed that the permeability in this direction may be much smaller than the one in the radial direction. The axial dependence of the solution is thus given by the parameters and boundary conditions.

The radially averaged effectiveness factor (referred to internal surface conditions) is

$$\eta = \frac{1}{\upsilon}\int_0^1 (1+\varepsilon\, r)\, c\, dr = \frac{1}{\phi^2\,\upsilon}\left[(1+\varepsilon)\left.\frac{\partial c}{\partial r}\right|_{r=1} - \left.\frac{\partial c}{\partial r}\right|_{r=0}\right] + (1-c_2)\,\frac{P}{\phi^2\,\upsilon}. \tag{5.68}$$

5.7.2 Perturbation solution for specified surface concentration and pressure profiles

A simplified solution is obtained below for the following parameter magnitude relationship: $(\alpha\,\varepsilon)^2$, $P_{ax}(\alpha\,\varepsilon)^2 << \varepsilon << 1$. There is no need to restrict the magnitude of ϕ^2, P and c_2, since the kinetic law is linear and an analytical solution is possible without further simplification. We take ε as a small parameter and look for a perturbation expansion for the concentration profile of the following form:

$$c(r) = c_0(r) + c_1(r)\,\varepsilon + O(\varepsilon^2). \tag{5.69}$$

The first two subproblems extracted from Eqs.(5.66) give the solution to the coefficients $c_0(r)$ and $c_1(r)$:

$$O(\varepsilon^0): \qquad \frac{\partial^2 c_0}{\partial r^2} - (P-\varepsilon)\frac{\partial c_0}{\partial r} - \phi^2\, c_0 = 0 \tag{5.70a}$$

$$c_0(r=0) = 1 \tag{5.70b}$$

$$c_0(r=1) = c_2 \tag{5.70c}$$

$$O(\varepsilon^1): \qquad \frac{\partial^2 c_1}{\partial r^2} - (P-\varepsilon)\frac{\partial c_1}{\partial r} - \phi^2\, c_1 = -(P-\varepsilon)\, r\,\frac{\partial c_0}{\partial r} \tag{5.71a}$$

$$c_1(r=0) = 0 \tag{5.71b}$$

$$c_1(r=1) = 0 \tag{5.71c}$$

A convenient redefinition of Peclet number with curvature effects is suggested by Eqs. (5.70a) and (5.71a): $P_C = P - \varepsilon$. The corresponding perturbation series for the effectiveness factor is

$$\eta = \eta_0 + \varepsilon\,\eta_1 + O(\varepsilon^2). \tag{5.72a}$$

Table 5.3: Maximum relative error between $\eta(\phi^2)$ calculated numerically (gPROMS®) and from Eq.(5.73) with $c_2 = 1$. The numbers in brackets correspond to the value of Thiele modulus where the maximum is observed.

ε \ P_C	0.1	1	5	10	100
0.1	0.0004% (16)	0.003% (15)	0.007% (28)	0.02% (67)	0.06% (136)
0.5	0.006% (12)	0.04% (11)	0.13% (31)	0.39% (67)	1.18% (128)
1	0.02% (12)	0.11% (11)	0.32% (31)	1.06% (64)	3.8% (122)

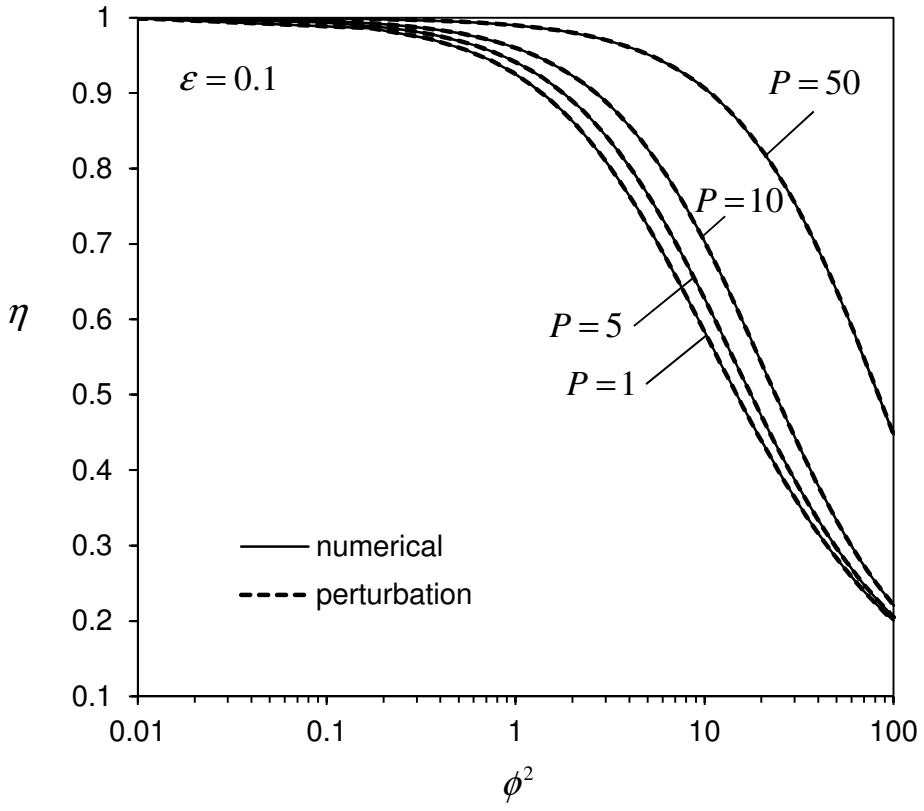

Figure 5.12: Effectiveness factor plot $\eta(\phi^2)$ in a hollow perfusive cylinder with $\varepsilon = 0.1$ and for several values of the intraparticular Peclet number. Full lines are the result of numerical simulation. Dashed lines represent the approximate solution (5.73).

The terms up to $O(\varepsilon^2)$ are calculated from

$$\eta_0 = \frac{1}{\phi^2 \upsilon}\left[(1+\varepsilon)\left.\frac{\partial c_0}{\partial r}\right|_{r=1} - \left.\frac{\partial c_0}{\partial r}\right|_{r=0}\right] + (1-c_2)\frac{P}{\phi^2\,\upsilon} \tag{5.72b}$$

$$\eta_1 = \frac{1}{\phi^2 \upsilon}\left(\left.\frac{\partial c_1}{\partial r}\right|_{r=1} - \left.\frac{\partial c_1}{\partial r}\right|_{r=0}\right). \tag{5.72c}$$

Solving Eqs.(5.70) to (5.72), the effectiveness factor becomes

$$\begin{aligned}\phi^2 \upsilon\,\eta = {} & \frac{1+c_2}{2}\frac{\xi}{\tanh(\xi/2)} - \frac{\xi}{2}e^{-P_C/2}\frac{c_2+e^{P_C}}{\sinh(\xi/2)} + P_C\frac{1-c_2}{2}\left(1-\frac{\varepsilon\,P_C}{\xi^2}\right) + \varepsilon(1-c_2) + \\ & + \frac{\varepsilon}{\sinh(\xi/2)}\left[\frac{2P_C(P_C-2)+\xi^2(P_C-4)}{8\,\xi\,e^{-P_C/2}} - \frac{c_2\,P_C\left(4-2P_C+\xi^2\right)}{8\,\xi\,e^{P_C/2}} - \right. \\ & \left. - \frac{c_2\,e^{-P_C/2}+e^{P_C/2}}{8\tanh(\xi/2)}(P_C-2)P_C + \frac{P_C(1+c_2)+4\,c_2\,\phi^2}{2\,\xi\,\mathrm{sech}(\xi/2)} + \frac{(1+c_2)(P_C-2)\,P_C}{8\sinh(\xi/2)}\right] + O(\varepsilon^2)\end{aligned} \tag{5.73}$$

where an auxiliary variable was defined as $\xi = \sqrt{P_C^2 + 4\,\phi^2}$. In particular, when $c_2 = 1$:

$$\begin{aligned}\phi^2 \upsilon\,\eta = {} & \frac{\xi}{\tanh(\xi/2)} - \xi\frac{\cosh(P_C/2)}{\sinh(\xi/2)} + \\ & + \frac{\varepsilon}{\sinh(\xi/2)}\left[\frac{2P_C(P_C-2)+\xi^2(P_C-4)}{8\,\xi\,e^{-P_C/2}} - \frac{P_C\left(4-2P_C+\xi^2\right)}{8\,\xi\,e^{P_C/2}}\right. \\ & \left. - \frac{\cosh(P_C/2)}{4\tanh(\xi/2)}(P_C-2)P_C + \frac{2P_C+4\,c_2\,\phi^2}{2\,\xi\,\mathrm{sech}(\xi/2)} + \frac{2(P_C-2)\,P_C}{8\sinh(\xi/2)}\right] + O(\varepsilon^2)\end{aligned} \tag{5.74}$$

The limiting forms are respected:

$$\eta = \frac{\tanh(\phi/2)}{\phi/2} \qquad \text{as } P \to 0 \tag{5.75a}$$

$$\eta = \frac{\xi}{\phi^2\tanh(\xi/2)}\left[1 - \frac{\cosh(P/2)}{\cosh(\xi/2)}\right] \qquad \text{as } \varepsilon \to 0\,. \tag{5.75b}$$

Eq.(5.75b) is equivalent to Nir and Pismen's solution (1977) with their flow parameter equal to $\lambda = P/2$ and Thiele modulus $\phi/2$ (due to difference in the length scales adopted). We have compared Eq.(5.73) with the numerical results from the full model (Eqs.(5.66) and (5.68)) using gPROMS®. The radial coordinate r was discretized by the orthogonal collocation on finite elements with a number of intervals between 500 and 1000. The maximum relative error for several values of the parameters is presented in Table 5.3. We should point out that in the numerical simulations with lower number of discretization points another maximum in the relative error was observed as $\phi \to \infty$, which disappeared as the number of intervals increased.

Therefore, Eq.(5.73) also avoids the numerical convergence issues in the diffusional controlled limit. The effectiveness factor curves $\eta\left(\phi^2\right)$ are plotted in Figure 5.12. For other values of c_2, the agreement between numerical and analytical solutions is comparable to this case.

It is important to note the good agreement observed even for reasonably high values of ε (note that our solution was conceived for small values of ε). At leading-order, the convection, diffusion and reaction problem in a slab catalyst is recovered, for which analytical solutions have been presented for a number of cases (e.g. zero-order kinetics (Rodrigues et al. 1984), consecutive-parallel reactions (Nir 1977; Cresswell 1985) and nonisothermal behavior (Cardoso et al. 2007), also discussed in Chapter 6 of this thesis). In certain limits, a curvature correction for these situations may also be obtained and added as a $O(\varepsilon)$ term.

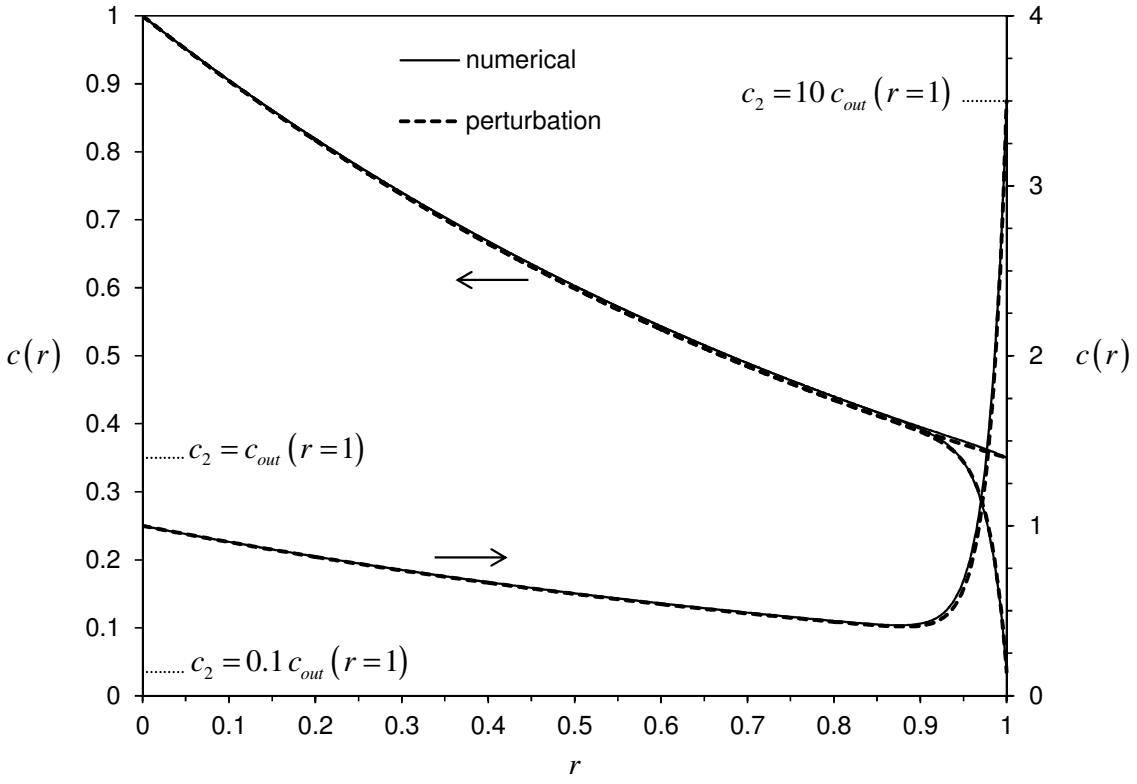

Figure 5.13: Concentration profile in the convection dominated regime for 3 values of the surface concentration at the outer surface of the cylinder. Comparison between perturbation composite solution (5.79) (dashed lines) and numerical solution (full lines). Parameters: $P_C = 50$, $\phi^2 = 50$, $\varepsilon = 0.1$ and $c_{out}\left(r=1\right) = 0.35$.

5.7.3 Performance enhancement

It is well-known (Nir et al. 1977; Rodrigues 1981; Rodrigues et al. 1991) that the effect of an additional mass transport mechanism is to increase the overall content of the pellet in reactant species, and therefore an increase in the effectiveness factor may be observed. The enhancement due to the intraparticular flow can be quantified by

$$\mathrm{E} = \frac{\eta\left(\phi^2, P\right)}{\eta\left(\phi^2, P=0\right)}. \tag{5.76}$$

There is a maximum in the $\mathrm{E}\left(\phi^2\right)$ curves with respect to the parameter ϕ^2, which increases as P increases (Figure 5.14). When $P >> 1$, the internal mass transport is dominated by convection, but for the effect to be visible in the observed reaction rate, kinetics should also be reasonable fast (otherwise no enhancement would be observed), so $\phi^2 >> 1$ (see Figure 5.14). The conditions under which maximum advantage is taken from the catalyst's permeability are detailed below. It is important to characterize this regime, since in others the enhancement is less pronounced. An approximate solution to the concentration profile can be built using the boundary layer method (Bender et al. 1978). For convection-dominated operation (diffusional limitation in the transport), the outer domain ($0 \le r < 1-\delta$) is described by

$$\frac{1}{1+\varepsilon\, r}\frac{\partial\, c_{out}}{\partial\, r} + \frac{\phi^2}{P_C}\, c_{out} = 0 \qquad (P >> 1,\ P \sim \phi^2) \tag{5.77a}$$

$$c_{out}\left(r=0\right) = 1, \tag{5.77b}$$

where it is assumed that the direction of the flow is from the lumen towards the exterior. The boundary condition at $r = 1$ only happens to be fulfilled by (5.77) if

$$c_{out}\left(r=1\right) = \exp\left[-\frac{\phi^2}{P_C}\left(1+\frac{\varepsilon}{2}\right)\right] = c_2$$

which does not happen in general. Therefore, a boundary layer exists at the external surface (from where flow exits the monolith). An appropriate description for this region ($1-\delta < r \le 1$) includes a convective-diffusive balance given by

$$\frac{\partial^2\, c_{in}}{\partial\, R^2} + \frac{\partial\, c_{in}}{\partial\, R} = 0 \tag{5.78a}$$

$$c_{in}\left(R=0\right) = c_2, \tag{5.78b}$$

with $R = P_C\left(1-r\right)$. Both solutions match in an intermediate domain ($c_{out}\left(r \to 1\right) = c_{in}\left(R \to \infty\right)$) to yield the following composite solution:

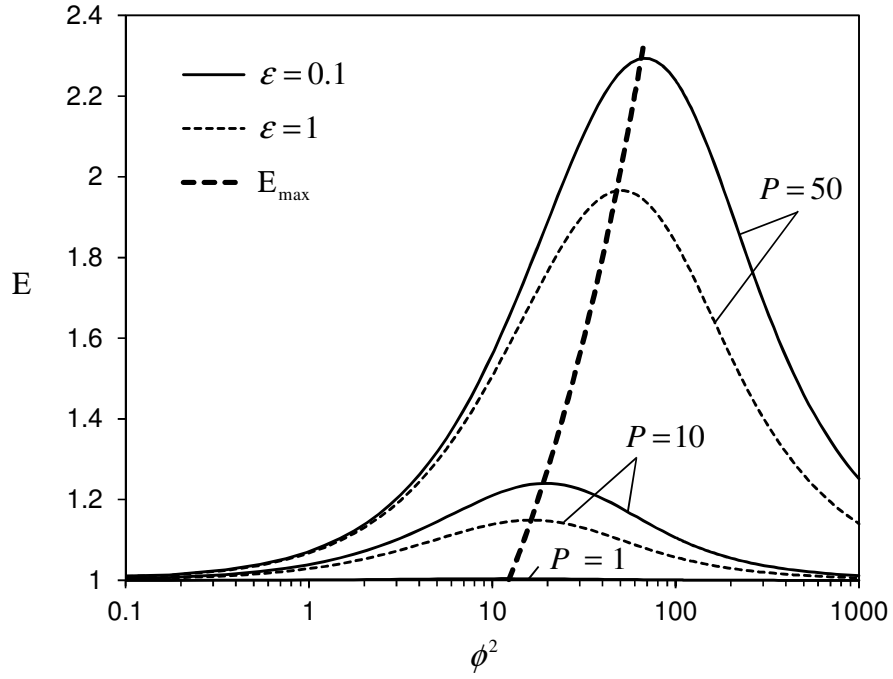

Figure 5.14: Enhancement curves $E(\phi^2)$ of the effectiveness factor in a hollow cylinder due to internal radial convection. Both surfaces are maintained at the same concentration and results for several values of P and ε are shown. The approximate relationship for the maximum effectiveness factor E_{max} in Eq.(5.82) is shown as a thick dashed line.

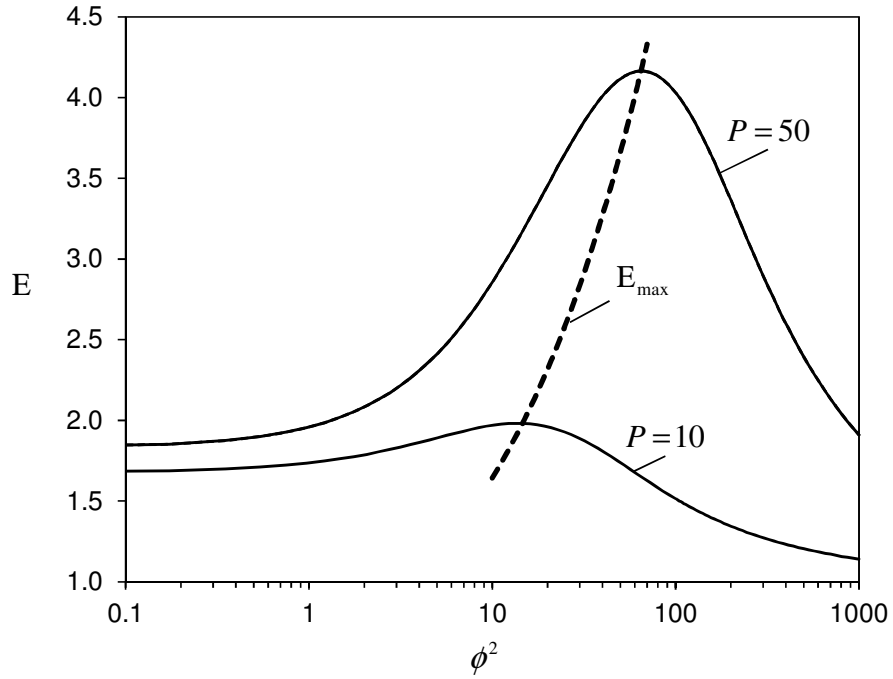

Figure 5.15: Effect of asymmetry in the boundary conditions on the enhancement curves $E(\phi^2)$. The concentration ratio is $c_2 = 0.1$ and results for several values of P and $\varepsilon = 0.1$ are shown. E_{max} from Eq.(5.82) is shown as a thick dashed line.

$$c(r) = e^{\frac{-\phi^2}{P_C} r\left(1+\frac{\varepsilon\, r}{2}\right)} + \left(c_2 - e^{\frac{-\phi^2}{P_C}\left(1+\frac{\varepsilon}{2}\right)} \right) e^{-P_C(1-r)} + O\left(P_C^{-1}\right) \qquad \text{with } \frac{\phi^2}{P_C} \sim O(1). \tag{5.79}$$

This solution is plotted in Figure 5.13 for $P = 50$, $\phi^2 = 50$ and $\varepsilon = 0.1$. For this case, $c_{out}(r=1) = 0.35$, and we choose three concentration profiles with: $c_2 = c_{out}(r=1)$, $c_2 = 10\, c_{out}(r=1)$ and $c_2 = 0.1\, c_{out}(r=1)$. The presence of boundary layers near $r = 1$ for the two latter cases is well described by the composite solution.

The corresponding effectiveness factor is according to Eq.(5.68):

$$\eta \sim \frac{P_C}{\upsilon\, \phi^2}\left[1 - (1+\varepsilon)\, e^{\frac{-\phi^2 \upsilon}{P_C}} + e^{-P_C - \frac{\phi^2 \upsilon}{P_C}} - c_2\, e^{-P_C} + \frac{1 + c_2\,(P_C - 1)}{P_C}\,\varepsilon \right] + \frac{1}{\upsilon\, P_C}\left[1 - (1+\varepsilon)^2\, e^{\frac{-\phi^2 \upsilon}{P_C}} \right]. \tag{5.80}$$

A simple estimate of the enhancement factor defined in (5.76) can be obtained in the limit of small ε and high P_C,

$$\mathrm{E} \sim \frac{P_C}{\upsilon\, \phi^2}\left[1 - e^{\frac{-\phi^2 \upsilon}{P_C}} + c_2\, \varepsilon \right] \frac{\phi}{(1+c_2)\tanh(\phi/2)}$$

The maximum of E with respect to ϕ is calculated from (for reasonably high ϕ but $\phi^2/P \sim 1$),

$$1 - e^{\frac{-\phi^2 \upsilon}{P_C}} = 2\,\frac{\phi^2\, \upsilon}{P_C}\, e^{\frac{-\phi^2 \upsilon}{P_C}} + O(\varepsilon)$$

and therefore, the optimum set of parameters ($\phi^2 \upsilon / P_C$) is approximately described by a constant ratio of the timescales for convection and reaction, with the following numerical value:

$$\frac{\upsilon\, \phi_{opt}^2}{P_C} = 1.2564 \qquad (P >> 1 \text{ and } \varepsilon << 1). \tag{5.81}$$

Eq.(5.81) gives a conservative estimate for P_C, which improves as $P >> 1$. This corresponds to a maximum enhancement of

$$\mathrm{E}_{\max} = \frac{0.5694\, \phi_{opt}}{(1+c_2)\tanh\left(\phi_{opt}/2\right)}. \tag{5.82}$$

Eqs.(5.81) and (5.82) give an approximate *loci* of the maxima points on the enhancement factor curves. These are plotted in Figure 5.14 for the symmetric case and in Figure 5.15 for the asymmetric case. In the latter case ($c_2 < 1$), the enhancement in the chemical regime is greater than 1, since the convective flow increases concentration significantly in comparison to the linear profile predicted by diffusion alone. In this case, the reactant is being transferred from the outer surface ($r = 1$) into the bulk, yielding $\eta(\phi \to 0) = (1+c_2)/2 < 1$. This limit corresponds to:

$$\mathrm{E}(\phi \to 0) = \frac{2}{1+c_2}\left(1+\frac{c_2-1}{P_C}\right) \qquad \text{for } P_C >> 1 .$$

Therefore, when a concentration difference exists the improvement brought by convection can be very significant. For moderate values of P_C, the estimates from (5.81) and (5.82) can still be useful. For a specified value of Thiele modulus, (5.81) overestimates the intraparticular Peclet number at which maximum enhancement is observed (given correctly by (5.82)). For a specified intraparticular Peclet number, ϕ_{opt} is underestimated. In both cases, a lower bound for the maximum enhancement is obtained from (5.82), while the actual improvement can be slightly larger. These differences become negligible in the convection dominated limit ($P_C >> 1$). Also, the result from (5.81) is quite insensitive to the values of c_2 (associated with ε).

5.8 CONCLUSIONS

We have addressed several questions related with the internal transport-reaction problem in a catalytic coating, using the classical effectiveness factor concept. First, we focused on the issue of the evaluation of the effectiveness factor itself and proposed an approximate calculation procedure with the following characteristics:

(a) A very simple expression based on a typical geometrical characteristic found in wall-coated microreactors was derived, and is valid for all values of Thiele modulus. This compares very favorably with methods presented in current literature where more complex shape factors are obtained for low and high ϕ^2, resulting sometimes in a fragmented analysis.

(b) For some classes of nonlinear kinetics, our solution fulfills the asymptotic behavior at small and large reaction rates, and presents small errors in the intermediate range. For this case, we presented a generalization of the Thiele modulus which includes the classical normalizations in their ranges of validity.

(c) An arbitrary geometry is described by our solution by a measurable shape parameter (which combines the washcoat volume, surface area and thickness) and by the effectiveness factor of an equivalent slab.

(d) The performance of the 'slice method' (Papadias et al. 2000b) is improved, without introducing further complexity. This involved the consideration of a curvature correction, which reduced the relative error or the number of slices required to achieve a satisfactory approximation, especially in the intermediate regime of Thiele modulus.

(e) Despite the fact that our analysis was built for thin coatings, in some cases acceptable results were obtained even for $\varepsilon \sim 1$. Also, even though our main focus was on microchannel reactors, egg-shell catalyst particles and hollow cylinders can also benefit from our approach.

The second part of our work was concerned with the definition of operating regimes in wall-coated microchannels. We have extended previous analyses (Chapter 4) to consider the interplay between internal and external controlling processes. We have shown that, even though channel and washcoat domains are coupled, the solution of the full model is not required for estimation of boundaries between regimes. Even if variation of all properties with temperature needs to be accounted for, the problem can be reduced to the solution of a set of nonlinear algebraic equations. We predict that the process which determines the limiting behavior is governed by the ratio of 'diffusion velocity' in the washcoat and in the channel ($D_{eff} / (\varepsilon D)$). This has implications in experimental and modeling methods for measurement of intrinsic kinetics (requiring chemically controlled conditions) and operation in the mass transfer controlled limit. Current studies have neglected the role of this parameter and contradictory conclusions regarding the presence/absence of mass transfer limitations can be explained by taking it into consideration. Regime maps are presented with the parametric regions where channel and coating can be considered to operate under chemical and diffusional control (independently or together).

Finally, performance enhancement of a catalytic coating by intraparticular convection is explored. An approximation to the effectiveness factor in the case of radial convective flow is presented for a hollow cylinder and gives very acceptable results for a wide range of the parameters (including the ratio of surface concentrations at the inner and outer walls). We have also looked at the conditions under which the enhancement due to internal convection was more pronounced. The original work of Nir and Pismen (1977) identify these conditions as the ones where "the kinetics just becomes diffusion controlled". In their analysis this happened for Thiele modulus of order 1. However, considering a regime with fast convective transport, but where reaction is also fast enough, we have observed an optimum range of operation and design. When the rate of reactant consumption is able to keep up with strong convection, the pellet should be designed so that the (short) timescale for convection is approximately 1.26 times higher than the one for reaction. The observed enhancement is proportional to the square root of the intraparticular Peclet number:

$$\mathrm{E}_{\max} = \frac{0.6382}{1 + c_2} \sqrt{\frac{P_C}{\upsilon}}.$$

NOTATION

a	characteristic distance for diffusion in the channel
A	cross-sectional area of washcoat
B	permeability of the medium
Bi_m	mass Biot number
c	dimensionless concentration of reactant in the washcoat
c_2	ratio between concentrations at the surfaces
C	concentration of reactant in the channel
D	diffusivity in the bulk
D_{ax}	effective diffusivity in the coating (axial)
D_{eff}	effective diffusivity in the coating (transverse)
Da	Damköhler number
E	activation energy
E	enhancement factor
${}_2F_1$	hypergeometric function
k_0	pre-exponential factor in reaction kinetics
K	kinetic parameter
L	length of the channel
LHS	left hand side
m	order of reaction
p	kinetic parameter
P	intraparticular Peclet number
$\nabla\hat{P}$	pressure gradient vector
r	dimensionless transverse coordinate
R	reaction rate
RHS	right hand side
R_G	ideal gas constant
S	area of the channel-coating interface
Sh	Sherwood number
t_w	thickness of the catalytic coating
T	temperature
$\hat{u}_i$	interstitial (pore) velocity
V	washcoat volume
w_i	fraction of the washcoat volume correspondent to a slice
z	dimensionless axial coordinate

Greek letters

α	aspect ratio of the channel
$\frac{\alpha Pe_m}{z}$	Graetz parameter
ε	ratio of the characteristic distances for diffusion in the coating and in the channel
ε_P	porosity of catalytic coating or membrane
ϕ	Thiele modulus
μ	dynamic viscosity
η	effectiveness factor
$\overline{\eta}$	global effectiveness factor
σ	shape parameter
τ	timescale
θ	degree of mass transfer control; angular coordinate
υ	volume to surface ratio, divided by characteristic dimension for diffusion

Superscripts

^	dimensional quantities
‘	normalized by inlet conditions

Subscripts

in	referred to inlet conditions
surf	referred to surface conditions
transv	transverse
V	per volume of washcoat

REFERENCES

Afeyan, N. B., S. P. Fulton, N. F. Gordon, I. Mazsaroff, L. Varady and F. E. Regnier (1990a). "Perfusion chromatography: An approach to purifying biomolecules." Nature Biotechnology **8**(3): 203-206.

Afeyan, N. B., S. P. Fulton and F. E. Regnier (1991). "Perfusion chromatography packing materials for proteins and peptides." Journal of Chromatography **544**(1-2): 267-279.

Afeyan, N. B., N. F. Gordon, I. Mazsaroff, L. Varady, S. P. Fulton, Y. B. Yang and F. E. Regnier (1990b). "Flow-through particles for the high-performance liquid chromatographic separation of biomolecules: Perfusion chromatography." Journal of Chromatography **519**(1): 1-29.

Aran, H. C., J. K. Chinthaginjala, R. Groote, T. Roelofs, L. Lefferts, M. Wessling and R. G. H. Lammertink (2011). "Porous ceramic mesoreactors: A new approach for gas-liquid contacting in multiphase microreaction technology." Chemical Engineering Journal **169**(1-3): 239-246.

Aris, R. (1975). The mathematical theory of diffusion and reaction in permeable catalysts. London, Oxford University Press.

Bakker, J. J. W., W. J. Groendijk, K. M. De Lathouder, F. Kapteijn, J. A. Moulijn, M. T. Kreutzer and S. A. Wallin (2007). "Enhancement of catalyst performance using pressure pulses on macroporous structured catalysts." Industrial and Engineering Chemistry Research **46**(25): 8574-8583.

Bakker, J. J. W., M. T. Kreutzer, K. De Lathouder, F. Kapteijn, J. A. Moulijn and S. A. Wallin (2005). "Hydrodynamic properties of a novel 'open wall' monolith reactor." Catalysis Today **105**(3-4): 385-390.

Bender, C. M. and S. A. Orszag (1978). Advanced Mathematical Methods for Scientists and Engineers. New York, McGraw-Hill.

Bischoff, K. B. (1967). "An extension of the general criterion for importance of pore diffusion with chemical reactions." Chemical Engineering Science **22**(4): 525-530.

Bouzek, K. and I. Roušar (1996). "Comparison of the effectiveness factors for a reaction at a pore wall calculated on the assumption of the Langmuir-Hinshelwood mechanism and according to a power equation." Journal of Chemical Technology and Biotechnology **66**(2): 131-134.

Burghardt, A. and A. Kubaczka (1996). "Generalization of the effectiveness factor for any shape of a catalyst pellet." Chemical Engineering and Processing: Process Intensification **35**(1): 65-74.

Cardoso, S. S. S. and A. E. Rodrigues (2007). "Convection, diffusion and reaction in a nonisothermal, porous catalyst slab." AIChE Journal **53**(5): 1325-1336.

Cedro III, V. and S. Srinivasan (1974). "Heat and mass transfer in a porous wall tubular reactor." International Journal of Heat and Mass Transfer **17**(11): 1413-1416.

Chen, G. and A. F. Palmer (2009). "Hemoglobin-based oxygen carrier and convection enhanced oxygen transport in a hollow fiber bioreactor." Biotechnology and Bioengineering **102**(6): 1603-1612.

Chen, X. B., Y. Sui, Y. P. Cheng, H. P. Lee, P. Yu, S. H. Winoto and H. T. Low (2010a). "Mass transport in a microchannel enzyme reactor with a porous wall: Hydrodynamic modeling and applications." Biochemical Engineering Journal **52**(2-3): 227-235.

Chen, X. B., Y. Sui, H. P. Lee, H. X. Bai, P. Yu, S. H. Winoto and H. T. Low (2010b). "Mass transport in a microchannel bioreactor with a porous wall." Journal of Biomechanical Engineering **132**(6).

Chou, C. T. and W. E. Stewart (1986). "Influence of coating geometry on the effectiveness of monolithic catalysts." Chemical Engineering Science **41**(1): 202-204.

CIM Convective Interaction Media(R) . Liquid Chromatography Redesigned™. www.monoliths.com. BIASeparations.

Coletti, F., S. Macchietto and N. Elvassore (2006). "Mathematical modeling of three-dimensional cell cultures in perfusion bioreactors." Industrial and Engineering Chemistry Research **45**(24): 8158-8169.

Cresswell, D. L. (1985). "Intra-particle convection: its measurement and effect on catalyst activity and selectivity." Applied catalysis **15**(1): 103-116.

Datta, R. and S. W. K. Leung (1985). "Shape generalized isothermal effectiveness factor for first-order kinetics." Chemical Engineering Communications **39**(1): 155 - 173.

De Lathouder, K. M., J. Bakker, M. T. Kreutzer, F. Kapteijn, J. A. Moulijn and S. A. Wallin (2004). "Structured reactors for enzyme immobilization: Advantages of tuning the wall morphology." Chemical Engineering Science **59**(22-23): 5027-5033.

Froment, G. F. and K. B. Bischoff (1979). Chemical Reactor Analysis and Design New York, Wiley.

Gavriilidis, A. and A. Varma (1992). "Optimal catalyst activity profiles in pellets: 9. Study of ethylene epoxidation." AIChE Journal **38**(2): 291-296.

Germani, G. and Y. Schuurman (2006). "Water-gas shift reaction kinetics over micro-structured Pt/CeO2/AI2O3 catalysts." AIChE Journal **52**(5): 1806-1813.

Gonzo, E. E. (2008). "Hydrogen from methanol-steam reforming. Isothermal and adiabatic monolith reactors' simulation." International Journal of Hydrogen Energy **33**(13): 3511-3516.

Gonzo, E. E. and J. C. Gottifredi (2011). "Heat and mass transfer limitations in monolith reactor simulation with non uniform washcoat thickness." Latin American Applied Research **40**(1): 15-21.

Görke, O., P. Pfeifer and K. Schubert (2009). "Kinetic study of ethanol reforming in a microreactor." Applied Catalysis A: General **360**(2): 232-241.

Gottifredi, J. C. and E. E. Gonzo (1986). Application of perturbation and matching techniques to solve transport phenomena problems. Advances in Transport Processes. A. Mujumdar and R. A. Mashelkar. New Delhi, Wiley Eastern. **IV:** 419-464.

Gottifredi, J. C. and E. E. Gonzo (2005a). "Approximate expression for the effectiveness factor estimation and a simple numerical method for concentration profile calculation in porous catalyst." Chemical Engineering Journal **109**(1): 83-87.

Gottifredi, J. C. and E. E. Gonzo (2005b). "On the effectiveness factor calculation for a reaction - Diffusion process in an immobilized biocatalyst pellet." Biochemical Engineering Journal **24**(3): 235-242.

Gottifredi, J. C., E. E. Gonzo and O. D. Quiroga (1981). "Isothermal effectiveness factor-I. Analytical expression for single reaction with arbitrary kinetics. Slab geometry." Chemical Engineering Science **36**(4): 713-719.

Groppi, G., W. Ibashi, M. Valentini and P. Forzatti (2001). "High-temperature combustion of CH4 over PdO/Al2O3: Kinetic measurements in a structured annular reactor." Chemical Engineering Science **56**(3): 831-839.

Hayes, R. E. and S. T. Kolaczkowski (1994). "Mass and heat transfer effects in catalytic monolith reactors." Chemical Engineering Science **49**(21): 3587-3599.

Hayes, R. E., B. Liu, R. Moxom and M. Votsmeier (2004). "The effect of washcoat geometry on mass transfer in monolith reactors." Chemical Engineering Science **59**(15): 3169-3181.

Hayes, R. E., B. Liu and M. Votsmeier (2005). "Calculating effectiveness factors in non-uniform washcoat shapes." Chemical Engineering Science **60**(7): 2037-2050.

Haynes Jr, H. W. (1986). "An explicit approximation for the effectiveness factor in porous heterogeneous catalysts." Chemical Engineering Science **41**(2): 412-415.

Horvath, C. and J. M. Engasser (1973). "Pellicular heterogeneous catalysts. A theoretical study of the advantages of shell structured immobilized enzyme particles." Industrial and Engineering Chemistry **12**(2): 229-235.

Jensen, K. F. (2001). "Microreaction engineering-is small better?" Chemical Engineering Science **56**(2): 293-303.

Joshi, S. Y., M. P. Harold and V. Balakotaiah (2010). "Overall mass transfer coefficients and controlling regimes in catalytic monoliths." Chemical Engineering Science **65**(5): 1729-1747.

Joshi, S. Y., Y. Ren, M. P. Harold and V. Balakotaiah (2011). "Determination of kinetics and controlling regimes for H2 oxidation on Pt/Al2O3 monolithic catalyst using high space velocity experiments." Applied Catalysis B: Environmental **102**(3-4): 484-495.

Kalluri, R. R., D. R. Cahela and B. J. Tatarchuk (2009). "Comparative heterogeneous contacting efficiency in fixed bed reactors: Opportunities for new microstructured systems." Applied Catalysis B: Environmental **90**(3-4): 507-515.

Kapteijn, F., R. M. De Deugd and J. A. Moulijn (2005). "Fischer-Tropsch synthesis using monolithic catalysts." Catalysis Today **105**(3-4): 350-356.

Kapteijn, F., T. A. Nijhuis, J. J. Heiszwolf and J. A. Moulijn (2001). "New non-traditional multiphase catalytic reactors based on monolithic structures." Catalysis Today **66**(2-4): 133-144.

Keegan, S. D., N. J. Mariani, S. P. Bressa, G. D. Mazza and G. F. Barreto (2003). "Approximation of the effectiveness factor in catalytic pellets." Chemical Engineering Journal **94**(2): 107-112.

Keegan, S. D., N. J. Mariani, O. M. Martínez and G. F. Barreto (2005). "Behaviour of smooth catalysts at high reaction rates." Chemical Engineering Journal **110**(1-3): 41-56.

Kelsey, L. J., M. R. Pillarella and A. L. Zydney (1990). "Theoretical analysis of convective flow profiels in a hollow-fiber membrane bioreactor." Chemical Engineering Science **45**(11): 3211-3220.

Khassin, A. A., A. G. Sipatrov, G. K. Chermashetseva, T. M. Yurieva and V. N. Parmon (2005a). "Fischer-Tropsch synthesis using plug-through contactor membranes based on permeable composite monoliths. Selectivity control by porous structure parameters and membrane geometry." Topics in Catalysis **32**(1-2): 39-46.

Khassin, A. A., A. G. Sipatrov, T. M. Yurieva, G. K. Chermashentseva, N. A. Rudina and V. N. Parmon (2005b). "Performance of a catalytic membrane reactor for the Fischer-Tropsch synthesis." Catalysis Today **105**(3-4): 362-366.

Khassin, A. A., T. M. Yurieva, A. G. Sipatrov, V. A. Kirillov, G. K. Chermashentseva and V. N. Parmon (2003). "Fischer-Tropsch synthesis using a porous catalyst packing: Experimental evidence of an efficient use of permeable composite monoliths as a novel type of the Fischer-Tropsch synthesis catalyst." Catalysis Today **79-80**: 465-470.

Kiwi-Minsker, L. and A. Renken (2005). "Microstructured reactors for catalytic reactions." Catalysis Today **110**(1-2): 2-14.

Kolb, G., V. Hessel, V. Cominos, C. Hofmann, H. Löwe, G. Nikolaidis, R. Zapf, A. Ziogas, E. R. Delsman, M. H. J. M. de Croon, J. C. Schouten, O. de la Iglesia, R. Mallada and J. Santamaria (2007). "Selective oxidations in micro-structured catalytic reactors--For gas-phase reactions and specifically for fuel processing for fuel cells." Catalysis Today **120**(1): 2-20.

Kreutzer, M. T., F. Kapteijn and J. A. Moulijn (2006). "Shouldn't catalysts shape up? Structured reactors in general and gas-liquid monolith reactors in particular." Catalysis Today **111**(1-2): 111-118.

Lee, J. and D. H. Kim (2006). "An approximation method for the effectiveness factor in porous catalysts." Chemical Engineering Science **61**(15): 5127-5136.

Lee, W.-C., G.-J. Tsai and G. T. Tsao (1990). Radial-Flow Affinity Chromatography for Trypsin Purification. Protein Purification: From Molecular Mechanisms to Large-Scale Processes. M. R. Ladisch, R. C. Willson, C. C. Painton and S. E. Builder, American Chemical Society**:** 104-117.

Leung, D., R. E. Hayes and S. T. Kolaczkowskl (1996). "Diffusion Limitation Effects in the Washcoat of a Catalytic Monolith Reactor." Canadian Journal of Chemical Engineering **74**(1): 94-103.

Lewis, W. and S. Middleman (1974). "Conversion in a hollow fiber membrane / enzyme reactor." AIChE Journal **20**(5): 1012-1014.

Lu, Z. P., M. M. Dias, J. C. B. Lopes, G. Carta and A. E. Rodrigues (1993). "Diffusion, convection, and reaction in catalyst particles: Analogy between slab and sphere geometries." Industrial and Engineering Chemistry Research **32**(9): 1839-1852.

Magyari, E. (2008). "Exact analytical solution of a nonlinear reaction-diffusion model in porous catalysts." Chemical Engineering Journal **143**(1-3): 167-171.

Mariani, N. J., S. D. Keegan, O. M. Martínez and G. F. Barreto (2003). "A one-dimensional equivalent model to evaluate overall reaction rates in catalytic pellets." Chemical Engineering Research and Design **81**(8): 1033-1042.

Mariani, N. J., S. D. Keegan, O. M. Martínez and G. F. Barreto (2008a). "On the evaluation of effective reaction rates on commercial catalyst by means of a one-dimensional model." Catalysis Today **133-135**(1-4): 770-774.

Mariani, N. J., S. D. Keegan, O. M. Martínez and G. F. Barreto (2008b). "On the evaluation of effective reaction rates on commercial catalyst by means of a one-dimensional model." Catalysis Today **133-135**(1-4): 770-774.

Mariani, N. J., C. Mocciaro, S. D. Keegan, O. M. Martínez and G. F. Barreto (2009a). "Evaluating the effectiveness factor from a 1D approximation fitted at high Thiele modulus: Spanning commercial pellet shapes with linear kinetics." Chemical Engineering Science **64**(11): 2762-2766.

Mariani, N. J., C. Mocciaro, O. M. Martínez and G. F. Barreto (2009b). "Estimation of effectiveness factor for arbitrary particle shape and non-linear kinetics." Industrial and Engineering Chemistry Research **48**(3): 1172-1177.

Mocciaro, C., N. J. Mariani, O. M. Martínez and G. F. Barreto (2011). "A three-parameter one-dimensional model to predict the effectiveness factor for an arbitrary pellet shape." Industrial and Engineering Chemistry Research **50**(5): 2746-2754.

Mogalicherla, A. K. and D. Kunzru (2010). "Effect of gas and liquid superficial velocities on the performance of monolithic reactors." Industrial and Engineering Chemistry Research **49**(4): 1631-1641.

Motamedhashemi, M. M. Y., F. Egolfopoulos and T. Tsotsis (2011). "Application of a Flow-Through Catalytic Membrane Reactor (FTCMR) for the Destruction of a Chemical Warfare Simulant." Journal of Membrane Science **In Press, Accepted Manuscript**.

Nagy, E. (2010a). "Convective and diffusive mass transport through anisotropic, capillary membrane." Chemical Engineering and Processing: Process Intensification **49**(7): 716-721.

Nagy, E. (2010b). "Mass transfer through a convection flow catalytic membrane layer with dispersed nanometer-sized catalyst." Industrial and Engineering Chemistry Research **49**(3): 1057-1062.

Nan, H. S., M. M. Dias, J. C. B. Lopes and A. E. Rodrigues (1996a). "Diffusion, convection and reaction in catalyst particles: Analogy between slab and cylinder geometries." Chemical Engineering Journal and the Biochemical Engineering Journal **61**(2): 113-122.

Nan, H. S., M. M. Dias, V. G. Mata and A. E. Rodrigues (1996b). "Measurements of effective diffusivity in large-pore permeable pellets with various geometries using the chromatographic method." Chemical Engineering Communications **146**: 201-229.

Nir, A. (1977). "Simultaneous intraparticle forced convection, diffusion and reaction in a porous catalyst - 2. Selectivity of sequential reactions." Chemical Engineering Science **32**(8): 925-930.

Nir, A. and L. M. Pismen (1977). "Simultaneous intraparticle forced convection, diffusion and reaction in a porous catalyst." Chemical Engineering Science **32**(1): 35-41.

Ouyang, X., L. Bednarova, R. S. Besser and P. Ho (2005). "Preferential oxidation (PrOx) in a thin-film catalytic microreactor: Advantages and limitations." AIChE Journal **51**(6): 1758-1772.

Papadias, D., L. Edsberg and P. BjoÌˆrnbom (2000a). "Simplified method of effectiveness factor calculations for irregular geometries of washcoats a general case in a 3D concentration field." Catalysis Today **60**(1): 11-20.

Papadias, D., L. Edsberg and P. Björnbom (2000b). "Simplified method for effectiveness factor calculations in irregular geometries of washcoats." Chemical Engineering Science **55**(8): 1447-1459.

Pérez-Cadenas, A. F., M. M. P. Zieverink, F. Kapteijn and J. A. Moulijn (2005). "High performance monolithic catalysts for hydrogenation reactions." Catalysis Today **105**(3-4): 623-628.

Petersen, E. (1965). Chemical Reaction Analysis. New Jersey, Prentice-Hall Inc.

Platonova, G. A., E. G. Vlakh, N. D. Ivanova and T. B. Tennikova (2009). "A flow-through enzymatic bioreactor based on immobilized α-Chymotrypsin." Russian Journal of Applied Chemistry **82**(12): 2182-2186.

Podgornik, A., M. Barut, A. Strancar, D. Josic and T. Koloini (2000). "Construction of large-volume monolithic columns." Analytical Chemistry **72**(22): 5693-5699.

Podgornik, A., J. Jancar, M. Merhar, S. Kozamernik, D. Glover, K. Cucek, M. Barut and A. Strancar (2004). "Large-scale methacrylate monolithic columns: design and properties." Journal of Biochemical and Biophysical Methods **60**(3): 179-189.

Podgornik, H. and A. Podgornik (2002). "Characteristics of LiP immobilized to CIM monolithic supports." Enzyme and Microbial Technology **31**(6): 855-861.

Protasova, L. N., E. V. Rebrov, H. E. Skelton, A. E. H. Wheatley and J. C. Schouten (2011). "A kinetic study of the liquid-phase hydrogenation of citral on Au/TiO2 and Pt-Sn/TiO2 thin films in capillary microreactors." Applied Catalysis A: General.

Rebrov, E. V., A. Berenguer-Murcia, H. E. Skelton, B. F. G. Johnson, A. E. H. Wheatley and J. C. Schouten (2009a). "Capillary microreactors wall-coated with mesoporous titania thin film catalyst supports." Lab on a Chip - Miniaturisation for Chemistry and Biology **9**(4): 503-506.

Rebrov, E. V., A. Berenguer-Murcia, A. E. H. Wheatley, B. F. G. Johnson and J. C. Schouten (2009b). "Thin catalytic coatings on microreactor walls a way to make industrial processes more efficient." Chimica Oggi **27**(4): 4-7.

Rodrigues, A., B. Ahn and A. Zoulalian (1982). "Intraparticle Forced Convection Effect in Catalyst Diffusivity Measurements and Reactor Design." AIChE Journal **28**: 541-546.

Rodrigues, A. E. (1981). Scientific bases for the design of two-phase catalytic reactors. Multiphase Chemical Reactors - Design Methods. A. E. Rodrigues, J. M. Calo and N. H. Sweed. Rockville, M.D., NATO ASI Series E-52. **2:** 65-133.

Rodrigues, A. E., J. M. Loureiro and R. M. Quinta-Ferreira (1991). "Intraparticle Convection Revisited." Chemical Engineering Communications **00**: 13.

Rodrigues, A. E., J. M. Orfao and A. Zoulalian (1984). "Intraparticle convection, diffusion and zero order reaction in porous catalysts." Chemical Engineering Communications **27**(5-6): 327-337.

Santos, H. and M. Costa (2011). "On the quantification of the controlling regimes in automotive catalytic converters." AIChE Journal **57**(1): 218-226.

Scheuer, A., O. Hirsch, R. Hayes, H. Vogel and M. Votsmeier (2011). "Efficient simulation of an ammonia oxidation reactor using a solution mapping approach." Catalysis Today **In Press, Corrected Proof**.

Schouten, J. C., E. V. Rebrov and M. H. J. M. De Croon (2002). "Miniaturization of heterogeneous catalytic reactors: Prospects for new developments in catalysis and process engineering." Chimia **56**(11): 627-635.

Shah, R. K. and A. L. London (1978). Laminar flow forced convection in ducts. New York, Academic Press.

Shah, Y. T. and T. Remmen (1971). "Radial mass transfer effects in a porous wall tubular reactor." International Journal of Heat and Mass Transfer **14**(12): 2109-2124.

Soltan Mohammadzadeh, J. S. and A. Zamaniyan (2002). "Catalyst shape as a design parameter - Optimum shape for methane-steam reforming catalyst." Chemical Engineering Research and Design **80**(4): 383-390.

Tao, K., Y. Zhang, S. Terao, Y. Yoneyama, T. Kawabata, K. Matsuda, S. Ikeno and N. Tsubaki (2011). "Chemical and spatial promotional effects of bimodal pore catalysts for methane dry reforming." Chemical Engineering Journal **170**(1): 258-263.

Thiele, E. W. (1939). "Relation between catalytic activity and size of the particle." Industrial and Engineering Chemistry **31**(7): 916-920.

Thomsen, M. S. and B. Nidetzky (2009). "Coated-wall microreactor for continuous biocatalytic transformations using immobilized enzymes." Biotechnology Journal **4**(1): 98-107.

Tomasic, V., Z. Gomzi and S. Zrncevic (2002). "Reaction and mass transfer effects in a catalytic monolith reactor." Reaction Kinetics and Catalysis Letters **77**(2): 245-253.

Tomasic, V., Z. Gomzi and S. Zrncevic (2006). "Analysis and modeling of a monolithic reactor." Chemical Engineering and Technology **29**(1): 59-65.

Trilisky, E. I., H. Koku, K. J. Czymmek and A. M. Lenhoff (2009a). "Relation of structure to performance characteristics of monolithic and perfusive stationary phases." Journal of Chromatography A **1216**(36): 6365-6376.

Trilisky, E. I. and A. M. Lenhoff (2009b). "Flow-dependent entrapment of large bioparticles in porous process media." Biotechnology and Bioengineering **104**(1): 127-133.

Vita, A., L. Pino, F. Cipitì, M. Laganà and V. Recupero (2010). "Structured reactors as alternative to pellets catalyst for propane oxidative steam reforming." International Journal of Hydrogen Energy **35**(18): 9810-9817.

Vodopivec, M., A. Podgornik, M. Berovič and A. Štrancar (2003). "Characterization of CIM monoliths as enzyme reactors." Journal of Chromatography B: Analytical Technologies in the Biomedical and Life Sciences **795**(1): 105-113.

Vos, H. J., P. J. Heederik, J. J. M. Potters and K. C. A. M. Luyben (1990). "Effectiveness factor for spherical biofilm catalysts." Bioprocess Engineering **5**(2): 63-72.

Walter, S., S. Malmberg, B. Schmidt and M. A. Liauw (2005). "Mass transfer limitations in microchannel reactors." Catalysis Today **110**(1-2): 15-25.

Wang, G. and M.-O. Coppens (2008). "Calculation of the Optimal Macropore Size in Nanoporous Catalysts and Its Application to DeNOx Catalysis." Industrial & Engineering Chemistry Research **47**(11): 3847-3855.

Wang, G. and M.-O. Coppens (2010). "Rational design of hierarchically structured porous catalysts for autothermal reforming of methane." Chemical Engineering Science **65**(7): 2344-2351.

Wedel, S. and D. Luss (1980). "Rational approximation of the effectiveness factor." Chemical Engineering Communications **7**(4-5): 245-259.

Weisz, P. B. and C. D. Prater (1954). "Interpretation of Measurements in Experimental Catalysis." Advances in Catalysis **6**: 143-196.

Westermann, T. and T. Melin (2009). "Flow-through catalytic membrane reactors-Principles and applications." Chemical Engineering and Processing: Process Intensification **48**(1): 17-28.

Wijngaarden, R. J., A. Kronberg and K. R. Westerterp (1998). Industrial catalysis: optimizing catalysts and processes Weinheim, Wiley-VCH.

Yoon, S. K., G. W. Fichtl and P. J. A. Kenis (2006). "Active control of the depletion boundary layers in microfluidic electrochemical reactors." Lab on a Chip - Miniaturisation for Chemistry and Biology **6**(12): 1516-1524.

Yu, X., S. T. Tu, Z. Wang and Y. Qi (2005). "On-board production of hydrogen for fuel cells over Cu/ZnO/Al 2O3 catalyst coating in a micro-channel reactor." Journal of Power Sources **150**(1-2): 57-66.

Zhou, Z., T. Zeng, Z. Cheng and W. Yuan (2011). "Preparation and characterization of titania-alumina mixed oxides with hierarchically macro-/mesoporous structures." Industrial and Engineering Chemistry Research **50**(2): 883-890.

CHAPTER

SIX

NONISOTHERMAL EFFECTS IN PERFUSIVE CATALYST PARTICLES

From the examples given in Chapter 1, it is clear that the analysis of the interaction between transport phenomena and chemical reaction inside large-pore catalyst particles needs to include intraparticular convection as an additional mass/heat transfer mechanism. Examples of such particles were given in Chapter 1. In this chapter, we describe by a 3-D regime diagram the global behaviour of a permeable catalyst slab, where an exothermic, zero-order reaction is occurring. An order of magnitude estimate for the maximum temperature change is obtained by scaling techniques in each regime of operation. Specific operating regimes of fast mass/heat transport, dominant reaction and strong intraparticular convection, are then studied in more detail using perturbation analysis. The results include approximate concentration and temperature profiles, which allow the estimation of both the effectiveness factor and maximum temperature attained inside the catalyst in these regimes.

6.1 INTRODUCTION

'Large-pore' materials have been used in several reaction and separation engineering applications, namely as catalyst supports, HPLC packings, ceramic membranes or supports for mammalian cell culture and biomass growth. Examples of work in these areas have been given in Chapter 1. The interest in using these permeable materials arises from the non-negligible convective contribution to the total transport rate inside the particle when subjected to a pressure difference, as first recognised by Wheeler (1951). The presence of convective flow within the pores of a coarse-grained pellet was found to reduce internal mass transfer resistance, improving the overall performance of the reactor/separator. The enhancement observed in a catalyst particle with 'large-pores' was quantified analytically by Nir and Pismen (1977) for an

* The contents of this chapter are based on J. P. Lopes, S. S. S. Cardoso and A. E. Rodrigues (2009), AIChE Journal **55**(10): 2686-2699.

isothermal first-order reaction, where the effect of intraparticular convection was found to be visible only when kinetics just becomes diffusion controlled. Rodrigues et al.(1982) explained the beneficial effect of convection with the concept of 'augmented diffusivity'. He found that the behaviour predicted from a model including convection was equivalent to a conventional reaction-diffusion system, with apparent diffusivity $D_{app} = D/f(\lambda) > D$. An expression for $f(\lambda)$ was derived. Rodrigues et al. (1984) extended the analysis of simultaneous convection and diffusion inside slab-shaped catalyst particles, when an isothermal zero-order reaction occurs. The same problem was addressed by Stephanopoulos and Tsiveriotis (1989) for the spherical geometry in the context of reactions in biologically active pellets.

Actually, large pore materials have become extremely popular among biotechnological applications, for which the zero-order reaction is an important limit. Although they provide easy access for cell attachment and growth, since nutrient and biomass concentration gradients within the carriers are highly disadvantageous. In fact, cell culture scaffolds are severely limited by diffusional resistance, which coupled with low diffusivity and solubility in liquid-phase, make nutrients (such as oxygen) poorly available. Intraparticular convection can therefore be of utmost importance in assuring uniform high cell densities. Fassnacht et al. (1999) recognise the importance of convective flux through carriers with large pores and high porosity (SIRAN® beads with macropore size between $60-300\,\mu m$) for antibody production from immobilized hybridoma cells. The oxygen uptake rate was identified as the limiting factor and modelled as a zero-order reaction, since Michaelis-Menten constant was much lower than the bulk concentration value. Goldstein et al. (2001) also conclude that convective currents are essential for uniform and extensive utilization of porous PLGA foams, where osteoblastic cells are seeded. Young et al. (1987) reported the use of Verax VX-100 microspheres (with pore diameters in the range of $20 - 40\ \mu m$) as a support for mammalian cell culture. Oxygen supply and waste removal are of vital importance also for feasible in vitro fabrication of mammalian tissues for therapeutic uses (Martin et al. 2005), since high cell density is a fundamental requirement. The same challenges appear in plant root cultures for the production of pharmaceuticals and flavours. Prince et al. (1991) present experimental evidence of convective mass transfer rate as the controlling step for oxygen consumption within porous root culture clumps. They report significant enhancement in catalyst performance (effectiveness factor increased 100 times), when external flow velocity was around $1\,cm/s$. Again, oxygen uptake was described by a zero-order reaction. In addition to these examples, the importance of intraparticular convection has also been noticed in other perfusive bioreactors for cell culture (e.g. Coletti et al. (2006), Chung et al. (2007), Allen et al. (2003)) and in immobilized enzyme systems.

Most of the modelling work is focused exclusively on isothermal conditions. However, many chemical reactions are strongly heat-generating and the common assumption of negligible internal temperature gradients has to be carefully evaluated. In what concerns the problem of intraparticular convection, diffusion and reaction under nonisothermal conditions, most studies at particle level are numerical (Quinta Ferreira 1988; Lopes et al. 1995). Cardoso and Rodrigues (2007) presented a perturbation analysis for nonisothermal first-order reaction in a permeable catalyst slab. All previous results indicate that temperature inside the particle can reach values several times higher than its surface value, for typical parameter values. First and zero-order reactions are always attractive for analytical treatment, since the problems they give origin to, are easier to handle. On the other hand, they constitute the two well-known limits for more complex reaction kinetics expressions, like the Michaelis-Menten equation, used to describe consumption of substrates in biological media. This work intends to extend the approximate analytical analysis to zero-order reactions. The purposes of this approach are: (1) define operating regimes and understand the transitions between them; (2) provide effectiveness factor approximations for each regime; and (3) estimate the maximum temperature attained inside the catalyst. An improved understanding of convective enhancement on the performance of porous particles as catalysts/supports, coupled with nonisothermal effects, is extremely relevant for reactor design and carrier structure optimization. Simple estimates can be useful for preventing operation problems, such as crossing critical temperature limits. Finally, algebraic solutions for the effectiveness factor greatly simplify fixed-bed simulation, since the highly nonlinear equations that describe mass/heat transfer and chemical reaction inside the particle do not need to be solved at every point of the reactor.

6.2 OPERATING REGIMES

6.2.1 Governing equations and model parameters

We adopt a one-dimensional steady-state model for mass and energy transport in a permeable catalyst slab, undergoing an exothermic zero-order reaction, in an uniform flow field (with *a priori* specified fluid velocity, u). The conservation equations write as:

$$u\frac{d\hat{c}}{d\hat{x}} = D\frac{d^2\hat{c}}{d\hat{x}^2} - \begin{cases} k, & \hat{c} > 0 \\ 0, & \hat{c} = 0 \end{cases} \tag{6.1}$$

$$u\frac{d\hat{T}}{d\hat{x}} = \kappa\frac{d^2\hat{T}}{d\hat{x}^2} + \begin{cases} \dfrac{(-\Delta H)k}{\rho C_P}, & \hat{c} > 0 \\ 0, & \hat{c} = 0 \end{cases} \tag{6.2}$$

Since both sides of the slab are assumed to be at uniform surface concentration and temperature, the proper boundary conditions are

$$\hat{c}\left(\hat{x}=\pm L\right)=\hat{c}_s \text{ and} \tag{6.3}$$

$$\hat{T}\left(\hat{x}=\pm L\right)=\hat{T}_s . \tag{6.4}$$

Non-dimensionalization of equations (6.1)-(6.4) was accomplished using the following scales (Cardoso et al. 2006):

$$x=\frac{\hat{x}}{L};\qquad c=\frac{\hat{c}-\hat{c}_s}{\hat{c}_s};\qquad T=\frac{\hat{T}-\hat{T}_s}{\Delta\hat{T}} \tag{6.5}$$

where the characteristic length scale is the slab half-thickness (L) and the correct scale for temperature deviation from its surface value, $\Delta\hat{T}$, is so far unknown. In these variables, equations (6.1)-(6.4) become:

$$\frac{dc}{dx}=\frac{1}{Pe_m}\frac{d^2c}{dx^2}-\frac{\phi^2}{Pe_m}r\left(T\right) \tag{6.6}$$

$$\frac{dT}{dx}=\frac{1}{Pe_h}\frac{d^2T}{dx^2}+\frac{\phi^2}{Pe_m}\beta\frac{Pe_m}{Pe_h}\frac{\hat{T}_s}{\Delta\hat{T}}r\left(T\right) \tag{6.7}$$

subject to

$$c\left(x=\pm 1\right)=0 \text{ and} \tag{6.8}$$

$$T\left(x=\pm 1\right)=0 . \tag{6.9}$$

The reaction term $r\left(T\right)$ in (6.6) and (6.7) is only operative if reactant exists:

$$r\left(T\right)=\begin{cases}\exp\left[\dfrac{\varphi T}{1+\eta T}\right], & c>-1\\ 0, & c=-1\end{cases} \tag{6.10}$$

where $\eta=\Delta\hat{T}/\hat{T}_s$ and $\varphi=\gamma\eta$ are at most of $O\left(1\right)$. The Arrhenius parameter, $\gamma=E_{act}/\left(R\hat{T}_s\right)$, is related with the reaction activation energy $\left(E_{act}\right)$ and is referred to the surface temperature value $\left(\hat{T}_s\right)$. The properties for the fluid and solid phases are taken to be uniform. Therefore, the mass diffusivity D and thermal diffusivity $\kappa\left(=\lambda/\rho C_p\right)$, which are related by Lewis' number $\left(Le=\kappa/D\right)$, are fixed for a given system.

6.2.1.a *Timescales*

Assuming that concentration and temperature are correctly scaled in (6.6)-(6.10), the magnitude of the convective, diffusive and conductive terms in the mass and energy balances is given respectively by: 1, $1/Pe_m$ and $1/Pe_h$. In the presence of reactant, the order of the reaction term is ϕ^2/Pe_m from (6.6) and $\frac{\phi^2}{Pe_m}\beta\frac{Pe_m}{Pe_h}\frac{\hat{T}_s}{\Delta\hat{T}}$ from (6.7), since $r(T)\sim O(1)$. These dimensionless groups compare the characteristic time for the fluid to be convected over the scale for the spatial dimension (L), with all the other interacting processes. This can be seen if the coefficients preceding the terms in equations (6.6) and (6.7) are written explicitly in terms of timescales:

$$\frac{1}{Pe_m}=\frac{\tau_C}{\tau_D} \tag{6.11}$$

$$\frac{1}{Pe_h}=\frac{\tau_C}{\tau_H} \tag{6.12}$$

$$\frac{\phi^2}{Pe_m}=\frac{\tau_C}{\tau_R} \tag{6.13}$$

$$\frac{\phi^2}{Pe_m}\beta\frac{Pe_m}{Pe_h}\frac{\hat{T}_s}{\Delta\hat{T}}=\frac{\tau_C}{\tau_{RH}} \tag{6.14}$$

Therefore, the time constant for convection $(\tau_C=L/u)$ can be related with the one for diffusion of matter $(\tau_D=L^2/D)$ and conduction of heat $(\tau_H=L^2/\kappa)$, through the mass and heat intraparticular Peclet numbers $(Pe_m$ and $Pe_h)$. Similarly, the characteristic time for reactant consumption $(\tau_R=\hat{c}_s/k_s)$ and fluid temperature rise from heat generation by chemical reaction $\left(\tau_{RH}=\rho C_p\Delta\hat{T}/\left(k_s(-\Delta H)\right)\right)$ are compared with convection, as expressed in equations (6.13) and (6.14). These dimensionless groups are also written in terms of the more familiar parameters in reaction engineering analysis, namely the Thiele modulus $(\phi^2=\tau_D/\tau_R)$ and Prater's parameter, $\beta=\left((-\Delta H)D\hat{c}_s\right)/\left(\rho C_p\kappa\hat{T}_s\right)$. Because the maximum temperature change in the diffusive-reactive limit(Prater 1958) is $\Delta\hat{T}_{dif}=\beta\hat{T}_s$, equation (6.14) reads as $\Delta\hat{T}\sim\frac{\phi^2}{Pe_m}\frac{Pe_m}{Pe_h}\Delta\hat{T}_{dif}\frac{\tau_{RH}}{\tau_C}$ or as $\Delta\hat{T}\sim\frac{\phi^2}{Pe_m}\Delta\hat{T}_{ad}\frac{\tau_{RH}}{\tau_C}$, since $\Delta\hat{T}_{ad}=\Delta\hat{T}_{dif}\,Le$ (the adiabatic temperature change). Also notice that $\frac{\Delta\hat{T}}{\Delta\hat{T}_{ad}}\sim\frac{\tau_{RH}}{\tau_R}$. If the time required for the fluid to heat up by the characteristic temperature change is comparable with the one needed for reactant

concentration to experience an $O(1)$ variation (until it reaches its minimum value), then a balance between the two processes yields $\Delta\hat{T}_{ad}$ as a scale for temperature change and the most symmetric form of equations (6.6)-(6.7). The maximum temperature change will be below or above this value, whether the fluid increases its temperature faster $(\tau_{RH} << \tau_R)$ or slower $(\tau_{RH} >> \tau_R)$, in comparison with the time needed for the adiabatic temperature change to occur $(\tau_{RH} \sim \tau_R)$. A more complete scaling analysis for temperature change will be presented in the next section.

6.2.1.b *Effectiveness factor*

A measure for the overall performance of the catalyst slab is given by the effectiveness factor, which compares the average reaction rate with the one observed if reactant concentration and temperature in the whole particle equal surface conditions. We seek to understand the enhancement brought to this quantity which is defined as

$$Eff = \int_{-L}^{L} k\, d\hat{x} \Big/ \int_{-L}^{L} k_s\, d\hat{x} \tag{6.15}$$

where $k(\hat{T})$ is the kinetic constant evaluated at each point from the temperature profile, as long as reactant exists (the contribution of the regions where no reactant exists is zero). Using Gauss' divergence theorem and according to (6.5):

$$Eff = \frac{1}{2\phi^2}\left(\left.\frac{dc}{dx}\right|_{x=1} - \left.\frac{dc}{dx}\right|_{x=-1} \right). \tag{6.16}$$

Eq.(6.16) is somewhat more generic than Eq.(6.15), since any solution (even the ones including concentration annulment branches) guarantee profile and flux continuity.

6.2.2 Scaling and regime diagram

Although, the complete description of the system's behaviour depend on the interaction of all the previously identified mechanisms, particular regimes can be defined in which two important processes balance, being the others negligible at first approximation. We want to describe the global behaviour of the catalyst slab in each one of these regimes, i.e. $x \sim O(1)$, so the original (outer) scaling should be kept. Examining equation (6.6), the following possibilities arise:

- Dominant convection and diffusion for $Pe_m \sim 1$ and $\phi^2 / Pe_m << 1$,
- Dominant diffusion and reaction for $Pe_m << 1$ and $\phi^2 \sim 1$, and
- Dominant convection and reaction for $Pe_m >> 1$ and $\phi^2 / Pe_m \sim 1$.

Also, limiting regimes in which only one mechanism dominates are conceivable. Diffusion is dominant for $\left(\phi^2, Pe_m\right) << 1$, while reaction is the more important process for $\phi^2 >> \left(Pe_m, 1\right)$. In addition, for $Pe_m >> \left(1, \phi^2\right)$, the system can be described as purely convective. Since the only two parameters at play are Pe_m and ϕ^2, this information concerning mass conservation can be represented in a $\phi^2 - Pe_m$ plot (Figure 6.1).

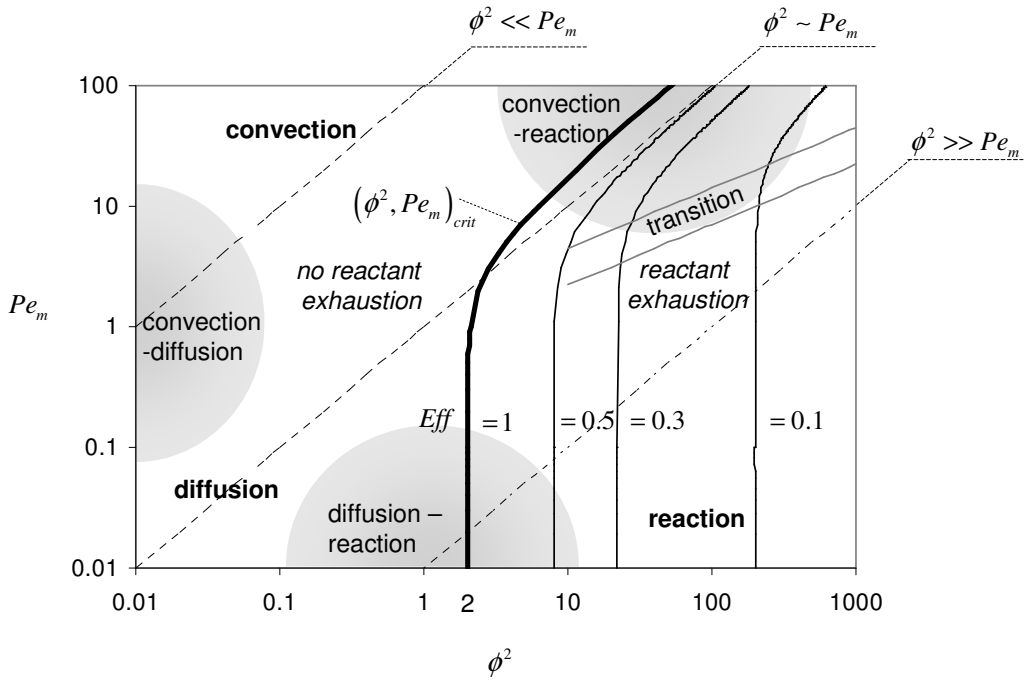

Figure 6.1: Regime diagram for convection, diffusion and zero-order reaction in an isothermal catalyst slab (analytical results from Rodrigues et al. (1984)). The boundary shown as a thick black line separates the situations of no reactant exhaustion (where $Eff = 1$) from the annulment region (where some iso-effectiveness factor curves at $Eff < 1$ are represented).

6.2.2.a *Isothermal zero-order reaction in permeable catalyst slab*

For an isothermal system, exact analytical solutions are available (Rodrigues et al. 1984). The calculation of the effectiveness factor and the condition that separates the situation of reactant exhaustion from the one where no concentration annulment occurs, are of particular interest. These important results are represented in Figure 6.1. For representation convenience, we choose a factor of 10^{-2} to express smallness in the above magnitude relations. The regions where the system behaves globally as purely diffusive, convective or reactive are shown, as well as the regimes described by a dominant balance between any of these two (grey areas). The thick black line separates the parametric sets that lead to concentration annulment anywhere inside the particle from the situations where no reactant exhaustion occurs. This line of $\left(\phi^2, Pe_m\right)_{crit}$ is also the iso-effectiveness factor curve for $Eff = 1$, when reactant concentration reaches zero only at a single point inside the slab. For $\left(\phi^2, Pe_m\right) < \left(\phi^2, Pe_m\right)_{crit}$, no annulment occurs and $Eff = 1$. Outside this region, catalyst performance decreases with increasing Thiele modulus, according to the curves of constant effectiveness factor in the $\left(\phi^2, Pe_m\right)$ plane. When $Pe_m \to 0$, the boundary tends to the well-known diffusive limit of $\left(\phi^2\right)_{crit} = 2$, and for $\phi^2 > 2$ the iso-effectiveness factor curves approach the value $Eff = \sqrt{2}/\phi$. The effect of convection is visible for high Pe_m, increasing the effectiveness factor for a given ϕ^2 (and also the value of $\left(\phi^2\right)_{crit}$ needed to achieve annulment), that is, the overall content in reactant inside the slab increases. The region around the grey lines represent the transition zone, above which, the effect of increasing the Peclet number (and therefore, convection) is particularly noticeable (this approximated criteria will be derived in section 6.3.3.c).

6.2.2.b *Scaling for temperature change in exothermic systems*

In order to study nonisothermal systems, in which β and γ are fixed, we have to consider the intraparticular heat Peclet number, Pe_h (through Lewis number, for example), in addition to ϕ^2 and Pe_m. A 3-D regime diagram can be constructed by adding this third axis ($Le = Pe_m / Pe_h$), as shown in Figure 6.2.

An order of magnitude estimation and scaling for the characteristic temperature change, $\Delta\hat{T}$, can be obtained by a balance between the terms corresponding to the dominant effects in the energy balance (Lin et al. 1988). To compare the magnitude between all terms in equation (6.7) we introduce a generic small parameter ε, which will express the relations between the

dimensionless groups. Therefore, for $Pe_h \sim \varepsilon$ (reaction-conduction dominant balance), $\Delta\hat{T}/\Delta\hat{T}_{ad} \sim \phi^2/Le$; while for $Pe_h \sim \varepsilon^{-1}$ (strong heat convection balanced by reaction), $\Delta\hat{T}/\Delta\hat{T}_{ad} \sim \phi^2/Pe_m$. When heat transport mechanisms dominate over reaction: $Pe_h \sim 1$ and $\Delta\hat{T}/\Delta\hat{T}_{ad} >> \phi^2/Pe_m$ (we will take $\Delta\hat{T}/\Delta\hat{T}_{ad} \sim \left(\phi^2/Pe_m\right)\varepsilon^{-1}$). In Figure 6.2a, the results of temperature scaling in the planes of slow conduction $\left(Le \sim \varepsilon\right)$, convection $\left(Pe_m \sim \varepsilon\right)$ and reaction $\left(\phi^2 \sim \varepsilon\right)$ are indicated by: isothermal (when $\Delta\hat{T} << \left(\Delta\hat{T}_{dif}, \Delta\hat{T}_{ad}\right)$); adiabatic ($\Delta\hat{T} \sim \Delta\hat{T}_{ad}$); diffusive ($\Delta\hat{T}_{dif} = \beta\hat{T}_s$) and 'explosion' (if $\Delta\hat{T} >> \left(\Delta\hat{T}_{dif}, \Delta\hat{T}_{ad}\right)$). In Figure 6.2b, the $Pe_m = \varepsilon^{-1}$ and $\phi^2 = \varepsilon^{-1}$ planes are shown. Since for a given system, Lewis number is approximately constant, we show in detail the planes for Le of order 1, ε and ε^{-1} (Figure 6.3). The boundaries between each region are schematic. The isothermal regions appear at regimes where reaction is slow and heat removal by conduction/convection is strong. The parameter sets where the characteristic temperature change is of the same order of the maximum temperature change observed in a diffusive-reactive system with concentration annulment are related to the ones leading to the adiabatic temperature change by the Lewis number, since $\Delta\hat{T}_{ad} = \Delta\hat{T}_{dif}\, Le$.

The indicated characteristic temperature changes are observed at an $O(1)$ scale inside the catalyst and they account for the existence of reaction throughout the slab. However, the existence of a reactant limitation (which puts an end to the heat-generating reaction) stops temperature from becoming unbounded in the 'explosion' areas. Since no physical solution for the steady-state mass and energy conservation equations (with the reaction term) can be found, the proper form of (6.6)-(6.7) includes also the branch of $r(T) = 0$ for $\hat{c} = 0$.

To obtain a correct estimate for temperature change, 'active' regions of thickness much smaller than 1 have to be considered (since the solution already includes an $O(1)$ branch from (6.6)-(6.7) with $r(T) = 0$). If the thickness of these inner regions is χ for concentration and τ for temperature, then we are interested in the cases where $\chi, \tau << 1$.

Rescaling x by χ and τ in the mass and energy conservation equations respectively, more insight into the 'explosive' regions can be achieved, if we choose the consistent dominant balances in each parameter set. So,

(a) For $Le \sim 1$ (Figure 6.3a) and $\phi^2 \sim \varepsilon^{-1}$, diffusive-reactive inner regions with thickness $\chi \sim \phi^{-1} \sim \sqrt{\varepsilon}$ in the concentration profile and $\tau \sim \sqrt{\varepsilon}\sqrt{\Delta\hat{T}/\Delta\hat{T}_{dif}}$ in the temperature profile are suggested. Since the two regions are comparable in extension ($\chi \sim \tau$), then $\Delta\hat{T} \sim \Delta\hat{T}_{dif}\left(\sim \Delta\hat{T}_{ad}\right)$.

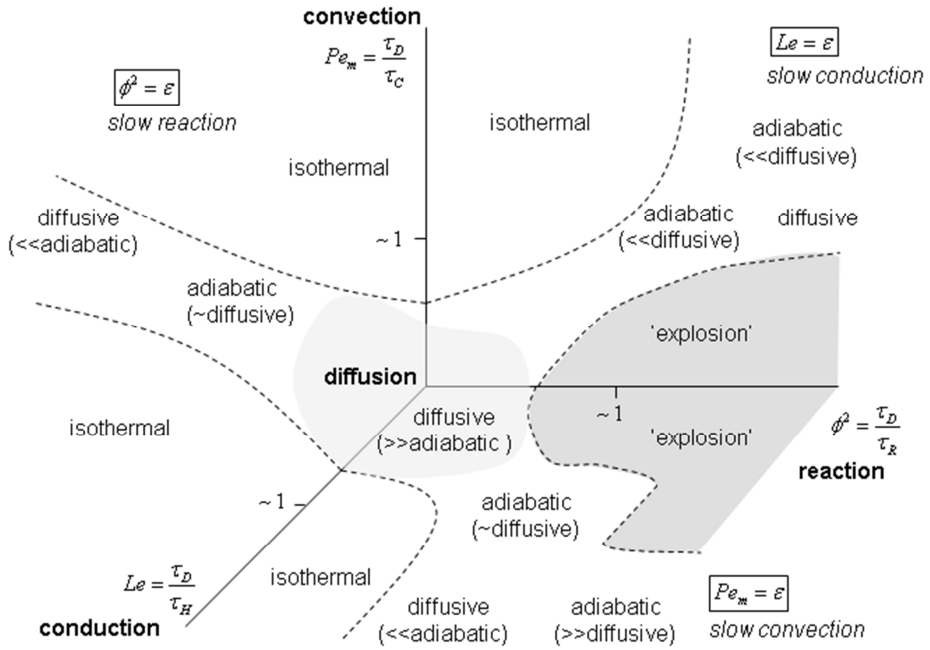

(a) $Le = \varepsilon$, $Pe_m = \varepsilon$ and $\phi^2 = \varepsilon$ planes.

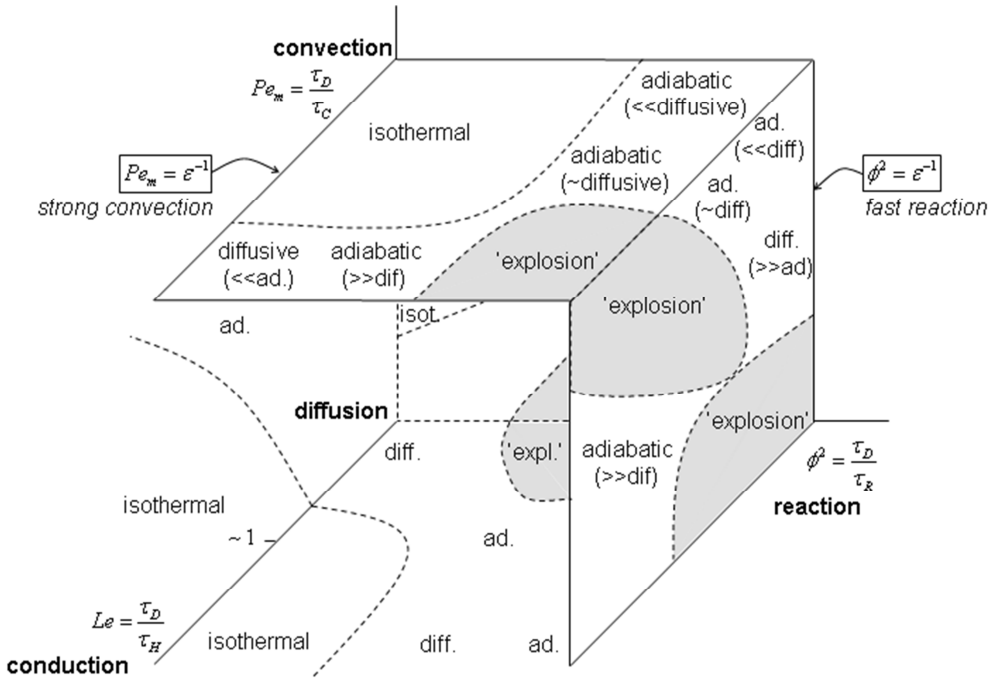

(b) $Pe_m = \varepsilon^{-1}$ and $\phi^2 = \varepsilon^{-1}$ planes.

Figure 6.2: 3-D regime diagram for convection, diffusion and exothermic reaction in a catalyst slab. The regions marked as isothermal present very small deviation from surface temperature. The adiabatic (ad.) limit is related with the characteristic temperature change under diffusive conditions (diff., $\Delta\hat{T}_{dif} = \beta\hat{T}_s$) by the Lewis number: $\Delta\hat{T}_{ad} = \Delta\hat{T}_{dif}\, Le$. When $\Delta\hat{T} >> \Delta\hat{T}_{ad}, \Delta\hat{T}_{dif}$, 'explosion' (expl.) occurs.

(b) In the plane of $Le \sim \varepsilon$ (Figure 6.3b), the 'explosive' regions are predicted at low intraparticular convection ($Pe_m \sim \varepsilon$). The diffusion-reaction balance (at $\phi^2 \sim \varepsilon^{-1}$) predicts again $\Delta\hat{T} \sim \Delta\hat{T}_{dif}$. On the other hand, at $\phi^2 \sim 1$, no consistent inner regions were found, so the only distinguished limit reproduces the outer solution: $\Delta\hat{T} >> \Delta\hat{T}_{ad}\,\varepsilon^{-1}$ or as in Figure 6.3b, $\Delta\hat{T} \sim \Delta\hat{T}_{ad}\,\varepsilon^{-2}$.

(c) When Lewis number is high ($\sim O\left(\varepsilon^{-1}\right)$, Figure 6.3c), the outer scaling shows an 'explosion' region at $\left(Pe_m, \phi^2\right) \sim \varepsilon^{-1}$. Introducing the new scales for the spatial dimension, we obtain inner layers of thickness ε in both concentration and temperature profiles and $\Delta\hat{T} \sim \Delta\hat{T}_{ad}\,\varepsilon^2$.

In the 'explosion' areas (with outer scaling), the predicted temperature change is unbounded. In the rescaled 'explosive' regions, the maximum temperature predicted in each one of the $Le = \text{constant}$ planes decreases from $\Delta\hat{T} \sim \Delta\hat{T}_{ad}\,\varepsilon^{-2}$ to $\Delta\hat{T}_{ad}$ and then to $\Delta\hat{T}_{ad}\,\varepsilon^2$, when Lewis number increases ($Le \sim \varepsilon, 1, \varepsilon^{-1}$). This can be explained by the increasingly stronger heat loss by conduction to the cold boundaries, compared to species diffusion rate to the reactive zones.

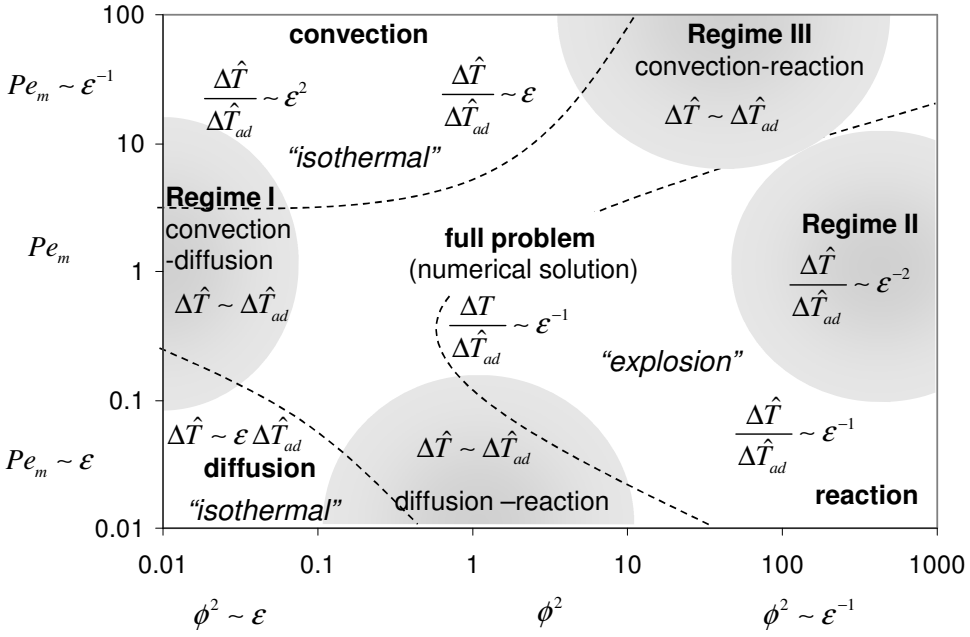

(a) $Le \sim 1$ ($\Delta\hat{T}_{ad} \sim \Delta\hat{T}_{dif}$)

Figure 6.3: Regime diagram for exothermic reaction inside permeable porous catalyst slab (planes for Le of order 1, ε and ε^{-1}).

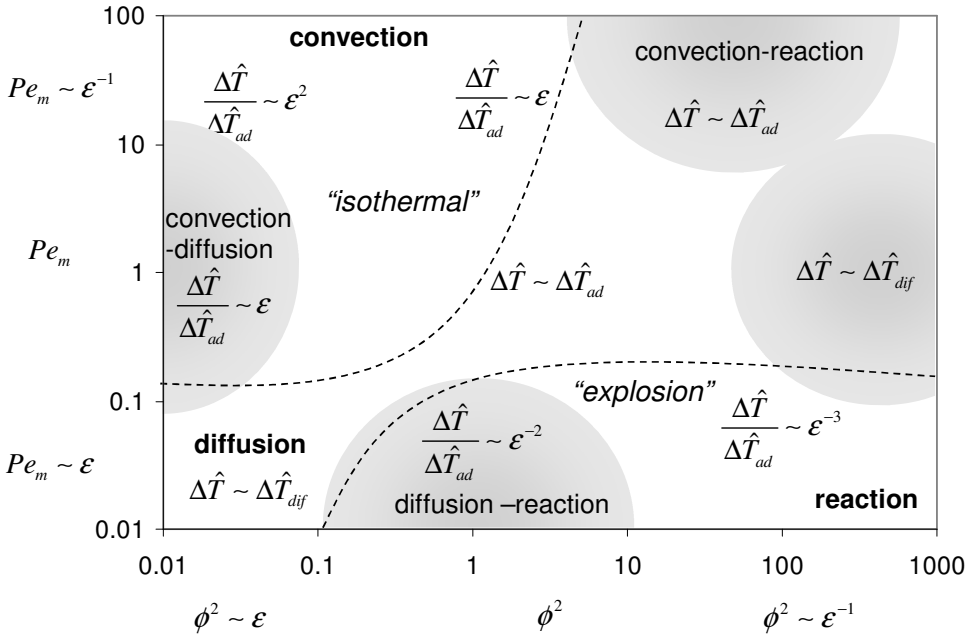

(b) $Le \sim \varepsilon$ $(\Delta\hat{T}_{ad} \sim \varepsilon \Delta\hat{T}_{dif})$

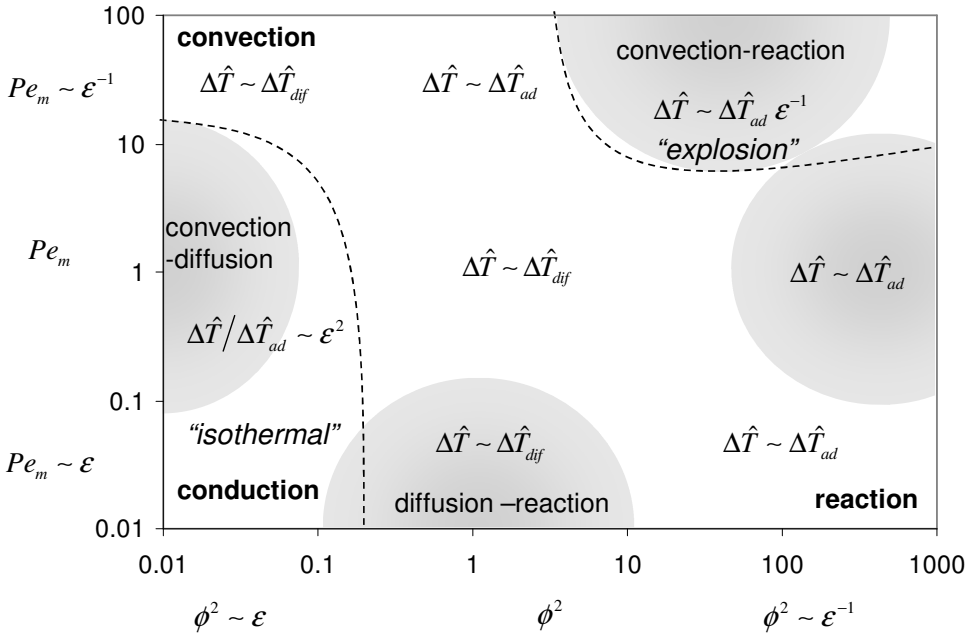

(c) $Le \sim \varepsilon^{-1}$ $(\Delta\hat{T}_{dif} \sim \varepsilon \Delta\hat{T}_{ad})$

Figure 6.3: Regime diagram for exothermic reaction inside permeable porous catalyst slab (planes for Le of order 1, ε and ε^{-1}).

Since the remaining of this work focuses on the particular case of $Le \sim 1$ (Figure 6.3a) we take $\Delta\hat{T}_{ad}$ as a scale for temperature change in the regimes of slow and fast reaction (Regime I and II respectively) and strong intraparticular convection (Regime III). We can also anticipate that in Regime II, non-uniformities will arise. With this scale, equations (6.6)-(6.7) become:

$$\frac{dc}{dx} = \frac{1}{Pe_m}\frac{d^2c}{dx^2} - \frac{\phi^2}{Pe_m} r(T) \tag{6.17}$$

$$\frac{dT}{dx} = \frac{1}{Pe_m}\frac{Pe_m}{Pe_h}\frac{d^2T}{dx^2} + \frac{\phi^2}{Pe_m} r(T) \tag{6.18}$$

The reaction term was assumed of $O(1)$:

$$r(T) = \exp\left[\frac{\varphi T}{1+\eta T}\right] = \exp\left[\frac{\gamma\beta LeT}{1+\beta LeT}\right] \sim \exp[\gamma\beta LeT]$$

for Le and $T \sim O(1)$. The product $\gamma\beta$ can also be taken close to unity for common exothermic reactions, since β rarely exceeds 0.3 and the typical range for γ is $\sim 10-30$ (Rodrigues 1981).

6.3 PERTURBATION ANALYSIS

The limiting cases discussed in the previous section can be analysed in more depth by considering appropriate parameter regimes and conducting a perturbation analysis (Bender et al. 1999). This involves the choice of a perturbation (small) parameter ε, against which all others should be compared. Concentration and temperature profiles are expanded as series of powers of ε and substituted into the governing differential equations and boundary conditions. An infinite set of determined problems is obtained when terms of the same order are collected in each equation. The leading-order problem reflects the assumed dominant balance, while higher order corrections account for the negligible mechanism. The results in the present work apply to $Le \sim O(1)$ and they intend to approximate the full solution of the complete problem in the limits of: fast mass/heat transport (Regime I), dominant reaction (Regime II) and strong intraparticular convection (Regime III). The diffusive regime for an exothermic zero-order reaction (diffusion-reaction grey area in Figure 6.3 and $Pe_m = 0$ plane in Figure 6.2a) was studied, among others, by Frank-Kamenetskii (1955), Hlavacek (1967) and Aris (1975) and it will be used to validate our solutions.

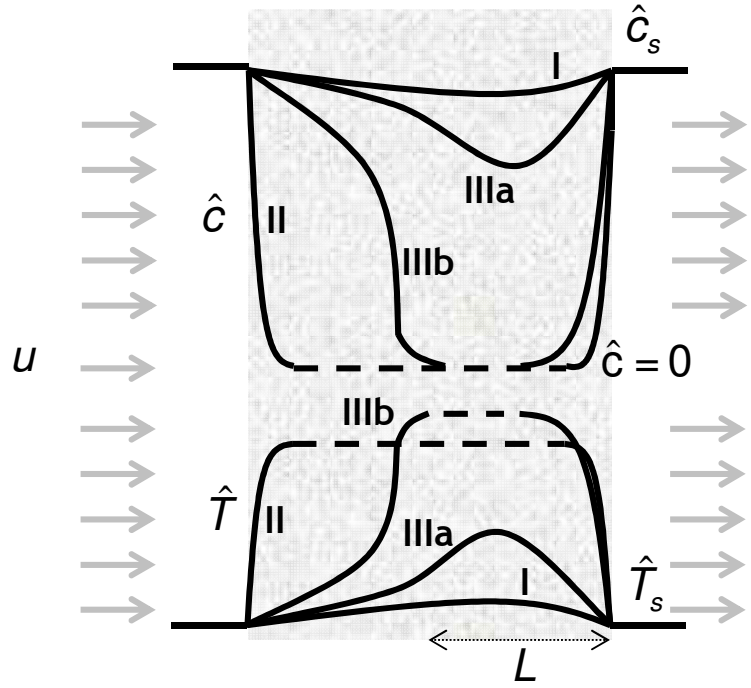

Figure 6.4: Schematic concentration and temperature profiles in a permeable catalyst slab, where an exothermic zero-order reaction occurs. The regimes studied are: slow and fast reaction (Regime I and II, respectively) and strong convection with and without (Regime IIIb and Regime IIIa, respectively) concentration annulment.

6.3.1 Regime I (Chemical regime)

When transport mechanisms are much faster than chemical reaction, concentration and temperature inside the slab depart little from its surface values (Figure 6.4). This corresponds to the case when Thiele modulus is low and to the classic chemical regime, in the presence of convection.

Assuming that the terms in Eqs.(6.17)-(6.18) are correctly scaled, we take $\varepsilon = \phi^2 / Pe_m$ as perturbation parameter and look for outer solutions (valid in $x = O(1)$) under the following conditions:

$$\frac{\phi^2}{Pe_m} << 1, \frac{1}{Pe_m}, \frac{1}{Pe_h} \tag{6.19}$$

Also, in this regime, concentration annulment is not expected to occur, so the appropriate form of mass and energy balances takes into account the reaction term:

$$\frac{dc}{dx}=\frac{1}{Pe_m}\frac{d^2c}{dx^2}-\varepsilon\exp\left[\frac{\varphi T}{1+\eta T}\right] \tag{6.20}$$

$$\frac{dT}{dx}=\frac{1}{Pe_h}\frac{d^2T}{dx^2}+\varepsilon\exp\left[\frac{\varphi T}{1+\eta T}\right] \tag{6.21}$$

subject to boundary conditions (6.8)-(6.9).

Since the reduced problem ($\varepsilon=0$) does not change the order of the differential equations (and therefore, the leading order solution is still able to fulfil both boundary conditions), this is a regular perturbation problem.

The uniformly valid solutions are assumed to be of the following form:

$$c(x;\varepsilon)=\sum_{n=0}^{\infty}c_n(x)\,\varepsilon^n\sim c_0(x)+c_1(x)\,\varepsilon+\ldots \text{ and} \tag{6.22}$$

$$T(x;\varepsilon)=\sum_{n=0}^{\infty}T_n(x)\,\varepsilon^n\sim T_0(x)+T_1(x)\,\varepsilon+\ldots. \tag{6.23}$$

Substituting (6.22)-(6.23) into (6.20)-(6.21) and regarding the resulting equations as identities in ε, the necessary subproblems arise, from which $c_n(x)$ and $T_n(x)$ functions can be calculated. The $O(1)$ problem represents the convective-diffusive balance, which yields the following solution: $c_0(x)=0$ and $T_0(x)=0$.

The effect of reaction is felt at $O\left(\phi^2/Pe_m\right)$, but since it is calculated from surface conditions (zero-order solution, $r(T_0)=1$), the order of the reaction is, so far, irrelevant. Therefore, these solutions equal the ones obtained for first-order reaction by perturbation techniques (Cardoso et al. 2007). The $O(\varepsilon^2)$ term, however, is dependent of the order of reaction, but its contribution was found to be negligible. This term carries also the information regarding the reaction rate sensitivity to temperature (activation energy). The concentration profile up to $O(\varepsilon)$ does not depend on any nonisothermal parameter (related with the reaction's heat or activation energy). In fact, it reproduces the solution for the problem of convection, diffusion and isothermal zero-order reaction in a slab (Rodrigues et al. 1984). Nevertheless, the two-term expansion is enough to represent concentration and temperature profiles accurately,

$$c(x)=\frac{\phi^2}{Pe_m}\left[\frac{2e^{Pe_m(x+1)}}{e^{2Pe_m}-1}-\frac{e^{2Pe_m}+1}{e^{2Pe_m}-1}-x\right]+O\left(\frac{\phi^4}{Pe_m^2}\right) \tag{6.24}$$

$$T(x)=\frac{\phi^2}{Pe_m}\left[\frac{2e^{Pe_h(x+1)}}{1-e^{2Pe_h}}+\frac{e^{2Pe_h}+1}{e^{2Pe_h}-1}+x\right]+O\left(\frac{\phi^4}{Pe_m^2}\right). \tag{6.25}$$

Concentration and temperature profiles (Eqs.(6.24) and (6.25)) are represented in Figure 6.5. Numerical results obtained with gPROMS (2007) are also plotted. The agreement is especially good for $\varepsilon \sim 0.01$.

For an exothermic reaction, the maximum temperature occurs at:

$$x_{\max}=-1+\frac{1}{Pe_h}\ln\left[\frac{e^{2Pe_h}-1}{2Pe_h}\right] \tag{6.26}$$

while the minimum concentration position is

$$x_{\min}=-1+\frac{1}{Pe_m}\ln\left[\frac{e^{2Pe_m}-1}{2Pe_m}\right]. \tag{6.27}$$

which is, in general, distinct from $x_{\max}$ (as long as $Le\neq 1$). The minimum concentration value in this regime is of order ε, and is given by:

$$c^{\min}=-\frac{\phi^2}{Pe_m}\left[\frac{2}{e^{2Pe_m}-1}-\frac{1}{Pe_m}+\frac{1}{Pe_m}\ln\left(\frac{e^{2Pe_m}-1}{2Pe_m}\right)\right] \tag{6.28}$$

Since thermal effects do not affect the concentration profile for weak reaction conditions, equations (6.27) and (6.28) reproduce the isothermal results (Rodrigues et al. 1984), when no annulment occurs. An estimate for maximum temperature will be given in section 6.4.

Although the dominant balance requires that $Pe_m \sim 1$ and $Pe_h \sim 1$, we expect that the presented solutions can also include the regimes where convection or diffusion is the only important mechanism. In the chemical regime, the limits of strong convection ($Pe_m, Pe_h >> 1$) or diffusion ($Pe_m, Pe_h << 1$) yield both: $c(x), T(x) \to 0$. However, convective transport suggests profile asymmetry ($x_{\min}, x_{\max} \to 1$), in contrast with the symmetry characteristic of diffusive profiles ($x_{\min}, x_{\max} \to 0$).

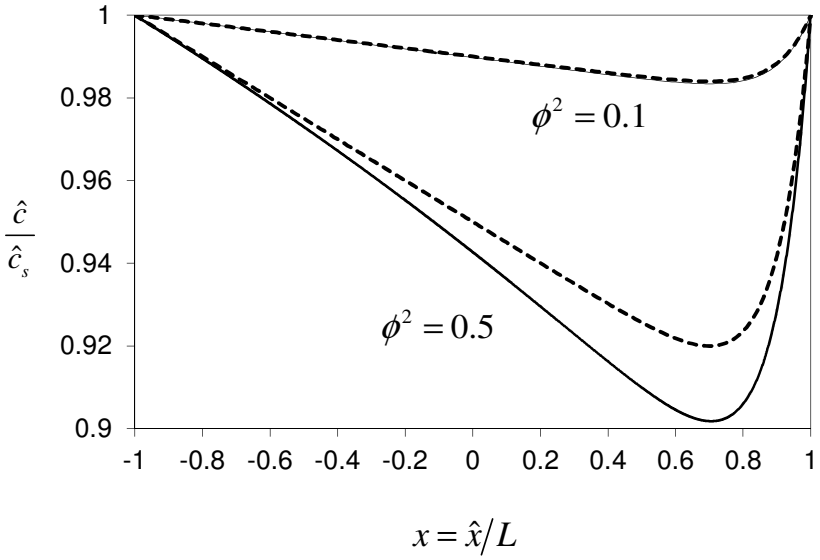

(a) Reactant concentration profile.

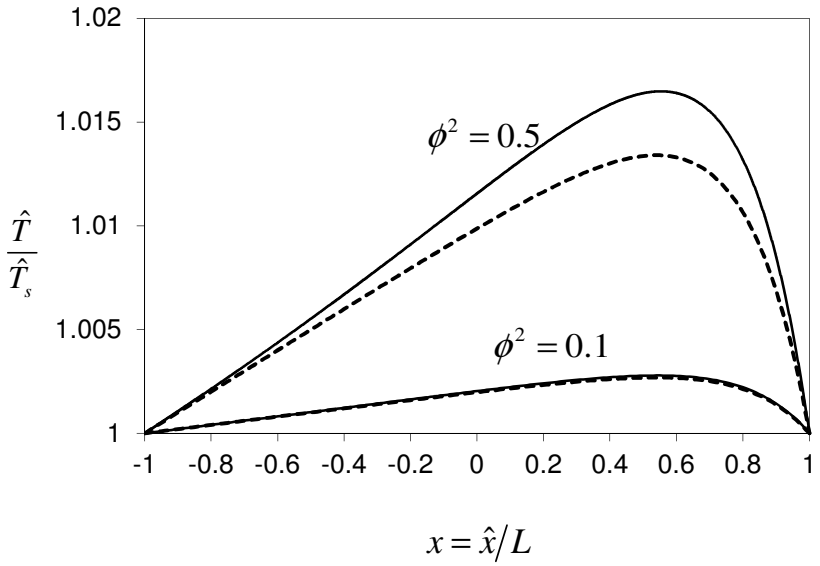

(b) Temperature profile.

Figure 6.5: Comparison of the perturbation solutions (equations (6.24)-(6.25), dashed lines) with numerical results from gPROMS® (solid lines) for $\gamma = 20$, $\beta = 0.1$, $Pe_m = 10$, $Pe_h = 5$, and $\phi^2 = 0.1$ ($\varepsilon = 0.01$) or $\phi^2 = 0.5$ ($\varepsilon = 0.05$).

6.3.2 Regime II (Diffusional regime)

The regime in which reaction is fast compared with transport mechanisms appears for large Thiele modulus. In order to study this diffusional regime (in the presence of convection), we set the perturbation parameter to: $\varepsilon = Pe_m / \phi^2$. Under the conditions:

$$\frac{\phi^2}{Pe_m} >> 1, \frac{1}{Pe_m}, \frac{1}{Pe_h} \tag{6.29}$$

the solution to (6.17)-(6.18) is obtained by conducting a singular perturbation analysis, since keeping the original scaling does not yield an uniformly valid result. We expect boundary layers to occur near the slab surfaces, where reactant concentration decreases and temperature increases sharply from the middle solution to surface values (Figure 6.4).

6.3.2.a *Middle region*

Looking for an outer solution with mass/energy equations that include chemical reaction leads to an $O(1)$ problem with no physical solution. That is, the reduced problem from

$$\varepsilon \frac{dc^m}{dx} = \frac{\varepsilon}{Pe_m} \frac{d^2 c^m}{dx^2} - \exp\left[\frac{\varphi T^m}{1 + \eta T^m} \right] \tag{6.30}$$

$$\varepsilon \frac{dT^m}{dx} = \frac{\varepsilon}{Pe_h} \frac{d^2 T^m}{dx^2} + \exp\left[\frac{\varphi T^m}{1 + \eta T^m} \right] \tag{6.31}$$

suggests that concentration and thermal boundary layers will develop at $\hat{x} = \pm L$ (as no boundary conditions can be fulfilled) and since $\exp\left[\varphi T^m / \left(1 + \eta T^m\right) \right] = 0$ is not possible, this should correspond to a 'dead core' situation where reactant vanishes and 'explosion' occurs. Consequently, chemistry-free equations should be used in this region. They are written as:

$$c^m(x) = -1 \qquad \text{for } x' \le x \le x^* \tag{6.32}$$

$$\frac{dT^m}{dx} = \frac{1}{Pe_h} \frac{d^2 T^m}{dx^2} \qquad \text{for } x' \le x \le x^*. \tag{6.33}$$

The solution from (6.33) is intended to represent the temperature profile in the region where reactant disappears (between x' and x^*). This equation is valid for all orders of the perturbation parameter and is free of ε. Therefore, all subproblems of order $O\left(\varepsilon^{n/2}\right)$ arising from (6.33) are identical and the expansion for the temperature profile in the middle section of the slab is:

$$T^m(x;\varepsilon)=\sum_{n=0}^{\infty}T_n^m(x)\,\varepsilon^{n/2}=\sum_{n=0}^{\infty}\left(\frac{h_n}{Pe_h}e^{Pe_h x}+j_n\right)\varepsilon^{n/2} \qquad \text{for } x'\le x\le x^*. \tag{6.34}$$

The shape of the temperature profile is exponentially increasing / decreasing or a plateau, depending on the value of $dT^m/dx=\sum_{n=0}^{\infty}\left(h_n e^{Pe_h x}\right)\varepsilon^{n/2}$ ($e^{Pe_h x}>0$, so the sign of dT^m/dx is independent of x). Since the nature of the regions at $x=\pm 1$ is such that surface temperature is brought monotonically to match the middle region profile, we expect that the derivative of these solutions to be null either at x' or x^* (where the maximum temperature occurs). These regions are described by equations (6.30)-(6.31), which are fundamentally different from (6.32)-(6.33). Therefore, we use perturbation analysis as an approximation procedure for boundary layers and require profile and flux continuity with the middle region. As a result of both derivative continuity and concentration annulment at x' and x^*, Eq.(6.34) has to predict a plateau with no temperature variation in the middle of the slab. This is a reasonable simplification for the conditions defined in this regime, and is confirmed by numerical simulations for the first-order reaction case (Quinta Ferreira 1988). Consequently, the maximum temperature is:

$$T^m(x;\varepsilon)=T^{\max}(\varepsilon)=T_0^{\max}+T_1^{\max}\sqrt{\varepsilon}+O(\varepsilon). \tag{6.35}$$

6.3.2.b *Right boundary layer*

At the inner layer near $x=1$, the following stretching transformation is introduced:

$$X=\frac{1-x}{\delta}. \tag{6.36}$$

The boundary layer thickness (δ) correctly rescales the convective, diffusive and reactive terms. A dominant balance between two of these terms yields the distinguished limit. In this case, the consistent option is a reaction-diffusion balance ($\delta\sim\sqrt{\varepsilon}$), being convection only important at $O\left(\sqrt{\varepsilon}\right)$. Equations (6.30)-(6.31) then become:

$$\frac{1}{Pe_m}\frac{d^2c^r}{dX^2}+\sqrt{\varepsilon}\frac{dc^r}{dX}-\exp\left[\frac{\varphi T^r}{1+\eta T^r}\right]=0 \qquad \text{for } 0\le X\le X^* \tag{6.37}$$

$$\frac{1}{Pe_h}\frac{d^2T^r}{dX^2}+\sqrt{\varepsilon}\frac{dT^r}{dX}+\exp\left[\frac{\varphi T^r}{1+\eta T^r}\right]=0 \qquad \text{for } 0\le X\le X^* \tag{6.38}$$

with boundary conditions:

$$c^r(X=0)=0 \text{ and} \tag{6.39}$$

$$T^r(X=0)=0. \tag{6.40}$$

Equations (6.37) and (6.38) suggest that we look for solutions of the form:

$$c^r(x) = \sum_{n=0}^{\infty} c_n^r(x)\,\varepsilon^{n/2} \quad \text{and} \tag{6.41}$$

$$T^r(x) = \sum_{n=0}^{\infty} T_n^r(x)\,\varepsilon^{n/2} \tag{6.42}$$

where $c_n^r(x) \equiv c_n^r(X)$, $T_n^r(x) \equiv T_n^r(X)$ and $X^* = (1-x^*)/\sqrt{\varepsilon}$.

6.3.2.c *Left boundary layer*

At the slab's 'entrance', the proper rescaling is given by:

$$Y = \frac{1+x}{\sqrt{\varepsilon}} \tag{6.43}$$

predicted from the diffusive-reactive nature of the boundary layer (same reasoning as for the boundary layer on the right). The equations for this region are:

$$\frac{1}{Pe_m}\frac{d^2c^l}{dY^2} - \sqrt{\varepsilon}\frac{dc^l}{dY} - \exp\left[\frac{\varphi T^l}{1+\eta T^l}\right] = 0 \qquad \text{for } 0 \le Y \le Y' \tag{6.44}$$

$$\frac{1}{Pe_h}\frac{d^2T^l}{dY^2} - \sqrt{\varepsilon}\frac{dT^l}{dY} + \exp\left[\frac{\varphi T^l}{1+\eta T^l}\right] = 0 \qquad \text{for } 0 \le Y \le Y' \tag{6.45}$$

subject to:

$$c^l(Y=0) = 0 \quad \text{and} \tag{6.46}$$

$$T^l(Y=0) = 0\,. \tag{6.47}$$

The form of the solutions that we are looking for is, again:

$$c^l(x) = \sum_{n=0}^{\infty} c_n^l(x)\,\varepsilon^{n/2} \quad \text{and} \tag{6.48}$$

$$T^l(x) = \sum_{n=0}^{\infty} T_n^l(x)\,\varepsilon^{n/2} \tag{6.49}$$

where $c_n^l(x) \equiv c_n^l(Y)$, $T_n^l(x) \equiv T_n^l(Y)$ and $Y' = (-1+x')/\sqrt{\varepsilon}$.

6.3.2.d *Profile and flux continuity at x^* and x'*

The problem is completely determined if two more types of conditions are provided: one from where the positions X^* and Y' can be calculated, and the remaining boundary condition for the problems defined by (6.37)-(6.40) and (6.44)-(6.47). Conditions for profile continuity at each order of the small parameter can be written as:

$$c_n^{\,r}(X^*) = c_n^{\,m}(x^*) = \begin{cases} -1, & n = 0 \\ 0, & n \geq 1 \end{cases} \tag{6.50}$$

and $T_n^{\,r}(X^*) = T_n^{\,m}(x^*) = T_n^{\max}$ (6.51)

at the right boundary layer, and

$$c_n^{\,l}(Y') = c_n^{\,m}(x') = \begin{cases} -1, & n = 0 \\ 0, & n \geq 1 \end{cases} \tag{6.52}$$

and $T_n^{\,l}(Y') = T_n^{\,m}(x') = T_n^{\max}$ (6.53)

at the left one.

To determine the annulment positions from gradient continuity between the boundary layers and the middle region, we have to solve nonlinear algebraic equations in X^* and Y'. An explicit approximate solution can be found if we expand these unknowns as:

$$X^* = \sum_{n=0}^{\infty} X_n^* \, \varepsilon^{n/2} = X_0^* + \sqrt{\varepsilon}\, X_1^* + O(\varepsilon) \text{ and} \tag{6.54}$$

$$Y' = \sum_{n=0}^{\infty} Y_n' \, \varepsilon^{n/2} = Y_0' + \sqrt{\varepsilon}\, Y_1' + O(\varepsilon). \tag{6.55}$$

After linearization around $\varepsilon = 0$, the coefficients X_n^* and Y_n' for ($n = 0, 1$) can be determined from:

$$\lim_{\varepsilon \to 0} \left. \frac{dc^r}{dX} \right|_{X^*, \varepsilon} = 0 \tag{6.56}$$

$$\lim_{\varepsilon \to 0} \left. \frac{dc^l}{dY} \right|_{Y', \varepsilon} = 0 \tag{6.57}$$

$$\lim_{\varepsilon \to 0} \frac{1}{\sqrt{\varepsilon}} \left[\left. \frac{dc^r}{dX} \right|_{X^*, \varepsilon} - \left. \frac{dc^r}{dX} \right|_{X^*, \varepsilon = 0} \right] = 0 \tag{6.58}$$

$$\lim_{\varepsilon \to 0} \frac{1}{\sqrt{\varepsilon}} \left[\left. \frac{dc^l}{dY} \right|_{Y', \varepsilon} - \left. \frac{dc^l}{dY} \right|_{Y', \varepsilon = 0} \right] = 0. \tag{6.59}$$

The problem is closed when the same equations are written for the temperature profile, and the coefficients in equation (6.35) can then be determined (maximum temperature estimate).

6.3.2.e *Approximate concentration and temperature profiles*

If expansions (6.41)-(6.42) and (6.48)-(6.49) are substituted into the equations for the boundary layers ((6.37)-(6.40) and (6.44)-(6.47)), and we collect same order terms, a sequence of sub-problems is obtained. The nonlinear term (6.10) is expressed by a Taylor series around $\varepsilon = 0$. At $O(1)$ the problem reduces to the following set of equations for the right boundary layer ($x^* < x < 1$):

$$\frac{1}{Pe_m}\frac{d^2 c_0^r}{dX^2} - \exp\left[\frac{\varphi T_0^r}{1+\eta T_0^r}\right] = 0 \text{ and} \tag{6.60}$$

$$\frac{1}{Pe_h}\frac{d^2 T_0^r}{dX^2} + \exp\left[\frac{\varphi T_0^r}{1+\eta T_0^r}\right] = 0 \qquad \text{for } 0 \le X \le X^* \tag{6.61}$$

with boundary conditions given by (6.39)-(6.40) and (6.50)-(6.51) for $n = 0$. Adding both equations, the well-known Damköhler relation in the diffusive limit is obtained, if the maximum temperature is $T_0^{\max} = Pe_h / Pe_m$ (in dimensional variables: $\hat{T}_{\max} = \hat{T}_s(1+\beta)$):

$$T_0^r = Pe_h / Pe_m \left(-c_0^r\right) \tag{6.62}$$

(or, in dimensional variables: $\hat{T}_0^r / \hat{T}_s = 1 + \beta\left(1 - \hat{c}_0^r / \hat{c}_s\right)$).

A similar leading-order problem can be extracted from the left boundary layer equations ((6.44)-(6.47) and (6.52)-(6.53)). Both these problems find simple analytical solution under the simplification:

$$\exp\left[\frac{\varphi T_0^r}{1+\eta T_0^r}\right] \simeq b^2 \tag{6.63}$$

The constant b^2 will be determined later by an integral approximation. Also, from equations (6.56)-(6.57), $X_0{}^*$ and $Y_0{}'$ can be estimated. Those results are written as:

$$c_0^r(X) = -\frac{X}{X^*} + \frac{Pe_m b^2}{2}(X - X^*)X \tag{6.64}$$

$$T_0^r(X) = T_0^{\max}\frac{X}{X^*} - \frac{Pe_h b^2}{2}(X - X^*)X \text{ and} \tag{6.65}$$

$$c_0^l(Y) = -\frac{Y}{Y'} + \frac{Pe_m b^2}{2}(Y - Y')Y \tag{6.66}$$

$$T_0^l(Y) = T_0^{\max}\frac{Y}{Y'} - \frac{Pe_h b^2}{2}(Y - Y')Y \tag{6.67}$$

with,

$$T_0^{\max} = \frac{Pe_h}{Pe_m}, \tag{6.68}$$

$$X_0^* = \sqrt{\frac{2}{Pe_m b^2}} \text{ and} \tag{6.69}$$

$$Y_0' = \sqrt{\frac{2}{Pe_m b^2}}\,. \tag{6.70}$$

The $O\left(\sqrt{\varepsilon}\right)$ problem takes into consideration the convective term influence. In the right boundary layer ($x^* < x < 1$), mass and energy conservation equations write as:

$$\frac{1}{Pe_m}\frac{d^2 c_1^r}{dX^2} - \frac{\varphi}{\left(1+\eta T_0^r\right)^2}\exp\left[\frac{\varphi T_0^r}{1+\eta T_0^r}\right]T_1^r = -\frac{dc_0^r}{dX} \text{ and} \tag{6.71}$$

$$\frac{1}{Pe_h}\frac{d^2 T_1^r}{dX^2} + \frac{\varphi}{\left(1+\eta T_0^r\right)^2}\exp\left[\frac{\varphi T_0^r}{1+\eta T_0^r}\right]T_1^r = -\frac{dT_0^r}{dX} \qquad \text{for } 0 \le X \le X^*. \tag{6.72}$$

with (6.39)-(6.40) and (6.50)-(6.51) as boundary conditions ($n = 1$). The corresponding problem at the left boundary layer appears from equations (6.44)-(6.47) and (6.52)-(6.53). In order to find a simple solution, the following simplifications are made:

$$\frac{\varphi T_1^r}{\left(1+\eta T_0^r\right)^2}\exp\left[\frac{\varphi T_0^r}{1+\eta T_0^r}\right] \simeq d \tag{6.73}$$

$$\frac{\varphi T_1^l}{\left(1+\eta T_0^l\right)^2}\exp\left[\frac{\varphi T_0^l}{1+\eta T_0^l}\right] \simeq f \tag{6.74}$$

Constants d and f will be estimated by an integral approximation. Finally, concentration and temperature profile corrections at $O\left(\sqrt{\varepsilon}\right)$ are:

$$c_1^r(X) = \frac{Pe_m}{2}X\left(X - X^*\right)\left[X^* + d - \frac{b^2 Pe_m}{3}\left(X - \frac{X^*}{2}\right)\right] \tag{6.75}$$

$$T_1^r(X) = \frac{X}{X^*}\left\{T_1^{\max} - Pe_h\left(X - X^*\right)\left[\frac{T_0^{\max}}{2} + \frac{d}{2}X^* + \frac{b^2 Pe_h}{6}X^*\left(-X + \frac{X^*}{2}\right)\right]\right\} \tag{6.76}$$

and

$$c_1^l(Y) = \frac{Pe_m Y}{2}\left(Y - Y'\right)\left[-\frac{1}{Y'} + f + \frac{b^2 Pe_m}{3}\left(Y - \frac{Y'}{2}\right)\right] \tag{6.77}$$

$$T_1^l(Y) = Y\left\{\frac{T_1^{\max}}{Y'} - Pe_h\left(Y - Y'\right)\left[-\frac{T_0^{\max}}{2Y'} + \frac{f}{2} + \frac{b^2 Pe_m}{6}\left(Y - \frac{Y'}{2}\right)\right]\right\} \tag{6.78}$$

The convective corrections in the annulment positions are calculated from (6.58)-(6.59):

$$X_1^* = -\frac{1}{b^2}\left(\frac{1}{3} + \frac{\sqrt{2}\,d}{2b\sqrt{Pe_m}}\right) \tag{6.79}$$

$$Y_1' = \frac{1}{b^2}\left(\frac{1}{3} - \frac{\sqrt{2}\,f}{2b\sqrt{Pe_m}}\right) \tag{6.80}$$

When similar equations are written for temperature, two estimates for the maximum temperature correction arise. They can be expressed by: $T_1^{\max} = \frac{\sqrt{2}\,Pe_h}{3b\sqrt{Pe_m}}\frac{Pe_h}{Pe_m}\left|1 - \frac{Pe_m}{Pe_h}\right|$.

6.3.2.f *Integral method for approximation at boundary layers*

The constants b^2, d and f are determined by an integral method where instead of requiring the energy balance to be satisfied at every point in the boundary layer, we force the boundary and profile continuity conditions to be fulfilled and the differential equation to be satisfied on average over the whole thickness of the boundary layer (this procedure is similar to the approximation for the momentum-integral equation of boundary layer theory (Schlichting 1979)).

We now write the energy balance equations ((6.61), (6.72) and their similar form for the left boundary layer) with less restrictive simplifications. In particular, we assume small η but non-negligible φ (this is justifiable, since $\varphi = \gamma\eta$, and typically $\gamma \sim 10-30$ (Rodrigues 1981)). So for $\eta T << 1$, the conditions for these constants determination are:

$$\int_0^{X_0^*}\left\{\frac{1}{Pe_h}\frac{d^2T_0^r}{dX^2} + \exp\left[\varphi T_0^r\right]\right\}dX = 0 \tag{6.81}$$

$$\int_0^{X_0^*}\left\{\frac{1}{Pe_h}\frac{d^2T_1^r}{dX^2} + \varphi\, b^2\, T_1^r + \frac{dT_0^r}{dX}\right\}dX = 0 \tag{6.82}$$

$$\int_0^{Y_0'}\left\{\frac{1}{Pe_h}\frac{d^2T_1^l}{dY^2} + \varphi\, b^2\, T_1^l - \frac{dT_0^l}{dY}\right\}dY = 0 \tag{6.83}$$

Integrating (6.81)-(6.83), after substitution of the previous approximate temperature profiles (Eqs.(6.65), (6.76) and (6.78)), yields:

$$b^2 = \frac{\sqrt{\pi}}{2}\exp(\gamma\beta)\frac{erf\sqrt{\gamma\beta}}{\sqrt{\gamma\beta}} \tag{6.84}$$

$$d = \frac{\varphi b\, Pe_h}{\sqrt{2\,Pe_m}}\frac{1+2\left|1-Pe_m/Pe_h\right|}{6\,Pe_m/Pe_h-\varphi} \text{ and} \tag{6.85}$$

$$f = -\frac{\varphi b\, Pe_h}{\sqrt{2\,Pe_m}}\frac{1-2\left|1-Pe_m/Pe_h\right|}{6\,Pe_m/Pe_h-\varphi}. \tag{6.86}$$

6.3.2.g *Complete solutions*

Rewriting equations (6.64)-(6.67) and (6.75)-(6.78) in terms of the original variables, it is possible to describe the concentration and temperature profiles by branches:

$$c(x;\varepsilon) = \begin{cases} c_0^l\left(\dfrac{1+x}{\sqrt{\varepsilon}}\right) + \sqrt{\varepsilon}\, c_1^l\left(\dfrac{1+x}{\sqrt{\varepsilon}}\right) + O(\varepsilon), & -1 \le x \le x' \\ -1, & x' \le x \le x^* \\ c_0^r\left(\dfrac{1-x}{\sqrt{\varepsilon}}\right) + \sqrt{\varepsilon}\, c_1^r\left(\dfrac{1-x}{\sqrt{\varepsilon}}\right) + O(\varepsilon), & x^* \le x \le 1 \end{cases} \tag{6.87}$$

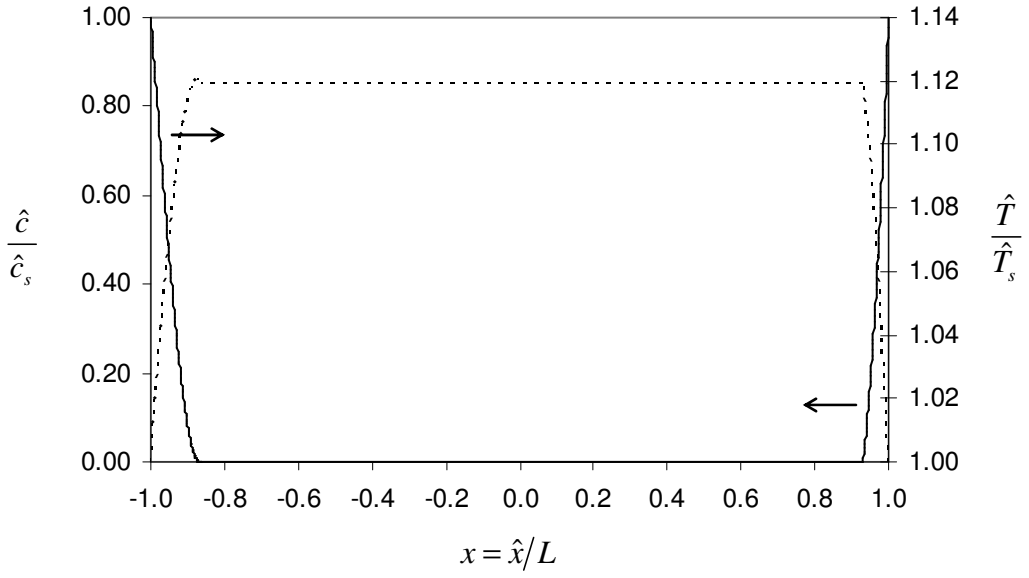

Figure 6.6: Concentration profile (solid line) and temperature profile (dashed line) at diffusional regime for $\phi^2 = 100$, $\gamma = 20$, $\beta = 0.1$, $Pe_m = 10$ and $Pe_h = 5$ ($\varepsilon = 0.1$).

$$T(x;\varepsilon)=\begin{cases} T_0^l\left(\dfrac{1+x}{\sqrt{\varepsilon}}\right)+\sqrt{\varepsilon}\,T_1^l\left(\dfrac{1+x}{\sqrt{\varepsilon}}\right)+O(\varepsilon), & -1\le x\le x' \\ T^{\max}(\varepsilon), & x'\le x\le x^*. \\ T_0^r\left(\dfrac{1-x}{\sqrt{\varepsilon}}\right)+\sqrt{\varepsilon}\,T_1^r\left(\dfrac{1-x}{\sqrt{\varepsilon}}\right)+O(\varepsilon), & x^*\le x\le 1 \end{cases} \tag{6.88}$$

The concentration annulment positions are calculated from (6.69)-(6.70) and (6.79)-(6.80):

$$x^*=1-\sqrt{\varepsilon}\,X^*=1-\sqrt{\varepsilon}\left(X_0{}^*+\sqrt{\varepsilon}\,X_1{}^*\right)+O\left(\varepsilon^{3/2}\right) \text{ and} \tag{6.89}$$

$$x'=-1+\sqrt{\varepsilon}\,Y'=-1+\sqrt{\varepsilon}\left(Y_0{}'+\sqrt{\varepsilon}\,Y_1{}'\right)+O\left(\varepsilon^{3/2}\right) \tag{6.90}$$

Solutions (6.87)-(6.88) are presented in Figure 6.6.

The leading-order problem in the boundary layers (e.g., Eqs.(6.60)-(6.61) for the right boundary layer) assumes a reaction-diffusion dominant balance, so the solution given by (6.64)-(6.70) and (6.84) can be directly compared with the exact analytical solutions at high Thiele modulus for the problem of exothermic zero-order reaction in a catalyst slab where mass/heat transfer occurs solely by diffusion/conduction. In particular, we compare concentration and temperature profiles (or simply temperature profiles, since for this order, they are both related by Eq. (6.62)) and concentration annulment points.

For slab geometry, when $\gamma\beta\phi^2>0.878$ (at high Thiele modulus), there is only one steady state solution for the diffusive-reactive problem (Frank-Kamenetskii 1955; Marek et al. 1968; Aris 1975) with

$$x^*=(-x')=1-\frac{\sqrt{2}}{\phi}\frac{\operatorname{sech}^{-1}e^{-\gamma\beta/2}}{\sqrt{\gamma\beta e^{\gamma\beta}}} \tag{6.91}$$

This result agrees with our perturbation solutions (6.69)-(6.70) if $b\sim\sqrt{\gamma\beta e^{\gamma\beta}}\Big/\operatorname{sech}^{-1}\left(e^{-\gamma\beta/2}\right)$, with b from (6.84). This comparison is plotted in Figure 6.7 for several values of $\gamma\beta$.

At high Thiele modulus, the temperature and concentration variation is concentrated in thin boundary layers, so the parabolic approximation (6.64)-(6.67) is a reasonable one, which proves to be in excellent agreement with exact analytical results (Aris 1975), as shown in Figure 6.8. The leading-order temperature profile in the middle region (Eq.(6.68)) is Prater's maximum temperature estimate for reaction-diffusion problems.

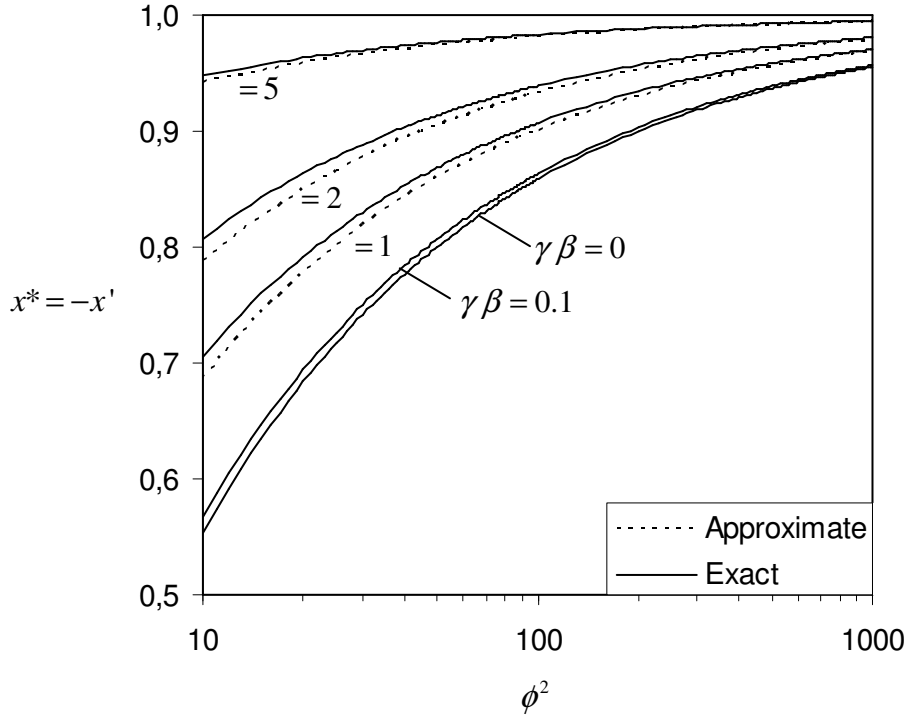

Figure 6.7: Concentration annulment positions in the diffusive limit for an exothermic zero-order reaction. Comparison between the exact analytical solution (Aris 1975) and perturbation solutions in the limit of negligible convection (Eqs.(6.69)-(6.70) with (6.84)). For $\gamma\beta \le 0.1$, exact and approximate results coincide.

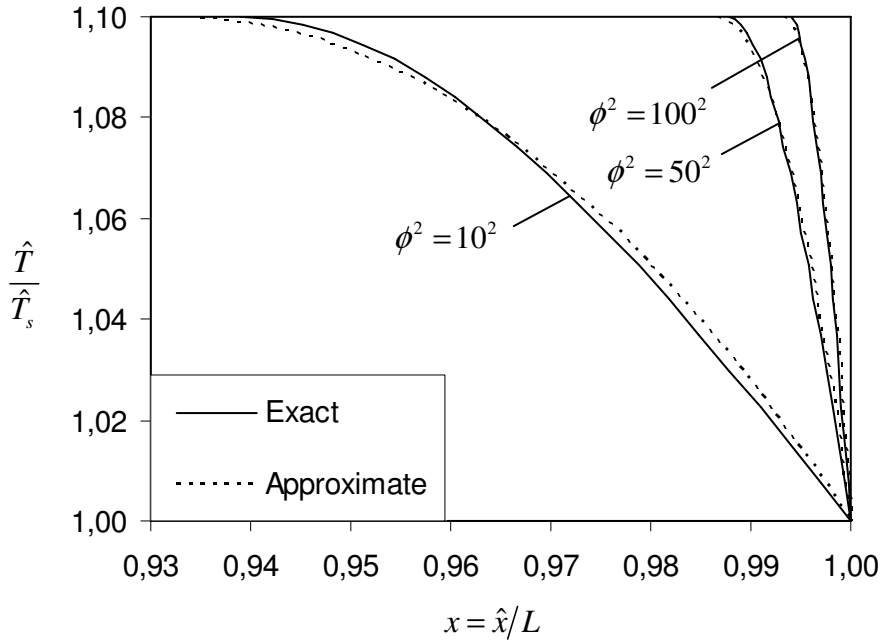

Figure 6.8: Temperature profiles in the right boundary layer (next to $x = 1$) in the diffusional regime for $\gamma = 20$, $\beta = 0.1$, $Pe_m = 10$ and $Pe_h = 5$ and $\phi = 10, 50, 100$. The leading-order perturbation solutions (dashed lines) are compared with the exact analytical results (solid lines) by e.g. Aris (1975).

In the isothermal limit ($\varphi \to 0$, $b^2 \to 1$ and $d, f \to 0$), equations (6.89)-(6.90) yield

$$x^* \to 1 - \sqrt{\frac{2}{Pe_m}}\sqrt{\varepsilon} + \frac{1}{3}\varepsilon + O\left(\varepsilon^{3/2}\right) \tag{6.92}$$

$$x' \to -1 + \sqrt{\frac{2}{Pe_m}}\sqrt{\varepsilon} + \frac{1}{3}\varepsilon + O\left(\varepsilon^{3/2}\right) \tag{6.93}$$

In the analysis of convection and diffusion with zero-order isothermal reaction, Rodrigues et al. (1984) calculate x^* and x' by solving numerically two nonlinear algebraic equations. We can find an approximate solution for those equations by perturbation techniques, for $\varepsilon = Pe_m / \phi^2 << 1$. The result of that calculation reproduces equations (6.92)-(6.93).

6.3.3 Regime III (Strong intraparticular convection regime)

A third regime, where intraparticular convection dominates mass and heat transport, can be studied for parameters obeying the following conditions:

$$\frac{\phi^2}{Pe_m} \sim 1 \text{ and } \frac{1}{Pe_h}, \frac{1}{Pe_m} << 1 \tag{6.94}$$

Therefore, $\varepsilon = 1/Pe_m$ is taken as the perturbation parameter (also $1/Pe_h \sim \varepsilon$). Since the reaction term in equation (6.10) is defined by two branches, the situation with concentration annulment (section 6.3.3.b) needs to be treated separately from the one where no reactant exhaustion occurs (section 6.3.3.a).

6.3.3.a *No annulment of reactant concentration inside the particle (Regime IIIa)*

Since reactant exhaustion never occurs within the slab (Figure 6.4), the mass and energy equations with their original scaling (x, $c(x)$ and $T(x)$ are assumed to be of $O(1)$) are:

$$\frac{dc^l}{dx} = \varepsilon \frac{d^2 c^l}{dx^2} - \frac{\phi^2}{Pe_m} \exp\left[\frac{\varphi T^l}{1 + \eta T^l}\right] \tag{6.95}$$

$$\frac{dT^l}{dx} = \varepsilon \frac{Pe_m}{Pe_h} \frac{d^2 T^l}{dx^2} + \frac{\phi^2}{Pe_m} \exp\left[\frac{\varphi T^l}{1 + \eta T^l}\right] \tag{6.96}$$

When $c^l(x)$ and $T^l(x)$ in equations (6.95) and (6.96) are expanded as a series in terms of powers of the small parameter, the leading-order problem (obtained setting $\varepsilon = 0$) is reduced to a first order ODE, which is in general, not able to fulfil both boundary conditions. In the thin

region next to the abandoned condition, a boundary layer will appear, bringing the concentration and temperature outer profiles to surface values. The only consistent option for matching between such two solutions is to drop the condition next to $x=1$. Equations (6.95)-(6.96) should then be solved with:

$$c_0^{\,l}\left(x=-1\right)=0 \text{ and} \tag{6.97}$$

$$T_0^{\,l}\left(x=-1\right)=0 \tag{6.98}$$

For $\eta T_0^{\,l} << 1$, the solution for the left/middle region of the slab is

$$T_0^{\,l}=-\frac{1}{\varphi}\ln\left[1-\frac{\varphi\phi^2}{Pe_m}\left(x+1\right)\right] \tag{6.99}$$

$$c_0^{\,l}=-T_0^{\,l}=\frac{1}{\varphi}\ln\left[1-\frac{\varphi\phi^2}{Pe_m}\left(x+1\right)\right]. \tag{6.100}$$

Because solutions (6.99)-(6.100) have a vertical asymptote, the existence of a bounded solution requires that $\frac{\varphi\phi^2}{Pe_m}\left(x+1\right)<1$.

Boundary layer next to $x=1$

To investigate the nature of the inner region near the slab's right surface, we introduce the following stretching transformation: $Y=\left(1-x\right)/\delta$. Comparing the substituted terms in equations (6.95) and (6.96), the distinguished limit (that doesn't reproduce the outer expansion) is a convective-diffusive balance in a thin layer of thickness $\delta\sim\varepsilon$. We will therefore calculate concentration and temperature profiles based on expansions of the form:

$$c\left(x\right)=\sum_{n=0}^{\infty}c_n\left(x\right)\varepsilon^n \text{ and} \tag{6.101}$$

$$T\left(x\right)=\sum_{n=0}^{\infty}T_n\left(x\right)\varepsilon^n\,. \tag{6.102}$$

The inner problem can be written as:

$$-\frac{dc^r}{dY}=\frac{d^2c^r}{dY^2}-\varepsilon\frac{\phi^2}{Pe_m}\exp\left[\frac{\varphi T^r}{1+\eta T^r}\right] \tag{6.103}$$

$$-\frac{dT^r}{dY}=\frac{Pe_m}{Pe_h}\frac{d^2T^r}{dY^2}+\varepsilon\frac{\phi^2}{Pe_m}\exp\left[\frac{\varphi T^r}{1+\eta T^r}\right] \tag{6.104}$$

with boundary conditions:

$$c^r\left(Y=0\right)=0 \text{ and } T^r\left(Y=0\right)=0 \qquad (6.105)\text{- } (6.106)$$

Substituting expansions (6.101)-(6.102) into the problem defined by (6.103)-(6.106) and collecting $O(1)$ terms, the leading-order solution is:

$$c_0{}^r\left(Y\right)=a_1\left[1-\exp\left(-Y\right)\right] \qquad (6.107)$$

$$T_0{}^r\left(Y\right)=a_2\left[1-\exp\left(-\frac{Pe_h}{Pe_m}Y\right)\right]. \qquad (6.108)$$

Integration constants a_1 and a_2 will be determined by matching with the outer solution (6.99)-(6.100). With $O(1)$ terms, the matching principle is simply (Bender et al. 1999):

$$\lim_{Y\to\infty} c_0^r=\lim_{x\to 1} c_0^l \qquad (6.109)$$

$$\lim_{X\to\infty} T_0^r=\lim_{x\to 1} T_0^l. \qquad (6.110)$$

Taking the limits of equations (6.99), (6.100), (6.107) and (6.108):

$$a_1=-a_2=\frac{1}{\varphi}\ln\left[1-\frac{2\varphi\phi^2}{Pe_m}\right] \qquad (6.111)$$

Matching between the two solutions is possible only if:

$$\frac{2\varphi\phi^2}{Pe_m}<1. \qquad (6.112)$$

If condition (6.112) is not met then a solution valid for the whole slab cannot be obtained. This suggests that, for typical parameter values, these solutions are only suitable for low Thiele modulus range. They will be useful for describing a regime near the 'chemical regime', but with strong convection. An additional term was calculated at $O(\varepsilon)$, but it was found to have negligible contribution to the complete solution.

Composite solution

The final composite solution, valid across the whole catalyst, is given by

$$c_0^{comp}\left(x\right)=c_0^l\left(x\right)+c_0^r\left(Pe_m\left(1-x\right)\right)-\lim_{Y\to\infty} c_0^r\left(Y\right) \qquad (6.113)$$

$$T_0^{comp}\left(x\right)=T_0^l\left(x\right)+T_0^r\left(Pe_m\left(1-x\right)\right)-\lim_{Y\to\infty} T_0^r\left(Y\right) \qquad (6.114)$$

Substituting (6.99)-(6.100) and (6.107)-(6.108) into (6.113)-(6.114):

$$c(x)=\frac{1}{\varphi}\ln\left[1-\frac{\varphi\phi^2}{Pe_m}\left(x+1\right)\right]-\frac{1}{\varphi}\ln\left[1-\frac{2\varphi\phi^2}{Pe_m}\right]e^{-Pe_m(1-x)}+O\left(\frac{1}{Pe_m}\right) \qquad (6.115)$$

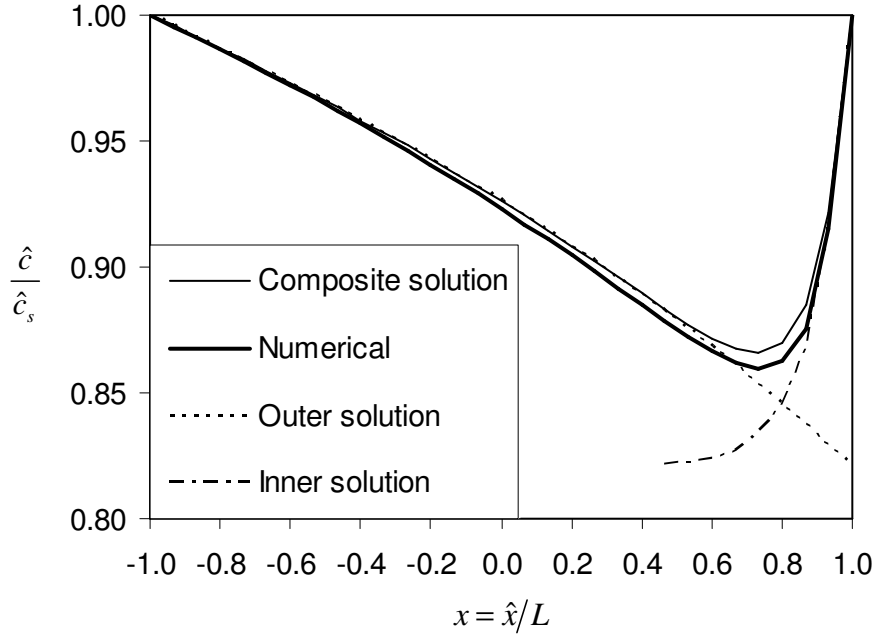

(a) Reactant concentration profile.

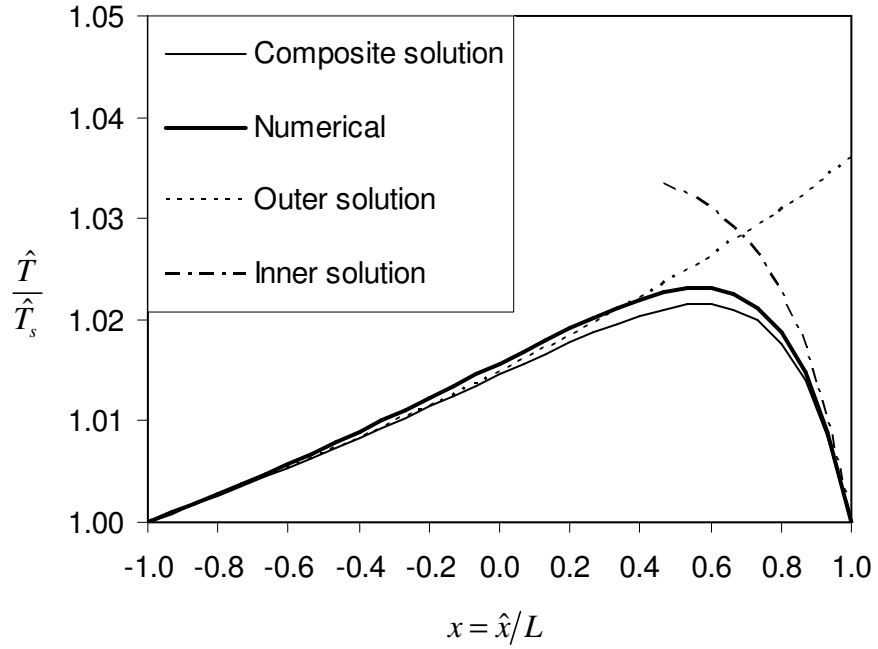

(b) Temperature profile.

Figure 6.9: Comparison between composite solutions (6.115)-(6.116), numerical results and contributions from outer and inner regions for $\varphi = 4$, $\phi^2 = 0.8^2$, $Pe_m = 10$ and $Pe_h = 5$.

$$T(x) = -\frac{1}{\varphi}\ln\left[1-\frac{\varphi\phi^2}{Pe_m}(x+1)\right]+\frac{1}{\varphi}\ln\left[1-\frac{2\varphi\phi^2}{Pe_m}\right]e^{-Pe_h(1-x)}+O\left(\frac{1}{Pe_m}\right). \quad (6.116)$$

Figure 6.9 provides a comparison of the analytical results (Eqs. (6.115)-(6.116)) with numerical solutions from gPROMS®. The outer and inner branches of the solution (equations (6.99)-(6.100) and (6.107)-(6.108), respectively) are also represented.

In this regime, we the expect minimum concentration to be close to surface concentration. We calculate it from $dc/dx\big|_{x_{\min}} = 0$, which yields

$$c^{\min} = \frac{1}{\varphi}\ln\left[1-\frac{\varphi\phi^2}{Pe_m}(x_{\min}+1)\right]-\frac{1}{\varphi}\ln\left[1-\frac{2\varphi\phi^2}{Pe_m}\right]e^{-Pe_m(1-x_{\min})} \text{ with} \quad (6.117)$$

$$x_{\min} = 1-\frac{1}{Pe_m}\ln\left\{\left(2-\frac{Pe_m}{\varphi\phi^2}\right)Pe_m\ln\left[1-\frac{2\varphi\phi^2}{Pe_m}\right]\right\}. \quad (6.118)$$

The maximum temperature will be calculated in section 6.4. In the isothermal limit ($\varphi \to 0$), equations (6.117)-(6.118) become:

$$x_{\min} \to 1-\frac{\ln(2Pe_m)}{Pe_m} \text{ and} \quad (6.119)$$

$$c^{\min} \to -\frac{\phi^2}{Pe_m}\left(2-\frac{\ln(2Pe_m)}{Pe_m}-\frac{1}{Pe_m}\right). \quad (6.120)$$

These results are in very good agreement with (6.28)-(6.27) (which reproduce exact analytical solutions for isothermal conditions (Rodrigues et al. 1984)).

6.3.3.b *Concentration annulment inside the particle (Regime IIIb)*

Another important situation is the one in which the reactant concentration is depleted in a region inside the particle (Figure 6.4). The outer solution for the left region (calculated in section 6.3.3.a) takes the zero concentration value at $\tilde{x} = -1 + Pe_m\left(1-e^{-\varphi}\right)/\left(\varphi\phi^2\right)$. For $x > \tilde{x}$, the solution should approach $c^m(x) = -1$ and the chemistry-free equations for temperature must be used. Finally, the diffusive-convective boundary layer (predicted from independent variable stretching in section 6.3.3.a) allows the right boundary condition to be fulfilled. This structure can only exist if $\tilde{x} < 1$ or

$$\frac{\phi^2}{Pe_m} > \frac{1-e^{-\varphi}}{2\varphi} \quad (6.121)$$

Concentration and temperature profiles will be approximated by expansions like (6.101) - (6.102) .

Solution structure

Since we are assuming the existence of a 'dead core', the concentration profile in the middle region is: $c_0^{\,m}(x) = -1$ and $c_n^{\,m}(x) = 0$, for subproblem n $(n \geq 1)$. The energy balance is written without the reactive term $(r(T) = 0)$ as

$$\frac{dT^m}{dx} = \varepsilon \frac{Pe_m}{Pe_h} \frac{d^2T^m}{dx^2} \tag{6.122}$$

with $\varepsilon = 1/Pe_m$ and $Le = Pe_m / Pe_h \sim O(1)$.

Introducing the expansion for temperature profile in terms of powers of ε and collecting the resulting subproblems, we get:

$$\text{At } O(1): \qquad \frac{dT_0^{\,m}}{dx} = 0$$

$$\text{At } O(\varepsilon^n): \qquad \frac{dT_n^{\,m}}{dx} = \frac{Pe_m}{Pe_h} \frac{d^2T_{n-1}^m}{dx^2} \qquad \text{for } n \geq 1. \tag{6.123}$$

Temperature will be uniform in the middle and this solution is valid for x from $\tilde{x}$ up to the boundary layer. Since the outer solution predicts $c_0^{\,l} = -T_0^{\,l}$, profile continuity between the two branches of the solution will require $T_0^{\,m} = 1$.

We will keep the solution for the left region given by equations (6.99)-(6.100) and the boundary layer at $x = 1$. However, the values of the integration constants in equations (6.107)-(6.108) are now: $a_1 = -a_2 = -1$ (from matching with the middle region). A smooth composite solution uniformly valid requires a more complex mathematical structure. Nevertheless, these three independent branches should be good estimates for the profiles in each region. We shall use these results to estimate the effectiveness factor in this regime (section 6.5).

In the isothermal limit of this strong convective regime, asymptotic expressions for the concentration annulment points are available (Rodrigues et al. 1984): $x' = -1 + Pe_m / \phi^2$ (left side) and $x^* = 1 - \ln\left(Pe_m{}^2 / \phi^2\right) / Pe_m$ (right side). The first result is in agreement with the isothermal limit of $\tilde{x}$ (for $\varphi \to 0$). A perturbation analysis of the exact nonlinear equation from which x^* is calculated, suggests rescaling of $(1 - x^*)$ by $\varepsilon = 1/Pe_m$, and is therefore consistent with the thickness of the boundary layer predicted in section 6.3.3.a.

6.3.3.c *Transition between Regimes II and IIIb*

Comparing the solution structure described above (for Regime IIIb) with the one built for diffusional regime (Regime II), it is possible to obtain simple order of magnitude relations concerning the transition between these two particular limits. Although both situations refer to high Thiele modulus, solutions (6.87)-(6.88) were found for $Pe_m, Pe_h \sim 1$, while the results obtained for Regime IIIb only have meaning when convection is high. Nevertheless, when the thicknesses of the regions near $x = -1$ become comparable ($x' \sim \tilde{x}$):

$$Pe_m \sim \sqrt{2}\,\phi \,\frac{\varphi}{b\left(1-e^{-\varphi}\right)} \tag{6.124}$$

with b given by (6.84).

In the isothermal limit, equation (6.124) yields $Pe_m \sim \sqrt{2}\,\phi$. This means that, at high Thiele modulus, the effect of convection is felt only for $Pe_m > \phi$. The corrective factor in equation (6.124) applies when an exothermic reaction is occurring, and increases the mass Peclet number needed for the effect of convection to be observed, when $Le > b/(\gamma\beta)$.

At the right surface, we require that the position x^* at diffusional regime to be of the same order of the diffusive-convective boundary layer thickness, when convection is strong $(1/Pe_m)$. This implies, $Pe_m \sim b\phi/\sqrt{2}$, or $Pe_m \sim \phi/\sqrt{2}$ (isothermal reaction). A transition region around these curves can be represented for the isothermal case (see Figure 6.1) and for the exothermic case (Figure 6.11).

6.4 MAXIMUM TEMPERATURE ESTIMATE

When mass/heat transfer occurs solely by diffusion/conduction, it is possible to establish a simple relationship between concentration and temperature profiles, from where an *a priori* estimate for the maximum temperature can be obtained (Damkohler 1943; Prater 1958). Such result provides a useful measure for internal nonisothermal effects, as well as an indication on whether the temperature exceeds some critical value for operation or not.

For the regimes outlined above, it is possible to obtain estimates for the maximum temperature attained in the particle, when convection is also present (see Table 6.1). At low Thiele modulus (Regimes I and IIIa), the temperature inside the particle is close to the surface value (equations (6.128) and (6.132)). For materials with high conductivity or when no convection exists ($Pe_h \to 0$), $\hat{T}^{\max} \to \hat{T}_s$. It can be shown that according to (6.128): $\hat{T}^{\max}/\hat{T}_s \to 1 + \beta\phi^2/2$ (for

$\phi^2 << 1$). On the other hand, for poorly conductive catalysts ($Pe_h \to \infty$), $\hat{T}^{\max}/\hat{T}_s \to 1 + 2\beta\phi^2/Pe_h$.

Under 'diffusional regime' conditions, the correction brought by convection to the diffusive leading-order result $\left(\hat{T}^{\max} = \hat{T}_s(1+\beta)\right)$ is of order $\sqrt{\varepsilon} = \sqrt{Pe_m}/\phi$. For $Le = 1$, the maximum temperature change (Eq.(6.130)) reduces to the characteristic diffusive value, which equals the adiabatic temperature rise.

In Regime IIIb, where convection is strong and the solution includes a region where annulment occurs, the maximum temperature is obtained at the same position where concentration reaches annulment (no increase is expected in the middle solution, which is a plateau, or in the boundary layer). It may be shown (Eq.(6.135)) that the maximum temperature change is equal to the adiabatic temperature rise after complete reaction in a catalyst slab with initial uniform surface-like reactant concentration $\left(T^{\max} \sim -c^{\min} \sim 1\right)$: $\hat{T}^{\max}/\hat{T}_s \sim 1 + \beta\, Pe_m/Pe_h$. This result confirms the scaling analysis in section 6.2.2. and was also obtained in the perturbation analysis for first-order reactions in the convective regime (Cardoso et al. 2007). The leading-order estimates for maximum temperature, in each regime, are indicated in Figure 6.11.

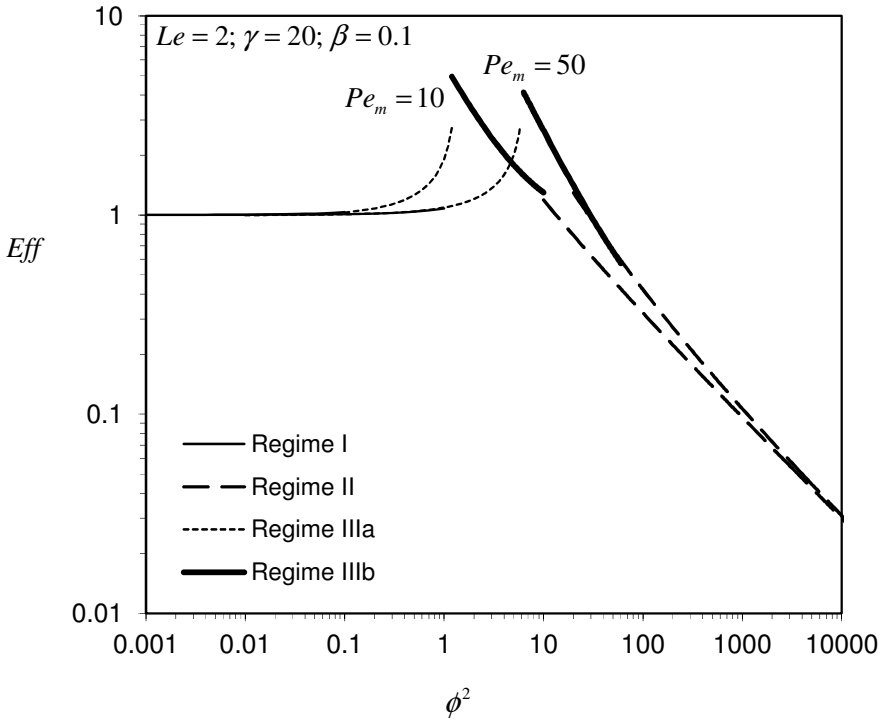

Figure 6.10: Effectiveness factor plot in the four regimes studied (Eqs. (6.127), (6.129), (6.131) and (6.134)).

6.5 EFFECTIVENESS FACTOR APPROXIMATION

The performance of the catalyst particle in the regimes described may be quantified by the effectiveness factor, defined by (6.15)-(6.16). In general, the calculation is rather straightforward, especially in the regimes with uniformly valid solutions. So, differentiation of equations (6.24), (6.87) and (6.115) yields direct estimates for the effectiveness factor in Regimes I, II and IIIa, as shown in Table 6.1.

In the 'chemical regime', the effectiveness factor is close to unity. Taking the limit of (6.127), when $Pe_h \to 0$ (when there is no convection or when the catalyst is highly conductive), gives

$$Eff \to 1 + \gamma\beta\phi^2/3$$

This result is also obtained by perturbation analysis for a zero-order reaction, with no convection, in the low Thiele modulus regime. For strong convection ($Pe_h \to \infty$) or under isothermal conditions ($\beta \to 0$), the leading-order estimate is again $Eff \to 1$. The results for Regime IIIa (Eq.(6.131)), where convection is strong, agree qualitatively with this result.

In the 'diffusional regime', the leading-order estimate for the effectiveness factor (from Eq.(6.129)) is

$$Eff = \frac{\sqrt{2}\,b}{\phi} \tag{6.125}$$

We expect this result to agree with the effectiveness factor calculated for the explosive branch (Aris 1975) of the diffusion-reaction problem. This is the case if $b^2 \sim \left(e^{\gamma\beta} - 1\right)/(\gamma\beta)$ agrees with Eq.(6.84). The agreement is indeed very good, especially for $\gamma\beta < 2$. The second-order term in (6.129) increases catalyst's performance if $\gamma\beta < 6$ (which is true for typical parameter values). In the isothermal diffusive limit, equation (6.129) retrieves the well-known result, $Eff = \sqrt{2}/\phi$.

For Regime IIIb, an approximate result was obtained by considering the solution structure that was described in section 6.3.3.b. If we use a two-term expansion to describe the concentration profile in each region, equation (6.16) yields:

$$Eff \simeq \frac{1}{2\phi^2}\left(\left.\frac{dc_0^r}{dx}\right|_{x=1} + \varepsilon \left.\frac{dc_1^r}{dx}\right|_{x=1} - \left.\frac{dc_0^l}{dx}\right|_{x=-1} - \varepsilon \left.\frac{dc_1^l}{dx}\right|_{x=-1} \right). \tag{6.126}$$

We note that $c_0^l(x)$ is given by (6.100) and $c_0^r(x)$ by (6.107) with $a_1 = -1$. To evaluate the remaining terms in (6.126), we calculate $c_1^l(x)$ from the $O(\varepsilon)$ subproblem that arises from

(6.95)-(6.96) and $dc_1^r/dx\big|_{x=1}$ is obtained integrating the $O(\varepsilon)$ mass balance from (6.103) over the boundary layer with thickness $\varepsilon \sim 1/Pe_m$. That is, for $\eta T_0^r << 1$:

$$\left.\frac{dc_1^r}{dx}\right|_{x=1} = \frac{1}{\varepsilon^2}\frac{\phi^2}{Pe_m}\int_{1-1/Pe_m}^{1} \exp\left[\varphi T_0^r\right]dx \simeq \frac{1}{\varepsilon^2}\frac{\phi^2}{Pe_m}\frac{e^{\varphi}+1}{2}\left(\frac{1}{Pe_m}\right)$$

where the integral on the right-hand side of this equation is evaluated using the trapezoidal rule between the surface and the maximum temperature values. Substituting these results into (6.126), gives an estimate for the effectiveness factor in Regime IIIb (equation (6.134)). If we take the limit of (6.134) for $\varphi \to 0$ ($\beta \to 0$), we obtain

$$Eff \sim \frac{Pe_m}{2\phi^2} + \frac{1}{Pe_m}$$

This solution is in excellent agreement with the asymptotic limit for high Pe_m (maximum error of 5% for $Pe_m \sim \phi^2 \sim 10$) presented by Rodrigues et al. (1984) for the isothermal case. Also, for strong convection the maximum effectiveness factor is given by $Eff \sim Pe_m/\left(2\phi^2\right)$. This result also appeared in the analysis for first-order reaction by Cardoso et al. (2007), although they were able to find the full concentration and temperature profiles in this regime. In these cases and when mass and thermal diffusivities are comparable, the performance of the catalyst depends at $O(1)$ on the Thiele modulus and intraparticular mass Peclet number, but not on any information regarding heat transfer or generation mechanisms (φ or Pe_h). Note that, for strong convective regimes, the contribution of the profile near $x=-1$ for the effectiveness factor is negligible, since reactant concentration decay is slow at the slab's entrance. All these results are summarised in Table 6.1 and plotted in Figure 6.10.

6.6 CONCLUSIONS

The analysis of simultaneous convection, diffusion and reaction is presented for an exothermic zero-order reaction occurring in a catalyst slab. Scaling techniques yield simple order of magnitude estimates for the characteristic temperature change experienced. We identified the regions in which the system behaves as isothermal, diffusive, adiabatic or 'explosive' by a 3-D regime diagram. In particular, we study the limits of chemical and diffusional regimes, in the presence of convection, as well as a strong convective regime, by conducting suitable perturbation analysis. For each regime, estimates of the effectiveness factor and maximum temperature are provided (Figure 6.11). They are consistent with the isothermal and diffusive limits, and agree with previous approximate analytical analysis (Cardoso et al. 2007).

When intraparticular convection is the dominating transport mechanism in a system with $Le \sim 1$, the performance of the catalyst depends (to a first approximation) on the mass Peclet number and Thiele modulus, but not on heat generation or transport. The maximum temperature was found to coincide with the adiabatic temperature change that one would observe after complete reaction, in a catalyst slab with initial uniform surface-like concentration and temperature.

Table 6.1: Effectiveness factor and maximum temperature approximations.

Regime I	$Eff = 1 + \varphi \frac{\phi^2}{Pe_m}\left[\frac{e^{2Pe_h}+1}{e^{2Pe_h}-1} - \frac{1}{Pe_h}\right] + O\left(\frac{\phi^4}{{Pe_m}^3}\right)$	(6.127)
$\frac{\phi^2}{Pe_m} << 1, \frac{1}{Pe_m}, \frac{1}{Pe_h}$	$\frac{\hat{T}^{\max}}{\hat{T}_s} = 1 + \beta \frac{\phi^2}{{Pe_h}^2}\left\{\frac{\ln\left[2e^{2Pe_h}\right]}{e^{2Pe_h}-1} + \ln\left[\frac{e^{2Pe_h}-1}{2Pe_h}\right] - 1\right\} + O\left(\frac{\phi^4}{{Pe_m}^2}\right)$	(6.128)
Regime II	$Eff = \frac{\sqrt{2}\,b}{\phi} + \varphi\frac{Pe_m}{\phi^2}\left\|1 - \frac{Pe_h}{Pe_m}\right\|\left(6\frac{Pe_m}{Pe_h} - \varphi\right)^{-1} + O\left(\frac{Pe_m}{\phi^4}\right)$	(6.129)
$\frac{\phi^2}{Pe_m} >> 1, \frac{1}{Pe_m}, \frac{1}{Pe_h}$	$\frac{\hat{T}^{\max}}{\hat{T}_s} = 1 + \beta\left(1 + \frac{\sqrt{2}Pe_m}{3b\phi}\left\|1 - \frac{Pe_h}{Pe_m}\right\|\right) + O\left(\frac{Pe_m}{\phi^2}\right)$	(6.130)
Regime III $\frac{\phi^2}{Pe_m} \sim 1$ and $\frac{1}{Pe_h}, \frac{1}{Pe_m} << 1$	IIIa: For $\frac{2\varphi\phi^2}{Pe_m} < 1$, $Eff = \frac{Pe_m}{2\varphi\phi^2}\left(e^{-2Pe_m} - 1\right)\ln\left[1 - \frac{2\varphi\phi^2}{Pe_m}\right] - \frac{1}{Pe_m}\left[1 - \frac{2\varphi\phi^2}{Pe_m}\right]^{-1} + O\left(\frac{1}{\phi^2 Pe_m}\right)$	(6.131)
	$\frac{\hat{T}^{\max}}{\hat{T}_s} = 1 - \frac{\beta}{\gamma}\ln\left[1 - \frac{\varphi\phi^2}{Pe_m}\left(x_{\max}+1\right)\right] + \frac{\beta}{\gamma}\ln\left[1 - \frac{2\varphi\phi^2}{Pe_m}\right]e^{-Pe_h\left(1-x_{\max}\right)}$	(6.132)
	with $x_{\max} = 1 - \frac{1}{Pe_h}\ln\left\{\left(2 - \frac{Pe_m}{\varphi\phi^2}\right)Pe_h \ln\left[1 - \frac{2\varphi\phi^2}{Pe_m}\right]\right\}$	(6.133)
	IIIb: For $\frac{\phi^2}{Pe_m} > \frac{1-e^{-\varphi}}{2\varphi}$, $Eff = \frac{Pe_m}{2\phi^2} + \frac{3+e^{\varphi}}{4Pe_m} + \frac{\phi^2}{Pe_m}\frac{\varphi}{2{Pe_m}^2} + O\left(\frac{1}{{Pe_m}^3}\right)$	(6.134)
	$\frac{\hat{T}^{\max}}{\hat{T}_s} \sim 1 + \beta\frac{Pe_m}{Pe_h} + O\left(\frac{\beta}{Pe_m}\right)$	(6.135)

where: $b^2 = \sqrt{\pi}\exp(\gamma\beta)\,erf\sqrt{\gamma\beta}\Big/\left(2\sqrt{\gamma\beta}\right)$ and $\varphi = \gamma\beta\,Pe_m/Pe_h$.

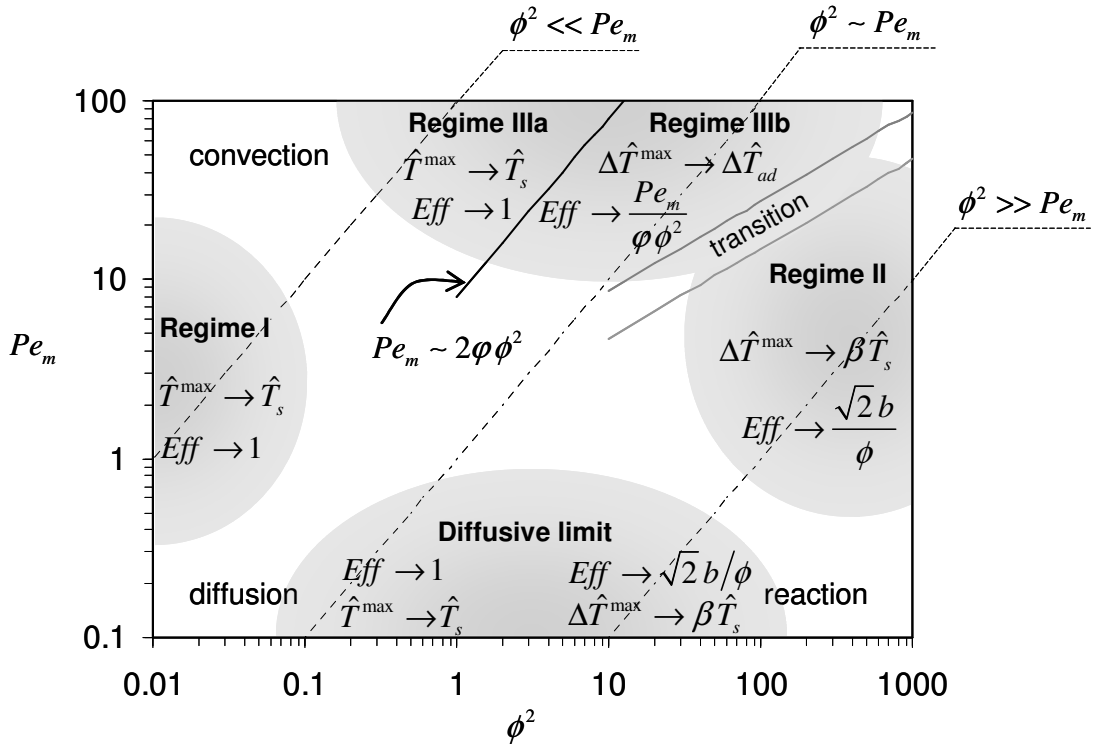

Figure 6.11: Regime diagram for an exothermic zero-order reaction in permeable catalyst slab. Shown are the leading-order estimates for the effectiveness factor and maximum temperature in each of the studied regimes, for $Le \sim 1$. Approximate boundaries between strong convective-reactive regimes are also presented.

NOTATION

a_1, a_2 integration constants

b parameter defined in eq. (6.63)

c dimensionless concentration of reactant

$c_n(x)$ perturbation function of order n for dimensionless concentration

$\hat{c}$ concentration of reactant

$\hat{c}_s$ concentration at the surface of the slab

C_p specific heat of the catalyst matrix filled with fluid

d parameter defined in eq. (6.73)

D effective reactant mass diffusivity

E_{act} reaction activation energy

Eff effectiveness factor

$erf(z)$ 'error function', defined by $erf(z) = \frac{2}{\sqrt{\pi}} \int_0^z e^{-t^2}\, dt$

f parameter defined in eq. (6.74)

$(-\Delta H)$ heat of the exothermic reaction

k intrinsic kinetic constant

k_s kinetic rate constant evaluated at the surface temperature of the catalyst

L semi-thickness of the slab

Le Lewis' number $(=\kappa/D)$

Pe_h intraparticular heat Peclet number $(=u\,L/\kappa)$

Pe_m intraparticular mass Peclet number $(=u\,L/D)$

$r(T)$ dimensionless reaction term

R ideal gas constant

T dimensionless temperature

$T_n(x)$ perturbation function of order n for dimensionless temperature

$\hat{T}$ temperature

$\hat{T}_s$ temperature at the surface of the slab

$\Delta\hat{T}$ characteristic temperature change

$\Delta\hat{T}_{ad}$ adiabatic temperature change

$\Delta\hat{T}_{dif}$ maximum temperature change observed in a diffusive-reactive system with concentration annulment

u superficial fluid velocity

x dimensionless transverse position within the slab

$\hat{x}$ transverse position within the slab

x' position where concentration reaches annulment on the left side of the slab

$x*$ position where concentration reaches annulment on the right side of the slab

$\tilde{x}$ point where outer solution takes zero concentration value

X stretched coordinate in the region near $x=1$

$X*$ stretched annulment position near $x=1$

X_n^* coefficients in the expansion for $X*$

Y stretched coordinate in the region near $x=-1$

Y' stretched annulment position region near $x=-1$

Y_n' coefficients in the expansion for Y'

Greek letters

β Prater's parameter $\left(=(-\Delta H)\,D\,\hat{c}_s/\left(\rho\,C_p\,\kappa\hat{T}_s\right)\right)$

δ thickness of the boundary layer

ε small (perturbation) parameter

ϕ Thiele modulus $\left(=L\sqrt{k_s/(\hat{c}_s\,D)}\right)$

$(\phi^2)_{crit}$ critical Thiele modulus value, above which concentration annulment occurs

γ Arrhenius parameter $\left(=E_{act}/\left(R\hat{T}_s\right)\right)$

η characteristic temperature change normalized by surface temperature $\left(=\Delta\hat{T}/\hat{T}_s\right)$

φ nonisothermal parameter $\left(=\gamma\eta\right)$

κ fluid-filled catalyst effective thermal diffusivity $\left(=\lambda/\rho C_p\right)$

λ effective thermal conductivity of the fluid-filled catalyst

ρ density of the catalyst matrix filled with fluid

Subscripts

max maximum

min minimum

n order of the perturbation function

Superscripts

$comp$ composite

l left

m middle

max maximum

min minimum

r right

REFERENCES

Allen, J. W. and S. N. Bhatia (2003). "Formation of steady-state oxygen gradients in vitro: Application to liver zonation." Biotechnology and Bioengineering **82**(3): 253-262.

Aris, R. (1975). The mathematical theory of diffusion and reaction in permeable catalysts. London, Oxford University Press.

Bender, C. M. and S. A. Orszag (1999). Advanced Mathematical Methods for Scientists and Engineers. New York, Springer-Verlag.

Cardoso, S. S. S. and A. E. Rodrigues (2006). "Diffusion and reaction in a porous catalyst slab: Perturbation solutions." AIChE Journal **52**(11): 3924-3932.

Cardoso, S. S. S. and A. E. Rodrigues (2007). "Convection, diffusion and reaction in a nonisothermal, porous catalyst slab." AIChE Journal **53**(5): 1325-1336.

Chung, C. A., C. W. Chen, C. P. Chen and C. S. Tseng (2007). "Enhancement of cell growth in tissue-engineering constructs under direct perfusion: Modeling and simulation." Biotechnology and Bioengineering **97**(6): 1603-1616.

Coletti, F., S. Macchietto and N. Elvassore (2006). "Mathematical modeling of three-dimensional cell cultures in perfusion bioreactors." Industrial and Engineering Chemistry Research **45**(24): 8158-8169.

Damkohler, G. (1943). "The excess temperature in contact grains." Zeitschrift Fur Physikalische Chemie-Leipzig **193**(1/3): 16-28.

Fassnacht, D. and R. Pörtner (1999). "Experimental and theoretical considerations on oxygen supply for animal cell growth in fixed-bed reactors." Journal of Biotechnology **72**(3): 169-184.

Frank-Kamenetskii, D. A. (1955). Diffusion and Heat Exchange in Chemical Kinetics. Princeton, Princeton University Press.

Goldstein, A. S., T. M. Juarez, C. D. Helmke, M. C. Gustin and A. G. Mikos (2001). "Effect of convection on osteoblastic cell growth and function in biodegradable polymer foam scaffolds." Biomaterials **22**(11): 1279-1288.

Hlavacek, V. and M. Marek (1967). "Modelling of Chemical Reactors .V. Heat and Mass Transfer within a Porous Catalyst Particle - Some Results of an Analysis for a Zeroth-Order Reaction." Collection of Czechoslovak Chemical Communications **32**(11): 4004-4017.

Lin, C. C. and L. A. Segel (1988). Mathematics Applied to Deterministic Problems in the Natural Sciences, SIAM.

Lopes, J. C. B., M. M. Dias, V. G. Mata and A. E. Rodrigues (1995). "Flow field and non-isothermal effects on diffusion, convection, and reaction in permeable catalysts." Industrial and Engineering Chemistry Research **34**(1): 148-157.

Marek, M. and V. Hlavacek (1968). "Modelling of Chemical Reactors .VI. Heat and Mass Transfer in a Porous Catalyst Particle; On the multiplicity of solutions for the case of an exothermic zeroth-order reaction." Collection of Czechoslovak Chemical Communications **33**(2): 506-517.

Martin, Y. and P. Vermette (2005). "Bioreactors for tissue mass culture: Design, characterization, and recent advances." Biomaterials **26**(35): 7481-7503.

Nir, A. and L. M. Pismen (1977). "Simultaneous intraparticle forced convection, diffusion and reaction in a porous catalyst." Chemical Engineering Science **32**(1): 35-41.

Prater, C. D. (1958). "The temperature produced by heat of reaction in the interior of porous particles." Chemical engineering Science **8**(3-4): 284-286.

Prince, C. L., V. Bringi and M. L. Shuler (1991). "Convective Mass Transfer in Large Porous Biocatalysts: Plant Organ Cultures." Biotechnology Progress **7**(2): 195-199.

Process Systems Enterprise (2007). gPROMS. London.

Quinta Ferreira, R. M. (1988). Contribuição para o Estudo de Reactores Catalíticos de leito fixo. Efeito da convecção em catalisadores de poros largos e casos de catalisadores bidispersos. University of Porto. PhD Thesis.

Rodrigues, A., B. Ahn and A. Zoulalian (1982). "Intraparticle Forced Convection Effect in Catalyst Diffusivity Measurements and Reactor Design." AIChE Journal **28**: 541-546.

Rodrigues, A. E. (1981). Scientific bases for the design of two-phase catalytic reactors. Multiphase Chemical Reactors - Design Methods. A. E. Rodrigues, J. M. Calo and N. H. Sweed. Rockville, M.D., NATO ASI Series E-52. **2:** 65-133.

Rodrigues, A. E., J. M. Orfao and A. Zoulalian (1984). "Intraparticle convection, diffusion and zero order reaction in porous catalysts." Chemical Engineering Communications **27**(5-6): 327-337.

Schlichting, H. (1979). Boundary-Layer Theory. New York, McGraw-Hill.

Stephanopoulos, G. and K. Tsiveriotis (1989). "Effect of intraparticle convection on nutrient transport in porous biological pellets." Chemical Engineering Science **44**(9): 2031-2039.

Wheeler, A. (1951). "Reaction Rates and Selectivity in Catalyst Pores " Advances in Catalysis **3**: 249-327.

Young, M. W. and R. C. Dean (1987). "Optimization of Mammalian-Cell Bioreactors." Bio-Technology **5**(8): 835-837.

CHAPTER

SEVEN

CONCLUSIONS AND PERSPECTIVES OF FUTURE WORK

This thesis proposes an analysis for some chemical engineering problems involving convection, diffusion and reaction. These phenomena occur at several scales: from a pore in a perfusive catalyst particle to a wall-coated channel in a microstructured reactor. Our approach was mainly based on approximate analytical methods, whose results were compared to the ones obtained from numerical simulation. Since neither numerical nor experimental work were considered in detail, it seems adequate that suggestions for future research should refer exclusively to developments accomplished by means of analytical techniques alone or in combination with others. In this chapter, we divide our contribution into eight topics, summarize main achievements and propose possible extensions in each.

7.1 FINITE REACTION RATES IN A WALL-COATED MICROCHANNEL REACTOR

Assuming that a reaction proceeds sufficiently fast in a coated microchannel, so that concentration annulment prevails at most part of its surface, may not be reasonable in many practical situations. This has been highlighted throughout the thesis. In Chapter 4, we have stressed that several studies in the literature reported to have incorrectly assumed operation under full mass transport control. We also derived boundaries for this regime, which placed the conditions for wall concentration annulment in a region corresponding to high values of the Damköhler number (Da). In fact for this to happen, highly active catalysts would be required, or alternatively high operating temperatures, as shown in Chapter 5 (which can lead to a change in the reaction mechanism or activation of homogeneous reactions). In analytical applications, this may require immobilization of a large quantity of ligand to guarantee that binding rates are sufficiently fast. In Chapter 1, we have mentioned a heuristic design rule: the microdevice

should be dimensioned so that transport rates 'match' reaction kinetics, or so that the former are not limiting (i.e. even faster than the latter). Therefore, in applications with miniaturized systems (with the purpose of reducing mass transfer resistance), the case of finite reaction rates compared to transport (i.e. finite Da) is relevant and is also the generic solution of the linear transport-reaction problem. Even when operation close to the asymptotes occurs, expressions for slow and fast reaction rates with $O(Da)$ and $O(1/Da)$ corrections improve the estimation of conversion significantly.

In Chapter 2, we have proposed simplified models for conversion calculation under finite values of Da in the two main mass transfer regimes. In the fully developed regime, conversion of reactant depends on Da through two quantities (the first eigenvalue λ_1 and the first weight w_1). We have proposed correlations to describe the variation of both quantities with Da. Our expressions were constructed from the correct asymptotic limits and shown to be reasonably accurate. They were also simple enough to be included in other quantities (namely conversion) and allowed for the effect of Da to be exhibited explicitly in appropriate limits. Moreover, the parameters in these correlations are dependent on the flow profile and geometry, and can be easily generalized for other channel cross-sectional shapes. This allows a direct comparison between different cases. When the concentration profile is developing, empirical formulas were also used to describe conversion according to Lévêque's analysis (which assumes a concentration boundary layer near the wall, in a planar channel with linear velocity profile) for all values of Da. These were shown to be accurate even for $Da \sim 1$, and valid for $\alpha\, Pe_m > (\sim 10)$.

The description of conversion with these results was compared with the numerical solution of the full problem and the following remarks can be made:

1. The accuracy of the fully developed regime decreases as expected with the magnitude of Graetz parameter (especially for $\alpha\, Pe_m / z > \sim 10$), but mainly for high values of Da;
2. Curvature decreases the range of validity of the fully developed profile at high $\alpha\, Pe_m / z$, especially for large Da, identifying the need for an higher order correction;
3. The empirical correlations describing the leading-order Lévêque solution have comparable or even better agreement with the numerical solution than the individual limits at high and low Da, from which they were constructed;
4. An higher order perturbation correction to the developing profile solution due to curvature in a channel with plug-flow is more important at high Da and can be written as a sum of two parcels of order $O(z/\alpha\, Pe_m)$ and $O\left(\sqrt{z/(Da\,\alpha\, Pe_m)}\right)$, where the latter (subdominant) accounts for finite (large) reaction rates. In the opposite limit (low values of Da), the correction is $O\left[(Da\, z/\alpha\, Pe_m)^2\right]$, which is very small at the inlet;

5. Nonlinearity of velocity profile near the wall in laminar flow has to be considered also at high Da and terms with order $O\left(z/\alpha\, Pe_m\right)$ and $O\left[z^{2/3} \Big/ \left(Da \left(\alpha\, Pe_m \right)^{2/3} \right) \right]$ should be added to the leading-order problem. At low Da, the correction is only of $O\left[Da^2 \left(z/\alpha\, Pe_m \right)^{5/3} \right]$;
6. Correction due to curvature in developing profile is more important than the one due to nonlinearities in the velocity profile, and both are more relevant for $Da >> 1$.

Additionally, it was exemplified how a channel can be dimensioned so that the required conversion is attained and how the results presented in Chapter 2 can avoid simulations in large parametric areas, or restrict the search for adequate design to particular configuration/operation sets. In comparison with the numerical solution, this also allowed the decoupling of effects such as geometry and flow profile.

7.1.1 Suggestions for future work

Extension of the work presented is possible for similar models to the one adopted, but encompassing other effects which may be important at the microscale. We refer specifically to viscous dissipation and simultaneous development of the velocity profile (Herwig 2008). In fact recently, Gundlapally et al. (2011) have used very similar techniques to the ones presented in Chapter 2 to predict the variation of Sherwood number with Graetz and Schmidt's numbers. They however considered uniform wall concentration and flux boundary conditions. It is possible that the effect of a reaction occurring at the wall may be superposed on these dependences and yield a more generic solution. In the case where flow is allowed to develop over the same distance of the concentration profile it would be interesting to evaluate how conversion is affected with Schmidt's number, namely if it changes from the plug-flow asymptote to the laminar flow one, and estimate the error introduced by taking these limiting models for channel flow. Concerning the effect of viscous dissipation, a great deal of work already exists, but it is mainly focused on the heat transfer problem and not in the nonisothermal reactive case (Aydin 2005; Morini 2005; Aydin et al. 2006; Barletta et al. 2006; Jeong et al. 2006; Magyari et al. 2006; Chiba et al. 2008).

7.2 APPROXIMATE SOLUTIONS FOR NONLINEAR KINETICS

There are not many available analytical treatments for the case of nonlinear wall kinetics. The most used strategies were reviewed in Chapter 2, but even the ones with a strong analytical character end up having to be evaluated numerically. With today's computational capabilities this actually makes the problem solution less straightforward than simply solving numerically the governing equations with appropriate boundary conditions.

In our work in Chapter 2, we have proposed a perturbation procedure to obtain analytical, explicit expressions for conversion as a function of the reaction order m in the case of a power-law kinetics. However, this introduced a limitation: intermediate values of Da may be satisfactorily approximated (and this indeed happens in some cases) but this is not guaranteed by the method, which predicts higher errors as Da increases/decreases from zero/infinity. This happens because the solutions were constructed from two limits associated with Da, which is the only parameter appearing next to the 'problematic' concentration nonlinear term in the kinetic law. Moreover, we have considered also the two main mass transfer regimes (developing and fully developed) to solve the mass balance in the simplest way possible. Nevertheless, it was possible to achieve some insight concerning the effect of the reaction rate law in conversion, namely:

1. The form of the perturbation expansion for mixing-cup concentration is different in the kinetic and in the mass transfer controlled limits: while in the former, the influence of m appears implicitly in the coefficients that are calculated; in the later there is also the explicit appearance of m in the order of the gauge functions of the perturbation parameter, which constitutes the expansion ($\langle c \rangle = \sum_{n=0} \langle c \rangle_n \varepsilon^{n/m}$).

2. For orders of reaction $m > 1$, the results for conversion normalize with the kinetic control asymptote up to higher values of Da. On the other hand for $m < 1$, deviation from the leading-order solution is negligible for small Da but gets more pronounced as the value of this parameter increases.
3. For orders of reaction $m < 1$, the orders of subsequent corrections to the Dirichlet leading-order term are much lower in magnitude ($O\left(\varepsilon^{n/m}\right)$), which means that the deviation from the full mass transfer control decreases sharply as $\varepsilon \to 0$ (i.e. better agreement with the Dirichlet limit for the same Da is observed).
4. Perturbation corrections are especially required when $m > 1$ in the mass transfer controlled regime, and in the kinetically controlled regime when $m < 1$.

5. In the determination of intrinsic reaction rate parameters, reactions orders with $m<1$ are expected to deviate the most from the normalization if low Da conditions cannot be assured.
6. When mass transfer controlled conditions are attained numerical integration may present some increased difficulties (e.g. when concentration near the wall oscillates to zero and the wall reaction is of 'power law' type with non-integer exponent; or when boundary layers near the wall exist). Therefore, analytical results are particularly convenient in this case.
7. The changes in behavior for $m<1$ and $m>1$ are related to kinetic / mass transfer control and the same trends were observed in the fully developed and developing limits. In the case of developing profile, the perturbation parameter was the rescaled Damköhler number detailed in Chapter 4. In this case, even though corrections due to curvature and velocity profile nonlinearities in a circular channel with laminar flow are important (as seen in section 2.3), accounting for the order of reaction reduces errors by one order of magnitude (e.g. for $Da^*=0.1$ and $\alpha\, Pe_m=100$, the maximum deviation for $m=2$ is 0.06%). Nevertheless, we note that the leading-order extended corrections from section 2.3 (accounting for curvature and nonlinear flow profile) are valid in these limiting cases too and can be added.

7.2.1 Suggestions for future work

Further analytical treatment on the effect of nonlinear reaction rates or more complex kinetics is likely to be more limited and demanding of numerical evaluation. However, the limiting solutions can be used in semi-numerical procedures suggesting a dependence of conversion on the governing parameters. For example, Spence et al. (1995) has noted the difficulties in the numerical solution of a one-dimensional model for power-law kinetics with non-integer reaction exponent m, when concentrations reach zero at the wall. To overcome this problem, an exponential substitution for the wall concentration is suggested, which helps the numerical evaluation if a coefficient in the argument of the exponential is set to 1000. This fitting relates directly to our analysis in section 2.4.2a. It is possible that our results can be used to improve numerical evaluation, based on a theoretical analysis and without the need for fitting coefficients. It would also be interesting to evaluate how the results presented can be employed in the determination of intrinsic kinetic parameters and rate expressions, and how available kinetics (determined from other methods) compare with these solutions.

7.3 UNIFORMLY VALID SOLUTION TO GRAETZ'S PROBLEM

We have pointed out that most literature analyzes transport-reaction problems in microchannels in one of two main mass (or heat) transfer regimes. We have also done so in Chapter 2, even though corrections to Lévêque's leading-order result were proposed to extend its validity to lower values of Graetz's parameter ($\alpha\, Pe_m / z$), for finite reaction rates. In Chapter 3, we reviewed several attempts to analytically describe the two simplified regimes in a single uniformly valid composite solution and have concluded that the existing approaches were unsatisfactory. Therefore, based on a feature of the eigenvalues on the exact solution, we propose the application of an asymptotic technique to obtain a general solution for concentration conversion (temperature change). Furthermore, we have identified in the obtained result the contributions of the fully developed and developing limits and two correcting functions accounting for the importance of each one in the composite solution. The overall quantity χ, which may be conversion of reactant X_R by an infinitely fast reaction (or also when kinetics is moderately fast but finite, $Da > 1$) or the reciprocal of Sherwood number in Neumann boundary condition ($1/Sh$), writes as:

$$\chi = \chi_{fd}\, \Theta_{fd} + \chi_{dev}\, \Theta_{dev} \tag{7.1}$$

where χ_{fd} is the value of χ in the fully developed regime (associated with the first term in an series of eigenfunctions), χ_{dev} is the solution when the concentration/temperature profile is considered only in a boundary layer near the wall. Moreover, Θ_{fd} is a function depending on the coefficients from the first term in Graetz series and accounts for the other terms that are not being retained in the fully developed limit. On the other hand, Θ_{dev} has the form of an incomplete Gamma function, whose arguments include the Graetz parameter and quantities depending on the shape of the channel, the flow profile and the boundary layer thickness.

The solutions of the form of (7.1) fulfill both limiting solutions and also yield very acceptable results in the transition regime, as it was shown for the channel geometries, flow profiles and boundary conditions studied in Chapter 3. No numerical evaluation is required and higher order terms don't need to be considered. The abundant information concerning the first term in Graetz series can be used to construct an uniform solution, with no additional information required. The same procedure was applied to the case of finite wall resistance (due to a finite reaction or nonzero thermal resistance). We believe that the combination of limiting models for heat/mass transfer in (7.1) is particularly important at the microscale, where both regimes can be found (millisecond contact times locate the operation at the inlet regime or at least a non-negligible entrance length inside the channel exists). It is also possible that, depending on the objective function for performance adopted in a particular application, the optimum operation is in the

transition region between the two models, which can be conveniently represented by our analytical solution.

7.3.1 Suggestions for future work

The Graetz problem is a classic one (the original solution by Graetz goes back to 1883), it is very fundamental in mass/heat transfer theory (Shah et al. 1978) and has been object of many modifications/extensions which are often referred as Graetz solutions (Weigand et al. 2007; Cossali 2009; Haji-Sheikh et al. 2009; Haji-Sheikh et al. 2010; Ray et al. 2010). The same comments apply to Lévêque's analysis (1928), and generalized Lévêque-type solutions are also present in the literature (Vera et al. 2011). Recently, these problems have gained an additional source of interest in the context of microchannel heat exchangers/reactors, for which a considerable number of studies are currently being published. We note that several reviews have reported that conventional macroscale theory is able to describe channel phenomena in the dimensions considered here, as long as microscale effects are considered. Inlet concentration/temperature boundary layers are one of these effects. Despite the fact that these problems constitute the basis of analysis of many diverse phenomena, the analytical treatment is generally the same (yielding an infinite series). This is a common characteristic shared with other linear partial differential equations, whose particular solutions are combined by the principle of superposition.

From the examples presented in this thesis, we believe that the application of asymptotic summation of series techniques (in particular, of the Euler-Maclaurin formula) may be of interest for a number of cases currently discussed in the literature. We note that this approach allows us to simultaneously obtain the corresponding Lévêque-type solution or correction, as this is a natural outcome of the procedure. Examples of possible extensions in the channel transport context include conjugate problems in heat transfer (Papoutsakis et al. 1981a; Papoutsakis et al. 1981b), axial diffusion effects (Acrivos 1980; Papoutsakis et al. 1980b; Papoutsakis et al. 1980a; Haji-Sheikh et al. 2009) and viscous dissipation (Aydin et al. 2010), among others. In particular, we propose three suggestions:

1. Considering axial diffusion in the problem, yields solutions with the same form of the problem considered in Chapter 3, but with coefficients which exhibit a more complex dependence on the governing parameters. However, it is possible to anticipate that by expansion of functions for plug-flow and WKB methods for laminar flow, the asymptotic behavior of these quantities can be obtained. For example, for Dirichlet boundary conditions with plug-flow between parallel plates,

$$\Delta\lambda^2 = \lambda_{n+1}^2 - \lambda_n^2 \sim Pe_m\,\pi - \frac{Pe_m^3}{8\,\pi\,n^2} + O\left(n^{-3}\right)$$

In this case, the spacing between eigenvalues also depends on the transverse Peclet number. At this stage, we recall the usefulness of empirical correlations to translate the parametric dependence of these quantities in a simple, but accurate manner. Then, with some additional assumptions the Euler-Maclaurin sum formula may still be an excellent tool to obtain a complete solution, with the advantages mentioned above. This results in an analysis which may be uniform in α^2 and $\alpha\,Pe_m$. Therefore, for channels without small aspect ratios general solutions can be obtained.

2. For the case of simultaneous development of the velocity profile, although the coefficients that appear in that case are also functions of other parameters, it would be interesting to understand if the same method applies.
3. In the case of a simultaneous homogeneous reaction (which may be activated at higher temperatures), the form of the solution is similar, but with coefficients that also depend on the bulk Damköhler number (defined with the homogeneous reaction rate at reference conditions). Developments in this problem may be expected.

7.4 DEGREE OF PROFILE DEVELOPMENT

One of the consequences of deriving a solution valid in all points of the domain and parametric space that we found particularly interesting was the estimation of boundaries for application of the well-known limiting solutions. This has been translated in the literature through several related quantities, e.g.: entrance length, incremental heat transfer number, thickness of boundary layer,... and has been determined in a number of ways, detailed in Chapter 3. Most of them are not explicit in the criterion, which at some point will have to be set arbitrarily. In our work, we have defined a degree of transverse control which measures the agreement with the fully developed asymptote. We concluded that the results were more insensitive to the formulated criterion in the fully developed boundary, whereas the inlet region depends more expressively on the level of agreement required with Lévêque's solution. Also, in the fully developed boundary the effect of flow profile is negligible. The transition region may occupy a large part of the channel domain. This can also be related with the pressure drop experienced in the system and the level of influence of inlet effects (which increase mass transfer) present in the system. In the case of a finite reaction rate, we have observed that for $Da > 1$, the entrance length is near the fast reaction asymptote, while for $Da \to 0$ the applicability of the 1-term Graetz solution increases up to the inlet.

7.4.1 Suggestions for future work

We have suggested that the uniformly valid solutions obtained in section 7.3.1 could be useful to analyze other problems. The definitions of transition boundaries would follow in the same terms. One adaptation of our results which would probably not require much additional effort is based on the idea behind one of the methods that are used for estimating the concentration profile length: analogy with the development of the velocity profile. This leads to the substitution of Reynolds number by Peclet number (i.e. multiplication by the Schmidt number) with negligible alteration of the numerical coefficients. Therefore the development of the velocity profile alone in a duct (with the shape normalization possibility pointed out in Chapter 3) could be treated in the same way. The effect of the simultaneous velocity and concentration/temperature development on these boundaries it is also of interest. Our ideas can be extended to a number of other cases. In particular and to highlight the effects of the microscale on the fluid dynamics, the results for finite wall resistance (finite *Da*) can share some similarities with the case of developing velocity slip (flow) in a channel with isothermal wall.

7.5 MAPPING OF OPERATING REGIMES AND THE CONCEPT OF "RESCALED DAMKÖHLER NUMBER"

In the previously identified contributions, the regimes proposed by the analysis were mainly concerned with the interaction of convection through the channel (in streamlines parallel to the surface defined by the wall) and transverse diffusion towards the catalyst coating. We proceeded to also incorporate the coupling of these transport mechanisms with the magnitude of reaction rate occurring at the channel wall. This was done in two parts. First, we focused on the external mass transport effects on a surface reaction in Chapter 4 (with internal phenomena lumped in the effectiveness factor). Then, the internal phenomena (at the catalytic coating level) was considered in more detail in Chapter 5.

Concerning the definition of external kinetically controlled and mass transfer controlled regimes the following was achieved (Chapter 4):

1. We have defined in line with what has been presented in the literature, a degree of mass transfer control θ, which is a concentration ratio;
2. Explicit expressions for θ were presented in the fully developed and developing limits for kinetic and mass transfer controlled regimes;
3. In each limit of the convection-transverse diffusion balance, correlations for θ were proposed to describe all values of Da;

4. Criteria for kinetic and mass transfer control valid for all values of the Graetz parameter and of the form $Da = Da\left(\theta, \alpha\, Pe_m / z\right)$ were proposed and describe very reasonably the results obtained from numerical simulations with gPROMS®;
5. Iso-θ curves were plotted in a $Da - \alpha\, Pe_m / z$ diagram, in particular for specified low and high specified values of θ (kinetic and mass transfer control, respectively);
6. The achievement of external mass transfer control required high values of Da, even for low $\alpha\, Pe_m / z$. Moreover, the effect of increasing the Graetz number is visible by demanding more severe conditions (translated e.g. into higher operating temperatures) to attain the same degree of mass transfer control observed in the fully developed regime, and
7. Previous criteria presented in the literature for specific values of θ (or related quantities) can be incorporated in our analysis and they all prove to be in agreement with our results, but are more limited or of less convenient evaluation.

The basis for defining these operating regimes has been the magnitude of the Damköhler number. In our opinion, this has happened for several reasons: this was how the very influential original work from Damköhler (1937) presented the problem; in many cases the effect of the entrance length is still not considered and in these conditions the degree of mass transfer control is indeed only a function of *Da*; simple magnitude relationships are attractive for the interpretation of experimental work; and from analogy with other problems such as the internal diffusion-reaction analysis based on the magnitude of Thiele modulus. However, we have seen that the entrance length needs to be accounted for in microchannels and has influence on mass transfer. Since this is an important parameter, we propose a modification based on the correct scaling of the wall boundary condition,

$$Da^* = Da\,\delta \tag{7.2}$$

where δ is the normalized thickness over which concentration decays in the channel. Most literature consider $\delta \sim 1$ (i.e. the scale for concentration change in the channel is e.g. the channel radius or the half spacing between parallel plates). However, we have shown that at the convection-dominated (Lévêque's) regime, this scale is not appropriate and the correct one should be applied in (7.2). In this case, the limiting conditions for absence of radial concentration gradients and wall concentration annulment are observed for $Da^* \to 0$ and $Da^* \to \infty$, and this is more rigorous than taking the $Da \to 0$ and $Da \to \infty$ limits. The parameter in (7.2) was named as the 'rescaled Damköhler number' and the variation of θ with Da^* in the developing profile limit is similar to the $\theta\left(Da\right)$ dependence on the fully developed profile asymptote. We have also shown that the concept can be applied when the thickness over which concentration changes is known as a result of other inner descriptions, incorporating different mechanisms (namely axial diffusion at the inlet, section 4.5). In this case,

concentration annulment at the wall near the inlet is also observed for high rescaled Damköhler number, and the iso-Da^* lines can also be plotted in a $Da - \alpha\ Pe_m$ diagram, so that the regions of influence of this effect are easily identified. Naturally, more severe conditions are required for concentration annulment to occur at the inlet, and in this case the remaining portion of the channel is also under full mass transfer control.

In Chapter 5, the interplay of these 'external' regimes with what is occurring inside the coating was considered. In particular, we showed that internal limitations may be controlling in the definition of a global (channel and washcoat) kinetic regime. This depends on the magnitude of a parameter involving bulk and catalyst diffusivities as well as the ratio between the length scales for diffusion at the channel and washcoat. It also explains why some studies observe internal limitations in the absence of external ones in the same ranges of temperature that others observe the opposite picture. Moreover, we have identified how the parameters relate to each other in the transition between regime definition from internal and external phenomena, which apart from geometrical and kinetic-related quantities is given by

$$\frac{D_{eff}}{\varepsilon\ D\ Sh} = \frac{D_{eff}}{t_w\ k_m},$$

where k_m is the mass transfer coefficient, D_{eff} the effective diffusivity in a coating with thickness t_w.

The boundaries were plotted in terms of the operating variable of interest, in this case temperature, as a function of a dimensionless parameter. However, this is just done for convenience since this dimensionless variable can be converted to a geometric feature of the design, if other quantities are kept fixed. Several expressions for the limiting temperatures which bound different regimes were proposed and are of convenient evaluation. These results make use of two quantities that can be set by the user as desired: the degree of mass transfer control θ (defined in Chapter 4) and the effectiveness factor (for which approximations in Chapter 5 were provided), which express the mass transfer resistances in the channel and coating, respectively.

7.5.1 Suggestions for future work

As mentioned in Chapter 1, microdevices open the possibility of operating in new parametric windows. It would be interesting to identify some of those regions in the constructed parametric map, once more information concerning production-scale technologies becomes available. On the other hand, it would also be of interest to draw the path of the chain of process development

in the proposed regime diagram: from kinetic studies (at low *Da*) to chemical production at different scales.

In the case of axial diffusion being also considered in the analysis of the extended Graetz problem, a third axis should be added to the diagram, corresponding to the aspect ratio (which governs the magnitude of axial diffusion effects to the transverse diffusion one). The case of nonisothermal systems would also add at least two parameters (concerning heat generation and conduction), assuming that others such as Arrhenius number with activation energy are kept fixed. The influence of inlet effects (in the sense detailed in section 4.5) should be also relevant in the investigation of local effects in fast reactions and ignited states. The results of our simplified new description for the boundary layer could be pursued in this context.

7.6 EVALUATION OF THE EFFECTIVENESS FACTOR IN A THIN CATALYST COATING

In the previous topics, external transport (in the channel) and its interaction with reaction were discussed while effects at the catalyst coating level were lumped by an effectiveness factor (η) and incorporated into the Damköhler number. As in most literature, we adopt the effectiveness factor concept as the basis for the analysis of the internal transport-reaction competition. Other related quantities (concentration ratios, linear driving force coefficients, mass transfer coefficients) imply a linearization of the concentration profile near the wall and in terms of evaluation are of comparable difficulty. Concerning our approach for the calculation of η, the main achievements in Chapter 5 were:

1. We wrote a reduced order model to represent reaction and diffusion in a catalytic coating with arbitrary shape. The general 3D equations were reduced to a 2D model by making use of a transformation to the curvilinear orthogonal coordinate system, as described elsewhere (Datta et al. 1985; Mariani et al. 2003). The resulting mass balance is further simplified by applying a perturbation method for thin coatings, reducing the problem to a 1D domain.
2. The concentration profile inside the catalytic coating (normalized by its value at the surface) depends on the following parameters: Thiele modulus ϕ^2 (defined with the characteristic length for diffusion, i.e. the maximum distance in the direction normal to the fluid-solid interface); the ratio of length scales for diffusion in the coating and in the channel (ε); and the ratio of washcoat volume to interfacial area and to the internal diffusion length scale (υ).
3. The concentration distribution and the effectiveness factor can be written as a series in powers of ε, assuming small values of this parameter. We consider the first two terms in

this expansion. This has proven to be reasonable in some cases even for $\varepsilon \sim O(1)$. Note that considering more terms in the perturbation series may improve the approximation near $\varepsilon = 0$, but may cause serious divergence as ε increases. Therefore, our two-term solution is appropriate.

4. The obtained result for η can be written in terms of the aforementioned geometry-related parameter (υ) and of the effectiveness factor for an equivalent slab (η_{slab} with the same length scale for diffusion). This was shown to be rigorously true in the case of perturbation solutions with linear kinetics (valid for all values of ϕ^2) and arbitrary geometry (as long as $\varepsilon < 1$). Nevertheless, reasonable agreement with numerical solutions is obtained even for $\varepsilon \sim 1$.
5. Based on the analysis for high and low ϕ^2, we speculated that the previous expression for η would also apply to the case of a reaction rate expression with arbitrary form. This was confirmed by comparison with the numerical solution for several 'normal' kinetics. In this case, the evaluation of η_{slab} has to be done for the particular reaction law. An approximate procedure for this was proposed, which is based on the solution for linear kinetics with a modified Thiele modulus Φ^2, including the classical normalization at high reaction rates and the correct behavior in the chemical regime.
6. The same result was also shown to improve the calculation of η in nonuniform geometries. Namely, by introducing a correction to the 'slice method' from Papadias et al. (2000), the error associated with this approximation decreases, especially in the intermediate region of ϕ^2.
7. The analysis was also applied to thin catalytic coatings supported on impermeable/inert particles to model egg-shell catalysts. It was found that the same expression was valid not only for uniform surface concentration conditions, but also when external mass transfer resistance was present.

7.6.1 Suggestions for future work

It would be interesting to further extend the perturbation techniques here employed to the cases where angular diffusion needs to be considered. This would allow a better description of nonuniform coatings and eventually provide analytical expressions for the local differential effectiveness factor, as defined by Hayes et al. (2005). This also relates to the more general case of a reaction-diffusion problem in a nonuniform geometry with peripheral variation of surface concentration (which is likely to be found in irregularly coated channels). The suitability of our approximation for η in the case of abnormal kinetics or with solution multiplicity also deserves

further investigation. However, since these effects usually manifest themselves in an intermediate range of the Thiele modulus, it is possible that the corrections in the chemical and diffusional limits can still be applicable. Other natural extensions of this work would include nonisothermal systems and systems with multiple reactions (for which the validity of the one-dimensional cylindrical model was already discussed in Keegan et al. (2005)). Taking into account the good description of the finite mass transfer resistance case in egg-shell catalyst particles, it can also be suggested that global effectiveness factors in a microchannel geometry should be considered.

Solutions based on the 'thin layer' assumption and consequent perturbation corrections should be useful to a number of other systems, e.g. related with pellicular adsorbents. Specific problems may include the measurement of diffusivities from chromatographic methods (where the effectiveness factor in the steady-state problem is related to the transfer function in Laplace's domain of the transient non-reactive problem). Multilayer egg-shell particles (catalyst or adsorbents) could benefit from this approach as well, even if the solution also requires some numerical evaluation.

7.7 PERFUSIVE COATINGS AND MONOLITHS

The second main direction for process intensification we have focused on is the improvement of mass transfer by promotion of an additional transport mechanism in porous catalytic bodies: intraparticular forced convection. In Chapter 5, we have applied a perturbation method conceived for thin coatings to a permeable curved wall, which can be the surface of a perfusive monolith for example. We developed an approximation for the effectiveness factor for this case, which described correctly the numerically obtained solution, for several values of the intraparticular Peclet number P, Thiele modulus ϕ^2, ratio of surface concentrations c_2, and channel/coating diffusion length scales ratio ε (including ε near 1).

We then examined a regime described by dominance of intraparticular convection and reaction, where we have found the most expressive enhancement of the effectiveness factor compared to a nonpermeable (negligible convection) catalyst in the same conditions. The combination of parameters at which the improvement was maximum was derived explicitly. This was found to be an increasing function of $\sqrt{P}$, but reaction rate should also 'match' with the increased transport rates, according to $\phi^2 \sim P$.

7.7.1 Suggestions for future work

In this case, we believe that considering external mass transfer will lead to much more complicated analytical expressions, and one can doubt of its usefulness. Nevertheless, some progress may occur with the simplified analysis in section 5.7.3.

It would be perhaps more interesting to incorporate our results at the single channel level into the (probably numerical) solution of more complex systems. This may appear e.g. in a specified arrangement of channels, where interaction between them happens due to suction/injection through the wall.

7.8 MAXIMUM TEMPERATURE RISE IN PERFUSIVE CATALYST PARTICLES

We continued to explore the effects of intraparticular convection on the behavior of catalytic porous solids in Chapter 6. In this case, the problem of an exothermic reaction in a slab-shaped catalyst particle was considered. This added transport and generation of heat to the mass transfer-reaction interaction. We conducted a scaling analysis to reach the following conclusions:

1. According to the mass balance, three dominant regimes can be identified. Each one reflects a balance between two mechanisms (convection, diffusion and reaction). These are related with the limiting regimes defined from the energy balance by assuming an order of magnitude for Lewis number.
2. The scale for temperature change $\Delta\hat{T}$ due to the occurrence of an exothermic reaction is predicted in several areas of the 3D parametric diagram formed by Thiele modulus, intraparticular mass Peclet number and Lewis number.
3. Different behaviors concerning $\Delta\hat{T}$ were observed, namely: isothermal (where temperature rise is negligible); diffusive (where Prater's relationship (Prater 1958) for non-permeable catalyst holds); adiabatic (where the adiabatic temperature rise is observed); and 'explosion' (where concentration annulment occurs and rescaling is required).

A perturbation analysis was then applied to the three main operating regimes to estimate concentration and temperature profiles, effectiveness factor and maximum temperature attained inside the catalyst. In particular, we note that

1. In the transport dominated case (chemical regime), a regular perturbation expansion expressed the small deviation of concentration and temperature from their surface values.

2. In the diffusional regime, concentration (and temperature) variation only occurs at thin boundary layers near the surface, where reaction dominates with diffusion (the core of the catalyst is free from reactant). The effect of convective transport in these regions is of the order of $\sqrt{Pe_m}/\phi$. This is also the order of the correction to Prater's limit (Prater 1958) in the maximum temperature estimate.
3. In the limit of strong convection, two distinct situations are considered depending on whether concentration annulment occurs or not. In the latter case, the problem is described at most part of the domain (starting from the inlet) by a smooth variation of concentration/temperature. Then, near the 'exit' of the slab (downstream) a relatively sharper decrease from surface values may be observed (in a region with thickness $1/Pe_m$). However, maximum concentration and temperature changes are small.
4. When concentration reaches annulment in a 'dead core' inside the slab, we consider the same structure for the boundary layer near the exit of the slab, but matched with the annulment branch of the solution. A boundary separating this regime from the diffusional one was provided. The transition between convection dominated regimes (with and without annulment) was also estimated analytically.
5. When convection is strong, but reaction is also fast enough to cause some annulment in the reactant's concentration, maximum effectiveness factor and temperature change are observed. Namely, the adiabatic temperature rise is obtained at leading-order and the effectiveness factor presents a very similar dependence to the optimum enhancement conditions in Chapter 5, with a contribution accounting for nonisothermal behavior (both analyses refer to the convection-reaction dominant balance).

The adiabatic temperature limit is frequently found as the maximum temperature in systems with coupled processes. For example, in the case of premixed flames from combustion theory (Law 2006). The same result was also found in catalyst particles with negligible intraparticular convection. Belfiore (2007a; 2007b) considered strongly exothermic reactions (Prater's parameter, $\beta \to 1$) with Dufour and Soret effects, and temperature dependence of physicochemical properties. The adiabatic temperature rise was found and named as a 'generalized Prater equation'.

7.8.1 Suggestions for future work

Extensions of this topic may include examination of other catalyst geometries. It could also be interesting to evaluate how kinetic normalization (e.g. the generalized Thiele modulus defined in Chapter 5) applies in the presence of internal convection. The effect of finite mass/heat

resistance and analytical bounds for the range where steady-state multiplicity occurs are also possible topics for future research.

REFERENCES

Acrivos, A. (1980). "The extended Graetz problem at low Peclet numbers." Applied Scientific Research **36**(1): 35-40.

Aydin, O. (2005). "Effects of viscous dissipation on the heat transfer in a forced pipe flow. Part 2: Thermally developing flow." Energy Conversion and Management **46**(18-19): 3091-3102.

Aydin, O. and M. Avci (2006). "Viscous-dissipation effects on the heat transfer in a Poiseuille flow." Applied Energy **83**(5): 495-512.

Aydin, O. and M. Avci (2010). "On the constant wall temperature boundary condition in internal convection heat transfer studies including viscous dissipation." International Communications in Heat and Mass Transfer **37**(5): 535-539.

Barletta, A. and E. Magyari (2006). "Thermal entrance heat transfer of an adiabatically prepared fluid with viscous dissipation in a tube with isothermal wall." Journal of Heat Transfer **128**(11): 1185-1193.

Belfiore, L. A. (2007a). "Effects of the collision integral, thermal diffusion, and the Prater number on maximum temperature in macroporous catalysts with exothermic chemical reaction in the diffusion-controlled regime." Chemical Engineering Science **62**(3): 655-665.

Belfiore, L. A. (2007b). "Soret diffusion and non-ideal dufour conduction in macroporous catalysts with exothermic chemical reaction at large intrapellet Damköhler numbers." Canadian Journal of Chemical Engineering **85**(3): 268-279.

Chiba, R., M. Izumi and Y. Sugano (2008). "An analytical solution to non-axisymmetric heat transfer with viscous dissipation for non-Newtonian fluids in laminar forced flow." Archive of Applied Mechanics **78**(1): 61-74.

Cossali, G. E. (2009). "Analytical solution of Graetz problem in pipe flow with periodic inlet temperature variation." International Journal of Heat and Mass Transfer **52**(13-14): 3396-3401.

Damköhler, G. (1937). "Einfluss von Diffusion, Strömung, und Wärmetransport auf die Ausbeute in Chemisch-Technischen Reaktionen." Chem.-Eng.-Tech **3**(Part 1, Chapter 2): 359-485.

Datta, R. and S. W. K. Leung (1985). "Shape generalized isothermal effectiveness factor for first-order kinetics." Chemical Engineering Communications **39**(1): 155 - 173.

Graetz, L. (1883). "Ueber die Wärmeleitungsfähigkeit von Flüssigkeiten." Annalen der Physik und Chemie **18**: 79-94.

Gundlapally, S. R. and V. Balakotaiah (2011). "Heat and mass transfer correlations and bifurcation analysis of catalytic monoliths with developing flows." Chemical Engineering Science **66**(9): 1879-1892.

Haji-Sheikh, A., J. V. Beck and D. E. Amos (2009). "Axial heat conduction effects in the entrance region of circular ducts." Heat and Mass Transfer/Waerme- und Stoffuebertragung **45**(3): 331-341.

Haji-Sheikh, A., W. J. Minkowycz and S. Manafzadeh (2010). "Axial conduction effect in flow through circular porous passages with prescribed wall heat flux." Heat and Mass Transfer/Waerme- und Stoffuebertragung **46**(7): 727-738.

Hayes, R. E., B. Liu and M. Votsmeier (2005). "Calculating effectiveness factors in non-uniform washcoat shapes." Chemical Engineering Science **60**(7): 2037-2050.

Herwig, H. (2008). Momentum and Heat Transfer in Microsized Devices. Micro Process Engineering: Fundamentals, Devices, Fabrication, and Applications. N. Kockmann. Weinheim, Germany, Wiley-VCH Verlag GmbH**:** 47-70.

Jeong, H. E. and J. T. Jeong (2006). "Extended graetz problem including axial conduction and viscous dissipation in microtube." Journal of Mechanical Science and Technology **20**(1): 158-166.

Keegan, S. D., N. J. Mariani, O. M. Martínez and G. F. Barreto (2005). "Behaviour of smooth catalysts at high reaction rates." Chemical Engineering Journal **110**(1-3): 41-56.

Law, C. K. (2006). Combustion Physics. New York, Cambridge University Press.

Lévêque, M. A. (1928). "Les lois de la transmission de chaleur par convection." Ann. Mines **13**: 201-299.

Magyari, E. and A. Barletta (2006). "Thermally developing Poiseuille flow with a non-uniform entrance temperature when the viscous heat generation is significant." Journal of Physics A: Mathematical and General **39**(14): 3829-3845.

Mariani, N. J., S. D. Keegan, O. M. Martínez and G. F. Barreto (2003). "A one-dimensional equivalent model to evaluate overall reaction rates in catalytic pellets." Chemical Engineering Research and Design **81**(8): 1033-1042.

Morini, G. L. (2005). "Viscous heating in liquid flows in micro-channels." International Journal of Heat and Mass Transfer **48**(17): 3637-3647.

Papadias, D., L. Edsberg and P. Björnbom (2000). "Simplified method for effectiveness factor calculations in irregular geometries of washcoats." Chemical Engineering Science **55**(8): 1447-1459.

Papoutsakis, E. and D. Ramkrishna (1981a). "Conjugated Graetz problems-I. General formalism and a class of solid-fluid problems." Chemical Engineering Science **36**(8): 1381-1391.

Papoutsakis, E. and D. Ramkrishna (1981b). "Conjugated Graetz problems-II. Fluid-fluid problems." Chemical Engineering Science **36**(8): 1393-1399.

Papoutsakis, E., D. Ramkrishna and H. C. Lim (1980a). "The extended Graetz problem with Dirichlet wall boundary conditions." Applied Scientific Research **36**(1): 13-34.

Papoutsakis, E., D. Ramkrishna and H. C. Lim (1980b). "Extended Graetz problem with prescribed wall flux." AIChE Journal **26**(5): 779-787.

Prater, C. D. (1958). "The temperature produced by heat of reaction in the interior of porous particles." Chemical engineering Science **8**(3-4): 284-286.

Ray, S. and D. Misra (2010). "Laminar fully developed flow through square and equilateral triangular ducts with rounded corners subjected to H1 and H2 boundary conditions." International Journal of Thermal Sciences **49**(9): 1763-1775.

Shah, R. K. and A. L. London (1978). Laminar flow forced convection in ducts. New York, Academic Press.

Spence, A., D. J. Worth and S. T. Kolaczkowski (1995). "The treatment of non-integer exponents in reaction rate expressions." Computers and Chemical Engineering **19**(11): 1169-1171.

Vera, M. and A. Liñán (2011). "Exact solution for the conjugate fluid-fluid problem in the thermal entrance region of laminar counterflow heat exchangers." International Journal of Heat and Mass Transfer **54**(1-3): 490-499.

Weigand, B. and G. Gassner (2007). "The effect of wall conduction for the extended Graetz problem for laminar and turbulent channel flows." International Journal of Heat and Mass Transfer **50**(5-6): 1097-1105.